Forschungszentrum Karlsruhe
Technik und Umwelt

Wissenschaftliche Berichte
FZKA 6271

High Pressure Chemical Engineering

Proceedings of the International Meeting of the GVC-Fachausschuß „Hochdruckverfahrenstechnik“

March 3 - 5, 1999, Karlsruhe, Germany

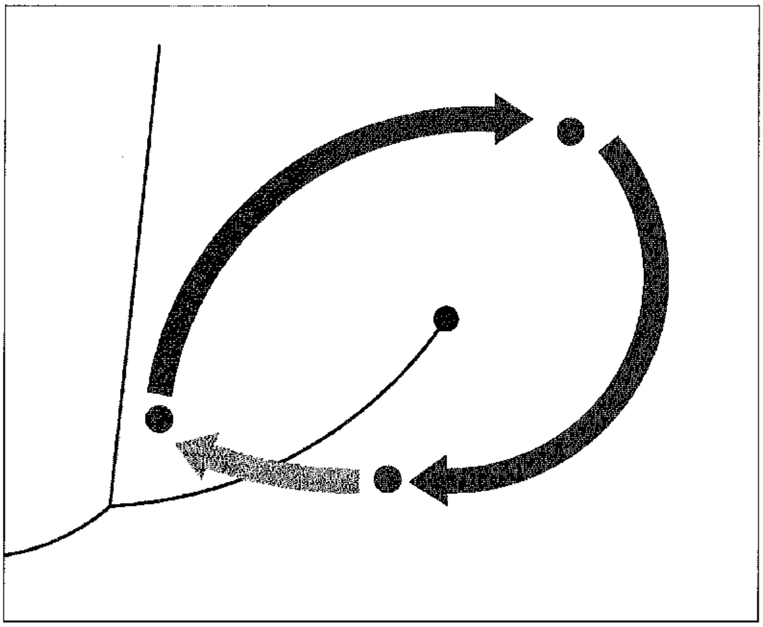

Institut für Technische Chemie

GVC
VDI-GESELLSCHAFT VERFAHRENSTECHNIK
UND CHEMIEINGENIEURWESEN

Juni 1999

Forschungszentrum Karlsruhe

Technik und Umwelt

Wissenschaftliche Berichte

FZKA 6271

High Pressure Chemical Engineering

Proceedings of the International Meeting
of the GVC-Fachausschuß "Hochdruckverfahrenstechnik"
March 3-5, 1999, Karlsruhe, Germany

N. Dahmen, E. Dinjus (Editors)

Institut für Technische Chemie

Forschungszentrum Karlsruhe GmbH, Karlsruhe
1999

Als Manuskript gedruckt
Für diesen Bericht behalten wir uns alle Rechte vor

Forschungszentrum Karlsruhe GmbH
Postfach 3640, 76021 Karlsruhe

Mitglied der Hermann von Helmholtz-Gemeinschaft
Deutscher Forschungszentren (HGF)

ISSN 0947-8620

Scientific Committee

Prof. Dr. E. Dinjus, Karlsruhe
Prof. em. Dr. Dr. h.c. E.U. Franck, Karlsruhe
Prof. Dr.-Ing. G. Brunner, Hamburg-Harburg
Prof. Dr.-Ing. G. Luft, Darmstadt
Dr. S. Maier, Ludwigshafen

Organization Committee

Forschungszentrum Karlsruhe
Institut für Technische Chemie
Chemisch-Physikalische Verfahren
P.O.Box 3640
D-76021 Karlsruhe, Germany

Prof. Dr. E. Dinjus,
Dr. N. Dahmen
Dipl.-Ing. A. Kögel
Dipl.-Chem. K. Wagner
E. Schröder
S. Bolz

GVC - VDI-Gesellschaft
Verfahrenstechnik und
Chemieingenieurwesen
P.O.Box 101139
D-40002 Düsseldorf, Germany

Dipl.-Ing. K. O. Schaller
Dipl.-Ing. R. Briel

Sponsors

B.E.S.T. Ventil+Fitting GmbH
DRÄGER TESCOM
FISHER ROSEMOUNT GmbH & Co.
Ernst Haage Apparatebau GmbH & Co. KG
Kempe Apparate und Maschinenbau
NWA analytische Meßgeräte GmbH
SCHMIDLIN Labor + Service GmbH
Schmidt, Kranz & Co. GmbH
SITEC-Sieber Engineering AG
WAGNER Meß- und Regeltechnik GmbH

Tagungsband der internationalen GVC-Fachausschußsitzung „Hochdruckverfahrenstechnik“, 3.-5. März 1999 in Karlsruhe

Die VDI-Gesellschaft Verfahrenstechnik und Chemieingenieurwesen (GVC) ist die Fachorganisation der auf dem Gebiet der Verfahrenstechnik und des Chemieingenieurwesens tätigen Ingenieure sowie der ihnen nahestehenden Berufsgruppen. Das Rückgrat der technisch-wissenschaftlichen Arbeit der GVC stellen die über 30 Fachausschüsse dar, in deren Sitzungen ein Erfahrungsaustausch zwischen Spitzenfachleuten aus den Universitäten und der Industrie stattfindet. Jüngeren Wissenschaftlern wird Gelegenheit gegeben, ihre Arbeiten zu präsentieren und auch noch nicht ausgereifte Überlegungen zur Diskussion zu stellen.

Der Fachausschuß „Hochdruckverfahrenstechnik“, z.Zt. unter Vorsitz von Prof. Dr.-Ing. G. Brunner, Technische Universität Hamburg-Harburg, tagt im jährlichen Wechsel an Hochschulen oder Forschungseinrichtungen, die sich mit Forschung und Entwicklung auf dem Gebiet der Anwendung hoher Drücke in der Technik beschäftigen. Die GVC·VDI veranstaltete seine diesjährige Fachausschußsitzung „Hochdruckverfahrenstechnik" zusammen mit dem Institut für Technische Chemie, Bereich Chemisch-Physikalische Verfahren im Forschungszentrum Karlsruhe, um den technischen Stand und wissenschaftliche Erkenntnisse zur Entwicklung von Hochdruckverfahren vor einem internationalen Publikum, vor allem aus Europa, zu präsentieren und zu diskutieren. Unter den 35 akzeptierten Vorträgen und 31 Postern fanden sich 19 bzw. 7 Beiträge aus Europa und den USA. Die Zahl der Teilnehmer betrug etwa 170, etwa 50 von ihnen kamen aus dem vorwiegend europäischen Ausland.

Eingeladene Vorträge wurden zu den Themenschwerpunkten Polymerisation und Polymermodifikation in nah- und überkritischen Fluiden (Prof. E. Kiran, University of Maine, Orono, USA), Reaktionen in heißem Hochdruckwasser (SCWO, Dr. H. Schmieder, Forschungszentrum Karlsruhe, D) und Herstellung von kleinskaligen Teilchen (Prof. E. Weidner, Ruhr-Universität Bochum, D) sowie zu den für viele Verfahrensentwicklungen notwendigen Grundlagen zu Phasengleichgewichten und Mischphasenthermodynamik (Prof. V. Majer, Université Blaise Pascal/C.N.R.S., Aubiere, F) gehalten. Weitere Themenschwerpunkte waren der Einsatz überkritischer Fluide in chemischen Reaktionen, zu Werkstoffen, zur Naturstoffbehandlung und in Trenntechniken.

Proceedings of the International GVC-Meeting on „High Pressure Chemical Engineering“, March 3-5, 1999, Karlsruhe, Germany

The VDI-Gesellschaft Verfahrenstechnik und Chemieingenieurwesen (GVC) is the organization of engineers and related scientists in the field of process and chemical engineering. The backbone of the scientific-technical work of the GVC are the more than 30 working parties; in their annual meetings experience and knowledge are exchanged between authorities from universities and industry. Young scientists have the chance to present and to discuss their work and even not completed considerations.

The working party „High Pressure Chemical Engineering“, chaired by Prof. Dr.-Ing. G. Brunner from the Technical University Hamburg-Harburg, meets annually at universities and other research facilities involved in research and development in the field of high pressure technical applications. This year, the GVC·VDI ran this meeting in an international surrounding together with the Institut für Technische Chemie at the Forschungszentrum Karlsruhe. State of the art and recent developments and results were presented and discussed in 35 oral presentations and 31 posters; 19 and 7 contributions, respectively, originated from european countries and the USA. From the 170 registrated participants 50 came mostly from european countries.

Invited lectures were given to the main topics polymerization and polymer modification in near- and supercritical fluids (Prof. E. Kiran, University of Maine, Orono, USA), on supercritical water oxidation (Dr. H. Schmieder, Forschungszentrum Karlsruhe, D), on particle generation (Prof. E. Weidner, Ruhr-Universität Bochum, D) and on fundamentals of phase equilibria and thermodynamics (Prof. V. Majer, Université Blaise Pascal/ C.N.R.S. , Aubiere, F). Further topics were concerned with the use of supercritical fluids in chemical reactions, materials, natural food processing and separation techniques.

Table of Contents

Polymers

Key Lecture: Polymerization and polymer modifications in near- and supercritical fluids
E. Kiran, Orono, MA, USA 5

The influence of inert gases on the high-pressure phase equilibria of copolymer-comonomer mixtures
G. Luft, M. Kinzl, Darmstadt, D 15

Free-radical polymerization in homogeneous phase of supercritical CO_2
S. Beuermann, M. Buback, Ch. Isemer, C. Schmaltz, A. Wahl, Göttingen, D 19

Production of elastomers in supercritical carbon dioxide
T.J. de Vries, M.A.G. Vorstman, J.T.F. Keurentjes, Eindhoven, NL 23

Mathematical modeling of dispersion polymerization of vinyl monomers in supercritical fluids
C. Kiparissides, N. Pagalos, Ch. Chatzidoukas, Ch. Mantelis, Thessaloniki, GR 27

Calculation of high pressure phase equilibria in polymer systems
S. Behme, G. Sadowski, W. Arlt, Berlin, D 31

Modeling of kinetics and structural properties in high-pressure fluid-phase polymerizations
M. Buback, M. Busch, H.C.M. van Boxtel, Göttingen, D 35

Polymer modification by supercritical impregnation
O. Muth, Th. Hirth, H. Vogel, Pfinztal, D 39

Preparation and evaluation of supercritical fluid bonded liquid chromatography stationary phase
M.M. Robson, R. Dmoch, I. Bromilow, K.D. Bartle, P. Myers, Leeds, UK 43

Posters:

Effect of cocatalysts on ethylene/1-hexene copolymerisation with metallocenes under high pressure
S. Schmitz, A. Rau, G. Luft, Ch. Götz, Darmstadt, D 47

Experimental investigation of phase equilibria in the system polystyrene/cyclohexane/carbon dioxide
B. Bungert, G. Sadowski, W. Arlt, Berlin, D 51

Modeling of two-phase ethylene polymerization in high pressure autoclaves
P. Pladis, C. Kiparissides, Thessaloniki, GR 55

Changing of properties of glassy polymers due to diffusion of supercritical CO_2
J. von Schnitzler, R. Eggers, Hamburg-Harburg, D 59

Investigation of the sorption and swelling behavior of Polymer/CO_2 systems by combined oscillometric-gravimetric measurements
H. Rave, R. Staudt, J.U. Keller, Siegen, D 63

Light Scattering Investigations of Polydimethylsiloxane in sc-CO_2
T. Berger, W. Steffen, Mainz, D 67

Materials

Poster:

High pressure surface plasmon- and optical waveguide spectroscopy (pressure dependence of thickness and refractive index of thin PMMA-films)
W. Knoll, G. Kleideiter, M.D. Lechner, Mainz, D 75

Hydrothermal Treatment

Key lecture: SCWO: facts and hopes
H. Schmieder, J. Abeln, Karlsruhe, D *83*

Production of hydrogen from wet biomass by supercritical water gasification
J.M.L. Penninger, Hengelo, NL *89*

Modeling, design and scale-up of an SCWO application treating solid residues of electronic scrap using a tubular type reactor – fluid mechanics, kinetics, process envelope
S. Pilz, Ulm, D *91*

Electrochemical aspects of inorganic film deposition from supercritical aqueous solutions
J.I. Brand, A.O. Sezer, Lincoln, NE, USA *97*

Posters:

Corrosion of titanium under SCWO-conditions – Recent results
N. Boukis, C. Friedrich, E. Dinjus, Karlsruhe, D *101*

The SCWO-destruction of organic compounds in the presence of salt in leachates from dump sites in the SUWOX-facility
H. Schmidt, S. Baur, V. Casal, Karlsruhe, D *103*

Simulation of the thermodynamic behavior of the pure components water, oxygen, nitrogen and carbon dioxide and of their mixtures for pressures up to 300 bar and temperatures up to 600°C
S. Pilz, Ulm, D *107*

Gasification of biomass and model compounds in hot compressed water
A. Kruse, J. Abeln, E. Dinjus, M. Kluth, G. Petrich, M. Schacht, E. Sadri, H. Schmieder, Karlsruhe, D *111*

Reactions

The dehydration of 1,4-butanediol to tetrahydrofuran in sub- and supercritical water
T. Richter, H. Vogel, Darmstadt, D *119*

Hydrolysis of some biopolymers with water and carbon dioxide at high pressures and temperatures
K. Liu, G. Brunner, Hamburg-Harburg, D *123*

Hydrogenation at supercritical conditions
M. Härröd, M.-B. Macher, S. van den Hark, P. Møller, Göteborg, S *127*

Chemical reactions in supercritical fluids as a continuous process
M. Poliakoff, F. Smail, N. Meehan, K.W. Gray, M.G. Hitzler, S.K. Ross, Nottingham, UK *131*

Sol-gel synthesis and characterization of various oxide aerogels and NiO and Pt supported on aerogels
Ž. Knez, Z. Novak, Maribor, SL *133*

Poster:

Pyrolysis and hydropyrolysis of a Turkish lignite under high pressures
M. Canel, Ankara, Turkey *137*

Phase Equilibria and Thermodynamics

Key lecture: New approaches to calculation of the Henry's constant of aqueous solutes at superambient conditions
V. Majer, Clermont-Ferrand, F *145*

A new apparatus for the investigation of the phase behavior of dilute, binary supercritical mixtures
M. Türk, A. Diefenbacher, Karlsruhe, D *151*

High-pressure apparatus for phase equilibria measurements: solubility of fatty acid ethyl esters in supercritical CO_2
G. Charbit, C. Crampon, E. Neau, Marseille, F *155*

Static solubility measurements of natural and synthetic dyestuffs in compressed gases
D. Tuma, G.M. Schneider, Bochum, D *159*

Posters:

High pressure equilibria of anthracene and octacosane between supercritical fluids and adsorbents
P. Harting, J. Germanus, Leipzig, D *163*

Correlation, prediction and experimental determination of gas solubilities
K. Fischer, M. Wilken, J. Gmehling, Oldenburg, D *167*

Pressure dependence of intradiffusion in binary mixtures with NH_3 resp. CO_2 as one component
T. Groß, N. Karger, L. Chen, H.-D. Lüdemann, Regensburg, D *173*

Phase equilibrium (solid-liquid-gas) in binary systems of polyethyleneglycols, polyethylenedimethylether with carbon dioxide, propane and nitrogen
V. Wiesmet, E. Weidner, Bochum, D *177*

Natural Food Processing

Extraction of carotenoid-rich oils by supercritical CO_2 and subcritical propane
H.G. Daood, P.A. Biacs, V. Illés, M.H. Gnayfeed, Budapest, H *185*

Extraction of natural products with superheated water
A.A. Clifford, A. Basile, M.M. Jiménez-Carmona, S.H.R. Al-Salidi, Leeds, UK *189*

Processing carotenoid-containing liquids with supercritical CO_2
R. Eggers, A. Pietsch, C.A. Lockemann, F. Runge, Hamburg-Harburg, D *193*

Posters:

Countercurrent extraction with supercritical carbon dioxide: behavior of a complex natural mixture
D. Buß, G. Brunner, Hamburg-Harburg, D *197*

Supercritical CO_2-extraction for production of extracts from plant materials containing cholagoga substances
T. Gamse, R. Marr, Graz, A *201*

Supercritical carbon dioxide extraction of essential oil: the case of two Romanian Lamiaceae
D. Barth, L. Philippon, E. Pop, Nancy, F *205*

Prepurification of Esterase EP-10 by treatment with supercritical carbon dioxide (SC-CO_2)
D.-J. Steinberger, A. Gießauf, T. Gamse, R. Marr, Graz, A *209*

Supercritical fluid extraction of the oil from the Tucumã Pulp (Astrocaryum vulgare Mart.) using carbon dioxide
L. F. de Franca, T. Christensen, G. Brunner, Hamburg-Harburg, D *215*

Particle Formation

Key lecture: Particle generation by high pressure spray processes
E. Weidner, Bochum, D *225*

Fine phospholipid particles formed by precipitation with a compressed fluid antisolvent
C. Magnan, N. Commenges, E. Badens, G. Charbit, Marseille, F *231*

Gas Antisolvent crystallization - from fundamentals to industrial applications
A. Weber, C. Weiss, J. Tschernjaew, R. Kümmel, Oberhausen, D *235*

Posters:

Understanding gas antisolvent processes of biocompatible polymers and drugs with supercritcal CO_2
A. Bertucco, P. Pallado, Padova, I 239

Experimental and theoretical investigations of the formation of small particles from the rapid expansion of supercritical solutions (RESS)
M. Türk, B. Helfgen, S. Cihlar, K. Schaber, Karlsruhe, D 243

Formation of submicron particles by rapid expansion of supercritical solutions
H. Kröber, U. Teipel, H. Krause, Pfinztal, D 247

Effect of process parameters on the supercritical antisolvent precipitation of microspheres of natural polymers
E. Reverchon, I. De Rosa, G. Della Porta, Salerno, I 251

Separation Techniques

Separation of fine chemicals through continuous supercritical fluid simulated moving bed (SF-SMB) chromatography
O. Di Giovanni, W. Dörfler, M. Mazzotti, M. Morbidelli, Zürich, CH 259

Alcohol reduction from excess wine by supercritical CO_2-extraction
T. Gamse, F. Steinkellner, R. Marr, Graz, A 263

Hydrodynamics in countercurrent packed columns at high pressure conditions
P.C. Simões, M.J. Cebola, R. Ruivo, M. Nunes da Ponte, Monte de Caparica, P 267

Synthesis of heavy hydrocarbons (C26 and C28) and purification by supercritical carbon dioxide extraction
D. Barth, S. Gandolfo, A.Brembilla, D. PetitJean, M. Dirand, Nancy, F 271

Present situation of research and technology of textile cleaning in compressed CO_2
J. Kurz, A. Hilbink, B. Gosolits, Hohenstein, D 275

Extrapolation of supercritical fluid processes from lab and pilot to production scale: problems and solutions
P. Mengal, J.-Y. Clavier, M. Perrut, Champigneulles, F 279

Posters:

Separation of stereoisomers in a SMB-SFC plant – determination of isotherms and simulation
T. Giese, A. Depta, M. Johannsen, G. Brunner, Hamburg-Harburg, D 283

Hydrodynamic behavior of aqueous systems in countercurrent columns at high pressures
R. Stockfleth, G. Brunner, Hamburg-Harburg, D 287

Trend evaluation for supercritical applications by patent statistics
E. Schütz, Trostberg, D 293

Natural and forced convection in precision cleaning autoclaves
V. Perrut, M. Perrut, Champigneulles, F 297

Cleaning of Metal Parts and Components by Compressed Carbon Dioxide
N. Dahmen, J. Schön, H. Schmieder, E. Dinjus, Karlsruhe, D 301

To Revert Grinding Sludge into Oil and Metal
- An Application for Supercritical Fluid Extraction in a Technical Scale -
U. Leffrang, K. Büttner and R. Schwing, Wiesbaden, D 305

Swagelok®

... a tradition of Excellence

Zwei-Klemmringverschraubung
Absperr- und Regulierventile
Nadelventile
Kugel- und Kükenhähne
Hochdruckbauteile
Rückschlag- und Überströmventile
Filter und Filterelemente
Manometeradapter
Gewindeadapter
Vakuum-Produkte

B.E.S.T. Ventil+Fitting GmbH
Heinrich-Hertz-Str. 5a
76694 Forst
Tel.: 07251 / 9722-0
Fax: 07251/ 9722-50
e-mail: swagelok@best-ka.de

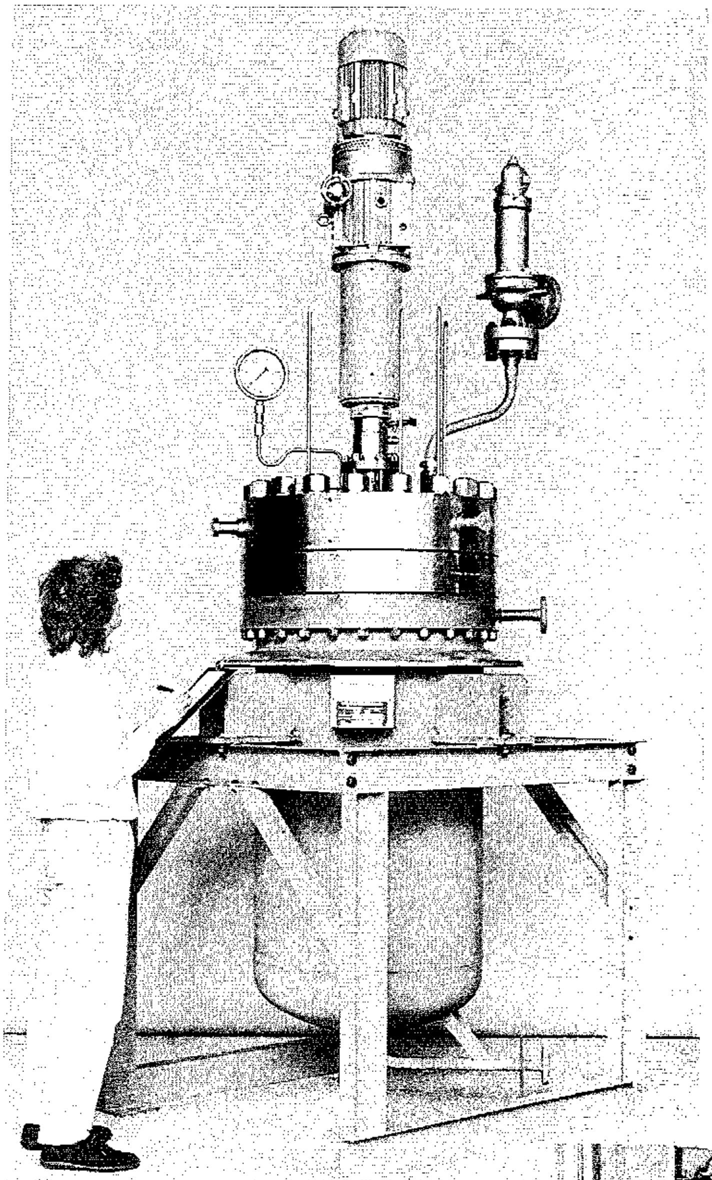

PRODUKTPROGRAMM

- **Laborautoklaven**
  Inhalt 0,15 - 7,5 ltr.
  Betriebsdruck bis 350 bar
  Betriebstemperatur bis 500 °C

- **Mikroautoklav**
  Inhalt 50 ml
  Betriebsdruck 350 bar
  Betriebstemperatur 350 °C

- **Sonderausführungen**
  Inhalt bis 5.000 ltr.
  Betriebsdruck bis 2.000 bar
  Betriebstemperatur bis 800 °C

- **Hochdruckarmaturen**
  bis 4.000 bar

Pilotanlagen

- mit Rohrreaktoren (Festbett)
- nach dem Schleifenprinzip
- Mikroreaktoranlagen

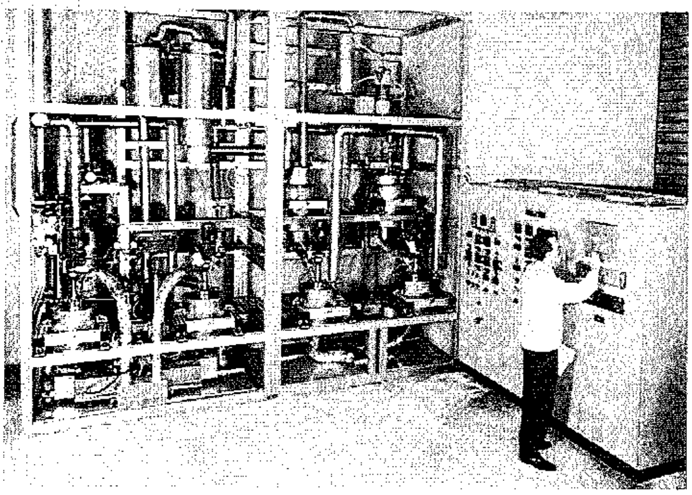

Ernst Haage Apparatebau GmbH & Co KG,
KG: Sitz Mülheim a. d. Ruhr, Amtsgericht Mülheim a. d. Ruhr, HRA 451.
Persönlich haftende Gesellschafterin: Ernst Haage Apparatebau Verwaltungs GmbH,
Sitz Mülheim a. d. Ruhr, Amtsgericht Mülheim a. d. Ruhr, HRB 2240.
Geschäftsführer: Karin Hesselmann, Alfred Hesselmann, Dipl. Kfm. Thomas Hesselmann

Ernst Haage Apparatebau GmbH & Co KG
Hauskampstraße 58 · D-45476 Mülheim an der Ruhr
Telefon 0208/40302-0
Telefax 0208/40302-77

2

Polymers

Polymerization and Polymer Modifications in Near- and Supercritical Fluids

Erdogan Kiran
Department of Chemical Engineering
University of Maine
Orono, Maine 04469-5737
E-mail: Kiran@maine.edu; Fax: 207-581-2323

This presentation is a review of the current state of high-pressure polymerization and polymer modifications in near- and supercritical fluids. The topics covered include homogeneous and heterogeneous polymerizations in pure fluids and fluid mixtures; polymer modifications through polymerization within swollen matrices of host polymers; polymer modifications through chain side group modifications; and depolymerization reactions. Future directions and research needs are also presented.

Introduction

Polymerization is the process of converting monomer(s) to long chain molecules. It is a basic process to produce materials with "microstructural" features. The microstructural consequences of polymerization are reflected in the molecular weight, molecular weight distribution, chain end groups, repeat unit orientation and chain regularity (as in tacticity), monomer sequence distributions (as in copolymers), branching, or crosslinking. The chain microstructure influences the ultimate properties of polymers that find ever increasing use in our everyday life.

Polymerization reactions proceed either by the "step growth" or the "chain addition" mechanisms. Step-growth polymerizations require monomers with at least two functional groups and are involved in the manufacture of several industrially important polymers such as polyamides, polyesters, and in the formation of biopolymers such as polysaccharides, proteins and polypeptides in nature.

The chain addition polymerizations require monomers with double bonds. They require free radical or ionic initiators to open the double bond and form the polymerization path in the manufacture of polymers such as polyethylene, polypropylene, polystyrene, and polyvinyl chloride which together constitute the majority of polymers, about 70 % of all polymers produced. A wide range of copolymers or terpolymers are produced by chain addition polymerization of two or three different monomers with double bonds.

Polymerization processes are carried out in bulk or in a solvent with or without added stabilizers, and may proceed under homogeneous or heterogeneous conditions. Polymerization in the presence of a solvent medium offers processing advantages in terms of lowered viscosity and elimination of localized heating that may lead to adverse polymerization rates. But the presence of traditional solvents introduces environmental issues in connection with solvent removal or recovery, kinetic issues related to chain transfer to solvent. Presence of stabilizers may introduce additional purity concerns if they need to be removed from the final polymer. Use of near and supercritical fluids as polymerization media is an alternative approach which may alleviate environmental issues by elimination of the use of traditional solvents, or help the solvent removal or purification steps while reducing the use of conventional solvents. Indeed, over the past 10 years there has been a remarkable increase in the interest in this area.

Several review articles on the use of near – or supercritical fluids as polymerization or polymer modification media have recently appeared [1-3]. The motivation and the rational are varied but include the following:

a) High pressures favor polymerization because polymerization usually involves a decrease in volume.

b) Precipitation thresholds or polymer molecular weights can be controlled because dissolving power of the supercritical fluids can be changed by density of pressure.
c) Polymerization rates can be fine-tuned towards producing polymers of desired properties because the propagation or termination rates can be modulated.
d) Monomer reactivity ratios may be tuned and thus monomer sequence distributions and the microstructure of copolymers may be controlled.
e) Intimacy of the ion pairs in propagating chains in ionic polymerizations can be adjusted to alter the rate of polymerization, or stereoregulation of the propagation because the dielectric constant of the reaction medium can be fine-tuned.
f) Reactions may be carried out in an environmentally more acceptable manner because reactions may be conducted in fluids such as carbon dioxide (with or without stabilizer additives or co-solvents depending upon the system), and the polymer end-product and the unreacted monomer(s) or solvents can be conveniently separated. Schemes can be devised to recover the polymer in powder form with minimal residual solvent entrapment.
g) Micro-structured composites and blends can be prepared because a polymer can be swollen in a supercritical fluid permitting infusion of another monomer and its in-situ polymerization.

This talk will present a state-of –the art review of the field with examples that have been selected to highlight the different methodologies that are used by different research groups (Buback at the University of Göttingen, Luft at Darmstadt University of Technology, DeSimone at University of North Carolina, Beckman at University of Pittsburgh, Kennedy at University of Akron, Watkins at University of Massachusetts, Erkey at University of Connecticut, Arai at Tohoku University, and Kiran at University of Maine). The talk is organized in two major parts. Part I will focus on polymerization reactions by chain addition and step growth mechanisms, while Part II will describe reactive modifications of polymers via side group modifications, reactive blending, or depolymerizations.

Part I. Polymerization Reactions

High-pressure polymerizations where the monomer is both a reactant and a solvent

Polymerization of ethylene. From a thermodynamic standpoint it has been long recognized that pressure favors polymerization. This is because successive additions of monomers to form a polymer chain normally involves a decrease in volume. Indeed, significant amount of literature exists on high-pressure polymerization in the liquid state, either in the bulk or in the presence of a liquid solvent [4, 5]. Polyethylene is historically the best example of commercial high-pressure polymerization where the monomer functions both as a reactant and a solvent and the conditions are supercritical for ethylene [6]. The polymerization is carried out in tubular reactors using organic peroxide initiators at temperatures above the melting temperature of polyethylene (typically in the range from 140 to 300 °C) and at pressures in the range from 1300 to 3000 bar [6-8]. Polymerization is controlled not to pass the solubility limit of the polymer in the monomer. At temperatures above 115 °C and pressures above 1900 bar, it is reported that miscibility of monomer and polymer is maintained at all conversions and polymerization of ethylene proceeds in the homogeneous supercritical state [6]. Miscibility and phase behavior of ethylene + polyethylene or its copolymer is receiving renewed interest and a comprehensive review has appeared [9]. A recent publication has reported on the critical points of ethylene + polyethylene wax (M = 1100) as a function of polyethylene concentrations up to 3.5 mol % in the temperature range of 413 to 513 K at pressure up to 93 MPa [10]. Such information is especially helpful in understanding and preventing fouling which is a concern in polyethylene reactors [7, 8].

A new development in polyolefin synthesis is the use of homogeneous single-site metallocene catalysts [11], which unlike traditional Ziegler-Natta catalysts contain just a single atom, usually titanium or zirconium. The catalysts are introduced in the gas, solution and emulsion processes to manufacture linear low density or high density polyethylene, isotactic polypropylene, and a host of polyethylene copolymers [12]. In homopolymerization of ethylene at 150 MPa and 453 K, productivity levels of 4400 kg of polyethylene (M_w of about 400,000 and PDI of about 2) per gram of catalysts is reported. These homogeneous metallocene catalysts permit the synthesis of polyolefins with better control of side chains, or controlling the properties of copolymers that are inaccessible with heterogeneous Ziegler-Natta type catalysts. [Ziegler –Natta catalysts are mixtures of solid and liquid compounds containing metal atoms, such as $TiCl_3$ on a carrier like $Mg\ Cl_2$ together with trialkylaluminum compounds such as $AlEt_3$]. Miscibility of polyethylene or its copolymers produced by using metallocene catalysis are expected to receive greater attention in the coming years.

Copolymerization of carbon dioxide. Copolymerization of carbon dioxide is another example where the monomer may function both as a reactant and a solvent. Historically, the interest in copolymerization of carbon dioxide has been in connection with a desire for carbon dioxide fixation [13, 14]. Recent interest however is in the use of CO_2 not only as a reactant, but also as a solvent and in the possibility of producing phosgene-free and thus environmentally desirable synthesis and recovery of polycarbonates.

In a recent study [15], carbon dioxide was used as the solvent for copolymerization of propylene oxide with carbon dioxide. Polymerizations were evaluated at pressures from 300 to 1200 psi at 60 °C using zinc (glutarate) catalyst. Polymerization leads to both the carbonate [-O-CO-O-] and ether [-O-] linkages in the chain. At pressures greater than 700 psi, high selectivity for poly (proylene carbonate) versus poly (propylene oxide) formation was noted, with fraction of polycarbonate linkages being in the range of 90-96 %. Carbon dioxide was shown be as effective a solvent as methylene chloride for these copolymerizations in terms of selectivity for polycarbonate versus polyether (polypropylene oxide) formation.

A more recent example where carbon dioxide has been used as a solvent and reactant is the copolymerization of carbon dioxide with cylohexenoxide to produce poly(cyclohexene carbonate) [16]. In this study, in contrast to earlier studies, a zinc-based but fluorinated catalyst that is soluble in supercritical carbon dioxide was developed and used. The catalyst has been shown to lead to high polymer yields (as high as 69 %). Polycarbonates containing greater than 90% polycarbonate linkages with molecular weights of 50,000 to 150,000 have been reported.

Free Radical Polymerizations

Homogeneous Solution Polymerization in Supercritical Carbon Dioxide. These polymerizations require that the monomer, the initiator and the polymer remain in solution throughout the reaction. Because carbon dioxide is not a very good solvent for majority of polymers, homogeneous solution polymerizations have been limited to either low conversion operations, or to a few special, mostly fluorinated, monomer/polymer cases that display high solubility in carbon dioxide. A well-known example is the polymerization of 1,1 dihydroperfluorooctyl acrylate (FOA) [3, 17]. Nearly 40 wt % monomer solution in carbon dioxide with AIBN initiator at 60 °C and 207 bar over 48 hr has been reported to lead to a polymer of molecular weight 270,000 with polymer yield of about 65 %. Styrenes with perfluoroalkyl side chains in the para position have also been polymerized via solution polymerization in supercritical carbon dioxide by the same group.

Another example is the polymerization of octafluoropentyl acrylate (OFP) with AIBN as initiator [18]. This monomer has been shown to be polymerized in carbon dioxide at 65 °C and 3000 psi, resulting in a polymer with a molecular weight of Mw = 5000 , with 45 % yield.

Homogeneous free-radical polymerizations of traditional monomers such as styrene start with the establishment of the phase boundaries for monomer + polymer + fluid [19]. A recent study [20]reports that to maintain homogeneous conditions in mixtures of polystyrene (11-13 %) + styrene (37-44 %) + carbon dioxide (43-51 %), one must maintain pressures higher than about 750 bar at 80 °C if the molecular weight of the polymer to be produced is 10,000. These compositions represent about 20 % monomer conversion starting with about 50 % monomer containing mixtures. For higher molecular weight polymers, much higher pressures are required. At 500 bar, with 45 % carbon dioxide, maximum monomer conversion allowable is about 10 %.

Heterogeneous Precipitation Polymerization. In these polymerizations, initially the monomer and the initiator are miscible in the fluid but the polymer that forms eventually phase separates. The treshhold polymer chain sustainable in the system depends on the fluid, and the P/T conditions. Phase separation is influenced by the solubility of the polymer in the fluid + unreacted monomer which may serve as a co-solvent.

Early examples include polymerization of styrene in supercritical ethane [21], propane, and butane [19, 22]. It was shown that polymerization of styrene in ethane at pressures in the range 12 to 25 MPa, and temperatures in the range 333 to 343 K and concentrations Of 3.33 – 6.66 wt % resulted in polystyrenes of low molecular weight, M = 1000, and low polydispersity (PDI = 1.2) [21]. In n-butane polymerizations at 160 °C, using t-butyl peroxide initiator, polymers with molecular weights in the range M w= 11,000 to 20,000 with PDI less than 2 were obtained in the pressure range from 6.9 to 27.6 MPa. In this study, using a recirculation loop, the polymers that reach the phase separation limit at a given pressure were precipitated and separated in a trap maintained at a lower pressure, while the one homogenous phase was recompressed and recirculated.

Recently, thermal and free radical precipitation polymerization of styrene has been carried out in supercritical carbon dioxide [23]. Thermal polymerizations conducted at a constant CO_2 density of 1.3 show that the yield would increase from about 10 % to 40 % with temperature in the range 170 to 200 °C, while the weight average molecular weight would decrease from about 40,000 to 15,000. At 200 °C, weight average molecular weight was noted to decrease from about 25,000 to 15,000 with increasing pressure from 4000 to 8000 psi. In the case of free-radical, AIBN-initiated polymerization at 65 °C and 5800 psi, the weight average molecular weight was about 15,000 with PDI in the range from 1.5 to 2.0.

Another example is the polymerization of acrylic acid in supercritical carbon dioxide (20 wt %) with t-butyl hydroperoxide as initiator [24]. The effect of initiator concentration (2 to 6%), temperature (160 to 350 °C) and pressure (2700 to 4700 psi) have been reported The polymerizations were conducted at 250 °C and 4500 psi. Contrary to conventional free radical polymerizations, in these polymerizations, it is reported that the initiator amount does not influence the molecular weight, even though in the absence of the initiator polymerization would not proceed. No explanation for this observation has been provided. Also, at a given temperature, molecular weight was found to decrease with pressure. For example, at 160 °C weight average molecular weight decreased from about 80,000 to 45,000 upon increase of the pressure from 2700 to 3700 psi while polydispersity was reduced from about 10 to 7. This behavior is somewhat similar to the thermal polymerization of styrene indicated above. No explanations for the unexpected pressure effect for these systems have been provided.

It should be noted that in a recent study on copolymerization of carbon dioxide and propylene oxide in 1,3 dioxolane, it was also reported [25] that the yield is enhanced with pressure from 200 to 600 psi, but with further increase in pressure there is a decrease in the yield. This unexpected affect of the increased pressure was attributed to the swelling (expansion) of the solvent as a result of greater dissolution of carbon dioxide in the solvent, which causes a reduction in the solubility of the copolymer. At pressures greater than 600 psi, molecular weight of the polymer was observed to decrease also.

These observations point to the complex nature of the phase behavior of these systems and possible solubility maximum for the polymer in the binary fluid system consisting of monomer plus carbon dioxide.

Heterogeneous Precipitation Polymerization in Binary Fluid Mixtures – Density modulation and Levitation. A recent approach in polymerization studies is the use of binary fluid mixtures of carbon dioxide with a traditional solvent to increase the precipitation thresholds and thus achieve higher molecular weights [26]. In this context AIBN initiated free-radical polymerization of styrene has been reported in mixtures of carbon dioxide with pentane, toluene and sulfur hexafluoride [26]. It has been however shown that up to 30 % level, pentane or toluene additions does not alter the relatively poor nature of the fluid mixture,as a solvent for polystyrene and molecular weights remain much lower than achievable in pure pentane or toluene. At 68 ° C and 56 MPa, the weight average molecular weights of the polymer produced in toluene, pentane, or carbon dioxide are 49, 000; 29,000 and 16,000, respectively. In 70/30-carbon dioxide/pentane or 70/30- carbon dioxide/toluene mixtures, the weight average molecular weights are 17,000 and 21,000. In these mixtures, the effect of pressure follows the expected trend, that is higher molecular weight polymer is obtained when pressure is increased. The polymerization trends in mixtures of carbon dioxide with SF_6 however show unique features. In these mixtures, at a given temperature, a wide range of fluid densities are obtainable at different pressures. This was used in a novel way to conduct polymerization by matching fluid mixture density to the density of polystyrene. This is referred to as *levitation* polymerization. The concept is to hinder precipitation of the polymer when the molecular weight increases to a level where the polymer is no longer soluble in the medium. This helps in producing even higher molecular weights. Indeed experiments conducted at 51 and 73 °C, show a maximum in the polymer molecular weight if polymerizations were carried out at pressures that would give a fluid density close to 1.05, the density of polystsyrene. For example, at 51 °C and 21 MPa, fluid density is 1.05 and the molecular weight of the polymer is 175,000.

As pointed out in the previous section, molecular weight maximum with pressure has been noted in some other systems, however the fluid mixture density information for those systems have not been reported to test if density plays a key role in those system also. The notion of solubility maximum has not been evaluated for the polymerization in the $SF_6 + CO_2$ mixtures.

The notion of levitation by density matching offers the possibility for a psuedo-dispersion polymerization process that is free of added stabilizers (such as surfactants) used in conventional dispersion polymerizations.

Heterogeneous Dispersion and Emulsion Polymerization. In dispersion polymerization, the monomer and the initiator are soluble in the continuous solvent phase, the polymer phase separates but is stabilized as a colloid with stabilizer additives. Polymerization proceeds to high degrees of polymerization and the end product is recovered as spherical particles. In emulsion polymerization, the initiator is preferentially dissolved in the continuous phase and not the monomer phase, and the monomer does not have high solubility in the continuous phase.

For dispersion polymerization in carbon dioxide, special stabilizer compounds have been developed. These molecules have *CO_2 - philic* segments that show high solubility in CO_2 and *CO_2-phobic* anchoring segments that are relatively insoluble in carbon dioxide. They are either homopolymers such as poly (FAO) which has an acrylic-like anchor and fluorinated CO_2-philic side chain, or block copolymers of polystyrene and poly (FAO), or block copolymers of polystyrene and Poly(dimethylsiloxane) where the FOA or siloxane blocks function as the CO_2-philic segments [3, 27]. Another group of stabilizers are the comblike graft copolymers, such as poly(methylmethacrylate-co-hydroxyethylmethacryalte)-graft-poly(perfluoropropylene oxide) [28].

These polymerizations have been successfully carried out in carbon dioxide with high polymerization rates to produce polymers of high molecular weight that are recovered as 1-3 micron spherical particles. For example, polymerization at 65 °C and 205 bar, with PFAO as stabilizer and using AIBN as initiator, polymethyl methacrylate of Mn =200,000 to 315,000 have been produced [27]. With a comb-like stabilizer at 65 °C and 380 bar polymethyl methacrylates in the molecular range 100,000 to 355,000 have been produced [28].

A recent study [29] demonstrates the dependence of dispersion polymerizations on solvent quality by conducting poly(FOA)-stabilized dispersion polymerization of methyl methacrylate in supercritical carbon dioxide in the presence of different amounts of added helium. It is shown that in the presence of helium, higher molecular weight polymer, higher yields, smaller particles sizes and a narrower particle size distributions are obtained. At 65 °C and 344 bar, polymer produced in pure carbon dioxide has a molecular weight of 204,000, and a particle size and particle size distribution of 1.93 microns and 1.29. In the presence of 10 mole % helium, molecular weight becomes 365,000, particle size reduces to 1.64 microns with a particle size polydispersity of 1.06. It is argued that in the presence of He, solvent quality is reduced, and as a result, critical chain length of PMMA in the continuous phase is reduced, and the polymer chain nucleates more effectively. When more nuclei are stabilized, a reduction in particle size is observed. Higher conversions and higher molecular weights in CO_2 + He mixtures are attributed to lower degree of swelling which in terns leads to higher viscosity and gel effect.

Ionic Polymerizations

Ionic polymerizations are either cationic where polymerization proceeds by adding monomers to a terminal carbocation, or anionic where monomers add to a negatively charged terminal carbon.

Cationic polymerizations are normally conducted at low temperatures to (-10 to –100 °C) in chlorinated hydrocarbon solvents that have sufficient polarity to promote active ion generation. Recently carbocationic polymerization of isobutylene in supercritical carbon dioxide has been reported. It has been demonstrated that at 32.5°C and 120 bar, using an initiator system of 2-chloro-2,4,4 trimethyl pentane / $SnCl_4$ or $TiCl_4$, isobutylene could be polymerized with 30 % conversion and result in a polymer with Mn = 2000 and PDI = 2 [30]. Other systems that have been reported include polymerization of 3-methyl-1-butene and 4-methyl-1-pentene and synthesis of phenol terminated polyisobutylene [31].

Some preliminary experiments on cationic dispersion polymerization of isobutylene in supercritical carbon dioxide in the presence of polymeric surfactants has also been reported [32].

Step-Growth Polymerizations

Even though not as extensive as chain addition polymerization, polymerization by step growth mechanisms in supercritical fluid media is also gaining attention.

By devising supercritical fluid based schemes to remove the byproduct from the condensation reactions, higher conversions are achievable. Even though water does not show high solubility in supercritical carbon dioxide, other condensation products (i.e., phenol, acetic acid) which may have higher solubility in carbon dioxide may be extracted from the reaction mixture with carbon dioxide and increase conversation. Removal with carbon dioxide would be a desirable path compared to vacuum methods employed in traditional condensation polymerizations.

In a recent study supercritical carbon dioxide has been explored as a medium for conducting melt phase transesterification of bisphenols with diphenyl carbonate to produce polycarbonate (at yields approaching 95 %) at temperatures around 270 °C and pressures of about 3000-4000 psi. [33-35]. Supercritical carbon dioxide provides a means of efficient extraction of phenol, which is the byproduct of reaction, and furthermore lowers the viscosity of the molten polycarbonate for easier handling. Swelling improves also the rate of polymerization by increasing the surface area available for condensate removal.

Even though water has a low solubility in carbon dioxide, it has been shown that it can also be effectively removed with supercritical carbon dioxide in formation of nylon 66 (a polyamide) [34]. In this polyamide formation, because of the reactivity of carbon dioxide with amines, instead of using hexamethylene diamine, reaction was carried out with a nylon salt. Carbon dioxide was shown to lower the melting point of the nylon salt and permit polymerization to proceed at lower temperatures. At temperatures around 270 °C and over a reaction time of about 3 hr at 3000 psi polyamides of high molecular weight (Mn = 25,000) have been produced.

Part II. Polymer Modification Reactions

Polymer modification through reactions in near- or supercritical water. Polymer modifications in near and supercritical fluids are being explored with different objectives.

An interesting case of polymer modification involves generation of functional groups on ethylene based copolymers [36]. Recently, a methodology has been described to convert the functional groups of ethylene-acrylate, -CH (COOR) - ethylene-acrylamide -CH ($CONH_2$) - and ethylene-acrylonitrile -CH (CN) - copolymers into an ethylene acrylic acid -CH(COOH)- type copolymer using near critical water (at temperatures of 250 and 300 °C and pressures of 300 to 1500 bar. An attractive feature of such modifications that result in reactive side groups is that these groups can then be reacted to produce terpolymers from binary copolymer materials.

It is shown that at 300 °C and 300 bar, nitrile group of butadiene-acrylonitrile copolymers are essentially all converted to amide (about 15 %) and acid groups (about 85 %) within about 4 hours. Mechanistically the nitrile groups are first converted to amide which is further hydrolized to the acid groups. In the *case* of ethylene-methlyacrylate copolymers, the ester groups were converted to acid groups in one step almost quantitatively at 275 °C and 300 bar within about 3 hrs. With ethylene-butyl acrylate copolymers conversion was slow, and after 60 hrs at 250 °C and 1500 bar, the content of –COOH groups reaching 80 % with acrylate groups remaining being at 20 %. These reactions are reported to proceed mostly under heterogeneous conditions, and it is indicated that full exploration of the potential modifications would require documentation of the phase behavior.

Another important area of polymer modification with subcritical and supercritical water is the hydrolysis of polycondensation polymers such as polyethylene terephthalate (PET), polyurethanes, and nylons for conversion to their monomers [37]. Specifically, in supercritical water, 91 % monomer recovery (terephthalic acid) is achieved at 400 °C and 40 MPa in less than 15 min reaction times [38]. Studies of these reactions using a hydrothermal diamond anvil cell to follow the phase changes during the reaction of PET in water demonstrate the complexities in terms of simultaneous reaction and dissolution processes.

Unlike polycondensation polymers, polymers of addition polymerization such as polyethylene and polypropylene when depolymerized in inert atmosphere (39) or in supercritical water (37) do not convert to just the monomer but, but a homologous series of oligomers (alkanes and alkenes). Compared to pyrolysis in argon, for polyethylene, the portion of the lighter products increases in supercritical water depolymerizations conducted at 693 K and water densities of 0.13 and 0.42 g/cm3. The 1-alkene to n-alkane ratio also increases in supercritical water and with density. These are attributed to the fact that in argon pyrolysis, the reaction proceed in the molten state of the polymer, whereas in supercritical water, some of degradation products are dissolved in supercritical water and further decomposes to smaller fragments, leading to differences in the reaction phase. Mechanistically, the increased alkene amount suggests that in supercritical water beta-sicssion is more prevalent than hydrogen abstraction reactions in the decomposition paths [37, 39].

These studies point to the possibilities for using supercritical fluids as reaction media to control product distributions.

Another example of polymer modification reaction is the hydrolysis of cellulose in subcritical and supercritical water [40]. Cellulose is shown to hydrolyze rapidly (<1 s) in supercritical water in the absence of any catalysts to glucose, fructose, and oligomers (cellobiose, cellotriose, etc) with a hydrolysis product yield of about 75 % at 400 °C and 25 MPa. The self catalyzed hydrolysis of lignocellulosic materials and wood in water + supercritical carbon dioxide mixtures has also been reported [41, 42].

Supercritical water and carbon dioxide have been used for controlled depolymerization of natural rubber and automotive tires at 380 °C and 276. It is shown that the extent of depolymerization and thus the molecular weight of the degraded polymer can be regulated by the selection of the fluid and reaction conditions. Indeed, it is shown that greater breakdown can be achieved in water compared to carbon dioxide [43].

Polymer Modifications in Supercritical Carbon Dioxide Medium. A number of different approaches are underway for modifying polymers in supercritical carbon dioxide medium. These are either chemical modifications such as side group derivatization, or physicochemical modifications such as in-situ blending.

Side group derivatization. Here advantage is taken of modification by swelling and adsorption of chemically reactive modifiers and catalysts into the polymer to generate different functional groups. It has been shown that the pendant hydroxyl groups of polyvinyl alcohol (PVA) and poly-2-hydroxy propyl methacrylate can partially be reacted with acetic or benzoic anhydride or phenyl isocyanate to form new structures [44], to form side groups with ester linkages. As a result a copolymer is produced. Extend of modification depends on the conditions and the swelling of the polymer in the fluids. At 40-60 C and 2000-5000 psi over 24 hours the modification is only about 2% for PVA (due to its high crystallinity) but 70 % for PHMPA. Extend of modifications is improved with addition of acetone as co solvent to carbon dioxide – this improves the solubility of the reactants.

The transformation of chitosan into branched chitosan derivatives by reductive alkylation in supercritical carbon dioxide has been reported as a new method to disrupt the hydrogen bonding and render this natural polymer water soluble [45].

Polymer blends and interpenetrating networks. A promising area of polymer modifications is the production of co-continuos phase blends by carrying out polymerization of a monomer in a host polymer swollen in supercritical fluid [46]. Polymer substrate is impregnated with a carbon dioxide solution of the monomer and initiator which is then polymerized. Phase morphologies different than melt-mixing or blending are produced. For example, if the polymer is semicrystalline, swelling with carbon dioxide opens up primarily the amorphous regions, and the polymerization proceeds in the amorphous domain of the host polymer.

In a recent study [47] of the polymerization of styrene in carbon dioxide swollen high density polyethylene at 100 °C and 240 atm using t-butyl peroxybenzoate as initiator has shown that more than 100 % mass uptake of polystyrene levels are reached within about 15 hr reaction time. The crystalline melting temperature of polyethylene in these blends is reported to be the same as the initial polyethylene, which is an indication of the styrene polymerization proceeding only in the amorphous regions of polyethylene matrix.

These polymer modification methodologies are now being explored in the broader field of interpenetrating networks, which are intimate combination of two polymers, often both in network form. At least one is synthesized or crosslinked in the presence of other, and therefore display interlocking configurations. In semi-interpenetrating networks, polymer I is crosslinked, but polymer II is linear. In thermoplastic IPNs, physical crosslinks are involved. These are offered by the glassy blocks of block copolymers, or crystalline segments of in semicrysalline polymers may act as physical crosslinks. A recent example is the thermoplastic IPN that has been produced by dissolving isotactic propylene and ethylene–propylene-diene(EPDN) terpolymer in supercritical propane and crosslinking EPDN with t-butyl peroxide at 170 °C and 680 bar [48].

Conducting polymers. A novel application area of polymer modification is the synthesis of conducting polymers. Polypyrrole is a relatively air-stable organic conducting polymer normally prepared by oxidative polymerization in water, ethyl acetate, acetonitrile, methanol or diethyl ether. Recently this polymer was synthesized in supercritical carbon dioxide and supercritical fluoroform (CHF_3) using pyrrole 2-carboxylic acid precursor monomer and ferric chloride $FeCl_3$ or ferric triflate Fe $(CF_3SO_3)_3$ as oxidants [49]. Even though $FeCl_3$ and the precursor monomer has limited solubility in supercritical carbon dioxide, pyrrole monomer and Fe $(CF_3SO_3)_3$ were indicated to be soluble in supercritical carbon dioxide, $FeCl_3$ being more soluble in supercritical fluoroform. The polymerization proceeds with the thermal decarboxilation (loss of CO_2) from the precursor monomer in supercritical carbon dioxide medium at 80-100 °C at pressures 70- 150 bar. Conductivities as high as 0.05 S/ cm were obtained – which are indicated to be higher than obtainable for polypyrrole prepared in conventional solvents. In contrast to globular morphology obtained in conventional precipitation polymerizations, the polypyrrole samples prepared in the supercritical carbon dioxide medium lead to fibrillar morphology.

Another unique approach to preparation of conductive polymers involves synthesis of the conductive polymer as part of a matrix through reactive blending. The motivation for this is to overcome the poor mechanical properties such as brittleness of conductive polymers such as polypyrrole. The methodology involves in-situ polymerization of pyrrole by exposing a polymer host (such as polyurethane foam) containing a suitable oxidant to pyrrole vapor. In a recent study [50] this methodology was extended to replace the traditional organic solvents with supercritical carbon dioxide for impregnation of the oxidant into the foam and for removing the by products of the pyrrole polymerization reaction form the foams. Polyurethane foams were impregnated with the oxidant ferric triflate Fe $(CF_3SO_3)_3$ dissolved in supercritical carbon dioxide at 45 °C/ 238 atm. The solubility of ferric triflate at these conditions is 0.01 wt %. The impregnated foams were then exposed to pyrrole vapor. Composites with about 3wt % conductive polymer displaying conductivity levels of 0.03 S/cm were prepared by this approach.

Future Trends

The interest in the polymerization and polymer modifications will clearly see a significant growth in the future. The trends in basic research and applied aspects will include

a) Generation of more detailed phase information on multicomponent systems which may include mixtures of a monomer, or monomers (in case of copolymerization), initiator, catalysts, stabilizers (in dispersion or emulsion poymerizations), solvent or solvent mixtures (i.e., carbon dioxide plus added co-solvent), a polymer or polymer network blends. There will be a greater level of interest in understanding the transient nature of the composition that continually changes during polymerization where monomer is depleted and the polymer forms and its molecular weight and the molecular weight distribution changes. The question of miscibility therefore needs to be addressed along the reaction coordinate in view of the changing nature of the chain length and microstructure of the polymer and the changing composition of the medium.

b) Generation of more information on swelling of polymers (being modified or synthesized) and the influence of the solvent on the lowering of the glass transition temperature or the melting/crystallization temperature of the polymer that forms.

c) Generation of more information on the viscosity of the reaction mixture during polymerization.

d) Generation of more information on kinetic parameters related to chemical and physical aspects, such as polymerization rates and rate of new phase formation and growth. Already significant activity is underway at University of Göttingen that uses pulsed laser polymerization technique to address these fundamental issues.

e) There will be significant effort to explore new approaches to better control of molecular weight, and molecular weight distribution, or chain sequence distributions. Greater exploitation of Metallocene catalysis, and adoption of Atom Transfer Radical Polymerization methodologies for high pressure and supercritical fluid media are just two examples. Copolymerizations will be a major focus area with emphasis on microstructure regulation via modulation of reactivity ratios. For example taking advantage of the differences in activation volumes has not yet been explored or exploited in this context.

f) Polymer modification area through in-situ polymerizations, side group modifications, or surface modifications via grafting or coatings, is expected to grow, opening new paths for producing microstructured composite or hybrid materials.

g) Polymerization with multifunctional monomers or in the presence of crosslinking agents to produce gels and crosslinked systems offer unique potentials that have not yet been explored to any significant extent.

h) Depolymerization or reactive schemes for recycling will continue to be an active area.

i) In terms of fluid medium, majority of the effort will continue to be in the use of carbon dioxide, alone or with another solvent. Polymerization in binary fluid mixtures will be an important area of activity.

j) From processing perspective, schemes that integrates polymerization with post processing steps (such as recovery of the polymer or polymer fractions in a target solvent- and / or impurity-free physical form) will be under intense consideration to make the processes economically more attractive.

Literature Citations

Reviews

1. K. M. Scholsky, *J. Supercritical Fluids*, 6, 103-128, 1993.

2. E. Kiran, in Supercritical Fluids, E. Kiran and J.M.H. Levelt Sengers, Eds., Kluwer Academic Publishers, Dordrecht, The Netherlands, 1994; pp. 541-588.

3. D. A. Canelas and J. M. DeSimone, Adv. Polym. Sci. 133, 103-140, 1997.

4. Y. Ogo, JMS-Rev. Macromol. Chem. Phys. C24(1), 1-48, 1984.

5. J. K. Beasley, in Comprehensive Polymer Science, G. Allen, Ed., Pergamon Press, New York, 1989; pp. 273-282.

Ethylene polymerization and copolymerization

6. P. Ehrlich and G. A. Mortimer, Adv. Polym. Sci., 7, 386-448, 1970.

7. B. G. Kwag and K. Y. Choi, Ind. Eng. Chem. Res. 33, 211-217, 1994.

8. M. H. Lacunza, P. E. Ugrin and A. Brandolin, Latin Am. Applied Res., 28, 101-106, 1998.

9. B. J. Folie and M. Radosz, Ind. Eng. Chem. Res. 34, 1501, 1995.

10. D. Huekelbach, and G. Luft, Fluid phase equilibria, 146, 187-195, 1998.

11. J. A. Ewen, Scientific American, May 1997, pp. 86-91.

12. C. Bergemann and G. Luft, J. Molec. Catalysis A: Chemical 135, 41-45, 1998.; also C. Bergemann, R. Copp and G. Luft, J. Molec. Catalysis A: Chemical 102, 1-5, 1995.

Copolymerization of carbon dioxide

13. S. Inoue, H. Koinuma and T. Tsurata, J. Polm. Sci. Polymer Letters 7, 287, 1969.

14. S. Inoue, Chemtech , 6, 588, 1976

15. D. J. Darensbourg, N. W. Stafford and T. Katsurao, J. Molecular Catalysis A: Chemical 104, L1-L4 , 1995.

16. M. Super, E. Berluche, C. Costello and E. Beckman, Macromolecules, 30, 368-372 (1997).

Homogeneous free-radical polymerizations

17. J. M. deSimone, Z. Guan and C. S. Elsbernd, Science, 257, 945-947, 1992.

18. J. Ryan, C. Erkey and M. Shaw, ACS Polymer Preprints, 38(2), 428-429, 1997.

19. E. Kiran and V. P. Saraf, J. Supercrit. Fluids, 3, 198-204, 1990.

20. S. Beuermann, M. Buback, C. Isemer and A. Wahl, Paper presented at the NATO ASI on Supercritical Fluids, Kemer, Antalya, Turkey, July 1998.

Precipitation polymerization

21. S. K. Kumar and U. W. Suter, ACS Polymer Preprints, 28(2), 286-287, 1987.

22. V. P. Saraf and E. Kiran, ACS Polymer Preprints, 31 (1), 687-688, 1990.

23. Y. P. Sun, H. W. Rollins, K. J. Simmons, ACS Polymer Preprints, 38(2), 448-449, 1997.

24. E. Dada, W. Lau, R. F. Merrit, Y. H. Paik, and G. Swift, ACS PMSE Preprints, 74, 427, 1996.

25. C. S. Tan and T. J. Hsu, Macromolecules, 3147-3150, 1997.

Levitation polymerization

26. E. Kiran and Z. Gokmenoglu, ACS PMSE Preprints, 74, 406-407, 1996.

Dispersion Polymerization

27. J. M. de Simone, E. E. Maury and Y. Z. Menceloglu, J. B. McLain, T. J. Romack and J. R. Combes, Science, 265, 356-359, 1994.

28. C. Lepilleur and E. J. Beckman, Macromolecules, 30, 745-756, 1997.

29. Y.-L. Hsiao and J.M. DeSimone, J. Polym. Sci. Polym. Chem. Ed., 35, 2009-2013, 1997.

Ionic polymerizations

30. T. Pernecker and J. P. Kennedy, Polymer Bulletin, 32, 537-5433, 1994.

31. T. Pernecker, Gy. Deak, and J. P. Kennedy, Macromolecular reports, A32 (suppl. 7), 969-978 (1995).

32. M. R. Clark and J. M. DeSimone, ACS Polymer Preprints, 37(1), 365-366, 1996.

Step growth polymerization

33. P. G. Odell and G. K. Hamer, ACS Polymer Preprints, 38(2), 470-471, 1997.

34. R. D. Givens, M. Jikei, and J. M. DeSimone, ACS Polymer preprints 38(2), 468-469, 1997.

35. A. L. Burke, R. D. Givens, M. Jikei and J. de Simone, ACS Polymer Preprints, 38(2), 387-388, 1997.

Polymer modifications

36. M. Buback, U. Elstner, F. Rindfleisch, Macromol. Chem. Phys. 198, 1189-1196, 1997.

37. M. Watanabe, H. Hirakoso, S. Sawamoto, T. Adschiri, and K. Arai, J. Supercritic. Fluids, 13, 247-252, 1998.

38. Z. Fang, R. L. Smith, H. Inomata, and K. Arai, J. Supercritical Fluids, in press.

39. E. Kiran and J. K. Gillham, J. Appl. Polm. Sci., 20, 2045-2068, 1976

40. M. Sasaki, B. Kabyemela, R. Malalulan, S. Hirose, N. Takeda, T. Adschiri, K. Arai, J. Supercritical fluids, 13, 261-268, 1998.

41. H. Balkan, High pressure extraction and delignification of red spruce with near and supercritical fluids, Ph. D. Thesis, University of Maine, 1993.

42. L. Li and E. Kiran, Ind . Eng. Chem. Research, 27, 1301, 1988.

43. D. T. Chen, C. A. Perman, M. E. Riechert and J. Hoven, J. Hazardous Materials, 44, 53-60, 1995.

44. J. L. Kerschner, S. H. Jueller, R. Harris, ACS PMSE Preprints, 74, 246-247, 1996.

45. M. Yalpani, Polymer, 34, 1102, 1993.

46. J. J. Watkins and T. J. McCarthy, Macromolecules, 28(12), 4067-4074, 1995.

47. E. Kung, A. J. Lesser and T. J. McCarthy, ACS Polymer Preprints, 38, 462-463, 1997.

48. S. J. Han, D. J. Lohse, M. Radosz, L. H. Sperling, ACS Polymer preprints, 38, 432-433, 1977.

49. F. M. Kerton, G. A. Lawless and S. P. Armes, J. Mater. Chem. 7(10), 1965-1966, 1997.

50. Y. Fu, D. R. Palo, C. Erkey and R. A. Weiss, Macromolecules, 30, 7611-7613, 1997.

The Influence of Inert Gases on the High-Pressure Phase Equilibria of Copolymer-Comonomer Mixtures

G. Luft*, M. Kinzl
Technische Universität Darmstadt, Institut für Chemische Technologie,
Petersenstraße 20, D-64287 Darmstadt, Germany
Email: luft@bodo.ct.chemie.tu-darmstadt.de
FAX: 06151 / 164214

Due to industrial and scientific interest the high-pressure phase equilibria of copolymer solutions in mixtures of highly compressed supercritical ethylene and comonomers have frequently been studied, whereas only few publications deal with the effect of the addition of inert compounds.
In this work we investigated the influence of nitrogen, carbon dioxide, helium, methane, ethane, propane and n-butane on the phase equilibria of such systems. The inert gases were added to solutions of poly(ethylene-co-vinyl acetate)- and poly-(ethylene-co-1-hexene)-copolymers in mixtures of the monomers ethylene and vinyl acetate or 1-hexene, respectively. Between 393 and 493 K we measured cloud point pressures and coexistence data in a wide range of mixture compositions. Helium, nitrogen, carbon dioxide and methane were found to reduce the copolymer solubility. At constant temperature, copolymer concentration and comonomer : ethylene ratio, the influence on cloud point pressures decreases in order helium > methane > nitrogen > carbon dioxide. Except methane, the alkanes did not act as antisolvents. Ethane did not have an observable effect on the phase behaviour, whereas the addition of propane and especially n-butane resulted in a reduction of cloud point pressures.

Introduction

Highly compressed supercritical ethylene is known as a good solvent for organic compounds. Several industrial processes, such as the polymerization of ethylene, take advantage of the solubility of polymers and copolymers in this medium [1]. The chain molecules formed during the reaction are dissolved in the monomer mixture. They can easily be separated from the reactants by depressurizing.

Whereas the influence of liquid comonomers like vinyl acetate or 1-hexene on the phase behaviour of polymer-ethylene and copolymer-ethylene systems has been investigated in detail [2,3,4,5], only few studies on the addition of inert compounds have been published [6,7]. The experimental data reported so far have been determined in a very narrow range of conditions.

This work contributes to the understanding of the impact of anorganic gases and alkanes on the phase equilibria of copolymer-monomer mixtures at technical conditions. Nitrogen, carbon dioxide, helium and alkanes like methane, ethane, propane and n-butane were added to solutions of poly-(ethylene-co-1-hexene) (EH) and poly(ethylene-co-vinyl acetate) (EVA) in mixtures of the monomers.

Using two different high-pressure autoclaves we systematically measured cloud point pressures and coexistence curves of these quasi-quaternary systems in dependence on temperature and mixture composition.

Materials and Methods

The copolymers were supplied by the Exxon Corporation, Houston, TX. The data are listed in Tables 1 and 2.

copolymer	EVA-copolymer
number average MW	61900 g/mol
weight average MW	167000 g/mol
polydispersity	2.70
incorporated vinyl acetate	27.5 wt%
melt index (463 K, 2.16 kp)	1.0 g/10 min

Table 1. Data of Poly(ethylene-co-vinyl acetate)

copolymer	EH-copolymer
number average MW	60000 g/mol
weight average MW	129000 g/mol
polydispersity	2.15
incorporated 1-hexene	16.1 wt%

Table 2. Data of Poly(ethylene-co-1-hexene)

The purities and sources of the inert compounds and the comonomers vinyl acetate and 1-hexene are given in Table 3.

1-hexene	97 wt%	Acros
vinyl acetate	99 wt%	Acros
ethylene	99.995 wt%	Linde AG
methane	99.5 wt%	Linde AG
ethane	99.95 wt%	Linde AG
propane	99.5 wt%	Linde AG
n-butane	99.5 wt%	Linde AG
nitrogen	99.996 wt%	Linde AG
carbon dioxide	99.995 wt%	Linde AG
helium	99.996 wt%	Linde AG
2,6-di-tert-butyl-4-methyl-phenol	99 wt%	Aldrich Corporation

Table 3. Purities and Sources of Materials

Apparatus and Procedure

The autoclave used for the cloud point measurement is designed for a maximum pressure of 250 MPa at a temperature of 513 K (see Fig. 1). In order to vary the inner volume and the pressure, the apparatus is equipped with a metal bellow (6, Fig. 1). Its extension, which is measured by means of a position transducer (2), can be changed by pumping the hydraulic oil isododecane into its interior. For that purpose, the metal bellow is connected to a hydraulic pump via a high-pressure tube. Valve 1 is used for the dosage of isododecane. The autoclave volume can be changed in the range of 14.5 to 19.0 ml. Depending on the pessure level, the corresponding pressure variation is up to 80 MPa.

In order to fill in exact amounts of ethylene and further compounds, two needle valves (5 and 8) are arranged at the top of the apparatus. Valve 5 is connected to the ethylene storage system from which compressed ethylene can be dosed into the autoclave. The temperature is adjusted by means of an electrical heater. Three thermocouples are arranged at the bottom of the apparatus.

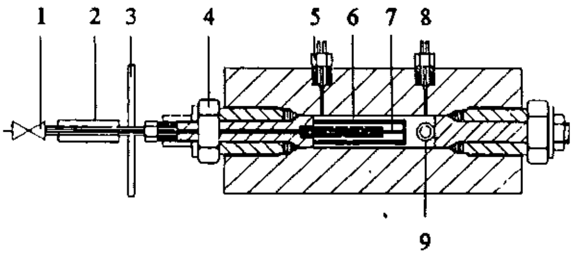

1 hydraulic valve
2 position transducer
3 thermal shield
4 high-pressure screwing
5 ethylene valve
6 metal bellow
7 metal stick
8 needle valve
9 sapphire window

Figure 1. The Small Autoclave

The cloud point pressures are measured optically. Two opposite sapphire windows are installed in the autoclave mantle. The interior of the apparatus is illuminated by a lamp, so that the phase state of the mixture can be observed.

At the beginning of a mixture preparation, the copolymer and 2, 6-di-tert-butyl-4-methyl-phenol, which is used as an inhibitor, are placed in the autoclave. After evacuation, the liquid comonomer is sucked into from a burette. Finally, the calculated amounts of the inert gas and ethylene are metered into it via a store vessel or, respectively, the ethylene storage system described above. While heating to the preset temperature, the apparatus is shaken in order to mix the components. The mixing process is accelerated by means of three metal plates placed around the metal bellow.

After homogenization, the pressure is reduced stepwise by means of the metal bellow, while the phase state is observed optically through the sapphire window. By the occurance of cloudiness the phase separation at the cloud point pressure is indicated. The procedure can be repeated at different temperatures in order to measure cloud point curves.

The measurement of coexistence data is performed in a similar autoclave which is shown in Fig. 2. In comparison with the apparatus described above there are two main differences. First, the autoclave is larger. The volume can be varied between 660 and 700 ml. Secondly, the apparatus is equipped with two special sampling valves (2 and 4, Fig. 2).

A mixture to be investigated is prepared the same way as described above. After homogenization it is demixed by a reduction of pressure. The autoclave is then fixed in vertical position, so that samples can be taken from the heavy and light phase by means of the valves 2 and 4. The liquid and gaseous parts are analyzed gravimetrically or, respectively, using gas chromatography.

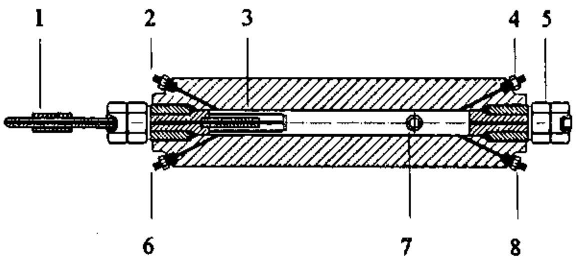

1 position transducer
2 sampling valve
3 metal bellow
4 sampling valve
5 screwing
6 outlet
7 sapphire window
8 ethylene valve

Figure 2. The Large Autoclave

Results and Discussion

In the following sections the influences of inert gas concentration, comonomer : ethylene ratio and temperature on the phase equilibria of EVA- and EH-copolymer solutions are discussed.

Cosolvent and Antisolvent Effects of Inert Gases

The addition of inert compounds to solutions of copolymers in supercritical ethylene can cause either an increase or a decrease of solubility. In Fig. 3 the cloud point pressures of the quasi-ternary systems EVA-copolymer / ethylene / inert gas are plotted versus inert gas concentration. Experiments were performed at a temperature of 433 K. The solutions contained 15wt% of the copolymer.

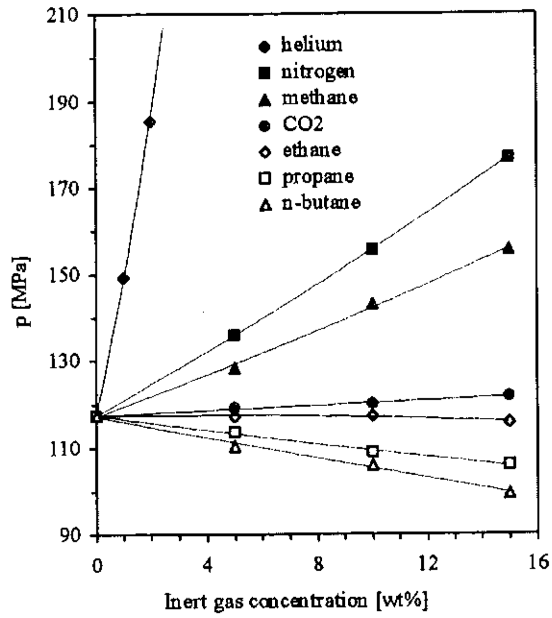

Figure 3. Cloud Point Pressures of the Systems EVA / Ethylene / Inert Gas T = 433 K; c(EVA) = 15 wt%

Helium, nitrogen, carbon dioxide and methane were found to act as antisolvents. The addition of 15 wt% of the gases caused a cloud point pressure increase of 59.4 MPa for nitrogen, 38.2 MPa for methane and 4.4 MPa for carbon dioxide. However, helium influenced the phase behaviour most distinctively. For the mixture containing 2 wt% helium the cloud point pressure rose by 68 MPa.

Except methane, the alkanes did not act as antisolvents. Ethane did not have an observable influence on the phase behaviour, whereas the addition of propane and n-butane resulted in a reduction of cloud point pressures. For the mixtures containing 15 wt% of the gases the pressures were 11.5 MPa, respectively 18 MPa lower.

All effects can be explained by means of Prigogine's rules [8]. If a compound is added to a mixture of two components in which it is solved similarly, it will act as cosolvent. Short-chain alkanes like propane and n-butane are soluble in ethylene as well as in copolymers. These gases meet the rule and cause a decrease of cloud point pressures. In contrast, the solubility of small N_2, CO_2 or methane molecules in copolymers is much lower than in ethylene. Thus, these inert gases are antisolvents.

The inert gas influences on the cloud point pressures of EH-copolymer solutions in ethylene were found to be similar to those described above. Fig. 4 shows the results obtained for a EH-copolymer concentration of 15 wt% and a temperature of 433 K.

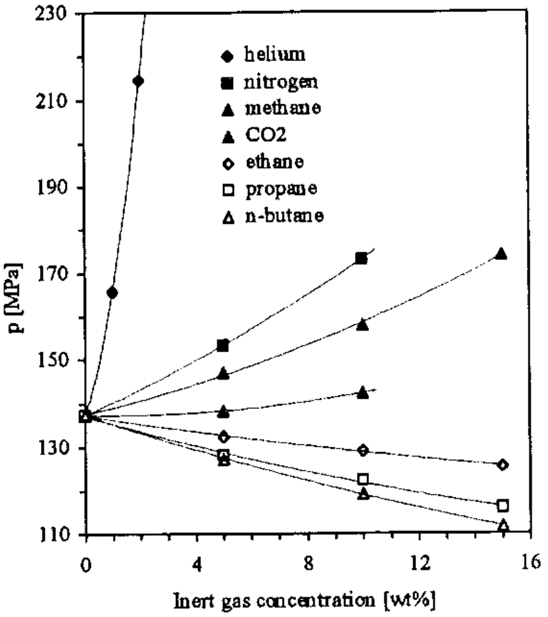

Figure 4. Cloud Point Pressures of the Systems EH / Ethylene / Inert Gas T = 433 K; c(EH) = 15 wt%

In contrast to the EVA systems, the addition of ethane, propane and n-butane results in a stronger reduction of cloud point pressures. Non-polar interactions between the alkanes and both the copolymer and ethylene lead to significant cosolvent effects.

Influence of the Comonomer : Ethylene Ratio

The addition of comonomers like vinyl acetate and 1-hexene to solutions of the corresponding copolymers in ethylene is known to improve the solubility [2,3,4,5] and hence to reduce cloud point pressures. As shown in Fig. 5, this rule is also valid in the presence of inert gases, e. g., nitrogen.

For constant concentrations of the copolymer (15 wt%) and of nitrogen (5 wt%) the cloud point pressures of the quasi-quaternary system EVA / vinyl acetate / ethylene / nitrogen decrease continously with rising comonomer : ethylene ratio. Due to their solubility both in the copolymer and in the solvent ethylene / nitrogen, vinyl acetate and 1-hexene were found to act as cosolvents for all mixture compositions and temperatures.

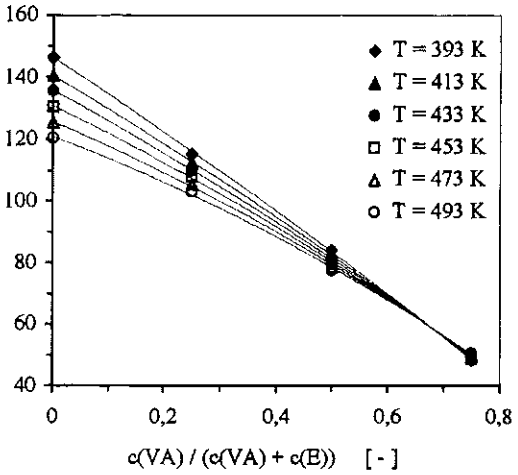

Figure 5. Cloud Point Pressures of the System EVA / Vinyl Acetate / Ethylene / N_2 c(EH) = 15 wt%; c(N_2) = 5 wt%

Temperature Dependence

As shown in Fig. 5, the temperature influence on cloud points depends on pressure level. At high pressures they decrease with rising temperature. In this region the molecular density of the solvent is liquid-like. Thus, the copolymer solubility increases with temperature. For higher vinyl acetate : ethylene ratios and lower pressures, the cloud point curves get closer and finally intersect at approximately 60 MPa. At lower pressures the opposite temperature effect is found. Under these conditions the solvent properties are gas-like and consistently the solubility of long-chain molecules decreases with rising temperature. The pressure-dependent temperature effect on cloud points was observed for all systems copolymer / comonomer / ethylene / inert compound.

Coexistence Curves

The effect of the addition of methane on the coexistence data of EVA-copolymer solutions in ethylene is demonstrated in Figs. 6 and 7. Experiments were performed at a constant temperature of 433 K. Similarly to the cloud points, the coexistence curves are shifted to higher pressures when methane is added. The maximum cloud point pressues are 120.2 MPa for the system EVA / ethylene and 145.5 MPa for the solutions containing 10 wt% of methane. Furthermore, the addition of the inert gas results in a decrease of the critical concentration from 19 wt% to 8 wt%, whereas the corresponding critical pressure rises from 114 to 144 MPa.

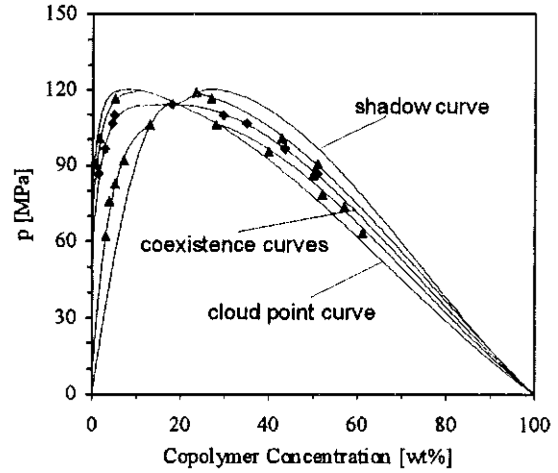

Figure 6. Phase Diagram of the System EVA / Ethylene; T = 433 K

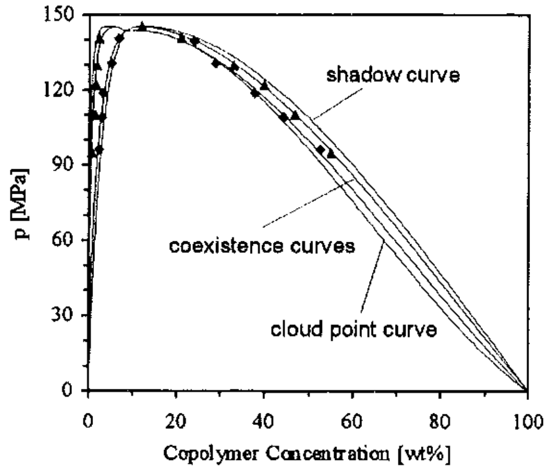

Figure 7. Phase Diagram (433 K) of the System EVA / Ethylene / Methane (10 wt%)

Conclusions

Whereas the cosolvent effect of comonomers on the copolymer solubility in supercritical ethylene has frequently been reported, this work shows the influence of the addition of inert compounds on such systems. Helium, nitrogen, methane and carbon dioxide were found to act as antisolvents. In contrast, n-butane, propane and, under certain conditions, ethane improve the copolymer solubility in mixtures of the corresponding monomers.

References

1. Radosz, M. *IECR* **1995**, *34*, 1501-1516.
2. Folie, B. *Fluid Phase Eq.* **1996**, *120*, 11-37.
3. Kunz, W. *Diplomarbeit TUD* **1983**, 38-59.
4. Raetzsch, M. *Z. Phys. Chem.* **1980**, *261*, 995.
5. Wohlfarth, C. *Acta Polymerica* **1984**, *35*, 498.
6. Constantin, D. *Eur. Polym. J.* **1978**, *14*, 703-708.
7. Dejmek, M. *Diplomarbeit TUD* **1995**, 62-92.
8. Prigogine, I.,*Chemical Thermodynamics* **1954**, VEB Leipzig.

Free-radical polymerization in homogeneous phase of supercritical CO_2

Sabine Beuermann*, Michael Buback, Christoph Isemer, Claudia Schmaltz, Almut Wahl
Institut für Physikalische Chemie, Georg August Universität Göttingen
Tammannstr. 6, 37077 Göttingen
E-mail: sbeuerm@gwdg.de, Fax: +49 - (0)551 - 393144

Although polystyrene (PS) is practically insoluble in supercritical (sc) CO_2, styrene polymerizations may be carried out in solution of CO_2, because of the cosolvent action of the styrene monomer. Experimental cloud point curves for ternary PS/styrene/CO_2 systems demonstrate a significant influence of polymer molecular weight on the solubility. Individual rate coefficients of the propagation and termination reaction, k_p and k_t, have been measured by pulsed-laser-assisted techniques and by conventional chemical initiation for both polymerization in bulk and in solution of scCO_2. For the homopolymerizations of butyl acrylate (BA), methyl methacrylate, and styrene only a moderate influence of CO_2 on the propagation rate are found. The termination rate coefficient is however strongly enhanced in the presence of scCO_2. These findings are assigned to the poor solvent quality of CO_2. A few copolymerization experiments have been carried out for the BA-styrene system. The data show no influence of CO_2 on the reactivity ratios.

Introduction

Supercritical carbon dioxide (scCO_2) has been demonstrated to be a promising alternate solvent medium for free-radical polymerizations [1]. Most studies so far refer to reactions in heterogenous phase. Very few studies have been carried out on homogeneous phase free-radical polymerizations in CO_2 of conventional monomers, such as (meth)acrylates and styrene. The associated polymers show only a very limited solubility in scCO_2 [2], with polystyrene (PS) being almost insoluble in scCO_2, even at polymer concentrations as low as 5 wt.%. Nevertheless it appeared rewarding to try to carry out such fluid phase reactions, because during a polymerization the ternary system with monomer, polymer, and CO_2 is present. As a consequence of some cosolvent activity of the monomer, a considerable range of monomer conversion should be accessible in homogenous phase of scCO_2. For the butyl acrylate (BA) system it has been demonstrated that BA significantly reduces cloud point pressures [3]. The intention of the present paper is to perform free-radical polymerizations of BA, methyl methacrylate (MMA), and styrene in CO_2 up to considerable monomer conversions and to measure propagation and termination rate coefficients. Pulsed-laser-assisted techniques are used in the majority of these experiments [4, 5, 6]. In addition, a few copolymerization experiments have been carried out for BA and styrene in CO_2 and reactivity ratios are determined. The kinetic information on individual rate coefficients and reactivity ratios is compared for polymerization in CO_2 and in bulk. To further extent the knowledge about polymerization in scCO_2 cloud point curves for PS/styrene/CO_2 systems differing in polymer molecular weight are performed.

Experimental Methods

Polymerization experiments are performed using pre-mixed solutions of monomer and CO_2. A schematic diagram of the experimental set-up for the preparation of the monomer/CO_2 mixture is given in Fig. 1 and has been detailed elsewhere [4]. The major components are a HPLC pump, a pressure intensifier, an optical high-pressure cell, and a mixing autoclave equipped with a magnetic stir bar and a cooling device. After filling monomer and CO_2 into the mixing autoclave, the mixture is stirred for one hour and subsequently fed into an optical high-pressure cell. During filling, the pressure is kept constant to avoid demixing of the solution. Once reaction pressure and temperature are reached, the high-pressure cell is disconnected from the pressure branch and inserted into the sample compartment of a FT-IR/NIR spectrometer (IFS 88, Bruker, Karlsruhe, F.R.G.). Initial monomer concentrations and the degree of monomer conversion during the reaction are determined via quantitative NIR spectroscopy in the region of the first overtones of the C-H stretching modes. Details are given elsewhere [4].

The application of PLP techniques towards the study of BA polymerization kinetics has already been described [4]. Termination rate coefficients for styrene are obtained from chemically initiated polymerizations using 2,2' azo(bis)isobutyronitrile as the initiator. Monomer conversion is monitored by means of on-line FT-IR/NIR spectroscopy [7]. The apparatus used to measure cloud point curves has been detailed in reference [8].

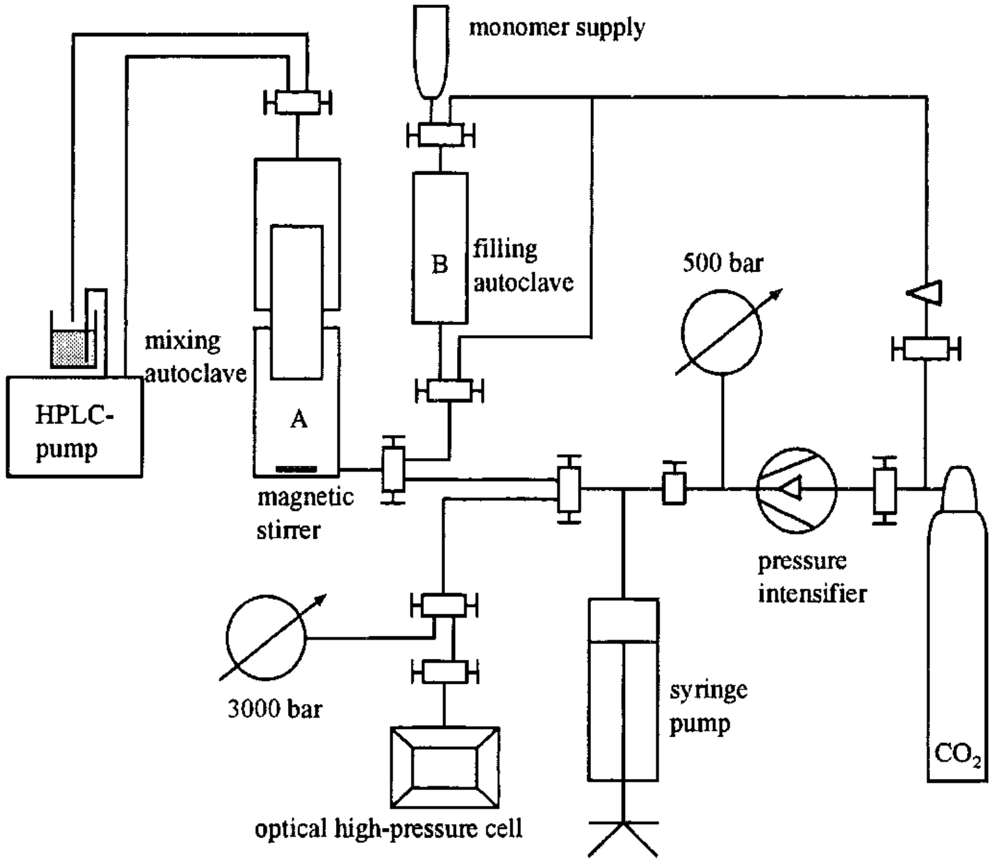
monomer supply
B
filling autoclave
500 bar
mixing autoclave
HPLC-pump
A
magnetic stirrer
pressure intensifier
3000 bar
syringe pump
CO_2
optical high-pressure cell

Figure 1. Experimental set-up for the preparation of reaction mixtures.

Results and Discussion

Cloud point measurements for polystyrene

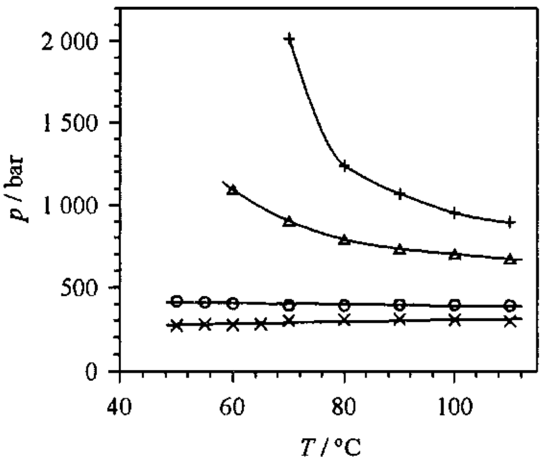

Figure 2. Cloud point curves for PS/styrene/CO_2 systems differing in polymer molecular weight (see text).

Cloud point measurements are performed for systems containing about 10 wt.% PS, 40 wt.% styrene, and 50 wt.% CO_2. The mixture serves as a model system for styrene polymerizations in 50 wt.% CO_2 at a monomer conversion of 20 %. Fig. 2 shows cloud point curves for PS samples of different molecular weights: M_W = 5900 (x), 8000 (o), 10800 (Δ), and 17500 (+).

Above the curves the system is homogeneous. A strong influence of polymer molecular weight on the polymer solubility is seen. For the two lowest molecular weights, an almost temperature independent cloud point pressure around 300 and 400 bar, respectively, is found. At higher molecular weights, the cloud point pressure steeply increase towards lower temperature. Even at M_W = 17500 homogeneity may be reached at 80°C by applying a pressure of 1500 bar.

Propagation rate coefficients for butyl acrylate and methyl methacrylate polymerizations in CO_2

From pulsed-laser initiated polymerization and analysis of the generated polymer by size-exclusion chromatography (SEC), the product of k_p and monomer concentration c_M is determined as a function of CO_2 content, of pressure, and of temperature [4]. Figure 3 gives the ratio of $k_p \cdot c_M$ values for polymerizations in CO_2 and in bulk as a function of the relative initial monomer concentration w_M (referring to the pure monomer density). Reaction pressures and temperatures were as indicated in Fig. 3. For each system a reduction of the propagation rate by 40 % is observed for the highest experimental CO_2 content. A similar reduction in k_p has also been reported in the literature [9]. From the pressure and temperature dependence of k_p measured for high CO_2 contents activation volumes and activation energies are calculated that are identical with the corresponding bulk data [10]. The observations are assigned to the poor solvent quality of CO_2 which is associated with more compact polymer coils as compared to the situation in bulk and with a lower monomer concentration in the vicinity of the free-radical site [4]. The observed decrease in $k_p \cdot c_M$ (see Fig. 3) is most probably due to a decrease in local monomer concentration rather than to a reduction in k_p. This explanation is in accordance with results from PLP-SEC experiments in CO_2, where low molecular weight material is produced. Under such conditions no influence on k_p was observed [5, 11].

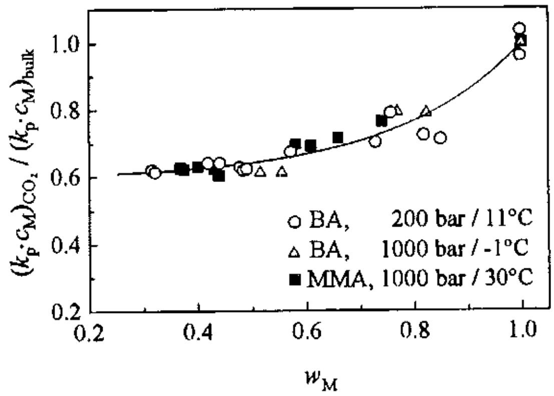

Figure 3. Ratio of $k_p \cdot c_M$ values for homopolymerizations in CO_2 and in bulk of BA and MMA. w_M is the weight fraction of initial monomer concentration relative to the corresponding bulk value.

Termination rate coefficients for butyl acrylate and styrene homopolymerizations in CO_2

Fig. 4 shows the conversion dependence of k_t for BA polymerizations in bulk and in 46 wt.% CO_2 at 40°C and 1000 bar. Over the entire conversion range k_t is higher in CO_2 solution. For polymerizations in bulk, k_t increases up to a monomer conversion of about 10 %, followed by a narrow plateau region. From 15 to 40 % of monomer conversion k_t decreases slightly. For polymerizations in CO_2 the initial k_t value is close to the bulk value. In contrast to bulk polymerizations, the increase in k_t is steeper and extends up to monomer conversions of about 20 %. For higher conversion, within experimental uncertainty a constant k_t is observed. The initial increase of k_t is supposed to be due to decreasing solvent quality associated with the consumption of monomer and with the increasing polymer concentration. The reduction in solvent quality results in more tightly coiled polymer molecules. Polymerization in $scCO_2$ leads to a more pronounced lowering of solvent quality and thus a stronger influence on k_t is observed. An enhancement of k_t originating from a decrease in solvent quality has already been discussed in the literature [e.g. 12, 13, 14].

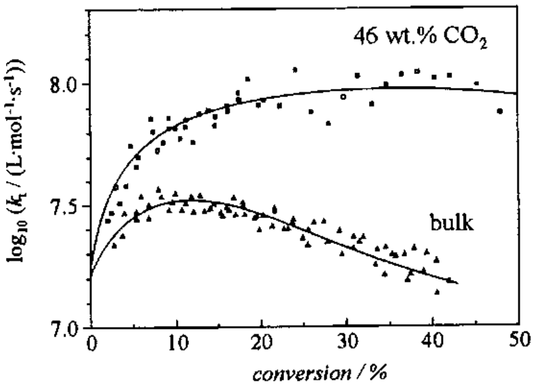

Figure 4. Conversion dependence of k_t for BA polymerizations at 40°C and 1000 bar [6].

The pressure dependence of k_t has been investigated for polymerizations in bulk and in $scCO_2$ (42 wt.%) at 40°C. The activation volumes are identical within experimental uncertainty. Investigations into the temperature dependence of k_t, however, resulted in slightly, but distinctly different activation energies. This difference is another indication of the impact that solvent quality has on the termination behavior.

Plotted in Figure 5 is the pressure dependence of k_t for thermally initiated styrene polymerizations at 80°C. The triangles refer to polymerizations in 41 wt.% CO_2 and the dashed line represents bulk data extrapolated from reference [15]. In the presence of CO_2, k_t values are by one order of magnitude higher than in bulk. The activation volume of k_t, $\Delta V^{\neq}(k_t)$ = 17 $cm^3 \cdot mol^{-1}$, is however identical for both reaction media [11]. The observed enhancement of k_t is more pronounced in styrene than in BA polymerizations, which is probably due to the lower solvent quality that CO_2 offers for PS.

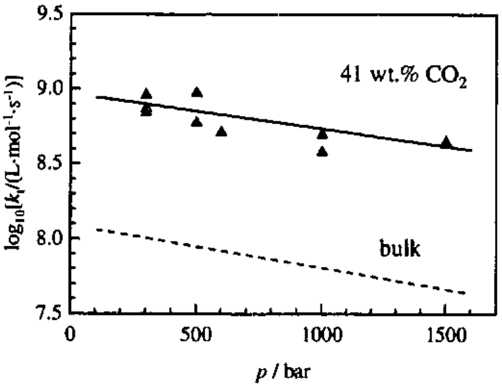

Figure 5. Pressure dependence of k_t for thermally initiated styrene polymerizations at 80°C. For details see text.

Copolymerization of styrene and butyl acrylate in scCO₂

Copolymerizations of styrene and BA are performed at 80°C and 300 bar in solution of CO_2 (41 wt.%) and in bulk. In order to avoid a noticeable composition drift, monomer conversions were limited to 4 %. Copolymer compositions are derived from ^{1}H-NMR spectra. Figure 6 shows a plot of styrene copolymer mole fraction, F_{St}, vs. styrene monomer mole fraction, f_{St}. Reactivity ratios r_{BA} and r_{St} are obtained via non-linear least squares fitting of these copolymer composition data. Within experimental uncertainty identical values of r_{BA} and r_{St} are obtained for copolymerizations in $scCO_2$ and in bulk. The full line in Fig. 6 represents the fit to the combined F_{St} - f_{St} data set.

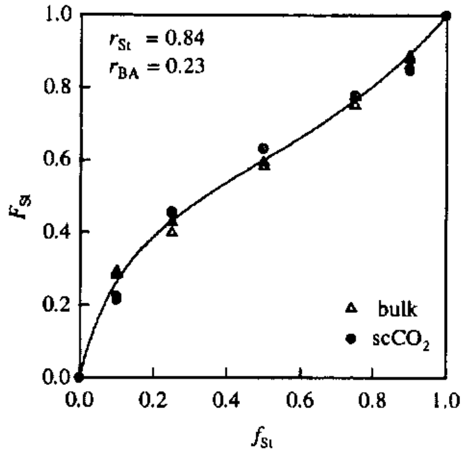

Figure 6. Styrene mole fraction of the copolymer, F_{St}, vs. styrene monomer mole fraction, f_{St}, for styrene-BA copolymerizations at 300 bar and 80 °C.

Conclusions

Because of the cosolvent activity of the monomer, free-radical homopolymerizations of BA and styrene may be carried out in homogeneous phase of CO_2 up to considerable degrees of monomer conversion. Whereas the termination reaction is strongly influenced by the presence of CO_2, propagation rate is only slightly different in bulk and in CO_2 solution. Investigations into copolymerizations of BA and styrene show that the reactivity ratios, r_{BA} and r_{St}, are not influenced by CO_2 to a significant extent.

Acknowledgements

Financial support of this work by the Deutsche Forschungsgemeinschaft (Schwerpunktprogramm: „Überkritische Fluide als Lösungs- und Reaktionsmittel" and Graduiertenkolleg "Kinetik und Selektivität chemischer Prozesse in verdichteter fluider Phase") is gratefully acknowledged. We thank the group of Prof. German at the TUE in Eindhoven for the measurement of molecular weight distributions.

References

1 Shaffer, K. A.; DeSimone, J. M. *Trends in Polym. Sci.* **1995**, *3*, 146
2 Rindfleisch, F.; DiNoia, T. P.; McHugh, M. A. *J. Phys. Chem.* **1996**, *100*, 15581.
3 McHugh, M. A.; Rindfleisch, F.; Kuntz, P. T.; Schmaltz, C.; Buback, M. *Polymer* **1998**, *39*, 6049
4 Beuermann, S.; Buback, M.; Schmaltz, C.; Kuchta, F.-D. *Macromol. Chem. Phys.* **1998**, *199*, 1209
5 v. Herk, A. M.; Manders, B. G.; Canelas, D. A.; Quadir, M. A.; DeSimone, J. M. *Macromolecules* **1997**, *30*, 4780
6 Beuermann, S.; Buback, M.; Schmaltz, C. *Ind. Eng. Chem. Res.*, submitted for publication
7 Beuermann, S.; Buback, M.; Isemer, C.; Wahl, A. *Macromol. Rapid Commun.*, **1999**, *20*, 26
8 Buback, M.; Busch, M.; Dietzsch, H.; Dröge, T.; Lovis, K. (1996) Cloud-Point Curves in Ethylene-Acrylate Poly(ethylene-co-acrylate) Systems, in R. v. Rohr and Ch. Trepp (eds), *Process Technology Proceedings 12, "High Pressure Chemical Engineering"*, Elsevier, Amsterdam, pp. 175-168
9 Quadir, M. A.; DeSimone, J. M.; v. Herk, A. M.; German, A. L. *Macromolecules* **1998**, *31*, 6481
10 Beuermann, S.; Buback, M.; Schmaltz, C. *Macromolecules* **1998**, *31*, 8069.
11 Beuermann, S.; Buback, M.; Isemer, C.; Lacík, I.; Wahl, A. in preparation for publication
12 North, A. M.; Reed, G. A. *Trans. Faraday Soc.* **1961**, *57*, 859
13 Mahabadi, H. K.; O'Driscoll, K. F. *Macromolecules* **1977**, *10*, 55
14 Kent, M. S.; Faldi, A.; Tirrell, M.; Lodge T. P. *Macromolecules* **1992**, *25*, 4501
15 Buback, M.; Kuchta, F.-D. *Macromol. Chem. Phys.* **1997**, *198*, 1455

Production of Elastomers in Supercritical Carbon Dioxide

T.J. de Vries*, M.A.G. Vorstman and J.T.F. Keurentjes
Department of Chemical Engineering and Chemistry, Dutch Polymer Institute & Process Development Group,
Eindhoven University of Technology, P.O. Box 513, 5600 MB Eindhoven, The Netherlands
Email: T.de.Vries@tue.nl, telefax: +31 40 243 93 03, telephone: +31 40 247 23 59

Experiments have been carried out aimed at the development of a new process design for the production of elastomers in supercritical carbon dioxide. The ternary phase behaviour of an ethylene-propylene-copolymer(EPM) with carbon dioxide and ethylene has been investigated. The results show that carbon dioxide is an antisolvent for EPM, but the antisolvent effect decreases significantly at higher temperatures.

A catalyst based on a late-transition-metal complex has been found to polymerise 1-hexene at high CO_2 pressure. The polymerisation has succesfully been carried out using a cationic palladium diimine complex as the catalyst. The influence of CO_2 on the catalyst activity has been investigated at low pressures and appears to have no significant influence. It is expected that lower α-olefins (ethylene, propylene) can be polymerised as well at supercritical conditions, since the catalyst proved to be active in polymerising 1-hexene at pressures and temperatures at which pure CO_2 would be supercritical and since the catalyst is known to be able to polymerise these monomers at atmospheric pressure in oganic solvents as well.

Introduction

Many polymers are currently being synthesised on a large scale in organic solvents, e.g. the production of EPDM in hexane. From an environmental point of view, these processes are undesired, due to inevitable losses of the solvent. Another major drawback of polymerisations in organic solvents is the inefficient removal and recovery of the solvents, see Fig. 1. One of the objectives of the present study is to avoid the recovery steps of the organic solvent in elastomer production by replacing the organic solvent by supercritical carbon dioxide ($scCO_2$). The CO_2 can easily be removed compared to organic solvents and CO_2 offers an environmentally benign, non-toxic, non-flammable and inexpensive alternative as a reaction medium.

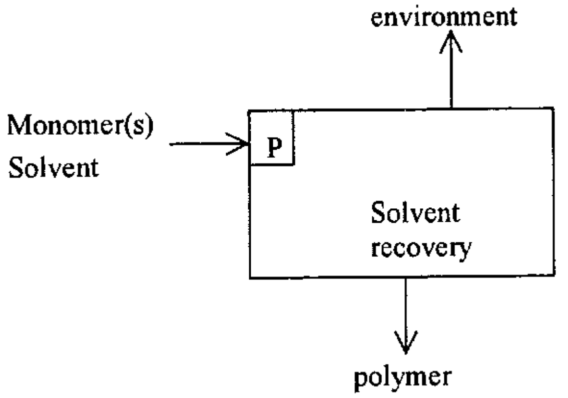

Figure 1: Visualisation of the relative effort required for polymerisation (P) and solvent recovery in traditional polymerisation processes.

In recent years, supercritical carbon dioxide has become an interesting medium for a range of polymerisation processes. Polymerisations using radical [1,2,3,4,5] and carbocationic [6,7] initiators and homogeneous catalysts [8] as well as polycondensations have already been carried out in $scCO_2$.

For a polymerisation process to be successful, phase behaviour plays a key role. Because of the very low dielectric constant ε and polarizability α/v of $scCO_2$, only volatile or relatively non-polar compounds are soluble in $scCO_2$ [9]. As for polymers, only fluorinated [5,10] or silicon- [11] based polymers and (perfluor-)polyethers [12,13] are soluble. Although some elastomeric polymers do exhibit strong swelling behaviour [14], their phase behaviour will lead to precipitation polymerisation when the polymer is not stabilised by surfactants [15]. Because literature on the phase behaviour of ternary mixtures is extremely rare, the phase behaviour of CO_2, ethylene and a random ethylene-propylene-copolymer, EPM, has been investigated and some preliminary results will be shown in the present contribution. Further experimental and modeling results of the ternary phase behaviour will be published [16].

Another important factor in a polymerisation process is the interaction of the solvent with the propagating species of the growing polymer chain. Ziegler-Natta and related catalysts based on early-transition-state metals are extensively used for the polymerisation of olefins. Although these catalysts can produce high molecular weight polymers of ethylene and α-olefins, they are incompatible with functionalized vinyl monomers, due to their highly oxophilic nature. For the same reason these catalysts are likely to be incompatible with CO_2. Catalysts based on late-transition-state metals (Pd, Rh) are less 'oxophilic' and are more likely candidates for polymerisation reactions of olefins in $scCO_2$. The use of homogeneous catalysts in $scCO_2$ is still rare, but is of increased interest [17,8,18,19]. A main point for the successful use of homogeneous catalysts in $scCO_2$ is the solubility of the catalyst. The solubility of a neutral or cationic homogeneous catalyst can be increased by modifying the ligands with perfluorated groups [19], whereas the solubility of cationic homogeneous catalysts can also be increased by highly soluble counter anions. Because $scCO_2$ has a low dielectric constant, the anion must also be good non-coordinating like tetrakis-(3,5-bis(trifluoromethyl)phenyl)borate (BArF), which has previously been used in $scCO_2$ [18]. This anion is also used in the present study.

Materials and Methods

High pressure phase behaviour

Materials: Carbon dioxide (Messer Nederland B.V., grade 4.5) and ethylene (Aga Gas B.V., grade 3.5) were used as received. Hydroquinone was added to prevent the polymerisation of ethylene.

Method: The ternary phase behaviour was examined in an optical high-pressure cell designed for pressures up to 4000 bar and temperatures up to 450 K. The cell, which is provided with sapphire windows and magnetic stirring is a modification of the one described by Van Hest and Diepen [20]. For a detailed description of this apparatus and of experimental techniques we refer to De Loos et al. [21].

The lower critical solution temperatures of the ternary system EPM, ethylene and CO_2 were measured as isopleths (P,T-sections for constant composition) by visual observation of the onset of phase separation of the homogeneous phase by lowering the pressure (the so-called cloud point pressure).

Catalyst

The catalyst used in this study was developed by Brookhart et al. [22] and was prepared according to literature procedures. The catalyst is shown in Fig. 2.

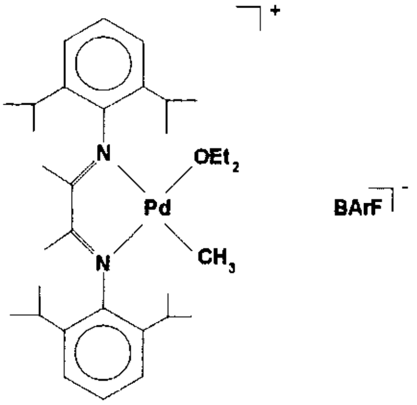

Figure 2: Structure of homogeneous palladium diimine catalyst used in this study

Polymerisations at low pressure

Materials: CH_2Cl_2 was distilled over CaH_2. 1-Hexene (97%, Aldrich) was dried over molsieves under an argon atmosphere. A stock solution of the catalyst was made in CH_2Cl_2, which was stored at -30°C under an inert atmosphere.

Method: The polymerisations were performed under an Argon or CO_2 (Hoek Loos, grade 4.5) atmosphere. The polymerisations were conducted as follows: a solution of 1-hexene with CH_2Cl_2 was heated to the required reaction temperature, followed by the addition of a known amount of catalyst stock solution. After the required reaction time, the polymerisation was terminated by injecting a small amount of concentrated HCl. The polymer was isolated by evaporating the solvent and monomer residu.

Polymerisations at high pressure

Materials: 1-Hexene (97%, Aldrich) was distilled over potassium. CO_2 (Hoekloos, grade 4.5) was used as received. The catalyst was powdered and was put in a glass ampul in a glove box.

Method: A glass ampulla containing the catalyst was put in a 75 mL high pressure reactor equiped with two sapphire windows, a stirrer bar and a heating jacket. The reactor was sealed and purged with CO_2. After purging, the reactor was filled with liquid CO_2 using a HPLC pump. The reactor was conditioned at the required reaction temperature at 85 bar. 1-Hexene was added to the reactor using a second HPLC pump. The reaction mixture was equilibrated using a magnetic stirrer. The pressure was raised by addition of liquid CO_2 until the required pressure was reached. After the required reaction time, the reactor content was vented through a gas trap. The glue-like polymer was collected, dissolved in n-hexane, filtered over Celite, evaporated under reduced pressure and dried under vacuum.

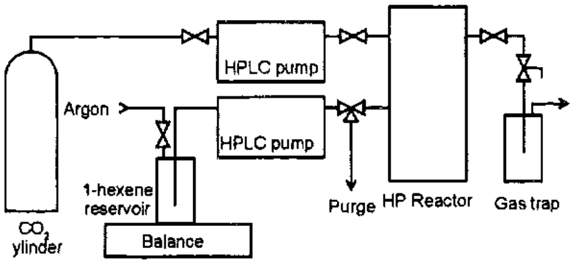

Figure 3: High pressure setup for polymerisation of 1-hexene

Results and discussion

High pressure phase behaviour

Fig. 4 shows the phase behaviour of a random ethylene-propylene-copolymer (EPM) in CO_2 and ethene. The results clearly show that CO_2 is a good antisolvent, as expected, especially at low temperature. However, at higher temperatures the antisolvent effect decreases. We also tested whether 10 wt% polymer could be dissolved in pure CO_2, but this proved to be impossible within a range of 1000 to 3000 bar and 40 to 170 °C.

Polymerisations of α-olefins in $scCO_2$ are therefore expected to be precipitation polymerisations.

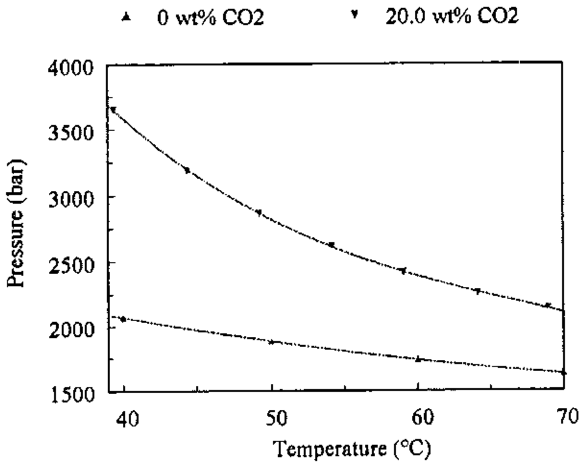

Figure 4: Cloud point pressures of 10 wt% EPM (Mn=46 kg/mole, Mw/Mn=2.5, 46 wt% ethylene), x wt% CO_2 and 90-x wt% ethylene as a function of temperature.

Polymerisations at low pressure

Preliminairy polymerizations of 1-hexene have been conducted to test whether the catalyst would be affected by CO_2. The results using the same catalyst stock solution are shown in table 1. The 1-hexene could not properly be dried over molsieves and proved to contain water. It is believed that the water reduces the activity of the catalyst significantly by complexation. Further differences in yield can be ascribed to slow deactivation of the catalyst over time as the experiments 1 to 4 were performed in that sequence. From these experiments, it was concluded that CO_2 does not inhibit or deactivate the catalyst to a large extent, although the results are not conclusive in this respect.

Table 1: Polymerization of 1-Hexene under Argon and low CO_2 pressure.

Experiment	Reaction condition[a]	Yield (g)
1	Argon, 1 bar	1.34
2	Argon, 1 bar	1.26
3	CO_2, 4.8 bar	1.23
4	CO_2, 4.8 bar	1.15

[a]Reaction conditions: 0.03 mmol catalyst, 50 mL 1-hexene, 50 mL CCl_2H_2, 25°C, 3 hours reaction time

Polymerisations at high pressure

Following the described method, a glass ampulla containing 0.045 g catalyst has been put in the reactor and 10.67 g 1-hexene is added subsequently. The mixture appears to be homogeneous above approximately 100 bar and 34.5 °C. After raising the pressure to approx. 150 bar, the homogeneous solution turned slightly yellow, indicating that the catalyst has at least partially been dissolved. The mixture turned opaque at the same time indicating the formation of an insoluble polymer phase. The pressure was further raised to 239 bar by adding CO_2. The reaction mixture turned more opaque during a reaction time of 2 hours and the pressure decreased to 227 bar. A rubberlike polymer has been obtained at a yield of 2.40 g.

As the palladium complex is able to polymerise a range of α-olefins and functionalized monomers in organic solvents, it is expected to do so in $scCO_2$ as well. In our view this opens the way to a whole range of new polymerisation processes.

Conclusions

The results of the investigated ternairy phase behaviour of EPM, ethene and CO_2 show that CO_2 is an antisolvent for the polymer. The antisolvent effect decreases as the temperature increases.

The preliminairy results regarding the catalyst indicate that the catalyst is not affected by CO_2 and that production of elastomers based on olefins can be performed using the catalyst investigated.

Acknowledgement

The advise and help of R. Duchateau with the synthesis of the palladium catalyst and E. Goetheer with the polymerisation experiments is greatly acknowledged. The high pressure phase behaviour measurements have been performed in the group of Th. De Loos at the Delft Technical University.

References

[1] Canelas, D.A., Betts, D.E., DeSimone, J.M. *Macromolecules* 29(8), 2818-2821, 1996.

[2] DeSimone, J.M., Maury, E.E., Menceloglu, Y.Z., McClain, J.B., Romack, T.J., Combes, J.R. *Science* 265, 356-359, 1994.

[3] Romack, T.J., Maury, E.E., DeSimone, J.M. *Macromolecules* 28, 912-915, 1995.

[4] Lepilleur, C. and Beckman, E.J., *Macromolecules* 30, 745-756, 1997.

[5] DeSimone, J.M., Guan, Z., Elsbernd C.S., *Science* 257, 945-947, 1992.

[6] Pernecker, T., Kennedy, J.P., *Polymer Bull.* 32, 537-543, 1994.

[7] DeSimone, J.M. Clark, M.R., *Macromolecules* 28, 3002-3004, 1995.

[8] Mistele, C.D., Thorp, H.H., DeSimone, J.M., *Pure Appl. Chem.* A33, 953-960, 1998.

[9] Yakoumis, I.V., Vlachos, K., Kontogeorgis, G.M., Coutsikos, P., Kalospiros, N.S., Tassios, D., *J. Supercrit. Fluids* 9, 88-98, 1996.
[10] Enick, R.M., Beckman, E.J., Yazdi, A.V., Krukonis, V., Schonemann, H., Howell, J. *J. Supercrit. Fluids* 13, 121-126, 1998.
[11] Mertsch, R. and Wolf, B.A., *Macromolecules* 27, 3289-3294, 1994.
[12] Enick, R.M., Beckman, E.J., Yazdi, A.V., Krukonis, V., Schonemann, H., Howell, J. *J. Supercrit. Fluids* 13, 121-126, 1998.
[13] O'Neill, M.L., Cao, Q. Cao, Fang, M., Johnston, K.P., Wilkinson, S.P., Smith, C.D., Kerschner, J.L., Jureller, S.H., *Ind. Eng. Chem. Res.* 37, 3067-3079, 1998.
[14] Zhang, Y., Gangwani, K.K., Lemert, R.M. *J. Supercrit. Fluids* (11), 115-134, 1997.
[15] Goetheer, E.G., Vorstman, M.A.G., Keurentjes, J.T.F., to be published in *Chem. Eng. Sci.*
[16] De Vries, T.J., Somers, P., Vorstman, M.A.G., De Loos, Th. W. , Keurentjes, J.T.F., to be published.
[17] Jessop, P.G., Ikariya, T., and Noyori, R., *Science* 269, 1065-1069, 1995.
[18] Burk, M.J., Feng, S., Gross, M.F., Tumas, W., *J.Am.Chem.Soc.* 117, 8277-8278, 1995.
[19] Kainz, S., Koch, D., Baumann, W., Leitner, W., *Angew.Chem.* 109(15), 1699-1701, 1997.
[20] Van Hest, J.A.M., Diepen, G.A.M., "The Physics and Chemistry of High Pressures", p. 10, Society of Chemical Industry, London, UK, 1962.
[21] De Loos, Th. W., Poot, W., Diepen, G.A.M., *Macromolecules* 16, 111, 1983.
[22] Johnson, L.K., Killian, C.M., Brookhart, M., *J.Am.Chem.Soc.* 117, 6414-6415, 1995.

Mathematical Modeling of Dispersion Polymerization of Vinyl Monomers in Supercritical Fluids

C. Kiparissides*, N. Pagalos, Ch. Chatzidoukas and Ch. Mantelis
Department of Chemical Engineering and Chemical Process Engineering Research Institute
Aristotle University of Thessaloniki , P.O. Box 472, 54006 Thessaloniki
cypress@alexandros.cperi.forth.gr, Fax: ++30 31 996198

Conventional dispersion polymerizations of unsaturated monomers are commonly conducted in aqueous or organic dispersing media. Supercritical CO_2 represents an environmentally sound alternative to both, eliminating the use of toxic and flammable organic solvents, and the generation of large volumes of aqueous waste. Using supercritical CO_2 as a medium for the free-radical dispersion polymerization of vinyl monomers, the polymer can be easily isolated as a free-flowing powder by simply venting the CO_2. The aim of the present work was to develop a comprehensive mathematical model for the quantitative prediction of the time evolution of the monomer conversion, molecular weight distribution and particle size distribution in the free-radical dispersion polymerization of MMA in supercritical CO_2. Simulation studies were carried out to determine the effect of process parameters (e.g. temperature, initiator concentration, etc.) on the time evolution of monomer conversion, pressure and number and weight average molecular weights. The predictive capabilities of the present model are demonstrated by a direct comparison of model predictions with reported experimental data on the polymerization of MMA in $scCO_2$.

Introduction

In the plastics manufacturing industry, more than 7 billions metric tons of organic and halogenated solvents are used worldwide each year as process aids, cleaning agents and dispersants. Thus, solvent-intensive industries are considering alternatives that can reduce or eliminate the negative impact that solvent emissions can have on the environment. In order to reduce the environmental burden, one has to find ways of making plastics that are environmentally friendly from the start. A more radical development would be to eliminate any source of harmful solvents and make quality polymers using a new kind of solvents (e.g. supercritical carbon dioxide) which is relatively harmless and inexpensive.

Conventional dispersion polymerizations of unsaturated monomers are commonly conducted in aqueous or organic dispersing media. Supercritical CO_2 represents an environmentally sound alternative to both, eliminating the use of toxic and flammable organic solvents, and the generation of large volumes of aqueous waste. Using supercritical CO_2 as a medium for the free-radical dispersion polymerization of olefinic monomers, the polymer can be easily isolated as a free-flowing powder by simply venting the CO_2. A free-radical dispersion polymerization [1] is a heterogeneous process by which latex particles are formed in the presence of a suitable stabilizer from an initially homogeneous reaction mixture. From a kinetic point of view the polymerization of MMA is considered to take place in three distinguished stages [2].

Stage 1: During the first stage, primary radicals formed by the thermal fragmentation of the initiator rapidly react with monomer molecules to produce polymer chains that are insoluble in the monomer phase. Aggregation of the closely spaced polymer chains results in the formation of unstable polymer microdomains. The reaction mixture consists mainly of pure monomer, since the polymer concentration is less than its solubility limit (e.g., monomer conversion $\leq 0.1\%$). Thus, the polymerization during this stage can be described as a solution polymerization.

Stage 2: Due to the very limited stability of the microdomains, they rapidly aggregate to form the primary particle nuclei, also called domains. From this point on, polymerization occurs in two phases, namely, the polymer-rich phase and the continuous, monomer-rich phase. This stage extends from the time of appearance of the separate polymer phase to a fractional monomer conversion, X_c, at which the monomer concentration in the continuous phase disappears. It is assumed that, during this stage, the rate of mass transfer of monomer and solvent from the continuous phase to the polymer phase is very fast so that the latter is kept saturated with monomer and CO_2. The overall polymerization rate is given by the sum of the polymerization rates in the two phases.

Stage 3: Finally, at higher monomer conversions ($X_c < X \leq 1.0$), polymerization continues only in the polymer-rich phase, which is swollen with monomer and CO_2, thus, the monomer mass fraction in the polymer phase decreases as the total monomer conversion approaches a final limiting value. During this stage, diffusion controlled phenomena (e.g., gel-effect and glass-effect) become very important.

The morphological properties (e.g., mean particle size, porosity, etc.) of the particulate product are directly related with the nucleation, growth and aggregation of the primary polymer particles formed during the early stages of dispersion polymerization. In the subsequent section the heterogeneous polymerization kinetics of MMA in $scCO_2$ are reviewed. Based on the postulated kinetic mechanism, dynamic molar species balances for the monomer, initiator, solvent, "live" and "dead" polymer chains, are derived. The calculation of monomer distribution in the two phases is the subject of section 3. Finally, in section 4, a comparison of model predictions with experimental results on the time evolution of monomer conversion, pressure and number and weight average molecular weights is presented.

Reaction Mechanism and Molar Species Balances

The free-radical dispersion polymerization mechanism of MMA in supercritical CO_2 can be described in terms of the following elementary reactions [2]:

Initiation:

$$I_j \xrightarrow{k_{d_j}} 2I_j^\bullet \tag{1}$$

$$I_j^\bullet + M_j \xrightarrow{k_{I_j}} R_{1,j}^\bullet \tag{2}$$

Propagation:

$$R_{x,j}^\bullet + M_j \xrightarrow{k_{pj}} R_{x+1,j}^\bullet \tag{3}$$

Chain transfer to monomer:

$$R_{x,j}^\bullet + M_j \xrightarrow{k_{fm_j}} P_x + R_{1,j}^\bullet \tag{4}$$

Termination by disproportionation:

$$R_{x,j}^\bullet + R_{y,j}^\bullet \xrightarrow{k_{td_j}} P_x + P_y \tag{5}$$

Termination by combination:

$$R_{x,j}^\bullet + R_{y,j}^\bullet \xrightarrow{k_{tc_j}} P_{x+y} \tag{6}$$

In the above kinetic scheme, the symbols I and M denote the initiator and monomer molecules, respectively. Primary radicals formed by the fragmentation of the initiator are denoted by the symbol $I^\bullet$. The symbols $R_x^\bullet$ and P_x are used to identify the respective "live" macroradicals and the "dead" polymer chains, containing x monomer units. It should be noted that the above elementary reactions can take place either in the monomer phase (j=1) or/and in the polymer phase (j=2).

Based on the above kinetic scheme, the differential equations describing the time variation of monomer, initiator, "live" and "dead" polymer chains in each phase can be derived:

$$\frac{1}{V_j}\frac{d([M]_j V_j)}{dt} = - k_{p_j}[M]_j \sum_{x=1}^{\infty} R_{x,j}^\bullet - k_{fm_j}[M]_j \sum_{x=1}^{\infty} R_{x,j}^\bullet \tag{7}$$

$$\frac{1}{V_j}\frac{d([I]_j V_j)}{dt} = -k_{d_j}[I]_j \tag{8}$$

$$\begin{aligned}\frac{1}{V_j}\frac{d([R_{x,j}^\bullet]V_j)}{dt} = {} & (2f\ k_{d_j}[I]_j + k_{fm_j}[M]_j \\ & \sum_{y=1}^{\infty}[R_{y,j}^\bullet])\varphi_j\delta(x-1) + k_{p_j}[M]_j[R_{x-1,j}^\bullet]\varphi_j \\ & \{[1-\delta(x-1)](k_{p_j} + k_{fm_1})[M]_j + \\ & (k_{tc_1} + k_{td_1})\sum_{y=1}^{\infty}[R_{y,j}^\bullet]\}[R_{y,j}^\bullet]\varphi_j\end{aligned} \tag{9}$$

$$\begin{aligned}\frac{1}{V_j}\frac{d([P_x]V_j)}{dt} = {} & \sum_{j=1}^{2}(k_{fm_j}[M]_j \\ & + k_{td_j}\sum_{y=1}^{\infty}[R_{y,j}^\bullet])\varphi_j[R_{x,j}^\bullet] \\ & + \frac{1}{2}\sum_{j=1}^{2}k_{tc_j}\sum_{y=1}^{x-1}[R_{y,j}^\bullet][R_{x-y,j}^\bullet]\varphi_j\end{aligned} \tag{10}$$

where δ(x) is the Kronecker's delta function:

$$\delta(x) = \begin{cases} 1 & \text{if } x = 0 \\ 0 & \text{if } x \neq 0 \end{cases} \tag{11}$$

and $\varphi_j = V_j / V$ is the volume fraction of the "j" phase. Equations (9) and (10) represent the net rate of production of "live" polymer chains of length x in phase j and the net rate of production of "dead" polymer chains of length x, respectively. These rates can be obtained by combining the reaction rates of the various elementary reactions describing the generation and consumption of "live" or "dead" polymer chains of length x.

To reduce the infinite system of molar species balance equations, for "live" and "dead" polymer chains, the method of moments [2] is invoked. Accordingly, the average molecular properties of the polymer (e.g., M_n, M_w) are expressed in terms of the leading moments of the "dead" polymer molecular weight distribution. Following the developments of Kiparissides et al. [2], the moments of the total number chain length distribution of "live" macroradicals and "dead" polymer chains are defined as:

$$\lambda_{i,j} = \sum_{x=1}^{\infty} x^i R_{x,j}^\bullet \ ; \ \mu_i = \sum_{x=1}^{\infty} x^i P_x \ , \ i = 0, 1, 2, .. \tag{12}$$

where λ_{ij} is the "i" moment of the "live" NCLD in the "j" phase and μ_i the "i" moment of the "dead" NCLD. The corresponding moment rate functions are subsequently obtained by multiplying each term of equations (9) and (10) by x^i and summing up the resulting expressions over the total range of variation of x. Accordingly we obtain the following moment rate equations:

"Live" polymer moment equations:

$$r_{\lambda i,j} = 2f\, k_{d_j}[I]_j \varphi_j + k_{fm_j}[M]_j \lambda_{0,j}\varphi_j + k_{p_j}[M]_j \{\sum_{k=0}^{i} \binom{i}{k} \lambda_{k,j}\}\varphi_j - -\{k_{p_i} + k_{fm_i})[M]_j + k_{t_i}\lambda_{0,j}\}\lambda_{i,j}\varphi_j \tag{13}$$

"Dead" polymer moment equations:

$$r_{\mu_i} = \sum_{j=1}^{2} (k_{fm}[M]_j + k_{td_j}\lambda_{0,j})\lambda_{i,j}\varphi_j + \frac{1}{2}\sum_{j=1}^{2} k_{tc_j} \sum_{k=0}^{i} \binom{i}{k} \lambda_{k,j}\lambda_{i-k,j}\varphi_j \tag{14}$$

The number and weight-average molecular weights can be expressed in terms of the moments of the NCLDs of "live" and "dead" polymer chains as follows:

$$M_n = MW_m \frac{\mu_1 + \lambda_{1,1} + \lambda_{1,2}}{\mu_0 + \lambda_{0,1} + \lambda_{0,2}} \cong MW_m \frac{\mu_1}{\mu_0} \tag{15}$$

$$M_w = MW_m \frac{\mu_2 + \lambda_{2,1} + \lambda_{2,2}}{\mu_1 + \lambda_{1,1} + \lambda_{1,2}} \cong MW_m \frac{\mu_2}{\mu_1} \tag{16}$$

Monomer Distribution

One of the major issues in the development of a comprehensive mathematical model for the dispersion polymerization of MMA in scCO$_2$ is the accurate prediction of the reactor pressure with respect to time. This requires a complete account of monomer and solvent distributions in the various phases, namely, the monomer-rich, and the polymer-rich phase. The separate monomer-rich phase will be present up to the critical monomer conversion, X$_c$, at which the monomer concentration in the continuous phase disappears. The monomer disappearance in the continuous phase is followed by a pressure drop in the reactor. In stage 2, the polymer-rich phase is saturated with monomer and solvent, thus, the monomer polymer ratio remains constant, reflecting the equilibrium solubility of monomer in the polymer phase. In what follows detailed mass balance equations are derived for the calculation of the MMA distribution in the two phases. As mentioned in the introduction, the MMA polymerization in scCO$_2$ is considered to take place in three stages.

Stage 1: $0<X\leq X_s$. In the first stage, the monomer mass distribution in the monomer-rich phase, M$_1$, and in the polymer-rich phase, M$_2$, will be given by the following equations:

$$M_1 = M_o(1-X); \quad M_2 = 0 \tag{17}$$

Stage 2: $X_s<X\leq X_c$. In the second stage, the monomer distribution in phases 1 and 2 will be given by the following equations:

$$M_1 = M_0\left[(1-X) - X/[X_c(1+K)] + X/(1+K)\right]\ ; \quad M_2 = M_0 X(1/X_c - 1)/(1+K) \tag{18}$$

$$X_c = \varphi_{2,p}\rho_p / [\varphi_{2,p}\rho_p + \varphi_{2,s}\rho_s + \varphi_{2,m}\rho_m] \tag{19}$$

where X$_c$ is the critical monomer conversion, $\varphi_{2,p}$, $\varphi_{2,s}$, $\varphi_{2,m}$ are the polymer, solvent and monomer volume fraction, respectively, and K relates the mass of solvent to the mass of the monomer in the swollen polymer-rich phase:

$$V_{2,s}\rho_s / (V_{2,m}\rho_m) = K \tag{20}$$

Stage 3: $X_c<X\leq 1$. In the third stage, the polymerization takes place only in the polymer phase under monomer starvation conditions. Accordingly, the monomer distribution in the two phases takes the following form:

$$M_1 = 0 \quad ; \quad M_2 = M_0(1-X) \tag{21}$$

Results and Discussion

In the simulation studies it was assumed that both the initiator decomposition rate constant, k$_d$, and the propagation rate constant, k$_p$, had the same values in the two phases. The swelling of polymer particles was attributed to the monomer and CO$_2$ solvent. Finally, the critical monomer conversion, at which the monomer disappears from the continuous phase was set equal to 40%.

At high monomer conversion, all the elementary polymerization reactions can become diffusion-controlled. Specifically, the diffusion-controlled initiation, propagation and termination reactions have been related to the well-known phenomena of cage, glass- and gel-effect, respectively. In the present study, the initiator efficiency, f, was assumed to be constant. Furthermore, the variation of propagation rate constant, k$_p$, with conversion was assumed to be negligible. The gel-effect has been attributed to the decrease of termination rate constant caused by a decrease in the mobility of polymer chains, due to a sharp increase of the reaction mixture viscosity. To take into consideration the variation of the termination rate constant with conversion, the following semi-empirical correlation was applied:

$$k_{t_2} = k_{t_{2o}} g(X,T) \tag{22}$$

where g(X,T) is a decreasing function of monomer conversion and temperature.

In order to achieve a direct comparison of model predictions with reported experimental data on the polymerization of MMA in scCO$_2$, the following polymerization conditions were considered [3], [4]. The reaction temperature was set equal to 338.15 K, while the initial pressure was equal to 380 bar. The initial reaction mixture consisted of MMA monomer (10.0 g), CO$_2$ (33.478 g), initiator (5 mg AIBN / g

MMA), and stabilizer (5.0358 g). The reaction was carried out in a constant volume cell of 55 cm^3.

In Figures 1, 2, 3 and 4 model predictions for monomer conversion, polymer phase volume, pressure and molecular weight averages are plotted with respect to the polymerization time. In Figure 1, the variation of monomer conversion is plotted as a function of time. The continuous line represents the model predictions while the discrete points represent the experimental conversion measurements [3]. The observed sharp increase in monomer conversion is due to the appearance of the gel-effect. Apparently, there is a good agreement between model predictions and experimental data.

In Figure 2, the volume of the polymer-rich phase is plotted with respect to time. Notice that the swollen polymer phase initially exhibits a sharp increase due to monomer-solvent absorption. This volume increase of the swollen phase continues up to the time at which the monomer concentration in the continuous phase disappears. Subsequently, the volume of the swollen polymer phase decreases due to the polymerization of the absorbed monomer. On the other hand, the non-swollen polymer phase exhibits a continuous increase with monomer conversion.

In Figure 3 the pressure model predictions and discrete experimental data are plotted with respect to time. Given that the polymer density is higher than the monomer density one would expect a monotone pressure decrease. Instead, an initial pressure increase is exhibited followed by a slow decrease of pressure with time. This anomalous behavior can be explained by the non-ideal behavior of the ternary (e.g. monomer-CO_2-polymer) system.

The model predictions of number and weight-average molecular weights are shown in Figure 4. The discrete points represent experimental values obtained by Hsiao et al. [3]. Apparently, there is a good agreement between model predictions and experimental data which demonstrates the predictive capabilities of the present model.

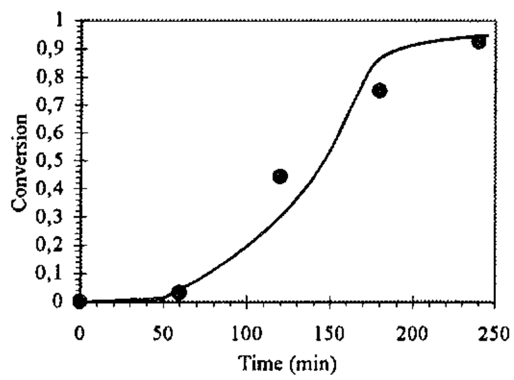

Figure 1: Variation of monomer conversion with reaction time (● : experimental data), [3].

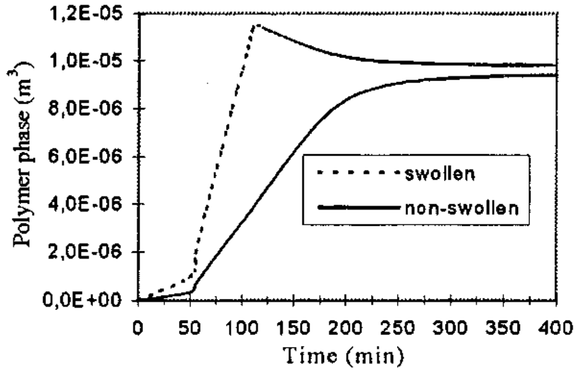

Figure 2 : Variation of the swollen and non-swollen polymer phase with reaction time.

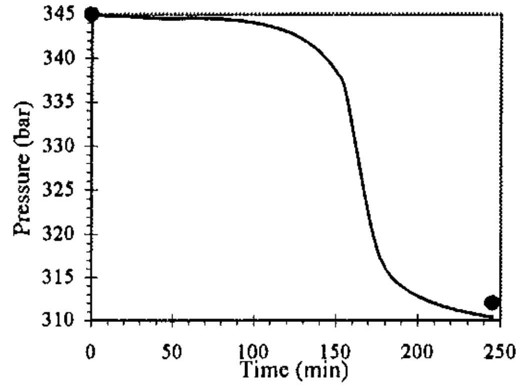

Figure 3 : Variation of the reactor pressure with reaction time (•: experimental data), [3].

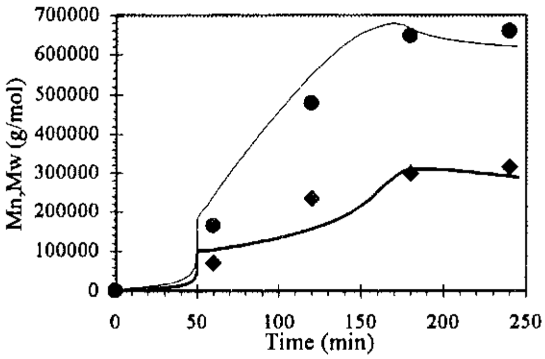

Figure 4 : Variation of the number- and weight average molecular weights with conversion (— : W.A.M.W., — : N.A.M.W., ● ◆ : experimental data), [3].

References

1. Barrett, K. E. J., *Dispersion Polymerization in Organic Media*; Wiley: London (1975).
2. Kiparissides, C., Daskalakis, G., Achillias, D. S. and Sidiropoulou, E., *Ind. Eng. Chem. Res.*, *36*, 1253-1267 (1997).
3. Hsiao, Y-L., Maury, E. E., DeSimone, J. M., Mawson, S. and Johnston, K. P., *Macromolecules*, , *28*, 8159-8166 (1995).
4. Lepilleur, C. and Beckman, E. J., *Macromolecules*, *30*, 745-756 (1997).

Calculation of High-Pressure Phase Equilibria in Polymer Systems

S. Behme, G. Sadowski, W. Arlt
Institut fuer Verfahrenstechnik, Fachgebiet Thermodynamik und thermische Verfahrenstechnik,
Technische Universitaet Berlin, Sek. TK-7, Strasse des 17. Juni 135, 10623 Berlin, Germany,
EMAIL : w.arlt@vt.tu-berlin.de, FAX : +49 30 314 22406

Abstract Calculations of high-pressure phase equilibria with the SAFT - equation of state are presented and compared to experimental data. Example systems are low-density polyethylene (LDPE) - ethylene, polyethyleneglycol (PEG) - propane and a ternary mixture of polystyrene (PS) - cyclohexane - carbon dioxide. Effects of the molecular weight distribution of the polymer on the phase equilibria are considered using the concept of pseudocomponents. The results show that SAFT is able to correlate and predict high-pressure phase equilibria for different types of polymers.

Introduction

Fluids with high volatility play an important role in polymer processing. They can combine good solubility at high pressures with good separability from the polymer by pressure release. In the near-critical region the solvent power of a fluid is well tuneable due to the big influence of the pressure on density. Supercritical gases are used as antisolvents in combination with normal technical solvents to affect the phase separation kinetics in order to yield certain particle structures. Dissolved gases in polymer solutions significantly decrease viscosity e.g. in spinning processes.

Calculations of phase equilibria for polymer systems at high pressures require a thermodynamic model which includes both, the temperature and pressure dependence of the chemical potential. Equation-of-state models fulfil this requirement in contrast to most of the common activity-coefficient models.

The present work gives calculation examples with the Statistical Associating Fluid Theory (SAFT) equation of state for three different polymer-solvent systems at high pressure: low-density polyethylene (LDPE) - ethylene, polyethyleneglycol (PEG) - propane and the ternary mixture of polystyrene (PS) - cyclohexane - carbon dioxide.

The influence of the molecular-weight distribution of the polymer is considered by the concept of pseudocomponents.

Theory

The SAFT-equation of state has been developed by Chapman et al. [1] and Huang and Radosz [2, 3]. SAFT is a perturbation theory which was derived from an expression for the free Helmholtz energy. Molecule segments of equal size and interaction energy are lined up to form a chain molecule. For each non-associating substance three pure-component parameters are required: the segment number (r), the segment volume (v_{00}) and the segment-segment interaction parameter (u_0/k). For each pair of substances there is one binary interaction parameter (k_{ij}). The different chain lengths of molecules of the same polymer type are specified by a different segment number r, while the other parameters are kept constant for all chain lengths.

Results

In the phase diagrams presented, the symbols denote experimental data and the full lines denote calculations with the SAFT-equation of state. Table 1 gives the pure-component parameters used for the calculations. The segment number is given in terms of the ratio M/r to clarify, that r is proportional to the molecular weight M. The binary k_{ij} parameter for LDPE - ethylene is 0.058, binary parameters for PEG - propane and PS - cyclohexane - carbon dioxide can be found in [4] and [5] respectively.

Table 1: Pure-component SAFT parameters used in this work

	M/r [g/mol]	v_{00} [cm^3/mol]	u_0/k [K]	reference
PS	21.969	12.000	226.50	[4]
LDPE	19.622	12.000	216.15	[2]
PEG	24.703	13.159	342.68	[5]
cyclohexane	21.199	13.502	236.41	[2]
ethylene	19.212	18.150	212.06	[2]
carbon dioxide	31.058	13.578	216.08	[2]
propane	16.356	13.457	193.03	[2]

LDPE - ethylene

Fig. 1 shows the phase equilibrium for the system LDPE - ethylene for two different LDPE's which are characterised by their weight-average molecular weight M_w. Experimental data and polymer characteristics are taken from de Loos et al. [6]. PE99 denotes a polydisperse LDPE with M_n = 56 kg/mol, M_w = 99 kg/mol and M_z = 185 kg/mol. PE8 denotes a polydisperse LDPE with M_n = 7.6 kg/mol, M_w = 8.8 kg/mol and M_z = 10.4

kg/mol. Table 2 gives the pseudocomponents which were used for the calculations and were obtained from a fit to the characteristical data M_n, M_w and M_z. Mp denotes the molecular weight of a pseudocomponent and xp their mol fraction within the pure polymer.

Table 2: Pseudocomponents and their mole fractions within the polymer

	LDPE8 kg/mol		LDPE99 kg/mol	
	Mp [g/mol]	xp	Mp [g/mol]	xp
1	213.7	$0.3443*10^{-10}$	775.0	0.000004
2	320.6	$0.2290*10^{-8}$	1370.0	0,000071
3	480.9	$0.1176*10^{-6}$	2422.1	0,000801
4	721.4	0,000004	4281.9	0,006134
5	1082.1	0.000117	7569.9	0.031297
6	1623.1	0.002006	13382.5	0.103903
7	2434.7	0,020610	23658.3	0.218863
8	3652,1	0,115550	41824.6	0,284819
9	5478,1	0.315918	73939,9	0,222620
10	8217.2	0.368537	130715.2	0.101433
11	12325.9	0.156560	231085.8	0.026102
12	18488,8	0.020071	408526.7	0.003668
13	27733.2	0.000621	722217.0	0.000271
14	41599,9	0.000003	1276776,5	0.000010
15	62399.8	$0.2774*10^{-8}$	2257158,4	$0.1878*10^{-6}$
16	93599.8	$0.2016*10^{-12}$	3990333.7	$0.1613*10^{-8}$

The experimental data as well as the calculated isotherm for LDPE99 (Fig. 1) show a bend at about 5 weight% polymer which is due to the occurrence of three-phase. This phenomenon was theoretically described for very polydisperse polymers by Šolc [7]. In contrast, it can be seen from the experimental data, that the cloud-point curve for the narrowly distributed polymer LDPE8 has a smooth curvature over the whole concentration range. Furthermore, the miscibility gap lies at much lower pressures than that of the large polymer. Both, the dependence of the phase equilibrium on the mean molecular weight and the occurrence of three-phase demixing are represented well by the calculations.

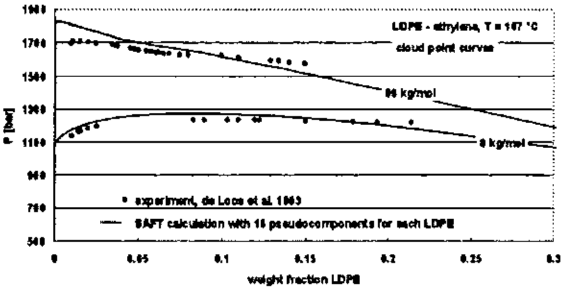

Fig. 1: Phase diagram for LDPE - ethylene for two different molecular weights and molecular weight distributions of LDPE (LDPE 8 kg/mol: M_w = 8.8 kg/mol, M_w/M_n = 1.18; LDPE 99 kg/mol: M_w = 99 kg/mol, M_w/M_n = 1.76) at 167°C. Symbols: experimental data [6], Lines: SAFT calculations.

PEG - propane

Fig. 2 presents the phase diagram for the monodisperse PEG 4000 (M_w = 4000 g/mol, M_w/M_n < 1.1) - propane system at 60°C and 120°C. The 60°C-isotherm increases slowly at low pressures. In this region a PEG-rich liquid phase coexists with a propane-rich vapor phase. After a sharp bend at about 23 bar the isotherm rises fast. At this point three phases coexist: a liquid PEG-rich phase, a liquid propane-rich phase and a vapor phase which almost exclusively contains propane. The abrupt change in solubility results from the change in solvent density as the system pressure exceeds the vapor pressure of the pure solvent. In contrast to 60°C the 120°C isotherm has a smooth course towards higher pressures. At this temperature the propane is supercritical ($T^c_{propane}$ = 96.65°C) and its density therefore changes continuously.

The SAFT calculations capture the described effects very well. Even a prediction (k_{ij} = 0) from pure component parameters results in qualitatively comparable isotherms. For the presented calculations the k_{ij} parameters for PEG - propane are -0,00089 for 60°C and -0,01210 for 120°C.

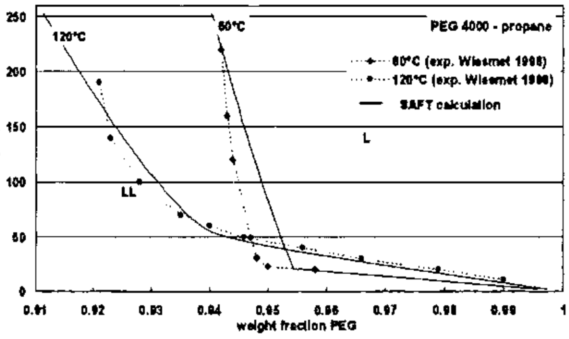

Fig. 2: Phase diagram for PEG (4 kg/mol) - propane for 60°C and 120°C. Symbols: experimental data [5], dashed lines are drawn for clarification. Full lines: SAFT calculations.

PS - cyclohexane - carbon dioxide

The influence of carbon dioxide on the solubility of polystyrene in cyclohexane can be seen in Fig. 3. The PS concentration lies between 7 and 11 weight% for all systems. Experimental data for a quasi-monodisperse PS (M_n = 93 kg/mol, M_w = 101 kg/mol) have been measured by Bungert et al. [8] and de Loos [9]. UCST data for the binary system PS - cyclohexane given as full points in Fig. 3 have been measured by Wolf et al. [10].

Starting from a CO_2 concentration of 0 weight% the LCST curve of the polystyrene - cyclohexane system is shifted to lower temperatures with rising

CO_2 content. At a concentration of 21.25% CO_2 the LCST curve detaches from the VL-transition line and merges with the UCST curve. The experiments show that in the region around 20% CO_2 the miscibility gap shifts dramatically to higher pressures; an addition of 1.11% carbon dioxide lifts the phase-separation pressure by 27 bar. This is because the free-volume effect of the dissolved carbon dioxide goes together with the enthalpic interactions responsible for UCST demixing.

The lines in Fig. 3 denote SAFT calculations. The numbers indicate the concentration (weight%) of carbon dioxide in the system. A prediction of the ternary system from pure-component and binary data leads to qualitatively correct results. The excellent quantitative result shown here for carbon dioxide concentrations between 0 and 16.5 weight% have been achieved by fitting the binary k_{ij} parameter of polystyrene - carbon dioxide to the ternary data. For higher carbon dioxide contents - in the region of very high sensitivity with respect to the gas influence - the demixing pressures are overestimated in comparison with the experimental data.

In addition to the good correlation for carbon dioxide concentrations up to 16.5% SAFT correctly predicts the merging of the LCST and the UCST curve and even the shape of the L-UCST curve is in remarkable conformity with the experimental data.

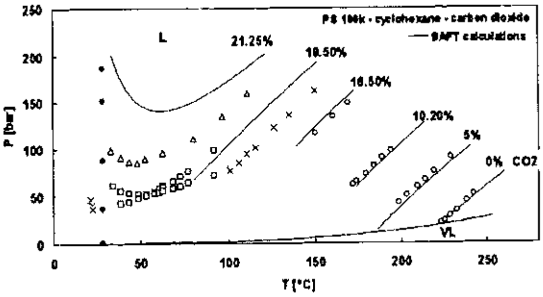

Fig. 3: Phase behavior of the polystyrene (100 kg/mol) - cyclohexane - carbon dioxide system. Symbols (experimental data) : ○ 0 weight% CO_2 content [8], 5% [9], 10.2% [9], 16.5% [8], x 19.5% [8], □ 21.25% VLE and LLE points [8], △ 22.36% [8], • 0% UCST curve [10]. Lines: SAFT calculations, CO_2 contents (weight%) as indicated.

Conclusions

Phase equilibria for three different applications in high-pressure polymer technology are calculated with the SAFT-equation of state.

SAFT is able to correlate and predict the influence of temperature, pressure and molecular weight for polymer-solvent systems with different polymers as polyethylene, polystyrene and polyethyleneglycol.

Gas solubilities in polymers and gas-antisolvent effects are well represented.

The influence of the polydisperse molecular-weight distribution of the polymer can be considered by the concept of pseudocomponents. The demixing of widely-distributed polymers in a mixture with a solvent is predicted in accordance with the experimental data.

List of Symbols

k_{ij}	binary interaction parameter of SAFT
M	molecular weight [g/mol]
M_n	number-average molecular weight [g/mol]
Mp	molecular weight of pseudocomponent [g/mol]
M_w	weight-average molecular weight [g/mol]
M_z	z-average molecular weight [g/mol]
r	segment number, SAFT parameter
xp	mol fraction of pseudocomponent with respect to the polymer [mol/mol]

Literature

[1] Chapman W. G., Gubbins K. E., Jackson G., Radosz M., Ind. Eng. Chem. Res. 1990, 29, 1709-1721

[2] Huang S.H., Radosz M., Ind. Eng. Chem. Res. 1990, 29, 2284-2294

[3] Huang S.H., Radosz M., Ind. Eng. Chem. Res. 1991, 30, 1994-2005

[4] Behme S., Sadowski G., Arlt W., *Modeling of the Separation of Polydisperse Polymer Systems by Compressed Gases*, accepted for publication in Fluid Phase Equilibria, 1999

[5] Wiesmet V. Weidner E., Behme S., Sadowski G., Arlt W., *Experiment and Modeling of High-Pressure Phase Equilibria in the Systems PEG - Propane, PEG - Nitrogen, and PEG - Carbon Dioxide*, submitted to Journal of Supercritical Fluids, 1999

[6] de Loos Th. W., Poot W., Diepen G. A. M., Macromolecules 1983, 16, 111-117

[7] Šolc K., Collect. Czech. Chem. Commun. 1970, 3(5), 665-673

[8] Bungert B., Sadowski G., Arlt W., Ind. Eng. Chem. Res. 1998, 37, 3208-3220

[9] de Loos Th. W., personal communication, 1994

[10] Wolf B. A., Geerissen H., Coll. Pol. Sci. 1981, 259, 1214-1220

Modeling of Kinetics and Structural Properties in High-Pressure Fluid-Phase Polymerizations

M. Buback, M. Busch, H. C. M. van Boxtel
Abteilung für Technische und Makromolekulare Chemie im
Institut für Physikalische Chemie der Universität
Tammannstraße 6
D-37077 Göttingen

Modeling polymer structure and molecular weight distribution is an attractive and powerful tool to gain insight into the kinetic details of elementary reactions determining these properties. Ethene (co)polymers are an ideal object for such investigations as all relevant types of elementary polymerization-related processes can be observed: initiation, propagation, chemically and diffusion controlled termination, transfer to polymer (including backbiting) and β-scission of secondary macroradicals. In copolymerizations with acrylates, branching becomes highly relevant due to the α-H atom on the acrylate monomer. ^{13}C-NMR spectroscopy which is carried out for the analysis of the branching structure, in addition provides monomer sequences in these copolymers which contain valuable information about propagation kinetics. Using a wide variety of analytical techniques, such as on-line infrared/near infrared spectroscopy, quantitative ^{13}C-NMR spectroscopy, elemental analysis and size exclusion chromatography (SEC) allows to deduce detailed kinetic information. The rate coefficients that have been determined by these techniques are introduced into models for homo- and copolymerizations which are capable of describing conversion and polymer properties simultaneously. For the ethene homopolymerization the focus is directed toward the description of polymerizations under widely differing reaction conditions. In copolymerizations the development of the kinetic model is more in focus. The simulations have been carried out using the program package PREDICI®.

Introduction

Ethene homopolymerizations may be regarded as the archetype of polyreactions carried out in supercritical fluid phase where reaction conditions may be continuously varied. Although being a well-established process with a production capacity of about 17 Mio. t/a this reaction still is of scientific interest. Current activities are directed toward describing the kinetics and polymer properties in ethene homo- and copolymerizations by simulations that are based on well-defined physically reasonable models using kinetic rate coefficients being derived from independent experiments. It is the enormous flexibility of the ethene polymerization carried out in supercritical fluid phase which asks for an adequate simulation of the kinetics and polymer properties to guide the optimization of the technical process. In copolymerizations with acrylate monomers, the homogeneous fluid phase range is further extended, as these comonomers act as cosolvents. Modeling of copolymerizations requires a lot of additional kinetic parameters to be known and also to test the applicability of copolymerization models. Within the subsequent text, after a brief discussion of the modeling of ethene homopolymerization, aspects of the simulation of ethene-methyl acrylate copolymerization will be outlined. The modeling of polymerization kinetics and (co)polymer structure has been exclusively carried out using the PREDICI® program package [1].

Kinetic Scheme of Ethene Polymerizations

Scheme 1 shows the set of elementary reactions of a model used for ethene homopolymerization. Initiation, propagation, termination, and transfer reactions to monomer and modifier follow the general scheme. For transfer reactions to polymer quite different approaches are reported in the literature. We use the concept that has been put forward by Lorenzini et al. [2] in which transfer to polymer and β-scission of the formed secondary macroradical are considered as sequential processes. This seems to be close to what is happening in reality.

For the initial propagation step of initiator-derived and modifier-derived radicals as well as for secondary macroradicals it is assumed that the rate coefficient of ordinary propagation may be used. These approximations do not introduce large uncertainties as has been tested by model calculations. Propagation and termination rate coefficients have been derived from time-resolved single pulse laser polymerization experiments [3]. The transfer rate coefficient to monomer is obtained from the average degree of polymerization of polyethylene samples prepared at low polymerization rate and conversion [4]. The modifier endgroups in the polymer backbone, as determined by infrared spectroscopy, are used to quantify the associated transfer reactions. Backbiting rate and transfer to polymer are quantified by the number of short- (SCB) and long-chain branches (LCB), as derived by quantitative ^{13}C-NMR spectroscopy. The full molecular weight distribution (MWD), measured by SEC, is used to fit the β-scission rate. It should be emphasized that the use of independent sensors for the determination of each individual rate coefficient is extremely important as polymer properties and conversion result from a complex coupling of the individual elementary reactions. For predictive purposes the rate coefficients should be represented as a function of temperature and pressure by physically reasonable models.

$$\mathrm{I} \xrightarrow{f \cdot k_\mathrm{d}} 2 \cdot \mathrm{R_I} \tag{1}$$

$$\mathrm{R_I} + \mathrm{E} \xrightarrow{k_\mathrm{SI}} \mathrm{R_1} \tag{1a}$$

$$\mathrm{R_X} + \mathrm{E} \xrightarrow{k_\mathrm{SX}} \mathrm{R_1} \tag{1b}$$

$$\mathrm{R_i} + \mathrm{E} \xrightarrow{k_\mathrm{p}} \mathrm{R_{i+1}} \tag{2}$$

$$\mathrm{R_i} + \mathrm{X} \xrightarrow{k_\mathrm{tr,X}} \mathrm{P_i} + \mathrm{R_X} \tag{3}$$

$$\mathrm{R_i} + \mathrm{E} \xrightarrow{k_\mathrm{tr,M}} \mathrm{P_i} + \mathrm{R_1} \tag{4}$$

$$\mathrm{R_i} \xrightarrow{k_\mathrm{SCB}} \mathrm{R_i} + SCB \tag{5}$$

$$\mathrm{R_i} + \mathrm{P_j} \xrightarrow{\mathrm{j} \cdot k_\mathrm{trP}} \mathrm{P_i} + \mathrm{R_{j,\,sec}} \tag{6}$$

$$\mathrm{R_{i,\,sek.}} + \mathrm{E} \xrightarrow{k_\mathrm{p}} \mathrm{R_{i+1}} + LCB \tag{7}$$

$$\mathrm{R_{i,\,sek.}} \xrightarrow{k_\beta} \mathrm{R_{i\text{-}k}} + \mathrm{P_k} \tag{8}$$

$$\mathrm{R_i} + \mathrm{R_j} \xrightarrow{k_\mathrm{t,\,comb}} \mathrm{P_{i+j}} \tag{9}$$

$$\mathrm{R_i} + \mathrm{R_j} \xrightarrow{k_\mathrm{t,\,disp}} \mathrm{P_i} + \mathrm{P_j} \tag{10}$$

Scheme 1: Elementary reactions in ethene homopolymerization: 1: initiation, 1a/b: initial propagation steps of initiator and modifier radicals, 2: propagation, 3: transfer to modifier, 4: transfer to monomer, 5: backbiting, 6: transfer to polymer, 7: propagation of secondary macro radicals, 8: ß-scission, 9/10: termination by combination/disproportionation

The kinetic scheme for copolymerizations is much more extended. At least two additional termination and three additional propagation steps need to be considered. Moreover, each elementary reaction of macroradicals splits into four reaction steps for the homo-reaction of the comonomers and the cross-reactions in-between the species. Propagation kinetics in bulk copolymerization can be adequately described by the penultimate unit model of Fukuda [5]. Ethene copolymerizations with acrylates can be nicely represented by the implicit penultimate unit model. For termination kinetics a variety of approaches exists [6,7] that are based on aspects of chemical and diffusion control. As the copolymerization takes place in an ethene-rich regime it is assumed that termination reactions are dominated by ethene-like reactions. The reactivity ratios can be determined applying the Mayo method. However, the evaluation of radical reactivities (see below), required by the implicit penultimate unit model, is less straight-forward. The analysis of monomer sequences in the copolymer provides information about propagation rates in copolymerizations. Models and experimental techniques to characterize branching structure and the full MWD in copolymers are rather scarce in the literature. Whereas some information on characterization of SCBs exists [8], the methodology for determining LCBs is not clearly worked out and examples of recent data will be presented below.

Polymer Properties in Ethene Homopolymerizations

Conversion profiles in ethene homopolymerizations can be simulated via PREDICI® in good quality for any reactor of known backmixing characteristics. This section focuses on the description of MWDs and branching indices. Fig. 1 shows a comparison of experimental MWDs with simulation results for ethene homopolymerizations carried out in an almost ideally mixed high-pressure vessel in the presence and in the absence of propionic aldehyde as modifier at moderate conversion.

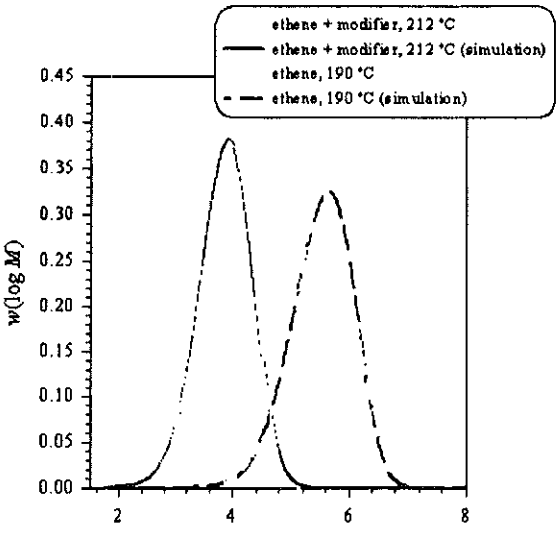

Figure 1: Comparison of simulated and experimental MWDs for polyethylene produced in an ideal mixed vessel at moderate conversion

Although the degree of polymerization is significantly different, both sets of experimental data are adequately described by using the same kinetic model and applying identical rate coefficients. The question arises, whether this is also true for a technical high-pressure tubular reactor. For a given pressure and temperature profile, excellent agreement of simulated and experimental MWDs is found, using the same model, rate coefficients and associated activation parameters. The only exception to this is a slightly different frequency factor for the β-scission rate.

The entire kinetic information on homopolymerization introduced up to this point goes into the subsequent modeling of copolymerization reactions.

Propagation Kinetics and Polymer Properties in Ethene Copolymerizations

In copolymerizations, the copolymer composition is controlled by the reactivity ratios r which characterizes the ratio of homo- to cross-propagation of a macroradical ($r_1 = k_{p,11}/k_{p,12}$; index 1 denotes ethene, index 2 comonomer). Applying the Mayo equation (Eq. 11) r_1 and r_2 can be derived from a plot of copolymer composition F (mole fraction) versus the mole fraction f of the monomer mixture.

$$F_1 = \frac{r_1 \cdot f_1^2 + f_1 \cdot (1 - f_1)}{r_1 \cdot f_1^2 + 2 \cdot f_1 \cdot (1 - f_1) + r_2 \cdot (1 - f_1)^2} \qquad (11)$$

Using the implicit penultimate model, propagation kinetics are additionally affected by radical reactivities s. These quantities reflect the influence of a penultimate unit on the homo-propagation step according to Eq. 12.

$$s_1 = \frac{k_{p,211}}{k_{p,111}} \qquad (12)$$

$$k_{p,11} = k_{p,111} \cdot \left(\frac{r_1 \cdot f_1 + f_2}{r_1 \cdot f_1 + \frac{f_2}{s_1}} \right) \qquad (13)$$

The propagation rate coefficient of a homo-propagation step is calculated via Eq. 13. For a large number of copolymerization systems these radical reactivities have been determined from average propagation rate coefficients measured by the PLP-SEC-technique. In evaluating reactivity ratios and radical reactivities for ethene copolymerizations, two difficulties have to be overcome. First, the synthesis of copolymer with a high acrylate content takes places in a very ethene-rich environment. This requires the acrylate content of the monomer mixture to be monitored with a high accuracy in order to determine the reactivity ratio of the acrylate, r_2, via Eq. 11. Second, the PLP-SEC technique, which is a powerful, IUPAC-recommended tool for measuring (average) propagation rate coefficients, can not be easily applied to such polymerization systems. Fortunately, a lot of kinetic information is contained in the sequence distribution of the copolymer. This is illustrated in Eq. 14 which relates the concentration ratio for two types of monomer triads, 122 and 121, with the reactivity ratio r_2. The triad sequence concentrations are determined by quantitative ^{13}C-NMR.

$$\frac{c(122)}{c(121)} = \frac{c_{R1} \cdot k_{p,12} \cdot c_2 \cdot k_{p,22} \cdot c_2}{c_{R1} \cdot k_{p,12} \cdot c_2 \cdot k_{p,21} \cdot c_1} = \frac{k_{p,22} \cdot c_2}{k_{p,21} \cdot c_1} = r_2 \cdot \frac{c_2}{c_1} \qquad (14)$$

The higher the acrylate content, the better is the accuracy of r_2. There exists more than one ratio of such triad concentrations, which serves for r_2 measurement and which, thus can be used as a consistency check. Eq. 15 gives the relation between the ratio of triad concentrations and the ratio of homo-propagation rates of the monomers.

$$\frac{c(121)}{c(221)} = \frac{c_{R1} \cdot k_{p,12} \cdot c_2 \cdot k_{p,21} \cdot c_1}{c_{R2} \cdot k_{p,22} \cdot c_2 \cdot k_{p,21} \cdot c_1} = \frac{F_1}{F_2} \cdot \frac{1}{r_1} \cdot \frac{k_{p,11}}{k_{p,22}} \qquad (15)$$

For known ethene propagation rates, which have been determined for high-temperature high-pressure conditions [3], the propagation rate of the acrylate is accessible. PLP-SEC experiments provide such data only up to about 15 °C. It is gratifying to note that the extrapolated value of methyl acrylate homopolymerization k_p derived from PLP-SEC experiments is in excellent agreement with the value derived from monomer triads in copolymer synthesized at 150 °C. Radical reactivities can be derived from combined fitting of composition data and average propagation rates. The confidence ellipsoid of these parameters for an ethene-methyl acrylate copolymerization at 150 °C and 2000 bar is shown in Fig. 2.

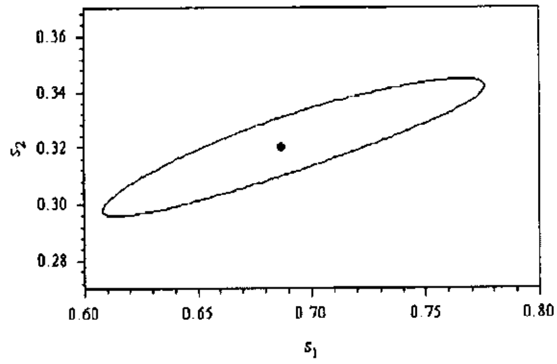

Figure 2: Radical reactivities in ethylene-methyl acrylate copolymerization at 150 °C and 2000 bar

^{13}C-NMR also provides access to the amount of SCBs and LCBs in the copolymers. The branching indices of copolymers synthesized at various conversions are shown in Fig. 3. As compared to ethene homopolymers, both indices are significantly higher than in polyethylene which is due to the action of the α-H atom on the acrylate. This comparison is illustrated by plotting the number of LCBs for ethene homopolymers synthesized at similar conditions as dashed line in Fig. 3.

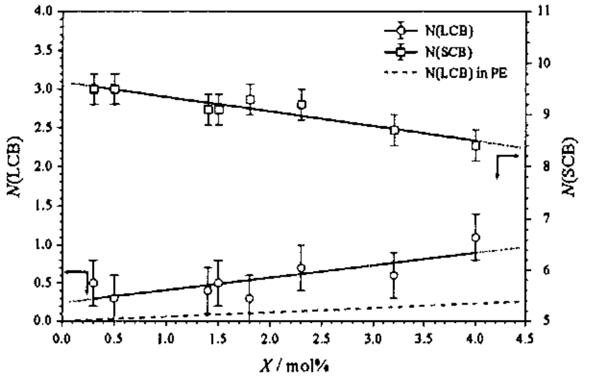

Figure 3: Short- and long-chain branching indices for ethylene-methyl acrylate copolymers synthesized at 150 °C and 2000 bar and various conversions X

It is interesting to see that the number of SCBs slightly decreases with conversion which is not found in ethene homopolymerizations. The reason for this type of behavior is not yet clear. To test whether the model can also describe copolymerization MWDs, Fig. 4 compares a calculated MWD with an experimental one.

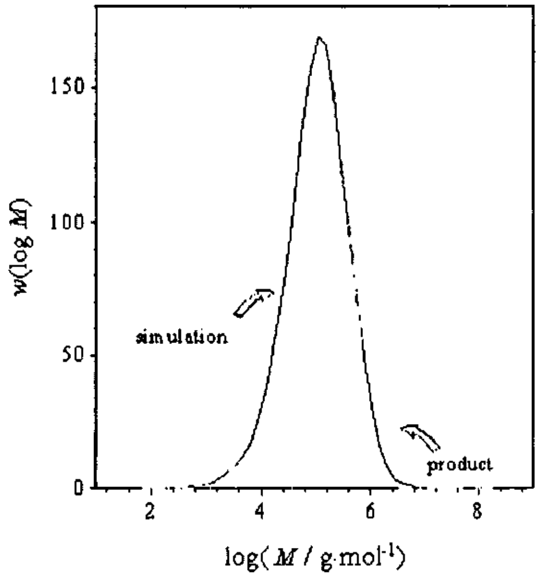

Figure 4: Comparison of simulated and experimental MWDs for a ethylene-methyl acrylate copolymer synthesized at 150 °C and 2000 bar with 15 mol% acrylate content

Considering the complexity of the kinetic scheme and the large number of model parameters which have to be determined independently, the agreement is rather satisfying. It turns out that acrylate repeat units undergo approximately 25 times more long-chain branching than ethylene units and about 2 times more β-scission reactions.

The data shows that modeling may be successfully applied to describe (co)polymerization parameters such as concentration profiles, structural properties of the polymer and MWD. Further work however remains to be done in order to fully model copolymerization kinetics and copolymer properties in extended ranges of pressure and temperature.

References

[1] Wulkow M., *Macromol. Theory Simul.* **1996** 5, 393

[2] Lorenzini P., Pons M., Villermaux J., *Chem. Eng. Sci.* **1992** 47, 3981

[3] Schweer J., *Dissertation*, Göttingen **1988**

[4] Buback M., Choe C.-L., Franck E.-U., *Makromol. Chem.* **1984** 185, 1699

[5] Fukuda T., Ma Y.-D., Inagaki H., *Macromolecules* **1985** 18, 17; Fukuda T., Ma Y.-D., Inagaki H., *Makromol. Chem. Suppl.* **1985** 12, 125

[6] Fukuda T., Kubo K., Ma Y.-D., *Prog. Polym. Sci.* **1992** 17, 875

[7] Buback. M., Kowollik C., *Macromolecules* in press

[8] McCord E. F., Shaw W. H. Jr., Hutchinson R. A., *Macromolecules* **1997** 30, 246

GVC-Fachausschuß „High Pressure Chemical Engineering“, March 3-5, Karlsruhe, Germany, 1999 GVC FZK '99

Polymer Modification by Supercritical Impregnation

O. Muth[1], **Th. Hirth and H. Vogel**[2]
[1]Fraunhofer Institut Chemische Technologie, Postfach 1240, D-76318 Pfinztal
e-mail: om@ict.fhg.de; Tel.: +49 (0)721/4640-152; Fax.: +49 (0)721/4640-111
[2]Technische Universität Darmstadt, Petersenstraße 20, D-64287 Darmstadt

Supercritical carbon dioxide ($scCO_2$) is used for polymer modification by the impregnation of polymer sheets with vinylic monomers and polymerization takes place inside the swollen polymers. The result of this process are new polymer blends with mixed gradients from the surface to the inner bulk, which are inaccessible by common techniques. For this reason the modification of poly(vinyl chloride) (PVC) with poly(methacrylic acid) (PMAA) was chosen as a model-system to evaluate the limits of supercritical impregnation. Up to 16 % (g g^{-1}) of the watersoluble PMAA could be generated inside the hydrophobic PVC. The opaque appearance and electron microscopic investigations of these blends indicated that both polymers formed a hetreogeneous mixture and the PMAA-phase existed of single sites (diameter < 200 nm) inside the PVC-matrix. Thermal analysis showed, that these blends are thermal unstable and therefore can not produced with common mixing methods like melt mixing. Another pecularity was the evidence of a mixing gradient, which was determined to be linear from the surface to the inner bulk. The maximum PMAA-impact reached 180 µm. Comparative experiments with impregnation under normal conditions demonstrated the necessity of $scCO_2$ during both the impregnation and polymerization processes. Without $scCO_2$ only a neglible mass gain could be achieved. Carbon dioxide acts as a low molecular mass plasticizer which does not enhance the compatibility between the polymeric substrate and the impregnating monomer, but accelerates the impregnation kinetics.

Introduction

Polymers are widely used in many sophisticated applications. Sometimes it is necessary to change the application profile by physical and chemical modifications. Commercial techniques like CVD (Chemical Vapor Deposition) or microwave plasma can only reach to the surface or sometimes cause much damage to the polymers and the modifying substances. Therefore thermally unstable components are disclosed from these modification techniques.

Materials and methods

Supercritical fluids (SCF), especially supercritical carbon dioxide have unique mass-transport properties, which are engaged during extraction and impregnation applications. With $scCO_2$ it is possible to obtain deep ranging polymer modifications by avoiding thermal stresses.

Watkins and McCarthy [1, 2] have developed a new process for polymer modification. In the following study this process was applied with some changes. It can be broken down into several steps shown in fig. 1. The first step is the impregnation of a substrate with vinylmonomers (styrene, acrylics) and a radicalic initiator (AIBN) in supercritical CO_2. In a second step after decompression the reaction is started by a rise in temperature within a CO_2-atmosphere. The impregnation- and reaction parameters control the modification results.

This work focused on bisphenol A poly(carbonate) (PC), poly(vinyl chloride) (PVC) and poly (tetrafluoro ethylene) (PTFE) as polymeric substrates and styrene (S), methyl methacrylate (MMA) and methacrylic acid (MAA) as impregnating monomers. The initiator was always AIBN. From the possible polymer / monomer-combinations the system PVC-(P)MAA was chosen as a model-system to investigate the limits of supercritical impregnation. This system seemed to be interesting because of the generation of a water soluble polymer PMAA inside a hydrophobic PVC-matrix. Furthermore, basic information for appropriate modification is necessary. For this purpose swellable polymers and process parameters for impregnation in the homogeneous phase had to

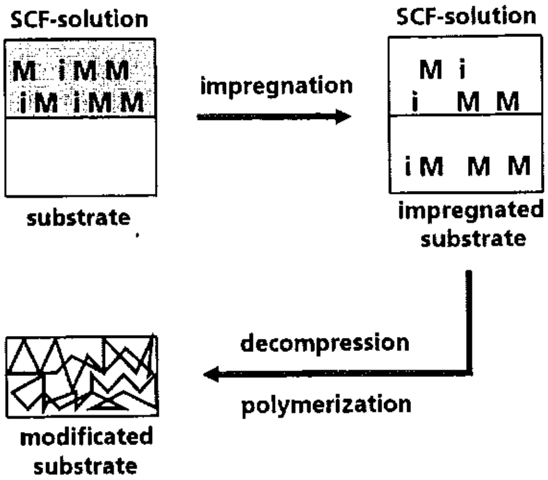

Figure 1. Scheme of the polymer modification, M = monomer, i = initiator.

be found and were topics of earlier investigations [3 - 6]. Experimental details are described there too.

Results and discussion

Table 1 gives the percentual mass gain (100 x g g^{-1}) of the original substrate after the modification. It can be seen, that PTFE showed the lowest mass increase, which concurs with the low swelling capability of PTFE with CO_2 alone. The highest mass gains are obtained in the modification experiments with PC and PVC as substrate and MMA and S as the impregnating monomers. This is due to the high compatability (PVC-MMA) and the increased swelling capability.

The exceptional system PVC-(P)MAA demonstrates the opportunities of this new modification process. Thermal analysis of these new blends showed a decomposition of the PMAA at temperatures > 130 °C. Therefore these blends cannot be produced with common methods like melt-mixing, because the PMAA would significantly decompose during the extrudation step.

Table 1. Percentual mass gain (100 x g g^{-1}) of PC, PVC and PTFE after modification with MMA, S and MAA.

	substrates		
monomers	**PC**	**PVC**	**PTFE**
MMA	50,4	101,7	4,7
S	117,4	76,7	4,0
MAA	8,3	11,1	< 0,1

PVC-PMAA-blends appear opaque because of the incompatibility of both polymers, which lead to heterogeneous blends. This was confirmed by electron microscopy. Fig. 2 shows ultra thin cuts of PVC-PMAA blends. After contrast with OsO_4 the PMAA-phase can be observed as black spots with a diameter of < 200 nm, indicating a separate PMAA-phase. The PMAA could partly be extracted with water. The extract showed a molecular mass of $1.27 \cdot 10^5$ g/mol and a polydispersity of 2.8. In comparison with virgin PVC, the modified PVC reacts hydrophilic and some samples can be completely wetted with water. By increasing the PMAA content the mixtures become more brittle.

Supercritical carbon dioxide enables not only unusual mixtures of polymers but also leads to blends with uncommon properties: X-ray surface investigations from cross sections of the blends gave information about the distribution of PMAA inside PVC. Fig. 3 shows the chlorine distribution of a cross section of PVC-PMAA blends. The low Cl-content on the surface indicates the distribution of PMAA, which means high concentrations on the surface and low concentrations in the bulk. Thus, these PVC-PMAA mixtures have linear gradients from the surface to the inner bulk with a maximum PMAA-impact of about 180 µm. Common polymer forming techniques would result in different layers and not in gradients.

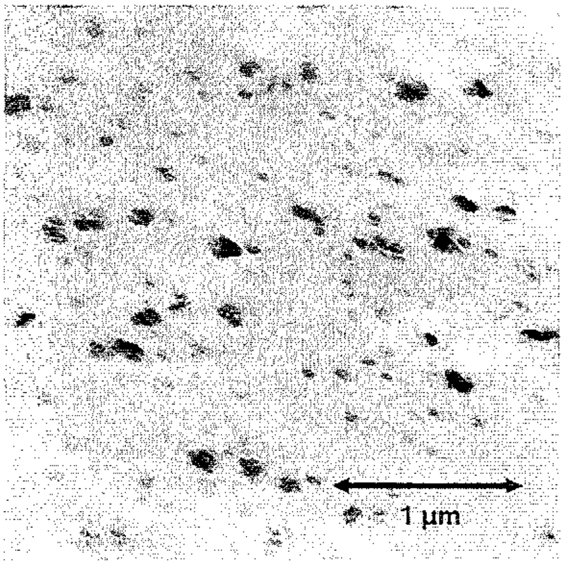

Figure 2. Electron microscopy of PVC-PMAA (93:7) with OsO_4-contrast.

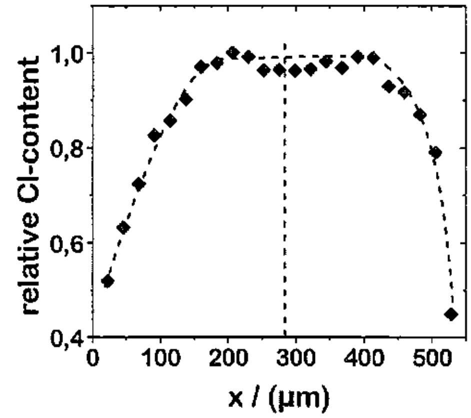

Figure 3. Relative chlorine content as a indicator for the PMAA destribution in PVC-PMAA.

In further experiments the SCF-impregnation was compared with an impregnation in neat MAA. Again the percentual mass gain was chosen as a criterion of successful modification. Fig. 4 shows the results of this comparison. It can be seen, that both impregnation and polymerization under supercritical conditions result in the highest mass increase (experiment A). On the other hand, impregnation in neat MAA and polymerization at ambient pressure results in a very small mass gain (experiment C). Therefore CO_2 acts as a low molecular plasticizer, which enhances the mobility of MAA inside PVC. A considerable diffusion of the monomer is only observable in plasticized PVC. The comparison between the experiments B and C indicates that even during the polymerization $scCO_2$ increases the mobility of the monomer, so that in order to obtain high mass increases both impregnation and polymerization should performed in supercritical swollen polymers. The relative low maximum mass gain of around 7 % also shows, that CO_2 only enhances the diffusion kinetics and not the compatibility between substrate and monomer.

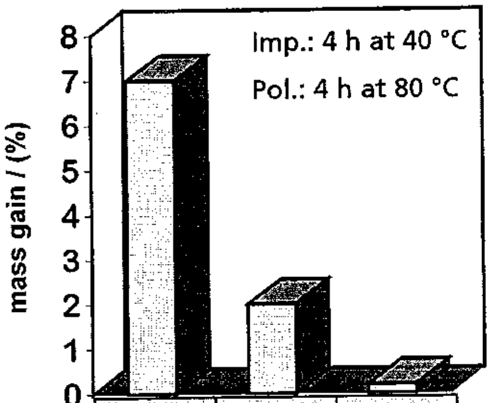

	A	B	C
p_{Imp}	250 bar	250 bar	1 bar
$c_{monomer}$	30 %	30 %	100 %
p_{Pol}	80 bar	1 bar	1 bar

Figure 4. Comparison of supercritical with common impregnation.

Conclusions

Supercritical carbon dioxide is a powerful tool to refine polymeric samples by impregnation techniques. It does not enhance the compatibility between substrate and modification species, but accelerates the impregnation kinetics. In this way it is possible to generate polymer blends, which are inaccessible by common techniques. For successful impregnation a swellable substrate and the solubility of the impregnation species is necessary. From the model-system PVC-PMAA it can be seen, that this process reaches sites close to the surface. So the impregnation with SCF is usefull for bodies with a large surface to volume ratio.

It was not the aim of this work to optimize the properties of PVC by modification, but to give clues for the use of supercritical carbon dioxide in the refinement of polymers. A future application field is the generation of membranes (separation, filtration) or the modification of ion exchange resins. A combination with common polymer-forming processes would enhance the application field of supercritical carbon dioxide.

Acknowledgements

This work is supported by *Ministerium für Wissenschaft, Forschung und Kunst Baden-Württemberg*. The autors would like to thank *Kalle-Pentaplast*, *Otto-Wolff GmbH* and *BASF-Ludwigshafen* for the free of charge polymer-samples.

References

1. J.J. Watkins, T. J. McCarthy; Macromolecules **27** (1994), 4845
2. J.J. Watkins, T. J. McCarthy; Macromolecules **28** (1995), 4067
3. A.R. Berens, G.S. Huvard; *Supercritical Fluid Science and Technology*, ACS Symposium Series 406, Washington D.C. (1989), chapter 14
4. R.G. Wissinger and M.E. Paulatis, J. Polm. Sci., Polm. Phys. Ed., **25** (1987), 2497
5. L. Merz, O. Muth and Th. Hirth, 4th Int. Symp. on Supercritical Fluids, May 11-14, Sendai, Japan (1997), 199
6. O. Muth, Ph. D. Thesis, Technische Universität Darmstadt (D 17), (1998)

Preparation and Evaluation of Supercritical Fluid Bonded Liquid Chromatography Stationary Phase

Mark M. Robson*, Richard Dmoch ,Ian Bromilow, Keith D. Bartle and Peter Myers
Express Separations Ltd, 175 Woodhouse lane, Leeds, LS ,UK

A new procedure has been devised for the bonding of alkoxy silanes to silica particles in supercritical carbon dioxide solvent. Stationary phases for HPLC are produced with high carbon loadings without the requirement of end capping. These have properties when tested with manufacturers test mixtures which shows them to be highly stable and reproducible, and comparable to conventionally bonded columns. The method is applicable to the manufacture of a wide range of stationary phases such as octadecyl, aminopropyl, cyanopropyl, and perfluoroalkyl silicas.

Introduction

Silica is the most commonly used support material in liquid chromatography and is used as polar packing in normal phase liquid chromatography or as a support material for the non-polar chemically bonded phases used principally for reversed phase liquid chromatography. A number of reactions have been used to bond groups to the silica surface so as to modify its surface and hence its chromatographic properties [1-3].

The preferred method, used to produce the majority of commercial stationary phases, uses either chloro or alkoxy (usually methoxy or ethoxy) silane derivatives with one, two or three reactive groups to produce a mono or oligomeric layer on the silica surface,

(surface) Si-OH + X-Si-R_3 $\rightarrow$ Si-O-Si-R_3,
where X is commonly Cl. A base such as pyridine is used to drive the reaction to the right resulting in a surface bond Si-O-Si-R

When a monofunctional ligand is used, surface coverage can be more predictable because only one surface hydroxyl is required for the reaction to proceed. The recent introduction of disopropyl octadecylsilane stationary phase with non-phosphate containing mobile phases has seen a significant increase in the stability [3] of silica based stationary phases. Monofunctional phases tend to be more sensitive to hydrolysis since it only requires one surface bond to be broken for the whole silane group to be lost; trifunctional silanes have the possibility of forming three surface bonds and are thus more strongly retained. However, trifunctional ligands are harder to bond reproducibly due to multiple bond formation with the surface, with the possibility of subsequent polymerisation. When the stationary phase is required to operate in moderately hydrolysing conditions then trifunctional ligands are normally used.

The work reported here describes the development of a supercritical fluid bonding technique using alkoxy silanes, to produce stationary phases with a high surface coverage without the requirement of end capping.

Experimental

All the experiments utilised supercritical CO_2 to dissolve the derivatising reagents followed by reaction with the silica surface. The effects of various parameters are investigated and detailed below. The following bonding reagents have been successfully bonded on to silica:
Trimethoxy octadecylsilane ($(MeO)_3SiOD$)
Methoxy dimethyloctadecylsilane ($MeO(Me)_2SiOD$)
Ethoxy trimethylsilane ($EtOSi(Me)_3$)
Trimethoxy 3,3,3-triflouropropylsilane ($(OMe)_3SiC_3F_3$)
where OD represents octadecyl.

Evaluation of the bonded phase was performed on a HPLC system comprising: a Waters 616 HPLC pump; Waters 600S controller; Waters 486 tunable absorbance detector; Waters WISP 710B auto sampler; Du Pont HPLC column oven; The chromatographic data was processed with a Waters Millenium data system. All solvents were degassed on line using a helium sparge.

Batch bonding of silica.

Bonded silica samples used in this work were prepared in a sealed autoclave. This consists of a thick walled stainless steel vessel with a Viton O ring seal and a connection to a SSI stainless steel valve.

Silica used for supercritical fluid bonding experiments.

This work used Waters Spherisorb S5W silica, batch H05229, particle diameter 5 µm, pore volume 0.5 mL g^{-1}, pore diameter 8 nm.

Waters high purity, high pore volume silica (denoted HP/HV) particle diameter 5 µm, pore diameter 10 nm.

Waters Spherisorb S3W silica, particle diameter 3 µm, pore volume 0.5 mL g^{-1}, pore diameter 8 nm.

The silica (10g) was mixed with 3g of the silane reagent to be bonded and 20 mL of pentane. The pentane was used to ensure homogeneous mixing of the bonding reagent and silica. The pentane was evaporated and the resulting silica slurry was added to the bomb. When highly porous silica designated (HP/HV) was bonded, an extra 10 mL of pentane was required to form a slurry.

The autoclave was part filled with silica and sealed, connected via an SSI valve to a ISCO CO_2 pump, and filled to the required pressure. The autoclave was then placed in a Carlo Erba Fractovap Series 4160 GC oven and heated at the reaction temperature for approximately twenty hours. The temperature was measured via a thermocouple (Pt-Rh) in physical contact with the autoclave.

Bonded silica clean up.

When the reaction was complete, the autoclave was removed from the oven while still at the reaction temperature and the supercritical CO_2 vented into a fume cupboard. After cooling the autoclave was opened and the bonded silica removed, washed three times with pentane (300 mL), and then allowed to dry at room temperature.

Results

Influence of reaction temperature and time on carbon loading

The conventional method of preparing bonded stationary phases utilises the reaction of chloro or methoxy silanes in a refluxing organic solvent and this therefore limits the temperature of the reaction. The maximum temperature is determined by the solvent used and therefore high temperature optimisation of the reaction cannot be used. The other disadvantage of using a liquid reaction medium is that the diffusion coefficient of the reactant is lower in a liquid than in a supercritical fluid, and it is therefore harder for the reactants to penetrate the silica pores.

Using supercritical CO_2 the optimum reaction temperature was measured by determining the variation in carbon loading of the stationary phases while keeping the pressure and reaction time constant (at approximately 20 hours) and varying the temperature between 117°C and 170°C. The optimum carbon loading was observed for a bonding temperature of 150°C.

Application of different bonding reagent

All the bonding reagents used in this work were alkoxysilanes. Methoxy or ethoxysilanes were used since it was necessary that the alcohols produced during the bonding process (MeOH and EtOH) were soluble under the reaction conditions and that the initial silane was soluble in supercritical CO_2.

Evaluation of supercritically bonded stationary phases using HPLC

The supercritically bonded stationary phases were evaluated by using a series of mixtures: a) standard test mixture; b) a metal activity test; and c) a mixture of base, neutral and acidic compounds. A number of the stationary phases were evaluated. The stationary phases were packed into 4.6 mm i.d. x 25 cm column by Phase Separations Ltd to ensure reproducible packing of the column

Standard test mixture

The test mixture comprises [4] dimethyl phthalate, nitrobenzene, anisole, diphenylamine and fluorene. This is a standard test mixture to determine the residual silanol activity and the chromatographic efficiency of the column.

The mobile phase was acetonitrile 70 %, water 30 % at a flow rate of 1 mL per minute; column temperature was ambient, and the detector wavelength was set at 254 nm.

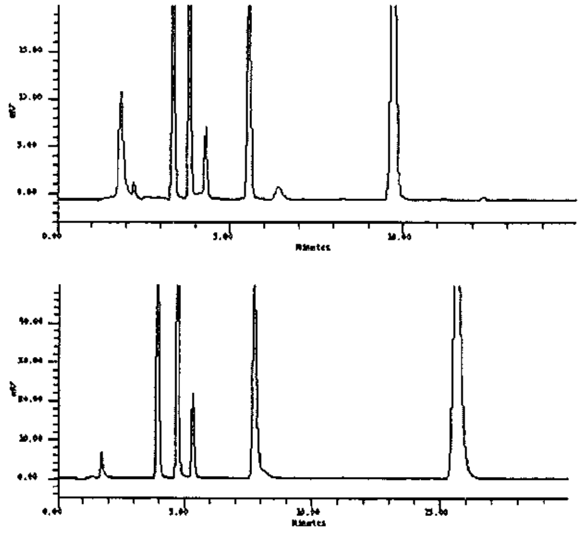

Figure 1. a-b Comparison of columns containing Waters Spherisorb S5W ODS2 and the stationary

phase from experiment B21/1 using the standard test mixture.

Figure 1 a,b compares the chromatograms from columns packed with Waters Spherisorb S5W ODS2 and the packing from experiment B21/1. Waters Spherisorb S5W ODS2 and B21/1 produced similar chromatograms; the peaks from neutral compounds are symmetrical while the basic compounds show tailing as would be expected for silicas containing approximately 1500 ppm sodium.

Metal activity test mixture

The metal activity test [5] is designed to reveal the degree of end capping; the trace metal activity of the stationary phase is determined from the ratio of the retention times of naphthalene (n) to 1-nitronaphthalene (nn) peaks (n/nn). A properly deactivated or end capped stationary phase should have a n/nn ratio of 1.4 or greater, while a non-deactivated stationary phase has an n/nn of less than 1.2

The test solution comprised of acetylacetone (20 µL per 100 mL), 1-nitronaphthalene (5 mg per 100 mL) and naphthalene (30 mg per 100 mL) in methanol.

The mobile phase was 60 % methanol, 40 % water containing 0.5 % sodium acetate at a flow rate of 0.5 ml per minute, column temperature was ambient and detector wavelength was set at 254 nm.

Figure 2 a,b shows the chromatograms obtained on columns packed with Waters Spherisorb S5W ODS2 and the packing material from experiment B21/1. It can be seen that Waters Spherisorb S5W ODS2 (n/nn = 1.52) is completely end capped compared to B21/1 (n/nn =1.28). It is interesting to note that the supercritical bonding process has improved the silica deactivation process slightly compared with a conventionally prepared non-end capped stationary phase. It is not possible, however, to end cap the supercritically bonded stationary phases and further deactivate the surface.

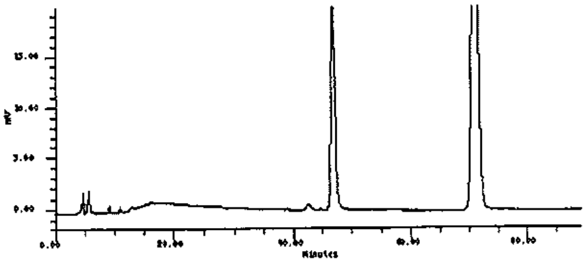

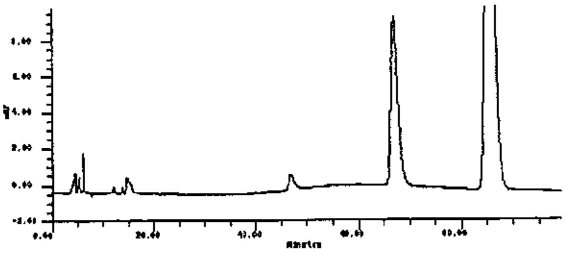

Figure 2. a-b Comparison of columns containing Waters Spherisorb S5W ODS2 and stationary phase from experiment B21 with the metal activity test mixture

Base/neutral/acid test mixture

The base/neutral/acid test [6] is designed to determine both residual silanol activity and chromatographic efficiency. The mixture consists of the following compounds: aniline, phenol, *o*-, *m*-, *p*-toluidine, N,N-dimethylaniline, methylbenzoate and toluene.

The mobile phase was 55 % methanol, 45 % water at a flow rate of 1.0 mL per minute, column temperature was ambient and the detector wavelength was set at 254 nm.

Figure 3 a,b compares the chromatograms for columns packed with Waters Spherisorb S5W ODS2 and material from experiment B21/1 which gave comparable separations but noticeable differences in peak shape. It is evident that a column packed with material from experiment B21/1 has significantly increased retention compared to Waters Spherisorb S5W ODS2.

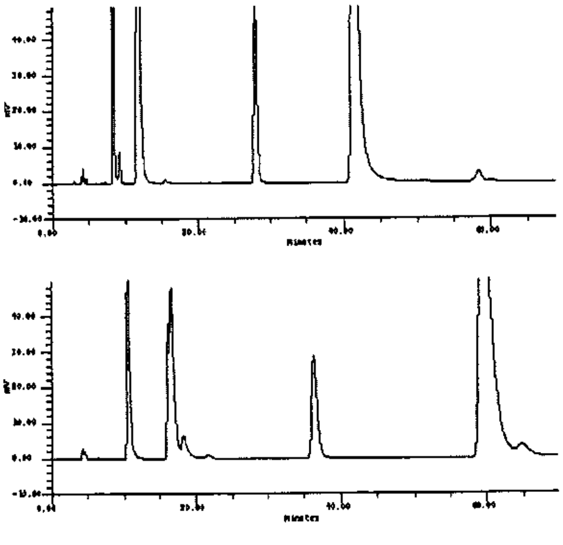

Figure 3. a-b Comparison of columns containing Waters Spherisorb S5W ODS2 and stationary phase

from experiment B21 with the base - neutral test mixture.

There is significant variability in the retention and symmetry of the N,N-dimethyl aniline peak on the supercritically bonded stationary phases, but the origin of this effect is unclear. The best supercritically bonded stationary phases in terms of carbon loading (from experiments B34 and 37) give comparable symmetrical peaks and hence silanol deactivation to that of Waters Spherisorb S5W ODS2.

Discussion

The measured surface area of Water Spherisorb S5W is 180 m^2 g^{-1}, the calculated surface area of an equivalent amount of 5 μm silica solid is < 1 % of the measured area, so that it can be concluded that the majority of the silane reacts inside the silica pores. The use of a higher reaction temperature and therefore an increased diffusion coefficient should allow the silane to diffuse deeper into the pores.

The majority of the supercritical bonding experiments were performed with silica as received, and since the surface water content was unknown therefore it is possible that the silane polymerised due to high surface water content. The silica was pretreated in air at 250°C for 24 hours to provide a surface comparable to that used in conventional bonding procedures and to remove the physically adsorbed water. The carbon loading from the silica heated to 250°C was 11.4 %. From this it is concluded that the increase in C_{18} carbon loading between conventionally and supercritically bonded silica (7 % compared to 12 %) is unlikely to be due to silane polymerisation.

The supercritically bonded stationary phases were comparable to Waters Spherisorb S5W ODS2 in the degree of silanol deactivation as measured by the symmetry of peaks from basic compounds. The degree of end capping as measured by the increase in n/nn ratio compared to a non end capped silica (1.28 to 1.20) suggests that a small amount of the increase in carbon loading can be attributed to end capping.

There is a significant increase in retentivity of the supercritically bonded; this confirms that there is a significant increase in C_{18} loading compared to Waters Spherisorb S5W ODS2, where a significant proportion of the carbon loading is due the end capping with trimethylsilyl.

Conclusions

A new stationary phase bonding technique has been developed which utilises the enhanced solubility and diffusion coefficients of silanes in supercritical CO_2. In this method silica is coated with a homogeneous layer of silane and heated in supercritical CO_2. The technique has the advantage of increased carbon loading, reduction in the quantities of organic solvents required and speed of manufacture.

Acknowledgements

The authors thank BP Chemicals Ltd for a CASE studentship (MMR), and the Engineering and Physical Sciences Research Council for financial support of RD and MMR. The support of Waters Phase Separations in the provision of silica and equipment is also gratefully acknowledged.

References

[1] C. F. Simpson, UK patent, **1,310,872.** (1975).
[2] D. C. Locke, J. T. Schmermund and B. Banner, *Anal. Chem.*, **44**, 90, (1972).
[3] J. J. Kirkland, *J. Chromatogr. Sci.*, **34**, 309 (1996).
[4] P. Myers, Waters Phase Separation, personnel communication (1997).
[5] M. Verzele and C. Dewaele, *Chromatographia*, **18**, 84 (1984).
[6] S. J. Schmitz, H. Zwanziger and H. Engelhardt, *J. Chromatogr.*, **544**, 381 (1991).

Effect of cocatalysts on ethylene/1-hexene copolymerization with metallocenes under high pressure

S. Schmitz, A. Rau*, G. Luft, Ch. Götz

Technical University Darmstadt, Department of Chemical Engineering, Petersenstr. 20, D-64287 Darmstadt, Germany, Email: alex@bodo.ct.chemie.tu-darmstadt.de

Today it is accepted that cations are the catalytically active species in metallocene polymerizations. The active cations are formed by the reaction of metallocene precursors with a cocatalyst. With only small modifications these catalyst systems could be introduced into existing high-pressure polymerization plants. This article shows the influence of the cocatalyst methylaluminoxane (MAO) and the cocatalyst system $Al(^iBu)_3/[NHMe_2(C_6H_5)]^+$ $[B(C_6F_5)_4]^-$ on the performance of ethylene/1-hexene copolymerizations in a continuously operated autoclave at 1500 bar, 210°C with a residence time of 240 s. The premixed solution of metallocene precursor and cocatalyst was continuously metered into the reactor by means of a syringe-type pump. The concentration of 1-hexene in the feed was varied between 0 and 70 mol%. Zirconocene-based catalyst systems showed a strong influence of the [Al]/[Zr] ratios on productivity with both cocatalysts. Up to certain [Al]/[Zr]-ratios the productivity increased with increasing [Al]/[Zr] ratios. To achieve the best productivity, catalysts based on zirconocene/$Al(^iBu)_3$/ $[NHMe_2(C_6H_5)]^+$ $[B(C_6F_5)_4]^-$ need much smaller [Al]/[Zr] ratios than MAO-based systems. Very low productivities were found with a titanocene/$Al(^iBu)_3/[NHMe_2(C_6H_5)]^+$ $[B(C_6F_5)_4]^-$ catalyst, while the analogue titanocene/MAO system produced the same amount of polymer as zirconocene-based systems. The productivity of MAO-based systems decreased with increasing comonomer concentration, whereas in one case the $Al(^iBu)_3/[NHMe_2(C_6H_5)]^+$ $[B(C_6F_5)_4]^-$-based catalyst showed a rate enhancement effect with small amounts of 1-hexene in the feed. The incorporation of 1-hexene into the polymer is not significantly influenced by the cocatalyst used.

Introduction

Since the discovery of Sinn and Kaminsky [1] that methylaluminoxane (MAO) is a very effective cocatalyst for metallocene-based catalysts in the polymerization of ethylene and other α-olefins many efforts have been made to use these highly active catalytic systems in an industrial polymerization process. The limiting factor is the high amount of cocatalyst required, which increases the costs of the catalytic system.

The syntheses of catalytically active systems using a metallocene dialkyl and a cation-forming agent like $[NHMe_2(C_6H_5)]^+$ $[B(C_6F_5)_4]^-$ opens the way to MAO-free catalysts. These catalysts show the same activity as MAO-based systems, but they are more sensitive towards impurities and require very pure monomers. Less sensitive and more easy to handle are ternary systems based on a metallocene dichloride, a certain amount of an aluminium alkyl and a cation forming agent. In these systems the aluminium alkyls are acting as a *scavenger* and as an alkylating reagent of the metallocene dichloride [2].

The purpose of this work is to study the influence of the aluminium-containing cocatalyst and of the comonomer 1-hexene on high pressure, high temperature polymerizations.

Experimental

All polymerizations were performed in a continuously operated high pressure autoclave of 100 ml capacity. In each experiment the pressure was 150 MPa and the average residence time was 240 s (Fig. 1). The temperature was adjusted to 483 K by the amount of catalyst in the feed and an electric heater. The mixtures of monomers were continuously fed into the reactor along the stirrer. The desired ratio between ethene and 1-hexene in the feed was adjusted by mass-flow controllers. Ethene (99.8%) was taken from bombs and further purified by molecular sieves and a copper catalyst. A two-stage compressor was used to pressurize ethene, while 1-hexene was metered by a membrane pump. The catalyst solution was fed into the reactor by a syringe-type pump. Due to the high concentration of the catalyst solution it was diluted with toluene before entering the reactor. Both toluene and 1-hexene were purified prior to use by refluxing and distillating with Na/K alloy.

The pressure was maintained constant by an motor-driven outlet valve controlled by the process computer. Behind the outlet valve, the pressure was released to normal. The polymer was separated in melted or powdered form from the unreacted monomers. When the steady state was attained within 10 min, the polymer samples were collected in different separators. The unit was operated by a computer, which recorded data such as temperature, pressure and mass flow during polymerization tests.

The catalysts based on MAO were prepared as follows: The metallocene dichloride was dissolved in toluene and the required amount of MAO was added to get the desired [Al]/[Zr] ratio.

The activation of the MAO-free catalytic systems based on the metallocene dichloride, triisobutyl aluminium and $[Me_2PhNH]^+ [B(C_6F_5)_4]^-$ is described by the following procedure. Metallocene dichloride was dissolved in toluene and mixed with 10-200 equivalents of triisobutyl aluminium. After 20 min, this solution was added to a solution of $[Me_2PhNH]^+ [B(C_6F_5)_4]^-$ in toluene. In each case, the ratio between borate and metallocene was 1.3 mol Bor /mol Zr.

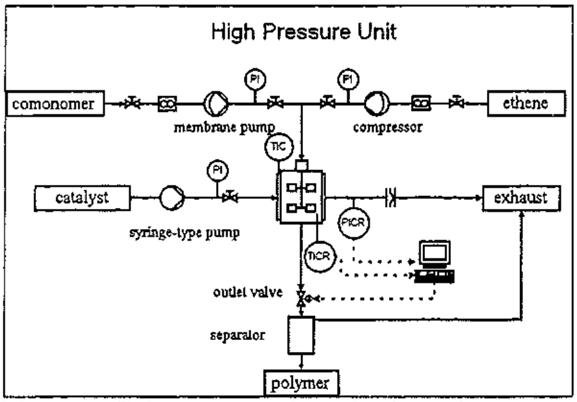

Figure 1: High pressure polymerization unit

Results and discussion

Influence of the [Al]/[Zr] ratio

In the first two series of experiments we studied the influence of the [Al]/[Zr] ratios for the two systems $Me_2Si[IndH_4]_2ZrCl_2/MAO$ and $Me_2Si[Ind]_2ZrCl_2/TiBA/[Me_2PhNH]^+[B(C_6F_5)_4]^-$. In Figure 2 the necessary [Al]/[Zr] ratios are compared. The solid black line with the black squares shows the conversion for the MAO-system in a homopolymerization with a catalyst concentration of 0.01 mol-ppm. As can be seen 22000 mol Al/mol Zr are required to get the maximal conversion. A further increase of the aluminium compound results in only a small influence on the conversion. For the MAO-free activated system only an [Al]/[Zr] ratio of 200 mol Al/mol Zr is needed to obtain the same conversion in a copolymerization with 20 mol% 1-hexene in the feed (catalyst concentration 0.5 mol-ppm). The amount of cocatalyst needed might be due to the so-called *scavenger effect* discussed in the literature [2]. But as shown recently it is not sufficient to adjust a minimum concentration of aluminium-alkyl in the reactor to obtain the best productivities. The zirconocene concentration in the reactor and the [Al]/[Zr] ratio of the premixed catalyst solution has to be additionally considered [3]. Both catalytic systems showed poor incorporation of the comonomer.

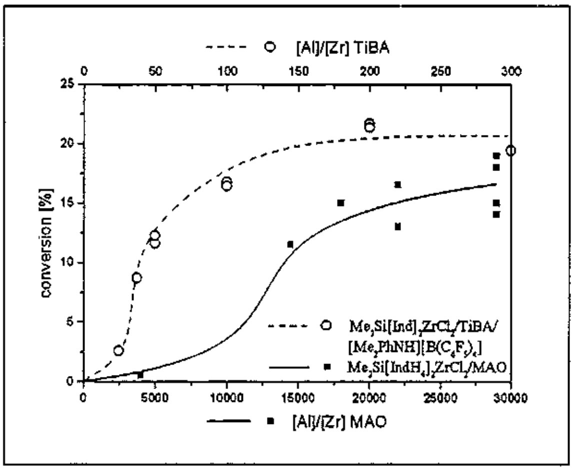

Figure 2: Influence of the [Al]/[Zr] ratio on conversion

Influence of 1-hexene

Halfsandwich catalysts with constraint geometry are well known to incorporate comonomers more easily. A new monocyclopentadienyl complex $^iPr(Cp)(2\text{-}PhO)TiCl_2$ was synthesized and tested in the pilot plant. High activities were achieved when activated with MAO, whereas low amounts of polymer were produced using the MAO-free activation method. Figure 3 shows the productivity of $Me_2Si[IndH_4]_2ZrCl_2/MAO$ and the $^iPr(Cp)(2\text{-}PhO)TiCl_2/MAO$ catalysts with respect to the 1-hexene ratio in the feed.

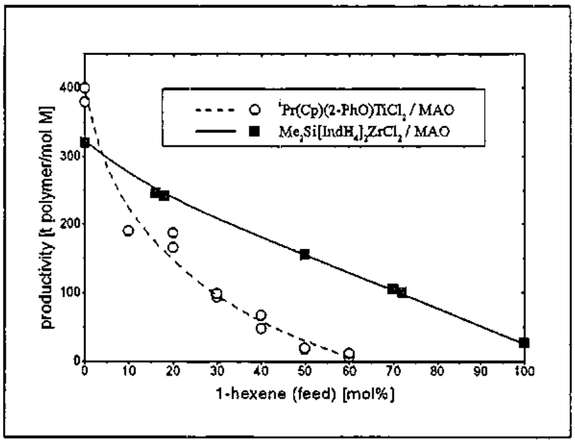

Figure 3: Influence of 1-hexene in the feed on productivity, [Al]/[Zr]=20000

The $^{i}Pr(Cp)(2\text{-}PhO)TiCl_2/MAO$ systems shows strong dependency on the amount of 1-hexene in the feed. With an increasing comonomer fraction the productivity sharply decreases from 400 to 10 t polymer/mol metal. The $Me_2Si[IndH_4]_2ZrCl_2/MAO$ system shows weaker dependency on the 1-hexene ratio. Even at 1-hexene homopolymerization 30 t polyhexene/mol metal can be obtained. The incorporation of 1-hexene in the polymers was determined by means of ^{13}C-NMR spectroscopy. According to the method of Fineman-Ross the copolymerization parameters were calculated as r_E=63, r_H=0.02 for the $Me_2Si[IndH_4]_2ZrCl_2/MAO$ and r_E=27.8 r_H=0.04 for the $^{i}Pr(Cp)(2\text{-}PhO)TiCl_2/$ MAO system. As already known from low pressure, low temperature polymerization processes the monocyclopentadienyl catalyst shows a better incorporation of the comonomer [4]. The product of $r_E * r_H = 1$ for both systems indicates that a statistically random copolymer is formed.

Copolymerization behaviour of the $Me_2Si[Ind]_2ZrCl_2/$ TiBA/ $[Me_2PhNH]^+[B(C_6F_5)_4]^-$ system in comparison with $^{i}Pr(Cp)(2\text{-}PhO)TiCl_2/MAO$

In an additional series of experiments we investigated the ethene/1-hexene copolymerization with a cationically activated metallocene dichloride. In Figure 4 the productivity of $Me_2Si[Ind]_2ZrCl_2/$ TiBA/ $[Me_2PhNH]^+[B(C_6F_5)_4]^-$ with an [Al]/[Zr]-ratio of 200 and of $^{i}Pr(Cp)(2\text{-}PhO)TiCl_2/MAO$ with [Al]/[Zr]=20000 are compared.

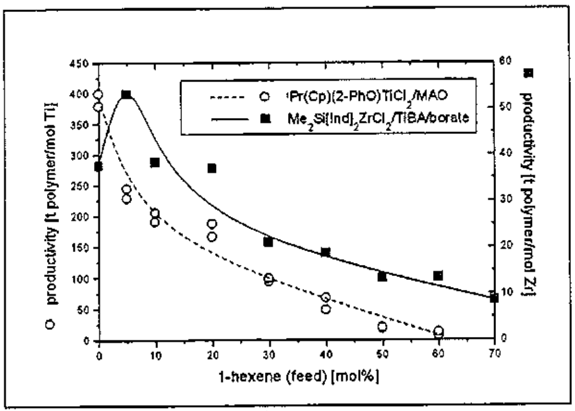

Figure 4: Productivity of $Me_2Si[Ind]_2ZrCl_2/TiBA/[Me_2PhNH]^+[B(C_6F_5)_4]^-$ versus $^{i}Pr(Cp)(2\text{-}PhO)TiCl_2/MAO$ in ethene/1-hexene copolymerizations

The productivity of the cationically activated $Me_2Si[Ind]_2ZrCl_2$ is about ten times lower than the MAO-activated catalyst. With small amounts of 1-hexene in the feed the productivity of the MAO-free catalyst system increases. With more than 10 mol% comonomer in the feed the productivity of both systems decreases. The copolymerisation parameters of the MAO-free system were close to those of the monocyclopentadienyl complex with values of r_E=28 and r_H=0.05. This might be due to the less bulky anion $[B(C_6F_5)_4]^-$ which allows the sterically demanding 1-hexene easier access to the zircon center.

The rate enhancement effect

As can be seen in Figure 5 the catalyst system $Me_2Si[Ind]_2ZrCl_2/$ TiBA/ $[Me_2PhNH]^+[B(C_6F_5)_4]^-$ shows an increase of the rate of ethene polymerization with small amounts of 1-hexene in the reactor. This phenomenon, which is discussed by several authors in regard to low pressure polymerizations, is called *rate enhancement effect*.

In a low pressure polymerization the system $Me_2Si[Ind]_2ZrCl_2/MAO$ showed an acceleration factor of 2.6 at a 1-hexene/ethene ratio of one [5]. As shown in Figure 5 in our process the rate of ethene polymerization is accelerated about 1.8 times at a [1-hexene]/[ethene] ratio in the reactor below 0.5. This could be due to the nearly solvent-free conditions in high pressure processes, which cause a higher comonomer concentration in the reactor. Higher ratios inhibit the rate of ethene polymerization.

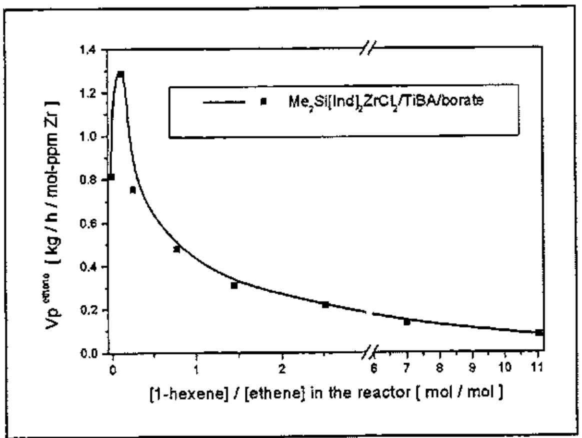

Figure 5: Rate enhancement effect

Copolymers are more soluble in the solvent used in slurry processes, and thus the homogeneous system avoids diffusion problems. The conditions used in the high pressure, high temperature polymerization results in a homogeneous, one-phase system. The acceleration effect can thus not be ascribed to a diffusion phenomenon.

A possible explanation for the rate enhancement in a homogeneous system is that 1-hexene is able to generate more catalytically active sites out of reversibly formed dormant sites.

Conclusions

The reported results show that ternary catalyst systems such as $Me_2Si[Ind]_2ZrCl_2$/ triisobutyl aluminium and $[Me_2PhNH]^+$ $[B(C_6F_5)_4]^-$ could replace metallocene/MAO-based catalysts in high temperature, high pressure polymerization. The copolymerization parameters for MAO-containing as well as MAO-free systems show that under high pressure, high temperature conditions the incorporation of 1-hexene in polyethylene is not favoured.

To gain a better insight into polymerizations with such catalyst systems, further investigation of the polymerization process and the activation method is underway.

The authors gratefully acknowledge financial support from the Bundesministerium für Bildung und Forschung and BASF AG.

Formulae

$Me_2Si[IndH_4]_2ZrCl_2$	dimethylsilyl-bis(tetrahydroindenyl)zirconium dichloride
$^iPr(Cp)(2\text{-}PhO)TiCl_2$	iso-propyl(η^5-cyclopentadienyl)(η^1-2-phenoxy)titanium dichloride
$Me_2Si[Ind]_2ZrCl_2$	dimethylsilylbis(indenyl)-zirconium dichloride
$[Me_2PhNH]^+[B(C_6F_5)_4]^-$	dimethylaniliniumtetrakis-(pentafluorophenyl)borate
MAO	methylaluminoxane
TiBA	triisobutyl aluminium

References

[1] Kaminsky W., Sinn H., Vollmer H.-J., Woldt R. *Angew. Chem.*, *92*, **1980**, 396.

[2] Ewen J.A., *Macromol. Chem., Macromol. Symp., 108*, **1993**, 179.

[3] Götz Ch., Luft G., Rau A., Schmitz S., *Chemie Ing. Tech.*, *70*, **1998**, 1424.

[4] Stevens J. C., in *Studies in Surface Science and Catalysis, Vol. 101*, ed. Hightower J.W., Delgass W.N., Iglesia E. and Bell A.T., Elsevier Science B.V., **1996**, p. 11-21.

[5] Fink G., Herfert N., *Polym. Mater. Sci. Eng.*, *67*, **1992**, 31.

Experimental Investigation of phase equilibria in the system polystyrene/cyclohexane/carbon dioxide

B. Bungert, G. Sadowski, W. Arlt
Institut fuer Verfahrenstechnik, Fachgebiet Thermodynamik und thermische Verfahrenstechnik,
Technische Universitaet Berlin, Sek. TK-7, Strasse des 17. Juni 135, 10623 Berlin, Germany,
EMAIL : g.sadowski@vt.tu-berlin.de

Abstract In the present work, the influence of a dense gas (carbon dioxide) on the phase behavior of polymer/solvent systems is examined. For this purpose, a high-pressure autoclave was built which allows measurements at temperatures up to 250°C and pressures up to 200 bar. Samples can be taken even from very high-viscous phases. At first, the influence of CO_2 on the LCST curve of the model system polystyrene/cyclohexane was investigated. An increasing amount of CO_2 shifts the LCST curve to lower temperatures and higher pressures. At a gas content of about 22 weight % the LCST curve merges with the UCST curve. The composition as well as the polymer distribution in each of the coexisting phases in the two-phase region was determined.

The elimination of a low-molecular-weight additive from the polymer using gas-induced liquid-liquid separation is examined for the model system polystyrene/dioctyl phthalate/ cycylohexane/carbon dioxide.

Introduction

Liquid-liquid phase separation induced by the addition of a compressed gaseous antisolvent to a liquid mixture is a well-known technique (SAS) that can be applied to the recovery of polymers as well as to molecular-weight fractionation of polymers.

For the design and evaluation of separation processes based on this effect, it is crucial to get a better insight in the underlying principles and phase equilibria. Especially in the investigation of complex systems such as polydisperse polymers with additives or impurities, it is necessary to get information on the composition of the coexisting phases. Therefore, in this work an apparatus is used which allows to take samples from all phases and to analyze them concerning composition and polymer distribution. The influence of the gaseous antisolvent (carbon dioxide) on the polymer solubility, on the polymer fractionation and on the additive content in the polymer is investigated.

Experimental

The experiments were performed in a variable-volume autoclave of about 1000 ml designed for vapor-liquid-liquid and vapor-liquid solid experiments at pressures up to 200 bar and temperatures up to 250°C. Two fused-glass windows allow for visual observation of the whole inner diameter. The volume is varied with a metal bellows. Samples can be drawn from the phases via short stainless steel capillary tubes. Mixing is achieved via rocking the autoclave at variable angles from the horizontal position. A detailed description has been given in [1].

For the experiments the autoclave is filled with polymer, solvent and gas and then equilibrated to the temperature of interest and to a pressure in the one-phase region. Once a homogeneous solution is established, the autoclave is moved to a vertical position and samples are taken from the top and the bottom to confirm proper mixing and the concentration. Then, the pressure is lowered until the solution becomes cloudy. Upon further lowering the pressure, samples are taken to determine the composition of the coexisting phases.

Materials

The experiments were performed with anionically synthesised polystyrenes from BASF (PS40: M_n=37.800 g/mol, M_w=42,700 g/mol; PS100: M_n=93,000 g/mol, M_w=101,400 g/mol; PS160: M_n=147,900g/mol, M_w=159,600 g/mol). The solvent was cycylohexane (Fluka, purity>99.5%). The gas was carbon dioxide (Linde, technical grade, purity>99.5%).

General Phase Behavior

Fig. 1 shows the general phase behavior of a polymer solution with the two regions of liquid-liquid phase separation at low temperature (UCST) and high temperature (LCST). At constant polymer concentration and for a given temperature the cloud-point curve indicates the pressure which is needed to form a homogeneous mixture. At low pressures a part of the solvent evaporates forming a vapor phase. The corresponding VLE line is almost identical with the vapor-pressure curve of the pure solvent. The adding of a gas to the system shifts the LCST curve to lower temperatures and higher pressures whereas the UCST curve is not much effected. At a certain gas content the LCST and the UCST merge to form a single two-phase region (L-UCST behavior). At this gas concentration the L-UCST curve touches the VLE line.

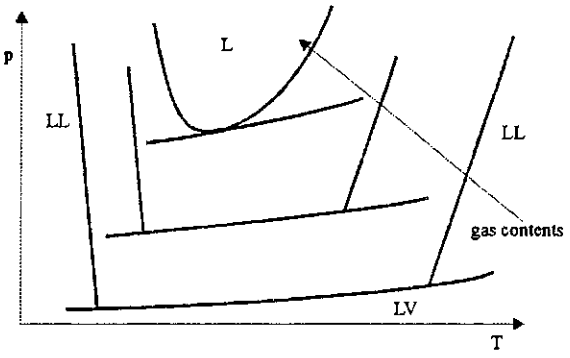

Fig. 1 General phase behavior of a polymer solution with increasing gas contents

Fig. 2 shows the experimentally determined phase behavior for the system polystyrene/cyclohexane /carbon dioxide.

As it can be seen the LCST curve is dramatically shifted to lower temperatures with about 40K per 5wt% gas added to the system. At the same time higher pressures are needed to keep the gas in the solution. At a gas content of 21.3 wt% the LCST curve and the UCST curve merge.

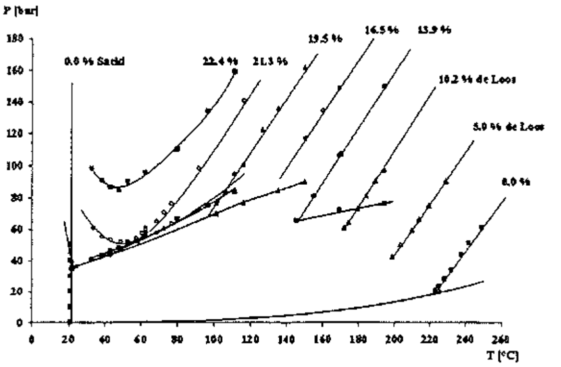

Fig. 2: Phase behavior of the PS100 - cyclohexane - carbon dioxide system. Symbols are experimental data at different CO_2 contents as indicated: 5% de Loos [2], 10.2% de Loos [2], 0% UCST curve Saeki et al. [3], all other data this work.

The phase behavior becomes evident from the ternary phase diagrams which were measured for different pressures at a temperature of 170°C (Fig.3). In pure polystyrene only about 4 wt% carbon dioxide dissolve [4]. An increasing amount of cycylohexane increases the solubility of the CO_2. On the other hand, an increasing amount of gas causes a liquid-liquid phase separation of the former homogeneous polymer solution. Therefore, a three-phase vapor-liquid-liquid area appears. While lowering the pressure from 135 bar until 71.2 bar the gas solubility in the liquid phases decreases and the vapor-liquid region becomes larger. At the same time the liquid-liquid region becomes smaller until it disappears at a lower pressure.

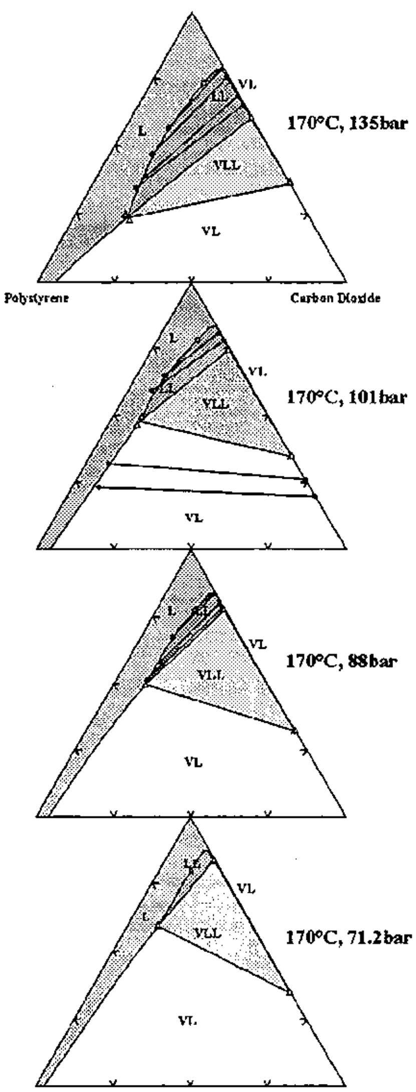

Fig. 3: Ternary phase diagrams for PS100-cyclohexane-carbon dioxide at 170°C and different pressures. The carbon dioxide solubility in pure polystyrene is interpolated using data from [4]. Full circles denote two-phase liquid-liquid coexistence data, triangles denote three-phase VLLE separation.

Molecular-Weight Fractionation

Whereas the experiments described above were carried out with a very narrow molecular-weight distributed polystyrene now the effect of molecular-weight fractionation is investigated. For this purpose polystyrene was used which was a 50/50 mixture by weight of two monodisperse samples PS40 and PS160. Experiments were carried out at 170°C and different pressures(Fig. 4). Starting from a bidisperse feed solution the polystyrene-rich phase contains most of the long chains whereas the polystyrene-lean phase contains most of the short chains at higher pressures. When further lowering the pressure the polymer-lean phase is essentially free of long chains.

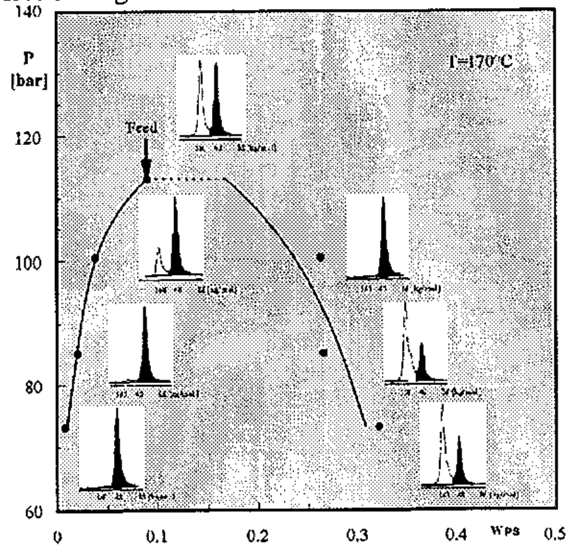

Fig. 4: Pressure vs. polymer-weight-fraction diagram for the LLE region for polystyrene (mixture of PS40 and PS160) in the mixed solvent cyclohexane+carbon dioxide at 170°C. Feed composition: 9.4 weight % PS (PS40 : PS160 = 1:1), 13.4 weight% CO_2, 77.2 weight% cyclohexane. Full circles denote coexisting polymer concentrations, the SEC curves show the polymer distributions in the coexisting phases (white area: PS160; black area: PS40).

Partitioning of additives

To investigate the separation of a low-molecular-weight component (additive) from a polymer by gas-induced liquid-liquid demixing the partitioning of a model substance (dioctyl phthalate DOP) on the two liquid phases was determined. Measurements were carried out for the system polystyrene (9.6wt%) /cyclohexane (75.75 wt%) /carbon dioxide (14wt%) /DOP (0.65 wt%) at a temperature of 170°C and a pressure of 100bar.

Fig. 5 shows the concentrations in the two phases and the SEC analysis of the solvent-free polymer (including DOP). The DOP contents in the polymer-rich phase was found to be significantly lower than in the solvent-rich phase.

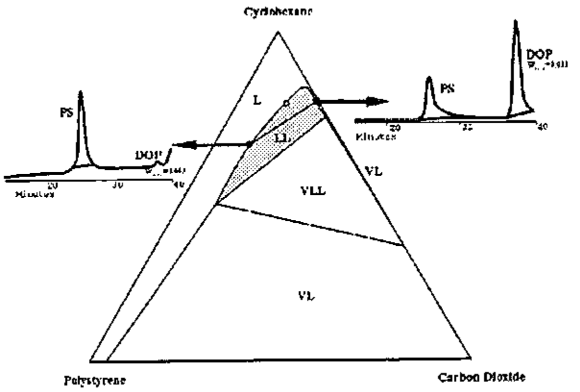

Fig. 5: Partitioning of DOP (dioctyl phthalate) in the polystyrene-cyclohexane-carbon dioxide system. Full circles denote the composition of the two liquid phases. SEC diagrams show the DOP contents in the solvent-free polymer.

Thus, the DOP contents in the solvent-free polymer could be decreased from 6.3 wt% in the feed to 2.2 wt% in the polymer-rich phase.

Conclusions

The influence of CO_2 on the phase equilibrium in polystyrene/ cyclohexane was investigated. With increasing gas contents the LCST curve was shifted to lower pressures and merged with the UCST curve at a CO_2 contents of about 21.3 wt%. The liquid-liquid phase separation induced by the addition of the gas results in an almost polymer-free solvent-rich phase and a polymer-rich phase. Depending on pressure and initial polymer concentration a separation of the polymer by chain length can be accomplished. Especially, it is possible to cut-off the short-chain end of the molecular-weight distribution. Using the same effect, low-molecular-weight components (additives) can be separated from the polymer.

Acknowledgements

This work was supported by the Deutsche Forschungsgemeinschaft under grant AR 236/2-2.

References

[1] B. Bungert, R. Tippl, G. Sadowski, W. Arlt High Pressure Chemical Engineering, von Rohr R., Trepp C. (editors) Elsevier 1996, 519-524
[2] de Loos Th. W., personal communication, 1994
[3] S. Saeki, N. Kuwahara, M. Nakata, M. Kaneko. Macromolecules 1973, 6, 246-250
[4] Y. Sato, M. Yurugi, S. Takishima, H. Masuoka Fluid Phase Equilib. 1996, 125, 129-138

Modeling of Two-phase Ethylene Polymerization in High Pressure Autoclaves

P. Pladis and C. Kiparissides*
Department of Chemical Engineering and Chemical Process Engineering Research Institute
Aristotle University of Thessaloniki, P.O. Box 472, 54006 Thessaloniki
cypress@alexandros.cperi.forth.gr, Fax: ++30 31 996198

The polymerization of ethylene in high pressure autoclaves is usually carried out in a single-phase. However, under certain pressure and temperature conditions, a two phase-system can be formed. In the present study, a comprehensive mathematical model is developed to describe the two-phase high pressure free-radical polymerization of ethylene in an autoclave. The thermodynamic phase behaviour of the ethylene-polyethylene mixture is calculated based on the Sako-Wu-Prausnitz equation of state. The effect of initiator and solvent partition coefficients on the polymer molecular properties is investigated and model predictions are compared with available experimental data. Although the present study is limited to a simple CSTR, the model can easily be extended to more complex reactor configurations by means of a generalized compartment approach.

Introduction

The high pressure free-radical ethylene polymerization is an industrial process of significant economic importance. Two reactor technologies, namely, tubular and autoclaves, are currently employed in the production of low density polyethylene (LDPE). High-pressure LDPE reactors typically operate at high temperatures (150 - 330 °C) and pressures (1200 - 3500 atm). Under these conditions, the reaction mixture behaves as a supercritical fluid.

An autoclave is a constantly mixed vessel made up of two or more reaction zones in series, separated by disks and stirred by a vertical stirrer shaft. Despite the large specific power input to the reacting system (20 - 100 kW/m^3) effected by high agitation rates, the zones are not considered perfectly mixed due to the very fast reaction kinetics. The polymerization of ethylene in autoclaves is practically carried out in an adiabatic way. Cooling of the reaction mixture is effected by the introduction of cold monomer at several side-feed points along the reactor. The reaction temperature in a zone is controlled by manipulating the corresponding initiator feed rate. It is important to point out that cautious reactor control is required because the reactor usually operates at an open-loop unstable steady-state.

The polymerization of ethylene in high pressure autoclaves is usually carried out in a single-phase. However, under certain reduced pressure and temperature conditions, a two phase system is formed. One phase, the polymer-rich phase, contains primarily polyethylene and the other, the monomer-rich, contains mainly ethylene. The presence of a viscous polymer-rich phase increases the probability of forming hot spots and can result in runaway reactions (e.g., ethylene and polyethylene decomposition reactions). Thus, the termination reaction in the polymer-rich phase can become diffusion-controlled leading to an increase of the ratio of propagation rate constant to the termination rate constant k_p/k_t (gel-effect). Nevertheless, in many cases, it is desirable to carry out the polymerization in the two-phase region. It has been reported that LDPE produced in a two-phase system exhibits better film properties because the polymer has a narrower MWD and a lower degree of long chain branching (LCB). However, in a two-phase system, the initiator consumption rate is in general higher than that in a single phase system. Phase separation in autoclave reactors is usually achieved by lowering the pressure of the reactor or by adding an inert gas such as N_2 to the reaction mixture which acts as an antisolvent.

To model the molecular and compositional developments in an LDPE autoclave, a comprehensive kinetic mechanism describing the free-radical polymerization of ethylene is considered. Dynamic mass, molecular species, macromolecular properties and energy balance equations are derived for each volume segment of the multizone autoclave reactor to simulate the transient reactor behaviour. The method of moments based on the statistical representation of the number chain length distribution is employed to reduce the infinite number of molecular species balances into a low-order system of moment differential equations.

The paper is organized as follows: In section 2 some computational aspects concerning the thermodynamic phase equilibrium of the ethylene-polyethylene mixture are presented. In section 3 the kinetic mechanism of the ethylene polymerization is described and the reaction rate functions are derived for a two-phase polymerization system. In section 4 the effect of initiator partition coefficient on model responses is investigated and a comparison of model predictions with available experimental data is carried out.

Thermodynamic Phase Equilibrium Calculations

The phase behaviour of LDPE-ethylene mixture is of great importance in any modeling study involving a two-phase system. The polymerization of ethylene in high pressure autoclaves is usually carried out in a single-phase. However, if the pressure and temperature are reduced, a two-phase system is formed.

In this work the Sako-Wu-Prausnitz equation of state [1] was employed to study the phase behaviour of the ethylene-polyethylene mixture.

$$P=\frac{RT(V-b+bc)}{V(V-b)}-\frac{a}{V(V+b)} \qquad (1)$$

where a, b and c are the parameters of the EOS. For c = 1 the SWP equation reduces to the Soave-Redlich-Kwong EOS. The third parameter c extends the applicability of the equation to system containing large molecules. It should be emphasized that SWP EOS is not a simple three-parameter EOS because the third parameter c has a strict physical meaning, since the product 3c denotes the total number of external degrees of freedom per molecule.

It has been shown both experimentally and theoretically that the phase behaviour of a polymer-solvent mixture depends on the polymer's MWD. In Figure 1, model predictions of the LDPE-Ethylene cloud point temperature are compared with experimental data of Luft and Lindler [2] at 130 °C for a polyethylene with M_v=11000. As can be seen, the model results are in good agreement with the experimental data. Figure 2 depicts the molecular weight distributions in the vapor and liquid phases as well as the overall polymer MWD for a two-phase system at 1500 bar. It is apparent that the MWD of LDPE in the vapor phase contains the lower molecular weight polymer fractions of the overall MWD.

In the presence of solvent(s) or other inert compounds the phase equilibrium behaviour of the multi-component mixture can be very complex. In such a case, one needs to know accurately the values of the various interaction parameters, calculated from phase equilibrium experimental data. Unfortunately this kind of information is not always available or/and cannot easily be obtained.

Kinetics of Ethylene Polymerization

At high pressures and temperatures, ethylene will undergo free-radical polymerization in the presence of an initiator (e.g., peroxide, oxygen, azo-compounds). A general kinetic mechanism describing the free-radical polymerization of ethylene in a high-pressure reactor includes initiation and propagation reactions, termination by both combination and disproportionation, molecular weight control by transfer to monomer and to CTA, long chain branching (LCB) formation by transfer to polymer, short chain branching (SCB) formation by intramolecular transfer and double bond formation by β-scission of tert- and sec- radicals.[3], [4], [5]:

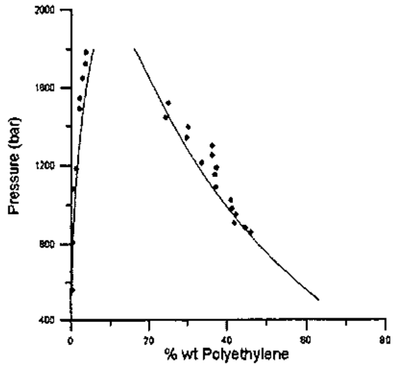

Figure 1: Model predictions and experimental measurements of cloud point pressures for the ethylene-LDPE system

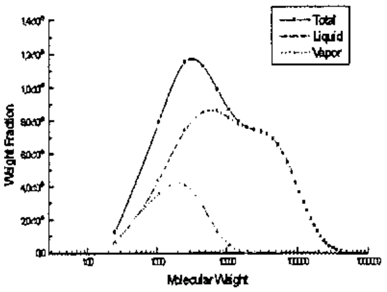

Figure 2: Model predictions of the liquid and vapour MWDs for the ethylene-LDPE system

Calculation of the rate functions for two-phase system

For the modeling of a two-phase ethylene polymerization reactor, the corresponding molar species rate functions in each phase have to be known. The total polymerization rate will be given by the sum of the respective polymerization rates in the two phases. To model the two-phase ethylene polymerization the following assumptions are made: (i) The two phases are in thermodynamic equilibrium; (ii) The total reaction volume will be given by the sum of the volumes of the two phases; (iii) The concentrations of monomer, initiator(s), solvent (and chain transfer agents) in the polymer phase can be expressed in terms of the respective partition coefficients and concentrations of the individual species in the monomer phase. The termination reaction becomes diffusion-controlled leading to an increase of the ratio (k_p/k_t).

To calculate the reaction rates of the various molar species in each phase it is necessary to know concentrations of respective species in each phase.

Using the SWP EOS one can calculate the weight fraction of polyethylene in each phase at a given temperature and pressure.

Let us assume that W_p, W_m and W_s denote the total mass of polymer, monomer and solvent, respectively in a two-phase polymerization mixture. The superscripts I and II denote the respective polymer and monomer phases. The polymer mass fractions φ_p^I and φ_p^{II} will be given by:

$$\varphi_p^I = \frac{W_p^I}{W_m^I + W_s^I + W_p^I} \quad ; \quad \varphi_p^{II} = \frac{W_p^{II}}{W_m^{II} + W_s^{II} + W_p^{II}} \quad (2)$$

Assuming that the values of W_p, W_m and W_s are known (e.g., from the solution of the model mass balances) and the values of φ_p^I and φ_p^{II} can be obtained from an EOS, the mass fractions of monomer and solvent in the two phases can be calculated:

$$W_m^I + W_s^I = \left(W_p - \left(\frac{\varphi_p^{II}}{1-\varphi_p^{II}} \right) (W_m + W_s) \right) \Big/ \left(\frac{\varphi_p^I}{1-\varphi_p^I} - \frac{\varphi_p^{II}}{1-\varphi_p^{II}} \right) \quad (3)$$

where

$$W_s^I = \frac{\varphi_p^I}{1-\varphi_p^I} * \left(W_s - \left(\frac{\varphi_s^{II}}{1-\varphi_s^{II}} \right) (W_m + W_p) \right) \Big/ \left(\frac{\varphi_s^I}{1-\varphi_s^I} - \frac{\varphi_s^{II}}{1-\varphi_s^{II}} \right) \quad (4)$$

$$\begin{aligned} &W_p + W_m + W_s = 1 \quad ; \quad W_p^I + W_p^{II} = W_p \\ &W_m^I + W_m^{II} = W_m \quad ; \quad W_s^I + W_s^{II} = W_s \end{aligned} \quad (5)$$

Accordingly, the volumes of the two phases will be given by the following equations:

$$\begin{aligned} &V^I = \frac{W_m^I}{\rho_m} + \frac{W_p^I}{\rho_p} + \frac{W_s^I}{\rho_s} \quad ; \\ &V^{II} = \frac{W_m^{II}}{\rho_m} + \frac{W_p^{II}}{\rho_p} + \frac{W_s^{II}}{\rho_s} \quad ; \quad V_t = V^I + V^{II} \end{aligned} \quad (6)$$

Finally, the initiator and solvent concentrations in the two phases can be expressed in terms of the respective partition coefficients:

$$K_I = [I]^I / [I]^{II} \quad ; \quad K_s = [S]^I / [S]^{II} \quad (7)$$

The total polymerization rate will be equal to the sum of the polymerization rates in the two phases.

[Total Rate of Polymerization] =

Polymerization Rate in Phase I] +

[Polymerization Rate in Phase II] =

$$r_p^I V^I + r_p^{II} V^{II} = k_p [M]^I [R^\bullet]^I V^I + k_p [M]^{II} [R^\bullet]^{II} V^{II} \quad (8)$$

The total moment rate functions of the "live" and "dead" polymer chain distributions as well as the rate functions of all other species are derived in a similar way.

Results and Discussion

In this section the effect of the initiator partition coefficient, K_I , on the polymer properties is investigated. It is assumed that the autoclave has a volume of 1 m^3 and operates at a pressure of 1300 bar and of temperature of 250 °C. For simplicity, the autoclave is represented by a single CSTR with a mean residence time of 30 sec. The weight fraction of the solvent (n-hexane) is assumed to be 7.5 % of the total feed stream. Furthermore, it is assumed that the solvent partition coefficient is equal to the partition coefficient of ethylene. The ethylene distribution in the two phases is calculated from the solution of the Sako-Wu-Prausnitz EOS.

In Figure 3 the total specific initiator consumption rate is plotted with respect to the initiator partition coefficient. As can be seen, the total initiator consumption rate decreases as K_I increases (e.g., the amount of initiator in the polymer phase increases). In Figure 4 the variation of the polymer polydispersity index is plotted with respect to the partition coefficient, K_I. As the initiator concentration in the polymer phase increases the polydispersity index increases. Finally, Figure 5 depicts the effect of the solvent partition coefficient on the weight average molecular weight. Notice that an increase of the solvent partition coefficient leads to a decrease of the weight average molecular weight, in agreement with the free-radical kinetics theory.

In Figures 6-8 model predictions are compared with reported experimental data [6] on the two-phase high pressure ethylene polymerization in an autoclave. The experimental reactor had a volume of 0.9 lt, and the ethylene feed rate was equal to 39 kg/hr. The experiments were carried out at a constant pressure of 1200 bar and two different temperatures (230 and 240 °C) in the presence of t-butyl-peroxybenzoate. No solvent was used. Phase separation was induced by the use of an inert gas (N_2).

In Figures 6-8, the effect of the % weight N_2 in the feed stream on the WAMW, polydispersity index and LCB content is shown for two different values of the initiator partition coefficient. The lines (e.g., continuous and broken) represent model predictions while the discrete points correspond to experimental measurements. Despite the large variability in the experimental measurements, the model predictions follow satisfactorily the experimental observations.

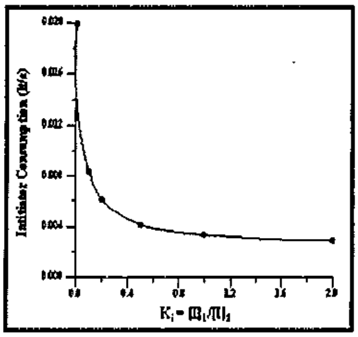

Figure 3: Effect of initiator partition coefficient on the specific initiator consumption

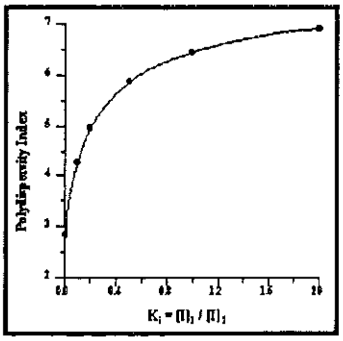

Figure 4: Effect of initiator partition coefficient on polydispersity index

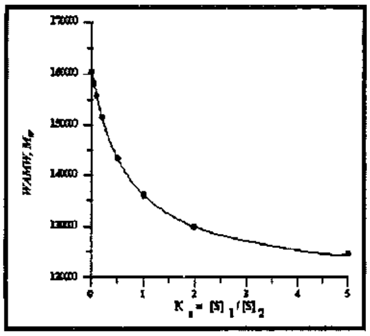

Figure 5: Effect of solvent partition coefficient on weight average molecular weight

Constantin and Machon [6] showed that phase separation occurs as soon as small amounts of nitrogen are added to the reaction mixture. Under these conditions (e.g., two-phase system), polymerization of ethylene does not lead, as one can expect, to the formation of high molecular weight polymer chains with increased long chain branching. It is likely that a decrease in ethylene concentration, due to the presence of nitrogen, results in an increase of the radical concentration in order to maintain a constant polymerization rate, which, in turn, causes a decrease of the average chain length. This is in agreement with the observed [6] increase in the specific initiator consumption rate (e.g., g of initiator/Kg of LDPE) with respect to the nitrogen concentration.

The present analysis represents a first attempt to simulate the two-phase ethylene free-radical polymerization. Current efforts are focused on the prediction of the MWDs in the two phases.

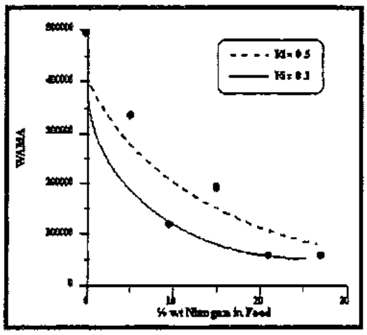

Figure 6: Effect of % wt nitrogen in the feed stream on weight average molecular weight

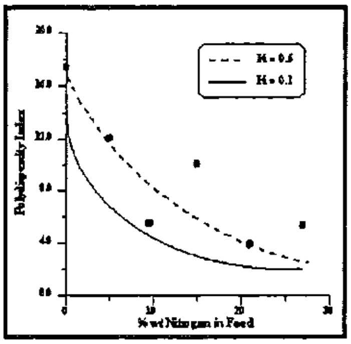

Figure 7: Effect of % wt nitrogen in the feed stream on polydispersity index

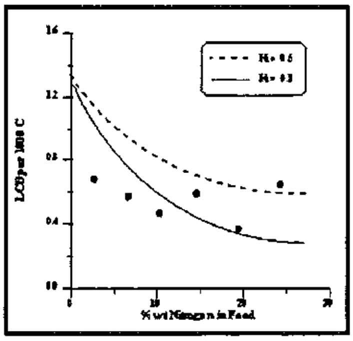

Figure 8: Effect of % wt nitrogen in the feed stream on long chain branching per 10^3 carbon atoms

Comparison of model predictions with experimental data obtained for a two-phase LDPE autoclave is in progress.

References

1. Sako T., Wu A.H. and Prausnitz J.M., *J. Appl. Polym. Sci.*, **38**, 1839 (1989)

2. Luft G. and Lindner A., *Die Angewadte Makromolekulare Chemie*, **56**, 99 (1976)

3. Goto S., Yamamoto K., Furui S. and Sugimoto M., *Journal of Applied Polymer Science: Applied Polymer Symposium*, **36**,21 (1981)

4. Kiparissides C.,Verros G.and McGregor J.F., *J.M.S-rev. Macromol. Chem. Phys.*, **C33**(4) 437 (1993)

5. Pladis, P., Kiparissides, C., *J. Appl. Polym. Sci.*, in press (1999).

6. Constantin D and Machon J.P., *European Polymer Journal*, **14**, 703 (1978).

Changing Properties of Glassy Polymers due to Diffusion of supercritical CO_2

J. v. Schnitzler, R. Eggers*
TU Hamburg-Harburg, Eißendorfer Str. 38
21073 Hamburg, Germany
phone: +49-40-42878 3191, fax: -42878 2859
e-mail: R.eggers@tu-harburg.de

Recently some promising applications have been developed, where mass transfer in the polymer phase, by support of a supercritical fluid, is of main importance. Some examples are: The dyeing of Polyester with supercritical CO_2, membrane separations of gas/fluid mixtures and the treatment of polymers with supercritical fluids to change their properties (generation of foams, extraction of impurities etc) [1]. In order to get a better understanding of the behavior of glassy polymers in a supercritical CO_2 atmosphere, sorption of CO_2 in Poly(Ethylene-Terephthalate) has been investigated. Some properties of PET, such as the glass transition temperature and the polymer density, are changing due to the sorption of CO_2. These properties were determined by measuring the equilibrium values of the sorption and swelling at temperatures from 40 to 120 °C and pressures up to 300 bar. The experimental method, used in this work, is based on gravimetrical measurements of the mass transport with a simultaneous optical investigation of the swelling behavior on a single polymer sample. Some kinetic data of the diffusion of CO_2 in the polymeric matrix were measured in order to determine diffusion coefficients. The diffusion coefficients were calculated by a classical diffusion model for cylindrical solids. Finally, the behavior of PET in supercritical CO_2 was compared to the behavior of an other glassy polymer (Polycarbonate).

Introduction

At atmospheric conditions (20 °C and 1 bar) PET belongs to the kind of polymers that are in a glassy state. It is usually hard, brittle and has a restricted polymer chain mobility [2]. Mass transfer in a glassy polymer is commonly described by the dual mode sorption model. There are two populations of sorbed molecules: 1) adsorbed in microvoids and 2) dissolved in the polymer matrix. This dual mobility of the sorbed molecules is typical of glassy polymers that are in a state below the glass transition temperature. At normal pressure the glass transition temperature (T_G) for PET varies between 70 and 110 °C, depending on state and history of the polymer sample [3]. History means especially the mechanical and thermal "pre-treatment". Additional to the history dependency, there is an influence of the pressure on T_G, due to the quantity of absorbed gas: T_G decreases with increasing pressure [4]-[6]. Above the glass transition temperature, glassy polymers change their properties similar to those of rubbery polymers [2]. PET in a supercritical CO_2 atmosphere at 100 to 120 °C and pressures around 300 bar is in a state well above the glass transition point. The rate of diffusion is much less than that of relaxation. In this case, mass transfer can be described by Fick's law of diffusion [2].

Above the glass transition temperature, there is a higher increase of the swelling with rising temperature, due to the higher chain mobility in the polymer [4]. Therefore the glass transition temperature is determined by the change of the slope in the swelling vs. temperature diagram. By measuring the swelling and sorption, the density of the polymer can be investigated. To evaluate the mass transfer mechanisms it is important to know if there is no over-all volume change on mixing, i.e. if the increase in volume of the polymer sample is equal to the volume of the fluid sorbed at vapour pressure existing in the experiment [7].

Experiments

An experimental method [8] to measure mass transfer in solid materials at elevated temperatures (40-120 °C) and elevated pressure (up to 350 bar) has been used to investigate the changing properties of polymer samples. It is a combination of a gravimetrical determination of mass transfer, from a supercritical fluid phase to a solid phase, within a high pressure autoclave and a simultaneous optical control. As shown in Figure 1 the apparatus consists of a high pressure version of a magnetic coupled balance, MSW (Rubotherm, Germany), connected to two view cells (Sitec, Switzerland). The first view cell, directly mounted under the magnetic coupled balance, enables the determination of the change in volume of the solid sample, via a CCD camera, and with the second view cell the concentration of the solute in CO_2, can be monitored via a VIS - photometer. The high pressure part of the apparatus can be thermostated by a heating system to a constant temperature within ±1K.

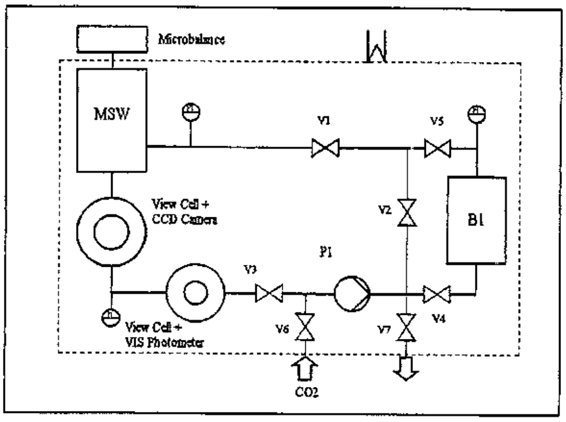

Figure 1: Flow sheet of the sorption apparatus

A combination of sorption and swelling measurements has been used to investigate the change of the polymer density. By placing a cylindrical polymer sample into the view cell, still connected to the MSW, the swelling could be measured via a video camera: The two-dimensional projection area of the rotationally symmetric sample has been recorded, from which the volume is calculated. Simultaneously, the change in weight of the polymer sample has been recorded. For all the swelling and mass transfer experiments of PET in this work, we used monofibers of about 1,3 mm in diameter.

Results and Discussion

Swelling of the Polymer

In order to examine the swelling behavior of the polymer in a supercritical CO_2 atmosphere, the thermal expansion of the material, the mechanical compression under pressure and the swelling through sorption need to be distinguished. Therefore the change in volume at atmospheric pressure and elevated temperatures was investigated first. The mechanical compression under pressure is comparatively small, so it was considered to be negligible. Finally the swelling by sorption could be distinguished from the other effects. Experiments were performed at 100 and 300 bar and different temperatures. For these experiments, the polymer samples have been preheated to eliminate the thermal expansion at atmospheric pressure. Figure 2 shows the measured volume changes for PET at both conditions for temperatures from 40 to 120 °C. It can be recognized, that the increase of the volume, due to mass transfer, at 300 bar is higher than that at atmospheric pressure. The increase of the slope indicates the glass transition temperature T_G, above which the swelling increases significantly. At atmospheric pressure this change of the slope can be determined at around 90 °C. At 300 bar, it can be recognized that the glass transition temperature (T_G) decreases to around 70 °C.

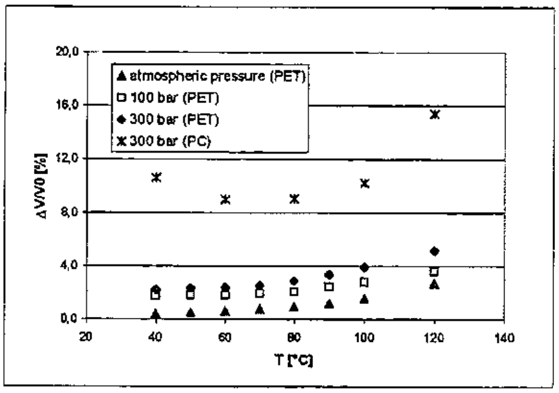

Figure 2: Swelling behavior of PET and PC in CO_2 at different conditions.

The swelling of PET in a high pressure CO_2 atmosphere is compared to an other glassy polymer: Polycarbonate (PC), shown in Figure 2. The swelling of PC reaches more than three times the values of PET over the range of 40 to 120 °C. At lower temperatures (40 to 60 °C), the swelling is decreasing with increasing temperature, due to the decreasing CO_2-density, which results in a decrease of sorbed CO_2. Whereas at higher temperatures (70 to 120 °C) the swelling is increasing with increasing temperature. In this temperature range, the positive temperature influence becomes dominant compared to the density influence. This results in a higher sorption and swelling behavior of the polymer. The glass transition temperature for PC at 300 bar is determined to be around 70 °C. It has been observed, that the swelling of both polymers is not totally reversible: After depressurisation the volumes of the samples do not totally return to their original state. This effect is also observed in the literature [2]. It seems, that the exposure of these materials to penetrants (such as CO_2) can induce permanent structural changes similar to those of mechanical and thermal treatment.

Sorption of supercritical CO_2

The sorption of supercritical CO_2 in PET was measured at temperatures from 80 to 120 °C and pressures from 50 to 350 bar.

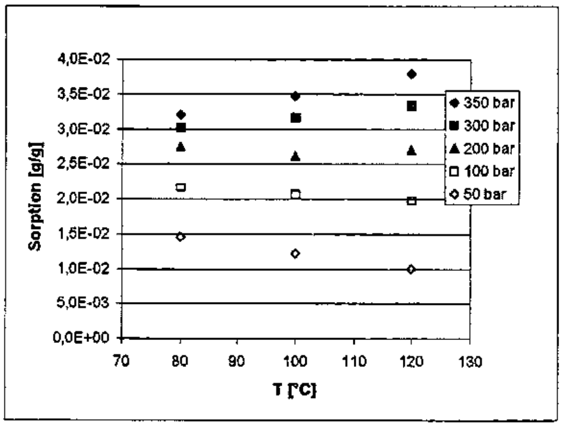

Figure 3: Sorption of CO_2 in PET

Results are shown in Figure 3. It can be recognized, that at lower pressures up to 200 bar, the sorption decreases with increasing temperature, whereas at pressures above 200 bar the sorption increases with increasing temperature.

Polymer density

The polymer density, calculated from sorption and swelling experiments, decreases with increasing pressure due to the increasing sorption of CO_2 (Figure 4). The calculated partial density (ρ_{p,CO_2}) of the sorbed CO_2 in the polymer phase is higher compared to the ambient density of the fluid (ρ_{CO_2}) at pressure existing in the experiment.

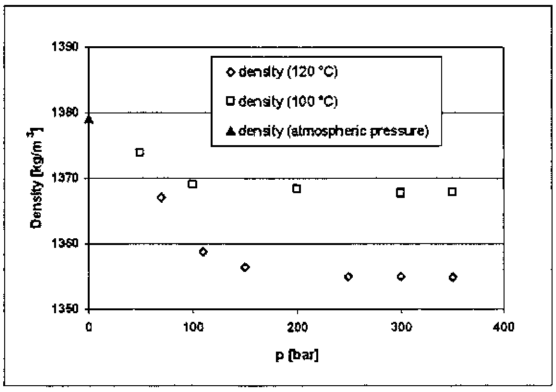

Figure 4: Change of the polymer density with pressure

Table 1 shows a selection of calculated partial densities compared to the ambient density of the supercritical fluid.

P [bar] / T [°C]	ρ_{CO_2} [kg/m³]	ρ_{p,CO_2} [kg/m³]
300 / 120	586,0	885,9
300 / 100	662,1	1102,2
100 / 120	166,9	757,3
100 / 100	188,1	1020,1

Table 1: Calculated partial density of sorbed fluid compared to ambient density of the fluid (CO_2)

Diffusion coefficients

In order to study the sorption behavior of CO_2 in the PET fiber, several experiments at different times have been performed. From the sorption data the diffusion coefficients have been calculated by a classical diffusion model for cylindrical solids, as described by Crank [7]. The diffusion coefficient has been determined as constant, at a single temperature and pressure combination, for all investigated times. The diffusion coefficients for 100 and 120 °C and various pressures, show a range from $3{,}5\times10^{-12}$ to $7{,}0\times10^{-11}$ [m²/s] (Figure 5). They increase with increasing temperature and pressure.

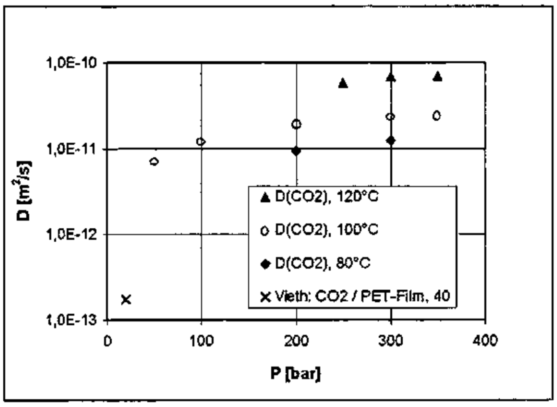

Figure 5: Diffusion coefficient of CO_2 in PET compared to literature [2]

Summary

The current paper shows some basic investigations on the behavior of glassy polymers in a supercritical CO_2 atmosphere. The results lead to a basis to various processes that are concerned in the treatment of polymers with supercritical fluids, e.g. the dyeing of polyester.

References:

[1] Krukonis, V., "Processing of Polymers with Supercritical Fluids", Polymer News, vol. 11 (1985) 7.

[2] Vieth, W. R.; "Diffusion in and through polymers: Principles and applications"; Hanser, Munich, 1991.

[3] Heffelfinger, C. J.; Schmidt, P. G.; "Structure and Properties of Oriented Poly (ethylene Terephthalate) Films", J. of Applied Polymer Science, 9 (1965) 2661.

[4] Wissinger, R. G.; Paulaitis, M. E.; "Swelling and Sorption in Polymer- CO_2 Mixtures at Elevated Pressures", J. Polym. Sci. B: Polymer Physics, 25 (1987) 2497.

[5] Shim, J. J.; Chang, S. H.; Park, S. C.; Lee, H., "Phase Equilibria of Supercritical Fluid-Polymer Systems", Proceedings of the 4th International Symposium on Supercritical Fluids, Japan, vol. B, 1997, p. 463.

[6] Lockemann, C. H.; Riede, Th.; Magin, P., "An Experimental Method to Determine the Sorption and Swelling Behavior of Solids at High Pressures", in: Ph. R. von Rohr, Ch. Trepp (Eds.), Proceedings of the 3rd International Symposium on High Pressure Chemical Engineering, 1996, p. 547.

[7] Crank, J., "The Mathematics of Diffusion", 2nd Edition, Oxford University Press, Oxford, 1975.

[8] von Schnitzler, J.; Eggers, R.; "Mass Transfer Phenomena in Polymers During Treatment in a Supercritical CO_2 - Atmosphere", Proceedings of the 5th Meeting on Supercritical Fluids, Nice (1998), p. 93.

GVC-Fachausschuß „High Pressure Chemical Engineering“, March 3-5, Karlsruhe, Germany, 1999

Investigation of the sorption and swelling behavior of Polymer/CO_2 systems by combined oscillometric-gravimetric measurements

H. Rave*, R. Staudt, J.U. Keller
Institute of Fluid- and Thermodynamics, University of Siegen, 57068 Siegen, Germany
Tel.: ++49-(0)271-740-4654, Fax: +49 (0)271 740 2360
email: rave@ift.maschinenbau.uni-siegen.de

Sorption phenomena of swelling sorbents like polymers cannot be measured adequately by either gravimetric or volumetric methods, since the volume needed for buoyancy correction or dead space determination, respectively, depends not only on pressure and temperature of the sorptive gas but also on the amount of gas absorbed.

The oscillometric method proposed here allows to determine the inertia of mass by measuring the oscillating motion of a disk filled with the sorbent. By combining this method with gravimetric or volumetric measurements it is possible to determine simultaneously the change in volume of the disk's filling and the amount of gas absorbed in the sorbent. The sample can be either pulverous, pelletlike or of dense cylindrical shape.

Combined oscillometric-gravimetric measurements have been carried out for the system polycarbonate/CO_2 in the pressure range $0 < p < 6$ MPa at $T = 293$ K. Sample data for the change in volume and the amount absorbed determined from these measurements are presented and discussed to a certain extend.

Introduction

The classical methods to measure sorption phenomena in swelling sorbents like polymers, i.e. gravimetric or volumetric measurements, require an information about the pressure, temperature and load dependent volume of the polymer sample for buoyancy correction or dead space determination.

The change in volume of a polymer due to sorption of gas is usually determined by measuring the change in length of a thin polymer film [1], thus allowing only to determine 1-dimensional changes of the polymer and requiring to manufacture a polymer film. An optical method developed recently allows on principle to determine changes in the cross-sectional area of a polymer drop [2], requiring a liquid like state of the polymer. However, changes of the 3-dimensional drop volume itself cannot be measured in this way.

In this paper a new oscillometric method is proposed to measure the inertia of mass by observing the oscillating motion of a disk filled with the sorbent. The use of a rotational pendulum leads to an additional information about the (3-dimensional) volume of the disk's filling. Combining this method with either gravimetric or volumetric measurements allows to determine the amount absorbed and the volume of the polymer sample simultaneously. Sample data for the sorption and swelling behavior of the system polycarbonate/CO_2 are presented.

Theory

The rotational pendulum basically consists of an oscillating disk suspended on a thin wire within a pressure vessel. A sketch of the setup is shown in Fig. 1. The disk's outer ring can be filled with a polymer sample of mass m^P and specific bulk volume V^*. The sample can be of either pulverous, pelletlike or dense cylindrical shape. A stem is attached to the disk for stabilization and a mirror to reflect a laser beam to detect pendulum's motion.

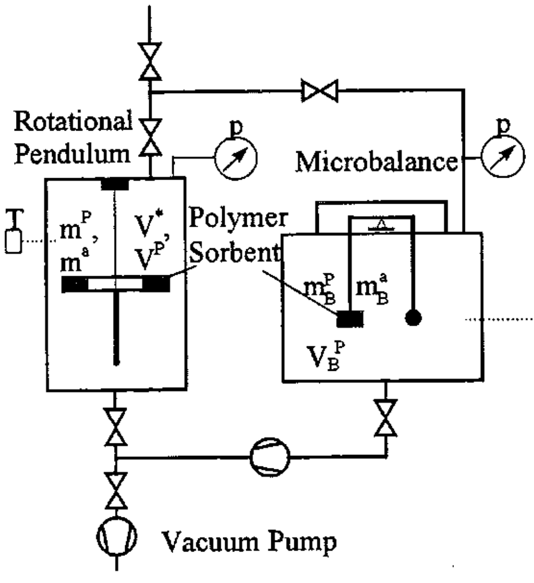

Figure 1: Experimental setup for oscillometric-gravimetric measurements.

Observing the pendulum's oscillating motion in vacuum and atmosphere, i.e. determining the angular frequency ω and the logarithmic decrement Δ of each damped harmonic oscillation, the moment of inertia of the disk can be calculated.

Taking into account the fluid mechanical relations holding for the flow induced by the disk's motion, the following relation between the parameters for each measurement can be derived [3, 4]:

$$\Omega_{osc} = \frac{\frac{1+\Delta_0^2}{1+\Delta_E^2}\left(\frac{\omega_0}{\omega_E}\right)^2 - 1}{1-\frac{\Delta_0\omega_0}{\Delta_L\omega_L}}. \qquad (1)$$

Here Δ_L and ω_L indicate the parameters of the empty disk in vacuum. Δ_0, ω_0 correspond to the loaded disk in vacuum and Δ_E, ω_E to the loaded disk under atmosphere. Ω_{osc} is defined by the ratio

$$\Omega_{osc} = \frac{m_{osc}}{m^P}, \qquad (2)$$

where m_{osc} is an effective mass accelerated in addition to the sample mass m^P and the mass of the empty disk m_L.

This effective accelerated mass consists of the total mass absorbed m, the mass of fluid not absorbed within the disk's filling m^f and an effective mass Δm^f corresponding to the moment of inertia of the boundary layer of fluid's flow around the disk. Relating these quantities to the mass of polymer sample one gets the working equation of the rotational pendulum [3, 4]:

$$\Omega_{osc} = m + \rho^f\left(V^* - V\right) + \rho^f \Delta V, \qquad (3)$$

where V^* is the specific bulk volume of the disk's filling, V is the volume of the dense polymer particle and ΔV an effective volume of the fluid flow's boundary layer which serves as a calibration function for the pendulum.

Gravimetric or volumetric measurements deliver the working equation:

$$\Omega_{grav} = m - V\rho^f \qquad (4)$$

Combining Eqns. (3) and (4) one can determine the bulk volume of the disk's filling, provided that the calibration function ΔV of the pendulum is known from measurements with inert materials, e.g. glass beads [5]:

$$V^* = \frac{1}{\rho^f}\left(\Omega_{osc} - \Omega_{grav}\right) - \Delta V \qquad (5)$$

Assuming the ratio $b = V/V^* = V_0/V^*_0$, determined from the values V_0 and V^*_0, respectively, in a reference state (i.e. vacuum or standard atmosphere), to be constant, one can determine the specific volume of the loaded sorbent:

$$V(p,T,m) = b \cdot V^*(p,T,m)\cdot \qquad (6)$$

With this result the mass absorbed m can be calculated from either oscillometric or gravimetric measurements through Eqns. (3) or (4), respectively. For gravimetric data one gets:

$$m = \Omega_{grav} + \rho^f V(p,T,m)\cdot \qquad (7)$$

Now, one has determined a complete data set (p,T,V,m), i.e. a single point of the thermal Equation of State of the loaded sorbent.

Apparatus and Materials

A schematic diagram of the experimental installation for simultaneous oscillometric-gravimetric measurements is given in Fig. 1. It consists of a microbalance (type 4104 S, Sartorius, Göttingen, Germany) and a rotational pendulum developed in our laboratory [3]. These elements are connected by proper tubing and complemented by auxiliary equipment like gas circulator, vacuum pump, thermostat, thermocouples, manometers, valves etc..

The rotational pendulum consists of the oscillating disk system and a surrounding pressure vessel withstanding pressures up to 10 MPa. Both parts of the installation are thermostated by means of a water bath allowing a temperature range of 293K<T<353K [5].

Determination of angular frequency (ω) and logarithmic decrement (Δ) of pendulum's motion is based on an optical system. A laser beam is reflected by the mirror attached to the stem of the oscillating system. Thus, pendulum's motion is imaged in a plane where the times (t_i) of the reflected laser beam passing through two photodetectors are recorded. The motion's parameters are then determined by fitting the parameters of a damped harmonic oscillation to the measured times (t_i). Details of this procedure, which is also well known from oscillating disk viscometers, are described elsewhere [3, 5].

Temperatures within pendulum's pressure vessel were measured with a platinum resistance thermometer with an uncertainty of ±0.1 K. Pressures were measured with a strain gauge (pressure range < 6.9 MPa) obtained from burster präzisionsmesstechnik (Gernsbach, Germany) with a relative uncertainty of ±0.1%.

Polycarbonate pellets of approx. 3 mm in diameter where obtained from the department of chemical engineering of the Technical University of Berlin, Germany (Prof. Arlt).

Carbon dioxide (purity 99.995%) was obtained from Messer Griesheim (Krefeld, Germany).

Experimental

Simultaneous oscillometric-gravimetric measurements were carried out for the system polycarbonate / CO_2 at 293 K in the pressure range $0 < p < 6$ MPa. The pendulum's disk was filled with 97.5 g of polycarbonate sample. The mass of sample in the microbalance was 2.67 g.

After evacuating the system to $p < 0.1$ Pa for 48 h, CO_2 was added to the apparatus in steps of approx. 1 MPa. Since, after increasing the pressure, even after 4 days no equilibrium was reached, every data point was taken after a time period of 48 h.

Results

In Fig. 2 the swelling isotherm of the system polycarbonate/CO_2 at 293 K calculated from eq. (6) is shown. While the oscillometric signal Ω_{osc} rises steadily, the gravimetric result Ω_{grav} is strongly curved and even becomes negative at higher pressures.

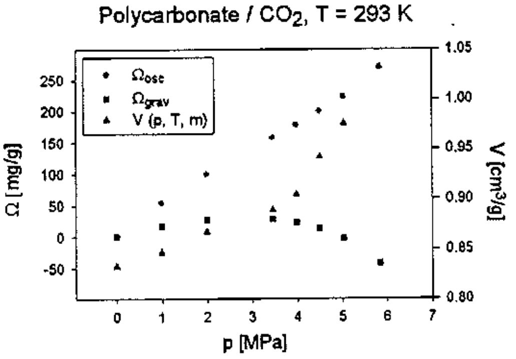

Figure 2: Swelling isotherm of polycarbonate/CO_2 at 293 K.

The swelling isotherm shows two linear branches. At lower pressures up to 3.5 MPa the volume (V) shows a slight increase with load. At higher pressures ($p > 4$ MPa) a larger slope of the swelling isotherm is observed, indicating a glass transition at this pressure. However, in interpreting the data in Fig. 2, it should be taken into account that they do not refer to equilibria states in strict sense but to quasi equilibrium attained after 48 h.

Fig. 3 shows the sorption isotherm of the system polycarbonate/CO_2 at 293 K calculated from eq. (7).

Additional measurements for different systems are underway in our laboratory and will be reported in due time.

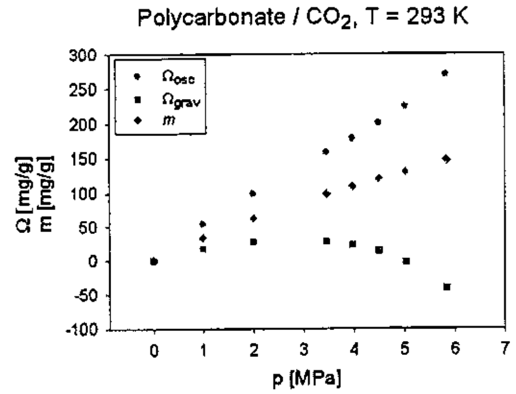

Figure 3: Sorption isotherm of polycarbonate/CO_2 at 293 K.

References

[1] Wissinger, R.G.; Paulaitis, M.E.; J. Polym. Sci., Part B: Polymer Physics, **1987**, 25, p. 2497-2510.

[2] Lockemann, C.A.: Experimentelle Methode zur Bestimmung des Sorptions- und des Quellverhaltens von Polymeren. presented at Arbeitssitzung GVC Fachausschuß „Hochdruck-Verfahrenstechnik", Garching, **1998**.

[3] Rave, H.; Keller, J.U.: Messung von Adsorptionsgleichgewichten reiner Gase mit Hilfe langsamer Schwingungen eines Rotationspendels. Arbeitsbericht zum Forschungsvorhaben DFG Ke334/18-1. Inst. Fluid- and Thermodynamics, University of Siegen, **1998**.

[4] Rave, H.; Staudt, R.; Keller, J.U.; Measurement of Gas Absorption in a Swelling Polymeric Material by a Combined Gravimetric - Dynamic Method. To be published, **1999**.

[5] Rave, H.; Dissertation, Inst. Fluid and Thermodynamics, University of Siegen, Germany, in preparation **1999**.

Light Scattering Investigations of Polydimethylsiloxane in sc-CO_2

T. Berger and W. Steffen*
Max-Planck-Institut für Polymerforschung, Ackermannweg 10, 55128 Mainz, Germany
email: berger@mpip-mainz.mpg.de, FAX: 0-(049)-6131-379-100

An optical high-pressure-cell was constructed for the investigation of the angular dependence of scattered light at different temperatures and pressures. With this set-up it is possible to either analyze the scattered light by photon correlation spectroscopy and obtain dynamic properties like hydrodynamic radii, or by the angular dependence of the total intensity to study static properties e.g. radii of gyration. Some preliminary results of polydimethylsiloxane dissolved in supercritical carbondioxide are presented.

Introduction

Supercritical Fluids (scf's) are of increasing importance in science and technology caused by the fact that their physical properties can be adjusted by variation of pressure and temperature. Supercritical carbondioxide (sc-CO_2) is on the one hand of special interest because of its environmentally and biologically benign nature[1,2] on the other hand because of the moderate critical parameters of T_c=31.1°C and p_c=73.8 bar.

Sc-CO_2 is due to its non-existing permanent dipole moment and the very low polarizability a very poor solvent. Based on this most of the polymers are insoluble except of some fluorinated polymers and polydimethylsiloxane (PDMS)[3]. About thermodynamic quantities of polymers in sc-CO_2 is not much known[4].

By light scattering techniques it is possible to investigate the hydrodynamic and thermodynamic properties of binary systems in dependence of composition, pressure and temperature[5,6]. Thus the application of light scattering techniques to these supercritical solutions are very desirable.

Theory and Data treatment

Static light scattering (SLS) is a fundamental method to determine the molecular weight, radius of gyration and the second osmotic virial coefficent of the solvent. By this technique the total intensity of the scattered light is measured in dependence of the scattering vector q and the concentration of the polymer.

In photon correlation spectroscopy (PCS) the time dependence of the scattered light is investigated by computing the intensity autocorrelation function $g^{(2)}(t)$[5]. From this the field autocorrelation function $g^{(1)}(t)$ has to be calculated by the *Siegert-relation*:

$$g^{(1)}(t) = \sqrt{\frac{g^{(2)}(t) - 1}{f}} \qquad (1)$$

where f is a factor which is due to the coherence of the scattered light. The autocorrelation function of a monodisperse sample in solution results in a simple exponential decay in our time-window.

$$g^{(1)}(t) = \exp\left\{\frac{t}{\tau}\right\} \qquad (2)$$

In many cases polymer samples show a distribution in their molecular weight. Such polydisperse samples can be described by a *Kohlrausch-Williams-Watts-function:*

$$g^{(1)}(t) = \exp\left\{-\left(\frac{t}{\tau}\right)^{\beta_{KWW}}\right\} \qquad (3)$$

The ensemble averaged value of the time $\langle\tau\rangle$ is given by:

$$\langle\tau\rangle = \frac{1}{\beta_{KWW}}\Gamma\left(\frac{1}{\beta_{KWW}}\right)\tau \qquad (4)$$

The correlation time $\langle\tau\rangle$ corresponds to the diffusion coefficient D by:

$$D = \frac{1}{\langle\tau\rangle q^2} \qquad (5)$$

where

$$q = \frac{4\pi\, n}{\lambda}\sin(\vartheta / 2) \qquad (6)$$

the scattering vector is with ϑ the angle between the incident and the scattered beam, λ the wavelength and n the refractive index of the solution. The hydrodynamic radius r_H is given by the *Einstein-Stokes relation:*

$$r_H = \frac{kT}{6\pi\eta D} \qquad (7)$$

with k the *Boltzmann-constant*, T the absolute temperature and η the viscosity.

Materials

PDMS has been synthesized by anionic polymerization and characterized by GPC. The number averaged molecular weight M_n is 113 kg/mol with a dispersity index of 1.21. This sample has been coded PDMS113. CO_2 (Linde, Germany) grade 4.5) was used without further purification.

Experimental

The complete set-up is illustrated in Fig. 1.

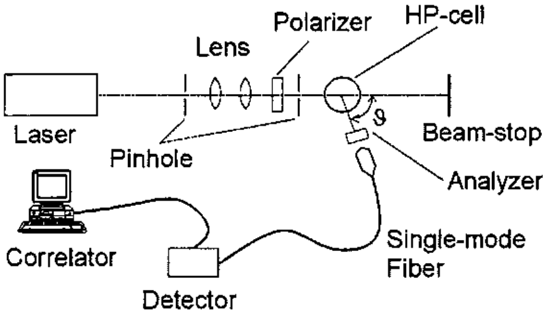

Fig. 1: Sketch of the complete light scattering set-up.

A frequency doubled Nd:YAG-Laser (Adlas, Germany) was used at a wavelength of 532 nm. The beam is collimated by two lenses and finally polarized. The scattered light is focused in an optical fiber and detected by a single photon detector (SO-SIPD, ALV, Langen, Germany) and analyzed by a correlator (ALV 5000/e, ALV, Langen, Germany). The polarization of the scattered light is due to different properties of the dissolved molecules. For the here introduced measurement both polarizers have been parallel, vertically to the table plane (VV-geometry) to investigate the translational diffusion.

The optical fiber with ist focusing lens is mounted on a goniometer stage to collect light at different angles ϑ.

High pressure light scattering cell

Our high pressure light scattering set-up is equipped with special features which are optimized for investigations of polymers in sc-CO_2. A vertical cross section of our cell is shown in Fig. 2.

The range of ϑ is given by the channels through the steel body from 0° to 180°. The window is cylindrical quartz. Fused quartz shows no anisotropic features like birefringence or pressure-induced birefringence. The maximum temperature is 120°C and maximum pressure in the experiment is 50 MPa where the steel body is constructed for 100 MPa. The temperature is controlled by a home-made controller which keeps the temperature constant within ±0,2 K.

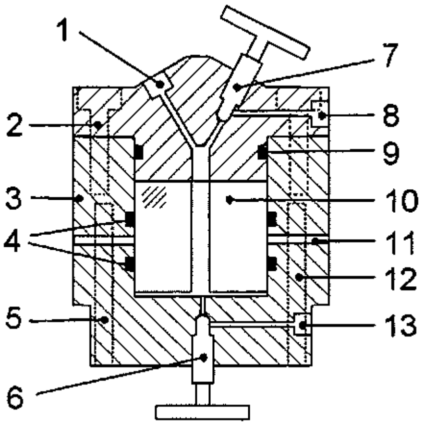

Fig. 2: Vertical cross section of the High-pressure cell. 1, 8, 13= G¼-connector, 2= M10 screw, 3=1.4701 steel-body, 4, 9=O-ring, 5, 12=heater, 6=inlet valve, 7=outlet valve, 10=cylindrical window, 11=channel for scattered light

Liquid CO_2 is pressurized by a programmable HPLC-pump(Jasco, 880-HP, USA). The solution inside is stirred by a magnetic stick stirrer from outside.

Results and Discussion

Fig.1 shows the PCS measurements of PDMS 113 in sc-CO_2.

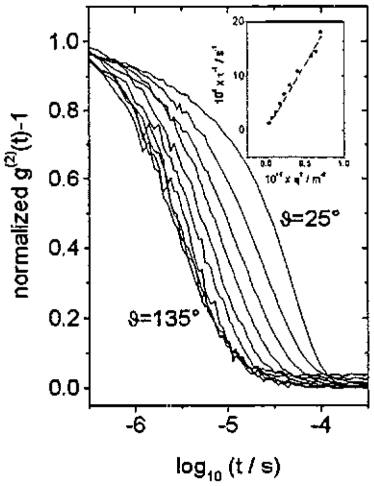

Fig. 1: Angular dependence of the correlation function of PDMS 113 in sc-CO_2 measured at 40,3 MPa and 316,15 K. The inset shows $1/\langle\tau\rangle$ vs. q^2.

The calculated radii and diffusion coefficents are summarized in Tab. 1.

Tab. 1: Summary of the PCS-data and evaluated quantities of PDMS113 in sc-CO_2 at 40.3 MPa and 316.15 K

Angel ϑ / °	Correlation time $\langle\tau\rangle$ / s	Diffusion coefficient D / m^2s^{-1}	Radius r_H / nm
25	$8,46 \times 10^{-5}$	$3,03\times 10^{-10}$	7,0
35	$5,42 \times 10^{-5}$	$2,44 \times 10^{-10}$	8,7
45	$3,41 \times 10^{-5}$	$2,39 \times 10^{-10}$	8,9
55	$2,24 \times 10^{-5}$	$2,51 \times 10^{-10}$	8,5
65	$1,61 \times 10^{-6}$	$2,59 \times 10^{-10}$	8,2
75	$1,30 \times 10^{-6}$	$2,50 \times 10^{-10}$	8,5
90	$1,00 \times 10^{-6}$	$2,39 \times 10^{-10}$	8,9
115	$7,94 \times 10^{-6}$	$2,12 \times 10^{-10}$	10,0
125	$7,76 \times 10^{-6}$	$1,97 \times 10^{-10}$	10,1
135	$7,01 \times 10^{-6}$	$2,00 \times 10^{-10}$	10,6

Haug et al. [7] as well as Mark [8] have published the following relation of the molecular weight dependency of the radius of gyration $r_{\Theta,g}$ in the Θ-state:

$$r_{\Theta,g} \,/\, \mathrm{nm} = 0{,}027 \cdot \sqrt{M_w \,/\, \mathrm{gmol}^{-1}} \qquad (8)$$

which results for PDMS113 in $r_{\Theta,g} = 9.1$ nm.

The found hydrodynamic radius r_H for the PDMS113 is in good agreement with the calculated $r_{\Theta,g}$ for Θ-conditions, but a bit smaller. This can be interpreted by a solvent effect. A smaller radius is obtained by a bad solvent with a negative second osmotic virial coefficient. This would indicate that under these conditions sc-CO_2 is not a good solvent for PDMS. The same result was found in a neutron scattering experiment by Melnichenko et al.[9].

Conclusions

The constructed cell and our set-up is suitable to investigate polymers in sc-CO_2. From the angle dependency of the carried out PCS measurements we obtained the diffusion coefficient and the hydrodynamic radius of PDMS in sc-CO_2. These values are a bit smaller but in good agreement to data from literature which have been obtain in conventional solvents in the Θ-state. This would indicate that sc-CO_2 under this conditions is still a bad solvent for PDMS.

On the other hand SLS investigations have to be carried out as well to get the radius of gyration and the thermodynamic properties like the pressure and temperature dependency of the second osmotic virial coefficient of sc-CO_2 to PDMS which is sensitive quantity of the solvent quality.

References

1. J. Kaiser, *Science* , **1996**, 274, 2013
2. H. Black, *Environ. Sci. Technol.*, **1996**, 30, 125A
3. E. Buhler, A.V. Dobrynin, J.M. DeSimone, M.Rubinstein, *Macromol.*, **1998**, 31, 7347
4. F. Rindfleisch, T.P. DiNoia, M.A. McHugh, *J. Phys. Chem.*, **1996**, 100, 15581
5. B.J. Berne, R. Pecora,''Dynamic Light Scattering'', Wiley, New York, 1976
6. M.D. Lechner, *Ber. Bunsenges. Physik. Chem.*, **1977**, 81, 992
7. A. Haug, G. Meyerhoff, *Makromol. Chem.*, **1962**, 53, 91
8. J.E, Mark,''Physical Properties of Polymers Handbook'', AIP Press, Woodbury, New York, 1996
9. Y. Melnichenko, E. Kiran, G.D. Wignall, H.D. Heath, S.Salaniwal, H.D. Cochran, M. Stamm, *submitted to Science*

DRÄGER TESCOM DT

Präzision -wir haben die Lösung!

Durch die RS-485 Schnittstelle kann mittels PC oder Userinterfaces auf die Regler zugegriffen werden.

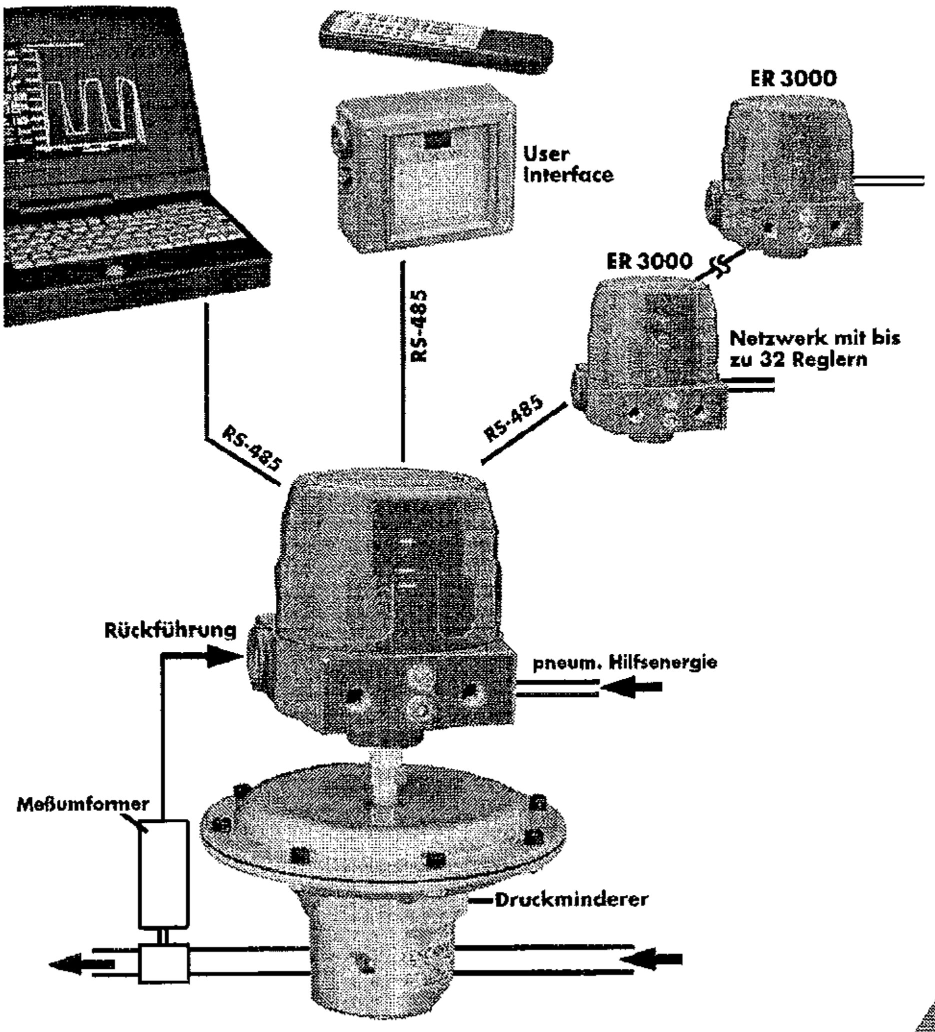
ER 3000
User Interface
ER 3000
RS-485
Netzwerk mit bis zu 32 Reglern
RS-485
RS-485
Rückführung
pneum. Hilfsenergie
Meßumformer
Druckminderer

ER 3000

Elektronischer Druckregler

- Drücke bis 1400 bar
- Durchflüsse bis Cv = 45
- Temperaturen bis 200°C
- verschiedene Dichtungsmaterialien

- verschiedene Sitz-Werkstoffe
- Sonderlegierungen
- Keramik-Ventileinsätze
- kundenspezifische Lösungen sind "standard" bei uns

Fernbedienbar

Automatisierbar

Höchste Präzision

Materials

High Pressure Surface Plasmon- and Optical Waveguide Spectroscopy
(Pressure Dependence of Thickness and Refractive Index of Thin PMMA-Films)

W. Knoll* a), G. Kleideiter a) b), and M.D. Lechner b)
a) Max Planck Institut für Polymerforschung, Ackemannweg 10,D-55021 Mainz
b) Institut für Chemie, Universität Osnabrück, Barbarastr. 7, D-49069 Osnabrück
knoll@mpip-mainz.mpg.de 06136-379360

Total internal reflection (TIR) and attenuated total reflection (ATR) measurements in the Kretschmann configuration have been performed at 25 °C with PMMA-film (of ca. 2.5 μm thickness) spincoated on top of a 50 nm thick gold layer, as a function of applied hydrostatic pressure, ranging from $p = 1 \cdot 10^5$ to $1050 \cdot 10^5$ Pa. The analysis of guided optical modes allows for the separate determination of the refractive index n and the thickness d of polymer films as a function of pressure. The pressure media in contact with the PMMA-films were water, ethanol and methanol. Thermodynamic theories for the density of solids and fluids in combination with the Lorentz-Lorenz-equation for their optical properties fit the experimental data quite well.

Introduction

Surface plasmon spectroscopy (SPS) or waveguide spectroscopy are optical methods to analyse thin [1),2)] and thick [2),3)] polymer films. The variation of temperature is standard to investigate e.g. the glass transition temperature T_G of ultrathin layers [4)].
Pressure technique are not combined with SPS so far. To our knowledge, the used set-up is the first one, that offers the possibility to study the thickness d and the refractive index n of polymer films at different pressures and temperatures. Additionally, we can measure the refractive index of any liquid (pressure medium) at pressures up to $1050 \cdot 10^5$ Pa.

Experimental

A thin (gold) metal layer is evaporated onto sapphire slide. Plasmon surface polaritons (or surface plasmons for short) are resonantly excited by the p-polarized light of a laser coupled via a prism in our set-up at an angle of incidence which corresponds to the energy- and momentum-matching conditions between the photon and the surface plasmon.[5,6,7)] The coupling prism was positioned on top of the sapphire window in the cylindrical high pressure cell (Fig. 1). As window material two sapphire are used. The optical axis is chosen in such a way as to avoid birefringence effects under applied pressure. Gold wire rings are used as sealing between the steel cell and the sapphire windows.
The sapphire prism (with the same orientation of its optical axis as that of the windows) was index-matched to the thin sapphire windows using a suitable index fluid. A small slit in the top cover of the cell allows for the coupling of the HeNe laser beam (λ=633nm) to the prism and after reflection fall onto the detector. All measurements were performed at a constant temperature, controlled by a thermostat.

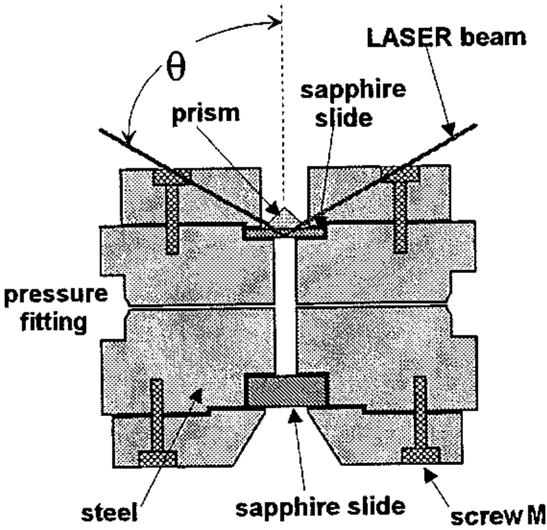

Sample preparation

For TIR measurements the sapphire window was in direct contact to the pressure medium, e.g., water, methanol, or ethanol. For the ATR investigations a 50 nm thick gold layer was evaporated directly onto one side of the 2.5 mm thick sapphire window in a vacuum chamber. Poly(methyl methacrylate) (PMMA) of molar mass M_w=150,000 g/mol was obtained from Fluka and used without further purification. The polymer was first dissolved in purified diethyleneglycoldimethylether at a concentration of 15-18 wt %. The solution was filtered two times. Polymer films were prepared by spincoating on top of the gold layer. Subsequently, all samples were dried for 12 h at T = 90 °C and heated up to T = 130 °C for several minutes in vacuum. By this treatment of the film at a temperature above the glass transition temperature T_G anisotropy effects due to the spin coating processes should be minimized.

Theory

In order to quantitatively analyse the experimental data a theoretical model will be presented that characterizes the behavior of the polymer films under hydrostatic pressure. This is achieved by combining standard equations of optics [8,9)] and thermodynamics [11),12)] in order to describe the dependencies of *n* and *d* of a polymer film on pressure. The Clausius-Mossotti equation describes the dielectric constant ε_r as a function of materials parameters. [8)]; Clausius-Mossotti equation:

$$\frac{\varepsilon_r - 1}{\varepsilon_r + 2} = \frac{\alpha' \mathrm{N_A}}{3\mathrm{M}} \cdot \rho \qquad (1)$$

with $\alpha' = \alpha/(4\pi\varepsilon_0)$ the polarizability volume, $\varepsilon_0 = 8.854 \cdot 10^{-7}$ $\mathrm{C^2/(Jm)}$ the dielectric constant in vacuum, M the molar mass, ρ the density, and $\mathrm{N_A}$ Avogadro's number. With $\varepsilon_r = n^2$ we obtain: [Lorentz-Lorenz equation]

$$R_{LL} = [(n^2 - 1)/(n^2 + 2)] \cdot (\upsilon_{sp}) \qquad (2)$$

with $R_{LL} = (4\pi/3) \cdot \alpha' \cdot \mathrm{N_A}$ the so called Lorentz-Lorenz-constant, and $\upsilon_{sp}(p,T) = 1/\rho$ the specific volume depending on temperature T and pressure p.

Alternative expressions to the Lorentz-Lorenz-equations have been introduced by Eykman or Gladstone and Dale, respectively [9)].

$$R_{GD} = (n-1) \cdot \upsilon_{sp} = \text{const} \qquad (3)$$

$$R_E = (n^2-1)/(n-0.4) \cdot \upsilon_{sp} = \text{const} \qquad (4)$$

The pressure and temperature dependence of R_{LL} (and likewise of R_E, and R_{GD}) are neglected in these simple theoretical approaches. Values for $\upsilon_{sp}(p,T)$ can be found in the literature or estimated with Tait's equation. The specific volume (the volume in general) changes with a variation in temperature or pressure according to:

$$\upsilon_{sp}(T,p) = \upsilon_{sp}{}^0 \, [1 + a_T - k_p] \qquad (5)$$

with $\upsilon_{sp}{}^0$ the specific volume at standard conditions ($p_0 = 1.013 \cdot 10^5$ Pa, $T_0 = 25°\mathrm{C}$), a_T the thermal expansion, and k_p the compression of a material. The simplest approximation for a_T and k_p is a linear behavior, respectively:

$$a_T = (1/\upsilon_{sp}{}^0) \cdot (\partial \upsilon_{sp}/\partial T) \cdot [T - T_0] = \alpha_T \cdot [T - T_0]$$

$$k_p = (1/\upsilon_{sp}{}^0) \cdot (\partial \upsilon_{sp}/\partial p) \cdot [p - p_0] = \kappa_0 \cdot [p - p_0].$$

α_T is the thermal expansion coefficient and κ_0 is the bulk compressibility at standard conditions ($p_0 = 1.013 \cdot 10^5$ Pa, $T_0 = 25°\mathrm{C}$), respectively.

The bulk compressibility κ_0 (necessary to calculate k_p) is given by the volume change . The volume change is connected to the (measured) change in film thickness according to [11,12)]:

$$\frac{\partial \upsilon_{sp}}{\upsilon_{sp}^0} = \frac{\partial V}{\mathrm{V}^0} = 3 \cdot \left(\frac{\partial \mathrm{d}}{\mathrm{d}_0}\right) + 3 \cdot \left(\frac{\partial \mathrm{d}}{\mathrm{d}_0}\right)^2 \qquad (6)$$

V is the total volume, d is the film thickness, V_0 is the volume and d_0 the film thickness at standard conditions, respectively.

A more general approach, which is due to Tait [13,14,15)], considers deviations from this linear behavior. The compression is no longer linear in p, and depends on T, too. This leads to Tait's equation:

$$\frac{\partial \mathrm{k_p}}{\partial \mathrm{p}} = \frac{\kappa_0 \mathrm{B(T)}}{\mathrm{B(T)} + \mathrm{p}} \qquad (7)$$

$B(T)$ is a temperature depending parameter, as shown in the literature [13,14,15)].

The solution of this differential equation is:

$$\mathrm{k_p} = \kappa_0 \mathrm{B(T)} \cdot \ln\left[\frac{\mathrm{B(T)} + \mathrm{p}}{\mathrm{B(T)} + \mathrm{p_0}}\right] \qquad (8)$$

Introducing a power series according to Yamashita [12)], and inserting Eq. (8) into Eq. (5) leads to:

$$\upsilon_{sp}(\mathrm{p,T}) = \upsilon_{sp}^0 \left\{1 - \kappa_0 \mathrm{B(T)} \cdot \ln\left[1 + \frac{\mathrm{p}}{\mathrm{B(T)}}\right]\right\} \qquad (9)$$

The combination of Eq. (9) and the Lorentz-Lorenz-equation, Eq. (2), then gives the dependence of the refractive index n as a function of pressure and temperature:

$$\mathrm{n(p,T)} = \sqrt{\frac{\upsilon_{sp}^0(1 - \mathrm{k_p}) + 2\mathrm{R_{LL}}}{\upsilon_{sp}^0(1 - \mathrm{k_p}) - \mathrm{R_{LL}}}} \qquad (10)$$

Results and Discussion

The measured reflectivity scans were compared with calculations for a model layer system by using the transfer matrix algorithm, based upon Fresnel's equations [1)]. The variables in Fresnel's equations are the layer thickness and the dielectric constants of the materials. These parameters are varied until the measured reflectivity scans are fit by the simulated ones as good as possible. Firstly, we considered the pressure medium itself. Next, we checked the pressure dependence of the gold layer by modeling the surface plasmon resonance curve. Finally, we measured and modeled polymer films spincoated onto the Au layer.

Pressure Medium

Firstly, we recorded reflectivity scans of the system sapphire/water (alternatively sapphire/methanol and sapphire/ethanol) at several pressure values. One set of scans is shown in Fig. 2. The angular position of the edge for the total internal reflection (θ_{tot}) in the scans shown in Fig. 2, gives the ratio between the refractive indices of water and sapphire [8)], respectively: .

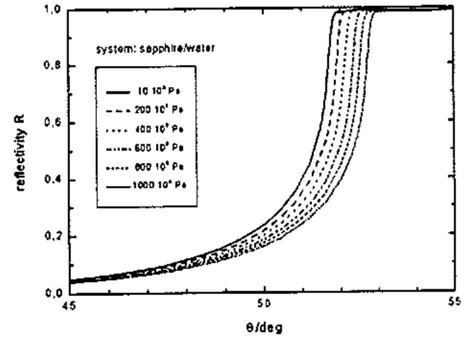

Fig.2

Here, θ_{tot} is the angle of total internal reflection within the prism, varying with the applied pressure, $n(H_2O)$ and n(sapphire) are the refractive indices of water and sapphire, respectively.

The sapphire window was always mounted with the same constant torque so that any mechanically induced change in n(sapphire) could be neglected. This set up then enabled us to measure refractive indices of fluids as a function of the applied pressure, with an accuracy of $\Delta n = \pm 0.003$. This was demonstrated for water, ethanol and methanol for a pressure range from $p = 1 \cdot 10^5$ to $1050 \cdot 10^5$ Pa, as shown in Fig. 3.

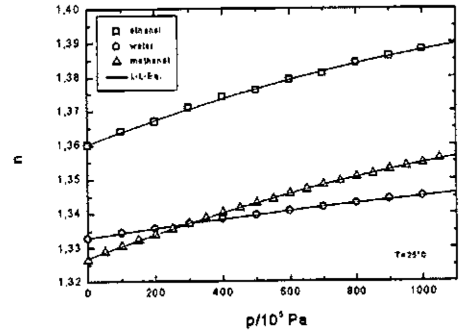

Fig.3

The measured data are compared with the theoretical prediction of Eq. (3). The constant R_{LL} ($R_{LL} = 0.2063$ cm^3/g for water; $R_{LL} = 0.2810$ cm^3/g for ethanol, $R_{LL} = 0.2191$ cm^3/g for methanol at T = 25°C, λ=633 nm) we take from the literature[16,19)].

Measurements of the refractive index of fluids versus pressure have been reported many times before [17,18,19)] with different methods. Our results are in good agreement with those basic experiments and with theoretical predictions given in those papers. We, too, find no significant difference in using the equations from Lorentz-Lorenz, Gladstone-Dale or Eykman for pressure values $p \leq 1050 \cdot 10^5$ Pa.

Gold Layer

The next step was to look at a pure gold layer under pressure (in this case water was the pressure medium). The measured reflectivity scans showed a shift in the resonance angle to higher values with an increase in pressure. This shift of these curves, however, can be completely modeled by changing $n(H_2O)$ only. Therefore, this effect is attributed to an increase of the pressure medium density and therefore to an increase of $n(H_2O)$ according to the Lorentz-Lorenz Eq. (2). The gold layer is stable and remains unchanged in its optical properties in aqueous environments up to pressures of $p = 1050 \cdot 10^5$ Pa.

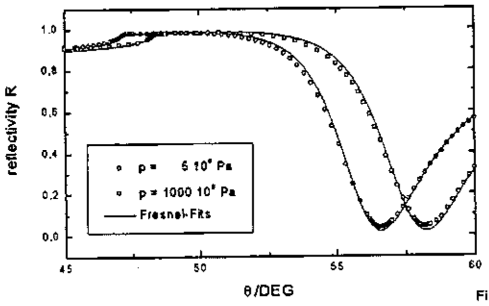

Fig.4

PMMA Films

Finally, polymer films and their optical and mechanical behavior under pressure were studied. Since the density of bulk PMMA is well known as a function of pressure [20,21,22,23)], we started our experiments with thick films ($d \approx 2.5$ μm) assuming that these films behave like bulk material. Therefore, the theoretical approach derived in Eq. (4)-(10) can be used. The knowledge of the specific volume as a function of pressure (and temperature) then enables us to calculate the refractive index of PMMA as a function of pressure with Eq. (10).

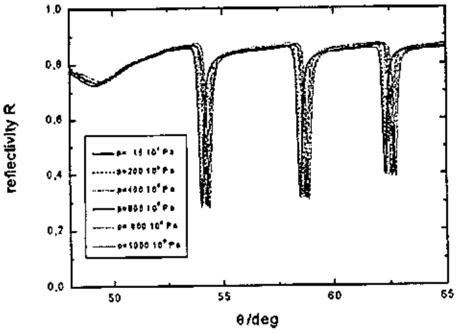

Fig.5

Fig. 5 shows reflectivity scans for such a thick PMMA film at 6 different pressure values, as indicated. Two contributions to the pressure induced shift of the guided modes have to be considered. The first is the increase of $n(H_2O)$ with the increase in p, as discussed above. The second is a density change in the PMMA film itself. Each scan (at a given pressure) allows then for the determination of a pair of data, one for the thickness and one for the refractive index value of the layer (n,d), provided $n(H_2O)$ was determined before as shown in Fig. 3.

Simulations of the waveguide mode spectra were performed using the transfer matrix algorithm, as mentioned above. The modeled thickness $d(p)$ and refractive index $n(p)$ of the polymer film thus obtained are shown in Figs. 6 and 7, respectively.

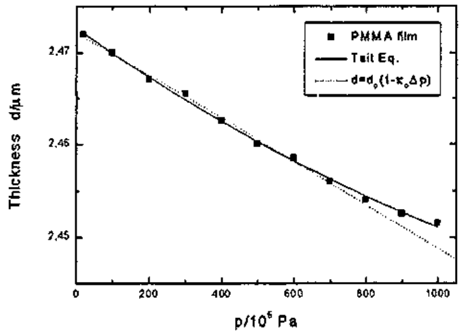

Fig.6

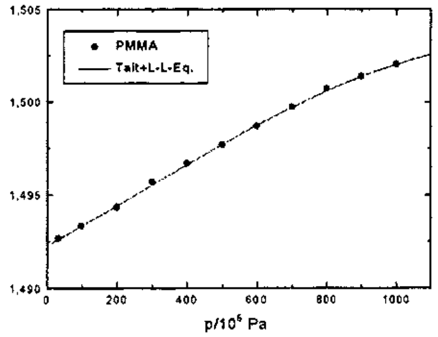

Fig.7

The linear approximation for the thickness decrease as a function of pressure , is valid for pressure values of $p \leq 800\ 10^5$ Pa [22)]. For higher pressures, only Tait's equation describes the data with sufficient accuracy.

From the data, we can calculate the PMMA bulk compressibility as: $\kappa_0 = 277 \cdot 10^{-12}$ /Pa, which is in good agreement with literature data of $\kappa_0 = 245 \cdot 10^{-12}$ /Pa [24)]. The parameter $B(T)$, was determined to $B(T{=}25°C) = 4724\ 10^5$ Pa.

Using Eq. (10) we then can calculate the refractive index of PMMA as a function of pressure, shown as the solid line in Fig. 7. For R_{LL} we used a value of 0.320 cm^3/g [22)]. In the pressure range investigated, once again we found that the empirical equations from Eykman or Gladstone and Dale are as good as the Lorentz-Lorenz-equation .

Conclusions

We built an experimental set-up for surface plasmon and waveguide spectroscopies and demonstrated its capability to measure the refractive index of fluids and thin dielectric films under hydrostatic pressure conditions. We chose a simple and well-known system (gold/ PMMA/water) to test our apparatus and compare our results with previous measurements with other techniques on bulk samples [16)-25)].

In a first set of experiments we determined the pressure dependence of the refractive indices for water, methanol, and ethanol. The results were in quantitative agreement with literature values and could be equally well described (within the experimentally accessible pressure range) by the theories given by Lorentz-Lorenz, Eykman, and Gladstone-Dale. For a PMMA-film of ca. 2.5 µm thickness, bulk behavior was confirmed up to pressure values of $p = 1050 \cdot 10^5$ Pa with a quantitative description of the thickness given by Tait's equation. The pressure dependence of the refractive index was again equally well described by Lorentz-Lorenz, Eykman, or Gladstone-Dale formulas.

References:

1.E.F.Aust, S.Ito, M.Sawodny, W.Knoll, *Trends in Polymer Science* **2**, 313 (1994),
2.W.Knoll, *Ann.Rev.Phys.Chem.* **49**,569-638(1998)
3. C.S.Mayo and R.B.Hallock, *Rev Sci. Instrum.* **60**,739 (1989)
4. O.Prucker, S.Christian, H.Bock, J.Rühe, C.W.Frank, W.Knoll,, *Macromol.Chem.Phys.* **199**,1435 (1998)
5.E.Kretschmann, *Opt. Commun* **6**,185 (1972)
6.J.G.Gordon II, *Opt.Commun* **22**,374 (1977)
7.J.D.Swalen, *J.Phys.Chem.***83**,1438 (1979)
8.M.Born and E.Wolf, *"Principles of Optics"*, Pergamon Press,London (1981)
9.W.Karthe,R.Mueller; *"Integrierte Optik"*,Akad. Verlagsbuch. Leipzig (1991)
10.O.Bodmann, *Die Makromolekulare Chemie* **122**, 196 (1969)
11.P.Heydemann, and H.D.Guicking; *Kolloid-Zeitschrift und Zeitschrift für Polymere* **193**,16 (1963)
12.T.Yamashita, *Jap. J.Appl.Phys.* **33**, 4025 (1994)
13.J.H.Dymond and R.Malhotra, *Int. J. Thermophys.***9**,41(1988)
14.J.S.Rosen, *J.Opt.Soc. Am.* **37**, 932 (1947)
15.R.E.Gibson and O.H.Loeffler, *J.Am.Chem.Soc.***63**, 898(1941)
16.M.D.Lechner, G.Hammel, *Eur.Polym.J.* **15**, 209 (1979)
17.H.Eisenberg *,J. Chem. Phys.* **43**, 3887 (1965)
18.K.Vendam and J.P.Limsuwan, *J.Chem.Phys.***69**, 4772 (1978)
19.D.Beysens, P.Calmettes, *J.Chem.Phys.* **66**, 766 (1977)
20.H.A.Spetzler, M.D.Meyer, *Rev. Sci. Instrum.* **45**, 911 (1974)
21.Y.Z.Wang, W.J.Chia, K.H.Hsieh, and H.C.Tseng, *J.Appl.Polymer Sci.* **44**, 1731 (1992)
22.K.-H.Hellwege, W.Knappe, P.Lehmann *Kolloid Zeitschrift und Zeitschrift für Polymere* **183**, 110 (1962)
23.K.Chan and A.L.Ruoff, *J.Appl.Phys.*. **52**, 5395 (1981)
24.W.Wunderlich, *"Physical Constants of Poly(methyl methacrylate)"*, in *Polymer Handbook*, p VII/77ff., J.Brandrup, E.H.Immergut, Eds., J.Wiley & Sons, New York (1975)

High-Pressure Equipment for Institutes and Industry

...and your ideas will come true.

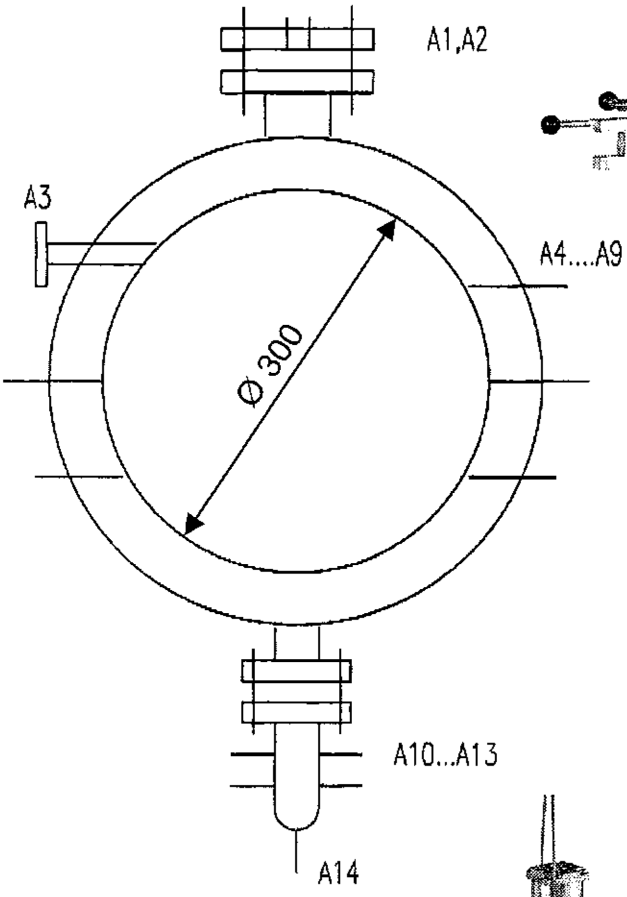

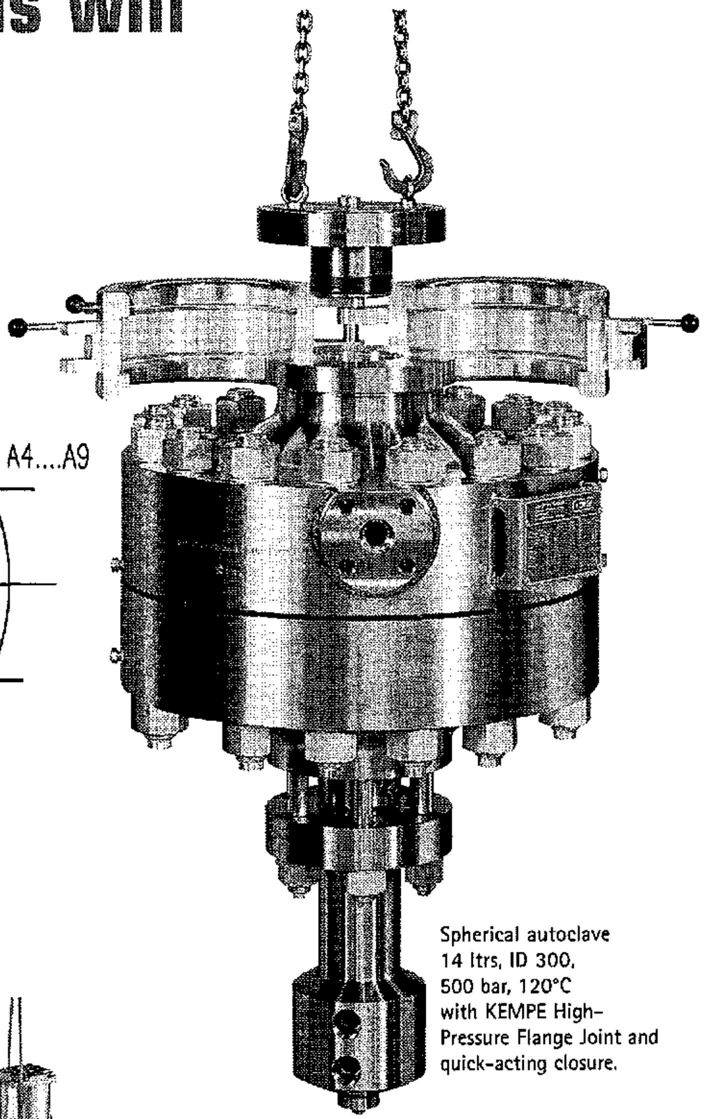

Spherical autoclave
14 ltrs, ID 300,
500 bar, 120°C
with KEMPE High-Pressure Flange Joint and quick-acting closure.

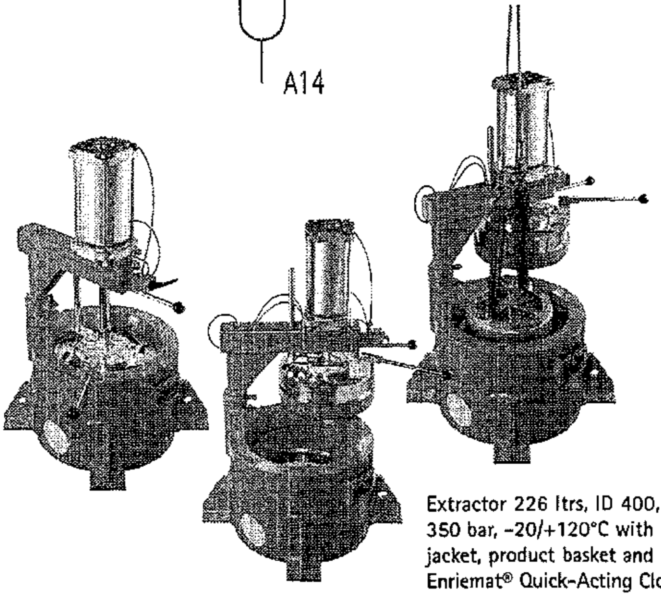

Extractor 226 ltrs, ID 400,
350 bar, -20/+120°C with heating jacket, product basket and KEMPE Enriemat® Quick-Acting Closure.

kempe

Siegfried Kempe
Apparate und Maschinenbau
Benzstraße 8
D-74193 Schwaigern
Telefon 07138/9881-12
Telefax 07138/9881-52
E-Mail tkempe3411@aol.com

Hydrothermal Treatment

GVC-Fachausschuß „High Pressure Chemical Engineering“, March 3-5, Karlsruhe, Germany, 1999 GVC FZK '99

SCWO: Facts and Hopes

H. Schmieder* and J. Abeln

Forschungszentrum KA, Institut für Technische Chemie-CPV, P.O. Box 3640, 76021 Karlsruhe, Germany
Fax: (+)7247/82-2244; e-mail: helmut.schmieder@itc-cpv.fzk.de

1 Introduction

After the experiments by M. Modell and S. Amin to convert carbohydrates in supercritical water at the Massachusetts Institute of Technology [1] in the mid 1970's the potential of the supercritical water oxidation process was recognised, and a very active chemical and engineering R & D began in the eighties especially at National Laboratories and Universities in the US. At this time the subcritical Wet Air Oxidation (WAO) has already been successfully used but the new process promised significant advantages [2]:

- higher oxidation efficiency by higher reaction temperature and density,
- very much lower residence time caused in part by the one-phase mixture of reactants which avoids interfacial transport inhibitions leading to much more compact reactors, and
- to meet the release standards in one process step for the gaseous and aqueous effluents without additional process steps as needed for the WAO.

From the engineering point of view two additional challenges emerged under supercritical operating conditions:

- more strength corrosion of reactor and heat exchanger construction materials, and
- drastically decreased solubility of salts resulting in precipitations within reactor and feed preheater causing fouling and even the possibility of plugging.

Figure 1 shows a simplified engineering diagram of the process containing the main components.

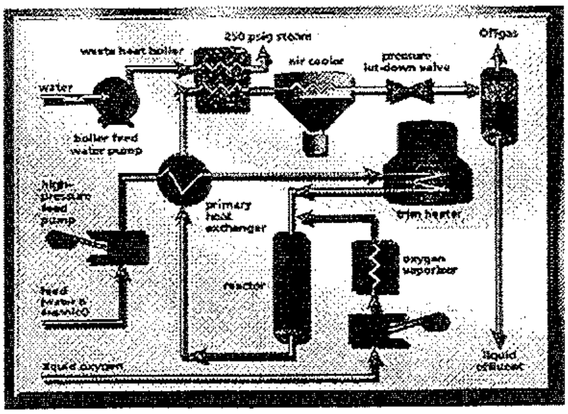
250 psig steam
waste heat boiler
air cooler
pressure let-down valve
Offgas
water
boiler feed water pump
high-pressure feed pump
primary heat exchanger
trim heater
oxygen vaporizer
reactor
feed (water & organic)
liquid oxygen
liquid effluent

Fig. 1: Simplified SCWO process diagram, [3]

It includes the preheater for efficient recovery of heat from the reactor effluent indispensable for commercial (civil) use regarding the competitiveness with traditional waste treatment (incineration, landfill storage etc.).

To achieve the desired conversion efficiency of 98 % (for some hazardous wastes much higher) temperatures of 500 to 600 °C at pressures between 25 to 35 MPa (economic compromise) and a reactor residence time of up to one minute are used. Essentially three reactor concepts (Figure 2) were developed and studied: tubular reactor [4,5], tank reactor with the reaction zone in the upper part and a cool zone in the lower part of the tank to dissolve the salts [6] and the "transpiring wall reactor" with an inner porous pipe which is rinsed with subcritical water to prevent salt deposits at the wall [7].

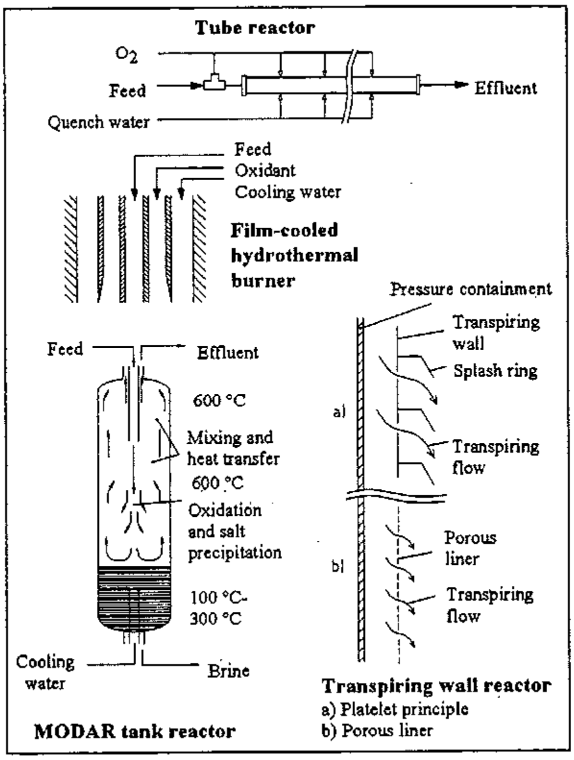
Tube reactor
O_2
Feed
Quench water
Effluent
Feed
Oxidant
Cooling water
Film-cooled hydrothermal burner
Pressure containment
Transpiring wall
Splash ring
a)
Transpiring flow
b)
Porous liner
Transpiring flow
Feed
Effluent
600 °C
Mixing and heat transfer
600 °C
Oxidation and salt precipitation
100 °C-300 °C
Cooling water
Brine
MODAR tank reactor
Transpiring wall reactor
a) Platelet principle
b) Porous liner

Fig. 2: Reactor concepts

A fourth concept also shown in Figure 2 is the hydrothermal burner which cools the wall by coaxial introduction of high amounts of water [8]. As oxidants mainly air, oxygen and hydrogen peroxide were tested. Mostly, Ni based alloys were used as reactor construction material.

Besides the investigations of numerous model compounds real wastes from chemical, pharmaceutical and food industry, municipal sewage, military and nuclear waste simulates were tested in bench and pilot scale plants [9].

2 R&D Basis

The physico-chemical fundament of the Supercritical Water Oxidation Process is based to an important part on the work started in the fifties by E. U. Franck and his collaborators [10,11,12]. Much experimental work to determine the destruction efficiencies and kinetic data for the oxidation of organic and inorganic model compounds under SCWO conditions was performed since the 80's. Examples are listed below (table 1).

These data allow conversions of more than 99 % under typical supercritical conditions in less than 1 minute residence time. It was seen very fast that the „oxidation chemistry" is not a the problem for this process.

Table 1: Destruction efficiencies (D.E.) for the oxidation of selected compounds [13]

Compound	D.E. / %
2,4-Dinitrotoluene	83-99
Acetic Acid	<99,9
Ammonia	20,3-99,99
Aniline	19,9
Carbon monoxide	
Cyanide	86,1
Dichloromethane	97,6-100
Ethanol	99,03-99,997
Formic Acid	92,8-93,3
Hexachlorocylohexane	99
Hydrogen	22,8-99,9
Methane	
Phenol	85-99,993
PVC	100
Pyridine	4-99.99
Thiophene	44,9
Toluene	97-99,999
Trichlorethylen	99,99-99,999
1,1,1-Trichloroethan	10-99,4

Even the oxidation of dioxines with high destruction efficiencies is documented in [14]. The partly de novo formation of dioxins is supressed at sufficient high temperatures [15].

The analysis of the effluents indicates a bottle neck for the destruction of only some small (and harmless) organics like acetic acid. Besides these some other, notoriously bad to oxdise compounds are: pyridine, urea, ammonia, acetonitril, aniline.

It can be seen that in general the oxidation chemistry is working very well. Studies with respect to the efficiency of the oxidants like air, O_2, H_2O_2, $KMnO_4$, $KMnO_4$+ O_2 are described in [16].

The global kinetic data were complemented by modeling the kinetics with elementary reaction pathways [17,18] adapting free radical mechanisms to SCWO conditions.

Tab. 2: Destruction efficiencies (D.E.) for the oxidation of halogenated aromatic compounds [13]

Compound	D.E. / %
2,4-Dichlorobenzene	99,7
2,4,6-Trichlorophenol	99,995
Tetrabromobisphenol A	99
3-Chlorobiphenyl	99,99
2-Chlorophenol	99,0
4-Chlorophenol	99,99
PCB	99-99,999
PCB	99,9999
PCB	99,99
Pentachlorophenol	99,99
Dioxines	99,99999

In order to demonstrate the high potential of SCWO as an end of pipe process many real waste waters were treated in bench sclae and pilot plants with very high destruction efficiencies. Table 3 shows some applications.

Table 3: Destruction efficiencies (D.E.) of real waste effluents treated with SCWO [13]

Waste	D.E. / %
Activated sludge	50-99,8
Brewery effluents	bis > 99,99
Electronic scrub	>99,9
Hanford waste	>99,9
Sewage sludge	85-99,4
Municipal sludge	> 99,99
Navy hazardous wastes	95-99, 92
Paper mill effluents	81,37-99,98
Percolate	96,5-99,8
Chemical & pharmaceutical industry	<99,997
Chemistry	85-99,99
Polymers	99,95-99,92
Rocky Flats	>99,9

Some of these applications are covered by lab- and bench-scale experiments carried out at FZK [19,20]. Results for SCWO of real waste effluents at 260 bar are put together in table 4.

Tab. 4: Results with industrial wastes in the bench scale plant at FZK

Waste water	Feed-TOC ppm	Conv. %	Temp. °C	Solids
Pharma	1.000	86	450	-
	7.000	83	410	-
	20.000	97	550	-
Chemistry	23.000	99,99	550	-
	4.500	99,98	550	-
Paper	2.000	98	450	+
	2.000	99	500	+
	11.000	97	500	+
Sewage Works	1.000	85	500	+
	630	98	550	+
	5.400	99,8	550	++

Extensive investigations were performed concerning the corrosion behavior of different metals, alloys and ceramics up to high pressures and high temperatures by the group of Latanision [21] and Boukis [22] who will present recent results on this conference.

3 Current Status of SCWO

United States:
The only commercial plant for civil waste treatment is operated in Texas since 1994 by the Huntsman Corporation [4]. The plant is designed and constructed by ECO Waste Technology (EWT) supported by the comprehensive development work done at the University of Texas [23]. Figure 1 shows a scheme of the process. The tubular reactor made of a non specified incolloy has a length of 200 m and works at temperatures between 540 and 600 °C at 250 to 280 bar. The nominal throughput amounts to 1100 kg/h. The feed is mainly a mixture of alcohol and amines. The total organic carbon, TOC in the aqueous feed amounts to more than 50 g/l. Typical organic concentrations are given with 10 w%. TOC oxidation efficiencies of 99.988 and 99.929 % for the amines corresponding to 10 and 3 mg/l TOC in the aqueous effluent are achieved. These values meet the standards for direct release. Nitrate is found with 6.4 and ammonia with 2.7 mg/l in the effluent low enough to meet even the German standards (Abwasser V, Anh. 22). In the off-gas 0.6 vppm NO_x, 60 vppm CO, 200 vppm CH_4 and 0.12 vppm SO_2 are measured as typical concentrations. The German standards (17. BImSch) require for low hydrocarbons an important lower release than 200 vppm; the CO value is near the limit. The plant is not suited for processing wastes with higher chlorine content and salt containing waste. EWT operates a pilot plant, however, where such material was successfully treated. The company does not describe the reactor type used for the pilot plant. By comparison with traditional waste treatment costs EWT concludes that the costs for SCWO amount only to one third of the incineration costs in the US.

Tab. 5: Cost estimations by EWT [24]

Raw Flow Rate Organic Conc. Plant Flow Organic Conc. as run	0,3 t/h 35 % 0,9 t/h 10 %
Unit costs	2 114 744 $
Operating Costs	313 000 $/year
Credits	34 000 $/year
Net Operating Costs	313 000 $/year
Operating Cost 365 d/yr 250 d/yr	 110 $/t raw waste 160 $/t raw waste
Capital Recovery Cost 10 yr life, i = 8 %	 120 $/t raw waste
Total Treatment Cost 365 d/yr 250 d/yr	 230 $/t raw waste 280 $/t raw waste
Total Treatment Cost 250 d/yr,waste: 50 % C	 1600 $/t C

Cost estimations by M. Modell gave values from 151-621 US $ per dry ton for a 5-100 tons per day system [25], relating to 500-2100 US $ per ton Carbon assuming 30 % carbon in the dry substance.

Today the main activities in the US are directed towards hazardous wastes from the defence sector. Such wastes include propellants, explosives, smokes, dyes, poisons and nuclear waste. The programs are executed in a tight collaboration between the institutions of the US Forces and National Laboratories, Universities and the industry [26].
At the Los Alamos National Laboratory the treatment of radioactively contaminated ion exchange resins and other wastes is tested with a lean vessel reactor (stainless steel, Ti lined) at 46 MPa and 540 °C. For explosives after a hydrolytic pretreatment a 150 m long tubular reactor is used at 110 MPa (!) and a rather low temperature of 450 °C to increase the salt solubility.
Wastes coming from the Air Force will be treated in a tubular reactor built by General Atomics. The plant has a throughput of 450 l/h; start up was planned for 1998. General Atomics, ECO Waste Technologies and the University of Texas are the partner of the Air Force program.
At the US Army about 10 000 t of colored smokes and dyes (polyaromatics, salt) wait for treatment by SCWO. The plant is designed to treat 36 kg waste per hour at 600 °C with a residence time of only 10 sec. The transpiring wall reactor built by a consortium led by the Foster Wheeler Corp. was previously tested at Sandia National Laboratory [27]. The Army also plans to treat the nerve gas VX by SCWO.

The US Navy tested for the disposal of Naval vessel wastes (sewage, shower water, paint, solvents, fuels) two SCWO demonstration plants (140 kg/h feed) in test in 1998. One plant uses a tubular reactor built by General Atomics [28] and the other a transpiring wall reactor designed by Foster Wheeler/Aerojet.

Europe:
Most of the European development work is done in Germany. Besides the R&D activities described above at FZK a film-cooled two-zone reactor (porous inner pipe rinsed with cool water to avoid salt deposits) is in test (EU collaboration) since 1998 [29]. Another double pipe reactor with an inner pipe made of alumina is used for the treatment of halogenated hydrocarbons [30].
The Fraunhofer Institute ITC develops a tubular reactor for treatment of electronic scrap in collaboration with Daimler Benz, Ulm, and built a mobile plant (20 l/h) to treat hazardous waste at the source of generation [31].
The Technical University Hamburg Harburg has investigated a combination of soil extraction by supercritical water followed by SCWO of the pollutants [32]. Former activities at the Technical University of Munich [33] and by MODEC together with a consortium of pharmaceutical companies (200 m tubular reactor with high flow velocity to transport particles, 90 l/h feed) [34] were terminated in 1996.
In Sweden Chematur Engineering, AB has built a 250 kg/h pilot plant (EWT license) for pulp and paper mill sludge and other wastes and is planning a larger plant for treatment of electronic scrap.
In France C.N.R.S. (University Bordeaux) together with Elf-Aquitaine plans the construction of a pilot plant [35].
At the University of Valladolid in Spain a film-cooled reactor filled with alumina balls with a volume of 15 l is operated at 20 kg/h feed (8-18 %w organics) and 600-700 °C. It is planned to treat industrial wastes in an up-scaled pilot plant [36].

Japan [37]:
Organo Corp. in Tokyo has acquired licenses of MODAR (acquired 1996 by General Atomics) and MODEC and built the first plant in Japan. Together with the Japan Sewage Agency detoxification of sludge is obviously a major task. The Japanese companies Hitachi and NGK are also licensees of MODEC. The Shinko Pantec Co.in Kobe has signed a cooperative agreement with EWT to develop the technology for the Japanese market. The companies Komatsu & Kurita have an agreement concerning technical support by General Atomics.
For recycling of residues from plastic production Kobe Steel has developed a hydrolytic "monomerisation" process in supercritical water and built a commercial plant in 1997. A similar process for treatment of radioactively contaminated resins is investigated by Mitsubishi Heavy Ind.. Kubota, Sumitomo Heavy Industry and Toshiba are other companies active in SCWO.
R & D work supporting the industrial activities is done for example at the Tohoku National Industrial Research Institute (PCB's, polymers), at the Kumamoto University (sewage) and at the Tokyo University (kinetics).

4 Further R&D Need

One of the most outstanding problems to be solved is possible plugging and corrosion caused by precipipitated solids, particularly by salts.
There are, in general, two types of salt phase behaviour depending on wether the solubility curve does intersect the critical curve (Type I) or not (Type II) [38]. Type I systems are often salts soluble in water at ambient conditions: NaCl-H_2O is a typical example, and its solubility curve is shown in Fig. 1:

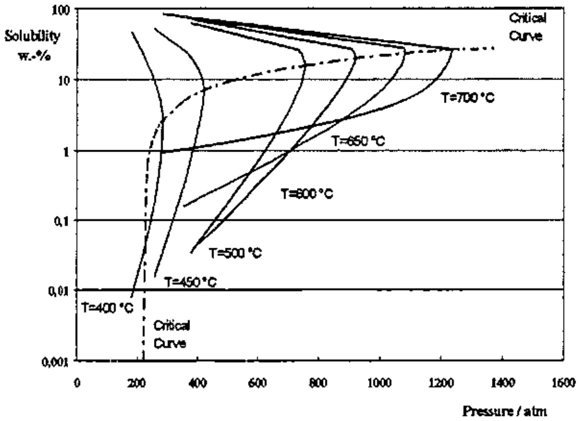

Fig. 1: NaCl solubility in water as function of pressure and temperature [39]

Type II salts - Na_2SO_4, K_2SO_4, Na_2CO_3, $CaSO_4$ – are generally less soluble; the solubility of Na_2SO_4 in SCW is about 1 ppm at 250 bar and 450 °C about thus 3 orders of magnitude less than that of NaCl. The solubility of $CaSO_4$ at 250 bar and 450 °C is only about 1 ppb [40].
For a better understanding of these problems more systems have to be studied in detail, particularly the dynamics of the nucleation process. Nucleation kinetics was studied for the system NaCl-Na_2SO_4-H_2O by the Tester group at MIT [41]. Besides the many salt-water binary phase systems determined until now, ternary (salt1-salt2-water) systems have to be determined. The determination of the binary and ternary phase diagrams has to be completed with data of the kind of the precipitate, e.g. morphology, stickiness, transportabilty, and with the corrosion activity including phosphate, nitrate and other halogens than chlorine.
Nevertheless it will be necessary to develop salt separation systems and/or new concepts to ensure a sufficient long continous operation time for wastes containing high contents of salt.

Another challenge connected with deposits of insoluble material and suppressing fouling is to make available an efficient heat exchanger to recover the heat in an economic way.

5 Spin Off - Further Applications

The path of the hydrothermal non-oxidizing treatment of organic wastes was followed since the late eighties. The main objective of the work at the Batelle Pacific Northwest Laboratory [42] was the gasification of wet organic wastes and biomass waste preferably at subcritical conditions. Under these conditions the major gas products are methane and carbon dioxide. Residence times of more than 10 min. are required to achieve conversions of 90 % and higher. The effect of different catalysts on the reaction paths, conversion efficiency and tar and soot formation was studied.

Antal [43] has investigated the gasification of wet biomass (aquatic plants etc.) under supercritical conditions using coke catalysts. At pressures >22 MPa and temperatures of up to 650 °C hydrogen and carbon dioxide with small amounts of methane and carbon monoxide are found in the product gas at residence times of about 30 sec.

At the Forschungszentrum Karlsruhe the gasification of model compounds, wet organic wastes and biomass is systematically investigated in batch experiments and tubular flow reactors since 1994. At temperatures of 600°C and pressures of up to 35 MPa the feed can be completely gasified to hydrogen and carbon dioxide as main products suppressing tar and soot formation. Contained or added alkali metals have a significant influence on the gasification efficiency and the reaction paths. Kruse et al. will report our results and Penninger will present an engineering concept for the production of hydrogen from wet biomass at this conference.

A further development that could be considered as a spin-off of the SCWO R&D are the investigations of the high pressure incineration in carbon dioxide instead of water. The experiments in a tubular flow reactor with different model compounds (alcohols, aromates, amines) at typical SCWO conditions show that comparable high oxidation efficiencies of 98 % (TOC) and higher can be achieved in carbon dioxide [44]. Only small differences are observed concerning the ignition behaviour and the reaction paths. The understanding of the surprising findings shall be improved by elementary reaction modelling. The results have also a considerable potential of application. A clean-up of liquid or solid material (catalysts, absorber etc.) by sc-CO_2 extraction could directly follow the integrated high pressure incineration step.

6 Literature

[1] M. Modell, Fundamentals of Thermochemical Biomass Conversion, Elsevier, Amsterdam, 1985, p. 95

[2] E.F. Gloyna, L. Li, R.N. Brayer, Water Sci. Tech., 9, 1994, p. 1-10

[3]www.jumpnet.com/~ewt/chart.jpg

[4]www.jumpnet.com/ewt/analysis.htm

[5] Info Package ECO WASTE TECHNOLOGIES, 2305 Donley Dr., Suite 108, Austin Texas, 78758

[6] H.E. Barner et al, J. Hazardous Mat., 31, 1992, p. 1-17

[7] Th.G. McGuiness, 1st Intern. Workshop on Supercritical Water Oxidation, Jacksonville, Fl, Febr. 6-9, 1995

[8] H.L. LaRoche, M. Weber, Ch. Trepp, 1st Intern. Workshop on Supercritical Water Oxidation, Jacksonville, Fl, Febr. 6-9, 1995

[9] E.F. Gloyna, L. Li, Waste Management, 13, 1993, p. 379-94

[10] E.U. Franck, Angew. Chem. 73, 1961, p. 309-322

[11] G.M. Schneider, in I. Prigogine and S.A. Rice (eds.) Advances in Chemical Physics, Vol. XVII, John Wiley, New York, 1970, p. 39

[12] W. Schilling, E.U. Franck, Ber. Bunsenges. Phys. Chem., 92, 1988, p. 631-36

[13] J. Abeln, H. Schmieder et al.: „Studie zum Stand von Wissenschaft und Technik der Oxidation in überkritischem Wasser", Proj.-Nr. 0324 3705, December 1997

[14] M. Modell; G.G. Gaudet; M. Simson; G.T. Hong; K. Biemann: „Supercritical Water Testing Reveals New Process Holds Promise, Solid Wastes Management, August 1982, p. 26-28 & p. 76

[15] Blaney, C.A.; Li, L.; Gloyna, E.F.; Hossain, S.U.: „Supercritical Water Oxidation of Pulp and Paper Mill Sludge as an Alternative to Incineration", ACS Symp. Ser. 608, 1995, p. 444-455

[16] K.-C. Chang; L. Li; E.F. Gloyna: „Supercritical Water Oxidation of Acetic Acid by Potassium Permanganate", Journal of Hazardous Materials 33, 1993, p. 51-62

[17] H.R. Holgate; J.W. Tester: „Oxidation of Hydrogen and Carbon Monoxide in Sub- and Supercritical Water. Experimental Results", J. Phys. Chem. 98, 1994, p. 800-809 and p. 810-822

[18] P.E. Savage; S. Gopalan; T.I. Mizan; C.J. Martino; E.E. Brock: „Reactions at Supercritical Conditions: Applications and Fundamentals", AIChE Journal 41, 1995, p. 1723-1778

[19] J. Abeln; H. Goldacker; M. Kluth; G. Petrich; H. Schmieder: „The Oxidation of Hazardous Waste in Supercritical Water", 4th Colloquium Supercritical Fluids and Environment, Lyon, 20.-21.1.1997

[20] H. Schmieder, E. Dinjus, H. Goldacker, A. Kruse, Proc. of the 4th Italian Conf. on Supercritical Fluids and their Applications, Sept. 1997, Capri, p. 343-48

[21] R.M. Latanisson; D.B. Mitton; S.-H. Zhang; J.A. Cline; N. Caputy; T.A. Arias; A. Rigos: „Corrosion and Corrosion Mechanisms in Suoercritical Water Oxidation Systems for Hazardous Waste Disposal“, in: S. Saito; K. Arai (Eds.), The 4th Int. Symp. On Supercritical Fluids, Sendai, 11.-14.5. 1997, p. 865-868

[22] P. Kritzer; N. Boukis; E. Dinjus: „Corrosion of Alloy 625 in High-Temperature, High-Pressure Sulfate Solutions“, Corrosion 54, 1998, p.689-699

[23] E.F. Gloyna, L. Li, Waste Management 13, 1993, p. 379-94

[24] Continuuing Engineering Studies: Supercritical Water Oxidation,February 26-27, 1998, Section G

[25] M. Modell: „Treatment of Pulp Mill Sludges by Supercritial Water Oxidation“, DOE/CE/40914-T1 (DE91002626), July 1990

[26] R.W. Shaw, N. Dahmen, NATO ASI Supercritical Fluids, July 12-24, 1998, Kemer, Turkey, in press

[27] B.L. Haroldsen et al, Sandia Report 96-8255 UC-702, 1996

[28]US-European Workshop on Thermal Treatment for Naval Vessels, 29-31 Oct. 1997, Brussels, Belgium, Eule & Partners, B-3080 Tervuren

[29] J. Abeln: „Cost Effective Destruction of Toxic Organic Wastes by Supercriitcal Hydrothermal Oxidation“, European Workshop on Environmental Technologies 1998, Darmstadt, 16-19 June, 1998

[30] V. Casal, H. Schmidt, Journal of Supercritical Fluids, 13, 1998, p. 269-76

[31] S. Pilz, this conference

[32] A. Firus, G. Brunner, in R. von Rohr, C. Trepp (eds) "High Pressure Engineering", Elsevier Science, 1996, p. 179-84

[33] H. Tiltscher et al, BayFORREST Report 2, 1994, p. 189

[34] M. Modell, S. Mayr, S. Kemna, Off. Proc. 56th Int. Water Conf. 1995, p. 479

[35] N. Bonneton et al, Proc. 5th Meeting on Supercritical Fluids, March 1998, Nice, p. 861-66

[36] private communication

[37] Shinko Pantec Co, private communication

[38] M.I. Ravich, Russian J. Inorg. Chem. 9(4), 1964, p. 520

[39] S. Sourirajan; G.C. Kennedy: The System H_2O-NaCl at Elevated Temperatures and Pressures, American Journal of Science 260, 1962, p. 115-141

[40] O,I. Martinowa: „Solubility of Inorganic Compounds in Subcritical and Supercritical Water“, in: D.G. Jones, R.W. Staehle (Eds.): „High Pressure, High Temperature Electrochemistry in Aqueous solutions“, National Association of Corrosion Enineers, Houston, Texas, 1976, p. 131-138

[41] F.J. Armellini; J.W. Tester: Experimental Methods for Studying Salt Nucleation and Growth from Supercritical Water“, The Journal of Supercritical Fluids 4, 1991, p. 254-264

[42] L.J. Sealock, D.C. Elliott, E.G. Baker, R.S. Butner, Ind. Eng. Chem. Res., 32, 1993, p. 1535-41

[43] D. Yu, M. Aihara, M.J. Antal, Energy Fuels, 7, 1993, p. 5

[44] A. Kruse, H. Schmieder, Environmental Progress, AIChE, 17, 1998, p. 234-39

Production of Hydrogen from wet biomass by Supercritical Water Gasification.

Johannes M.L. Penninger*
SPARQLE International B.V.
18 Boerhaavelaan, 7555 BC Hengelo-The Netherlands
e-mail spql@introweb.nl
fax +31.74.250/5285

Water, in its critical state (T >374 C, P > 22 MPa) is a potent medium for the conversion of organic substrates. It has been shown by Antal et al. [1] that biomass-type materials can be converted completely into a fuel gas which is rich in hydrogen. This was achieved by treating an aqueous slurry or solution of the organic precursor in a continuous flow reactor at 600 C and 30 MPa and maintaining a reaction time of 1 minute or less.

These observations provided the basis for a feasibility study [2], supported by an EU Exploratory Research Award, into the technical and economic potential of SWG.

The results show that aqueous rest biomass in particular holds potential as a feedstock for fuel gas production by SWG. A survey shows that rest biomass is abundantly produced throughout the EU countries, as a by-product of agriculture and industrial activities and could replace in some EU countries as much as 10 % of the natural gas consumption when SWG would have come into practice.

This presentation deals with some aspects of the feasibilty study, in particular the chemistry of SWG and the conceptual process which needs to be developed. The supply potential and the prevailing economic constrains of SWG are illustrated.

References

1. Antal, Jr. M.J., "Hydrogen production from high-moisture content biomass in supercritical water" pers. comm. **1996.**
2. Penninger, J.M.L. , "Clean fuel gases from aqueous biomass – a feasibilty study" Stage 1 EU Proposal JO-ST-3042 **1998.**

Modeling, Design and Scale-Up of an SCWO Application Treating Solid Residues of Electronic Scrap Using a Tubular Type Reactor
- Fluid Mechanics, Kinetics, Process Envelope

Stephan Pilz*

DaimlerChrysler
Research and Technology (FT4/TP)
P.O. Box 2360
89013 Ulm (Germany)
e-mail: Stephan.Pilz@DaimlerChrysler.com FAX: +49 (0)731 505-4231

The design of a tubular suspension reactor for supercritical water oxidation of a complex solid waste consisting of polymers, ceramics and metals was investigated. The work focuses on solid particle behavior within the system and thermo-chemical considerations. Computing settling velocities for all of the experienced conditions in an SCWO process provides an idea of particle motion. Furthermore, models are deployed in order that the minimum velocities required to convey the particles through the tube may be estimated. Measured chemical kinetic data on the degradation of the organic portion was utilized to assess the thermo-chemical operation in a large scale plant. Finally, a process envelope in which the further design studies can be carried out was set up.

Introduction

Electrical appliances and electronic support are still well on their way to becoming the technical standard in households, in industry, in cars and for professional purposes. Since the innovation cycle for new products is extremely short, the amount of resulting electrical and electronic scrap feeds a market on its own. While electrical applications such as vacuum cleaners do not cause environmental problems, the printed circuit boards do.

Daimler-Benz has designed and established a new plant for the mechanical processing of printed circuit boards [1]. Basically, the scrap is crushed and ferro-magnetic components are removed. The next stage of process is a cryogenic grinding and a classification using sieves. The gained particle classes are forwarded separately into an electrostatic separator which is optimized with respect to each specific particle size range. The smallest class (<100µm) is not processed for economical reasons. We receive an extremely rich metal fraction (>97%) and a mixed fraction consisting of polymers, ceramics, glass and metals. The recovery rate for metals is very high, e.g. for copper about 95%. The ferro-magnetic fraction and the metal fraction are sold to a metallurgical plant and recycled. However, the dust fraction and the mixed fraction cannot be treated in blast furnaces, or in standard incinerators, nor can they be landfilled [2].

For the further treatment, conventional thermal processes such as pyrolysis and gasification were investigated, but they do not meet all of the requirements with respect to economical, ecological and technical concerns. A monitoring of new thermal processes resulted in Super-Critical Water Oxidation (SCWO) as a favorable option [3]. Feasibility studies at the Fraunhofer-ICT demonstrated the total destruction of the organic content. Research on the design of such an SCWO application which treats residues of electronic scrap has been underway since then – as a joint project between Fraunhofer-ICT, Pfinztal, and DaimlerChrysler, Ulm.

Figure 1 shows the scaled, basic flowsheet of an SCWO unit processing a 10 wt.-% suspension with an oxygen supply exceeding stoichiometric demand.

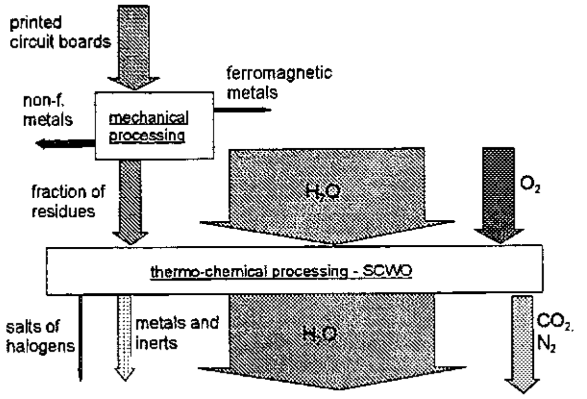

Figure 1. Basic flowsheet for the recycling of electronic scrap according to the DB concept, scaled with respect to mass flow

We decided to operate the SCWO unit continuously and to use a plug flow reactor (PFR) system. Here, we present several basic considerations for the design of such a plant with the main focus on the solid particles. We consider the described waste merely as an example since the concepts can be transferred to other complex solid mixtures.

Geometric Dependency

In addition to three standard relations for designing the geometry of PFR system, equation (2, 3 and 4), we have to take the sensitivity of the fluid density (1) into account.

Table 1. Equation for design of the geometry of a PFR system

$\rho = f(T,p)$ (1)	$\dot{V} = \dot{M}/\rho$ (2)
$v = 4\dot{V}/\pi d_i^2$ (3)	$L_{PFR} = \tau_{Reac} v$ (4)

Figure 2 illustrates that changing operating conditions or design parameters by only a small factor might result in dramatic changes to other numbers, e.g. the reactor length varies by an order of magnitudes.

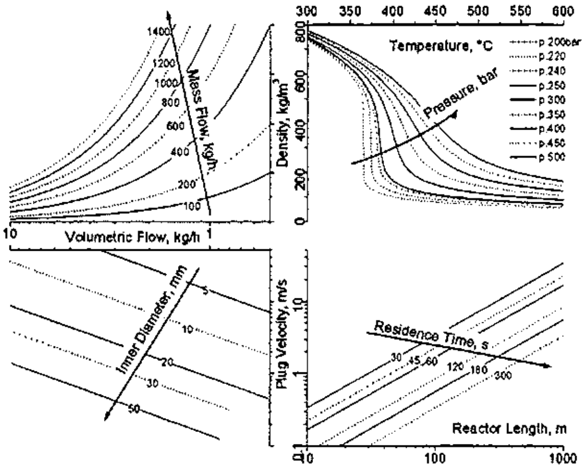

Figure 2. Nomogram for SCWO design - starting point is the temperature

Results and Discussion

Fluid Mechanics

One major obstacle when treating solids deploying SCWO is the sedimentation. The drag coefficient C_D for different flow regimes is calculated according to Table 2.

Table 2. Flow regimes and their drag coefficients for spherical particles

Regime	Re	C_D
General		$C_D = f(\mathrm{Re})$ (5)
Stokes	Re<1	24/Re (6)
Intermediate	1<Re<1000	$\frac{A}{\mathrm{Re}} + \frac{B}{\sqrt{\mathrm{Re}}} + C$ (7)
Intermediate, linearized	1<Re<1000	$12/\sqrt{\mathrm{Re}}$ (8)
Newton	Re>1000	approx. 0.5 (9)

Setting up a force balance on a single particle and solving it for the settling velocity, we obtain the following:

$$u = \sqrt{\frac{4g}{3C_D} \frac{\Delta\rho}{\rho_F} d_S} \qquad (10)$$

Since the Reynolds number is dependent on the velocity, it was necessary to run iterations and take care in implementing the appropriate approximation.

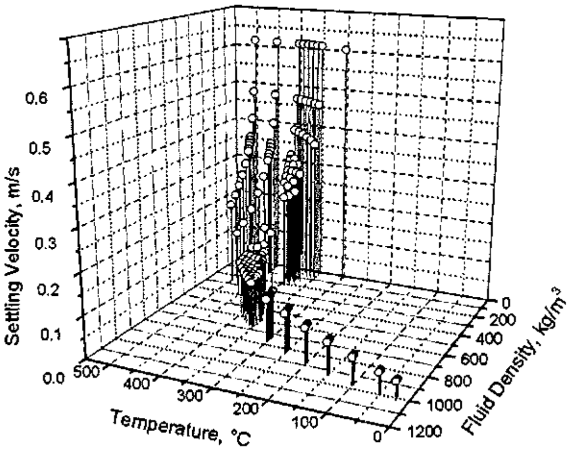

Figure 3. Settling velocities from ambient to supercritical conditions

The settling velocities are determined for temperatures and pressures ranging from ambient to 600°C and 300bar, respectively. The fluid is considered as pure water, and the properties are calculated using NBS steam tables [4]. The exemplary chosen solid is a spherical particle consisting of copper and has a diameter of 100μm.

The settling velocity is plotted in Figure 2 over the temperature and the fluid density. Therefore, the plot relates three important figures within the SCWO of solids: the temperature which has a significant effect on the destruction kinetic and, hence, on the length of the reactor; the density which affects the size of the plant; and the settling velocity which is an indicator for solid behavior within the process. The spreading of the data points reflects the supercritical behavior, as the density is dependent on both temperature and pressure.

As a result of this investigation, we found that the settling velocity can increase by a factor of six. For less dense particles, of course, the effect is even more dramatic since the difference in density between solid and fluid is slighter.

Further investigation was carried out on the transport of solids through the suspension flow reactor. The density of the suspension ρ_m depends on the mass concentration c_m, the fluid density ρ_F and the solid density ρ_S and can be expressed as follows:

$$\rho_m = c_V \rho_S + (1 - c_V)\rho_F \tag{11}$$

whereby the volumetric concentration is given as follows:

$$c_V = \frac{1}{1 - \frac{\rho_S}{\rho_F} + \frac{\rho_S}{\rho_F} c_m} . \tag{12}$$

There are several models for determining the critical velocity at which the suspension is carried through the pipe without saltation and with about the same velocity as the fluid described in the literature. Two of them were chosen to predict the slurry flow behavior:

- model 1 according to Spells for keeping particles in suspension – for horizontal pipes of 0.025m to 0.30m diameter d_i [5]:

$$v_c^I = \left(0.0251 \left(d_i \frac{\rho_m}{\eta_F} \right)^{0.775} g d_S \left(\frac{\rho_S - \rho_F}{\rho_F} \right) \right)^{\frac{1}{1.225}} \tag{13}$$

- model 2 developed by Davies, and Oroskar and Turian [6,7] and success-fully used for an SCWO application treating solids [8]

$$v_c^{II} = f_{Susp} \left(\frac{\rho_F}{\eta_F} \right)^{0.09} \left(2g \frac{\rho_S - \rho_F}{\rho_F} \right)^{0.54} d_i^{0.46} \tag{14a}$$

where

$$f_{Susp} = 1.08 (1 + \chi c_m)^{1.08} (1 - c_m)^{(0.55n)} d_S^{0.18} . \tag{14b}$$

The plug flow velocity is given by equation (3).

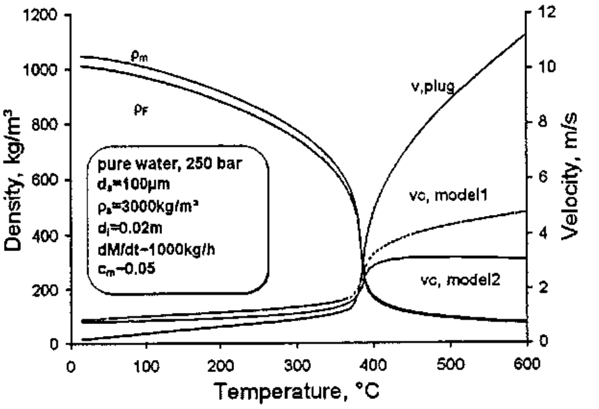

Figure 4. Fluid and suspension density and tube and critical velocities over temperature

Although the settling velocity increases with elevating temperature due to the changes in fluid density and viscosity, the plug flow velocity inside the PFR is far enough away from the critical velocities with respect to both models at supercritical temperatures at all times. In fact, the bottleneck for conveying the solids through a suspension reactor is not the supercritical region but, instead, the region at ambient or subcritical temperatures at which the fluid is still a liquid. This characteristic was also experienced at the ICT bench scale plant.

Kinetics

Degradation during SCWO is usually modeled by means of a power law for the reaction rate [9,10]:

$$r = k[Org]^a [H_2O]^b [O_2]^c \tag{15}$$

with the Arrhenius expression

$$k = k_\infty \exp(-E_A / \Re T) . \tag{16}$$

For our specific complex waste, the kinetic was investigated in MIT's CSTR system, which is described in detail in [11]. The temperature was varied from 400° to 480°C while the pressure was kept constant at about 275bar. The waste concentrations were so low that the generation of water was negligible. The supply factor of oxygen based on the stoichiometric amount was set as two or slightly higher. The residence time was, as a rule, approx. 1.2min.

The kinetic parameters were regressed to the following values as a preliminary result using a very simple model with $a=1$ and $b=c=0$ and with no further dependency [12]:

$k_\infty = 1.6 \cdot 10^5$ and $E_A = 41 kJ/mol$.

Once we also know the heat value and roughly the chemical composition of the waste, especially of the reacting constituents, we can simulate the operation of the PFR. The results are shown in Figure 5. The SCWO system is modeled with a cold stream injection which prevents gluing and sticking of the polymers. The water-oxygen stream is heated to 400°C and the system pressure is set at 275bar. Any heat transfer and any heat capacity, e.g. of the inerts and the metals in the sludge, are neglected. It turns out that the concentration should not exceed 10 wt.-% in order that the temperature constraint of 600°C for the commonly used tubing material Inconel 625 may be observed.

One might argue that cooling the reaction part of the tube allows a higher concentration to pass through the SCWO system. However, not only would the reaction be slower but also the conversion into CO_2 would drop, as Figure 6 indicates.

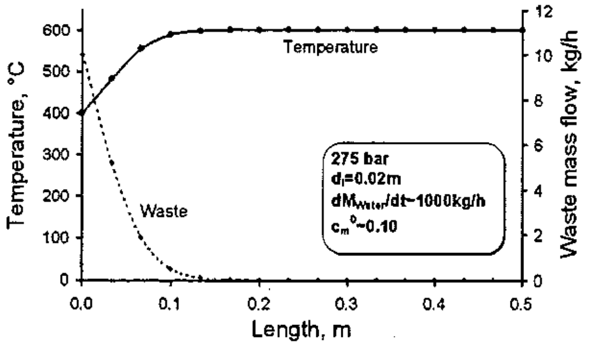

Figure 5. Profiles of the temperature and of the waste concentration along the tubular reactor

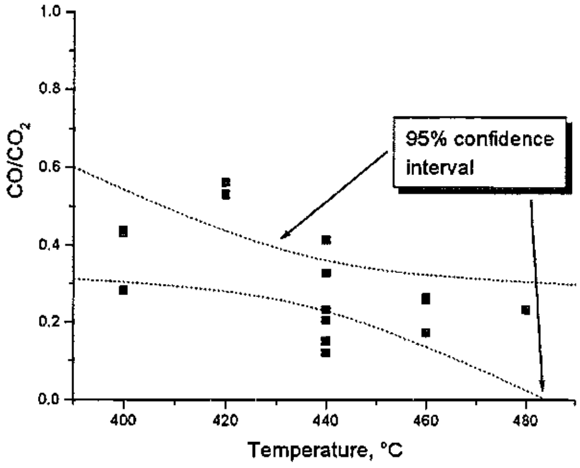

Figure 6. Measured CO/CO_2-ratio for the observed reaction

Process Envelope

Two major parameters which are of interest are waste concentration and mass flow. The limitation on the concentration has already been shown. Furthermore, depending on the concentration, we can obtain minimum mass flow rates by calculating the minimum velocities at which particles are conveyed through the cold part of the tube; see Figure 7.

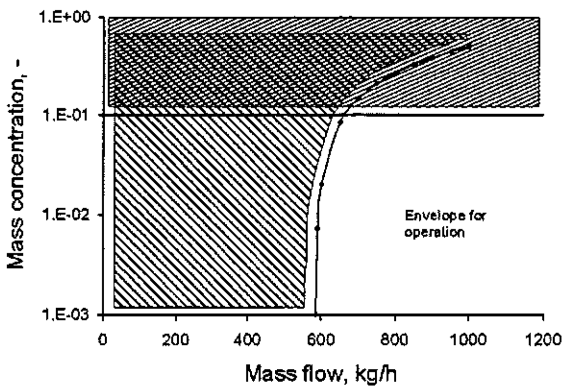

Figure 7. Process envelope for solids and geometry as per Figure 4 at 300°C and 275bar

In order to allow a minimum residence time but also to keep the transportation of the solids feasibly long, small tubular reactors are the best choice.

Cooling of the reaction zone is an option in order to increase the concentration. However, it results in a longer residence time, and hence in a longer reactor tube. Basically, this requires an economic trade-off study.

Conclusions

The above considerations and models enable us to move towards an optimal system, observing decisions on the basic configuration made earlier. We can vary the geometry and the operating conditions and simulate the general response. Of course, there some shortcomings remain to be overcome, in particular the extrapolation of the kinetics at higher temperatures and the fact that we neglected heat transfer and heat capacities in our first approach. However, a process envelope may be given and design studies performed.

References

1. Haepp, H.J.; Melchiorre, M.; Jakob, R.; *Umwelt*, **1996**, 26(11/12)

2. Melchiorre, M.; Jakob, R.; Daimler-Benz AG, Internal Report, 1995

3. Pilz, S.; In. VDI-Seminar „Technologien zur stoff-lichen/energetischen Verwertung von Abfällen in metallurgischen/thermischen Prozessen"; September 24-25, 1998; Düsseldorf, Germany

4. Haar, L.; Gallagher S.; Kell, S. "NBS/NRC Steam Tables", Hemisphere Publ. Corp.; Washington; 1984

5. Spells, *Trans Inst. Chem. Eng.*; **1955**; 33, 97-84

6. Davies, J.T.; *Chem. Eng. Sci.;* **1987**, 42(7), 1667-1670

7. Oroskar, A.R.; Turian, R.M.; *AIChE Journal*, **1980**, 26 (4), 550-558

8. Modell, M.; In: 2nd Int. Conf. On Solvothermal Reactions, December 18-20, 1996, Takamatsu, Japan

9., Li, L.; Chen, P.; Gloyna E.F.; *Supercritical Fluid Engineering Science Fundamentals and Applications*; ACS Symp. Series No. 514, 24, 306-313, 1993

10. Meyer, J.C.; Marrone, P.A., Tester, J.W.; *AIChE J.*, **1995**, 41(9), 2108-2121

11. Marrone, P.; Ph.D. Dissertation, MIT, Cambridge, MA, 1998

12. Pilz, S.; Vogel, F., Peters, W.A., Tester J.W.; "Supercritical Water Oxidation of printed circuit boards – Degradation efficiencies and product yields for a continuously operated stirred tank reactor", in preparation

Electrochemical Aspects of Inorganic Film Deposition from Supercritical Aqueous Solutions

Jennifer I. Brand* and Ali O. Sezer
Department of Chemical Engineering
University of Nebraska
Lincoln, NE 68588-0126 USA
jbrand@unl.edu FAX (402) 4726989

Significant electrical potentials can develop during the deposition of films and particles from supercritical water solutions. The source of these potentials can be process-induced electrokinetics or externally applied voltages. Results of previous experiments from this research group have shown that electrokinetic potentials and applied biases affect the crystallinity, morphology, and deposition rates of ceramic and carbon films from aqueous supercritical jets. These potentials can be predicted by electrokinetic theory when there is a charge transfer between the double layer in a fast flowing fluid and its conduit.

One standard method to investigate the effect of potentials in electrochemical solutions is to construct "Pourbaix diagrams" which are basically phase diagrams presenting the Gibbs free energy in terms of pH and electrical potentials. Pourbaix diagrams are difficult to construct for aqueous solutions at high pressures and temperatures. This work also introduces the rigorous calculations of high pressure and temperature Pourbaix diagrams needed to describe the supercritical deposition process.

Introduction

Inorganic species dissolved in near-critical or supercritical water were first investigated by Hannay and Hogarth over a century ago [1-4]. In addition to their scientific interest, such solutions have great economic importance in a variety of fields. Naturally occurring mineral-rich waters or brine solutions at high temperatures and pressures are important in the formation of geological features such as ore deposits. In power production, near-critical and supercritical solutions occur in turbines and nuclear reactors, where dissolved solids cause materials problems by both deposition and corrosion. Similar problems are encountered in the oxidation processes for the destruction of organics in wastewaters. An environmentally benign process to deposit ceramic films and particles from supersonic jet expansions of such solutions is being perfected at the University of Nebraska Supercritical Fluids Processing Laboratory. The deposition process is merely a rapid expansion of an undersaturated aqueous supercritical solution[5]. The expansions in high pressure turbines and other flowing systems can be viewed as analogous in many respects, with a major difference being that the deposition products are unwanted scale and corrosion.

In the film deposition process, as in power generation processes, the expanding high temperature, high pressure solutions are moving rapidly over "stationary" surfaces. Electrokinetic theory predicts that in such cases, a double layer will be created at the interface of the stationary solid and the flowing fluid. Charge transfer will occur as this double layer is sheared. The magnitude of the "streaming potential" created by this flow is given by:

$$\Delta\Phi = \frac{\varepsilon\varsigma}{\kappa\eta}\Delta P \qquad (1)$$

where Φ = streaming potential, ς = zeta potential, κ = solution conductivity, ε = permittivity, ΔP = the pressure drop in the fluid, and η = viscosity [6]. In expansion processes of supercritical solutions, pressure drops can be high (over 30 MPa), viscosity low (10^{-6} poise), and the other properties will depend on the concentration of ionic species in the water. Even for pure water, the generated potentials in supercritical expansions can be quite significant.

Experimentally, it is easier to measure streaming currents than streaming potentials. Streaming currents in water jets have been reported and modelled in the literature[7,8,9]. In the supercritical system, the existence of the double layer shearing was confirmed by streaming current measurements. These measurements gave streaming currents up to 2 orders of magnitude higher than expected from the dissociation of water alone based on pH predictions using Marshall and Franck[10].

Electrochemical influences on the deposition process would be expected to manifest themselves in two ways: 1) the thermodynamic equilibrium within solution being expanded might shift under the influence of these fields, and 2) any deposition at the surface-solution interface might be influenced by induced or applied biases on the surface or by electrokinetic changes of the species in the expansion.

The experimental work at Nebraska, which included applied bias voltages as well as the electrokinetic, flow-induced voltages, has verified that both effects occur. This paper will concentrate on the theoretical and computational methods developed to predict these effects, using the carbon-water system as an example. The method should be generally applicable.

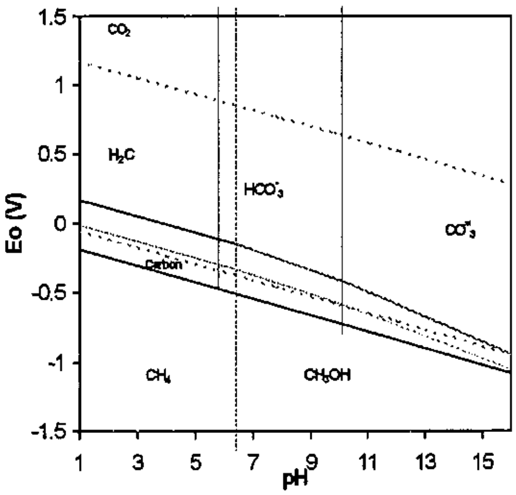

Figure 1. The carbon-water system at 25 C and 0.1 MPa

Experimental Methods

Film and particle deposition equipment has been described in detail elsewhere[5]. Pressurized water is heated before entering a dissolving cell where it contacts an inorganic solute at supercritical conditions, forming a solution, which is then expanded through a nozzle to form a free jet. After expansion, the solution and condensates can be either be collected as a film or passed on to a quadrupole mass spectrometer for time-of-flight or compositional analysis. The temperature of the substrate on which the films are grown may be regulated. Streaming current was measured at the nozzle using a Keithly electrometer.

Computational Methods

One common method to investigate the effect of potentials in electrochemical solutions is to construct "Pourbaix diagrams"[11]. Pourbaix diagrams are phase diagrams of aqueous systems constructed by writing the Gibbs free energy in terms of pH and electrical potentials. Pourbaix diagrams are routinely used by electrochemists to study corrosion, electrodeposition, and similar processes. On Pourbaix diagrams, regions of corrosion and passivation are delineated by the indicated regions of thermodynamic stability of various dissolved species.

Pourbaix diagrams are routinely constructed for conditions at 25 C and 0.1 MPa.. For the near-critical and supercritical systems, there are few published calculations, in part because the rigorous calculations are not trivial [12,13]. When high temperature diagrams have been published, pressure effects have often been assumed to be negligible. If the rigorous calculations are done to describe the equilibria in the high pressure, high temperature solutions, it becomes apparent that the pressure effects can be significant.

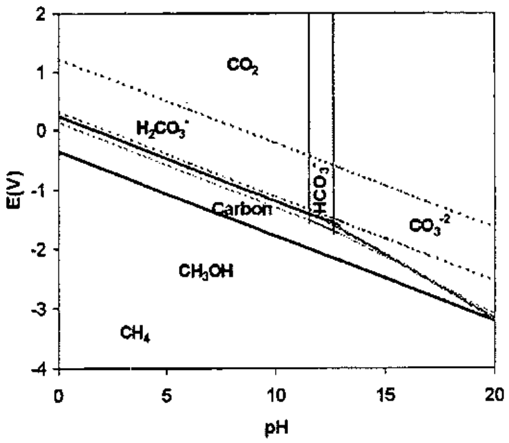

Figure 2. The carbon-water system at 400 C and 50 MPa

In order to calculate the diagrams, the species and reactions of interest must be determined. After they are determined, the rigorous calculations, using the HKF method, can be done using SUPCRT92 [14]. For any species not in the data base, literature values must be found and used for Gibbs free energy of formation. For the Pourbaix diagrams shown below, only C_1 species were considered, both as CO combinations and as methane and methanol. With the hydrogen and oxygen combinations, a total of 12 species and 14 reactions were specified.

Results and Discussion

Figs. 1 and 2 are the Pourbaix diagrams for the carbon-water system at 25 C and 0.1 MPa and 400 C and 50 MPa, respectively. In the calculations, the pressure effects were found to be higher for charged than neutral species. One of the most striking aspects of the comparison of the two figures is that in the high pressure, high temperature figure, the stability region of water is considerably reduced.

For the film deposition process, this reduced stability region for water means that operating with a small negative potential can mean the products would be expected to be anhydrous, in spite of the overwhelming preponderance of water in the system. Indeed, experimental analysis of the films produced confirms this.

There are also implications for other applications, especially where corrosion and scaling are to be avoided. Both of these are functions of the ionic species present, as well as the free hydrogen ions. Investigating the existing species in the water might indicate how controlling potentials may lead to passivation protection from corrosion.

In addition to the anhydrous nature of the films, with the applied negative biases, films became more diamond like, as shown by Raman, x-ray diffractions, and transmission electron microscopy. Adhesion to the deposition substrate varied directly with the hyperbolic sine of the bias, in agreement with the adhesion theory of Derjaguin[15].

Conclusions

Electrochemistry is very important in high pressure, high temperature water systems. The self-induced electrokinetic potentials in flowing systmes can influence both the reactions which occur in solution, as well as those at the interfaces of the fluid and the solid, where corrosion, scaling, or desired product formation takes place. The HKF scheme for calculating the equilibrium Pourbaix diagrams at temperature and pressure is a useful tool in predicting system behavior and optimizing operating conditions.

References

1. Hannay, J. B. and James Hogarth. "On the Solubility of Solids in Gases (Preliminary Notice)". *Proc. of the Royal Society of London.* **29**(1879) 324-326.

2. Hannay, J. B. and James Hogarth. "On the Solubility of Solids in Gases. I" *Proc. of the Royal Society of London* **30**(1880) 178-188.

3. Hannay, J. B. "On the Artificial Formation of Diamond". *Proc. of the Royal Society of London.* **30**(1880) 188-189.

4. Hannay, J. B. and James Hogarth "On the Solubility of Solids in Gases. II" *Proc. of the Royal Society of London* **30**(1880) 484-489.

5. Brand, J. I. and D. R. Miller. "Ceramic Beams and Thin Film Growth," *Thin Solid Films* **166**(1988)139-148.

6. Brett, C.M.A and A. M. O. Brett *Electrochemistry: Principles, Methods, and Applications.* Oxford Science Publications. Oxford. 1993.

7. Faubel, M. and B. Steiner. "Strong Bipolar Electrokinetic Charging of Thin Liquid Jets Emerging from 10 µm PtIr Nozzles" *Ber.Bunsenges. Phys.Chem.***95**(9) 1993

8. Kolgatin, S. N. "Simple model for investigating the dynamics of the developed stage of fast electrical discharge in gases and liquids". *Tech Phys.* **40**(7) 1995.

9. Shiryaeva, S. O. and A. I. Grigor'ev.. "Applicabitiy of variational principles in calculations on the electrohydrodynamic spraying and flow of liquids". *Tech Phys.* **40**(2) 1995.

10. Marshall, William L. and E. U. Franck "Ion Product of Water Substance, 0-1000 C, 1-10,000 Bars". *New International Formulation and Background Journal of Physical Chemistry Reference Data* **10**(2) 295-304. 1981.

11. Pourbaix, M *Altas of Electrochemical Equilibria in Aqueous Solutions.* NACE. Houston. 1974.

12. Cubicciotti, D. "Pourbaix Diagrams for Mixed Metal Oxides--Chemistry of Copper in BWR Water" *Corrosion* **44**(12) 875. 1988.

13. Kriksunov, L. and D. D. Macdonald. "Potential-pH Diagrams for Iron in Supercritical Water."

14. Johnson, J. W.E. H. Oelkers, H. C. Helgeson "SUPCRT92: A software package for calculating the standard molal thermodynamic properties of minerals, gases, aqueous pecies and reactions from 1 to 5000 bar and 0 to 1000 C" *Computers & Geosciences* **18** (1992) 899.

15. Derjaguin, B. V. and V. P. Smilga "Electronic Theory of Adhesion" *Journal of Applied Physics* **38**(12) 4609. 1967.

Corrosion of Titanium under SCWO – Conditions.
Recent Results.

N. Boukis, C. Friedrich, E. Dinjus
Forschungszentrum Karlsruhe, Institut für Technische Chemie CPV, P.O. Box 3640,
D- 76021 Karlsruhe, Germany
EMAIL: nikolaos.boukis@itc-cpv.fzk.de
FAX : +49 7247 82 2244

Abstract

The Super Critical Water Oxidation process is very effective in destruction of hazardous aqueous wastes containing organic contaminants. During oxidation of acidic chlorine, sulfur or phosphorus containing wastes the corrosion of reactor material proceeds very fast. Test tubes made of Ni-base alloys and lined with Titanium grade 2 are used as reactors and examined after experiment. Typical experimental conditions are temperatures up to 600 °C and pressures up to 34 MPa.

The corrosion of Titanium grade 2 in 0.1 - 0.2 mol/kg sulfuric acid solutions with 1.5 – 3 mol/kg O_2 under certain T, p conditions is too high for technical applications

Introduction

Organic compounds can be oxidized with oxygen in the Supercritical Water Oxidation process (SCWO). Due to the low density and dielectric constant of supercritical water ($T \geq 374°C$, $p \geq 22.1$ MPa), its solvancy for organic compounds and oxygen is high and the conversion of organics into carbon dioxide and water is fast. In the presence of heteroatoms, the corresponding mineral acids are formed additionally.

The common heat resistant materials like Ni-Base alloys and stainless steel, failed in acidic solutions under SCWO conditions.

Titanium grade 2 has been found to be well corrosion resistant in oxygen containing ([O2]=3 mol/kg) hydrochloric acid solutions even under SCWO conditions [1, 2]. Only some general corrosion, far less than 40 µm/100 h was measured. In sulfuric or phosphoric acid solutions corrosion of titanium is considerably faster than in HCl of the same concentration. In both cases acid concentration was up to 0.2 mol/kg ([O2]=3 mol/kg) and no localized corrosion was observed [2]. In the present work the results of the detailed metallographical analysis of the experiments with H2SO4 solutions are discussed.

Corrosion tests

Titanium grade 2 - lined tube reactors were used for the corrosion tests. By this experimental technique the whole temperature range from room temperature up to the maximal experimental temperature is covered in a single experiment and titanium is tested under typival SCWO - conditions.

The outer pressure tubes were made of a Ni-base alloy. The liners were thin-walled (0.5 mm) tubes made of titanium grade 2 with an ID of 7.4 mm and 1000 mm length. Both ends of the liner were welded or bonded to the outer pressure tube. The accuracy of the liner's wall thickness measurement is ± 25 µm.

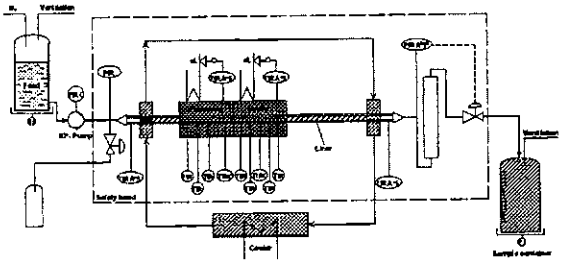

Experimental setup for the corrosion tests

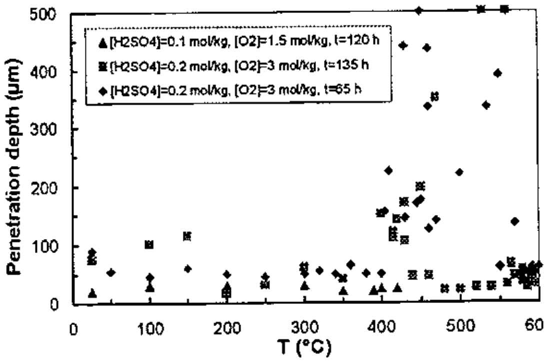

Corrosion penetration depth of Ti-liners after exposure to H_2SO_4 as function of the temperature, p ˜ 25 MPa

During the experiment, the temperature of the solution increased from ambient values at the entrance of the reactor up to the maximum temperature (450 or 600 °C) in the middle part of the reactor and falls again to ambient values in the outflow part.

The temperature of the reactor material is very close to the temperature of the solution due to the low flow velocity. The temperature profile of the reactor was measured.

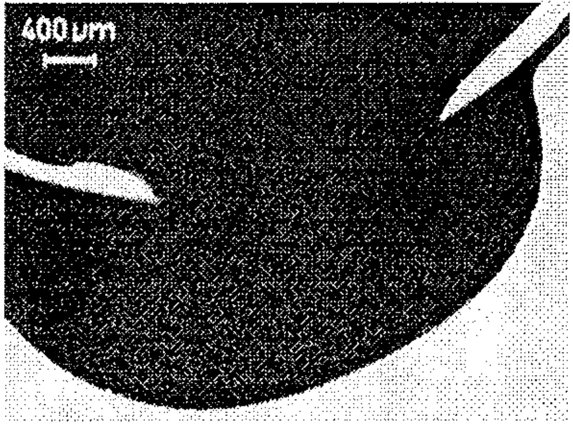

Cross section of the reactor after exposure to 0.2 mol/kg H_2SO_4 and 3 mol/kg O_2. T=450 °C, p=25 MPa, t=65 h.

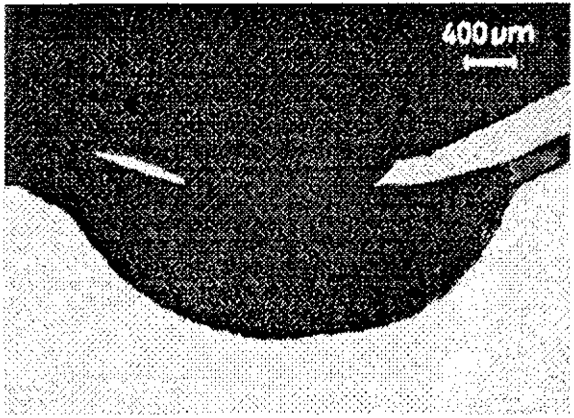

Cross section of the reactor after exposure to 0.2 mol/kg H_2SO_4 and 3 mol/kg O_2. T=530 °C, p=27 MPa, t=135 h.

Metallographical analysis of the entrance and middle part of the reactor shows acceptably low corrosion rates. The highest corrosion rates are measured in the outflow part of the reactor. There, at temperatures between 450 and 600 °C the upper part of the liner was completely dissolved. This behavior is still not completely understood and further experiments are necessary.

Conclusions

In 0.2 mol/kg sulfuric acid solutions titanium grade 2 shows corrosion rates in the order of 0.5 mm/100 h above 400 °C.

The use of liners made of this material is not recommended in the temperature range from 400 to 600 °C.

Literature

[1] Boukis, N.; Friedrich, C.; Dinjus, E.: Titanium as reactor material for SCWO applications. First experimental results. NACE, Corrosion '98, Paper Nr. 98417, USA, 1998.

[2] Friedrich, C.: Das Korrosionsverhalten von Titan und Titanlegierungen während der Oxidation in überkritischem Wasser. PhD Thesis, Universität Heidelberg, in press.

GVC-Fachausschuß „High Pressure Chemical Engineering“, March 3-5, Karlsruhe, Germany, 1999

The SCWO-Destruction of Organic Compounds in the Presence of Salt in Leachates from Dump Sites in the SUWOX-Facility

H. Schmidt*, S. Baur, V. Casal
Forschungszentrum Karlsruhe
Institut für Angewandte Thermo- und Fluiddynamik
P. O. Box 36 40, 76021 Karlsruhe, Germany
E-mail: secretary@iatf.fzk.de
Fax: +49 (0)7247 82-4837

The SCWO-process is accompanied with the inconvenience of the reactor material corrosion, and the precipitation of salts. For the treatment of hazardous aqueous waste the SUWOX-process presents the solution of both these problems.

Material corrosion is overcome by the development of a double wall reactor. In case of acid formation in the supercritical reaction, alumina is used as a suitable housing material.

The precipitation of salts is avoided by the appropriate adjustment of the operating conditions. In this way > 90 % of the salts dissolved in the investigated leachates pass the entire process. A minor portion of the salts requires the pre-separation before entering the process.

Introduction

The Supercritical Water Oxidation (SCWO-) process brings together water, the organic pollutant and oxygen at temperatures of 400 - 600 °C and pressures of >250 bar [1]. Under these conditions water possesses a high solubility for organics and a complete miscibility with oxygen [2]. A high reactive single fluid phase exists where the inherent transport limitations of multi-phase systems are absent. As a result, the oxidation rates are very rapid, and high destruction rates are obtained inside small volumes of fully contained systems [3]. Many of the hydrocarbons however, contain heteroatoms, such as chlorine or other halogens, sulfur and phosphorus which form acids. These acids together with oxygen dissolved in supercritical water represent a highly corrosive fluid system, and the pressure vessel materials available today do not withstand this attack [4]. The possible neutralization of the acids brings along the formation of salts. These salts and more important, the salts dissolved in the industrial and municipal organic waste water streams, precipitate at supercritical conditions causing blockages inside the components of the facilities [5]. These two problems of material corrosion and salt precipitation prevented, up to now, the practical application of the SCWO-process. At the Forschungszentrum Karlsruhe, a novel SUWOX- (Superkritische Wasser Oxidation) facility was developed which overcomes both of the problems and provides the technical requirements for an environmentally friendly destruction of hazardous aqueous waste in supercritical water.

Reactor Design

To cope with the problem of material corrosion a concentric double wall reactor was developed [6] consisting of an external pressure vessel and an inner reaction vessel (Fig. 1).

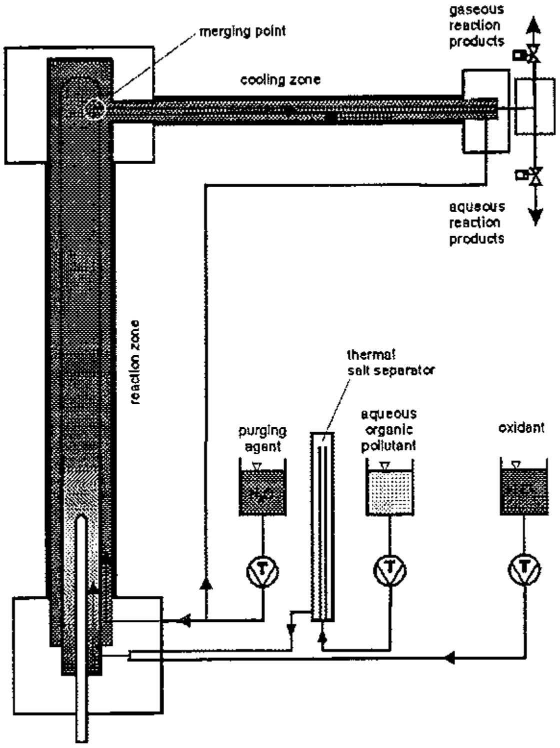

Figure 1. Scheme of the SUWOX-Facility

The pressure vessel is made of a licensed stainless steel or nickel base alloy. The confinement of the SCWO-reaction is ensured by an impermeable, corrosion-resistant reactor material, e. g. ceramic or metal. Between the inner wall of the pressure vessel and the external wall of the reactor vessel, a small annulus is located. Inside this annulus a sparse flow of inert water serves as a coupling medium between the two confinements with respect to pressure and temperature.

Both process streams, the organic pollutant solution and the hydrogen peroxide, used as the oxidant, are pumped to system pressure and intensively mixed just before entering the reaction vessel. In the first section of the vertical upward flow, they are heated up to the desired supercritical reaction temperature. The destruction of the pollutants takes place inside the vertical, temperature-controlled reaction zone.

In a horizontal effluent zone, heat is removed by a second concentric annular flow. Thus subcritical temperatures are reached inside the central, corrosion resistant effluent tube.

The two annular flow streams join at the top of the vertical part of the facility and penetrate the inner reactor housing via a small annular gap. They merge in the central upflow, and when joined together leave the rector through the horizontal effluent tube. Therefore this design of the facility ensures that the corrosion resistant parts are not exposed to mechanical load and the pressure vessel does not undergo chemical attack by the reaction products.

Operating conditions

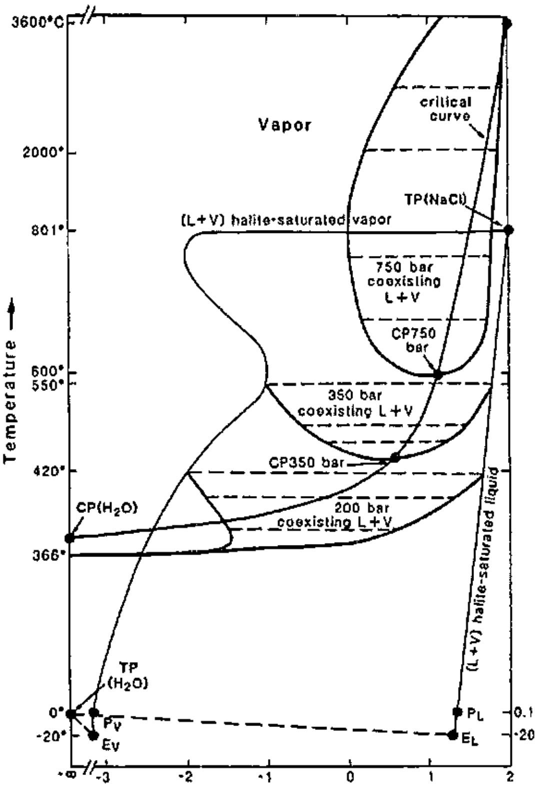

Figure 2. T-x Diagram, H_2O-NaCl [8]

The technical realization and the experimental testing of the SUWOX-facility was followed by extensive investigations of the influencing process parameters, using the industrial solvent dichloromethane as the pollutant. The experiments were carried out at pressures of 250 bar to 420 bar, and temperatures of 300 to 460 °C. High destruction rates of > 99.99 % are measured depending on the O_2-stoichiometry, and total oxidation to carbon dioxide is obtained at residence times between 40 and 220 sec [7].

In these experiments pH-values of ≤ 1 are achieved, thus demonstrating the save confinement of highly corrosive conditions and the practicability of the SUWOX-facility.

The second problem, the precipitation of salts at supercritical conditions, is managed by taking a process operational action: the increase of the system pressure. The slope of the critical curve of the system H_2O-NaCl is shown in Fig. 2, indicating a pressure-temperature-concentration-dependence [8]. The diagram shows the appearance of multiphase regions along the critical curve in which the precipitation of salt will occur. However, the diagram also shows that while the temperature is kept constant the area of homogeneous solution remains present with increasing pressure. This means that the precipitation of salt can be prevented by the augmentation of the system pressure, i. e. by increasing the density.

Salt concentration, Feed	10 % NaCl	13 % NaCl + H_2O_2	10 % NaCl + H_2O_2 + CH_2Cl_2	4,81 % (NaCl + Na_2SO_4)	4,67% (NaCl + Na_2SO_4)
Operating conditions					
p [bar]	400	400	402	400	481
T [°C]	420	421	423	421	422
O_2-stoichiometry	---	---	2	---	---
Input [g/h]					
NaCl	110	111	103	2.32	2.22
Na_2SO_4	---	---	---	2.32	2.22
H_2O_2	---	6.26	13.0	---	---
CH_2Cl_2	---	---	5.6	---	---
Output [g/h]					
NaCl	109	111	108	2.35	2.28
Na_2SO_4	---	---	---	1.30	2.25
CH_2Cl_2	---	---	$2 * 10^{-3}$	---	---
Material transfer					
NaCl [%]	99.1	100	105	101	103
Na_2SO_4 [%]	---	---	---	56.0	101
Destruction rate [%]	---	---	99.96	---	---

Table 1. Solubility of Salt at T = 420 °C, p = 400 bar and 480 bar

As shown in Tab. 1 the NaCl is kept in soluble state at p = 400 bar and T = 420 °C, and the simultaneous destruction of dichloromethane is obtained. In the presence of an additional salt component, Na_2SO_4, augmenting the pressure to p = 481 bar, i. e. increasing the density from $\rho_{400} = 0.42$ g/cm^3 to $\rho_{480} = 0.5$ g/cm^3, is required to maintain both salts in the supercritical solution. The necessity of a high fluid density to keep the salts in solution during the SCWO-process, requires operating conditions at which the number value of the system pressure (in bar) is located above the reaction temperature (in °C) ($p > T$). This means a turn-around of the operation parameter values with respect to the "normally considered" SCWO-process operating conditions ($T > p$). Our experiments and the literature indicate that the efficient destruction of the pollutants under these changed operating conditions further exists.

Experimental Results

The aim of the experimental investigations is to prove the destruction of authentic harmful substances in the SUWOX-facility. Therefore, the leachates from dump sites are considered to be the suitable subject for testing. These aqueous species of waste are characterized by the load of organic pollutants and of inorganic salts. Successful testing requires the proper adjustment of the operating variables to achieve complete destruction of the organics and to prevent the precipitation of salts.

The experiments were started using the leachates of a municipal dump site as the pollutant. These waste waters are less characterized by high, or in particular dangerous load of pollutants - the DOC-value is in between 360 to 660 mg/l - but rather by the presence of salts in the range of g/l.

In the first experiment, the operating conditions were adjusted to a system pressure of 480 bar and a reaction temperature of 425 °C. The O_2-stoichiometry was 2.7 and the residence time was between 4 to 5 min. Under these conditions, the expected results could not be achieved. Neither the complete destruction of the organic compounds, nor the throughput of the salts in aqueous solution was obtained.

The destruction rate is analyzed to be 93 % in the aqueous phase. The main oxidation product, however, is CO_2, smaller portions of CO, CH_4 and H_2 are measured in the effluent of the gas phase. The amount of sulfate analyzed in the aqueous effluent is 62 %, and the precipitation of salt is observed inside the reactor.

The augmentation of the system pressure to 500 bar, while keeping the reaction temperature constant at 425 °C, leads to a significant improvement of the experimental results. A material destruction rate of 99.32 % is attained, and the components in the gaseous effluent are analyzed exclusively as CO_2 and O_2. The measured TE-values of PCDD/F are in the range of the facility's bank value. The main constituents of the salts: chloride, sulfate, nitrate, sodium and potassium ions remain in solution and thus are passing the facility. The calcium and magnesium ions remain, to a certain amount, in the solution. The missing portions of the latter ions are detected as thin, locally restricted areas of precipitation in the heating zone of the reactor. They are analyzed as $CaSO_4$ and $Mg(OH)_2$, with minor portions being Ca-Mg-Si-mixed oxides.

A considerably more demanding medium tested in the SUWOX-facility is the leachate water of an industrial dump site. It is characterized by the high concentration of dissolved salts of 200 g/l. The DOC-value is 6 g/l and the COD-value reaches 15 g/l. About 5 % of the dissolved organic compounds consist of highly environmentally dangerous pollutants, such as: aromatic hydrocarbons, volatile halogenated hydrocarbons, chlorobenzenes, chlorophenols, polychlorinated biphenyls and chloroanilines. The TE-value of PCDD/F is 2 ng/l. This pollutant, not being diposed in Germany, is considered to be a tough milestone for the demonstration of feasibility of the SUWOX-process. To avoid any risks in the first experiment, the leachate is diluted by the factor of ten before processing.

Due to installation reasons, the operating conditions are set to the maximum possible system pressure of 500 bar. The process temperature is set to 426 °C to obtain a high solubility of salts in the supercritical state. The very high supply of oxygen (18-fold O_2-stoichiometry) and the long residence time (8.5 min) are adjusted to gain complete destruction of the pollutants.

Operating conditions	Pressure:	500 bar
	Temperature:	426°C
Effluent		
Gas phase	Oxidation products:	CO_2, O_2, << N_2
Aqueous phase	Input DOC:	503 mg/l
	Destruction rate:	> 99.2 %
Material balance	Oxygen:	100 %
	Carbon:	105 %
Inorganics:	Input [mg/l]	Output [%]
total:	19822	91
compounds:		
- Chloride	11497	88
- Sulfate	317	55
- Calcium	95.0	42
- Silicon	6.3	42
- Magnesium	35.0	94
- Sodium	5345	98
- Potassium	2520	95
pH-value	6.7	6.3

Table 2. Destruction of the Pollutants in Leachates from an Industrial Dump Site

The experimental results are listed in Tab. 2. In the effluent of the gas phase, considerable amounts of the remaining oxygen are analyzed. Besides traces of nitrogen, only carbon dioxide is found. The desired conversion of the organic matter to CO_2 and H_2O is obtained. The rate of destruction is measured to >99.2 % referred to the DOC-amount in the input of the aqueous phase. The quantities of PCDD/F are effectively destroyed. The values attained are located slightly above those of the facility's blank value, and fall below the limitation of direct discharge set by the supervising agency.

The behavior of the inorganic components is also shown in Tab. 2. Besides listing the amount of ions and the pH-value of the input flow of the pollutant, the recovery rates of the ions, and the pH-value in the aqueous effluent leaving the SUWOX-facility are listed. The total amount of ions analyzed in the feed solution is 19.8 g/l, and in the effluent solution 18 g/l of this amount is retained, i. e. 91 % of the salts are passing through the process. About 60 % of the calcium precipitates form a thin layer of $CaSO_4$ in the heating zone of the reactor.

To avoid this undesired deposit of salt the installation of a pressure and temperature controlled pre-precipitation, of the low soluble salts in the organic feed stream, is installed (see Fig. 1). The experimental investigations of the system containing chloride, sulfate, calcium and sodium ions in an aqueous solution, indicate that the precipitation of $CaSO_4$ is attained, whereas the solubility of NaCl and Na_2SO_4 is fully retained (Fig. 3). In this diagram the system pressure is set to 500 bar, and the temperature at which the precipitation occurs is 150 °C. When the system pressure is set to 250 bar, the experimental finding is that a temperature of about 320 °C is required to attain salt precipitation. This indicates that with increasing system pressure the required temperature decreases to achieve the precipitation of $CaSO_4$.

The issues of further investigations in the SUWOX-facility are the behavior of salts in dependence of pressure and temperature, and the demand of oxygen and the required residence time to achieve the complete destruction of the pollutants.

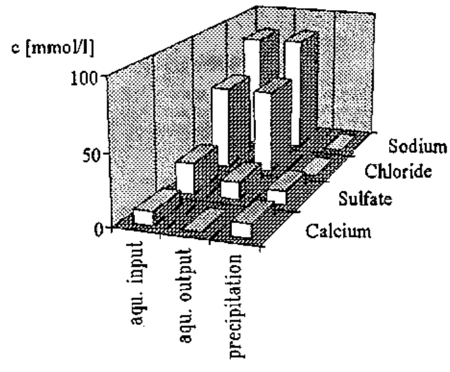

Fig. 3: Precipitation of $CaSO_4$ at $p = 500$ bar, $T = 150$ °C in a salt pre-separator

Conclusions

The SUWOX-reactor is designed in a way that in dependence on the expected problem of corrosion, caused by the components of the pollutants, the appropriate corrosion resistant reactor material can be installed. In cases of the formation of mineral acids during the SCWO-reaction, it has been proven that the use of alumina as a reactor material withstands pH-values < 1 (with the exception of hydrofluoric acid formation) without corrosive damage. Moreover, it is shown that the precipitation of salts at supercritical conditions is substantially prevented augmenting the system pressure. The increase of the water density in the supercritical state to ρ-values of about 0.5 g/cm^3 causes the main components of the salts (s. a. NaCl and Na_2SO_4), being dissolved in the investigated leachates from dump sites, to remain in solution during the supercritical process. At operating conditions of 500 bar and 426 °C, complete destruction of organic pollutants is nearly obtained while >90 % of the salt load passes through the SUWOX-process. The low soluble salts (s. a. $CaSO_4$) precipitate in the heating zone of the reactor. This causes the need to prevent them from entering the process. That can be achieved by a pressure and temperature controlled pre-precipitation of these salts in a small salt separator installed into the organic feed stream before they enter the SUWOX-reactor.

The experiments are continued pursuing the effect of further system pressure increase on the solubility of salts. Furthermore, the requirements of oxygen supply and residence time, to obtain high destruction rates, are investigated.

References

1. Modell, M.: Processing Methods for the Oxidation of Organics in Supercritical Water, U. S. Patent, No. 4, 338, 199, July 6, 1982.

2. Franck, E. U.: Fluids at High Pressures and Temperatures, *J. Chem. Thermodynamics* **1987,** 19, 225-254.

3. Tester, J. W. et al.: Supercritical Water Oxidation Technology, ACS Symposium Series Paper, Atlanta, Georgia, October 1-3, 1991.

4. Latanision, R. M.; Shaw, R. W.: Corrosion in Supercritical Water Oxidation Systems, Workshop, Summary, The Energy Laboratory, MIT, May 6-7, 1993.

5. Armellini, F. J.; Hong, G. T.; Tester, J. W.: Precipitation of sodium chloride and sodium sulfate in water from sub- to supercritical conditions: 150 °C to 550 °C, 100 to 300 bar, *Journal of Supercritical Fluids* **1994,** 7, 147-158.

6. Brans, J.; Casal, V.; Gegenheimer, M.; Schmidt, H: Verfahren zum Schutz innerer Behälterwandungen bei der überkritischen Wasseroxidation, Patentanmeldung P4443078.7, 3. Dez. 1994.

7. Casal, V.; Schmidt, H.: SUWOX - A Facility for the Destruction of Chlorinated Hydrocarbons, *Journal of Supercritical Fluids* **1998,** 7, 269-276.

8. Bischoff, J. L.; Pitzer, K. S.: Liquid-vapor relations for the system $NaCl-H_2O$: Summary of the P-T-x surface from 300 to 500 °C, *American Journal of Science* **1989,** 289, 217-248.

GVC-Fachausschuß „High Pressure Chemical Engineering“, March 3-5, Karlsruhe, Germany, 1999 GVC FZK '99

Simulation of the Thermodynamic Behavior of the Pure Components Water, Oxygen, Nitrogen and Carbon Dioxide and of Their Mixtures for Pressures up to 300bar and Temperatures up to 600°C

Stephan Pilz*
DaimlerChrysler
Research and Technology (FT4/TP)
P.O. Box 2360
89013 Ulm (Germany)
e-mail: Stephan.Pilz@DaimlerChrysler.com FAX: +49 (0)731 505-4231

An equation of state (EOS) based on the well-known cubic Redlich-Kwong-Soave equation (RKS) with three modifications was regressed and used to model thermodynamic properties of pure species and mixtures from ambient to supercritical conditions. These changes involve a volume-translation, an α-function with polar parameters and more sophisticated mixing rules. For all of the investigated substances (H_2O, CO_2, N_2, O_2), inaccuracies occurred close to the critical points and, for higher pressures, around the critical temperatures. However, the average errors of the simulations were remarkably slight in general. The expansion to mixtures was also possible. The simplicity of the EOS and its stability lead to fast and reliable representations of the thermodynamic behavior of these four key substances within the process of supercritical water oxidation (SCWO). Hence, the EOS and its regressed parameters enable simulation of SCWO with only one EOS throughout the whole process. The accurate and easy prediction of the thermodynamic properties is of major interest for setting up mass and energy balances, for performing chemical kinetic investigations, and carrying out flow studies.

Introduction

A major step when modeling chemical processes is the identification of the running conditions and finding an appropriate equation of state to represent the physical properties to a certain extent of accuracy. Modeling of supercritical processes involves some general problems independently of the single process.

High pressure applications move the system away from ideal gas behavior. The system is quite sensitive around the critical point. Neither EOS developed for liquid substances nor EOS developed for gaseous substances have the right background for modeling species in the supercritical region where they exhibit either liquid-like or gas-like behavior depending on the physical property.

Systems involving water experience those problems even more gravely as the system pressure is higher than for other typical supercritical fluids, e.g. carbon dioxide. Also, the sensitivity of water around the critical point is extremely high due to the fact that the hydrogen bonding is partially dismissed and water changes its strong polar attitude into a moderate one [1].

The aim of this work is to support the process modeling of an SCWO application by providing a fairly accurate representation of the physical properties. The scope of the process simulation includes calculation of mass and energy balances for the overall SCWO process (black box) and also for single steps or even along the fluid pathway (glass box).

Considerations for the Equation of State

The process conditions of interest are temperatures and pressures ranging from ambient to 600°C and 300bar, respectively. The main, and dominating, component is water, and its density varies within the process from 1000kg/m^3 to 0.5kg/m^3.

The EOS should represent the density and the enthalpy/heat capacity of pure substances over a wide range of temperatures and pressures fairly well, especially for water. It should be extendible to mixtures of water, hydrocarbons and gases while keeping a reasonable accuracy.

The EOS should be simple in terms of the mathematical configuration in order to keep numerical changes of the parameters predictable. Therefore, it should be explicit either in pressure or in volume. This also enables the calculation of derived properties, e.g. fugacity. Furthermore, the EOS should have just a few adjustable parameters. This keeps the equation stable and the computation fast – a great advantage since the calculation of the physical properties is supposed to support the appropriate simulation of the process, including sensitivity studies and optimization routines, and not to hinder it.

Selected Equation of State

In order to meet the above requirements, a cubic EOS based on the van-der-Waals equation was chosen. The basic structure is a Redlich-Kwong-Soave equation (RKS) [2,3], yet the specific volume is translated through c in order to represent the density more accurately [4,5]:

$$p = \frac{\Re T}{v + c - b} - \frac{a_c \alpha}{(v + c)(v + c + b)} \qquad (1)$$

with the volume translation

$$c = c_0 + \frac{c_1}{1 + c_2 - T_r}, \qquad \text{if } T_r \le 1 \qquad (2)$$

$$c = b + \frac{\left(\frac{(c_0 - b)c_2}{c_1} + 1\right)^2 c_1}{1 + c_2\left(\frac{(c_0 - b)c_2}{c_1} + 1\right) - T_r} \qquad \text{if } T_r > 1 \text{ and } c_1 \ne 0 \qquad (3)$$

$$c = c_0, \qquad \text{if } T_r > 1 \text{ and } c_1 = 0. \qquad (4)$$

Instead of the original RKS-α-function, a function developed by Boston and Mathias (BM) involving polar parameters p_i was used [6]:

$$\sqrt{\alpha} = 1 + m(1 - T_r^{0.5}) - p_0(1 - T_r)(1 + p_1 T_r + p_2 T_r^2), \qquad \text{if } T_r > 1 \qquad (5)$$

$$\alpha(T_r) = \left(e^{c_d(1 - T_r^d)}\right)^2, \qquad \text{if } T_r \le 1 \qquad (6)$$

$$\text{with } c_d = 1 - 1/d \qquad (7)$$

$$\text{and } d = 1 + 0.5m - p_0(1 + p_1 + p_2). \qquad (8)$$

The parameter m shows a slightly different dependency on the azentric factor ω compared to the RKS equation:

$$m = 0.48508 + 1.55191\omega - 0.15613\omega^2. \qquad (9)$$

For the extension to mixtures, Schwartzentruber and Renon (SR) introduced new mixing rules [6]:

$$a = \sum_i \sum_j x_i x_j (a_i a_j)^{1/2}\left[1 - k_{a,ij} - l_{ij}(x_i - x_j)\right] \qquad (10)$$

$$b = \sum_i \sum_j x_i x_j \frac{b_i + b_j}{2}\left(1 - k_{b,ij}\right) \qquad (11)$$

where the temperature-dependent binary interaction parameters are calculated as follows:

$$k_{a,ij} = k_{a,ij}^0 + k_{a,ij}^1 T + k_{a,ij}^2 / T \qquad (12)$$

$$k_{b,ij} = k_{b,ij}^0 + k_{b,ij}^1 T + k_{b,ij}^2 / T \qquad (13)$$

$$l_{ij} = l_{ij}^0 + l_{ij}^1 T + l_{ij}^2 / T \qquad (14)$$

with

$$k_{a,ij} = k_{a,ji}, \quad k_{b,ij} = k_{b,ji} \text{ and } l_{ij} = l_{ji}. \qquad (15a,b,c)$$

The selected and regressed EOS will be referred to as the VTBMSR equation.

Regression Procedure

The literature tabled below was utilized as reference data for the pure substances water, oxygen, nitrogen and carbon dioxide.

Table 1. Reference data for the regression

Species	Source	Number of data points
Water	NBS/NRC Steam Table, 1984 [7]	1232 (v), 977(h), 911 (c_p)
Oxygen	Nat. Std. Ref. Data of the USSR, 1987 [8]; IUPAC, 1976 [9]	720 575
Nitrogen	IUPAC, 1977 [10]	324
Carbon Dioxide	IUPAC, 1973 [11]	2935

There is also some reference data on these conditions available for the binary aqueous mixtures [12,13,14,15] and for the gas mixture N_2-CO_2 [16]. Due to the lack of extensive data on the H_2O-O_2 -system, its similarity to the H_2O-N_2 system has been taken advantage of [17, 18].

The software package AspenPlus^{TM} [19]was used for the regression of the parameters and for the computation of the physical properties, making use of the obtained parameters.

As the temperature and pressure were varied at the same time, the regression was quite likely to be unstable or to abort completely. Hence, the strategy was to regress all three c_i-parameters first and, subsequently, the three polar parameters p_i. Finally, the interaction parameters were gained.

The results are plotted over the intensive numbers as a relative error which is defined as follows:

$$rel.error = \frac{calculated\ value - reference\ value}{reference\ value}. \qquad (16)$$

Results and Discussion

Pure Substances

As mentioned above, water is the key component in terms not only of molefraction but also of its characteristic of changing its thermodynamic behavior dramatically when entering the supercritical region. Therefore, our work focused on this substance.

In Figure 1, the L-V coexistence curve for pure water is plotted according to NBS and several EOS. In addition to the VTBMSR-EOS, the approaches of RKS and Peng-Robinson (PR) [20] were chosen since they are often declared as good high pressure EOS [21]. Furthermore, the Rackett equation [22] is also shown although it is not really an EOS but a density model for liquid phases. The ideal gas correlation is plotted for the saturated gas. The figure demonstrates the power of the VTBMSR-EOS. It is far more accurate than the two other cubic equations. Only for densities close to critical is the Rackett equation superior to the VTBMSR-EOS. This indicates reasonable phase equilibria calculations using the regressed VTBMSR-EOS.

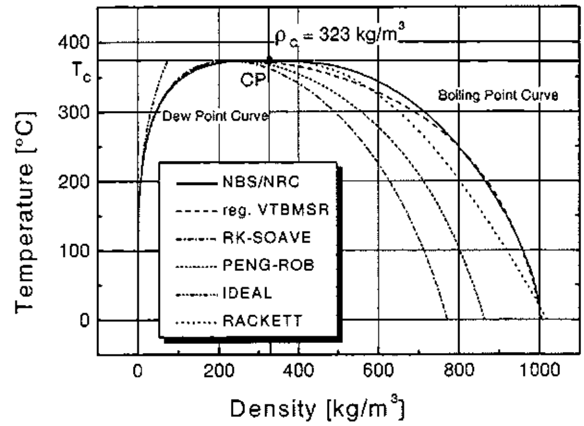

Figure 1. Density predictions for several EOS for H_2O along the L-V coexistence curve

Figure 2 shows the relative error for density calculations using the VTBMSR-EOS and the regressed parameters over the whole range of pressures and temperatures. While the error is largest around the critical temperature, it does not exceed 14%. In the supercritical region, the relative error is approximately 5%.

The approach for the heat capacity of water, which is plotted in Figure 3, is, in general, quite effective. However, for supercritical pressures and around the critical temperature, the error reaches 30%. This is caused by the extreme heat capacity peak at this temperature for supercritical pressure (theoretically, c_p converges to infinity at the critical point [23]). Nevertheless, the VTBMSR-EOS still simulates the behavior best [24].

For the other three components, the errors are slighter or even negligible. Yet, the representation of the thermal and caloric properties reveals some deficiencies of the EOS around the critical point for all of the substances. For oxygen and nitrogen this does not lead to any drawbacks as their critical points are far away from the operating conditions of SCWO. The higher critical values of carbon dioxide might cause inaccuracies when calculating the gas phase separation after the oxidation.

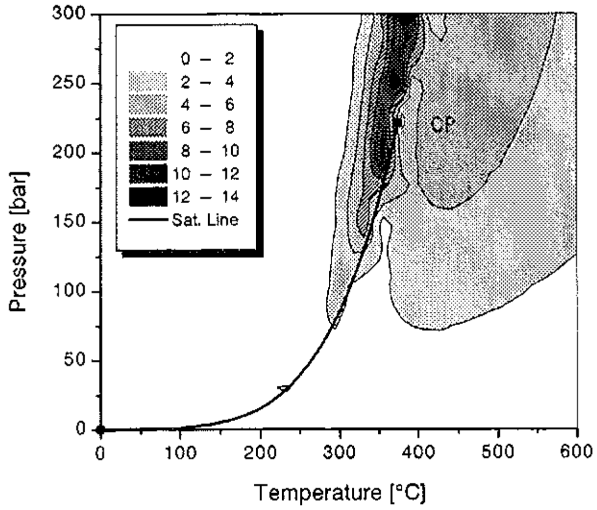

Figure 2. Relative error in specific volume of H_2O

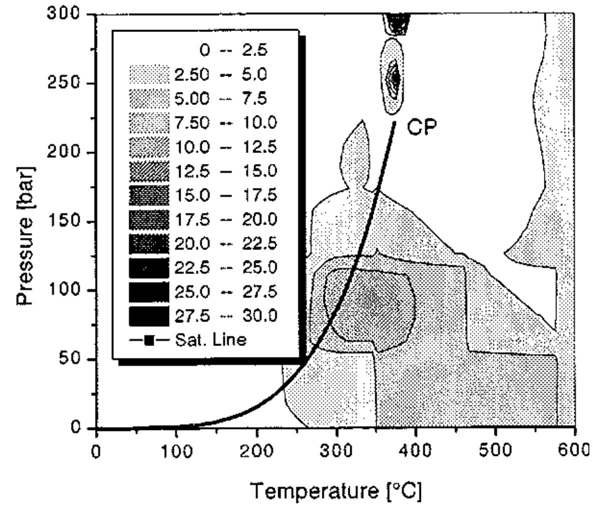

Figure 3. Relative error in the heat capacity of H_2O

Mixtures

Figure 4 illustrates the need for regressing of interaction parameters: the specific volume and the heat capacity of the water-carbon dioxide mixture (x_{CO2}=0.05) are calculated by taking the data of the pure components from the literature and weighting them by the molefraction. The resulting numbers are compared to the reference data of the mixture [13] by computing the relative error. While the specific volume shows a maximum error of about 35% and rapidly converges toward zero at higher temperatures, the heat capacity starts off with substantially greater errors and converges at higher temperatures. However, from approx. 500°C on, the mixtures demonstrate behavior similar to that of an ideal mixture.

Figure 5 sets out the improvement in the simulation of thermodynamic behavior by the VTBMSR-EOS compared to its basic model, the RKS equation. The more sophisticated α-function pushes the calculated caloric values for pure components closer to the real ones [24], but the more advanced mixing rules and the regression of their parameters also contribute greatly to this considerable accuracy.

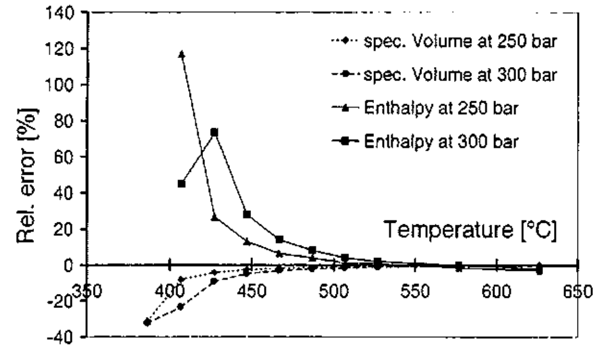

Figure 4. Relative error when calculating properties of the mixture H_2O-CO_2 with x_{CO2}=0.05 by weighting the pure values compared to reference data

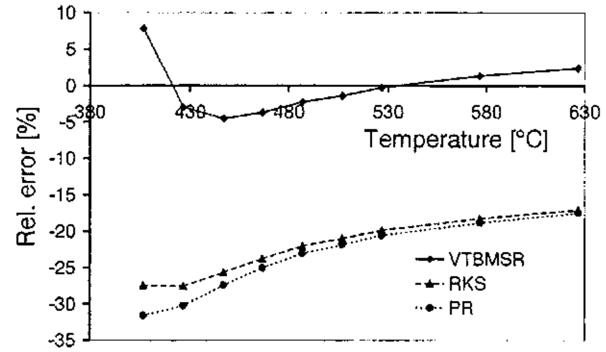

Figure 5. Relative error on the enthalpy of the H_2O-CO_2 system (x_{CO2}=0.05), 300bar

Conclusions

It has been shown that the proposed EOS, involving a volume-translation, a sophisticated α-function with polar parameters and more complicated mixing rules, specifies reasonable accuracy for the modeling of the thermodynamic behavior of aqueous mixtures at elevated pressures and temperatures – even in the supercritical region. Around the critical points, their closeness to the real values drop but only for small regions.

The structure of the EOS is relatively simple and the parameters c_i and p_i can be related to density and caloric properties, respectively, although there are some interactions. Therefore, only slight effort is required to predict the physical properties. This enables the EOS to be deployed usefully in process modeling and simulation.

Acknowledgement

The author would like to thank his former students Jens-Martin Doering and Martin Junginger for their major contribution to this work made by performing the regressions and computing the results.

References

1. Clifford, A.A. In: Clark, J.H. (ed.), "Chemistry of Waste Minimization", 1995
2. Redlich, O; Kwong, J.N.S. *Chem. Rev.* **1949**, 44, 233-244
3. Soave, G. *Chem. Eng. Sci.* **1972,** 27, 1197-1203
4. Martin, J.J.; *Ind. and Eng. Chem. Fundam.* **1976,** 15; 59-64
5. Péneloux, A.; Rauzy, E.; Fréze, R. *Fluid Phase Equilibria*, **1982**, 8, 7-23
6. Boston, J.F.; Mathias, P.M. In: Proc. of the 2nd Int. Conf. on Phase Equilibria and Fluid Prop. in the Chem. Process Ind., West Berlin, 823-849, **1980**
7. Schwartzentruber, J.; Renon, H., *Ind. Eng. Chem. Res.*, **1989**, 28, 1049-1055
8. Haar, L.; Gallagher S.; Kell S. "NBS/NRC Steam Tables"; Hemisphere Publ. Corp.; Washington; 1984
9. Wagner, W.; de Rueck, K.M.; "International. Tables of the Fluid State – 9: Oxygen"; IUPAC; Pergamon Press, 1976
10. Sychev, V.V.; Vassermann A.A.; Kozlov A.D.; Spiridonov, G.A.; Tsymarny, V.A.; "Thd. Properties of Oxygen; Nat. Std. Ref. Data Service of the USSR"; Hemisphere Publ. Corp.; Washington; 1987
11. Angus, S.; de Rueck, K.M.; Armstrong, B.; "Int. Thermodynamic Tables of the Fluid State – 6: Nitrogen", IUPAC, Pergamon Press, London, 1977
12. Angus, S.; de Rueck, K.M.; Armstrong, B.; "International Tables of the Fluid State: Carbon Dioxide", IUPAC, Pergamon Press, London, 1973
13. Gallagher, J.S.; Crovetto, R.; Levelt Sengers, J.M.H. *J. Phys. Chem. Ref. Data*, **1993**, 22(2), 431-
14. Gallagher J.S.; Levelt Sengers, J.M.H.; Abdulagatov, I.M. NIST Technical Note 1404, 1993
15. Japas, M.L.; Franck, E.U. *Ber. Bunsenges. Phys. Chem.*, **1985**, 89, 1268-1275
16. Japas, M.L.; Franck, E.U. *Ber. Bunsenges. Phys. Chem.*, **1985**, 89, 793-800
17. Johns, A.I. et al., *Int J. Thermophys.*, **1988**, 9(1), 3-19
18. Franck, E.U. *Pure&Appl. Chem.*, **1985**, 57(8), 1065-1070
19. Aspen Technology Inc., AspenPlus™ User's Manual, Release 9, Cambridge, MA, USA
20. Peng, D.-Y.; Robinson, D.B. Ind. Eng. Chem. Fundam., **1976**, 15(1), 59-64
21. Dohrn, R. Berechnung von Phasengleichgewichten, Vieweg, Braunschweig, 1994
22. Rackett, H.G. *J. Chem. Eng. Data.*, **1970**, 15, 514-
23. Shaw R.W; Brill, T.B.; Clifford, A.A:; Eckert, C.A.; Franck E.U., *Chemical Engineering News*, **1991**, 69 (51)
24. Pilz, S.; Ph.D. Thesis; RWTH Aachen, to be submitted in 1999

Gasification of Biomass and Model Compounds in Hot Compressed Water

A. Kruse*, J. Abeln, E. Dinjus, M. Kluth, G. Petrich, M. Schacht, E. Sadri, H. Schmieder
Forschungszentrum Karlsruhe, Institut für Technische Chemie CPV, P.O.Box 3640,
D- 76021 Karlsruhe, Germany
EMAIL : andrea.kruse@itc-cpv.fzk.de
FAX : +49 7247 82 2244

Experimental results of the gasification of biomass (straw, wood, sewage sludge) and model compounds in supercritical water are presented. The experiments were carried out in three batch and two tubular reactors in a temperature range of 300-600°C and pressures up to 70 MPa. Glucose and sucrose were chosen as model compounds for cellulose. Vanillin and pyrocatechol as aromatic compounds are model compounds for lignin. The influence of salt addition and solid catalysts on the gasification was also investigated.

Introduction

For the growing future energy demand, energy from biomass may contribute in a non negligible amount. Such a strategy would avoid the net increase of carbon dioxide in the atmosphere and it would help to fulfil the obligations of the European Union to reduce the carbon dioxide release.

Today the main part of energetic use of biomass consists in incineration of wood with a rather low energy yield. An increase of the efficiency can be expected by gasification and use of the fuel gases in turbines or even fuel cells. For wet biomass and wastes the less investigated gasification in hot compressed water shows considerable potential advantages [1, 2].

Experimental

In this paper, experiments carried out in three batch and two tubular reactors are reported. The reason for using different reactors is to study whether differences like unequal heating rates and surface to volume ratios influence the results. Real biomass can be investigated only in batch reactors up to now because feeding of small flows of suspensions is difficult.

Batch reactor I is made of Inconel 625 and has an internal volume of 1000 ml. It is constructed for pressures up to 28 MPa at temperatures up to 500°C and equipped with a stirrer. The experiments were carried out with vanillin and sucrose as model compounds (0.25-0.75 mole/kg) mainly in the presence of NaOH (0.25-0.75 mole/kg) and a solid catalyst (1.7-6 g/kg Raney Nickel, pellets of Nickel etc.). The temperature was adjusted between 300-490°C and the pressure between 10-27 MPa. Typical results are given in table 1.

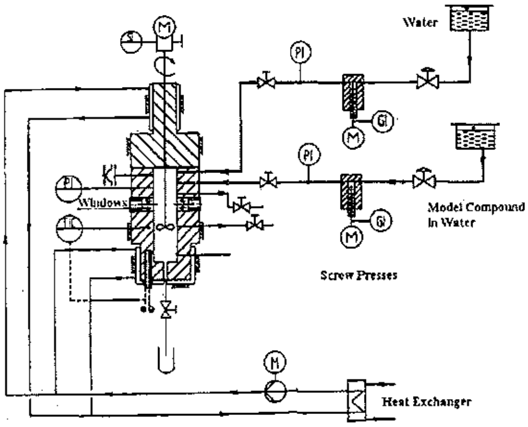

Fig. 1: Experimental set-up of batch reactor II

Batch reactor II (up to 700°C and 100 MPa, fig. 1) has an internal volume of 100 ml and is made of Nimonic 110. A stirrer with magnetic coupling is used for mixing. In this reactor, mainly the reactions of model compounds (0.25-0.5 wt.% vanillin and lignin) were studied in the range of 350-600°C, 20-70 MPa and residence times up to 4 hours. In some experiments K_2CO_3 (0.02-0.46 wt.%) was added.

Batch reactor III (up to 500°C and 50 MPa, fig. 2) is a tumbling autoclave with an internal volume of 1000 ml and is mainly used for the study of the chemical behavior of common biomass feedstocks like wood, straw, and sewage sludge (1 wt.%). For comparison also experiments with vanillin (1 wt.%) with and without K_2CO_3 addition were conducted. In most experiments the temperature was 450°C and the pressure 35 MPa.

In the experiments carried out in batch reactor I and batch reactor III, the model compounds or biomass were heated up together with water. In the experiments carried out in batch reactor II, the model compounds were injected in the reactor when the water had reached the desired temperature.

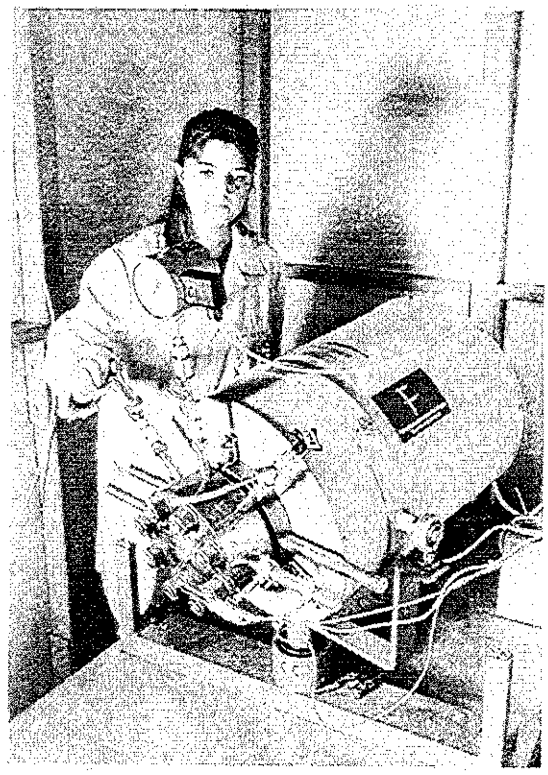

Fig. 2: Picture of the tumbling reactor (batch reactor III)

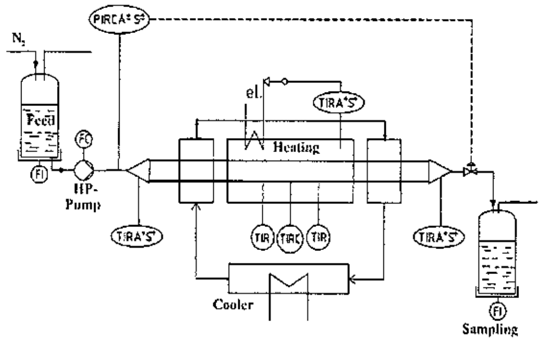

Fig. 3: Experimental set-up of tubular reactor II.

Tubular reactor I (up to 600°C and 32 MPa) is constructed for oxidizing aqueous wastes in supercritical water (description see [3]). Here, the degradation of vanillin and glucose (0.1-0.4 mole/kg) was studied in the presence of K_2CO_3 (0.001-0.002 mole/kg) and KOH (0.002-0.02 mole/kg) at 550 and 600°C, in the pressure range of 27-31 MPa and with residence times up to 2 min. Selected results are given in table 2.

A second flow reactor (tubular reactor II) was constructed to study special aspects of the hydropyrolysis of model compounds like pyrocatechol, glucose and glycine in the range of 400–600°C, 25-30 MPa, in the presence of KOH (0.002 mole/kg) and a residence time of 2 min.

After all experiments the gas phase was measured by gaschromatography and the total organic carbon content (TOC) of the liquid phase is determined. In selected experiments the composition of the liquid effluent was determined by mass spectrometry and quantified by SPME-GC.

Results

At temperatures below 500°C the model compounds (e.g. sucrose) are not completely gasified in the absence of alkali compounds like K_2CO_3 and KOH, even if the residence time is 4 hours (batch reactor I). In these experiments, a lot of soot and tar is formed and the CO content is significantly higher than in the presence of alkali compounds (table 1).

The use of Raney nickel leads to a further increase in the gasification efficiency and to a increased formation of methane at 400°C (batch reactor I). This was expected because nickel is a catalyst for hydrogenation and hence increases the reaction rate of the hydrogenation of CO to methane. At higher temperature hydrogen is the favorite product and therefore nickel influences the gas composition to a much smaller extent. Some solid catalysts based on Fe_2O_3 were also studied, they lead to a comparable high conversion like nickel but to higher CO formation.

In order to understand what kind of compounds are included in the residual TOC and how the composition in the liquid phase is influenced by temperature, pressure and salt presence, experiments with vanillin and lignin were carried out. The reason for the low gasification rate of the model compounds in the absence of salts is, that in the studied temperature range up to 550°C the aromatic rings are not degraded completely. The reaction of vanillin in hot compressed water leads to a variety of other aromatic compounds like different phenols. At 400°C the main product is pyrocatechol, which is the hydrolysis product of vanillin. The yield of pyrocatechol increases with pressure (fig. 4) which is in accordance with the assumption that the ability of water to be a reaction medium for hydrolysis increases with density.

The gas phase composition after the gasification of biomass (straw and wood, batch reactor III) is similar to the composition after the reaction of model compounds in the presence of potassium salts (table 1). The influence of salt addition to the reaction of biomass is of minor importance compared to the degradation of model compounds, because these materials contain salts. In table 1 is shown that the addition of K_2CO_3 decreases drastically the CO content after gasification of vanillin, while the CO content after wood gasification was influenced to a much smaller extend. The salt content of straw is higher than of wood, therefore the addition of K_2CO_3 has no significant influence on gas phase composition and gasification efficiency. Sewage sludge is an exception, despite of the relative high salt content, the CO-content is high and the gasification efficiency low. This has to be investigated in further studies at higher temperatures.

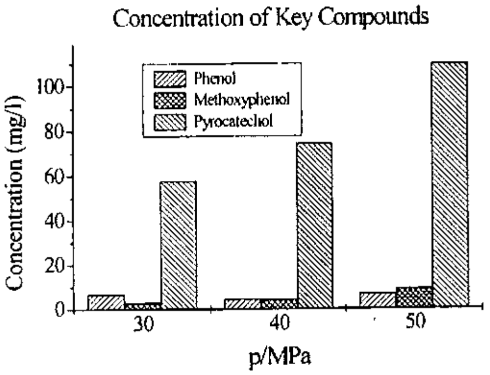

Fig. 4: Concentration of phenol, methoxyphenol and pyrocatechol after reaction of vanillin in supercritical water as a function of pressure. (Batch reactor II, 400°C, 2 h reaction time).

Table 3: Influence of the reaction time (600°C, 25 MPa, 0.2 mole/kg pyrochatechol, 0.0018 mole/kg KOH, tubular reactor II)

Time /sec.	H_2 Vol.%	CH_4 Vol.%	CO Vol.%	CO_2 Vol.%	TOC / %
30	66.1	1.4	0.5	32.1	0.6
60	66.4	1.9	0.6	30.1	0.3
120	63.1	2.4	0.5	32.1	< 0.1

As mentioned above, the addition of alkali salts to the model compounds leads to a decrease in CO formation. The reason for this influence is likely the known catalysis of the water- gas shift reaction (I) by alkali compounds [2]. The maximum hydrogen yield is given by stoichiometry. For example in the case of glucose the optimum hydrogen yield can be achieved if 6 molecules of water react with one glucose molecule (II).

$$CO + H_2O \rightarrow CO_2 + H_2 \qquad \text{(I)}$$
$$C_6H_{12}O_6 + 6\ H_2O \rightarrow 6\ CO_2 + 12\ H_2 \qquad \text{(II)}$$

For illustration to which extent water participates in the reaction, a stoichiometric factor y is calculated, which gives the number of water molecules per carbon atom reacting via equations analogous to equation (III).

Example glucose:

$$1/6\ C_6H_{12}O_6 + y\ H_2O \rightarrow (y+1)\ H_2 + y\ CO_2 + (1-y)\ CO \qquad \text{(III)}$$

In the case of vanillin the addition of K_2CO_3 increases the stoichiometric factor from 0.52 to 0.98 (table 1: 450°C, batch reactor III).

The influence of the alkali compounds on the gas phase composition was also confirmed for the model compounds vanillin and glucose by flow experiments (tubular reactor I, table 2). In both cases the CO formation is decreased and the conversion as well as the stoichiometric factor is increased by KOH or K_2CO_3. Similar results are found for pyrocatechol: if KOH is added than pyrocatechol is gasified completely in two minutes (table 2 and 3). The liquid effluent has no color, no odor and no measurable organic carbon content. Very good gasification efficiency is also found for glycine, which was used as model compound for amino acids and proteins. The nitrogen contained in glycine reacts nearly complete to $[NH_4]_2CO_3$ found in the aqueous effluent.

Table 4: Influence of concentration (glucose, tubular I, 2 min. reaction time)

Glucose mole/ kg	Salt mole/kg	H_2 Vol.%	CH_4 Vol.%	CO Vol.%	CO_2 Vol.%	TOC %
		550°C, 31 MPa, K_2CO_3:				
0.1	0.001	40.5	4.5	0.9	54	8.1
0.2	0.002	34.0	6.6	0.3	59.1	17.0
		600°C, 30 MPa, KOH:				
0.1	0.002	32.7	3.0	0.2	58.8	0.14
0.2	0.02	63.3	10.9	0.5	25.2	0.25
0.4	0.02	65.5	11	0.5	23	0.20

The gas composition of the pyrocatechol gasification changes only to a small extent with reaction time (table 3). Only the methane yield increases and the TOC in the liquid effluent decreases significantly after a longer reaction time.

Higher concentrations usually lead to lower hydrogen yields and higher residual TOC content. This effect vanishes at higher temperatures and higher alkali concentrations (examples in table 4). If KOH is added, the gas composition is influenced by the formation of K_2CO_3. Therefore the CO_2 content in the gas phase is lower than in the cases K_2CO_3 is added before reaction (table 2,4).

Outlook

A pilot plant for the gasification of biomass is planned. For a technical process, the following aspects has to be studied:

- Feeding of the solid biomass.
- Selection of hydrogen-resistant materials.
- Efficient heat exchange.

Table 1: Batch experiments

Reactant	T °C	p MPa	t min	H_2 Vol.%	CH_4 Vol.%	CO Vol.%	CO_2 Vol.%	TOC % (1)	Soot,Tar % of TC_0	Y (2)
Batch reactor I (48 experiments):										
Sucrose (0.5 mole/kg)	390	26	240	8	8	14.4	71	97 (3)	88.9	n.d. (4)
Sucrose (0.25-0.5 mole/kg)	400	26	240	29	11	1.6	53	81 (3)	34.6	n.d.
+ NaOH	480	20	240	58	11	1.4	24	54 (3)	5.6	n.d.
Sucrose	300	10	240	22-64	2-23	0.3-5	30-67	53-79 (3)	≤40	n.d.
(0.25-0.75mole/kg)	400	26	240	26-49	12-28	≤0.5	27-50	0-32 (3)	0-34	n.d.
+ NaOH, + Raney Ni	480	26	240	58	14	≤0.3	26	<0.1 (3)	<0.1	n.d.
Vanillin	390	26	240	44-61	21-35	<0.1	15-20	19-33(3)	≤13.9	n.d.
(0.25-0.75mole/kg)	450	26	240	72-73	10-11	≤0.04	14-17	<0.1 (3)	≤6.6	n.d.
+ NaOH, + Raney Ni	480	26	240	73-74	8-11	0.05	14-18	<0.1 (3)	0-19.6	n.d.
Batch reactor III (15 experiments):										
Vanillin	450	35	120	22.3	13.3	39.4	25.1	71.8	n.d.	0.52
(10g/kg)	500	31.5	120	40.9	13.1	7.4	38.7	29.5	n.d.	0.86
Vanillin (10g/kg)	450	35	120	45.9	15.0	0.5	38.6	26.5	n.d.	0.98
+K_2CO_3	500	31.5	120	40.9	14.6	1.5	43.0	21.9	n.d.	0.90
Wood (10g/kg)	450	35	120	28.9	19	3.3	48.8	8.2	n.d.	0.49
Wood (10g/kg) +K_2CO_3	450	35	120	34.2	15.3	0.7	50	18.8	n.d.	0.57
Straw (10g/kg)	450	35	120	32.8	18.5	1.4	47.2	16.5	n.d.	0.55
	500	31.5	120	35.0	18	0.4	46.7	7.6	n.d.	0.58
Straw (10g/kg) +K_2CO_3	450	35	120	42.7	16.5	1.0	39.7	17.9	n.d.	0.68
	500	31.5	120	43.7	15.6	0.12	40.6	7.5	n.d.	0.65
Sewage Sludge (10g/kg)	450	35	120	48.8	17.0	2.8	31.3	45.17	n.d.	0.79

(1): % TOC = 100 • mole organic C in the liquid effluent/ mole C in reactant; (2): Calculated stoichiometric factor; (3): TOC not measured but estimated from solid carbon content and gas phase composition;(4): n.d. = not determined

Table 2: Flow experiments

Reactant	T °C	p MPa	t min	H_2 Vol.%	CH_4 Vol.%	CO Vol.%	CO_2 Vol.%	TOC % (1)	Soot,Tar % of TC_0	Y (2)
Tubular reactor I (52 experiments):										
Glucose (0.1mole/kg)	550	27	2	26.0	7.5	29.3	36	40.6	n.d. (4)	0.38
	600	31	2.1	33.1	6.0	28.9	31.9	8.23	n.d.	0.38
Glucose (0.1-0.3	550	31	2.3	29-47	1.9-8.7	0.1-1.9	46-69	4.8-19	n.d.	0.64-0.82
mole/kg)+ K_2CO_3	600	31	2.3	28-37	2.3-7.3	0.2-4.1	55-67	3-9.2	n.d.	0.72-0.81
Glucose (0.1-0.4mole/kg)+ KOH	600	30	2	35-66	3-11	0.1-0.6	22-65	0.2-2.4	n.d.	0.267-0.76
Vanillin	600	27	1.75	35.9	8.9	38.4	16.8	32.2	n.d.	0.75
(0.07 mole/kg)		30	2	37.8	9.6	32.3	20.2	31.9	n.d.	0.80
Vanillin(0.07 mole/kg)+	600	27	1.75	46.2	15.8	1.2	36.8	18.2	n.d.	1.00
K_2CO_3		30	2	43.4	17.3	1.8	37.5	21.1	n.d.	0.98
Tubular reactor II (20 experiments):										
Glucose	400	30	2	4.1	1.5	41.2	45.1	65	23	-0.14 (6)
(0.2 mole/kg)+ KOH	500	30	2	15.1	5.3	53.4	21.8	38	16	-0.12 (6)
	600	25	2	57.2	3.7	0.5	33	<0.1	<0.1	1.12
Pyrochatechol (0.2 mole/kg)+ KOH	600	25	2	63.1	2.4	1.4-6.3	32.1	0.1	<0.1	1.5
Glycine 5 (0.6 mole/kg)+ KOH	600	25	2	57	1.8	0.8	41 (5)	1.5	<0.1	n.d. (3)

(5): The nitrogen contained in the glycine is converted completely to $[NH_4]_2CO_3$, therefore the CO_2 yield is low;
(6): Negative values because in equation (III) the equilibrium $C + CO_2 \leftrightarrow 2\ CO$ was not considered.

References:

[1] S. Ramayya, A. Brittain, C. DeAlmeida, W. Mok, M. J. Antal, Jr., *Fuel* **66**, 1364 (1986).

[2] D. C. Elliott, M. R. Phelps, L. J. Sealock, Jr., E. G. Baker, *Ind. Eng. Chem. Res.* **33**, 566 (1994).

[3] H. Goldacker, J. Abeln, M. Kluth, A. Kruse, H. Schmieder, G. Wiegand, *Proceedings of 3rd International Symp. High Pressure Chemical Engineering, 7-9 Oct. 1996, Zürich, Switzerland.*

PlantWeb
FIELDBUS
PLANTWEB
PRODUKTE
www.fisher-rosemount.com/fieldbus

Die PlantWeb™-Architektur läßt den FOUNDATION™ Fieldbus schon heute für Sie arbeiten.

Der Feldbus ist da - wo soll er hin?

Egal, ob Sie einen neuen Produktionsbereich automatisieren, oder eine existierende Anlage aufrüsten wollen, die PlantWeb-Produkte bieten Ihnen die richtige, langfristige Lösung und garantieren sofortige Einsparungen und Effizienzsteigerungen.

Wir haben die Lösung - jetzt sind Sie an der Reihe.
Die feldbasierte PlantWeb-Architektur eröffnet völlig neue Möglichkeiten für die feldbusfähige Produktpalette von Fisher-Rosemount.
Wir bieten Ihnen eine umfassende, integrierte Lösung inklusive verteilter Intelligenz und umfassendem Informationszugriff.

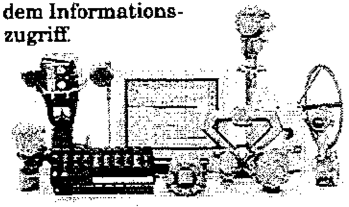

Felderprobt und einsatzbereit.
Fisher-Rosemount hat bereits über 1000 feldbusfähige Geräte im harten, täglichen Einsatz. Wann dürfen wir Ihnen die Vorteile der Feldbus-Technologie liefern?
Worauf warten Sie noch? Zögern Sie nicht länger – fordern Sie noch heute weitere Informationen von uns an.

☞ **Neue deutsche Homepage: www.fisher-rosemount.de**

Fisher-Rosemount GmbH & Co.
Argelsrieder Feld 3
D-82234 Weßling
Telefon (08153) 939-0
Telefax (08153) 939-172

FISHER-ROSEMOUNT
Managing The Process Better.

Reactions

The dehydration of 1,4-butanediol to tetrahydrofuran in sub-and supercritical water

Dipl.-Ing.Thomas Richter, Prof. Dr.-Ing. Herbert Vogel*,
Technische Universität Darmstadt, Fachbereich Chemie, Institut für Chemische Technologie,
Chemische Technologie I, Petersenstraße 20, D-64287 Darmstadt
Fax: 06151 / 163465, e-mail: hervogel@hrz1.hrz.tu-darmstadt.de

Water plays an important role in many chemical reactions: as a solvent, a reaction partner or a catalyst. Many organic substances do not react or react only insufficiently with or within water at lower temperatures. This behaviour changes dramatically when the temperature is increased. A broad scope of the properties of the aqueous reaction-mixture (e.g. ρ, ε, pK_w, c_p), especially near the critical point, can be changed through minor temperature- and pressure variations. This can provide alternative reaction pathways, i.e. the chemical environment can be adapted without the need to find alternatives for the solvent water. One cause is the change of the intermolecular interaction of water molecules during the transition into the supercritical condition. In order to investigate the synthesis-potential of supercritical water (SCW), hydration- and dehydration reactions of various model compounds were carried out under sub- and supercritical conditions. These reactions were carried out without involving catalysts (acids, bases) to overcome the disadvantages of common reaction-conditions (e.g. use of mineral-acids, salt-yields and low space-time-yield). 1,4-butanediol dehydrates in sub- and supercritical water selectively to tetrahydrofuran (THF), without the addition of an acid catalyst. No other products were detected. THF has proved to be stable under the applied reaction conditions. The conversion increases significantly with the temperature. At 300 °C (25 MPa) a conversion rate of 10 % was obtained, which increases to 70 % at 380 °C (25 MPa) with 2 minutes residence time.

Introduction

Today, the production of tetrahydrofuran (THF) via dehydration of 1,4-butanediol (BTD) is carried out in liquid-phase at elevated temperatures in the presence of a dehydrating agent, e.g. a mineral acid [1,2,3]. The disadvantages of using a mineral acid are the waste disposal of the soiled acid and the high costs of a corrosion-resistant reactor.

The reaction mechanism under conventional conditions is well known [4,5]:

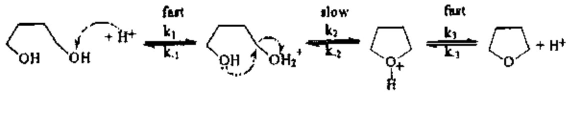

Many examinations about the dehydration of alcohols in SCW are known in literature; mostly monohydric alcohols e.g. ethanol [6,7,8] or propanol [9,10] are described there. In most cases the reaction products were olefins. These examinations were carried out in small batch- or plug-flow reactors (volumes < 5 ml) where there was no exclusion of catalytic wall effects. The measurements in this paper were carried out in a plug-flow reactor with "technical" dimensions.

Methods

A mini plant with a plug-flow reactor was built. The plug-flow reactor has a length of one meter and a volume of 50 ml. A flow sheet of the plant is given in Fig. 1. Detailed information about the mini plant and the analytics are given in [11].

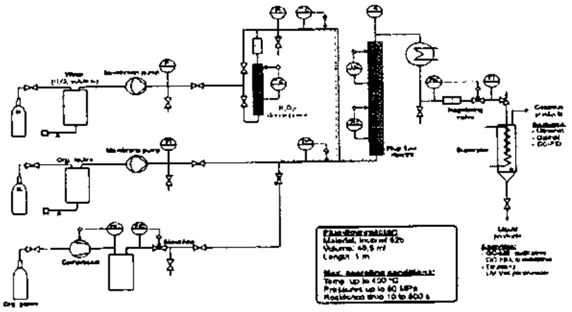

Figure 1. Flow sheet of the high pressure plant.

The reaction temperature was varied from 300 to 400 °C and the reaction pressure from 23 to 35 MPa. The residence times were adjusted from 15 to 165 s.

Results and Discussion

By changing the reaction medium to sub- and supercritical water (SCW), it is possible to discard the use of a mineral acid. The dehydration of BTD to THF in SCW has a selectivity of nearly 100 %. Only traces of CO_2 and CO were detected. THF has proved to be stable under the applied reaction conditions.

Increasing the temperature from 300 to 380 °C one can notice a rise in the conversion rate at all pressures, reaching a maximum at 380 °C. A further rise in the temperature will cause the conversation rate to decrease (Fig. 1). The addition of 1 % (g g^{-1}) acetic acid will cause the conversion rate and the rate constant to increase, which can be explained by the ionic mechanism. Furthermore, the maximum of the conversion rate shifts from 380 to 400 °C (Fig. 2).

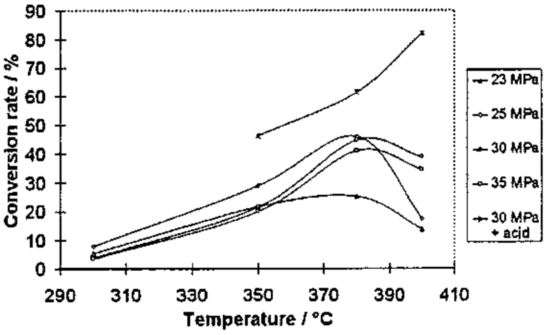

Figure 2. The conversion rates of the dehydration of BTD to THF showing the dependence on the temperature at various pressures.

At subcritical conditions the pressure dependence of the conversion rate is small (Fig. 3). The maximum of the conversion rate at 300 and 350 °C are at 25 MPa in both case. At near-critical conditions (380 °C) there is a strong pressure dependence at low pressures; at supercritical conditions (400 °C) at high pressures. The maximum of the conversion rate shifts at 400 °C to a pressure of 30 MPa (Fig. 3).

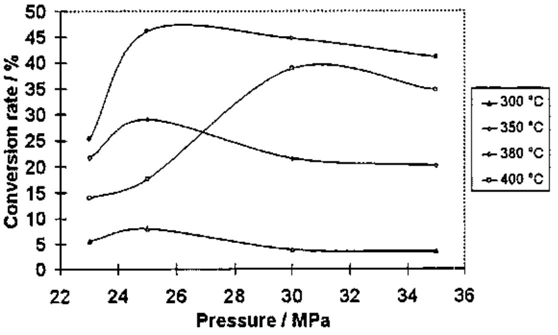

Figure 3. The conversion rates of the dehydration of BTD to THF showing the dependence on the pressure at various temperatures.

Based on the ionic mechanism the dissociation constant of water should show an influence on the conversation rate and on the rate constant. For the first step of the reaction (the protonation of the 1,4-butanediol) the presence of protons is crucial. Approaching the critical point, the pK_w value increases and therefore the self-dissociation of water decreases accompanied by a reduction of density. In Fig. 4 the interdependence of the conversion rate at 25 MPa and the K_W-value is shown.

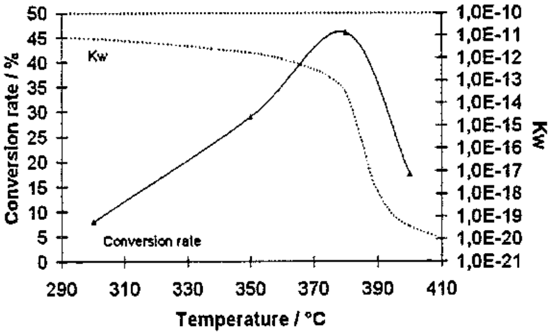

Figure 4. Conversion rate at 25 MPa and at various temperatures compared with the K_W-value of water.

It could be unmistakeably shown that the addition of acetic acid results in an increase of the conversation rate at all temperatures. The shift of the maximum of the conversation rate from 380 °C to 400 °C was particularly apparent. The reason for this can be tracked down to the pK_w value which only plays a minor role for the supply of protons due to the presence of acid.

The rate constants were calculated via a first order equation. They are given in Tab. 1.

Table 1. Rate constants of the dehydration of BTD to THF.

Pressure / MPa	Temperature / °C	Rate constant / 10^{-3} s^{-1}
23	300	0,62 (9)
23	350	4,4 (2)
23	380	6,9 (8)
23	400	3,8 (7)
25	300	0,91 (9)
25	350	4,1 (5)
25	380	8,8 (5)

25	400	3,8 (6)
30	300	0,66 (3)
30	350	3,7 (2)
30	380	9,8 (2)
30	400	8,4 (3)
35	300	0,50 (3)
35	350	3,5 (2)
35	380	9,9 (6)
35	400	6,4 (4)

The activation energies which are calculated from the rate constants are shown in Fig 5. They rise with increasing pressure.

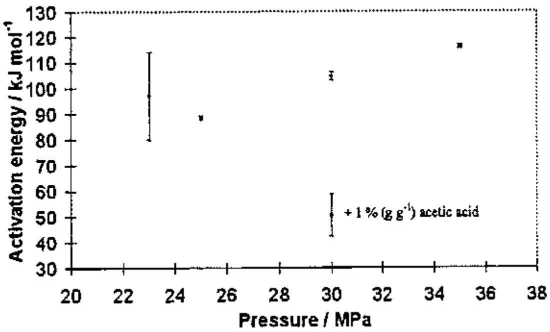

Figure 5. The activation energies of the dehydration of BTD to THF at various pressures.

The ionic mechanism, which predominates under conventional conditions, could be confirmed by measurements in the subcritical as well as in supercritical state. Homolytic mechanisms dominates in "non" dissociated water (high pKw values). The addition of an acid should counteract a reaction, which has a homolytic mechanism. This was not observed. Furthermore, there were no other products detected. Therefore no hints of change in the mechanism were revealed.

Conclusions

The dehydration of BTD to THF is a successful reaction under common conditions, but has some disadvantages based on the use of mineral acids. These problems can be solved by using SCW. With a maximum conversion rate of 75 % (380 °C, 30 MPa, 140 s residence time) without the addition of an acid and up to 90 % (400 °C, 30 MPa, 120 s residence time) with an addition of 1 % (g g^{-1}) acetic acid the dehydration in SCW is an appropriate alternative. The selectivity of THF is always nearly 100 %.

References

[1] BASF; *DT* 1043342, 1957.

[2] I.G. Farbenind.; *D.R.P.* 696779, **1937**.

[3] Gen. Aniline & Film Corp.; *U.S.P.* 2251292, **1938**.

[4] Schmoyer, L.F.; Case, L.C.; *Nature*, **1960**, *187*, 592-593.

[5] Hudson, B.G.; Barker, R.; *J. Org. Chem.*, **1967**, *32*, 3650-3658.

[6] Antal, M.J. et al.; *Supercritical Fluids* (Squires and Paulaitis Hrg.), Washington DC, ACS Symposium Series 329, **1987**, 77-86.

[7] Ramayya, S.; Brittain, A.; DeAlmeida, C.; Mok, W.; Antal, M.J.; *Fuel*, **1987**, *66*, 1364-1371.

[8] Xu, X.; De Almeida, C.; Antal, M.J.; *J. Supercrit. Fluids*, **1990**, *3*, 228-232.

[9] Narayan, R.; Antal, M.J.; *Supercrit. Fluid Sci. Tech.*, Washington DC, ACS Symposium Series 406, **1989**, 226-241.

[10] Narayan, R.; Antal, M.J.; *J. Am. Chem. Soc.*, **1990**, *112*, 1927-1931.

[11] Krammer, P.; Mittelstädt, S.; Vogel, H.; *Chem. Ing. Tech.*, **1998**, *12*, 1559-1563.

Hydrolysis of some Biopolymers with water and carbon dioxide at high pressures and temperatures

Kaiyue Liu*
UHDE Hochdrucktechnik, Buschmühlenstr. 20, 58093 Hagen, Germany, LiuK@uht.krupp.com
Gerd Brunner
Technische Universtaet Hamburg-Harburg, Arbeitsbereich Thermische Verfahrenstechnik
Eissendorferstr. 38, 21073 Hamburg, Germany, brunner@tu-harburg.de

To our knowledge the hydrolysis of starch with water and carbon dioxide at elevated pressure and temperature has not yet been investigated. We have therefore carried out these experiments with the aim of optimizing the reaction conditions to obtain a maximum yield of the valuable products such as maltose, glucose and fructose. The hydrolysis of starch was performed in a tubular reactor measuring 4.02 m in length and having an inner diameter of 6 mm. Experimental conditions were such that the temperature ranged from 170 to 300 °C and the pressure was varied between 60 and 240 bar. An increase in the yield of products was observed when carbon dioxide was used as a catalyst. But only the dissolved and dissociated carbon dioxide has an influence on the hydrolysis of starch. The temperature is the parameter which has the strongest influence on the hydrolysis of starch in water. The glucose yield varied only little with the initial starch concentration, eventhough this was, in one case, increased by a factor of 50. The kinetic study was carried out with the assumption, that the type of all reactions are the first order. The activation energy and frequecy factor for the decomposition of starch and formation of products were calculated. We present in this article the hydrolysis of starch with carbon dioxide as catalyst as an alternative to the traditional acid catalyzed process. Comparing with the traditional acid catalyzed process the hydrolysis of starch with carbon dioxide as catalyst has the advantage, that two process units, one for neutralizing the solution and a second one for removing the resulting salt with ion exchangers, could be eliminated.

Introduction

The hydrolysis of many biopolymeres at high pressure and high temperature is already examined. The studies on the hydrolysis of glucose were carried out within a range of temperature from 150 to 300°C [1][2][3]. A detailed kinetic investigation of the hydrolytic reactions of glucose near the critical point was done by Kabymela [4]. Mok examined the acid catalyzed hydrolysis of cellulose at a pressure of 345 bar and at a temperature ranging from 190 to 225 °C [5]. However, to our knowledge the hydrolysis of starch, though being the economically most important biopolymere, has not been investigated so far. The goal of our work is to determine the best conditions for the formation of the valuable products like maltose, glucose and fructose. Instead of traditional acid catalyzed process the hydrolysis of starch was carried out with carbon dioxide as catalyst. The advantage is that two process units, one for neutralizing the solution and a second one for removing the resulting salt with ion exchangers, could be eliminated.

About 70 % of the annual 17 million tons world production of starch is converted to glucose-containing sweeteners [6]. Starch is usually converted to glucose by using either an acid catalyzed or an enzymatic process. The initial suspension for the acid catalyzed process is a 40 wt. % starch suspension which is acidified to a pH of 4 - 5, usually using hydrochloric acid. After the hydrolysis the solution is neutralized and the resulting salt is removed using an ion exchanger.

Starch is an alpha-linked polysaccharide. Furthermore it is composed of two components with different molecular weights: 20 - 30 % of linear amylose and 70 - 80 % of branched amylopectin (see Fig. 1). The hydrolysis of starch is an acid catalyzed hydrolytic decomposition where a C-O-C linkage is cracked between two glycopyranose units and a water molecule is inserted.

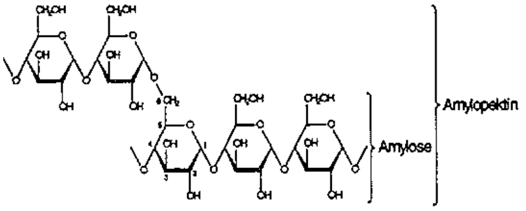

Figure 1. Sketch of a starch molecule

Apparatus and experimental procedure

The experiments were carried out in a tubular reactor of 4.02 m length an inner diameter of 6 mm and an outer diameter of 10 mm. The used Inconel 600 tubes were made of a corrosion resistant and hightemperature resistant nickel-based alloy (2.4816). The flow chart of the whole apparatus is shown in Figure 2.

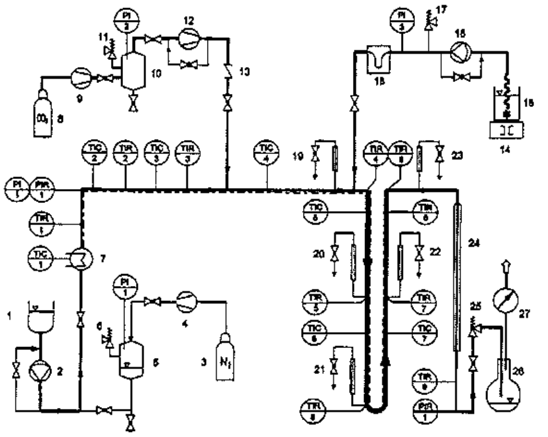

Figure 2. Scheme of experimental apparatus
1. water storage tank 2. Pump 3. nitrogen storage tank 4. compressor 5. pressure compensator 6. check valve 7. preheater 8. carbon dioxide storage tank 9. compressor 10. plenum chamber 11. check valve 12. high-precision pump 13. backflow check valve 14. magnetic stirrer 15. starch suspension storage tank 16. pump 17. check valve 18. mass flow measuring instrument 19-23. sample port with cooling system 24. heat exchanger 25. pressurizing valve 26. separator 27. gasometer

Analysis

The concentration of liquid products, maltose, glucose, fructose, 1,6-anhydro-β-D-glucopyranose (Levoglucosan) und 5-hydroxymethylfurfurol (HMF) were analyzed by HPLC. The HPLC equipment consisted of a pump (Merck-Hitachi-L7100), an autosampler, and an integrator. The used ET 300/7.8 NUCEOGEL SUGAR Na carbohydrate column contains 300*7.8 mm bed packed with a calcium-exchange polymer in Na+ form. The HPLC was operated at a floe rate of 0.5 mL/min demineralized water. The oven (Sykan S4110) was operated at a temperature of 72°C. The detector used was a RI detector (RI-IV LDC Analytical). The products of hydrolysis of corn starch that were identified by HPLC are shown in Fig. 3.

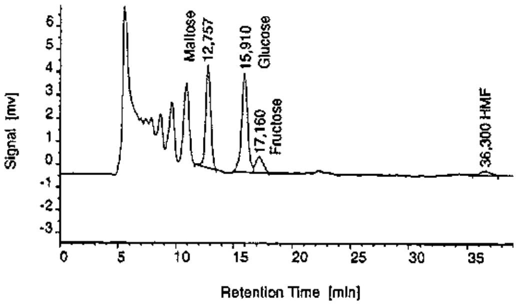

Figure 3. HPLC chromatograms of a liquid sample from corn starch hydrolysis at 250°C, 240 bar and the residence time of 50 sec.

Results and discussion

Hydrolysis of starch with carbon dioxide

In the course of this work the hydrolysis of corn starch, the most important kind of starch, in water and CO_2 at high pressures and temperatures was investigated. The experiments were performed at a temperature between 170 and 300 °C and a pressure between 60 and 240 bar. Concentration of starch varied from 0.2 up to 10 wt. % and the residence time varied from 0.4 up to 20 min.

In this work the added quantity of carbon dioxide is expressed in degree of saturation, which is the ratio of the added carbon dioxide by the maximum soluble quantity of carbon dioxide in water at given conditions. A degree of saturation of more than 100 % means that carbon dioxide is in excess. Figure 4 exemplary shows the results of the hydrolysis of starch at 230°C and 240 bar. The initial starch concentration was 0.2 wt. %. The water was saturated with nitrogen to exclude the influence of oxygen.

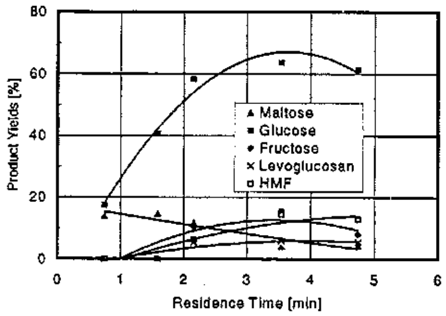

Figure 4. Product yields under influence of carbon dioxide as a function of residence time

Influence of the concentration of carbon dioxide

The influence of the concentration of carbon dioxide on the formation of glucose is shown in Figure 5.

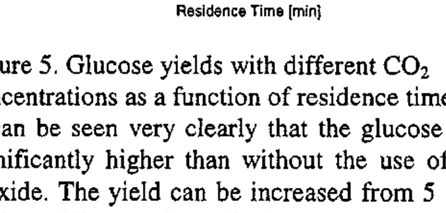

Figure 5. Glucose yields with different CO_2 concentrations as a function of residence time

It can be seen very clearly that the glucose yield is significantly higher than without the use of carbon dioxide. The yield can be increased from 5 % to 60 % by adding carbon dioxide. The effect on the formation of glucose increases with increasing carbon dioxide concentration. However, the formation of glucose at 96 % and 153 % degree of saturation of CO_2 is almost the same. This is caused by the H+ ions being the real catalyst in the acid catalyzed hydrolysis. Therefore only the dissolved and dissociated carbon dioxide has an effect on the hydrolysis of starch. The excess carbon dioxide stays in the gas phase and has no direct influence on the hydrolytic reaction. However, the density of carbon dioxide is about a third of the water density even at elevated pressures and temperatures. Since the massflowrate of liquid phase is constant, the excess carbon dioxide affects the residence time obviously.

Influence of temperature

It was discovered that the temperature, compared with the other variables like pressure and concentration of acid, had the strongest influence on the hydrolysis of starch in water [7]. The influence of different experimental temperatures, on the formation of glucose is shown in Figure 6. It can be seen that at the beginning period the hydrolysis reaction is faster at higher temperatures than it is at lower temperatures, thus more glucose is formed. Likewise the decomposition of glucose is faster at the end of hydrolysis at increased temperatures. The reason is that the higher temperature accelerates both formation and further decomposition of glucose. This effect increases with increasing temperature.

The maximum yields of glucose at 190 °C and 210 °C occurring late were not measured because of the limitation of the apparatus. However, with regard to previous experiments [8] there are reasons for assuming that the maximum yield occurs earlier when increasing temperature. The self-dissociation-constant of water increases at elevated temperature, therefore both hydrolysis of starch and further decomposition of glucose are accelerated.

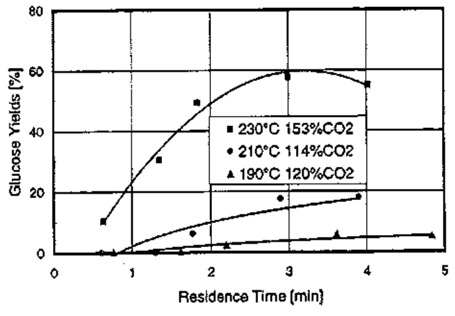

Figure 6. Influence of temperature on the glucose yield when hydrolyzing corn starch with an excess of carbon dioxide

Influence of pressure

Previous work [9] confirmed that the pressure itself has no influence on the hydrolysis of corn starch. The effect of changing the pressure within our experiment's range on the dielectric-constant and self-dissociation constant of water is so small that the hydrolysis of starch is hardly influenced. Further the hydrolysis of starch is strongly influenced by the dissolved and dissociated carbon dioxide. The solubility of carbon dioxide is dependent on the pressure and temperature, like Figure 7 shows. Therefore the hydrolysis of starch is indirectly by the pressure influenced.

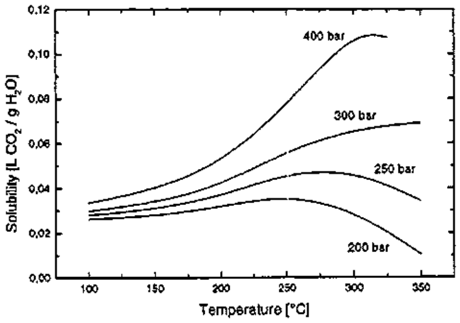

Figure 7. The solubility of carbon dioxide as function of the pressure and temperature [9]

The experiments were carried out in the aqueous phase at pressures of 60, 120, 180 and 240 bar, to ensure that the hydrolysis of starch prevails over the pyrolysis. The influence of pressure on the hydrolysis of corn starch when adding carbon dioxide is shown in Figure 8. All experiments shown in Figure 8 were carried out with excess carbon dioxide at 230 °C and an initial starch concentration of 0.2 wt. %. However, previous investigations showed, that the hydrolysis of starch was not influenced by degree of saturation, if the saturation degree is more than 100 %.

The glucose yield increases with an increase in pressure, because the maximum solubility of carbon dioxide in the aqueous phase increases with increasing pressure. More dissolved carbon dioxide accelerates the hydrolysis of starch and produces more glucose.

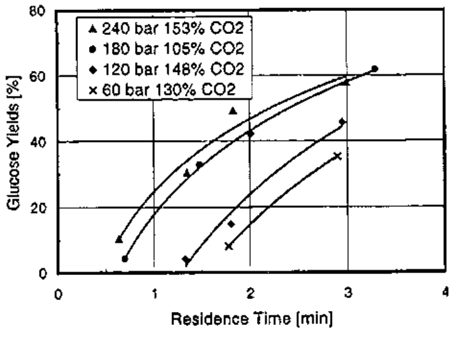

Figure 8. The influence of pressure on the glucose yield with excess carbon dioxide

Influence of initial starch concentration

For industrial applications the space-time yield of the product is of major importance. The experimental results are shown in Figure 9 as glucose yields as function of residence time. The glucose yields are in a narrow range even when increasing the initial starch concentration 10 or 50 times. This leads to the conclusion that the results, which were obtained in this work with the low initial concentration, are transferable to higher initial starch concentration conditions.

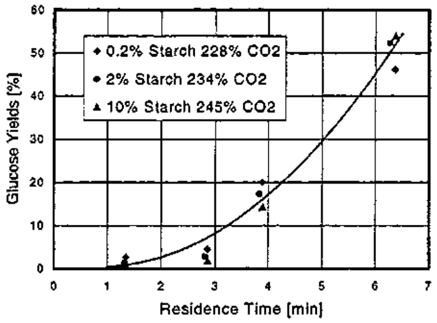

Figure 9. Glucose yields at different initial starch concentrations

Kinetic modeling

The kinetic study of hydrolysis of starch in near critical water was carried out by assuming the first order reactions. The reaction scheme is considered as follows.

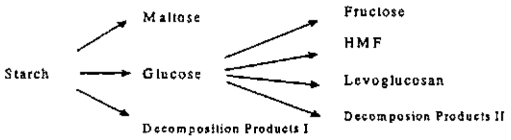

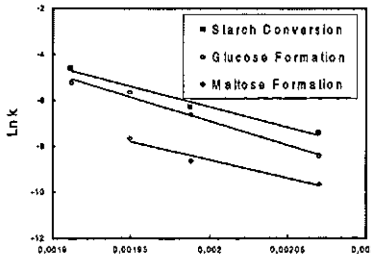

Figure 10. Arrhenius plot for the hydrolysis of starch

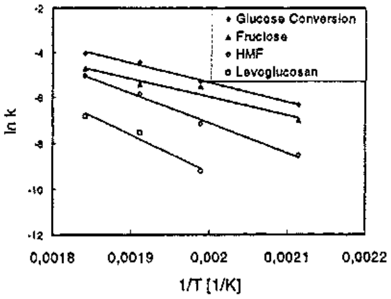

Figure 11: Arrhenius plot for the further hydrolysis of glucose

Figure 10 and 11 show the arrhenius plot for the hydrolysis of starch and further decomposition of glucose. The activation energy Ea and frequecy factor k0 for different reactions were evaluated.

Conclusion

The hydrolysis of starch with water and carbon dioxide at elevated pressure and temperature has been investigated. An increase in the yield of products was observed when carbon dioxide was used as a catalyst. But only the dissolved and dissociated carbon dioxide has an influence on the hydrolysis of starch. The temperature is the one parameter which has the strongest influence on the hydrolysis of starch in water. The yields obtained for glucose varied only little with the initial starch concentration, eventhough this was, in one case, increased by a factor of 50. The kinetic study was carried out with the assumption, that the type of all the reactions are the first order. Comparing with the traditional acid catalyzed process the hydrolysis of starch with carbon dioxide as catalyst has the advantage, that two process units, one for neutralizing the solution and a second one for removing the resulting salt with ion exchangers, could be eliminated.

References

1. Bobleter, O.; Pape, G. „Hydrothermal Decomposition of Glucose“, Monatsh. Chem. 99, **1968**, 1560
2. Amin, S.; R.C. Reid and M., ASME Paper #75-ENAs-21, Intersociety Conf. On Environ. Systems, San Francisco (July 21-24,**1975**)
3. Bonn, G.; Schwald, W.; Bobleter, O., Hydrothermolysis of Short Rotation Forestry Plants; Energy from Biomass (Hrsg.: Palz, W.; Coombs, J.; Hall, D.O.), Elsevier, London **1985** 953-958
4. Kabyemela, B.M.; Adschiri, T.; Malaluan, R.M.; Arai, K. *Ind. Eng. Chem. Res.* **1997,** 36, 1552-1558
5. Mok, W.S.L.; Antal, M.J., Jr.; Jones, M., Jr., J. *Org. Chem.* **1989,** 54, 4596
6. Schenck,F.W.; Hebeda,R.E. „Starch hydrolysis products“ VCH Publischers, ISBN 1-56081-055-6
7.Liu, K; Brunner,G, Proceeding of AIChE Annual Meeting **1998,** Session-Reaction in supercritical fluids
8. Liu, K.; „Zur Hydrolyse von Biopolymeren in Wasser und Kohlendioxid unter erhoehten Druecken und Temperaturen“; Dissertation, Technische Universitaet Hamburg-Harburg, **1999**
9. Liu, K.; Brunner, G. DECHEMA-Jahrestagung, **1998,** Band II, 362
10. Toedheide, K.; Franck, E.U. *Zeitschrift fuer Physikalische Chemie Neue Folgen* **1963**, 37, 387-401

Hydrogenation at Supercritical Conditions

Magnus Härröd*[a] Maj-Britt Macher[a] Sander van den Hark[a] and Poul Møller[b]
[b] Augustenborggade 21B, DK-8000 Aarhus C, Denmark
[a] Chalmers University of Technology, Department of Food Science,
c/o SIK, PO Box 5401, SE-402 29 Göteborg, Sweden
E mail: magnus.harrod@fsc.chalmers.se fax: +46-31-83 37 82

In hydrogenation of liquids, hydrogen is mixed with the liquid and brought in contact with a catalyst. The reaction rate is limited by the concentration of hydrogen at the catalyst surface. The reasons are the transport resistances for the hydrogen: between the gas phase and the liquid phase; through the liquid phase; and between the liquid phase and the catalyst.
By adding a suitable solvent to the reaction mixture, we can bring the whole mixture to a supercritical or near-critical state. Under these conditions the solvent dissolves both the substrate and the hydrogen and a substantially homogeneous phase is formed, in which the transport resistances are eliminated. Therefore, the hydrogen concentration at the catalyst surface can be greatly increased and extremely high reaction rates achieved. Hydrogenation at supercritical conditions can improve both the process economy and the product quality.
At this meeting we will present the basic principles for hydrogenation at supercritical conditions. We will demonstrate the principles using our results from reactions for production of hydrogenated oils and fatty alcohols. Reaction rates up to 1000 times higher than in traditional processes have been achieved. An example of improved product quality is that in partially hydrogenated fat the *trans*-fatty acid content was dramatically reduced.

Introduction

With hydrogenation at supercritical conditions greatly improved product quality and tremendously increased reaction rates have been achieved for both liquid and solid substrates. A solvent is used to dissolve the substrate and the hydrogen into a single phase. The solvent has to be rather close to its critical temperature and the whole mixture of substrate, product, solvent and hydrogen is in a near-critical or supercritical state. Therefore we call the new technology hydrogenation at supercritical conditions. This technology has a great potential to produce products at lower costs and with improved quality.
In this paper we compare the basic principles for the traditional hydrogenation and for hydrogenation at supercritical conditions. To do that we use phase diagrams and concentration profiles. We will demonstrate the benefits of the new process with experimental results from: hydrogenation of fatty acid methyl esters aiming for hardening of fats for margarine and shortening; and hydrogenation of fatty acid methyl esters for fatty alcohol production.

Traditional hydrogenation processes

Hydrogenation is used for production of a wide range of products in areas like: food-, petrochemical-, fine chemical- and pharmaceutical-industry. The total added value for these hydrogenation processes is in the range of 10 billion US$/year.

Many metals can be used as catalysts, e.g. Ni, Cu, Zn, Cr, Pd, Pt, Rh and others. Each catalyst has a certain ignition temperature. This temperature decides whether the substrate is a gas, a liquid or a solid.

When the substrate is a liquid at the reaction temperature a three phase system is used: a gas phase (hydrogen), a liquid phase (substrate, product and eventually solvent) and a solid phase (catalyst). Fig. 1 shows a general concentration profile for such a hydrogenation process. For hydrogen there is equilibrium between the gas phase and the surface of the liquid. Good mixing of the gas and the liquid can reduce the concentration drop in the film between the surface and bulk. The drop between the bulk and the surface of the catalyst can be reduced by rapid flow of the liquid over the catalyst and reduction of the thickness of the liquid film at the catalyst. The concentration drop in the catalyst depends on the diffusion of hydrogen into the pores of the catalyst. This drop can be affected by the design of the catalyst.

The substrate concentration is also described in Fig. 1. A concentration drop occurs in the film at the surface of the catalyst. However, the concentration of the substrate is high and there is always a lack of hydrogen at the catalyst surface. The limited solubility of hydrogen in the liquid and the transport resistances restrict the hydrogen concentration at the

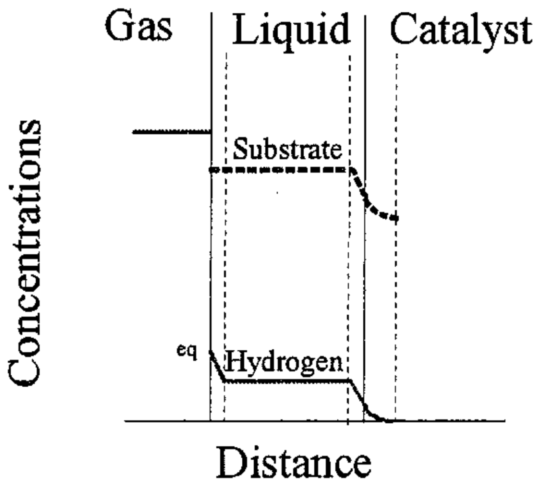

Figure 1. General concentration profiles during *gas/liquid* hydrogenation

catalyst surface. This concentration controls the reaction rate and the kinetics of the reaction.

To illustrate the hydrogenation processes, we will focus on hydrogenation of oils, i.e. triglycerides, for production of margarine and shortening. The annual production of hydrogenated triglycerides is about 25 million ton [1, 2]. Most of them are produced in batch processes using large slurry reactors (5 - 20m^3) with strong agitation, at high temperatures and low pressures and long reaction times (140 - 200°C, 1 - 3bar, 2h) [3]. In these reactors the reaction rates are very low (SubHSV<1000 $kg_{substrate}/m^3_{reactor}h$).
The rates are limited by the low concentration of hydrogen at the catalyst surface. Furthermore, inadequate hydrogen supply to the catalyst surface promotes the formation of *trans*-fatty acids. [4-7].

Important process parameters. The solubility of hydrogen in an oil is low. It increases when the pressure increases and it is affected only to a minor extent by temperature [8, 9]. Thus, by increasing the pressure the reaction rate increases. The technical economical pressure limit for large plants is about 300bar. Up to this pressure standard materials can be used for the reaction vessels and the compressors.

Temperature is the other main parameter. When the temperature is increased by 10°C all reaction rates normally increase with a factor of 2. When side reactions occur it is important to balance reaction rate and yield of the desired product. For optimised continuous reactors the SubHSV can be up to 10 000 $kg_{substrate}/m^3_{reactor}h$.

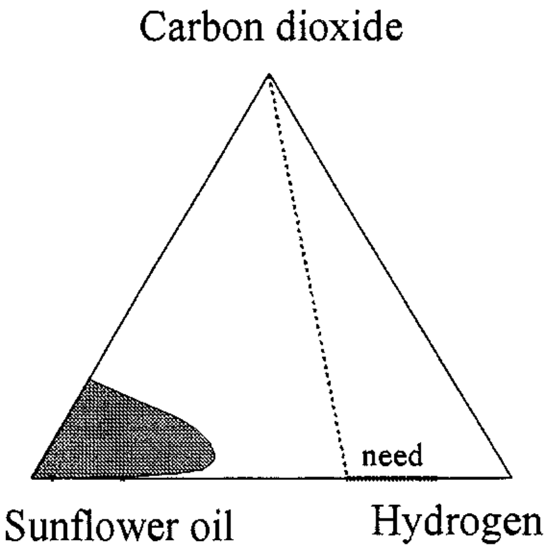

Figure 2. Phase diagram for sunflower oil, CO_2 and hydrogen at 100bar and 100°C (mol%).
▩ Single phase ☐ Two phases

For small molecules increased temperature may lead to gas phase hydrogenation instead of liquid phase hydrogenation. This leads to a dramatically increased SubHSV. For example during hydrogenation of cyclohexene at 350°C an SubHSV of 400 000 $kg_{substrate}/m^3_{reactor}h$ has been achieved [10]. However, increasing the temperature can only be utilised in this way when no side reactions occur because the pure thermal effect is tremendously high.

Solvents can also be used to affect the reaction. In these processes it is important to analyse the phase behaviour and the viscosity effects of the interactions between the substrate, the solvent and the hydrogen at different concentrations, temperatures and pressures. In general the solvents reduce the viscosity and increase the solubility of hydrogen.

The first one to propose CO_2 as a solvent in a hydrogenation process was Zosel [11]. The substrate was triglycerides. A phase diagram for this system is presented in Fig. 2. The solubility of triglycerides in carbon dioxide is below 1 wt.% (0.05 mol%) at 80°C and 300bar [12]. Supercritical CO_2 is miscible with H_2. Therefore the single-phase area with CO_2/triglyceride/H_2 is so small that it is not visible in Fig. 2, and a very large mixing gap occurs between the CO_2/H_2 phase and the CO_2/triglyceride/H_2 phase (see Fig. 2).

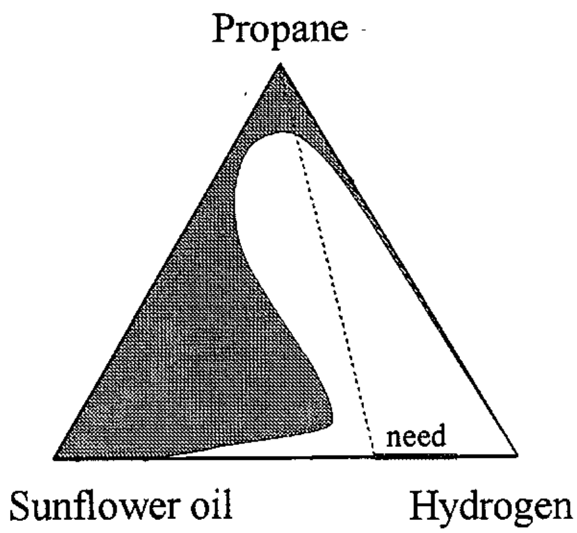

Figure 3. Phase diagram for sunflower oil, **propane** and hydrogen at 100bar and 100°C (mol%).
▩ Single phase ☐ Two phases

The solubility of H_2 in oil can be seen at the baseline between the oil and the hydrogen in Fig. 2 and Fig. 3. It is the same as illustrated by "eq" in Fig. 1. The stoichiometric need of hydrogen depends on the reaction, but generally it is above 50mol%. This means that one gas phase and one liquid phase have to be present in the reactor (see "need" between oil and hydrogen in Fig. 2 and 3). This ratio between oil and H_2 has to be maintained even when a solvent is added. Thus, the composition of the feed to the reactor has to be to the right of the dotted line in Fig. 2 and 3. In practice, the stoichiometric ratio has to be exceeded to some extent for technical reasons; we call it a "technical need".
As can be seen in Fig.2, using CO_2 as a solvent does not reduce the number of phases during the hydrogenation. However, it is reasonable to expect that the addition of CO_2 reduces the viscosity. This may lead to increased reaction rates, but the SubHSV is always below 10 000 $kg_{substrate}/m^3_{reactor}h$ [10, 11, 13-16].

Solvents are not preferred in commercial processes where the substrate is liquid, because the hydrogenation rates are not increased enough to motivate the costs required to recover the solvent [9].

Hydrogenation at supercritical conditions
The basic idea behind the new supercritical technology is that the substrate and the required hydrogen are in one single phase. This is achieved by adding a suitable solvent, which dissolves both the substrate and the hydrogen [17-20].

As before we use the hydrogenation of fats and oils as an example. For this kind of substrates propane is a good solvent. In Fig. 3 we describe the phase behaviour of such a mixture at different concentrations. Propane can be made miscible with oil [21] (see the oil/propane line in Fig. 3).

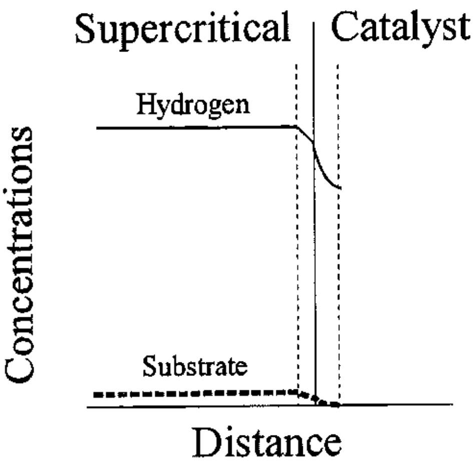

Figure 4. General concentration profiles during hydrogenation at *supercritical* conditions.

Supercritical propane is miscible with hydrogen (see the propane/H_2 line in Fig. 3). Based on literature [22, 23] and own experiments we have estimated the curve in Fig. 3.

To achieve the desired composition of the feed to the reactor one has to combine the required ratio of hydrogen to oil and the single-phase range in Fig. 3. At the top of the figure, to the right of the "need"-line a large favourable range can be found. From economical point of view it is important to have a high loading of oil in the feed, otherwise both the investment and the running costs for a plant will be high. Thus, the most favourable composition of a feed to a plant is the intersection between a "technical need" line and the phase border line.

Fig. 4 describes the concentration profiles during hydrogenation at supercritical conditions. Around the catalyst there is only one single phase. This makes it possible to choose the hydrogen concentration at the catalyst as required. In the traditional process described in Fig. 1. this concentration is always zero. At supercritical conditions the substrate can become the restricting component (see Fig. 4). This can be utilised to control the kinetics of the reaction.

In our experiments, we have achieved tremendous reaction rates, SubHSV >100 000 $kg_{substrate}/m^3_{reactor}h$ [17-20]. If we express the reaction rate as

mol/$g_{catalys}$h, we have achieved reaction rates similar to the highest rates achieved in a gas phase reactor [20]. Note that at the supercritical conditions the substrate molecule was much larger.
The supercritical technology provides a new tool to achieve new product qualities. As an example we can mention that during partial hydrogenation of rape seed fatty acid methyl esters we have been able to reduce the *trans* fatty acid concentration to below 5% at a an IV of 60 [19]. This is a dramatic reduction, which is impossible to achieve with traditional technology.

The main reason for these good results is the very high hydrogen concentration at the catalyst surface. However, reduced viscosity and increased diffusivity may also contribute.

We have achieved loadings of 15wt.% and good product quality for different lipids. We know that this loading can be increased further. High loading is desired because it reduces the solvent recovery costs. All hydrogenation reactions are strongly exothermic. This heat gives a strong temperature rise. Using a solvent the temperature rise is reduced. A high reaction temperature gives frequently undesired side products. Thus, we think that in the end there will be a balance between loading, product quality and solvent recovery costs.

The very high SubHSV can be used in different ways. Firstly, it leads to a dramatic reduction in reaction time, from hours in the traditional process to seconds at supercritical conditions. In turn this leads to less time-thermal degradation of sensitive products. Secondly, it can be partly sacrificed by running the process at a lower temperature. This may lead to less thermal degradation and a reduction of side products. Thirdly, it leads to small plants also when the solvent recovery plant is included. Small plants leads to small buildings and low investments. Fourthly, small plants means reduced risks. The value of pressure times volume is reduced when the hydrogenation is performed at supercritical conditions.

Outlook

Hydrogenation at supercritical conditions can improve the product quality and at the same time reduce the production costs. The technology can be applied to a wide range of products. However, a lot of research is required on topics like: solubility data for different substrate/solvent/hydrogen systems at different pressures and temperatures; catalyst and reactor design; process optimisations to achieve the desired product quality at low costs; fundamental kinetic research; separation processes including solvent recovery; and design of production plants.

Some processes are developed so far that decisions to build large plants will be taken in the near future. Other processes require a lot of work to reach this stage but the potential tremendous.

Acknowledgements

Our work is financed by the Swedish Council for Forestry and Agricultural Research (SJFR) and daka a.m.b.a., Løsning, Denmark.

References

1. Mielke, S.; *Inform,* **1992**, 3:695.
2. Fitch Haumann, B., *Inform* **1994**, 3:668.
3. Hui, Y.H. (ed.), "Bailey's Industrial Oil and Fat Products", Vol. 4, 5th edn., John Wiley & Sons Inc., New York, NY, 1996.
4. Horiuti, I.; Polanyi, M. *Trans. Faraday Soc.* **1934**, 30:1164.
5. Allen, R.R. *J.Am.Oil Chem.Soc.*, **1986**, 63:1328.
6. Hsu, N.; Diosady, L.L.; Rubin, L.J. *J.Am.Oil Chem.Soc.*, **1989**, 66:232.
7. Berben, P.H.; Blom, P.J.W.; Sollie, J.C. **1995** *Proceedings of AOCS meeting.*
8. Wisniak, J.; Albright, L.F. *Ind. Eng. Chem.* **1961**, 53:375.
9. Veldsink, J.W.; Bouma, M.J.; Schöön, N-H.; Beenackers, A.A.C.M. *Catal.Rev.-Sci.Eng.*, **1997**, 39(3), 253-318.
10. Hitzler, M.G.; Smail, F.R.; Ross, S.K.; Poliakoff, M. *Organic Process Research Development,* **1998**, 2(3), 137-146.
11. Zosel, K. *US patent 3 969 382*, **1976**
12. McHugh, M.A.; Krukonis, V.J. "Supercritical Fluid Extraction: Principles and Practice", 2nd ed., Butterworth-Heinemann, Stoneham, MA, **1994**, p. 300.
13. Pickel, K-H.; Steiner, K. *Proc. 3rd Int. Symp. Supercritical Fluids,* Strasbourg, **1994**, 3:25
14. Tacke, T.; Rehren, C.; Wieland, S.; Panster, P.; Ross, S.K.; Toler, J.; Hitzler, M.G.; Smail, F.R.; Ross, S.K.; Poliakoff, M. *17th conf Catalysis Organic Reactions,* New Orleans, **1998**.
15. Devetta, L.; Canu, P.; Bertucco, A.; Steiner, K. *Chem.Eng.Sci.* **1997**, 52(21/22), 4163-4169.
16. Minder, B.; Mallat, T.; Pickel, K-H.; Steiner, K.; Baiker, A. *Catalysis Letter,* **1995**, 34,1-9.
17. Härröd, M.; Møller, P. *PCT patent application,* **1996**, WO 96/01304.
18. Härröd, M.; Macher, M-B.; Högberg, J.; Møller, P. *4th Italian Conf. on Supercritical Fluids and their Applications,* Capri, **1997**, 319-326.
19. Macher, M-B.; Härröd, M.; Møller, P. **1999**, *submitted.*
20. van den Hark, S.; Härröd, M.; Møller, P. **1999** *submitted.*
21. Brunner, G., *Fette-Seifen-Anstrichmittel* **1986** 88:464.
22. Schiemann H., PhD thesis, Univ. Erlangen-Nurnberg, Erlangen, **1993**.
23. Coorens, H.G.A.; Peters, C.J.; De Swaan Arons, J. *Fluid Phase Equilibria,* **1988**, 40, 135-151.

Chemical Reactions in Supercritical Fluids as a Continuous Process

Martyn Poliakoff*, Fiona Smail, Nicola Meehan, Keith W. Gray, Martin G. Hitzler
and Stephen K. Ross.
School of Chemistry, University of Nottingham, Nottingham, NG7 2RD, ENGLAND
email; Martyn.Poliakoff@nottingham.ac.uk; fax. +44 115 951 3058
http://www.nottingham.ac.uk/supercritical/

Supercritical fluids (SCFs) offer a wide range of opportunities as media for chemical reactions and supercritical CO_2, $scCO_2$, is becoming increasingly important as a benign replacement for more toxic solvents.[1] High pressure reactions, however, are more capital intensive than conventional low pressure processes. Therefore, supercritical fluids will only gain widespread acceptance in those areas where the fluids give real chemical advantages as well as environmental benefits. This lecture gives a brief account of the use of flow reactors for continuous reactions in supercritical fluids, particularly those of interest for the manufacture of fine chemicals.

We initially became involved with SCFs via inorganic and organometallic chemistry, a field which we have comprehensively reviewed very recently.[2] We were among the first to recognise that the miscibility of H_2 with SCFs could be exploited for new chemistry and we generated a number of previously unknown organometallic dihydrogen complexes.[3] This miscibility of H_2 has since been widely exploited by other groups for supercritical homogenous catalysis.[4-6] More recently we developed the use of miniature flow reactors to isolate new, highly labile alkene and dihydrogen complexes from SCF solution.[7,8]

Our work on H_2-complexes and flow reactors led to our interest in the supercritical hydrogenation of organic compounds and initiated a fruitful collaboration between the University of Nottingham and Thomas Swan & Co. Ltd. The attraction of $scCO_2$ is that it offers new possibilities in chemical processing as well as being cleaner. In particular, it offers the possibility of converting from batch to continuous processes, with the advantages of smaller reactors, lower inventories of chemicals and increased safety. Several groups have reported the use of continuous reactors for hydrogenation,[9-18] Our own work has focused on the hydrogenation of compounds of interest to the fine chemicals industry. We have shown that $scCO_2$ and supercritical propane can be used as solvents for the ***continuous supercritical hydrogenation of a wide range of organic functionalities***.[13,14] The organic substrate, H_2 and $scCO_2$ are mixed by the stirrer, and are then passed over a heterogeneous catalyst bed, such as Pd/Deloxan (a polyamino-siloxane support from Degussa). Depressurization of the system downstream gives phase separation of the CO_2 and organic products. Conditions can be optimised to give very high selectivity and efficiency in such a reactor. This opens up the possibility of continuous "on demand" manufacture of fine-chemicals without the need to stock-pile chemicals which is inherent in batch processes. In this lecture, we will show how this concept can be extended to other organic reactions, for example Friedel Crafts alkylation, using a solid acid catalyst.[19] In each reaction, $scCO_2$ appears to offer significant advantages, as well as process intensification. Thus, supercritical hydrogenation of isophorone gives 99.6% selectivity for dihydro-isophorone,[14] better than is achieved in most commercial hydrogenation processes for this compound. In the Friedel-Crafts reaction, there is high

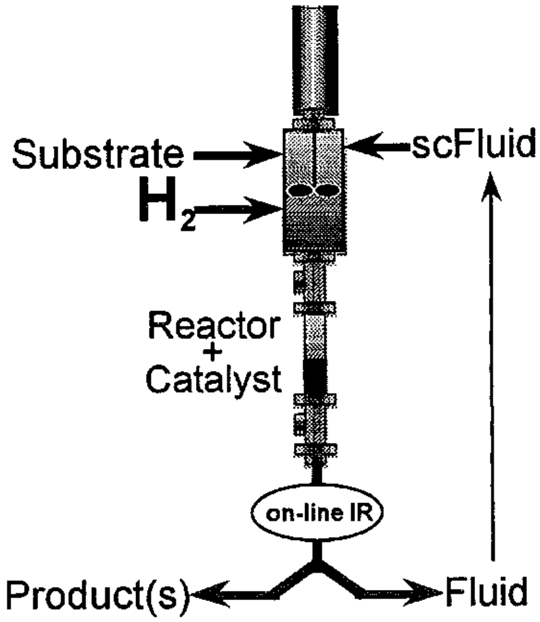

selectivity for mono-alkylation and long catalyst lifetime.[19] In all of the reactions, the products are recovered free from any liquid solvent, which greatly simplifies the subsequent work-up. *We thank EPSRC, the Royal Academy of Engineering, Thomas Swan & Co Ltd and Degussa AG for their support.*

References

(1) *Green Chemistry: Frontiers in Benign Chemical Synthesis*; Anastas, P. T.; Williamson, T. C., Eds.; Oxford University Press, **1998**.

(2) Darr, J. A.; Poliakoff, M. *"New Directions in Inorganic and Metal-Organic Coordination Chemistry in Supercritical Fluids" Chem. Rev.* **1999**, *99*, 495.

(3) Howdle, S. M.; Healy, M. A.; Poliakoff, M. *J. Am. Chem. Soc.* **1990**, *112*, 4804.

(4) Jessop, P. G.; Ikariya, T.; Noyori, R. *Nature* **1994**, *368*, 231.

(5) Rathke, J. W.; Klingler, R. J.; Krause, T. R. *Organometallics* **1991**, *10*, 1350.

(6) Klingler, R. J.; Rathke, J. W. *J. Am. Chem. Soc.* **1994**, *116*, 4772.

(7) Banister, J. A.; Lee, P. D.; Poliakoff, M. *Organometallics* **1995**, *14*, 3876.

(8) Lee, P. D.; King, J. L.; Seebald, S.; Poliakoff, M. *Organometallics* **1998**, *20*, 524.

(9) Pickel, K.-H.; Steiner, K. Proc. 3rd Int. Symp. on Supercritical Fluids,, Strasbourg, France, **1994**, 25.

(10) Härröd, M.; Møller, P. In *High Pressure Chemical Engineering*; Rudolph von Rohr, P., Trepp, C., Eds.; Elsevier: Netherlands, **1996**, 43.

(11) Härröd, M.; Macher, M.-B.; Högberg, J.; Møller, P. Proc. 4th Conf. on Supercritical Fluids and Their Applications, Capri, Italy, **1997**, 319.

(12) Tacke, T.; Wieland, S.; Panster, P. In *High Pressure Chemical Engineering*; Rudolph von Rohr, P., Trepp, C., Eds.; Elsevier: Netherlands, **1996**, 12.

(13) Hitzler, M. G.; Poliakoff, M. P. *Chem. Commun.* **1997**, 1667.

(14) Hitzler, M. G.; Smail, F. R.; Ross, S. K.; Poliakoff, M. *Org. Proc. Res. Dev.* **1998**, *2*, 137.

(15) Bertucco, A.; Canu, P.; Devetta, L.; Zwahlen, A. G. *Ind. Eng. Chem. Res.* **1997**, *36*, 2627.

(16) Devetta, L.; Canu, P.; Bertucco, A.; Steiner, K. *Chem. Eng. Science* **1997**, *52*, 4163.

(17) King, J. W. In *NATO AS Institute on Supercritical Fluids, Kemer, Turkey*; Kluwer Academic Publications: Dordrecht, **1998**, to be published.

(18) Devetta, L. PhD, Padua, Italy, **1998**.

(19) Hitzler, M. G.; Smail, F. R.; Ross, S. K.; Poliakoff, M. *Chem. Commun.* **1998**, 359.

Sol-gel synthesis and characterization of various oxide aerogels and NiO and Pd supported on aerogels

Ž. Knez*, Z. Novak
Faculty of Chemistry and Chemical Engineering, University of Maribor, Smetanova 17,
SI-2000 Maribor, Slovenia
E-mail: zeljko.knez@uni-mb.si, Fax: +386 62 22 77 74.

The preparation and characterization of aerogels of metal oxides (SiO_2, Al_2O_3 and TiO_2), binary mixed oxides (SiO_2-Al_2O_3 and SiO_2-TiO_2), and various NiO aerogels (NiO-Al_2O_3, NiO-SiO_2 and NiO-SiO_2-Al_2O_3) and Pd aerogels (Pd-Al_2O_3 and Pd-SiO_2-Al_2O_3) is presented.

The preparation of aerogels includes several steps: sol-gel synthesis, drying and, finally, thermal treatment. Excellent properties of aerogels, obtained with the sol-gel synthesis, were preserved with supercritical drying with CO_2. Due to this fact, supercritical drying was carried out at the conditions above the binary critical curve of the solvent - CO_2, where the solvent and CO_2 are completely miscible.

All produced aerogels were characterized by means of nitrogen physisorption at 77 K, single point BET surface area measurements (adsorption of argon-nitrogen gas mixture), X-ray diffraction and thermal analysis.

Introduction

Silica aerogels, as well as other metal oxide (alumina, titania, zirconia, stannic or tungsten oxide or mixture of these oxides) aerogels, are extremely porous high-tech materials with very high specific surface areas. They possess an ultrafine pore size (< 100 nm) and due to their high porosity (up to 99% for SiO_2), aerogels show a few highly interesting physico-chemical properties: very high specific surface area (500-1000 m^2g^{-1}), low bulk density (0.003-0.35 gcm^{-3}), low thermal conductivities (0.014 $Wm^{-1}K^{-1}$ at atmospheric pressure and 0.004 $Wm^{-1}K^{-1}$ at reduced pressure), sound velocity in the order of 100 ms^{-1} and refractive index between 1.008 and 1.4 (for SiO_2 1.008 -1.05).

Due to these remarkable properties many aerogels could serve as especially active catalysts and catalyst supports [1-3], precursors for glasses and glass-ceramic materials [4,5], for superinsulation [6,7] and some other applications such as: gellifying rocket propellants [8], as insect killers [9], for the capture of pollution gases [10].

Experimental methods

Sol-gel transformation. The apparatus used for the sol-gel syntheses was already presented in our articles [11,12]. It consists of two-piece glass reactor with a water cooled condenser for the reflux of solvent and a dropping funnel for the addition of different reactants during sol-gel synthesis. To perform the sol-gel synthesis in an inert atmosphere, nitrogen was supplied from a gas cylinder.

Supercritical carbon dioxide drying. Aerogels with their special properties can only be produced when the solvent is removed in the absence of capillary forces in the gel pores, because even small capillary forces collapse the gel structure [13]. In supercritical carbon dioxide drying, alcohol is replaced by carbon dioxide. The main idea is the extraction of alcohol with carbon dioxide at conditions above the critical conditions of CO_2 ($T_C = 31.1°C$, $P_C = 7.36$ MPa).

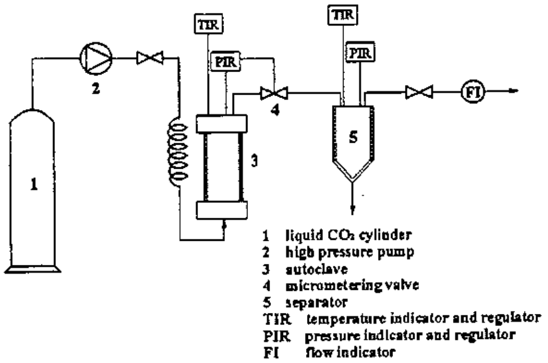

Figure 1. Schematic representation of supercritical carbon dioxide drying equipment.

Thermal treatment. All produced aerogels were thermally treated for three hours in air at two different temperatures: 400°C and 800°C.

Characterization. The physico-chemical properties of the aerogels were characterized by means of nitrogen physisorption, X-ray diffraction (XRD), thermal analyses (TG, DSC) and single point BET surface area measurements.

Results and discussion

Single and mixed oxide aerogels.

Three different single oxide (SiO_2, Al_2O_3 and TiO_2) aerogels were prepared to determine some physico-chemical properties. These are necessary for better understanding of the preparation of mixed oxide aerogels (SiO_2-Al_2O_3 and SiO_2-TiO_2 aerogels).

Table 1. Oxide aerogels designations and corresponding sol-gel synthesis conditions.

Aerogel	Composition wt (%)	Sol-gel system[a] alkoxide-solvent	H_20[b] r_w	Appearance
SM	100% SiO_2	$Si(OMe)_4$-MeOH	4	transparent gel
AB30SM	30%Al_2O_3 - 70% SiO_2	$Si(OMe)_4$-MeOH $Al(sec\text{-}OBu)_3$-sec-BuOH	4 3	gel
AB60SM	60% Al_2O_3 - 40% SiO_2	$Si(OMe)_4$-MeOH $Al(sec\text{-}OBu)_3$-sec-BuOH	4 3	gelatinous precipitate
AB	100% Al_2O_3	$Al(sec\text{-}OBu)_3$-sec-BuOH	3	precipitate
TiB	100% TiO_2	$Ti(OBu)_4$-BuOH	4	precipitate
TiB30SM	30% TiO_2 - 70% SiO_2	$Si(OMe)_4$-MeOH $Ti(Obu)_4$-BuOH	4 4	gel

[a] 10 wt% solutions of alkoxides in solvent

[b] mole of water/mole of alkoxide

Adsorption/desorption cumulative surface areas (S_{cum}), pore diameter (d) and pore volumes (V) of mesopores were estimated using the method of Barrett-Joyner-Halenda (BJH) [14]. The assessments of microporosity were made from t-plot constructions, using the Harkins-Jura relation. Micropore diameter was estimated by the Horwath-Kawazoe calculations using both, a model for cylindrical pore geometry and a model for slit pore geometry.

Table 2. N_2 physisorption results for different silica aerogels.

Aerogel	S_{BET} (S_{mic})[a] (m^2/g)	Ads. S_{cum}(m^2/g)	Des. S_{cum}(m^2/g)	V (cm^3/g) meso/micro	d (nm)[b] meso/micro
SM	1065 (170)	914	1114	6.3/0.072	10-20/1.5
AB30SM	620 (243)	360	398	1.1/0.117	10-15/1.5
TiB30SM	569 (295)	238	345	0.8/0.149	10-12.5/1.5

[a] (S_{mic}) in parenthesis specific micropore area

[b] cylindrical pore geometry

As can be concluded from the isotherm curves for all aerogels, samples consist of micropores and mesopores (type of isotherm number IV). Single silica aerogel (SM) has large specific surface area and high pore volume but small level of microporosity confirmed by both low micropore area and volume.

If two mixed oxide aerogels are compared to silica aerogel, BET surface areas are lower and also $S_{cum} << S_{BET}$, which indicates both the presence of micropores and the possibility of numerous spherical cavities. Specific areas of micropores indicate high level of microporosity in both mixed oxide aerogels. For all samples, a micropore diameter, estimated by using a model for slit pore geometry, is about 1 nm. Silica aerogel has also very narrow and symmetrical pore size distribution of mesopores. Pore size distribution is within the interval of 10 and 20 nm.

Independently from N_2 physisorption, the specific surface areas (BET) were measured by the adsorption of mixed gas (30% N_2 and 70% Ar) to determine their behavior dependent on thermal treatment.

Tab. 3 shows the morphological properties of raw single oxide aerogels. If compared to those, obtained for silica aerogels, the loss of weight is much higher for all three aerogels. These weight losses determined up to 500°C originate from water (desorption of physisorbed water, dehydroxylation) and organic residues (alkoxy groups).

Table 3. Properties of raw alumina and titania aerogels.

Aerogel	S_{BET} (m^2/g)	Weight loss (%)[a]	XRD (raw aerogel)
SM	664	7,97	Amorph.
AB30SM	577	30,3	Amorph.
AB60SM	287	44,3	Amorph.
AB	453	46,0	Amorph.
TiB	469	37,3	Amorph.
Ti30SM	392	34,9	Amorph.

[a] Weight loss of raw aerogel derived from thermal analysis up to temperature 500°C

Weight losses of mixed SiO_2-Al_2O_3 aerogels increase with the increasing of the content of Al_2O_3. Fig. 2 shows the decrease of BET specific surface area while the content of Al_2O_3 in mixed silica-alumina aerogels increases. This decrease does not depend on the fact whether the aerogels are calcinated or not. The minimum of BET surface area appears at the content of 60 mol% of Al_2O_3, afterwards the area slightly increases to single (100 mol%) Al_2O_3.

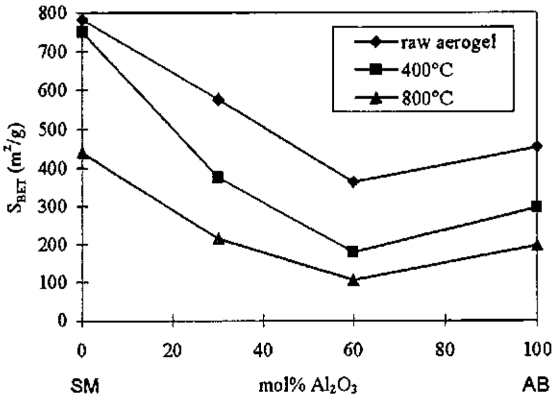

Figure 2. BET surface areas vs. content Al_2O_3 in mixed silica-alumina aerogel.

In comparison to silica aerogel, single titania aerogel is extremely unstable even at low calcination temperature. A sharp drop in specific surface area to almost neglected 17 m^2/g was observed at 400°C (and 2 m^2/g at 800°C). The addition of silica stabilizes TiO_2 aerogels with regard to thermal treatment. The drop of specific surface area is gradual and more linear than for single TiO_2 aerogel (250 m^2/g at 400°C and 100 at 800°C).

NiO supported on silica and alumina aerogels. Nickel acetoacetat, crystallized with four moles of water ($Ni(OOC-CH_3)_2 \bullet 4H_2O$), was used for producing NiO aerogels with composition as shown in Tab. 4.

Table 4. NiO aerogels designations and corresponding sol-gel synthesis conditions.

Aerogel	Sol-gel system Alkoxide-solvent	Ratio Ni/(Al or Si)	Appearance[a]	Bulk density (g/L)
NiOSM	$Si(OMe)_4$-MeOH	3/5	Gel	65.04
NiOAB(x)[b]	$Al(sec\text{-}OBu)_3$-sec-BuOH	1/5 2/5 3/5	Precipitate	82.62 98.80 106.57
NiOAB30SM	$Si(OMe)_4$-MeOH $Al(sec\text{-}OBu)_3$-sec-BuOH	3/5	Sol	58.59

[a] ageing 6 days

[b] x = 0.2, 0.3 and 0.6

From isotherm curves (type of isotherm number IV) of both NiO aerogels it is obvious that the samples consist of micropores and mesopores. $S_{cum} < S_{BET}$ for NiOSM aerogel indicates the presence of micropore with micropore specific area and volume quite similar to that of silica aerogel. The specific surface area and volume of mesopores are slightly lower but still high in comparison to all other mixed silica aerogels. From these results it is obvious that including NiO in silica aerogel does not have a lot influence on the physico-chemical properties of silica aerogel.

Table 5. N_2 physisorption results for $NiO-SiO_2$ and $NiO-Al_2O_3$ aerogels.

Aerogel	S_{BET} (S_{mic})[a] (m^2/g)	Ads. S_{cum} (m^2/g)	Des. S_{cum} (m^2/g)	V (cm^3/g) meso/micro	d (nm)[b] meso/micro
NiOSM	809 (161)	542	591	2.3/0.072	15-20/2
NiOAB	316 (22)	268	292	0.8/0.009	25-30/2

[a] (S_{mic}) in parenthesis specific micropore area derived from t-plot analyses

[b] cylindrical pore geometry

Fig. 3 shows specific surface areas of different NiO aerogels after calcination for 3 hours at 400°C in air.

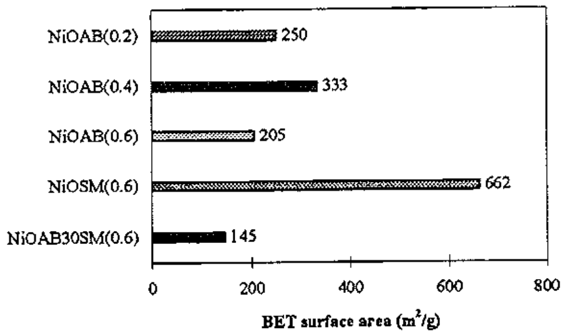

Figure 3. Bet surface areas of different NiO aerogels.

These results are in close agreement with those obtained for single and mixed oxide aerogels. Only one unexpected result for the sample NiOAB30SM(0.6) appeared. BET surface area is lower than expected, which is probably due to the fact that no gel or precipitate has been formed and the precipitation of this aerogel from sol has occurred during supercritical CO_2 drying process. Despite different ways of preparation, weight losses of all $NiO-Al_2O_3$ aerogels are similar, about 50%. Weight loss of $NiO-SiO_2$ aerogel is about 25%.

Fig. 4 shows X-ray diffraction patterns for $NiO-SiO_2$ aerogel at different temperatures up to 800°C. All patterns indicate that the aerogel sample NiOSM is totally amorphous after drying and calcination up to temperature 800°C. Two peaks on each pattern belong to Pt-carrier in X-ray diffractometer.

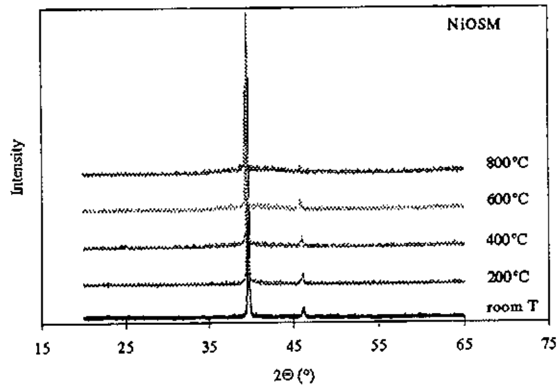

Figure 4. X-ray diffraction patterns for $NiO-SiO_2$ aerogel.

Pd supported on Al_2O_3 and Al_2O_3-SiO_2 aerogels. Several different Pd supported on silica and alumina aerogels were also prepared as shown in table 6. Palladium was introduced during the sol-gel synthesis by adding the solution of $PdCl_2$ in apropriate solvent.

Table 6. Pd aerogels designations, sol-gel synthesis, conditions and results.

Aerogel[a]	Gelation and ageing[b]	Appearance	S_{BET}[c] (m^2/g)	Bulk density (g/L)
PdAB	8 days	precipitate	385	83.20
PdABac	8 days	precipitate	409	82.70
PdABetac	12 days 50°C	sol	335	208.33
PdABSM	8 days	precipitate	346	144.73
PdABSMetac	12 days 50°C	gel	430	75.44

[a] metal loading 2 wt%

[b] at room temperature, if otherwise, noted

[c] after calcination for 3 hours at 400°C in air

Catalytic properties of $Pd-Al_2O_3$ aerogels. $Pd-Al_2O_3$ aerogels were used as catalysts in the reaction of hydrogenation of soybean oil. Their activities were compared to commercial one (Heraeus).

PdABac-400-act.:
- Pd-Al_2O_3 aerogel- palladium content 2 wt%,
- thermally treated at temperature 400°C,
- activation: 26 hours in hydrogen atmosphere at temperature 145°C.

Fig. 5 shows the refractive index during the hydrogenation process. The refractive index of Pd-Al_2O_3 aerogel catalysts decrease more sharply than the commercial one.

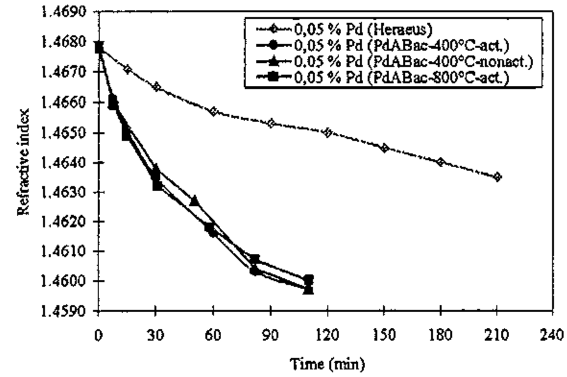

Figure 5. Refractive index vs. time of hydrogenation.

From slopes of linearized parts the initial reaction rates of hydrogenation were calculated.

Table 7. Initial reaction rates of hydrogenation of soyabean oil

Init. Rate	Heraeus	PdABac-400-act.	PdABac-400-nonact.	PdABac-800-act.
$r_0 = \frac{mol}{s \cdot g}$	$9{,}09 \bullet 10^{4}$	$13{,}13 \bullet 10^{4}$	$13{,}47 \bullet 10^{4}$	$16{,}11 \bullet 10^{4}$

From Tab. 7 it is obvious that sample PdABac, calcinated at 800°C, shows higher activity that the same one, calcinated at 400°C. The initial reaction rates of both PdABac-400-act. and PdABac-400-nonact. indicate that no activation is necessary. At the end, in this particular reaction it was found out that our aerogel catalyst PdABac-800-act. shows 77 % more activity than the compared commercial one.

Conclusion

The preparation of aerogels includes several steps: sol-gel synthesis, drying and thermal treatment. Excellent properties of aerogels, obtained with the sol-gel synthesis, are preserved with supercritical drying with CO_2. Due to this fact, supercritical drying has to be carried out at the conditions above the binary critical curve of the solvent - CO_2, where the solvent and CO_2 are completely miscible.

All produced single and mixed oxide aerogels have very high specific surface areas after supercritical drying. The calcination of these aerogels causes the decrease of specific surface area.

Thermal analyses of the samples of produced aerogels indicate a series of inert materials with regard to thermal sensibility. Similarly, X-ray analyses show that aerogels are totally amorphous even up to the temperature of 800°C.

Nitrogen physisorption shows that both single oxide and mixed binary oxide aerogels consist of micro and mesopores.

Despite including NiO and Pd into single and binary oxide aerogels, high specific surface areas, up to 800 m^2/g, were preserved.

In case of model reaction of hydrogenation of soyabean oil, Pd-Al_2O_3 aerogel, calcinated at the temperature of 800°C, used as a catalyst, showed 77% more activity than the compared commercial catalyst.

References

[1] Fricke, J. (ed.): "Aerogels", Proceedings of the 1st International Symposium on Aerogels, ISA1, Würzburg 1985, Springer Proceedings in Physic, Vol. 6, Springer-Verlag, Berlin, 1986
[2] Cauqui, M.A.; Rodriguez-Izquierdo, J.M.: J. Non-Cryst. Solids, 147&148 (1992), 724
[3] Pajonk, G.M.: Appl. Catal., 72 (1991), 217
[4] Zarzycki, J.; Woignier, T.; in: [1], p. 42
[5] Woignier, T.; Phalippou, J.; Hdach, H.; Larnac, G.; Pernot, F.; Sherer, G.W.: J. Non-Cryst. Solids, 147&148 (1992), 672
[6] Schmitt, W.J.; Greiger-Black, R.A.; Chapman, T.W.: The preparation of Acid Catalyzed Aerogels, annual meeting AICHE, New Orleans, 1981
[7] Henning, S.; in: [1], p. 38
[8] Pajonk, G.M.; Teichner, S.J.; in: [1], p. 193.
[9] San-Sarma; Mishra, S.C.: Indian J. Entour., 38 (1976), 11
[10] Attia, Y.A.; Ahmed, M.S.; Zhu, M.; in:, "Sol-Gel Processing and Applications", Proc. Int. Symp. on Advances in Sol-Gel Processing and Applications (Ed. Y.A. Attia), Plenum, New York, 1993, p. 311
[11] Novak, Z.; Knez, Z.: Chem. Tech. 49 (1997), 106
[12] Knez, Z.; Novak, Z.; in: Proc. 5th Meeting on Supercritical Fluids, Tome 1, Nice, 1998, p. 13
[13] Novak, Z.; Knez, Z.: J. Non-Cryst. Solids 221 (1997), 163
[14] Lecloux, A.: Mémoires Société Royale des Sciences de Liége, 6e Série, Tome I, Fach. 4, 1971, p. 169

GVC-Fachausschuß „High Pressure Chemical Engineering", March 3-5, Karlsruhe, Germany, 1999 GVC FZK '99

Pyrolysis and Hydropyrolysis of A Turkish Lignite Under High Pressures

Muammer Canel
Ankara University Science Faculty Department of Chemistry 06100 Besevler-Ankara/TURKEY
Fax : 00 - 90 - 312 - 223 23 95

Pyrolysis and hydropyrolysis of a turkish lignite has been performed in nitrogen and hydrogen atmospheres in a flow through reactor. The influence of ambient gas atmosphere (inert, reactive) and the pressure on the yield of products have been investigated. The yield of liquid and gas products is significantly influenced by the type of gaseous atmosphere. The tar and gaseous products obtained by hydropyrolysis are greater than those obtained by pyrolysis under the same conditions. The tar yield in hydropyrolysis increases substantially as the pressure increases. An increase of pressure for both pyrolysis and hydropyrolysis leads first to an increase in the yield of gaseous products than a decrease at high pressures. As a result of the reaction of char with the H_2 gas existing in the reactor in hydropyrolysis the amount of CH_4 and C_2H_6 present in the gaseous products are substantially higher than those exist in pyrolysis. The formation rates of tar and the total gaseous products obtained by hydropyrolysis are higher than those obtained by pyrolysis

Introduction

The thermal decomposition of organic compounds of coal above 300 ^{0}C in an oxygen-free medium is called pyrolysis. Pyrolysis of coal is a basic reaction in gasification, hydrogenation, combustion and carbonization. It is also an additional method for the production of liquids from coal. Among the methods of producing liquids from coal pyrolysis represents a fourth way besides gasification followed by Fischer-Tropsch synthesis, direct coal hydrogenation and supercritical extraction with different solvents. The kind and the amount of the pyrolysis products depend on the coal used and the experimental process conditions. If the pyrolysis is realized under hydrogen atmosphere it is called hydropyrolysis. It is especially possible to obtain high conversion of coal to liquid products in hydropyrolysis [1]. For this reason besides the gasification, liquefaction and extraction processes, extensive studies on the production liquid products by hydropyrolysis are being realized in the recent years [2-5]. The main objective of pyrolysis or more specifically of hydropyrolysis is to produce the liquid chemicals that are used in medicine, in the prevention of plants from microorganismus, in cosmetic industry and in paint industry. ¼ th (~30 million tons/year) of the aromatic chemical materials produced in one year in the world are obtained from coal tar. 15 % of benzene production and 95 % of heteroaromatic compounds are also produced from tar [6]. The aromatic compounds benzene, toluene and xylene which are known as BTX-aromatics are especially important as raw materials. One of the objection of pyrolysis is to obtain BTX compounds.

The aim of this study was to investigate the effect of pressure and pyrolysis atmosphere on the total conversion and the product yield and furthermore to determine the formation rates of the products as a function of temperature and pressure. In the literature the coals that contain more than 30% of volatile matter are defined as 'suitable for pyrolysis'. The Tunçbilek lignite ,which contains 43% volatile matter, being a solid fuel suitable for pyrolysis was submitted to experimentation.

Materials and Methods

The pyrolysis and hydropyrolysis experiments were carried out with a high volatile Tunçbilek lignite from West-Turkey. The analysis of Tunçbilek lignite is shown in Table 1.

Table 1 Analysis of Tunçbilek Lignite

Proximate analysis (wt %)		**Ultimate analysis (wt % daf)**	
Moisture	10.5	C	73.0
Ash (db)	15.7	H	5.4
Volatile matter (daf)	43.2	N	2.4
Maceral analysis (vol %)		S	2.1
Vitrinite.	69.0	O(diff.)	17.1
Exinite	15.0	H/C (atomic)	0.89
Inertinite	1.0		
Minerals	15.0		

The experiments were performed in a system with pressurized thermobalance. The system with the thermobalance to which pressure can be applied is shown schematically in Fig. 1.

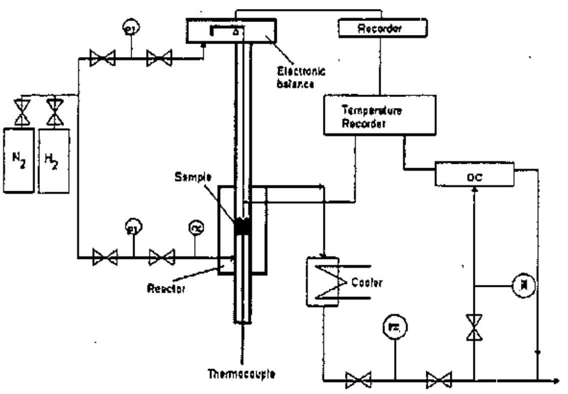

Figure 1. Experimental Setup Scheme

The lignite sample (~2 g, particle size 0.5mm-0.8 mm) was heated up in a pressurised thermobalance from 120°C to 950°C at a heating rates of 3°C/min. The pyrolysis products were discharged from the reactor by means of carrier gas (flow rate 3.5 L (NTP)/min). The amount of the solid, liquid and gaseous products as a function of temperature and inert gas (N_2) and hydrogen pressures in the range of 0.5 MPa up to 10 MPa were determined. The gaseous products (CH_4, C_2H_6, C_2H_4, CO, CO_2 and H_2O) and BTX aromatics were analysed by the gas chromatography which is coupled to the system. The mass equilibrium is established using the gaseous products, the moisture present at the beginning and the tar obtained and the residual char. Formation rate curves were obtained from the amount of each gas determined by gas chromatography. The total gas formation curve was obtained from those curves. The difference between the weight loss due to the formation of the non-condensable total and weight loss of the sample recorded continuously with the thermobalance showed the corresponding curve of tar formation rate depending on temperature.

Results and Discussion

The variation of mass with temperature at 5 MPa inert gas pressure is shown as an example in Fig. 2. The weight loss differential curve consist of a steep peak with a subsequent shoulder. It can clearly seen that in an inert atmosphere the substantially mass loss occurs in the range of 350°C and 800°C. In this temperature range decomposes the high molecular organic compounds into the tar, gases and residual char. The yield of tar and gaseous products at different pressures in pyrolysis and hydropyrolysis are shown in Fig. 3. The yield of the liquid and gaseous products is significantly influenced by the type of gaseous environment. When the tar and gaseous product yields obtained at different pressures in pyrolysis and hydropyrolysis are compared, it is observed that the tar and gaseous product yields obtained by hyropyrolysis are greater than those obtained by pyrolysis under the same conditions. In the presence of hydrogen the pyrolysis reaction mechanism changes substantially and the additional formation of methane and tar compounds takes place at the expend of solid product. Especially in hydropyrolysis the tar yield increases substantially as the pressure increases. Concerning the amount of total gaseous products, at first an increase, then a decrease observed when the pressure increased.

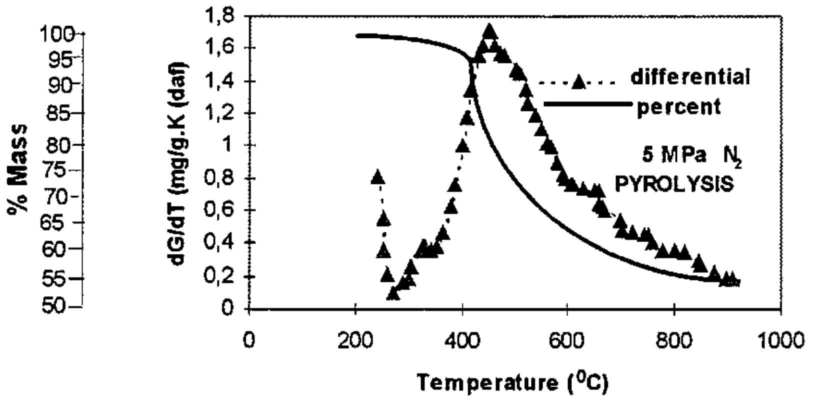

Figure 2. Thermogravimetric Analysis of Lignite

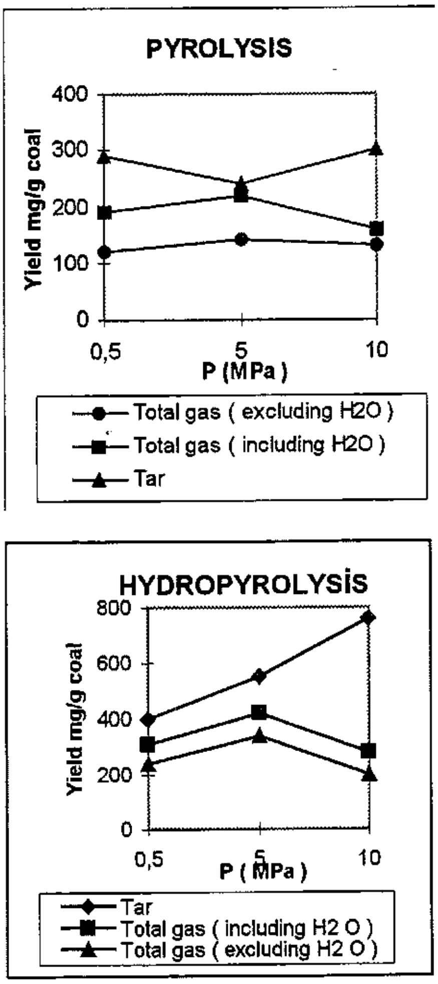

Figure 3. Product Yields Versus Pressure

Fig. 4 shows the effect of pressure on the yield of each gaseous products. In hydropyrolysis, as a result of the gasification of char with H_2 in the reactor, there is an important increase in CH_4 and C_2H_6 yields with respect to pyrolysis.

The dependence of the tar formation rates on temperature during pyrolysis and hydropyrolysis are given in Fig. 5. The weight loss of lignite during pyrolysis and hydropyrolysis begins around 350°C and continues up to 900°C. The maximum of weight loss during pyrolysis at 0.5 MPa and at 5 MPa are at 450°C and at 500°C respectively, whereas at 10 MPa it is at 800°C. The possible reason for this is as follows:

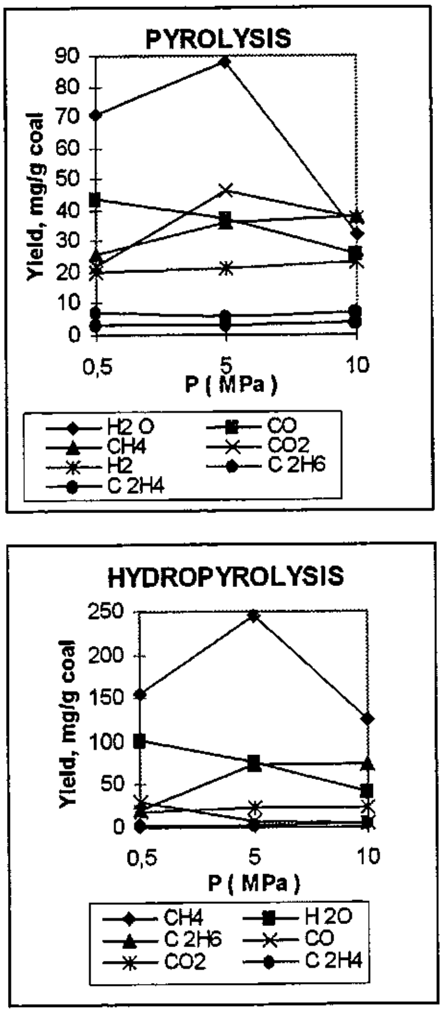

Figure 4. Gas Yields Versus Temperature

Low pressures promote the transport of primary volatiles out of the coal particle and thereby out of the reaction zone, whereas increasing pressure extends the residence time inside the coal particle. In this latter case enhancing the temperature from 500°C to 800°C causes the formation of tar compounds by the cracking of coal which could come out of the pores only at high temperatures. In hydropyrolysis as a result of the stabilisation of the radicals by H_2 the tar formation and its separation from coal is completed between 400°C-700°C. .Fig. 6 shows the variation of the total amount of gaseous products with temperature and pressure in pyrolysis and hydropyrolysis. In pyrolysis, the gas formation begins around 300°C and shows some peaks between 400°C and 700°C.

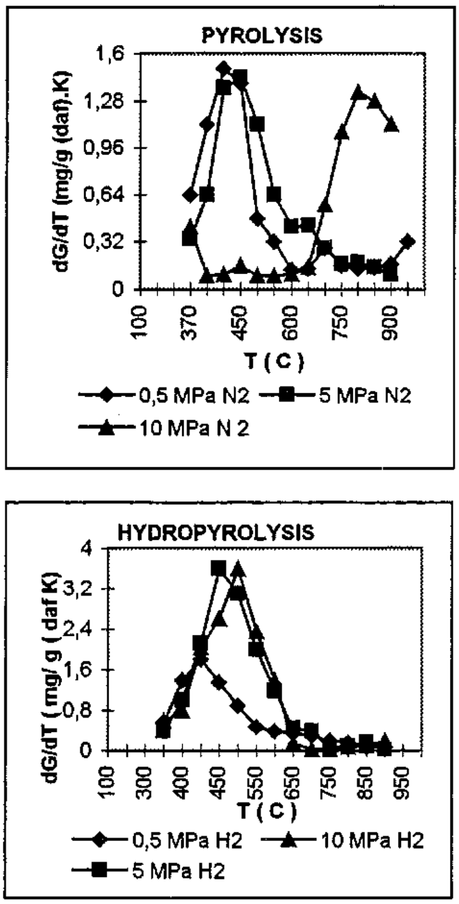

Figure 5. Tar Formation Curves

The effect of pressure on the total gas formation rate can be explained by the individual gas formation rate of each gas. In hydropyrolysis, a variation similar to that of pyrolysis is observed up to 700°C. At higher temperatures than 700°C as a result of the reaction of char with H_2 existing in the medium to give more CH_4 and C_2H_6 a considerable increase in gas formation rate occurs.

Conclusions

The results show that higher tar and gaseous product yields are obtained under the same conditions in hydropyrolysis when compared to those obtained in pyrolysis. In the presence of hydrogen the pyrolysis mechanisms change substantially with additional formation of tar, gaseous products such as methane and ethane at the expense of residual char.

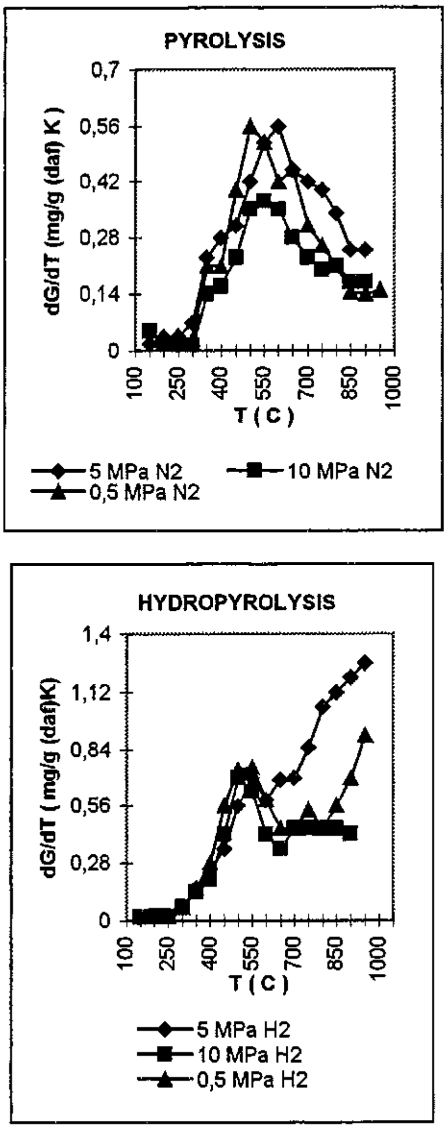

Figure 6. Gas Formation Yields

References

1 van Heek, K.H., Wanzl, W. *Erdöl-Erdgas-Kohle*, **1989**, 30-36.

2. Stanczyk, K., Kisielow, W. *Fuel*, **1994**, 73(5), 660-664

3 Mae, K., Maki, T., Okutsu, H., Miura, K. *Proc. 9th Intern. Conf. .on Coal Science, Essen*, **1997**, 195-198 .

4 Liu, Y., Hodek, W., van Heek, K.H. Proc. *9th Intern. Conf. on Coal Science , Essen*, **1997**, 127-130.

5 Canel, M., Wanzl, W. *Fuel*,**1994**, 73 (1), 137 - 138

6 Collin, G. *Erdöl und Kohle, Erdgas-Petrochemie*, **1985**, (38), 489-496.

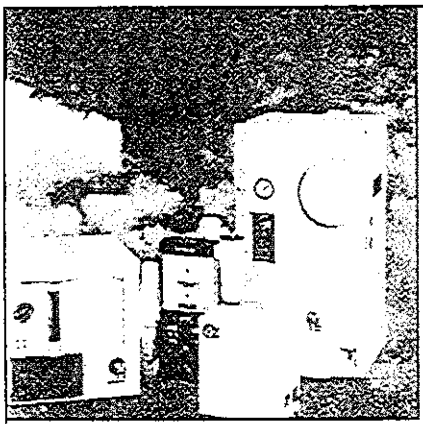

Gasgeneratoren
Stickstoff, Wasserstoff, synthetische Luft, Null-Luft

Analysatoren
TOC (Hochtemperatur, UV-Persulfatoxidation), TX, AOX, EOX
Gesamtstickstoff, Nitrat, Nitrit

Statischer, dynamischer Headspace, Thermodesorption

Festphasenextraktion

Laborbedarf
Filter, Flaschen etc.

SCHMIDLIN Labor + Service GmbH
Stuttgarter Straße 3, 73525 Schwäbisch Gmünd, Tel. 0 71 71 /1803-0, Fax 0 71 71 /1803-20
email: schmidlin.gmbh@t-online.de

Phase Equilibria
and
Thermodynamics

New Approaches to Calculation of the Henry's Constant of Aqueous Solutes at Superambient Conditions

Vladimir Majer
Laboratoire de Thermodynamique et Génie Chimique,
Université Blaise Pascal / CNRS,
Avenue des Landais, 63177 Aubière Cedex, France
Email: Majer@cicsun.univ-bpclermont.fr, Fax: +33 (0)473407185

Chemical and environmental engineers are using the Henry's constant (K_H) for description of the dissolution of sparingly soluble compounds in water at ambient conditions or along the vapour-pressure curve of a solvent. The solubility data are the main source for calculating K_H and empirical relationships are used for the description of its temperature dependence. Several alternative approaches to the calculation of the Henry's constant are presented, based on the link of K_H (and its temperature and pressure derivatives) with the thremodynamic functions of hydration. Three models are tested on four aqueous hydrocarbons by correlating simultaneously the solubility data below 423 K and the derivative properties for solutes (enthalpies, heat capacities and volumes) up to the 623 K and 40 MPa.

Introduction

The Henry's law is a useful tool for expressing fugacity f_s' of a sparingly soluble nonelectrolyte in aqueous phase. The constant of proportionality between the fugacity and concentration is the Henry's constant defined as:

$$K_H(T,p) = \lim_{x_s \to 0} \frac{f_s'}{x_s}. \qquad (1)$$

This constant is used in calculations of solubility based on the relation ship:

$$f_s'' = f_s' = K_H x_s \gamma_s^{HL} \quad (x_s \to 0, \gamma_s^{HL} \to 1) \qquad (2)$$

where f_s'' corresponds to the fugacity of a solute in an nonaqueous phase which is either a pure substance (for solids) or a fluid mixture where the component s often prevails. This fugacity can be obtained as a multiple of the vapour pressure of pure substance, fugacity coefficient and the Poyinting correction (when $p \neq p_{sat}$). Then the solubility calculation is straightforward especially for systems where the activity coefficient γ_i^{HL} (defined on the basis of the asymetric standard state convention) is close to unity. Chemical engineers use the Henry's constant mainly for expressing the solubility of gases at the saturation line of a solvent $(x_s \to 0,\ p \to p_{sat})$.

The general one phase definition of the Henry's constant (1) allows to express K_H as a function of two state variables. Use of the standard state of an ideal gas at a reference pressure of 0.1 MPa for the solute leads to the equation:

$$K_H(T,p) = p\varphi_s^\circ \qquad (3)$$

showing how the Henry's constant can be related to an equation of state. The reliable calculation of the fugacity coefficient at infinite dilution φ_s° in the aqueous phase is, however, a challenge equations of state are rarely able to meet with success for nonpolar electrolytes.

When using the standard state of a pure liquid solute equation (1) takes the form:

$$K_H(T,p) = f_s^{\bullet l} \gamma_s^\infty \quad (x_s \to 1, \gamma_s^{RL} \to 1). \qquad (4)$$

This relationship connects the Henry's constant with the fugacity of the pure liquid (which can be hypothetical in the case of gases and solids) and the activity coefficient at infinite dilution γ_s^∞ for the symmetrical standard states convention. The latter type of data is generated for the use of engineering thermodynamics by a variety of experimental methods and is useful in calculations of K_H for condensed solutes.

The Henry's constants are now frequently used in environmental chemistry and geochemistry for calculating equilibrium concentrations of pollutants and trace components in aquatic systems and geological fluids. It is also convenient to use K_H in engineering calculations involving equilibria between nonelectrolyte and aqueous phases at superambient conditions. Therefore it is desirable to have models allowing correlation and possibly also prediction of K_H as a function of temperature and pressure. Most equations available in literature are, however, of empirical character and usually permit to calculate the Henry's constant only along the saturation line of a solvent. The thermodynamic functions of hydration having an exact physico-chemical meaning present a better founded alternative and permit to model the Henry's constant as a function of two independent variables.

Henry's constant and thermodynamic functions of hydration

Thermodynamic functions of hydration relate to the transfer of 1 mole of a solute from an ideal gas state to the ideal aqueous phase defined by the Henry's law:

$$X^{\circ}_{\mathrm{hyd}} = \overline{X}^{\circ}_{\mathrm{s}}(T,p) - X^{\mathrm{ig}}_{\mathrm{s}}(T,p_{\mathrm{r}}) \qquad (5)$$

where p_{r}=0.101 MPa. It can be easily shown that K_{H} is directly linked with the Gibbs free energy of hydration $\Delta G^{\circ}_{\mathrm{hyd}}$ as follows:

$$\begin{aligned} RT\ln\left(K_{\mathrm{H}}/p_{\mathrm{r}}\right) &= \overline{G}^{\circ}_{\mathrm{s}}(T,p) - G^{\mathrm{ig}}_{\mathrm{s}}(T,p_{\mathrm{r}}) \\ &= \Delta G^{\circ}_{\mathrm{hyd}}(T,p). \end{aligned} \qquad (6)$$

The temperature derives connect the Henry's constant with the enthalpy and heat capacity of hydration

$$RT^2\left(\frac{\partial \ln K_{\mathrm{H}}}{\partial \mathrm{T}}\right)_p = -\,\Delta H^{\circ}_{\mathrm{hyd}}(T,p) \qquad (7)$$

$$\left(\frac{\partial}{\partial T}\left[RT^2\,\frac{\partial \ln K_{\mathrm{H}}}{\partial T}\right]\right)_p = -\,\Delta C^{\circ}_{p\,\mathrm{hyd}}(T,p) \qquad (8)$$

which can be calculated from the calorimetric data for aqueous phase (heats of solution ΔH_{sol}, specific heat capacities c_p) extrapolated to infinite dilution and properties of pure solute (residual enthalpy $\Delta H_{\mathrm{res}} = H_{\mathrm{s}}(T,p) - H^{\mathrm{ig}}_{\mathrm{s}}(T)$, C^{ig}_p). It holds:

$$\Delta H^{\circ}_{\mathrm{hyd}} = \Delta H^{\circ}_{\mathrm{sol}} + \Delta H_{\mathrm{res}} \qquad (9)$$

where $\Delta H^{\circ}_{\mathrm{sol}}$ can be obtained as

$$\Delta H^{\circ}_{\mathrm{sol}} = \overline{H}^{\circ}_{\mathrm{s}} - H_{\mathrm{s}} = \lim_{x_{\mathrm{s}}\to 0}\left(\Delta H_{\mathrm{sol}}/x_{\mathrm{s}}\right) \qquad (10)$$

and similarly for $\Delta C^{\circ}_{p\mathrm{hyd}} = \overline{C}^{\circ}_{p\mathrm{s}} - C^{\mathrm{ig}}_{p\mathrm{s}}$

$$\overline{C}^{\circ}_{p\mathrm{s}} = c_{p\mathrm{w}}M_{\mathrm{s}} + M_{\mathrm{w}}\lim_{x_{\mathrm{s}}\to 0}\left(\frac{c_p - c_{p\mathrm{w}}}{x_{\mathrm{s}}}\right) \qquad (11)$$

where subscript w relates to properties of solvent. The pressure derivative of K_{H} leads directly to the partial molar volume at infinite dilution

$$RT\left(\frac{\partial \ln K_{\mathrm{H}}}{\partial p}\right)_T = \overline{V}^{\circ}_{\mathrm{s}}(T,p) \qquad (12)$$

available from densimetric measurements at low concentrations:

$$\overline{V}^{\circ}_{\mathrm{s}} = \frac{M_{\mathrm{s}}}{\rho_{\mathrm{w}}} - \frac{M_{\mathrm{w}}}{\rho^2_{\mathrm{w}}}\lim_{x_{\mathrm{s}}\to 0}\left(\frac{\rho - \rho_{\mathrm{w}}}{x_{\mathrm{s}}}\right) \qquad (13)$$

Several types of instruments were constructed over the past fifteen years or so allowing to obtain the experimental values of derivative properties (enthalpy, heat capacity and volume) for dilute aqueous solutions of nonelectrolytes as a function of temperature and pressure. This makes it possible to calculate the Henry's constant at superambient conditions by combining the solubility data near 300 K and atmospheric pressure with $\Delta H^{\circ}_{\mathrm{hyd}}$, $\Delta C_p{}^{\circ}_{\mathrm{hyd}}$ and $\overline{V}^{\circ}_{\mathrm{s}}$ derived from calorimetric and densimetric measurements.

For both practical and theoretical reasons it is necessary to have models allowing to correlate and possibly to predict the thermodynamic properties of hydration and hence the Henry's constant as a function of temperature and pressure. Two approaches can be used depending on the choice of the reference state as apparent from the Figure 1.

In the first approach a model is used for expressing the difference between the standard Gibbs free energy of a solute at T and p and that. at the reference state of T_{r} and p_{r}.. Then with the use of equation (6) the Henry's constant can be calculated as

$$\begin{aligned} RT\ln\left(K_{\mathrm{H}}(T,p)/p_{\mathrm{r}}\right) &= \left[\overline{G}^{\circ}_{\mathrm{s}}\right]^{T,p}_{T_{\mathrm{r}},p_{\mathrm{r}}} \\ &\quad + RT_{\mathrm{r}}\ln\left(K_{\mathrm{H}}(T_{\mathrm{r}},p_{\mathrm{r}})/p_{\mathrm{r}}\right) \\ &\quad - \left[G^{\mathrm{ig}}_{\mathrm{s}}\right]^{T,p}_{T_{\mathrm{r}},p_{\mathrm{r}}} \end{aligned} \qquad (14)$$

where the first term is obtained from a model, the second is calculated from the Henry's constant at the reference state of T_{r} and p_{r} and the third term refers to the Gibbs free energy difference for a solute in an ideal gas state.

Figure 1. Thermodynamic pathways

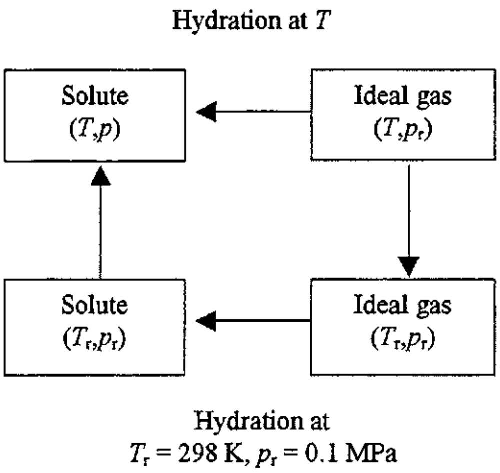

The second approach uses as a reference state an ideal gas at T and p_{r}, then the Gibbs free energy of hydration is directly yielded by a model allowing straightforward calculation of K_{H} by equation (6). The typical models are reviewed below.

Modelling the difference $\overline{G}^{\circ}_{\mathrm{s}}(T,p) - \overline{G}^{\circ}_{\mathrm{s}}(T_{\mathrm{r}},p_{\mathrm{r}})$

The geochemists at the U. of Califiornia at Berkeley have developped a model (HKF) [1,2] available as a software SUPCRT92 [3] which has become widely used for calculating the standard state properties over a wide range of temperatures and pressures. Standard thermodynamic functions of an aqueous solute are obtained as a combination of the so-called solvation contribution (s) derived from the Born equation expressing ionic solvation and a nonsolvation contribution (n) of empirical nature:

$$\overline{X}^{\circ}_{\mathrm{s}} = \overline{X}^{\mathrm{n}}_{\mathrm{s}} + \overline{X}^{\mathrm{s}}_{\mathrm{s}} \qquad (15)$$

The basic equations for heat capacity

$$\overline{C}^{\circ}_{ps} = c_1 + \frac{c_2}{(T-\Theta)^2} + \omega T\left(\frac{\partial}{\partial T}\frac{1}{\varepsilon_{\mathrm{w}}^2}\left(\frac{\partial \varepsilon_{\mathrm{w}}}{\partial T}\right)\right)_p \quad (16)$$

at $p = p_{\mathrm{r}}$ and volume

$$\overline{V}^{\circ}_{\mathrm{s}} = a_1 + \frac{a_2}{\psi + p} + \left(a_3 + \frac{a_4}{\psi + p}\right)\left(\frac{1}{T-\Theta}\right) - \frac{\omega}{\varepsilon_{\mathrm{w}}^2}\left(\frac{\partial \varepsilon_{\mathrm{w}}}{\partial p}\right)_T \quad (17)$$

allow to obtain all other thermodynamic properties by integration. The symbols a, c and ω stand for seven adjustable parameters, ε_{w} is the dielectric constant (relative permitivity) of water, Θ =228 K and Ψ = 260 MPa. For the Gibbs free energy difference it holds:

$$\left[\overline{G}^{\circ}_{\mathrm{s}}\right]^{T,p}_{T_{\mathrm{r}},p_{\mathrm{r}}} = (T_{\mathrm{r}} - T)\overline{S}^{\circ}_{\mathrm{s}}(T_{\mathrm{r}}, p_{\mathrm{r}}) + \int_{T_{\mathrm{r}}}^{T}\left(\overline{C}^{\circ}_{ps}\right)^{p_{\mathrm{r}}} \mathrm{d}T - T\int_{T_{\mathrm{r}}}^{T}\left(\overline{C}^{o}_{ps}\right)^{p_{\mathrm{r}}} \mathrm{d}\ln T + \int_{p_{\mathrm{r}}}^{p}\left(\overline{V}^{\circ}_{\mathrm{s}}\right)^{T} \mathrm{d}p \quad (18)$$

where the superscripts denote the property constant at the path of the integration and $\overline{S}^{\circ}_{\mathrm{s}}(T_{\mathrm{r}}, p_{\mathrm{r}})$ is the entropy of an aqueous solute in the reference state. The model was originally proposed for aqueous electrolytes and it has been used by analogy also for nonlectrolytes [4-5] although any theoretical foundation is missing. This aproach has some difficulties to describe derivative properties of aqueous organics and when extrapolating towards the critical point of water.

An effort has been recently made to keep the same concept but to modify the model in order and to make it compatible with the theories of near-critical solutions. Nonsolvation terms are simplified and the dielectric properties of water are replaced by the pVT properties [6]. A density model (DEN) proposed recently at LTGC Clermont-Ferrand [7] formulates analogues to equations (16) and (17) as follows:

$$\overline{C}^{\mathrm{o}}_{ps} = c + \frac{c_T}{T-\Theta} + (\omega + \omega_T T)T\left(\frac{\partial^2 \rho_{\mathrm{w}}}{\partial\, T^2}\right)_p + 2\omega_T T\left(\frac{\partial \rho_{\mathrm{w}}}{\partial T}\right)_p \quad (19)$$

$$\overline{V}^{o}_{\mathrm{s}} = a + a_T T - (\omega + \omega_T T)\left(\frac{\partial \rho_{\mathrm{w}}}{\partial p}\right)_T \quad (20)$$

with six adjustable parameters. The Gibbs free energy difference for a solute can be calculated by equation (18) leading to a a somewhat simpler relationship compared to the HKF model.

Modelling the Gibbs free energy of hydration

$$\Delta G^{\circ}_{\mathrm{hyd}} = \overline{G}^{\circ}_{\mathrm{s}}(T,p) - G^{\mathrm{ig}}_{\mathrm{s}}(T,p_{\mathrm{r}})$$

These models lead directly to the value of the Henry's constant without use of the three steps (14) depicted in the thermodynamic cycle (Figure 1). Levelt-Sengers and Japas [8] analyzed behaviour of the fugacity coefficient of an infinitely dilute solute near the solvent's critical point. Using equation (3), they have derived a relationship linear in density representing K_{H} along the vapour pressure curve of a solvent with the correct asymptotic near critical behaviour. Levelt-Sengers and collaborators [9,10] have added an empirical term exponential in temperature to allow calculation of the Henry's constant down to 273 K. In addition they showed that their relationship has general validity (not restricted to the solvent's saturation curve) permitting to express K_{H} as a function of T and p and to calculate derivative properties. For an aqueous solution it has a simple form:

$$RT\ln(K_{\mathrm{H}}(T,p)/f^{\bullet}_{\mathrm{w}}) = A + B(\rho_{\mathrm{w}} - \rho_{\mathrm{cw}}) + CT\rho_{\mathrm{w}}\exp((273.15-T)/50) \quad (21)$$

where A,B,C are adjustable parameters and $f^{\bullet}_{\mathrm{w}}$ is the pure water fugacity. The equation correlates in fact the difference between the Gibbs free energy of hydration of a solute and an analogous function for a solvent. It has a correct ideal gas limit and was used with good results for correlating the Henry's constant of gases in water up to the critical region. The simple form of the relationship does not allow, however, a reliable correlation of derivative properties as shown for volume by Majer et al. [11]. Introduction of an additional parameter N (multiplying a pure water property) analogous to that introduced below was necessary for getting a reasonable fit of experimental data.

A different approach is that making use of the fluctuation solution theory (FST). It can be shown [12] that the spatial integral of the infinite dilution solute-solvent direct correlation function C°_{sw} is linked with the dimensionless parameter $\overset{\circ}{A}_{\mathrm{sw}}$ (called sometimes the generalised Krichevskii parameter)

$$1 - C^{\circ}_{\mathrm{sw}} = \frac{\overline{V}^{\circ}_{\mathrm{s}}}{\kappa_{\mathrm{w}} RT} = \overset{\circ}{A}_{\mathrm{sw}} \quad (22)$$

which is well behaved in the critical region of water (κ_{w} stands for water compressibility). After a rearrangement this parameter can be also expressed in terms of a virial expansion:

$$\overset{\circ}{A}_{\mathrm{sw}} = \lim_{n_{\mathrm{s}}\to 0}\left(\frac{\partial(pV/RT)}{\partial n_{\mathrm{s}}}\right)_{T,V} = 1 + (2/M_{\mathrm{w}})\rho_{\mathrm{w}} B_{\mathrm{sw}} + \ldots \quad (23)$$

where B_{sw} is the cross virial coefficient. An analogous procedure can be adopted for pure water where the water-water direct correlation function is linked with the A_{ww} parameter and a similar virial expansion is obtained. By comparing the virial expansions for an aqueous solute and pure water one obtains the relationship

$$A^{\circ}_{\mathrm{sw}} - NA_{\mathrm{ww}} = (1-N) + \rho_{\mathrm{w}}(2/M_{\mathrm{w}})(B_{\mathrm{sw}} - NB_{\mathrm{w}}) + \ldots \qquad (24)$$

where N is an adjustable scaling factor related to the difference between the volume of solute and that of water. Several equations are now under development differing by expressions used for approximation of the virial terms.

A promising example is the relationship [11,13]

$$\begin{aligned}\bar{V}^{\circ}_{\mathrm{s}} - NV_{\mathrm{w}} &= (1-N)RT\kappa_{\mathrm{w}} \\ &+ RT\kappa_{\mathrm{w}}\rho_{\mathrm{w}}[a + b\exp\left[\frac{\Theta}{T}\right] + c(\exp[\vartheta.\rho_{\mathrm{w}}]-1) \qquad (25) \\ &+ \delta(\exp[\lambda.\rho_{\mathrm{w}}]-1)]\end{aligned}$$

with five adjustable parameters N, a, b, c, δ and three predetermined constants Θ=1500 K, ϑ=5 cm^3/g and λ=-10 cm^3/g. When extrapolating towards low densities relationship (20) decays to the virial expansion limited to the second virial coefficient. This is a considerable advantage over the HKF model and its analogues in description of volatile solutes where the constraint of ideal gas limit is meaningful. Then any standard thermodynamic property of an aqueous solute can be obtained as a combination of the ideal gas value at T and p_{r} and the corresponding hydration function which can be calculated using the above volumetric equation. The relationship for the Gibbs free energy of hydration

$$\Delta G^{\circ}_{\mathrm{hyd}} = \int_{p_{\mathrm{r}}}^{0} RT\mathrm{d}\ln p + \int_{0}^{p} \bar{V}^{\circ}_{\mathrm{s}}\mathrm{d}p \qquad (26)$$

can be directly used for calculating the Henry's constant using equation (6). Relationships analogous to (26) permit to connect the model with other hydration properties :

$$\Delta H^{\circ}_{\mathrm{hyd}} = \int_{0}^{p} \left(\bar{V}^{\circ}_{\mathrm{s}} - T\left(\frac{\partial \bar{V}^{\circ}_{\mathrm{s}}}{\partial T}\right)_{p} \right) \mathrm{d}p \qquad (27)$$

$$\Delta C^{\circ}_{p,\mathrm{hyd}} = -T\int_{0}^{p} \left(\frac{\partial^{2} \bar{V}^{\circ}_{\mathrm{s}}}{\partial T^{2}}\right)_{p} \mathrm{d}p \qquad (28)$$

accessible from experimental data.

Thermodynamic data for hydrocarbons(aq) as a function of temperature and pressure

It is clearly apparent from the above analysis that the data on standard thermodynamic properties of solutes can be useful in prediction of the Henry's constant over a wide range of temperatures and pressures; this is demonstrated below for aqueous hydrocarbons. Reliable literature data for solutions of hydrocarbons in water are, however, scarce in literature although they are sorely needed for technological, environmental and geochemical applications. At near-ambient conditions the information is in most cases confined to the solubility data as most other techniques are inhibited by very low concentrations of a solute. Miscibility of hydrocarbons and water increases with increasing temperature but literature data on phase equilibria are fragmentary and sometimes contradictory. Exception are reliable measurements of compositions along the three phase equilibrium line resulting from the project at Exxon Research Engineering Co. [14].

Derivative properties were till recently practically non-existent in literature except the results for $\bar{C}^{\circ}_{p}$ and $\bar{V}^{\circ}_{\mathrm{s}}$ of benzene and toluene up to 353 K [15,16] and a series of measurement of heats of solution at near ambient conditions [17] for a variety of aqueous hydrocarbons. We have developed at the University Blaise Pascal a flow instrument [18] combining in one thermostatted environment a heat compensation mixing calorimeter and a vibrating tube densimeter allowing simultaneous determination of enthalpic and volumetric properties up to 673 K and 40 MPa. This *calodensimeter* is particularly useful for measurements with systems exhibiting increasing miscibility with temperature. The solution is "prepared" directly in the hot zone of the instrument which allows to work at sufficiently high concentrations where the measurements are feasible. We have used this instrument for measuring enthalpies of solution and densities for benzene(aq), toluene(aq), cyclohexane(aq) and hexane(aq) between 473 K and 685 K and pressures up to 30 MPa [7]. In addition, the reliability of the data was checked on another calorimeter and densimeter which allowed to expend the measurements of volumetric data for aqueous benzene down to 373 K. The new values were combined with the literature data on derivative properties at near ambient conditions originating from different sources (most data being from references [15,16,19]). As no low temperature data were found in literature for $\bar{C}^{\circ}_{p}$ and $\bar{V}^{\circ}_{\mathrm{s}}$ of hexane(aq) and cyclohexane(aq) we have made estimates near 298 K based on the analogy with aromatics(aq) and properties of pure compounds. The two figures below show the values of $\Delta H^{\circ}_{\mathrm{sol}}$ and $\bar{V}^{\circ}_{\mathrm{s}}$ resulting from our measurements at temperatures up to 623 K at 10 and 30 MPa, the low temperature data [15] at 0.1 MPa are also presented on the volumetric plot. Both enthalpies and volumes become increasingly positive at high temperatures due to repulsive forces between solute and solvent and are proportional to the water expansivity and compressibility, respectively.

Figure 2. Enthalpic data obtained by extrapolation

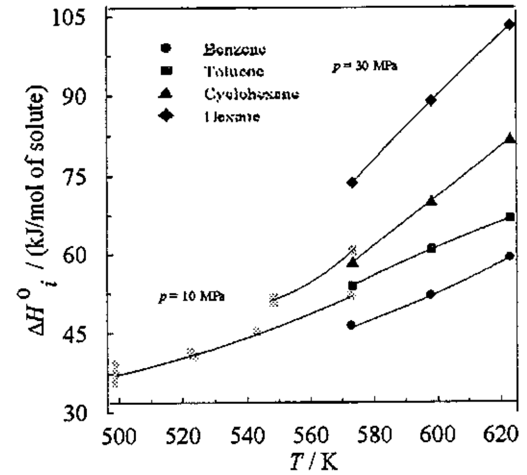

Figure 3. Volumeric data obtained by extrapolation

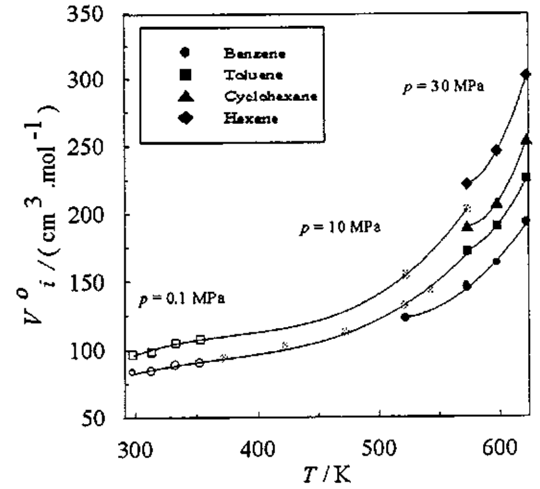

In the next step the data on derivative properties were combined with the selected solubilities at ambient and moderately elevated temperatures. For benzene(aq), cyclohexane(aq) and hexane(aq) it was possible to compare the solubility data recommended by IUPAC [20] with the data presented in reference [14] as the Henry's constants along the vapour pressure line of water and the mole fractions of hydrocarbon in the aqueous phase along the three phase line. After appropriate conversion the data were found basically consistent. For convenience the K_H values [14] were directly used for the above three solutes between 273 and 423K while for toluene the Henry's constants had to be calculated from the recommended solubilities [20] available only at near ambient conditions.

The established database served for testing the models described above at temperatures up to 623 K supposing that for most engineering applications this limit is rarely exceeded. When a suitable model is selected the Henry's constant can be generated as a function of temperature and pressure. An information on the number of data points for individual properties and the corresponding temperature intervals are in Table 1.

Table 1. Data base for thermodynamic properties of hydrocarbons(aq).

Repartition of data points $T\in[288 - 623\mathrm{K}], p \in[0.1 - 30\ \mathrm{MPa}]$		
System	$\overline{V}^\circ_s$	ΔH°_{sol}
Benzene	27 (298-623K)	16 (288-623K)
Toluene	19 (298-623K)	10 (288-623K)
Cyclohexane	11 (298-623K)	9 (298-623K)
Hexane	9 (298-623K)	6 (288-623K)
System	$\overline{C}^\circ_{ps}$	K_H
Benzene	6 (298-353K)	16 (273-423K)
Toluene	5 (278-353K)	9 (273-328K)
Cyclohexane	2 (310-340K)	16 (273-423K)
Hexane	2 (310-340K)	16 (273-423K)

Testing of models, calculation of the Henry's constant

The described database was used in a simultaneous correlation using three models:

1. HKF model, equations (16) to (18)
2. Density model, equations (18) to (20)
3. FST model, equations (25) to (28)

The minimized objective function had the form:

$$S=\sum_{i=1}^{u}\frac{\left(\overline{V}_s^{\circ\exp}-\overline{V}_s^{\circ\mathrm{cal}}\right)_i^2}{\sigma_i^2\overline{V}_s^\circ}+\sum_{i=1}^{v}\frac{\left(\Delta C_{p\mathrm{hyd}}^{\circ\exp}-\Delta C_{p\mathrm{hyd}}^{\circ\mathrm{cal}}\right)_i^2}{\sigma_i^2\Delta\overline{C}_{p\mathrm{hyd}}^\circ}+\sum_{i=1}^{t}\frac{\left(\Delta H_{\mathrm{hyd}}^{\circ\exp}-\Delta H_{\mathrm{hyd}}^{\circ\mathrm{cal}}\right)_i^2}{\sigma_i^2\Delta H_{\mathrm{hyd}}^\circ}+\sum_{i=1}^{z}\frac{\left(\Delta G_{\mathrm{hyd}}^{\circ\exp}-\Delta G_{\mathrm{hyd}}^{\circ\mathrm{cal}}\right)_i^2}{\sigma_i^2\Delta G_{\mathrm{hyd}}^\circ} \tag{29}$$

where the quantities with superscript exp are obtained from the experimental data data using equations (6) and (9) to (12). Symbol σ^2 denotes variances in correlated properties (estimated from experimental errors) which are reciprocal values of weighting factors. The quantities with superscript were obtained from model. In the case of the HKF and density models $\Delta G^\circ_{\mathrm{hyd}}$ is calculated by combining equations (6), (14) and (18); the enthalpy difference $\overline{H}^\circ_s(T,p)-\overline{H}^\circ_s(T_r,p_r)$ is calculated from an analogue of equation (18) and the thermodynamic cycle (Figure 1) is used to obtain $\Delta H^{\circ}_{\text{hyd}}$.

The results of correlation are given in Table 2 listing for the three models the overall standard weighted deviations (s.w.d) and the average weighted deviation for individual properties (*a.w.d.).* The values near unity indicate that the model is fitting the data within the margins of experimental errors.

Table 2. Testing of models, results of correlation

Systems		Ben (aq)	Tol (aq)	Cyhe (aq)	Hex (aq)
MODEL	m_p		s.w.d		
Prop.			*a.w.d.*		
HKF	7	4.2	3.0	2.4	2.2
V		*5.4*	*2.9*	*1.7*	*1.4*
C_p		*2.8*	*2.2*	*1.2*	*0.5*
H		*3.2*	*2.2*	*2.4*	*1.9*
G		*2.0*	*3.2*	*2.4*	*2.3*
DEN	6	1.2	1.7	0.7	1.4
V		*1.3*	*0.9*	*0.5*	*0.8*
C_p		*1.2*	*1.2*	*0.3*	*0.6*
H		*1.1*	*1.2*	*0.6*	*1.5*
G		*0.6*	*2.9*	*0.6*	*1.4*
FST	6	1.0	1.4	1.9	1.5
V		*0.7*	*0.7*	*0.9*	*0.8*
C_p		*1.0*	*1.3*	*0.1*	*0.6*
H		*1.3*	*1.2*	*2.3*	*1.5*
G		*1.0*	*2.2*	*1.9*	*1.6*

m_p number of adjustable parameters
s.w.d. = standard weighted deviations
a.w.d. = average weighted deviations

It is clearly apparent from the table that the density and FST models give better results in correlation than the HKF model. The difference is particularly pronounced for benzene(aq) where experimental data were relatively more abundant and of better accuracy.

The FST model was used to generate the recommended values of the Henry's constant as a function of temperature and pressure. As an example K_H is plotted in Figure 4 for benzene(aq) and hexane(aq) which exhibit the lowest and highest values from the four studied hydrocarbons. The Henry's constants are plotted up to 523 K and at three pressures to 30 MPa. . The figure illustrates a typical flat extreme on the $K_H(T)$ curve corresponding to $\Delta H^{\circ}_{\text{hyd}} = 0$ *i.e.* $\Delta H^{\circ}_{\text{sol}} = \Delta H_{\text{res}}$ (see equations 7 and 9). Also apparent is a sizable increase of the Henry's constant with pressure which is governed by the partial molar volume of solute at infinite dilution (see equation (12).

Acknowledgement: This text was prepared with the technical help of Laure Pacynski and Lorette Rochette-Jardy

Figure 4. Plot of the Henry's constant at three pressures (0.1, 10 and 30 MPa).

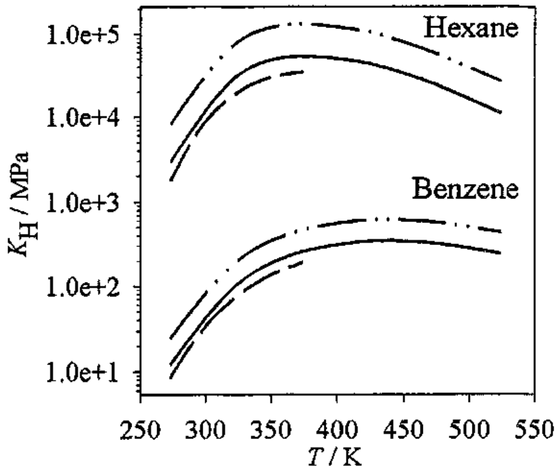

References

1. Helgeson, H. C.; Kirkham, D. H.; Flowers, G. C. *Amer. J. Sci.* **1981**, 281, 1249-1516.
2. Tanger IV, J. C.; Helgeson, H. C. *Amer. J. Sci.* **1988**, 288, 19-98.
3. Johnson, J. W.; Oelkers, E. H.; Helgeson, H. C. *Computers and Geosciences* **1992**, 18, 899-947.
4. Shock, E. L.; Helgeson, H. C.; Sverjensky, D. A. *Geochim. Cosmochim. Acta* **1989**, 53, 2157-2183.
5. Shock, E. L.; Helgeson, H. C. *Geochim. Cosmochim. Acta* **1990**, 54, 915-945.
6. Schulte, M. D. "Synthesis and processing of aqueous organic compounds during water-rock reactions". Ph.D. Thesis, Washington University, Saint Louis, Missouri **1997**.
7. Degrange, S. "A New Procedure for Simultaneous Determination of Enthalpic and Volumetric Properties of Fluid Systems: A Study of Aqueous Hydrocarbons up to the Critical Region of Water" , Ph.D. Thesis, University Blaise Pascal, Clermont-Ferrand **1998**.
8. Japas, M.L.; Levelt-Sengers, J.M.H. *AIChE J.* **1989**, 35, 705-713.
9. Harvey, A.H.; Levelt-Sengers, J.M.H. *AIChE J.* **1990**, 36, 539-546.
10. Harvey, A.H.; Levelt-Sengers, J.M.H.; Tanger IV, J.C. *J. Phys. Chem.* **1991**, 95, 932-937.
11. Majer, V.; Degrange, S.; Sedlbauer, J. *Fluid Phase Equilib.* **1999**, in press.
12. O'Connell, J.P. *Mol. Phys.*, **1971**, 20, 27-33.
13. Sedlbauer, J.; O'Connell, J. P.; Wood, R. H. *Chem. Geology*, **1999**, in press.
14. Tsonopoulos *et al.* AIChE J. **1983**, 29, 990-999 ; **1985**, 31, 376-384 ; **1997**, 43, 535-546.
15. Makhatadze, G.I.; Privalov, P.L. *J. Chem. Thermodyn.* **1988**, 20, 405-412.
16. Sakurai, M. *Bull. Chem. Soc. Jpn.* **1990**, 63, 1695-1699.
17. Series of measurements by I. Wadsö *et al.* at the U. of Lund and S.J. Gill *et al.* at the U. of Colorado published in JCT and JPC between **1975** and **1988**.
18. Hynek, V.; Degrange, S.; Polední• ek ; M., Majer, V.; Quint, J. ; Grolier J.-P. E. *J. Solut. Chem.* in press.
19. Gill, S.J.; Nichols, N.F.; Wadsö, I. *J. Chem. Thermodyn.* **1975**, 7, 175-183 ; **1976**, 8, 445-452.
20. "Hydrocarbons with water and sea water", Shaw, D.G. Editor, Part 1 Hydrocarbons C_5 to C_7, IUPAC Solubility Data Series, Pergamon Press, Oxford **1989**.

GVC-Fachausschuß „High Pressure Chemical Engineering", March 3-5, Karlsruhe, Germany, 1999 GVC FZK '99

A New Apparatus For The Investigation Of The Phase Behaviour Of Dilute, Binary Supercritcal Mixtures

M. Türk* and A. Diefenbacher
Institut für Technische Thermodynamik und Kältetechnik, Universität Karlsruhe (TH)
Richard Willstätter-Allee 2, D-76128 Karlsruhe, F.R.G.

A new static equilibrium apparatus for the investigation of the phase behaviour of dilute supercritical fluid mixtures is presented. The view cell apparatus was tested by measurements of the three-phase S_2LG line and the critical mixture curve of the $CO_2(1)$/naphthalene(2)- system. The upper critical end point (UCEP) location is estimated from the experimental data. The results are discussed in comparison with previously published data by various authors.

Introduction

Experimental investigations and thermodynamic modelling of the solubility and the phase behaviour of organic solutes in supercritical solvents are of special interest for supercritical fluid processes such as the supercritical fluid extraction (SFE) or the continous formation of small particles by rapid expansion of supercritical solutions (RESS).

Frequently the triple point temperature of the organic solute (component 2) is markedly higher than the critical temperature of the solvent (component 1). These asymmetric mixtures generally show the phase behaviour schematically depicted in figure 1.

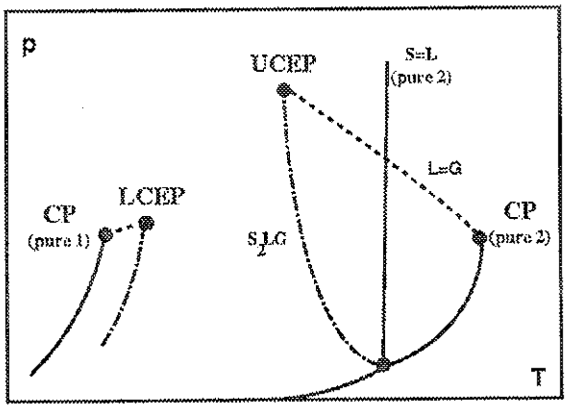

FIGURE 1: Schematic pT-projection of the pTx-diagram for an asymmetric binary mixture.

The three-phase S_2LG line interrupts the critical mixture curve (L=G). The two distinguished points of intersection are called lower critical end point (LCEP) and upper critical end point (UCEP) [1,2]. Between the LCEP- and the UCEP-temperature only a solid-fluid equilibrium exists. In the vicinity of these critical end points, small changes in pressure and temperature result in a substantial change of the composition. Because of the higher solid solubilities in the UCEP region, this region is of major economic interest in comparison to the LCEP region.

For many processes, such as the RESS process, it is desired to take advantage of the increased sensitivity of the solubility with respect to pressure near the UCEP, but to avoid the formation of a liquid phase. The knowledge about the phase behaviour is one of the basics for modelling such processes. Furthermore, when using supercritical fluid mixtures as solvent, the knowledge about the influence of mixture composition on the solubility and the location of the UCEP is indispensable.

Materials and Methods

A new equilibrium apparatus, shown in figure 2, was designed for measurements of the phase behaviour and the solubilities of solid solutes in supercritical solvents. The apparatus can be used for pressures up to 50 MPa and for temperatures up to 100 °C. The static equilibrium cell of 1310 cm^3 inner volume is installed in a thermostatted chamber, in which with controlled cooling and heating it is possible to maintain a constant temperature in the limits of ± 10 mK for many hours. The test fluid can be observed during the measurement through two saphir windows at both ends of the cylindrical cell.

The temperature in the equilibrium cell is measured with a Pt-100 thermometer, which is calibrated against a Pt-25 thermometer (Rosemount) provided with a National Bureau of Standards certificate (ITS-90). The accuracy of the temperature measurement is within $\Delta T_{Meas} = \pm 30$ mK.

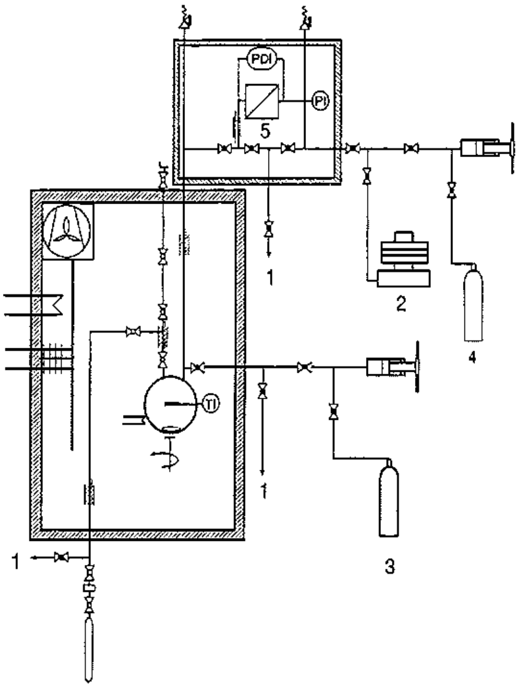

FIGURE 2: Scheme of the apparatus (1: to vacuum pump; 2: dead-weight pressure gauge; 3: solvent; 4: nitrogen; 5: pressure null indicator)

The pressure is measured by a high-precision standard dead-weight gauge (Desgranges & Hout) provided with a National Bureau of Standards certificate, which is separated from the test fluid in the equilibrium cell by a thermostatted pressure null indicator. By means of a very sensitive displacer, the pressure difference at the null indicator is adjusted to less than ±0.01 kPa. The total uncertainty of the pressure measurement is within $\Delta p_{Meas.} = \pm 6$ kPa.
At the present state samples of the upper phase of the test fluid can be taken at the top of the equilibrium cell by blocking of a sample volume, which is small compared to the cell volume. The composition of the sample is determined by gaschromatographic and gravimetrical analysis. An improvement of the sampling unit, using HPLC equipement, is under design.

The apparatus and the experimental procedure for the determination of the three-phase line and the critical mixture curve were tested using naphthalene (purum) supplied by C. Roth, FRG and carbon dioxide with a volume fraction purity of 0.99995 delivered by Messer Griesheim, FRG.

Results and Discussion

The three-phase S_2LG line for CO_2/naphthalene-mixture was determined by observing the first melting point at various pressures. The experimental results are listed in table 1.

At each starting pressure the temperature was slowly raised until the onset of melting was observed. This procedure was repeated many times in order to reduce the temperature span of heating in which melting took place iteratively to less than 200 mK. For this reason the total uncertainty of the first melting point temperatures can be limited to less than ±250 mK.
For the estimation of the total experimental uncertainty of the melting point pressure, both the uncertainty of the pressure measurement and the uncertainty resulting from the assignment of a particular measured temperature to the pressure on the S_2LG line must be taken into account:

$$\Delta p = \Delta p_{Meas.} + \underbrace{\left(\frac{\partial p}{\partial T}\right) \cdot \Delta T_{Meas.}}_{\Delta p_{Assign.}} \qquad (1)$$

In general this assignment uncertainty exceeds the uncertainty of the measurement by far, especially at higher pressures.

p / MPa	T / K
13.363 ±0.06	332.94 ±0.25
24.11 ±0.12	333.31 ±0.25
25.012 ±0.125	333.45 ±0.25
25.845 ±0.125	333.53 ±0.25
26.123 ±0.125	333.43 ±0.25
26.347 ±0.125	333.52 ±0.25

TABLE 1: Experimental pressure-temperature data for the CO_2/naphthalene S_2LG line.

The critical mixture curve was determined with an analogous iterative experimental procedure. While slowly decreasing the temperature from slightly above the critical mixture temperature, the occurence of the liquid surface was noted. As the liquid formation appears much more abrupt than a first melting point, it was possible to limit the temperature span of cooling to less than 100 mK. In addition the experimental results listed in table 2 were also verfied by observing the disappearance of the liquid surface, while slowly raising the temperature from values slightly below the critical mixture temperature. The values measured by raising and by lowering the temperature coincided within the accuracy of the temperature measurement, which is ±30 mK. The total experimental uncertainty of the determination of the critical mixture temperature can be limited to less than ±150 mK. The experimental uncertainties of the critical mixture pressures listed in table 2 were estimated in consideration of an assignment uncertainty according to eqn.(1).

p / MPa	T / K
26.877 ±0.085	334.02 ±0.15
26.868 ±0.085	334.54 ±0.15
26.851 ±0.085	335.03 ±0.15
26.853 ±0.085	336.07 ±0.15
26.859 ±0.085	337.34 ±0.15

TABLE 2: Experimental pressure-temperature data for the CO_2/naphthalene critical mixture curve.

The pT-projection of the pTx-diagram for the CO_2/naphthalene-system is shown in figure 3. Besides the present experimental results, literature data from various authors are also depicted for comparison. An enlargement of the UCEP region with errorbars representing our total experimental uncertainties is shown in the upper right corner of figure 3.

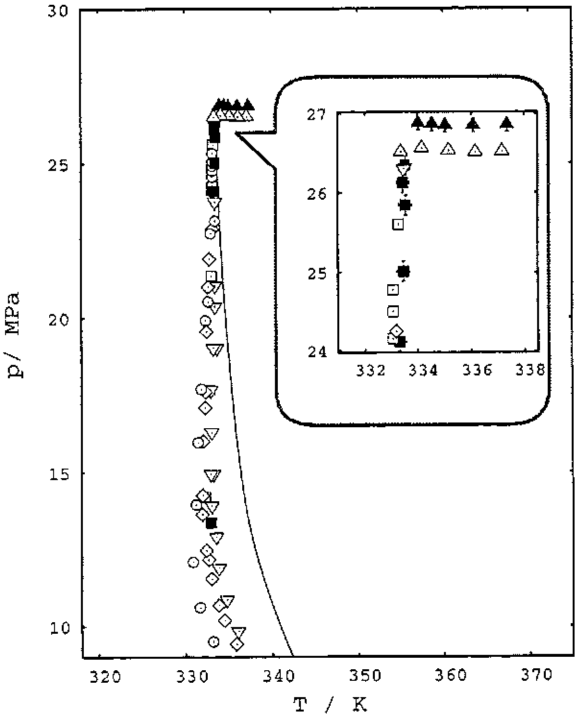

FIGURE 3: pT-projection of the pTx-diagram for the CO_2/naphthalene-system; experimental data for the S_2LG-line: ■: this work; ▽: [3]; □: [4]; ◇: [5]; ∘ [2] experimental data for the critical mixture curve: ▲: this work; △: [3]
The solid line is calculated using the Peng-Robinson equation of state [6].

While experimental data for the S_2LG line is abundant (e.g. [2,3,4,5,7]), information about the critical mixture curve is scarce. Our results for the S_2LG line are in good agreement with the previously published data. The determined melting point temperatures coincide with the literature values [3,4,5] within our experimental uncertainty. However, the values measured for the critical mixture curve pressures are systematically (1 to 1.5) per cent higher than the previously published data by Lemert and Johnston [3]. This discrepancy can not be explained, since it is not within our experimental uncertainty.

The UCEP in the CO_2/naphthalene-system is estimated from our experimental data by locating the intersection of the three-phase S_2LG line and the critical mixture curve. A good agreement of the UCEP temperature with previously published data summarized in table 3 is noticed.

T_{UCEP} K	p_{UCEP} MPa	year	reference
333.45 ±0.25	26.6 ±0.2	1999	this work
333.25 ±0.2	26.3 ±0.2	1989	[3]
333.45 ±0.2	26.3 ±0.2		[3]
333.25	22.6	1986	[7]
333.25	25.6	1984	[4]

TABLE 3: Pressure p_{UCEP} and temperature T_{UCEP} at the UCEP of the CO_2/naphthlene-system.

In the work of Lemert and Johnston [3] two differing values of the UCEP temperature are given. Both values, one given in the text and one given in a table of experimental results, are listed in table 3. The UCEP pressure estimated in this work agrees with the pressure determined by Lemert and Johnston within the combined uncertainties. The UCEP pressure given by Lamb et al.[7] was estimated from the solubility isotherm at 58.5°C, because it was not possible to determine directly the UCEP pressure with the NMR technique used by these authors. McHugh and Yogan [4] determined the location of the UCEP by observing the critical opalescence. As reprorted by Lemert and Johnston, a critical opalescence near the UCEP can be observed over a pressure range of 1 to 1.5 MPa. This observation can be confirmed by our experiments. Since the critical opalescence observed in the vicinity of the UCEP of the CO_2-naphthalene system was not as distinct as it is familiar from homogeneous binary fluid mixtures [8,9], this might lead to a larger experimental uncertainty in the UCEP pressure determination. Small changes of temperature and pressure in the vicinity of the UCEP caused enormous changes in the ratio of supercritical fluid phase, liquid phase, and solid phase present in the equilibrium cell, as already reported by McHugh and Yogan.

A first qualitative approach of the experimental data along the three-phase S_2LG line is made by means of the Peng-Robinson equation of state (PR-EoS)[6]. The S_2LG line is determined by solving the equations (2) to (4), which represent the three phase equilibrium.

$$f_1^g(T,p,y_1) = f_1^l(T,p,x_1) \qquad (2)$$

$$f_2^g(T,p,y_2) = f_2^l(T,p,x_2) \qquad (3)$$

$$f_2^{\overset{0}{s}}(T,p) = f_2^g(T,p,y_2) \qquad (4)$$

In equation (2) to (4) f^g and f^l represent the fugacity in the gas and liquid phase, respectively. The solid phase, whose fugacity is represented by $f_2^{\overset{0}{s}}(T,p)$ in equation (4), is treated as a pure substance. For the calculations with the PR-EoS simple van-der-Waals mixing rules with two binary interation parameters, one in the attraction and one in the repulsion term, are used. These parameters are fitted exclusively to the experimental data in the UCEP region.

Although the fitted interaction parameters are treated as independent from temperature, the PR-EoS is also used to calculate solid solubilities in a supercritical solvent according to equation (5).

$$y_2 = \frac{p_2^{subl}(T)}{\phi_2^{scf} \cdot p} \cdot exp\{\frac{(p - p_2^{subl}) \cdot v_2^{\overset{0}{s}}}{R \cdot T}\} \qquad (5)$$

In equation (5) ϕ_2^{scf} denotes the fugacity coefficient in the supercritical phase, and p_2^{subl} and $v_2^{\overset{0}{s}}$ denote the sublimation pressure and the molar volume of the pure solid. Results from these calculations are plotted in figure 4.

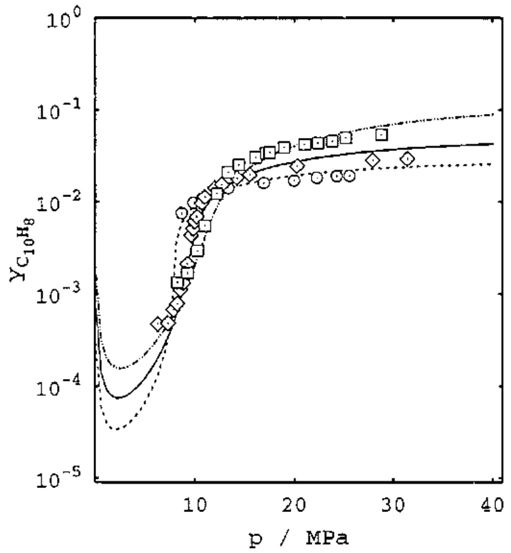

FIGURE 4: Solubilities of naphthalene in CO_2. The plotted lines are correlated using the PR-EoS at the corresponding temperatures.
□, McHugh and Paulaitis 328 K [10]; ◇, Tsekhanskaya et al. 318 K [11]; ○, McHugh and Paulaitis 308 K [10]

The deviations of the solubilities calculated with the PR-EoS using the binary interaction parameters fitted to the UCEP region from the experimental data are in the same order of magnitude as those obtained by fitting the binary interaction parameters directely to solubility data.

Conclusions and Outlook

The solubility of solid solutes in supercritical fluids in the vicintity of the UCEP is very sensitive with respect to pressure and temperature. This feature is advantageously used in many applications. For certain processes, such as RESS, experimental data not only of the solubility, but also of the phase behaviour in the UCEP region is desirable.

In further work chemically diverse organic solutes in supercritical solvents will be investigated. The ablility to manipulate the UCEP location, the melting point depression, and the solubility by the use of binary fluid mixtures as supercritical solvents will be focussed. The critical data of such binary solvent mixtures eligible have already been subject of previous investigations [10,11]. The experimental data are represented by means of cubic equations of state, which have already been sucessfully applied to potential supercritical solvent mixtures as well as to asymmetric mixtures, such as the CO_2/naphthalene-system presented in this work.

Acknoledgements

The investigation was supported by the grants Tu 93/2-1, 2 and 3 of the Deutsche Forschungsgemeinschaft which is gratefully acknowledged.

References

1. VanGunst, C.A.; Scheffer, F.E.C.; Diepen, G.A.M. *J. Phys. Chem.* **1953**, 57, 578-581
2. Paulaitis, M.E.; McHugh, M.A.; Chai, C.P "Chemical Engineering at Supercritical Conditions ", p.139, Ann Arbor Science, Michigan, 1983
3. Lemert, R.M.; Johnston, K.P. *Fluid Phase Equilibria* **1989**, 45, 265-286
4. McHugh, M.; Yogan, T.J. *J. Chem. Eng. Data* **1984**, 29, 112-115
5. Cheong, P.L.; Zhang,D.; Ohgaki, K.; Lu, B.C.-Y. *Fluid Phase Equilibria* **1986**, 29, 555-562
6. Peng, D.Y.; Robinson, D.B. *Ind. Eng. Chem. Fundam.* **1976**, 15,59-64
7. Lamb, D.M.; Barbara, T.M.; Jonas, J. *J. Phys. Chem.* **1986**, 90, 4210-4215
8. Diefenbacher, A.; Crone, M.; Türk, M. *J. Chem. Thermodynamics* **1998**, 30, 481-496
9. Diefenbacher, A.; Türk, M. *J. Chem. Thermodynamics in press*
10. *McHugh, M.; Paulaitis, M.E. J. Chem. Eng. Data* **1980**, 25, 326-329
11. Tsekhanskaya, Yu.V.; Iomtev, M.B.; Mushkina, E.V. *Russ. J. Phys. Chem.* **1964**, 38, 1173-1176

High-Pressure Apparatus for Phase Equilibria Measurements: Solubility of Fatty Acid Ethyl Esters in Supercritical CO_2

G. CHARBIT*, C. CRAMPON, E. NEAU#
*Laboratoire d'Etudes et d'Applications de Procédés Séparatifs
Université d'Aix-Marseille III, Av. Escadrille Normandie Niemen,
13397 Marseille, Cedex 20, France.
Phone number: 33 4-91-28-86-43/ Fax number: 33 4-91-02-35-72
Email: gerard.charbit@leaps.u-3mrs.fr
#Laboratoire de Chimie Physique de Marseille
108, av. de Luminy
13288 Marseille Cedex 08, France.

A high-pressure apparatus was designed to perform phase equilibria measurements under the synthetic mode. The efficiency of both the apparatus and the procedure were first checked through preliminary experiments related to a system widely studied, CO_2/methyl oleate. The good agreement between our results and those already published, allowed us to study other binary systems involving CO_2 and some ethyl esters, more precisely the ethyl palmitate, myristate and stearate. For each systems the measurements were obtained at three different temperatures 313.1, 323.1 and 333.1 K and at pressures ranging from 1 to 20 MPa. The data were correlated using the modified Peng-Robinson equation of state with the classical quadratic mixing rules.

Introduction

The design of an extraction or fractionation operation needs key parameters such as solubilities or equilibrium data at the operating conditions.

The main features of methods used to measure phase equilibria were summarized by Brunner [1], Staby [2] and McHugh and Krukonis[3]. Three different ways are usually used to perform experimental studies of phase equilibria: synthetic, dynamic and static modes. Contrary to analytical methods, the synthetic procedure does not need any sampling and the phase transitions resulting from pressure variations are studied by direct visualization.

The study undertaken had the objective to design a simple apparatus according to the synthetic mode, allowing a low consumption of substance combined with precise measurements. The data thus obtained will serve to tune interaction parameters for thermodynamic models.

The present work describes the apparatus, the measurement method, and reports data related to four esters, at three temperatures 313.1, 323.1 and 333.1 K in a wide range of pressures. In order to check the efficiency of both the set-up and the method, it was necessary to perform measurements on a system already studied. Since the binary mixture CO_2/methyl oleate has been the object of several works [4-6], it was taken as reference.

Experimental section

Apparatus.

The experimental set-up shown in Figure 1 consists in a high-pressure view cell with variable volume, built of stainless steel, a magnetic stirrer, a thermostatic water bath, a camera (Model #1352-5000, from COHU Inc.), a TV monitor, temperature and pressure gauges. The cell was designed by TOP INDUSTRIES S.A.. A three hand screw-type manual pump was set to a thermostated chamber, equipped with a sapphire window to enable a direct visualization of the medium.

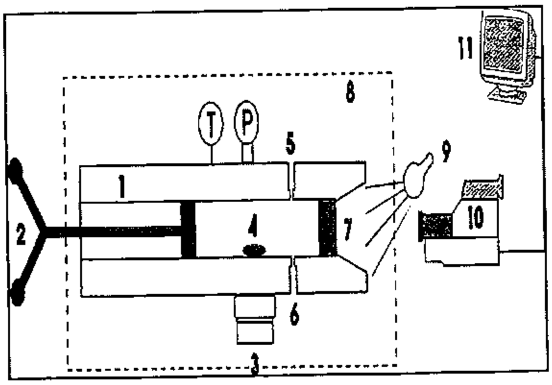

Figure 1: Experimental set-up. 1. Cell; 2. Piston; 3. Magnetic stirrer; 4. Magnetic bar; 5. Vapor sampling port; 6. Liquid sampling port; 7. Sapphire window; 8. Water bath; 9. Lamp; 10. Camera; 11. TV set.

Preliminary calibrations showed that the global volume of the cell might vary from 4.05 to 14.35 cm^3; these values take into account the dead volumes generated by the different equipments of the apparatus. Each revolution of the manual pump was registered by a counter and induced a 0.3 cm^3 variation of the cell volume.

The pressure is measured by an electronic transmitter (HAENNI ED 510); overpressures are prevented by a rupture disc. The front zone of the apparatus is heated by circulation of water coming from a thermostated bath. The screw filler cap at the top of the cell includes a port for a platinum resistance. A purge drain is fitted at the base of the cell for an easy cleaning.

The cell may work both in the synthetic and the analytical modes. For the latter, it is equipped with two sampling ports at the upper and lower parts of the chamber, each sampling line including a three-way micro-valve.

Materials.

CO_2, pure at 99.9% was supplied by "l'Air Liquide". The methyl and ethyl esters from SIGMA had a stated purity higher than 99%.

Procedure.

The experimental procedure is as follows:

First, a known amount of ester is loaded in the cell.

The air being purged, the cell is closed and a known amount of CO_2 is brought into the cell by a high-pressure calibrated bomb which is weighed before and after the introduction of CO_2. The mixture thus obtained has a known composition and the medium is biphasic at this pressure level. As soon as the system is equilibrated at the chosen temperature, as indicated by the pressure remaining constant, the piston is progressively moved in order to increase the pressure and thus bring the biphasic system to a monophasic one. Once the pressure is stabilized, it is slowly decreased until a second phase appears. The medium is thus successively compressed and decompressed in order to define the most narrow range of pressure for the phase transition. The stabilization has to be reached after each modification of pressure, but due to the small cell volume and to the efficiency of the stirring, the equilibration does not require more than three hours, which is a relatively short time as compared to those reported in the literature.

For a given global composition, different increasing temperatures are studied.

The second point of an isotherm which corresponds to a higher CO_2 mole fraction, is obtained by the following method. An additional weighed amount of CO_2 is introduced in the cell, thus modifying the composition of the previous mixture. Measurements of the transition pressures are performed as described above. After three additions of CO_2 it is considered that the cumulative errors due to the successive weighings, induce an inadequate uncertainty of the composition. As a consequence, the cell is drained off, and a new amount of ester is introduced for further measurements.

Accuracy of the measurements.

The uncertainty in the gravimetric measurements is in the order of ± 5mg for the carbon dioxide and 0.05 for the ester. The uncertainty on the binary composition is essentially due to CO_2 because it is weighed with the less good precision.

Taking account of the respective uncertainties on the CO_2 and esters weights, and the cumulative errors due to the method we could calculate that uncertainties never exceed 0.003 on CO_2 mole fractions:

The cell pressure measurement is accurate to $\pm 2.10^{-2}$ MPa and the temperature is known to within ±0.2K.

Experimental results and correlation

Experimental results.

The compounds chosen for this study were:

- methyl oleate, widely studied, in order to check the experimental set-up,
- then, ethyl myristate, palmitate and stearate as new data.

For each system, the equilibrium transitions were isothermally measured at three temperatures: 313.1, 323.1 and 333.1 K.

The transition points were easily obtained and were reproduced to within 5.10^{-2} MPa. Our experiments were performed in a large range of pressures and compositions, however the present experimental set-up did not enable us to perform measurements at low pressures (less than 1 MPa). As a consequence the lower part of the equilibrium curves was not obtained. It must be noticed that our procedure allowed measurements around the critical point.

Data correlation.

The experimental P-x data were correlated using the modified Peng-Robinson equation of state [7].

$$P = \frac{RT}{v-b} - \frac{a(T)}{v^2 + 2bv - b^2} \qquad (1)$$

where the equation parameters a and b are defined from the critical properties.

$$b = 0.07780\frac{RT_c}{P_c} \qquad (2)$$

$$a(T) = 0.45724\frac{R^2T_c^2}{P_c}\Psi(T,\omega) \qquad (3)$$

$$\Psi(T,\omega) = \left[1 + m\left(1 - \left(\frac{T}{T_c}\right)^{0.44507}\right)\right]^2 \qquad (4)$$

m is calculated from

$$m = m_0(m_1 - 1) \qquad (5)$$

$m_0=6.8126$

$m_1=\sqrt{1.1275 + 0.5173\omega - 0.0037\omega^2}$

ω is the acentric factor

As the ethyl esters used in this study decompose before reaching the critical temperature, the pseudocritical properties have been estimated through the Ambrose group contribution method [8, 9] using the normal boiling point calculated from

AMP correlation [10,11]. ω is calculated from the Edminster equation.

For a mixture of p components, the classical quadratic mixing rules was used:

$$a = \sum_{i}^{p}\sum_{j}^{p} x_i x_j \sqrt{a_i a_j}\left(1 - k_{ij}\right) \qquad (6)$$

$$b = \sum_{i}^{p}\sum_{j}^{p} x_i x_j \frac{b_i + b_j}{2}\left(1 - l_{ij}\right) \qquad (7)$$

x_i, b_i, a_i are respectively the composition, covolume and temperature function of pure component i.

k_{ij} and l_{ij} are the binary interaction parameters which must be tuned on experimental data.

The results of the correlation appear on Figures 2 to 7.

CO_2/methyl oleate mixture.

As mentioned above the CO_2/methyl oleate has been the subject of some previous papers [4-6]. Data are reported in Figures 2 to 4.

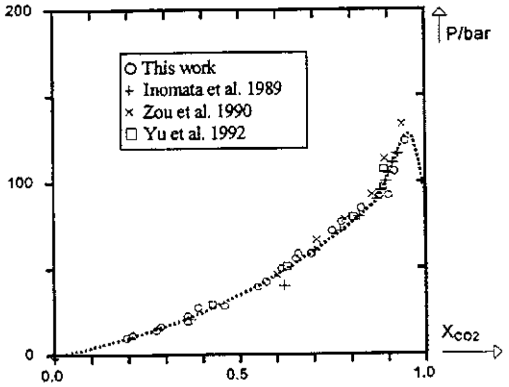

Figure 2: Phase equilibria for the system CO_2/methyl oleate at 313.1 K. Experimental data and correlation curve using kij=0.0521, lij=0.0226.

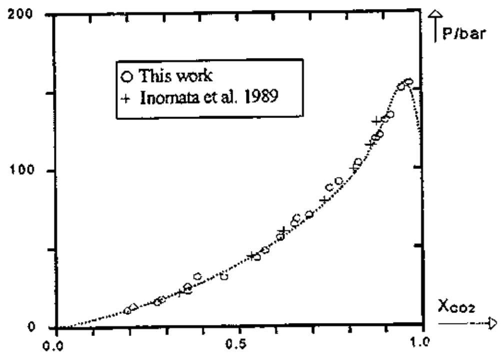

Figure 3: Phase equilibria for the system CO_2/methyl oleate at 323.1 K. Experimental data and correlation curve using kij=0.0529, lij=0.0253.

It may be observed that our data are in good agreement with all those already published. At the very near of the critical point, measurements are difficult to achieve and a certain scattering is observed. That is probably the reason why except for Zou *et al.*, few data are given by the other authors.

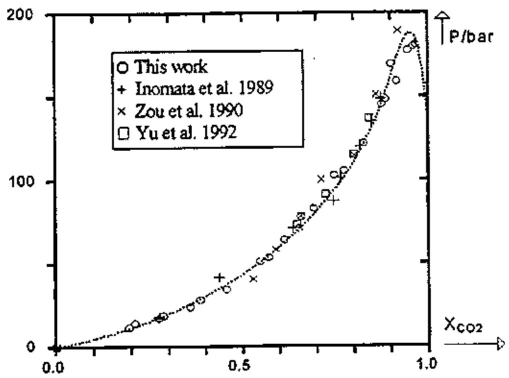

Figure 4: Phase equilibria for the system CO_2/methyl oleate at 333.1 K. Experimental data and correlation curve using kij=0.0559, lij=0.0352.

Other esters.

As concerns the myristic, palmitic and stearic acid ethyl esters, the experimental data are shown in Figures 5 to 7.

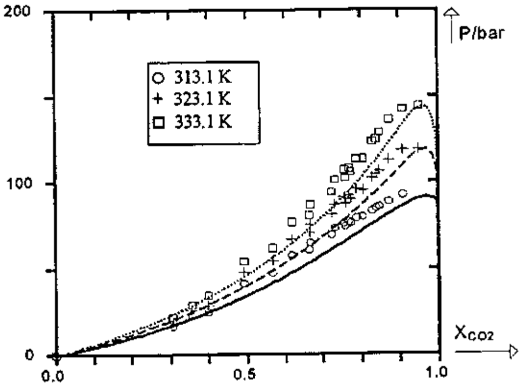

Figure 5: Phase equilibria for the system CO_2/ethyl myristate at different temperatures. Experimental data and correlation curves using kij=0.0435, lij=0.0202.

Another interesting feature of this new apparatus is the slight weight of solute required to investigate the whole range of composition. The small volume of the cell and the absence of sampling, make the experiments being carried out with less than 30 grams of each ester. This characteristic should be attractive in the case of studies devoted to high price compounds.

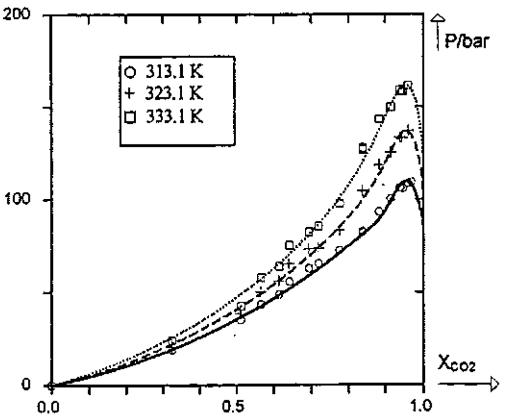

Figure 6: Phase equilibria for the system CO_2/ethyl palmitate at different temperatures. Experimental data and correlation curves using kij=0.0492, lij=0.0190.

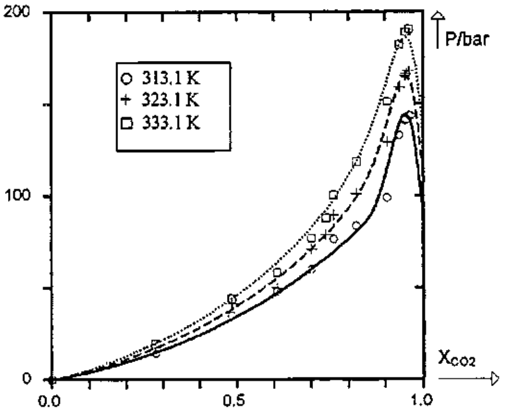

Figure 7: Phase equilibria for the system CO_2/ethyl stearate at different temperatures. Experimental data and correlation curves using kij=0.0533, lij=0.0224.

Conclusion and perspectives

A new apparatus has been designed to perform measurements of equilibria involving fatty acids esters and CO_2. The synthetic method was chosen for this study, though the set-up could operate in the analytical mode.

Several advantages were reached with this method. As sampling is avoided, it offers an easy use. The charasteristics of the optical cell combined with the specificity of the synthetic method enable the collection of numerous data with a low consumption of solute. Reproducible data could be obtained, fitting correctly with those already published.

References

(1) G. Brunner, Gas Extraction: An Introduction to Fundamentals of Supercritical Fluids and the Applications to Separation Processes, Springer, New York, 1994.

(2) A. Staby, Application of Supercritical Fluid Techniques on Fish Oil and Alcohols, Thesis of the Technical University of Denmark, Lyngby, 1993.

(3) M. MacHugh, V. Krukonis, Supercritical Fluid Extraction: Principles and Practice, 2nd Edition, Butterworths, Boston, 1994.

(4) M. Zou, Z.R. Yu, P. Kashulines, S.S.H. Rizvi, and J.A. Zollweg, Fluid-Liquid Phase Equilibria of Fatty Acids and Fatty Acids Methyl Esters in Supercritical Carbon Dioxide, The Journal of Supercritical Fluids, 3(1990), p. 23.

(5) H. Inomata, T. Kondo, S. Hirohama, K. Arai, Y. Suzuki, and M. Konno, Vapour-Liquid Equilibria for Binary Mixtures of CO_2 and Fatty Acid Methyl Esters, Fluid Phase Equilibria, 46(1989), p. 41.

(6) Z.R. Yu, and S.S.H. Rizvi, Phase Equilibria of Oleic Acid, Methyl Oleate, and Anhydrous Milk Fat in Supercritical CO_2, The Journal of Supercritical Fluids, 5(1992), p. 114.

(7) A. Péneloux, E. Rauzy, A consistent correction for the Redlich-Kwong-Soave volumes, Fluid Phase Equilibria, 8 (1982), p. 7.

(8) D. Ambrose, Correlation and estimation of vapor-liquid critical properties. I. Critical temperatures of organic compounds, NPL Rep. chem. 92. National Physical Laboratory: Teddington, 1978.

(9) D. Ambrose, Correlation and estimation of vapor-liquid critical properties. I. Critical pressures National Physical laboratory: Teddington. 1979.

(10) A.B. Macknick, J.M. Prausnitz, Vapor pressures of heavy liquid hydrocarbons by group-contribution method. Ind. Eng. Chem. Fundam., 18(1979), vol. 4, p. 348.

(11) A.B. Macknick, J. Winnick, J.M. Prausnitz, Vapor pressures of liquids as a function of temperature. Two parameters equation based on kinetic theory of fluids. Ind. Eng. Chem. Fundam. 16(1977), vol. 3, p. 392.

Static Solubility Measurements of Natural and Synthetic Dyestuffs in Compressed Gases

Dirk Tuma and Gerhard M. Schneider*
Ruhr-Universität Bochum, Physikalische Chemie
D-44780 Bochum, Germany
Fax: + 49 234 7094 293
E-mail: gerhard.schneider@ruhr-uni-bochum.de

Solubility data of 1,4-bis-(octylamino)-9,10-anthraquinone (AQ08) in CO_2 and Disperse Red 60 (DR60) in CO_2 are presented and discussed with respect to the applicability of a density-based solvato complex model proposed by Chrastil. The isotherms in the system CO_2 + AQ08 were measured between $285.9 < T/K < 324.7$ and $6 < p/MPa < 90$, those of CO_2 + DR60 between $303.1 < T/K < 332.7$ and $7.2 < p/MPa < 97.6$, respectively. In both cases it came out that in the low as well as in the high peripheral pressure (density) regions this model does not give a reliable description of the phenomena. Furthermore, for all-trans β-carotene in CO_2 at 307.6 K a method to estimate stereomutation kinetics was tested by which isomerization was found to be dependent on pressure.

Introduction

Since several years we focus our activities on systematic measurements of the solubility behavior of dyestuffs in near- and supercritical fluids as a function of temperature and pressure [1–7]. Solubility data over a large temperature and pressure range is pertinent to both technical applications (e.g. planning and performance of extractions) and thermodynamic considerations relating to phase behavior as well, the latter being linked to solubility modeling and its development.

The static analytical method is an ideal tool for investigation of those regions (primarily high and ultrahigh pressures), which are normally beyond a technical application. If you have designed a cell being operable for any particular pressure and temperature conditions, the experimental requirements for both the lowest and highest pressures will remain more or less the same, whereas a flow method equipment for very high pressures strongly differs from that what is normally used in SFE or SFC [8].

For applications there are two major demands for solubility modeling, namely that it can be based on experimental data merely from the interesting region with the implication that scarcely known or doubtful additional thermodynamic information of the individual system (such as calculations from EOS do require, see e.g. [9]) can remain unconsidered and that nevertheless reliable results are obtained. In literature, for example, we sometimes find the semi-log and the log-log relationship between solubility and density often resulting in linear or at least near-linear behavior [10–12].

The static method with its possibility to work at high pressures, is able to test and discuss such a plot on the basis of data covering a large pressure range. In this contribution a survey of own recent results is presented which are correlated by Chrastil's method [11]. The outcoming results are interpreted with special consideration of this correlation method.

Materials and Methods

Our equipment consists of an optical high-pressure autoclave coupled to a spectrophotometer by fiber optics. Two similar setups were used, on the one hand a cell constructed for a maximum pressure of 200 MPa and a temperature range from approximately 273 to 383 K, respectively, being coupled to a Perkin-Elmer Lambda 18 spectrophotometer (no. 1), and on the other hand a similar cell for use up to 100 MPa and at about 273 to 413 K coupled to a Perkin-Elmer Lambda 9 instrument instead (no. 2). Facts and details of device no. 1 are reported in Refs. [1,5,7,13] and of device no. 2 in Refs. [14,15], respectively.

CO_2 (99.995 vol.%) and N_2O (99.0 vol.%) were purchased from Messer Griesheim GmbH. All-trans β-carotene came from Sigma Chemical Co. (synthetic, crystalline, purity 97.1 % (HPLC)), Disperse Red 60 (1-amino-4-hydroxy-2-phenoxy-9,10-anthraquinone) was delivered by LG Chemical Co., Seoul, Korea, and had a purity of 99.4 % (SFC) [13,16].

Source and purity of the 1,4-bis-(n-alkylamino)-9,10-anthraquinones are given in Refs. [4–7,13,16]. For details of the measuring technique for determining equilibrium solubilities see again Refs. [4–7,13,16]. In the case of the 100 MPa-autoclave, which was not described there, the experimental performance was exactly the same [13]. To summarize briefly, the anthraquinone derivatives did not undergo any changes under test, whereas β-carotene showed significant stereomutation and therefore had to be treated differently. In contrast to the anthraquinone derivatives where isothermal equilibrium could be determined by a stepwise increase of pressure, β-carotene required separate gas-fillings for each single pressure to see how isomerization behaved.

Results and Discussion

As reported previously [5,7,13], solubility of AQ08 in CO_2 is a monotonous function of solvent density at a constant pressure in the region where we did our measurements. The corresponding log-log plot in Fig. 1, however, shows two remarkable deviations from linearity. The first is in the region near the liquid-vapor boundary (low pressures), the second occurs at liquid like solvent densities when the curvature of the concentration (density) isotherm (see Ref. [13]) changes its sign.

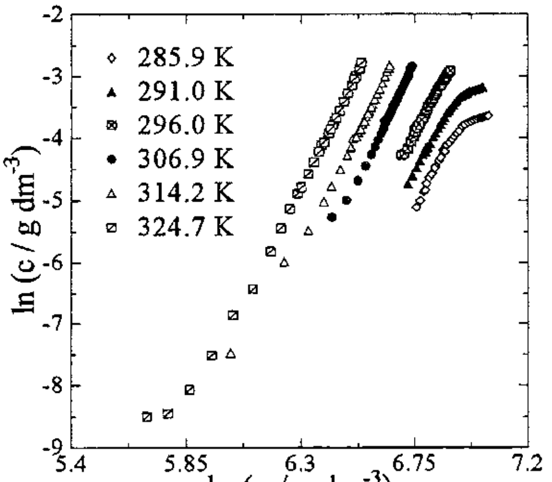

Figure 1. Solubility of AQ08 in CO_2. Solvent Densities Were Calculated from the EOS Given by Span and Wagner [17]

Wagner et al. [6] and Kautz et al. [4] used a modified SFC-apparatus (maximum operating pressure 20 MPa) for this substance and other homologous 1,4-bis-(alkylamino)-9,10-anthraquinones having shorter alkyl chains (from methyl to pentyl) in CO_2. Their results proved to be linear in the temperature range chosen, when plotted in this way.

Chrastil derived a relationship correlating the solubility of a solute to the density of the solvent through the formation of a solvato complex, which is in equilibrium with the gas. The main assumption is that one molecule (here dyestuff) associates with a fixed (even non-stoichiometric) number of solvent molecules at a given temperature and that this complex is in equilibrium with its surroundings. Thus, we get

$$c = \rho^k \exp\left(\frac{a}{T} + b\right) \qquad (1)$$

where c is the dyestuff concentration in g dm^{-3}, ρ is the solvent density in g dm^{-3}, k is the aforementioned constant giving the average number of solvent molecules present in the solvato complex, and a and b are constants derived from the solvation enthalpy and molar mass of the two components, respectively [11].

For CO_2 + AQ08, in the linear region k is only slightly increasing to higher temperatures but towards the bordering region to high densities k becomes distinctly smaller. When approaching the solubility extremum with increasing density, the partial molar volume of the dissolved dyestuff in the fluid phase V_2^g grows from lower values until it equals the molar volume of the pure solid component $V_{m,2}^{s*}$ at the solubility maximum [1,18]. This indicates that there should be more solvent molecules in the solvato complex here what seems to be plausible but is in contradiction to Chrastil's model. Since $(\partial \ln c / \partial \ln \rho)_T = 0$ at the solubility maximum, then in Eqn. 1 k equals zero which is physically unreasonable.

Another behavior is shown by the system CO_2 + DR60 (Fig. 2). Besides the high-density drop, the slope of the function decreases also with increasing temperatures. Sung and Shim report similar findings [12]. Further own investigations of this system are underway.

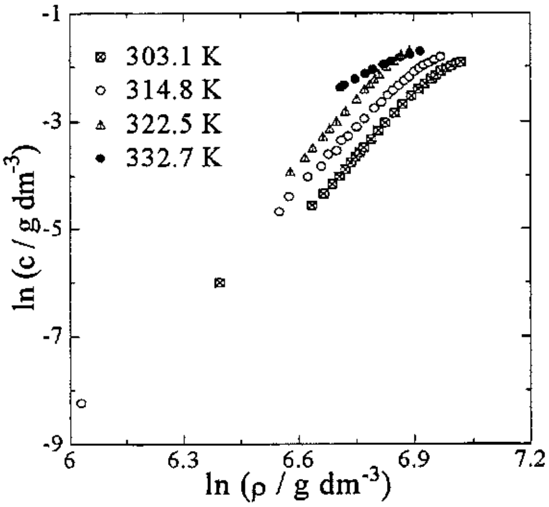

Figure 2. Solubility of DR60 in CO_2

The main accompanying effect in doing solubility measurements of β-carotene and carotenoids in general is stereomutation or rather isomerization arising from the inherent instability. Since we record an absorption spectrum in situ to determine the particular solubility and do not take a sample to analyze it separately (e.g. by means of chromatography), we always see an indefinite number of cis isomers being present in the equilibrium mixture. This effect, not welcome but unalterable, complicates the correct detection of the all-trans isomer. The extinction coefficients of the cis forms are smaller than that of the all-trans compound. A special feature of the formation of cis isomers, however, is the appearance of an additional peak (the "cis peak") in the UV-region, actually between 320 and 380 nm. As the spectra strongly overlap, it is not possible to quote values for each isomer in a mixture. Therefore, the only remaining possibility to determine the cis isomer contamination in equilibrium is to express it in terms of % III/II and % D_B/D_{II} which have been introduced by Liaaen-Jensen [19,20]. Here, the height (III) of the longest wavelength absorption band is expressed as a percentage of that of the λ_{max} absorption band (II), the base line in each case being the minimum between the two maxima. The % D_B/D_{II} relation is the maximum absorption of the cis peak expressed as a percentage of that of λ_{max}. Usually, all-trans compounds (this rule is applicable for carotenoids in general) are characterized by a low % D_B/D_{II} and a high % III/II ratio while the reverse is true for cis isomers. Individual values for a great variety of components and solvents are tabulated [20].

The following spectroscopic effects can be observed during the solubility experiment: On a time scale, the cis peak and the total absorption spectrum are gradually increasing since cis isomers are more soluble than the all-trans compound. Besides, isomerization is a dynamic process as cis isomers also can revert to an all-trans configuration [21,22]. The most important promoter of cis-trans rearrangements aside from the solvent is temperature. Consequently, at higher temperatures the isomer contribution at the beginning of the measuring run will be higher (resulting in a lower % III/II ratio at t = 0). The analysis of the % III/II and % D_B/D_{II} ratios of the spectra as a dependence of time proved to be practicable.

Fig. 3 shows a plot for CO_2 + β-carotene at 307.6 K where % III/II for different pressures is given on a time scale. At low concentrations the tendency to isomerize is higher than when more molecules are dissolved. Starting from low pressures upwards, the % III/II ratio first increases parallel to the increasing solubility. At pressures between 20 and 40 MPa, the peak ratio is between approximately 30 and 35. When going to higher pressures (especially in the region of retrograde solubility at pressures exceeding 60 MPa [3,13]), however, the % III/II ratio decreases again. Now, the isomer contribution increases both with pressure and time. The better soluble cis isomers remain in solution whereas preferably the all-trans β-carotene is "squeezed out".

For N_2O, no significant pressure dependence of % III/II can be found because of the drastically better solubility of β-carotene limiting the spectroscopically accessible pressure range to 8 to 15 MPa in the temperature region between 308 and 323 K [7]. Furthermore, the % III/II ratio is independent from concentration and it gave a constant value for the spectra obtained during calibration (heptane: 36.4, cyclohexane: 34.1, THF: 25.8).

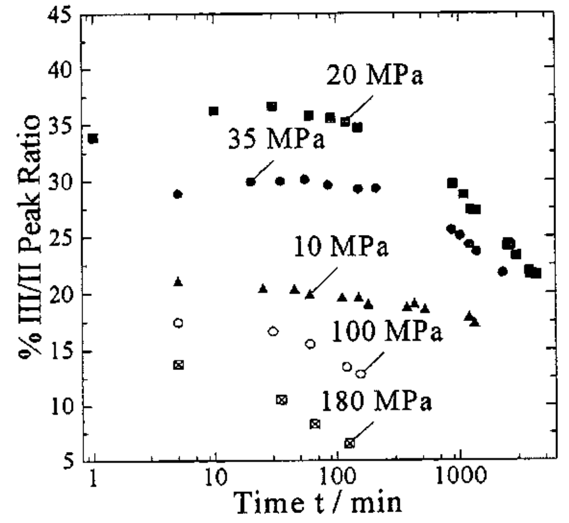

Figure 3. % III/II Peak Ratio for β-Carotene in CO_2 at T = 307.6 K

Conclusions

On the basis of our investigations of anthraquinone dyestuffs in various solvents, for which a large amount of solubility data had been collected, we tried to correlate the data using a log-log solubility-density relationship proposed by Chrastil [11]. It could be shown that a plot of ln c vs. ln ρ exhibits a satisfactorily straight line only in a specified density region, i.e. at such conditions where the solvent clustering about a dyestuff molecule might be regarded as a constant. Anyway, this simplification becomes inaccurate the more the density region is expanded.

Secondly, for solubility measurements of β-carotene the p,T-dependent isomerization expressed in terms of spectral structure gave indications for the optimization of solubility measurements. For each data point it is to decide when equilibrium conditions have been achieved. First the % III/II ratio vs. time is about constant, then the value decreases because of progressive isomerization. Therefore, we think it is useful to record the spectrum at the point when the curve starts to deviate essentially from a constant value or to calculate the equilibrium solubility from the data measured at different times since the adjustment of equilibrium and isomerization are simultanously proceeding. The value for the integral absorbance is gradually increasing, at the beginning preferably through the solubility process, whereas later the contribution of isomerization becomes significant.

Acknowledgments

The authors thank Professor Jae-Jin Shim, Yeungnam University, Korea, for providing Disperse Red 60. Financial support of the Deutsche Forschungsgemeinschaft (DFG) and the Fonds der Chemischen Industrie e. V. is highly appreciated.

References

1. Haarhaus, U.; Swidersky, P.; Schneider, G. M. *J. Supercrit. Fluids* **1995**, 8, 100-106.
2. Swidersky, P.; Tuma, D.; Schneider, G. M. *J. Supercrit. Fluids* **1996**, 9, 12-18.
3. Schneider, G. M.; Kautz, C. B.; Tuma, D. in: Rudolf von Rohr, Ph.; Trepp, Ch. (Eds.) "Process Technology Proceedings 12, High Pressure Chemical Engineering", p. 259, Elsevier, Amsterdam, 1996.
4. Kautz, C. B.; Wagner, B.; Schneider, G. M. *J. Supercrit. Fluids* **1998**, 13, 43-47.
5. Tuma, D.; Schneider, G. M. J. *Supercrit. Fluids* **1998**, 13, 37-42.
6. Wagner, B.; Kautz, C. B.; Schneider, G. M. *Fluid Phase Equilibria* **1999**, in press.
7. Tuma, D.; Schneider, G. M. *Fluid Phase Equilibria* **1999**, in press.
8. Stahl, E.; Quirin, K. W.; Glatz, A.; Gerard, D.; Rau, G. *Ber. Bunsenges. Phys. Chem.* **1984**, 88, 900-907.
9. Deiters, U. K. *Fluid Phase Equilibria* **1985**, 20, 275-282.
10. Kumar, S. K.; Johnston, K. P. *J. Supercrit. Fluids* **1988**, 1, 15-22.
11. Chrastil, J. *J. Phys. Chem.* **1982**, 86, 3016-3021.
12. Sung, H.-D.; Shim, J.-J. submitted to *J. Chem. Eng. Data* **1999**.
13. Tuma, D. Dissertation, Ruhr-Universität Bochum, 1999.
14. Maiwald, M. Dissertation, Ruhr-Universität Bochum, 1997.
15. Schneider, G. M. in: Kiran, E.; Levelt Sengers, J. M. H. (Eds.) "Supercritical Fluids – Fundamentals For Application", NATO ASI Series E: Applied Sciences, vol. 273, p. 91, Kluwer, Dordrecht, Boston, London, 1994.
16. Wagner, B. Dissertation, Ruhr-Universität Bochum, 1998.
17. Span, R.; Wagner, W. *J. Phys. Chem. Ref. Data* **1996**, 25, 1509-1596.
18. Kurnik, R. T.; Reid, R. C. *AIChE J.* **1981**, 27, 861-863.
19. Liaaen Jensen, S. "The Constitution of Some Bacterial Carotenoids and Their Bearing on Biosynthetic Problems", p. 119, Det Kongelige Norske Videnskabers Selskabs Skrifter 8, Trondheim, 1962.
20. Britton, G. in: Britton, G.; Liaaen Jensen, S.; Pfander, H. (Eds.) "Carotenoids, Volume 1B – Spectroscopy", p. 13, Birkhäuser, Basel, 1995.
21. Chen, B. H.; Chen, T. M.; Chien, J. T. *J. Agric. Food Chem.* **1994**, 42, 2391-2397.
22. von Eggers Doering, W.; Sotiriou-Leventis, Ch.; Roth, W. R. *J. Am. Chem. Soc.* **1995**, 117, 2747-2757.

High Pressure Equilibria of Anthracene and Octacosane between Supercritical Fluids and Adsorbents

Peter Harting and Joachim Germanus
Institute of Non-Classical Chemistry
at the University of Leipzig
Permoserstr. 15, D-04318 Leipzig
E-Mail: inc@sonne.tachemie.uni-leipzig.de, Fax: +49 – (0)341–235 2701

This study provides an overview of experiments of dissolution and adsorption characteristics of substances with a high boiling point. Aromatic and aliphatic compounds in supercritical fluid phases are used as examples. A static high pressure equilibrium apparatus used for the determination of the phase equilibrium and the method of analysis are described. The results are discussed and, as far as possible, compared with previously published data.

Introduction

Separation processes based on high pressure gas extraction have gained considerable importance over the last few years in industrial extraction processing [1]. The application is currently mainly used in pharmaceutical production and food processing technology, where the relatively careful and selective extraction of substances and the further advantage of ultrapure and solvent-free products are of special importance.

However, the required characteristics of the applied compressed gases are generally only present in a supercritical or fluid state of the gases. Pressures and temperatures above the critical values for these gases must be applied. It is therefore obvious that gases such as carbon dioxide, ethane and propane with low critical values are generally preferred.

Gas mixtures, e.g. carbon dioxide with a low nitrogen content can also be used as extracting agents, as these mixtures have critical temperatures below room temperature.

In addition to the actual extraction process, the separation of the substances dissolved in supercritical fluids as well as the regeneration of the solvent are of great importance especially in industrial processing, as these processes often require high energy inputs and consequent costs.

Several different procedures are used for the separation of the substances dissolved in fluids. As the solubility of a substance in a supercritical fluid generally increases with the density of the fluid and the pressure respectively, the reduction of the density of the fluid phase by means of pressure reduction is a simple method for the separation of the dissolved substance. This approach though may result in high energy consumption as the fluid must be recompressed subsequently. An alteration of the gas composition by addition of a further suitable gas component may result in a reduced solubility and consequent separation of the desired component. In order to re-use the solvent, the added gas component must be subsequently separated.

Alteration of the miscibility gap by means of entrainers and liquid phase distillation of the compressed fluid (cooled to subcritical temperature prior to processing) are alternative separation and extraction methods. Separation methods with membranes were often unsuccessful, due to the insufficient mechanical stability of the membranes in technical processing [1]. According to Zosel [2], absorption processes can be used to decaffeinate aqueous coffee extract solutions. In this process, water, which shows a minimal solubility in carbon dioxide at high pressures and low temperatures, is used as an absorbent. However, there are only a few substances which are extractable with supercritical carbon dioxide and at the same time are water-soluble.

A barely researched method for the separation of substances from supercritical fluids is adsorption. This method can be carried out under isobaric conditions and does not require the expansion of the solvent, a considerable reduction of costs in a recirculation process is achievable.

Equipment, substances, method

The solubility and equilibrium concentrations of the dissolved substances in the fluid under the required conditions were determined after sampling and transfer of the substances into suitable organic solvents.

Figure 1 shows an outline of the experimental design of the high pressure autoclave system with its peripherals including the sampling unit (at the right). The sampling unit consists of a back-to-back valve with removable steel ampoule. Sampling is done by letting a small amount of the fluid flow into the steel ampoule by briefly opening the autoclave outlet valve. After subsequent closure of all valves, the sampling unit can be disconnected from the autoclave. The fluid contained in the steel ampoule is then expanded into a suitable solvent. Subsequently, the valve and steel ampoule are rinsed with the same solvent and a quantitative determination of the substance may be carried out with a suitable analysis method. UV-VIS spectrophotometry was used for the determination of anthracene, while octacosane is analysed by means of gas chromatography.

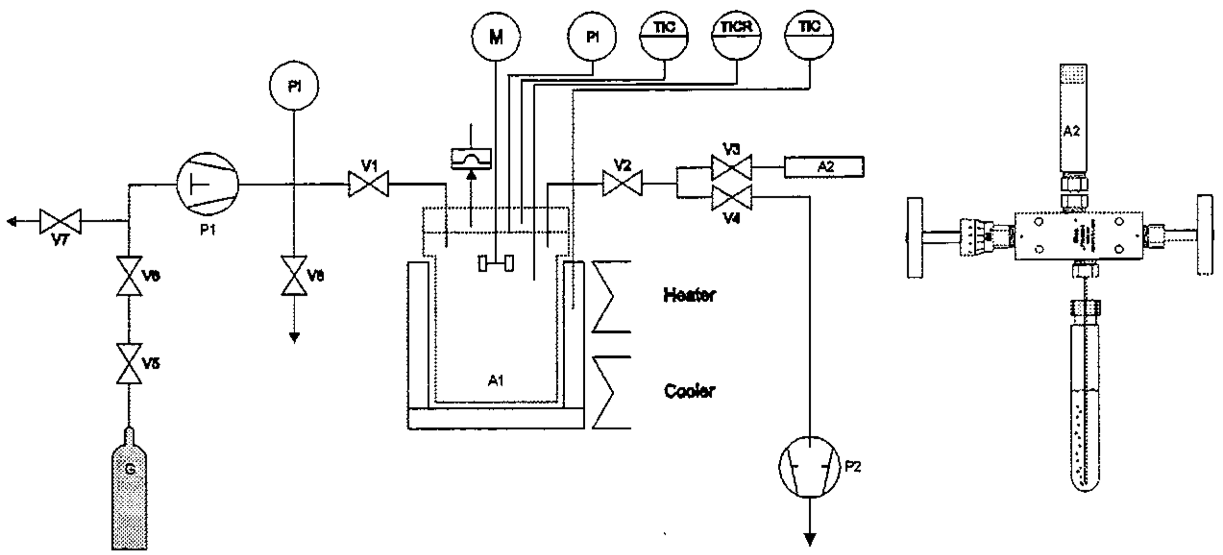

Fig. 1: General design of the high pressure equipment. V1-V8 high pressure valves, A1 high pressure autoclave, A2 sampling ampoule in steel, P1 compressor, P2 vacuum pump, G gas reserve, M stirring device, PI pressure indicator, manometer, TIC temperature indicator and control, TICR temperature indicator and control recording

In the experiments, carbon dioxide of purity class 4.5 and a mixture of carbon dioxide with 10 % nitrogen [3] were used. For various reasons, anthracene and octacosane were used as model substances. The melting points of these substances are sufficiently high in order to prevent a dissolution of the supercritical gas in the components. The components are further sufficiently stable at high temperatures and suitable as model substances for high-molecular aromatic and aliphatic compounds. The anthracene used was of a purity of 99 % with a melting point between 215 °C and 219 °C and boiling point of 340 °C [4]. Octacosane was of a purity of 99 % with a melting point between 61 °C and 63 °C and boiling point of 278 °C at 15 torr [4].
The following adsorbents were used: activated carbon of the type Norit R1 [5] and zeolite 13X (trade name Zeosorb) [6].
The zeolite was activated in a helium flow at a temperature of ca. 400 °C for 4 hours. The active carbon was activated at a pressure of approx. 5 bar under helium for 6 hours at 90 °C. Prior to the direct adsorption experiments for component separation from the supercritical fluid, the adsorbents were again activated in the autoclave under vacuum at 90 °C. Periods of at least 5 hours were necessary for the establishment of an equilibrium, and the fluid phase was agitated in order to gain improve distribution.
Table 1 presents an overview of the examined systems and the respective conditions.

Results and Discussion

Figures 2 and 3 illustrate a selection of experiment results regarding the solubility of anthracene and octacosane in the supercritical fluids.
Empirical correlation methods were used for the equalisation of the experiment data. For solubility results and the equilibrium load at simultaneous adsorption, the equations $\ln(c) = A+B*p$ and $\ln(c)= A+B*\rho$ respectively were used. In the equations, c is the concentration of the component of low volatility in the fluid phase, p is the pressure and ρ is

Component	Fluid	Investigation	Temperature
Anthracene	CO_2	Solubility	40 °C, 55 °C
Anthracene	CO_2 +10 % N_2	Solubility	25 °C, 40 °C
Anthracene / Norit R1	CO_2	Adsorption - Solubility - Equilibrium	40 °C, 55 °C
Anthracene / Zeosorb	CO_2	Adsorption - Solubility - Equilibrium	40 °C, 55 °C
Anthracene / Norit R1	CO_2 +10 % N_2	Adsorption - Solubility - Equilibrium	25 °C, 40 °C
Anthracene / Zeosorb	CO_2 +10 % N_2	Adsorption - Solubility - Equilibrium	25 °C, 40 °C
Octacosane	CO_2	Solubility	40 °C
Octacosane	CO_2 +10 % N_2	Solubility	40 °C
Octacosane / Norit R1	CO_2 +10 % N_2	Solubility	40 °C

Table 1: Overview of the examined systems at a pressure range from 0 to 500 bar

the density of the fluid under the required conditions.

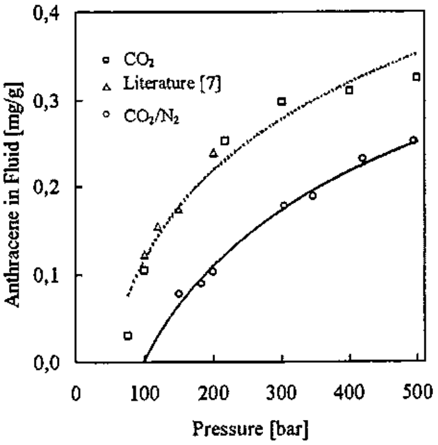

Fig. 2: Solubility of anthracene in carbon dioxide and carbon dioxide/nitrogen mixture at 40 °C.

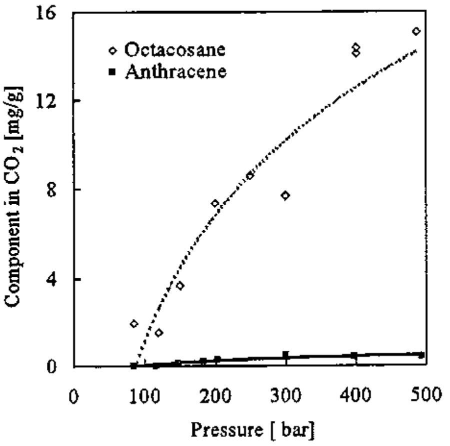

Fig. 3: Comparison of the solubility of anthracene and octacosane in carbon dioxide at 55 °C

The comparisons of the solubility data in different fluid compositions under otherwise equal conditions show clearly that carbon dioxide is the generally preferable solvent. The mixture of carbon dioxide with 10 % nitrogen though reaches similar solubility characteristics to that of the pure carbon dioxide at a pressure increase of approx. 100 bar. A comparison between the measured solubility values of anthracene in pure carbon dioxide and the data by Kwiatkowski [7], shows good consistency. The solubility values established by Rößling and Franck in 1983 [8] are approx. 30% lower for the same system.

Octacosane is considerably more soluble in the fluids than anthracene, as is shown clearly in the example of carbon dioxide as a solvent in Figure 3.

With the inclusion of the absorbents in the equilibrium system, the equilibrium load of the fluid phase is considerably reduced due to adsorption. Figures 4 and 5 show the results for carbon dioxide-absorbent-anthracene systems and adsorption on zeolite 13X and Norit R1 respectively.

In these diagrams, the coefficient K represents the ratio between absorbent mass and anthracene mass in the equilibrium system.

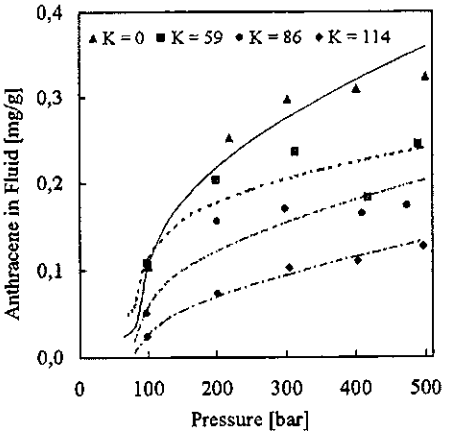

Fig. 4: Equilibrium load of the fluid phase (solvent: carbon dioxide) at simultaneous adsorption on zeolite 13X at 40 °C

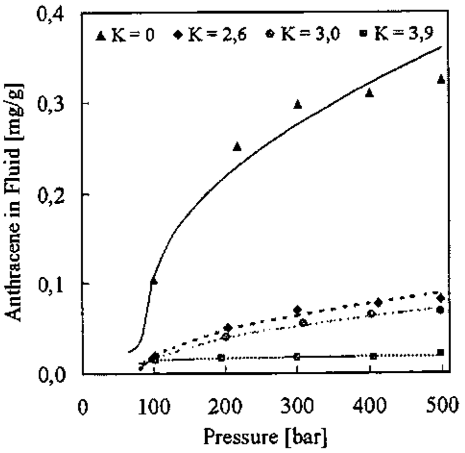

Fig. 5: Equilibrium load of the fluid phase (solvent: carbon dioxide) at simultaneous adsorption on active carbon Norit R1 at 40 °C

From the loads of the fluid phase and adsorbate phase, which were determined by means of weigh balance of the substances in the autoclave, the distribution coefficients of the systems $K_c=c''/c'$ can be calculated, c'' being the concentration of the component with low volatility, in the adsorbate phase and c' being the concentration of the fluid phase.

The distribution coefficients of the system with anthracene-zeolite-carbon dioxide in figure 6 show clearly that, supercritical fluids are not suitable for the subsequent desorption of the separated substances, even if high pressures are applied. Therefore, other more practical methods for the regeneration of the absorbents must be applied.

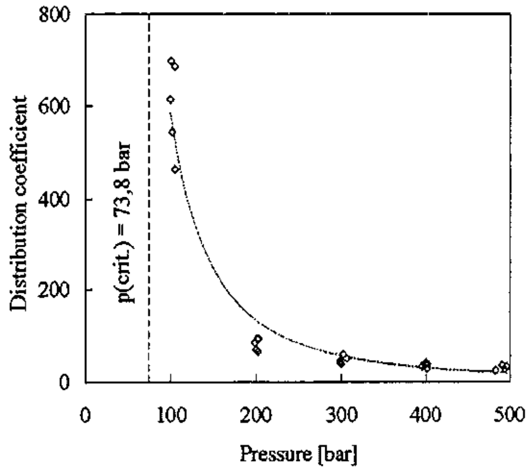

Fig. 6: Distribution coefficient of the system anthracene-zeolite-carbon dioxide at 55 °C with approximation curve ($K_c=9{,}8*10^6*p^{-2{,}11}$)

Acknowledgements

Financial support by the Deutsche Forschungsgemeinschaft is acknowledged.

References

[1] *Birtigh, A.; Brunner, G.:* Abscheidung von Stoffen aus überkritischen Gasen; Chem.-Ing.-Tech. 67, 829 (1995).

[2] *Zosel, K.:* Angew. Chem. Int. Ed. Engl. **17**, 702 (1978).

[3] Messer Grießheim GmbH, Industriegase Deutschland, Homerger Str. 12, Düsseldorf.

[4] Sigma-Aldrich Chemie GmbH, Grünwalder Weg 30, Deisenhofen.

[5] Norit, Product information
Norit R1, Postbus / P.O. Box 105, 38 AC Amersfoot, Netherland, 1986.

[6] Engelhard Process Chemicals GmbH, Karl-Wiechert-Allee 72 Hannover.

[7] *Kwiatkowski, J., Lisicki, Z., and Majewski, W.*, Ber. Bunsenges. Phys. Chem., **88**, 865 (1984).

[8] *Rößling, G. L.; Franck, E. U.:* Solubility of Anthracene in Dense Gases and Liquids to 200 °C and 2000 bar; Ber. Bunsenges. Phys. Chem. **87**, 882 (1983).

Correlation, Prediction and Experimental Determination of Gas Solubilities

Kai Fischer, Michael Wilken, Jürgen Gmehling
Universität Oldenburg, Technische Chemie, Fachbereich 9, Postfach 2503
26111 Oldenburg, Germany
e-mail: fischer@fb9tc.uni-oldenburg.de, fax ++49 441 798 3330

The correlation and prediction of (vapor or gas) + liquid equilibria is possible with cubic equations of state combined with so called G^E-mixing rules. They combine the advantages of the local composition G^E - models with those of cubic equations of state. Vapor-liquid equilibria at high or low pressure of multicomponent systems can be predicted using only binary interaction parameters, regardless of the polarity of the components and whether they are sub- or supercritical. Also group contribution approaches, e.g. UNIFAC can be used, so that the applicability of methods like for example the PSRK group contribution equation of state [1,2,3,4] is not restricted to systems, where experimental data are available.

Most of the available experimental information for gas solubilities is given in terms of solubility coefficients, which are based on the linearity of gas solubility with its partial pressure at low concentration and low pressure. They can be used to fit the interaction parameter for the classical mixing rules for cubic equations of state, but for the optimization of two or three parameters required for G^E-mixing rules, a larger composition and pressure range should be covered. Therefore in this ongoing work gas solubilities for different gases (CO, O_2, CO_2, H_2S, SF_6 and N_2) and a variety of solvents were investigated with the help of a static apparatus. These data together with literature data were used to fit the required interaction parameters for the PSRK-model. The results of the PSRK-model are compared with all the available experimental information. The predictive potential of PSRK is demonstrated by calculating the phase equilibrium behavior of multicomponent systems.

Introduction

Although group contribution methods are usually considered as predictive models, reliable experimental information is needed to fit the required group interaction parameters. In the Dortmund Data Bank (DDB) most of the worldwide available information on phase equilibria and other thermophysical data for mixtures and pure components is stored, and made easily accessible in an electronic form for the regression of the desired model parameters. DDB is an ideal tool for the development of reliable thermodynamic models. At the same time it allows to define, which additional experimental information is required to extend the different models for applications in new areas of interest. In the case of PSRK, the model was initially based on the UNIFAC method, where for most of the gases no structural groups had been available. The choice of the binary systems studied in this work is related mainly to the following two topics:

1. Absorption processes for the removal of H_2S and CO_2 from natural gas. Besides chemical solvents such as aqueous alkanolamine solutions, also selective physical solvents as for example cyclic amides (N-alkyl-2-pyrrolidones) are often used.
2. Air solubility in organic solvents. The knowledge about the air solubility in various liquids is of great interest for safety reasons for example in the storage and transport of liquids, where the system pressure, changing with temperature, should not exceed the given limits. Information about the single oxygen and nitrogen solubilities from air is needed for example for the estimation of the oxygen uptake in recycle streams open to the atmosphere.

Materials and Methods

The different solvents were degassed and distilled after drying over molecular sieve as described earlier [5], except water which was distilled twice and degassed. The gases were used without further purification. The static apparatus used was described previously in detail [5] and is shown in Fig. 1. Since it was previously used for the measurement of VLE in subcritical systems only, a few changes were necessary. The principle of the synthetic measurement is to inject precisely known amounts of the pure components into a thermostated equilibrium chamber, and to measure the system equilibrium pressure as a function of composition in the gas + liquid system. Known amounts of the pure liquids were accurately injected into the empty equilibrium cell using displacement pumps. The experimental pure solvent vapor pressures were measured in the beginning of each isothermal P,x measurement and compared with literature data. The agreement indicated that in all cases the solvents were sufficiently degassed. The injection of gases was realized using a constant volume (ca. 1 dm^3) gas container. It was filled directly from the gas bottles up to a pressure higher than the system pressure in the equilibrium cell. The temperature and pressure in the gas container at ambient temperature was monitored using a Pt 100 resistance thermometer (Hart Scientific) and a calibrated pressure sensor (Druck). The exact volumes of the gas injection system and the equilibrium chamber were determined by filling them with pure compressed water under vacuum. After recording the initial pressure in the gas injection system, the valve to the

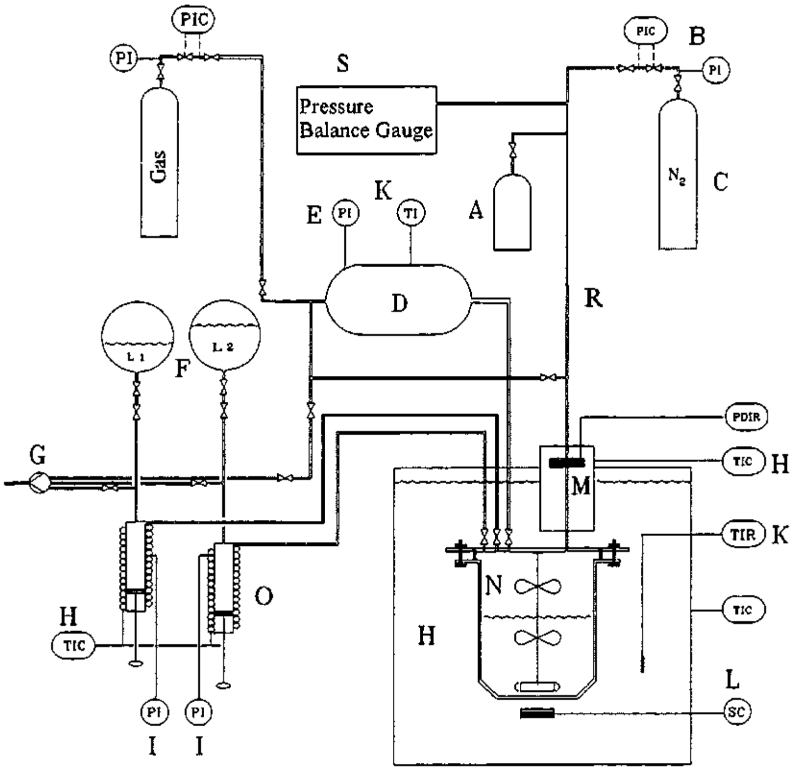

A: Buffer Volume
B: Pressure Regulator
C: Nitrogen Flask
D: Gas Container
E: Pressure Sensor
F: Container for Degassed Liquids
G: Vacuum Pump
H: Constant Temperature Bath

I: Bourdon Pressure Gauge
K: Pt 100 Resistance Thermometer
L: Rotating Magnetic Field
M: Differential Pressure Null Indicator
N: Equilibrium Cell
O: Piston Injectors
R: Pressure Balance Gauge

Figure 1. Schematic of the static apparatus

equilibrium chamber was opened for several seconds so that the pressure in the equilibrium chamber was equal to the pressure in the gas injection system. Then the valve was closed and the pressure of the gas injection system was measured again. From the PVT data before and after injection, the injected amount of the pure gaseous compound could be determined using the virial equation with the second virial coefficients recommended by DIPPR [6]. The injection of gas was repeated until the desired pressure range of P,x data was covered. After each injection, the pressure decreased until thermodynamic equilibrium was reached. Then pressure and temperature were recorded together with the feed amounts of the substances. Although a magnetically driven stirrer was used, the time for each point took between 1 and 2 h. The amount of solvent initially injected into the equilibrium chamber was chosen to be large enough to fill more than ca. 90% of the total volume of the equilibrium chamber, even more for systems with small gas solubilies or less for those with larger solubilities. This strategy was chosen in order to minimize the gaseous phase since a considerable part of the gas feed should be in the liquid phase.

The indirect measurement applied in this work gives all quantities temperature, system pressure and feed composition with high accuracy, but the composition of the coexisting phases must be determined by flash calculation. This procedure gives a small correction from the feed composition in the two phase region to the bubble point curve, providing experimental P,x data, whereas the vapor compositions cannot be considered as experimental values. Volume and mass balance equations must be solved in this data treatment, and special attention must be paid to a correct representation of the volume of the liquid phase, where both the liquid density of the solvents and the partial molar volume of the dissolved gas are of importance. For the liquid densities, reliable correlations are recommended by DIPPR [6], and the partial molar volumes of the gases can be calculated by a generalized method suggested by Cibulka and Heintz [7]. These values are in good agreement with the values implicitly calculated with the help of cubic equations of state simultaneously with the phase equilibrium behavior.

Results and Discussion

A few series of measurements have been performed in order to check the reliability of the experimental method by comparing the results with literature data. Typical results of experimental isothermal P,x data are shown in Fig. 1 and 2 for the system $CO_2 + H_2O$.

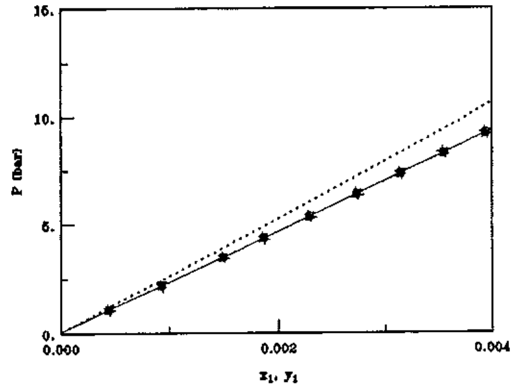

Figure 2. Experimental (• this work) and calculated (— PSRK/UNIQUAC; --- SRK/quadratic mixing rule; ····· PSRK/UNIFAC) VLE for the system carbon dioxide (1) + water (2) at 312.66 K.

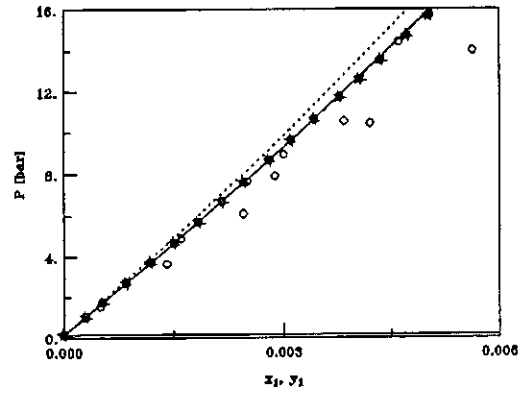

Figure 3. Experimental (• this work, o data from various authors taken from DDB at 323.15 K) and calculated (— PSRK/UNIQUAC; --- SRK/quadratic mixing rule; ····· PSRK/UNIFAC) VLE for the system carbon dioxide (1) + water (2) at 323.46 K.

Also literature data are shown in Fig. 3 and it can be seen, that the accuracy of the data from different authors changes significantly. For a more comprehensive representation of the solubility behavior as a function of temperature, the Henry coefficients were derived from the solubility data measured in this work (full circles) and are shown in Fig. 4 for the system $CO_2 + H_2O$, and in Fig. 5 for the system $CO + H_2O$ in comparison with literature data taken from DDB (open circles)

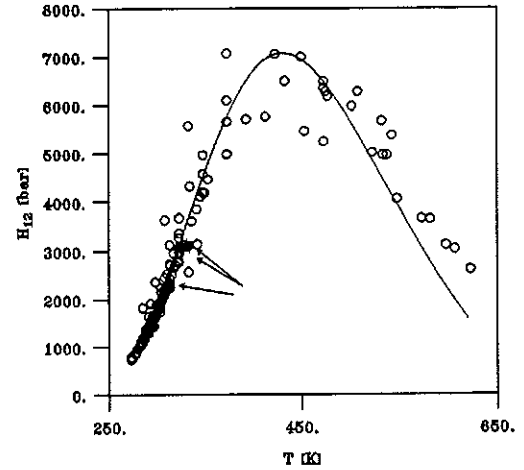

Figure 4. Experimental (• this work, o data from various authors taken from DDB) and calculated (— PSRK/UNIFAC) Henry coefficients for carbon dioxide (1) in water (2)

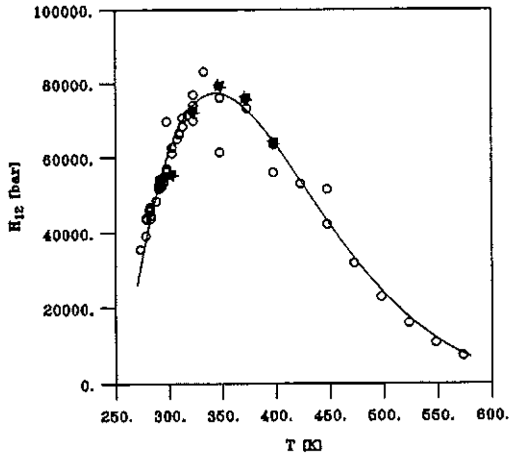

Figure 5. Experimental (• this work, o data from various authors taken from DDB) and calculated (— PSRK/UNIFAC) Henry coefficients for carbon monoxide (1) in water (2)

It can be seen from Fig. 2 – 5 that the data from this work agree well with the literature data, and moreover that a reliable representation is possible with the PSRK model. The two examples show furthermore the typical temperature dependence of the Henry coefficients, where often a marked maximum is observed. In Fig. 6, the system H_2S + benzene is shown as an example for larger gas solubilities. The results are compared with VLE data obtained by Laugier and Richon [8] using a direct analytical experimental method. A summary of the

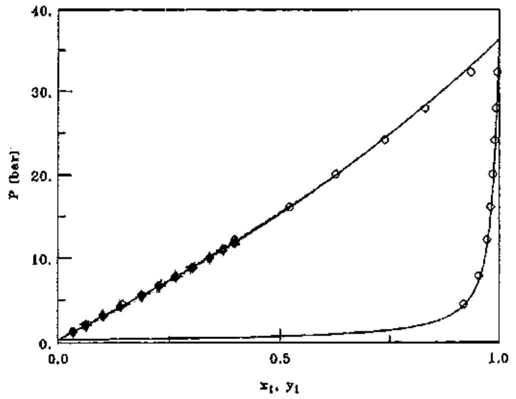

Figure 6. Experimental (● this work, o Laugier and Richon [8] at 323.15 K) and calculated (— PSRK/UNIQUAC; --- SRK/quadratic mixing rule; ····· PSRK/UNIFAC) VLE for the system hydrogen sulfide (1) + benzene (2) at 323.5 K.

data measured in this work is given in Tab. 1.

The experimental P,x data from this work as well as the data stored in DDB were used to fit several new PSRK / UNIFAC group interaction parameters. The current status of the required parameter matrix is shown in Fig. 7. For obtaining reliable interaction parameters between gases and solvent groups solubility data up to 20 - 40 bar should be present. If only gas solubility data at atmospheric pressure are used, the significance of the parameters get lost because 2 parameters are used to represent one quantity, the Henry coefficient. The significance for the solvent(2)-gas(1) parameter (A_{21}) is lower than for the gas(1)-solvent(2) parameter (A_{12}), because often the concentration of gases in solvents in limited. Therefore most of the gas solubility data measured in this work cover a large pressure range from the solvent vapor pressure up to 100 bar.

A great part of the binary systems listed in Table 1 have been investigated in order to extend the applicability of the PSRK method for the prediction of air solubilities in organic solvents. Currently the following solvent compounds are covered for air solubility calculations: Alkanes, aromatics, alcohols, water and ethers.

Conclusions

An isothermal static apparatus was used to determine gas solubility data for various binary systems. The data were correlated using cubic equations of state with different mixing rules, where for the sytems studied in this work no significant difference between the models was observed. Furthermore the data were used for the regression of group interaction parameters for the PSRK method, providing a predictive tool for phase equilibrium calculations in multicomponent systems.

For most of the missing parameters, no or not enough reliable experimental phase equilibrium information is available. For a further extension of the application range of PSRK, measurements have to be performed. The example of oxygen solubility measurements in this work shows that a few specific precise measurements are sufficient for a large extension of the range of applicability of PSRK.

Acknowledgement

The authors thank the "Bundesministerium für Wirtschaft" for financial support via "Arbeitsgemeinschaft industrieller Forschungsvereinigungen" (AiF project 10931N).

References

1. Holderbaum, T.; Gmehling, J. *Fluid Phase Equilibria* **1991** 70, 251-265
2. Fischer, K.; Gmehling, J. *Fluid Phase Equilibria* **1996**, 121, 185-206
3. Gmehling, J.; Li, J.; Fischer, K. *Fluid Phase Equilibria* **1997** 141, 113-127
4. Li, J.; Fischer, K.; Gmehling, J. *Fluid Phase Equilibria* 1998 143, 71-82
5. Fischer, K.; Gmehling, J. *J. Chem. Eng. Data* **1994** 39, 309-315
6. Daubert, T. E.; Danner, R. P.; Sibul, H. M.; Stebbins, C. C. Data Compilation "Physical and Thermodynamic Properties of Pure Compounds", DIPPR, AIChE, Taylor & Francis, New York, 1989
7. Cibulka, I.; Heintz, A. *Fluid Phase Equilibria* **1995** 107, 235-255
8. Laugier, S.; Richon, D. *J. Chem. Eng. Data* **1995** 40, 153-159

Table 1. Henry coefficients derived from P,x data measured in this work

gas	solvent	temperature [K]	Henry coefficient [MPa]
hydrogen sulfide	benzene	304.30	1.96
hydrogen sulfide	benzene	323.50	2.69
hydrogen sulfide	N-octyl-2-pyrrolidone	306.70	0.70
hydrogen sulfide	N-octyl-2-pyrrolidone	323.60	1.15
carbon dioxide	N-octyl-2-pyrrolidone	303.40	5.00
carbon dioxide	N-octyl-2-pyrrolidone	323.60	6.67
carbon monoxide	water	302.59	5560.
carbon monoxide	water	322.61	7247.
carbon monoxide	water	347.52	7932.
carbon monoxide	water	372.41	7591.
carbon monoxide	water	398.46	6400.
carbon dioxide	N-methyl-2-pyrrolidone	322.52	10.34
carbon dioxide	water	312.66	229.0
carbon dioxide	water	323.46	307.9
carbon dioxide	water	332.50	310.1
carbon monoxide	N-methyl-2-pyrrolidone	302.60	276.8
carbon monoxide	N-methyl-2-pyrrolidone	373.40	201.7
oxygen	benzene	302.85	122.9
oxygen	benzene	317.71	118.6
oxygen	benzene	332.63	114.3
oxygen	toluene	298.43	104.5
oxygen	toluene	323.30	96.38
oxygen	toluene	348.28	89.22
oxygen	n-octane	298.42	45.94
oxygen	n-octane	323.29	46.87
oxygen	n-octane	348.31	46.44
oxygen	di-n-butyl ether	298.32	47.63
oxygen	methanol	298.33	252.8
oxygen	methanol	323.31	257.5
oxygen	methanol	348.30	233.4
oxygen	1-propanol	298.20	150.2
oxygen	1-propanol	323.54	141.2
oxygen	1-propanol	348.19	139.7
nitrogen	1-propanol	298.34	254.0
nitrogen	1-propanol	348.18	213.9
nitrogen	1-propanol	398.00	164.2
nitrogen	ethanol	298.22	296.5
nitrogen	ethanol	348.20	252.3
nitrogen	ethanol	398.02	198.3

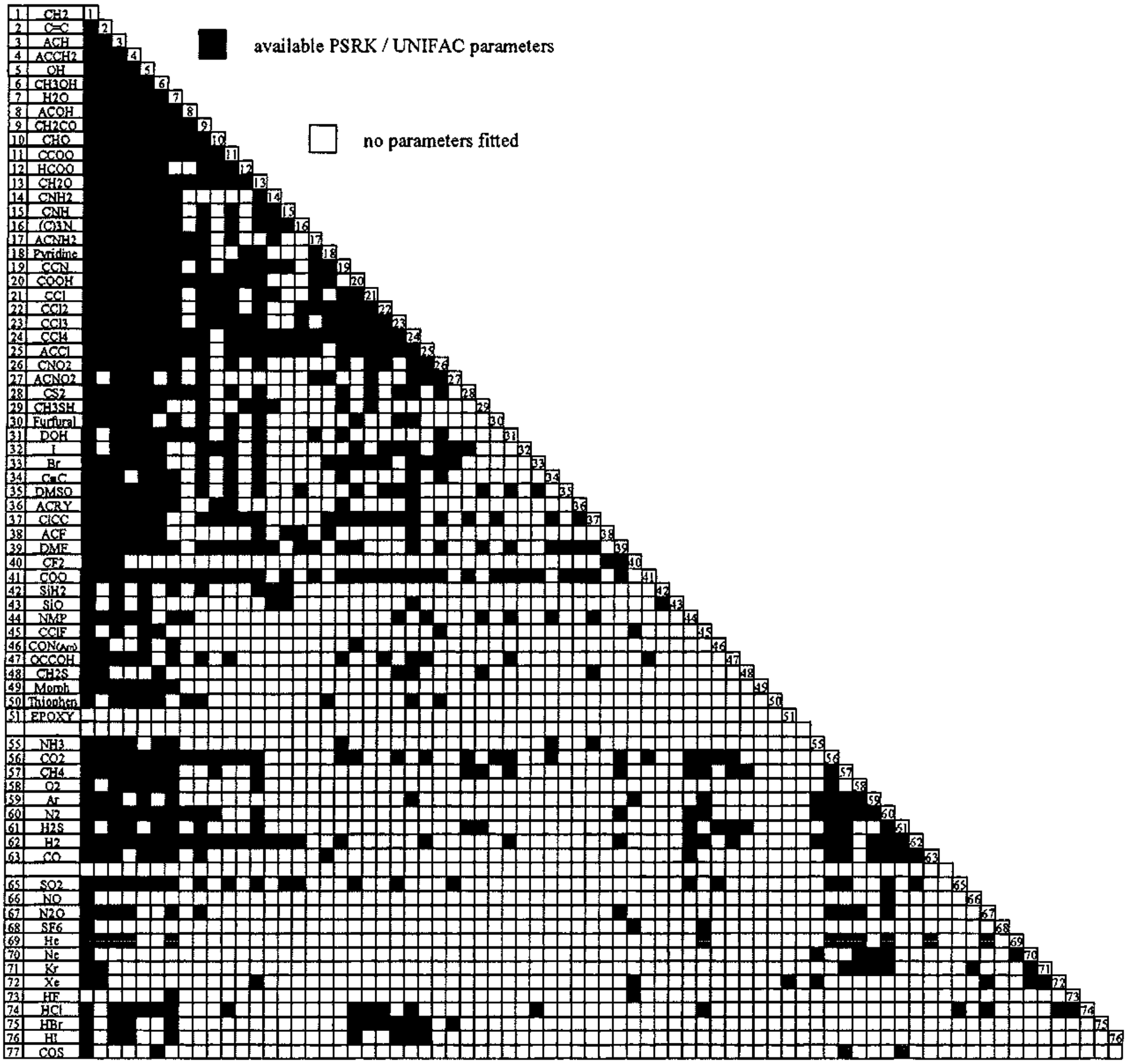

Figure 7. Current status of the PSRK / UNIFAC parameter matrix

GVC-Fachausschuß „High Pressure Chemical Engineering“, March 3-5, Karlsruhe, Germany, 1999

Pressure Dependence of Intradiffusion in Binary Mixtures with NH_3 resp. CO_2 as one Component

T. Groß, N. Karger, L. Chen, and H.-D. Lüdemann*
University of Regensburg, Institute of Biophysics and Biophysical Chemistry, D-93040 Regensburg, Germany
EMAIL: hans-dietrich.luedemann@biologie.uni-regensburg.de
FAX: ++49-941-9432479

The translational molecular mobility as described by the intradiffusion coefficient D_{ii} has been determined by nuclear magnetic resonance measurements for the binary systems ammonia/benzene, ammonia/methanol, carbon dioxide/benzene, and carbon dioxide/methanol. The D_{ii} were taken in the temperature range between the melting pressure curves and in part up to 423 K at pressures up to 200 MPa. Log D_{ii} vers x plots at constant p and T reveal interesting differences between the four systems: In the two mixtures containing benzene as one component a very regular behaviour is observed. The two D_{ii} vary almost linearly with composition. In both mixtures with methanol as one component a strong curvature is seen for these plots, leading at low temperatures to pronounced minima of the curves.

Introduction

For the quantitative characterization of the fluidity in liquids and mixtures the self- resp. intradiffusion coefficient is the most fundamental property. For the determination of D_{ii} at extreme conditions of temperature and pressure the NMR Hahn-spin echo method with application of pulsed field gradients has become the method of choice [1]. It can in principle be applied to all multicomponent systems. In continuation of older studies on neat fluids, which included ammonia [2], carbon dioxide [3], and methanol [4] we will present in the following first data collected for fluid solutions in CO_2 and NH_3 the two most applied solvents in supercritical fluid technology [5].

Experimental

The self diffusion coefficients were determined by the NMR pulsed field gradient method [1] in strengthened glass cells of the Yamada design [6]. Details of our modification of this type of high pressure cell have been given previously [7, 8]. The mixtures were prepared by weighing. Their concentration was controlled by integration of the NMR spectra. Concentrations are judged reliable to ±1 mole %. The data were collected at pressures up to 200 MPa. The pressure was determined with a strain gauge (Burster Präzisionstechnik, Gernsbach, FRG) connected directly to the sample side of the separation volume to ±0.5 MPa. Temperatures given are judged reliable to ±1 K. They were measured with a metal sheathed thermocouple (Thermocoax, Philips Industrie Electronic, Hamburg, FRG) just outside of the glass capillary and were stable to ±0.5 K. The D_{ii} were calculated from the amplitudes of the Fourier transformed second half of the spin echoes. The D_{ii} are judged reliable to ±5 % they were reproducable to ±2 %.

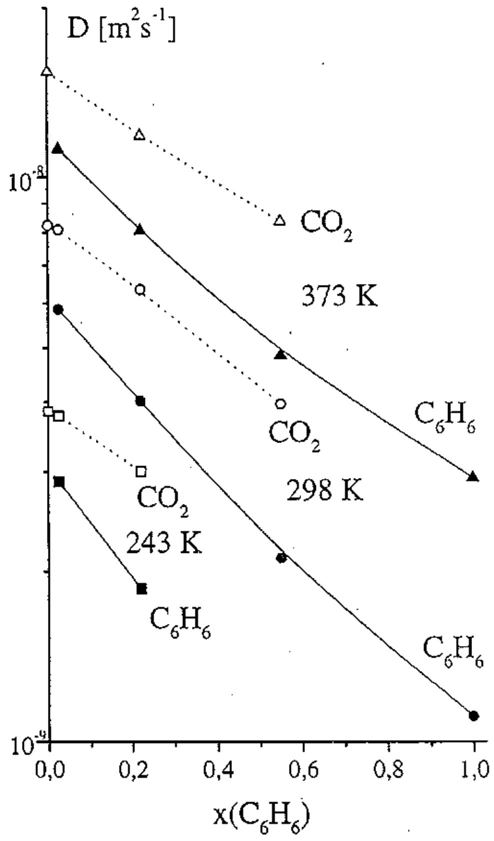

Figure 1.Intradiffusion Coefficients D_{ii} as Function of Mole Fraction $x(C_6H_6)$ in the System CO_2/C_6H_6. The Data of the Neat Fluids were taken from the Literature CO_2 [3], C_6H_6 [9]

Results and Discussion

Some typical data for the system CO_2/C_6H_6 are compiled in fig. 1. In these plots as well as for most of the other data collected the concentration dependence in the log D_{ii} vers x plot is almost „linear“, which appears to be the common behaviour for unpolar binary mixtures [10]. The same behaviour is seen in the mixture NH_3/C_6H_6 presented in fig. 2. Since in this system NH_3 is considered to be a hydrogen bonded liquid, this result is surprising, because it was expected that the unpolar diluent C_6H_6 should show an influence upon the arrangement and dynamics of the hydrogen bonds.

The mixtures NH_3/CH_3OH (fig. 3) in which both compounds may interact via hydrogen bonds show especially at low temperatures a very pronounced minimum in the translational mobility of the alcohol, which in our opinion can only be explained by the formation of hydrogen bonds between both compounds. By standard chemical reasoning ammonia can contribute 3 donors and 1 acceptor to hydrogen bonding while the stoichiometry for methanol is 2 acceptors and 1 donor. Hydrogen bonded associates involving both compounds should thus have a greater probability to form locally branched three dimensional networks. This qualitative attempt of an explanation should be supported by intradiffusion coefficient measurements for the ammonia molecules. Because of the chemical exchange between the N-H and O-H protons leading for most concentrations, temperatures, and pressures to one averaged ^{1}H-signal for these two types of protons these measurements cannot be done by ^{1}H-NMR. Experiments to measure D_{ii} by ^{15}N-NMR applying ^{15}N-enriched ammonia are in progress.

Also the dynamic behaviour of neat NH_3 [2] as revealed by the rough hard sphere analysis of the self diffusion coefficients [11] is in puzzling contrast to this observation. From this analysis no contribution of hydrogen bonds between ammonia molecules can be derived, which is on the other hand in agreement with our results for the NH_3/C_6H_6 mixture.

In fig. 4 the $D_{ii}(CH_3OH)$ for CO_2/CH_3OH are given. Here we find at low temperature and low mole fractions of methanol a very sleep decrease of $D_{ii}(CH_3OH)$ with concentration, while at higher mole fractions this value is almost concentration independent. Fig. 5 gives for some temperatures the concentration dependence of $D_{ii}(CO_2)$ and $D_{ii}(CH_3OH)$. $D_{ii}(CO_2)$ decreases almost linearly with mole fraction. With decreasing temperature the ratio $D_{ii}(CO_2)$ / $D_{ii}(CH_3OH)$ becomes larger. This ratio also increases with $x(CH_3OH)$. One could thus conclude that the CO_2 is not involved in any hydrogen bonding and that the translational mobility of CH_3OH is mostly dominated by the dynamics of the alcohol/alcohol hydrogen bonds. However with this

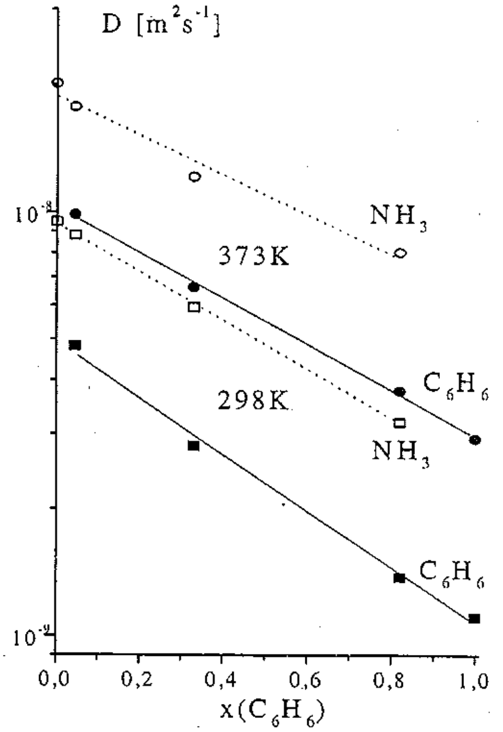

Figure 2.Intradiffusion Coefficients D_{ii} as Function of Mole Fraction $x(C_6H_6)$ in the System NH_3/C_6H_6. The Data of the Neat Fluids were taken from the Literature NH_3 [2], C_6H_6 [9]

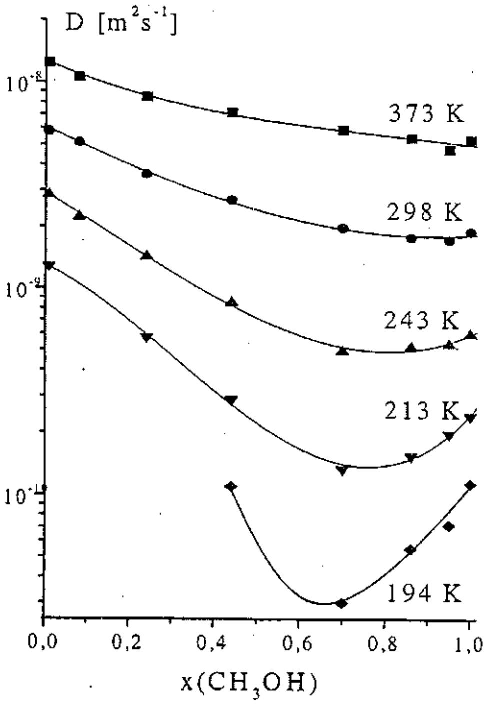

Figure 3.Intradiffusion Coefficients D_{ii} of CH_3OH as Function of Mole Fraction $x(CH_3OH)$ in the System NH_3/CH_3OH. The Data of the Neat Fluid was taken from the Literature CH_3OH [4

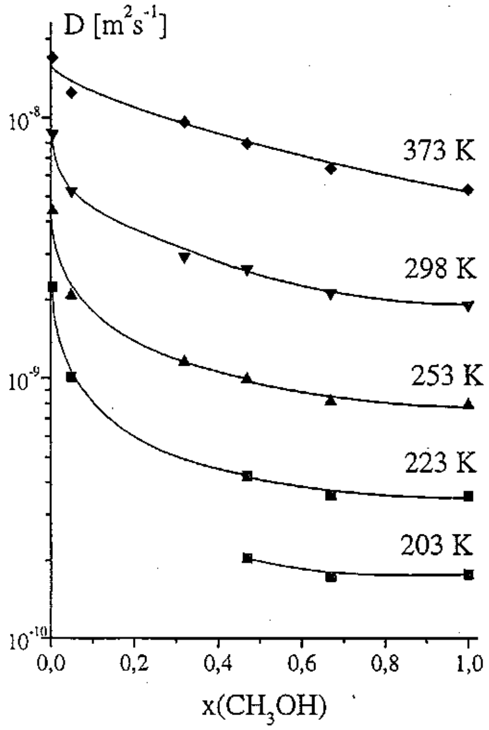

Figure 4.Intradiffusion Coefficients D_{ii} as Function of Mole Fraction x(CH_3OH) in the System CO_2/CH_3OH. The Data of the Neat Fluid was taken from the Literature CH_3OH [4]

assumption the missing concentration dependence of D_{ii} (CH_3OH) for $x > 0.5$, $T \leq 223K$ is hard to understand.

In a preliminary attempt to characterize the extent of hydrogen bond formation in the CO_2/CH_3OH system we determined the chemical shift of the hydroxyl proton as function of x(CH_3OH), temperature, and pressure. In fig. 6 some of the data are given. The chemical shift δ of the methyl group was used as an internal standard. Formation of hydrogen bonds shifts the difference $\Delta = \delta(O\underline{H}) - \delta(C\underline{H}_3)$ to more positive values. The temperature and pressure dependence of the difference Δ can be described in terms of hydrogen bond equilibria [12, 13]. Inspection of the curves for various x (CH_3OH) in fig. 6 shows that the dilution of the alcohol with CO_2 reduces the temperature at which Δ starts to decrease, which seems to indicate that CO_2 does not participate in the hydrogen bonding. Thus the experimental evidence for the moment appears to be contradictory.

Conclusions

The intradiffusion coefficients for the systems CO_2/C_6H_6 and NH_3/C_6H_6 show a very regular concentration, temperature, and pressure dependence.

In the two mixtures NH_3/CH_3OH and CO_2/CH_3OH hydrogen bonding leads especially at

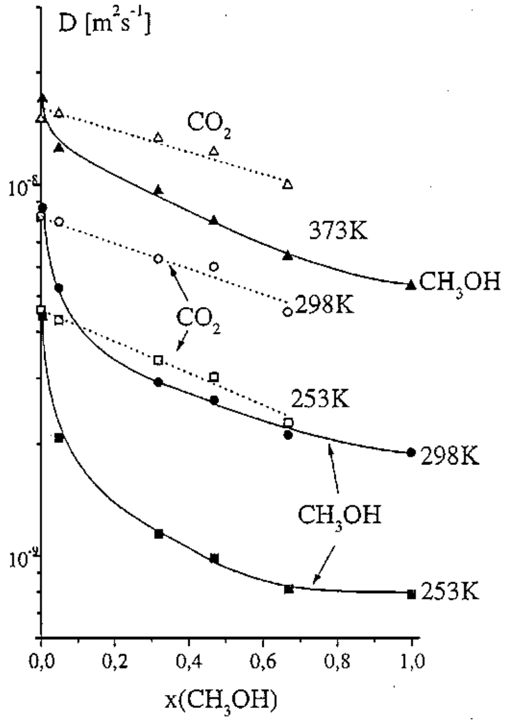

Figure 5.Some Intradiffusion Coefficients D_{ii} for both Compounds of the System CO_2/CH_3OH as Function of x(CH_3OH)

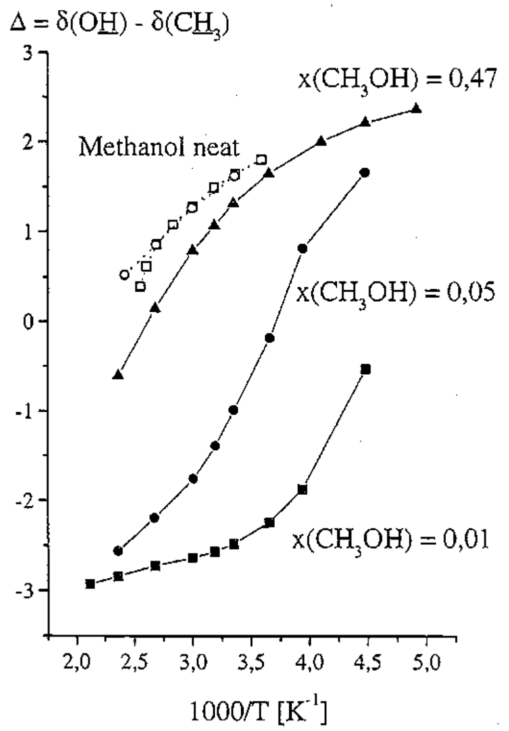

Figure 6.Temperature Dependence at 100 MPa for the Chemical Shift Difference $\Delta = \delta(O\underline{H}) - \delta(C\underline{H}_3)$ in CO_2/CH_3OH, values for Neat CH_3OH [12, 13]

lower temperatures to a much stronger temperature and concentration dependence for D_{ii} (CH_3OH). With the experimental evidence available at the moment it cannot be decided, whether and to which extent NH_3 and CO_2 participate in hydrogen bonding with the CH_3OH.

Acknowledgements

Financial support by the Deutsche Forschungsgemeinschaft is acknowledged. The technical skills of Mr. S. Heyn, R. Knott, G. Niesner, and G. Wührl made this work possible.

References

1. Stejskal, E. O.; Tanner, J. E. *J. Chem. Phys.* **1965**, 42(1), 288-292.
2. Groß, T.; Buchhauser, J.; Price, W. E.; Tarassov, I. N.; Lüdemann, H.-D. *J. Mol. Liq.* **1997**, 73/74 , 433-444.
3. Groß, T.; Buchhauser, J.; Lüdemann, H.-D. *J. Chem. Phys.* **1998**, 109(11), 4518-4522.
4. Karger, N.; Vardag, T.; Lüdemann, H.-D. *J. Chem. Phys.* **1990**, 93(5), 3437-3444.
5. Brunner, G. 'Topics in Physical Chemistry, Vol. 4, Gas Extraction,' Ed. Baumgärtl, H.; Franck, E. U.; Grünbein, W.; Springer, New York, 1994.
6. Yamada, H. in: Jonas, J. ed. 'NMR Basic Principles and Progress, High Pressure NMR' Vol. 24, p.233, Springer Verlag, Heidelberg, 1991.
7. Lang, E. W.; Lüdemann, H.-D. *Progress in NMR Spectroscopy* **1993**, 25, 507-633.
8. Price, W. E.; Lüdemann, H.-D. in: High Pressure Techniques in Chemistry and Physics: A Practical Approach. Holzapfel, W. B.; Isaacs, N. S. eds., Chapter 5, p. 225, Oxford University Press, 1997.
9. Parkhurst, H. J.; Jonas, Jr. and J. *J. Chem. Phys.* **1975**, 63(6), 2698-2704.
10. Tarassov, I. *Dissertation, Universität Regensburg,* **1996**.
11. Chandler, D. J. Chem. Phys. 1975, 62(4), 1358-1363.
12. Wallen, S. L.; Palmer, B. J.; Garrett, B. C.; Yonker, C. R. *J. Phys. Chem.* **1996**, 100(10), 3959-3964.
13. Schulman, E. M.; Dwyer, D. W.; Doetschman, D. C. *J. Phys. Chem.* **1990**, 94(20), 7308-7312.

Phase Equilibrium (solid-liquid-gas) in binary Systems of Polyethyleneglycols, Polyethylenedimethylether with Carbon Dioxide, Propane and Nitrogen

V. Wiesmet, E. Weidner
Lehrstuhl für Verfahrenstechnische Transportprozesse
Institut für Thermo- und Fluiddynamik der Ruhr-Universität Bochum
Universitätsstr. 150, D-44780 Bochum
Fax: 0234/7094 277 E-mail: weidner@vtp.ruhr-uni-bochum.de

Phase behaviour in binary polymer-gas systems containing Polyethyleneglycols (PEG) with molecular weights from 200 to 8000 g/mol respectively Polyethyleneglycoldimethylether with molecular weights of 200 and 2000 g/mol have been investigated. Gas components were carbon dioxide, nitrogen and propane. Experiments were performed in a temperature range from 298 K to 393 K and a pressure range from 1 bar to 300 bar. Melting points and qualitative phase behaviour were determined in a high pressure optical cell. Quantitative solubilities were measured in an autoclave using a static analytic method.
Phase behaviour with liquid polymers depends on the gas and it's state of aggregation (liquid/supercritical). Open and closed miscibility gaps are existing, as well as three phase areas.
The influence of a methylgroup at the beginning and the end of the polymerchain is strong for short-chained polymers like PEG 200 and PEGDME 200. For polymers with molecular weight higher than 1500 g/mol the influence of the functional end group on the phase behaviour is nearly negligible.
Melting points of the polymers under pressure are also influenced by the gas and it's state of aggregation. The solubility of gas in the molten polymer is a measure for the difference between the melting point of the pure polymer and the melting behaviour in the polymer-gas system.
Projection of the 3-dimensional p,T,x-phase behaviour into p-T-plane allows assignment of the experimental results to the classes of phase behaviour defined by Scott, van Konynenbourg and McHugh..

Introduction

Polymers are widely applied in several industrial processes. Polyethyleneglycols (PEG) are polymers, which, due to their physiological acceptance, are used in large quantities in chemical, pharmaceutical, cosmetic and food industry. Liquid PEGs are e.g. applied as lubricants in compressors due to their excellent fluiddynamic properties, which can be adjusted by the molar mass. Polyethyleneglycoldimethyether (PEGDME) is used as absorbent in gas cleaning. In both applications high pressure and sub-/supercritical gases are involved. Several authors [1-7] studied the solubility of polymers in supercritical fluids due to research on fractionation of polymers. For solubility of SCF in polymers and solid-liquid phase transitions only limited number of experimental data are available till now [2,3,8-10].

Polymers

The general formula of PEG is $H(OCH_2CH_2)_nOH$, where n is the number of ethylene oxide groups. By etherification of the hydroxyl-group at the beginning and the end of the PEG-chain PEGDME $CH_3(OCH_2CH_2)_nOCH_3$ is created. With variation of n polymers of different molar masses, with narrow size distribution can be obtained. In this work PEGs with molar masses of 200, 1500, 4000, and 8000 g/mol were used. PEG up to molar mass of 600 g/mol is liquid, while those with higher molar mass are solid. PEGDME with molar mass of 200 (liquid) and 2000 g/mol (solid) were used. PEG and PEGDME were obtained from Hoechst AG and used without further purification.

Experimental Equipment

Determination of Melting Point To observe the phase behaviour and for the determination of melting points under pressure a high pressure optical cell, presented in Figure 1, was used. It is designed for a pressure of 300 bar and a temperature of 423 K. The volume of the cell is 15,7 cm³. The construction allows to view the complete content. To lower the time to reach equilibrium a magnetic stirrer is fixed below the cell.

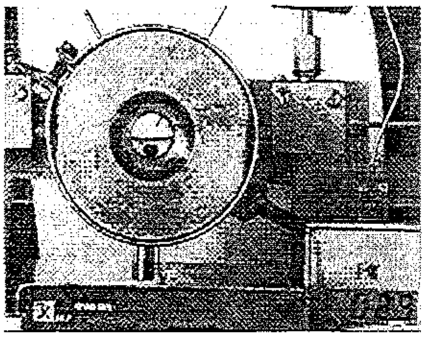

Figure 1: high pressure optical cell

Determination of solubility For determination of solubility of gases in liquid polymers an autoclave (volume 1 l) designed for a pressure of 500 bar and temperature of 423 K was used. The autoclave is shaken by an oscillating device to accelerate phase equilibrium. For experimental procedure a static-analytic method was used [11].

Results

PEG-Carbon dioxide Figure 2 shows the isotherms of the system PEG 4000-carbon dioxide. For all presented temperatures CO_2 is supercritical. With increasing temperature the solubility of CO_2 becomes smaller, thus the mixing gap becomes bigger. This phase behaviour is the same for all measured PEG-CO_2-Systems.

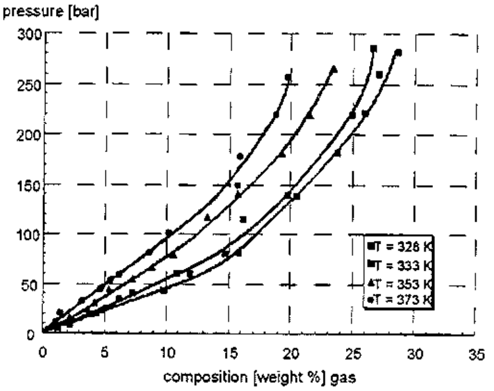

Figure 2: Solubility isotherms of CO_2 in PEG 4000

As can be taken from figure 3 pressure influences the melting point of PEG 4000. All melting points of the polymers under pressurised gas were measured by Z. Knez et.al. [12].

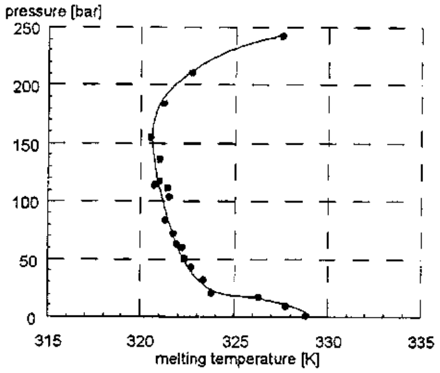

Figure 3: Melting curve of PEG 4000 in presence of CO_2

For all PEG samples the melting point increases as the pressure raises. After passing a maximal melting temperature the melting point decreases. At pressures over 220 bar it increases again. These phenomena could be explained with the competing effects of decreasing melting points of a solution and the increase of the melting point of a pure substance due to higher pressure. Nevertheless, it has to be admitted, that the sharp increase at pressures below approx. 10 bar (which was measured in independent apparatus by different authors) is not yet completely understood.

PEG-Nitrogen The solubility of N_2 in PEG is low and the maximum solubility is 0.7 weight%. The solubility measurements show an unusual trend: with increasing temperature at constant pressure the solubility of N_2 in PEG increases. At constant temperature with increasing pressure the solubility of N_2 increases for PEG samples of molar masses 1500 – 8000 g/mol.

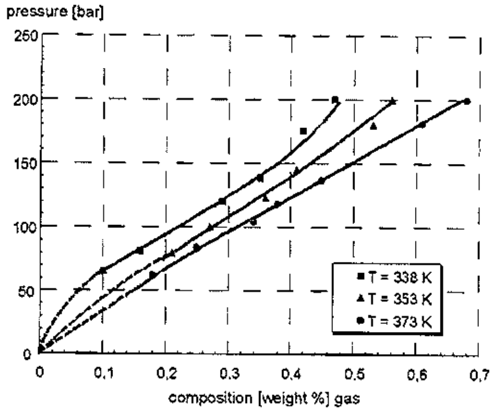

Figure 4: Solubility isotherms of N_2 in PEG 4000

The pressure influences the melting point of all measured PEG samples. The melting interval for all PEGs is relatively narrow - approx. 1°K. It seems that the melting point behaviour of the pure polymer in the p-T diagram is followed. In this pressure range the solubility of nitrogen in PEG is low and therefore liquefaction is dominated by the pressure effect.

PEG-Propane Figure 5 presents the solubility isotherms for the system PEG 4000 – propane. The maximal solubility of C_3H_8 in PEG is about 6 weight%.

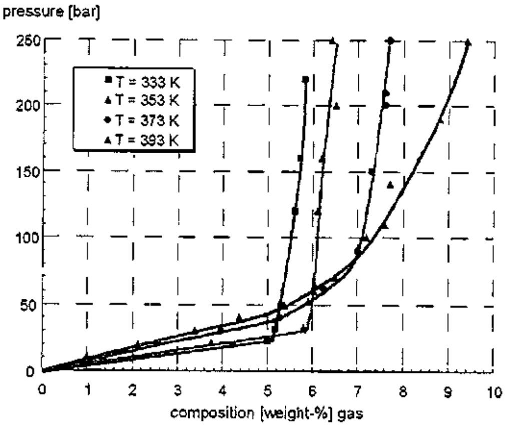

Figure 5: Solubility isotherms of C_3H_8 in PEG 4000

When temperature is below the critical temperature of propane, the isotherms show an increase at lower pressures. After a sharp bend the isotherms rises fast. At the point of the sharp bend three phases coexists: liquid PEG, liquid propane and gaseous propane. The 373 K- and 393 K-isotherm has a smooth course towards higher pressures. At these temperatures propane is supercritical. The isotherms crosses, thus the temperature-dependency of the solubility changes.

In Figure 6 the melting points in PEG – propane systems are presented. They depend on the state of aggregation of propane.

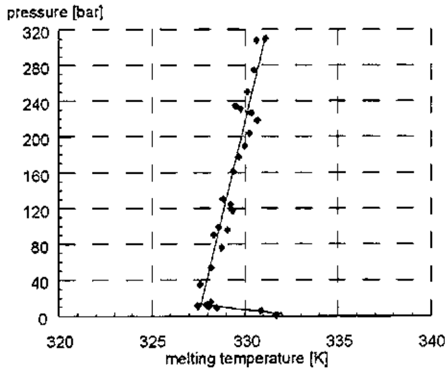

Figure 6: Melting curve of PEG 4000 in presence of C_3H_8

At lower pressures propane is gaseous and the melting point of PEG 4000 decreases. At the transition from gaseous propane to liquid propane there is a sharp bend in the melting curve and with increasing pressure the melting point increases.

Influence of functional group To show the influence of the methyl group at the end of the polymerchain the results are splitted in two parts. First Figure 7 presents solubility of carbon dioxide in the short chained polymers PEG 200 and PEGDME 200.

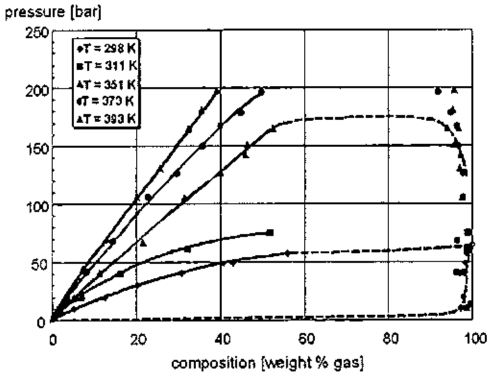

Figure 7: Solubility of CO_2 in short chained polymers

The system PEG 200/CO_2 shows a large miscibility gap with maximal 25 weight% CO_2 in the polymer. In the gas phase no PEG was measured. The system PEGDME 200 shows a totally different phase behaviour. The mutual solubility is much better and the miscibility gap closes at low temperatures and low pressures. The temperature-dependency is the same in both polymers: the miscibilty gap increases with increasing temperature.

The phase behaviour of the polymers with longer chains (PEG 1500 and PEGDME 2000) is almost the same. Both systems show large miscibility gaps. The solubility of carbon dioxide in PEG 1500 is lower than in PEGDME 2000. The influence of the temperature is the same in both systems.

The result demonstrate the strong influence of the functional group at the end of short chained polymers. PEG 200 and PEGDME 200 show different phase behaviour while those of the longer-chained species are almost identical. In this case the influence of the functional *chain-group* is predominant, while that of the functional *end-group* is negligible.

Classification of phase behaviour Scott and van Konynenbourg defined classes of phase behaviour [13-16]. To classify the systems of this work they have to be subdivided in systems with and without solid phases. Systems containing liquid and gaseous phases can easily be assigned to the classification. Figure 9 presents the p-T-projection of the phase behaviour of the system PEG 200/carbon dioxide.

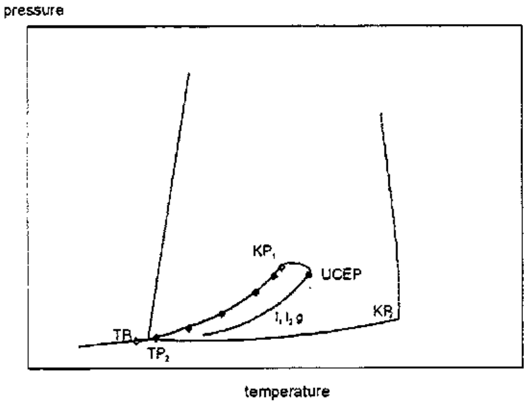

Figure 8: Class III of the system PEG 200/CO_2

The projection show the l-g-line of the pure component 1 (carbon dioxide) and component 2 (PEG 200) which ends in the critical points (KP_1 and KP_2). Because of the observation of three phases below the l-g-line of pure carbon dioxide the l_1-l_2-g-line, which ends in an UCEP (upper critical end point), exists. The l-g-line of pure PEG is at far higher temperatures. Scott and van Konynenbourg describe this type of phase behaviour as class III.

The same phase behaviour show for example CO_2/H_2O and Ethane/H_2O.

Systems with solid phases are splitted in two classes by McHugh [17, 18]. The system PEG 4000/CO_2 shows phase behaviour described as class A (Figure 10).

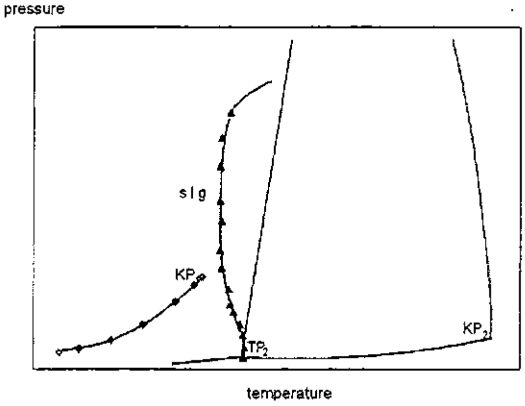

Figure 9: Class A of the system PEG 4000/CO_2

Beside the two l-g-lines of the pure components a s-l-g-threephaseline exists. It starts at the triple point of component 2 and has a temperature-maximum and –minimum. This kind of behaviour is described for the system n-Butanol/H_2O by McHugh.

Conclusion

The solid-liquid-gas-behaviour of binary systems containing pressurised carbon dioxide, nitrogen and propane as well as polyethyleneglycol and polyethyleneglycoldimethylether with different molar masses were studied. It was found that the phase behaviour depends on the kind of gas and its state of aggregation. The solubility of gas in the liquid polymer phase increases as follows: nitrogen ⇒ propane ⇒ carbon dioxide. The influence of a methylgroup at the beginning and the end of the polymerchain is strong for short chained polymers like PEG 200 and PEGDME 200 (open and closed miscibility gaps). For polymers with molecular weight higher than 1500 g/mol the influence of the functional group is nearly negligible.

Melting points of the polymers under pressure are also influenced by the gas and its state of aggregation. The amount of dissolved gas in the molten polymer determines the decrease of the melting point of the binary system in comparison to the pure polymer.

Projection of the 3-dimensional phase behaviour into p-T-plane allows classifications according to given classes in the literature by Scott, van Konynenbourg and McHugh.

Acknowledgments: The author wish to thank for the support by Deutsche Forschungsgemeinschaft, Deutsche Gesellschaft für Luft-und Raumfahrt (travel grants), Clariant and AGA (suppliers of polymers and gases) and by Prof. Knez and his group from the University in Maribor.

Literature

[1] Ali, S. Zeitschrift für Physikalische Chemie Neue Folge **1983**, 137, 13.
[2] Daneshvar, M.; Gulari, E. ACS Symp. Ser. (Supercrit. Fluid Sci. Technol.) **1989**, 406, 72.
[3] Daneshvar, M.; Kim, S.; Gulari, E. J. Phys. Chem. **1990**, 94, 2124.
[4] Kiran, E.; Saraf, V. P.; Sen, Y. L. Int. J. Thermophys. **1989**, 10(2), 437.
[5] Kumar, S. K.; Suter, U. W.; Reid, R. C. Fluid Phase Equilibria **1986**, 29, 373.
[6] McHugh, M. A.; Krukonis, V. J. Encycl. Polym. Sci. Eng.; Wiley Publisher: New York, **1989**; 16, 368.
[7] Tuminello, W. H.; Dee, G. T.; McHugh, M. A. Macromolecules **1995**, 28, 1506.
[8] Bonner, D. C. Polym. Eng. Sci. **1977**, 17(2), 65.
[9] Davis, R. A.; Menéndez, R. E.; Sandall, O. C. J. Chem. Eng. Data **1993**, 38,119.
[10] Garg, A.; Gulari, E.; Manke, C. W. Macromolecules **1994**, 27, 5643.
[11] Wiesmet, V.:Phasenverhalten binärer Systeme aus Polyethylenglykolen, Polyethylenglykoldimethylether und verdichteten Gasen, Diss, Erlangen, **1998**
[12] Knez, Z.; Kokot, K. Faculty of Chemistry and Chemical Engineering University of Maribor, Slowenia
[13] Scott, R. L.; van Konynenburg, P. H.; Van der Waals and Related Models for Hydrocarbon Mixtures; Discus. Faraday Soc., 40, **1970**, p. 87 – 97
[15] Scott, R. L.; The Thermodynamics of Critical Phenomena in Fluid Mixtures; Ber. Bunsenges. Phys. Chem., 76, **1972**, p. 296 – 308
[16] van Konynenburg, P. H.; Scott, R. L.; Critical Lines and Phase Equilibria in Binary van der Waals Mixtures; Philosophical Transactions of the Royal Society of London, 298, **1980**, p. 495 – 540
[17] McHugh, M. A.; Seckner, A. J.; Yogan, T. J.; High Pressure Phase Behavior of Binary Mixtures of Octacosane and Carbon Dioxide; Ind. Eng. Chem. Fundam., 23, **1984**, p. 493 – 499
[18] McHugh, M. A.; Krukonis, V. J.; Supercritical Fluid Extraction: Principles and Practice; Butterworths, Boston, **1986**, S. 23 - 49

MAXIMATOR®

Hohe Drücke– Kleine Mengen

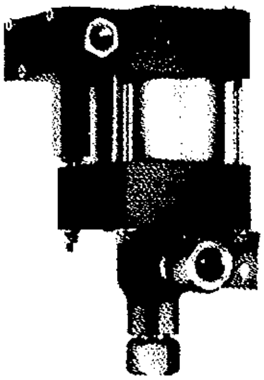

Pumpen 10–5500 bar

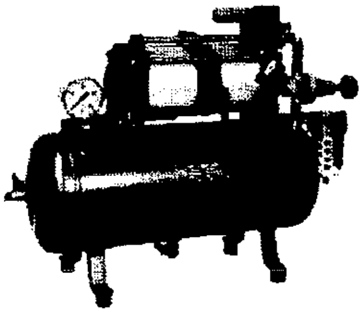

Kompressoren bis 40 bar

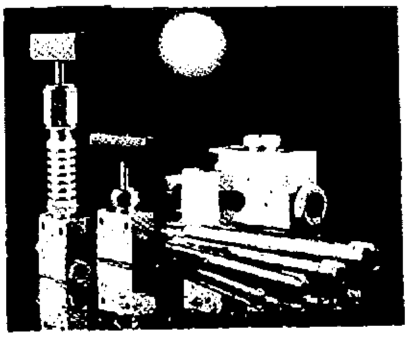

700–15000 bar

Komponenten für

- Prüfstände
  Automobil-, Anlagenbau
- Spannhydraulik
  Werkzeuge
- Hydraulikwerkzeuge
  Power Pack
- Überlastsicherung
- Druckerhöher
- Chemie / Kunststoff
  Maschinen / Anlagen
- Gummiindustrie
  Ausdorn und Prüfanlagen
- Offshore
  Test und Injektion

Schmidt, Kranz & Co. GmbH · Postfach 110348
42531 Velbert · Tel. (02052) 888-0 · Fax (02052) 888-44

Natural Food Processing

Extraction of Carotenoid–Rich Oils by Supercritical CO_2 and Subcritical Propane

H.G. Daood[a]*, **P.A. Biacs**[a], **V. Illés**[b] **and M.H. Gnayfeed**[a]
[a]* Central Food Research Institute, Herman Otto u. 15. 1022 Budapest, Fax: 361-3558928
[b] Dept. Chem. Engin. University of Veszprém, Veszprém, Hungary

The influence of supercritical and subcritical fluid extraction (SFE) conditions on the carotenoid content of oils from spice red pepper (paprika) and peels of citrus fruits. The carotenoids in the extracts and powders were analyzed by high-performance liquid chromatography. The different classes of carotenoids showed great differences in their solubility in SF-CO_2. Subcritical propane was found superior over SF-CO_2 in the extraction of carotenoids from different sources.

Introduction

Due to their bioantioxidant activity carotenoids have great biological and technological importance. Some studies have associated decreased risk of cancer and cardiovascular diseases with the increased or sufficient daily intake of carotenoids and other bioantioxidant such as tocopherols and vitamin C [1]. From the nutritional and technological points of view it became of interest to prepare oily concentrates that can easily be applied in food, pharmaceutical and cosmetic industries as a sources of vital carotenoids.

The widely used procedure for such a goal was organic solvent extraction that has limitations concerning safety and chemical alteration of carotenoids. Recently supercritical fluid extraction (SFE) has become superior over other techniques because of being non-toxic, non-corrosive, with no solvent residue and cost-effective [2-4]. Carbon dioxide (SF-CO_2) is widely used alone or with modifier in a fractional or sequential extraction [5].

In the present work behavior of different carotenoid classes during SF-CO_2 and subcritical propane was studied using two of the most important sources of food carotenoids, spice red pepper (paprika) and peels of citrus fruits.

Materials and Methods

CO_2 was technical grade and from Répcelak (Hungary). Highly pure propane (99%) were from MAFKI Institute (Veszprém, Hungary). Other organic solvents used for analysis were analytical or HPLC grade and purchased from Reanal (Hungary). Standard tocopherols and carotenoids were from Sigma (St.Lo. USA).

Ground paprika of about 200-300 µm particles was obtained from the spice paprika developing Rt. (Kalocsa, Hungary) while orange and mandarin fruits were obtained from the local markets in Budapest. The peels of citrus fruits were removed by hand, dried for 24hr at 50°C and milled by a coffee mill to pass a 20 mesh sieve.

The sub- and supercritical extractions were performed with high pressure, flow-up stream extraction apparatus described previously [6]. The pressure as adjusted between 50 and 400 bar by a back-pressure regulator. The solvents were compressed through the extractor with a flow rate of 1.0-1.5 $lmin^{-1}$. The solute-rich fluid departing from the extractor was expanded through a heated needle value to atmospheric pressure. The volume of solvent used in each experiment was normalized by the Peng-Robinson equation [7]. The density of SF-CO_2 and propane was determined by applying the equation of Bender [8]. The temperature of extraction was between 25°C and 55°C.

Organic solvent extraction (control) was carried out using 50 ml of mixture of 2:1:1 dichloroethane-acetone-methanol to recover lipid fraction from 0.5 gram of the ground sample. After shaking for 15 min the mixture was filtrate and the solvent removed under vacuum by rotary evaporator.

The carotenoids were separated and determined by high-performance liquid chromatographic (HPLC) method [9].

Results and Discussion

Fig.1 shows the results obtained from extraction trials on the ground paprika at 35°C and pressure between 200 and 300 bar using SF-CO_2. The amount of oil recovered from 100 g powder was plotted against the ratio of solvent to solid (solvent using up).

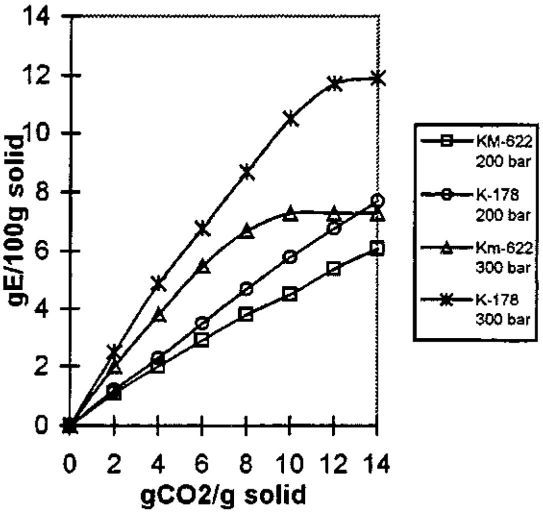

Figure 1: Extraction of ground paprika by SF-CO_2 at 35°C and two different pressures.

After an initial increase, extraction curves reached a plateau and approached the maximum. Solubility of oil in SF-CO_2 was increased with the increase of pressure towards 400 bar. The same held true at both 35°C and 55°C with the exception that the ratio of solvent to solid required for the complete extraction at 35°C is higher than at 55°C particularly at 200 bar. For implementation of complete extraction at 35°C and 55°C the ratio of solvent/solid was 10 and 7.5 respectively when the pressure was fixed at 400 bar.

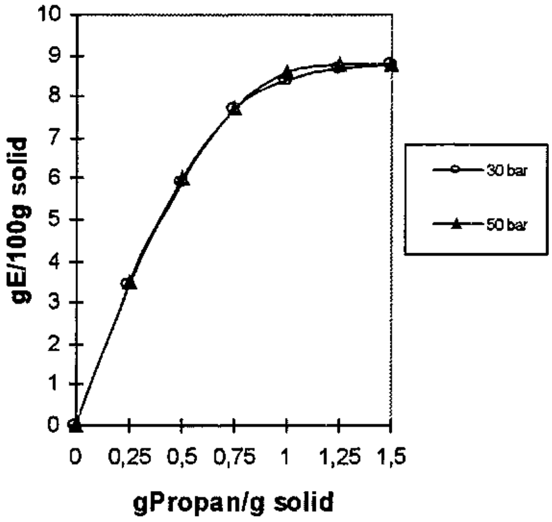

Figure 2: Extraction of ground paprika by subcritical propane at 25°C.

Under the given conditions the highest amount of oil obtained from 100 g of ground paprika (K-178 CV) was 11.4 g. This value is well above the 7.5 g recovered from 100 gram of powder from Km-622 cultivar under the same conditions (data not shown). As a function of increasing pressure the oil solubility in SF-CO_2 was increased.

In case of subcritical extraction with propane there was an initial steep increase in the solubility of the oil in the solvent followed by a plateau and the extraction curves reach the maximum (Fig.2). To achieve complete extraction of oil only 30-50 bar with a ratio of solvent/solid of 0.8 is required. These data revealed that subcritical propane has greater capability to solubilise paprika oil than SF-CO_2. The aforementioned advantages of propane make its highly applicable and cost-effective in the extraction of paprika oleoresin.

As shown in Fig. 3 and 4. The change in solubility of oil from citrus peels in SF-CO_2 and propane as a function of solvent/solid ratio was similar to that observed with the oil from spice paprika except that the ratio needed for complete extraction was well lower with the oil of citrus fruit peels. This indicates that the peels contain easy to solubilise oil in supercritical fluids. However, after extraction the powder, samples were not entirely decolorized even with propane that has solvating powder greater than SF-CO_2. It is believed that non-volatile lipids are strongly associated to structural constituents of the peel tissues and need higher pressure to be recovered from the powder.

Carotenoids extract of plant materials is diverse. This diversity is due to the occurrence of a wide variety of compounds in different forms varying in their chemical properties including solubility in supercritical fluids. The esterification of OH-containing carotenoids (xanthophylls) with fatty acids in a form of mono- or diesters alters their solubility properties and their association with the structural macromolecules. Extraction of each carotenoid from plant tissues depends on how easily or difficulty the solvent breaks their association with the tissues and solubilise them. Table 1 shows the data obtained from the extraction experiments of spice paprika oil and behavior of different carotenoid classes. It was evident that SF-CO_2 has low capability to solubilise the less polar diesters of the major

Table I. Effect of Type and Conditions of Supercritical Extraction on the Yield and Quality of Spice Paprika Oil

Type and fractions	Extraction parameters			Yield g/100g powder	Concentration of carotenoids µg/g			
	Pressure bar	T, °C	Extraction degree %		Capsanthin ME	β-carotene	Capsorubin DE	Capsanthin DE
Control*	1	25	100	9.0	319.3	436.5	100.7	670.4
$SF\text{-}CO_2$	100	35	14	1.1	0.69	7.1	0.1	0.5
Cumulative	200	35	100	7.3	13.5	231.7	3.1	22.4
	300	35	82	5.9	18.3	282.6	5.2	21.9
	400	35	100	7.4	30.5	313.9	8.6	33.9
	200	55	62	5.8	12.2	149.1	1.5	4.0
	300	55	93	6.4	29.8	364.1	6.5	25.5
	400	55	100	6.8	15.5	236.0	6.6	29.9
Fractional	200	35	37	2.6	3.0	93.4	3.5	11.1
	200	35	71	2.4	3.3	74.7	0.8	3.4
	200	35	93	1.5	3.6	95.2	0.9	2.1
Propane	30	25	100	8.9	187.2	374.9	88.5	526.3
	50	25	100	8.6	177.1	395.1	94.6	497.6
	80	25	100	8.5	144.9	295.5	69.8	374.6

* Control oil was prepared by organic solvent extraction using 2:1:1 dichloroethane–acetone–methanol.

Table II. Distribution of Carotenoids Between Recovered Oil and Residues as Well as Their Loss During Extraction at Different Conditions

Pigments	$SF\text{-}CO_2$ at 35°C			Supercritical propane
	100 bar (14%)*	200 bar (100%)*	300 bar (93%)*	30 bar (100%)*
Capsanthin ME				
in oil (µg)	0.69	13.46	18.28	187.15
in residues (µg)	220.92	33.60	121.92	91.84
total (µg)	221.61	47.06	140.20	278.99
found (%)	69.41	14.74	43.91	87.38
lost (%)	30.59	85.26	56.09	12.62
β-carotene				
in oil (µg)	7.03	231.73	282.57	374.86
in residues (µg)	353.21	47.36	48.00	18.56
total (µg)	360.24	279.09	330.57	393.42
found (%)	82.54	63.94	75.74	90.14
lost (%)	17.46	36.06	24.26	9.86
Capsorubin DE				
in oil (µg)	0.14	3.07	5.16	88.52
in residues (µg)	39.18	8.42	20.80	13.38
total (µg)	39.32	11.49	25.96	101.90
found (%)	39.04	11.41	25.77	101.16
lost (%)	60.96	88.59	74.23	-
Capsanthin DE				
in oil (µg)	0.50	22.37	21.99	526.32
in residues (µg)	360.18	123.20	114.56	Traces
total (µg)	360.68	145.57	136.55	526.32
found (%)	53.80	21.72	20.37	78.51
lost (%)	46.20	78.28	79.63	21.49

Quantities of carotenoids are in µg recovered from 1 g ground paprika.
*= between brackets the values of extraction degree under the used conditions.

red carotenoids (capsanthin and capsorubin). The solubility of most carotenoid could be improved by increasing the pressure to 400 bar. This improvement was clear on β-carotene and the polar pigments, but of slight influence on the less polar diesters. The low recovery of diesters is regarded as remarkable disadvantage because diester of red xanthophylls are the most important component of red pigment of paprika oleoresin.

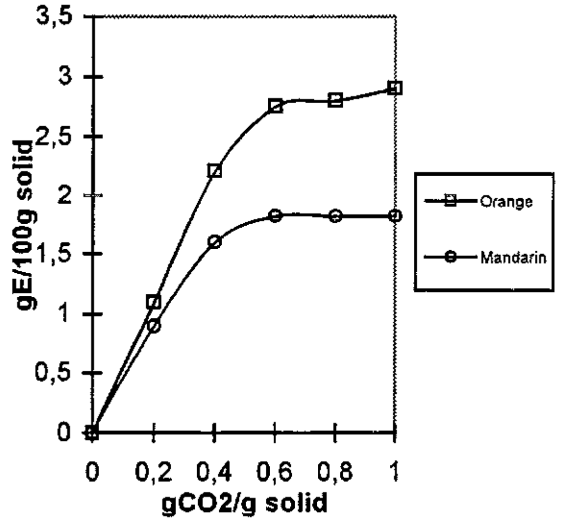

Figure 3: Extraction of citrus fruit peels by SF-CO_2 at 35°C and 250 bar.

To produce paprika oleoresin devoid of the aforementioned limitation use of less polar solvent such as propane even under subcritical conditions (25°C and 30-80 bar) was indispensable. Application of subcritical propane resulted in more than 90% recovery of all the carotenoid individual except unesterified xanthophylls.

To search after the reason of the low recovery of diesters by SF-CO_2 extraction, the residual carotenoids were determined in the powders. From the sum of residual and in-oil solubilised carotenoid the loss percentage could be calculated (Table 2). It could be concluded that there is a marked in-device loss of carotenoids during SFE by CO_2. Such a loss was not found when subcritical propane was used. These results were repeatedly confirmed when mandarin or orange peel were extracted to produce carotenoid rich preparation.

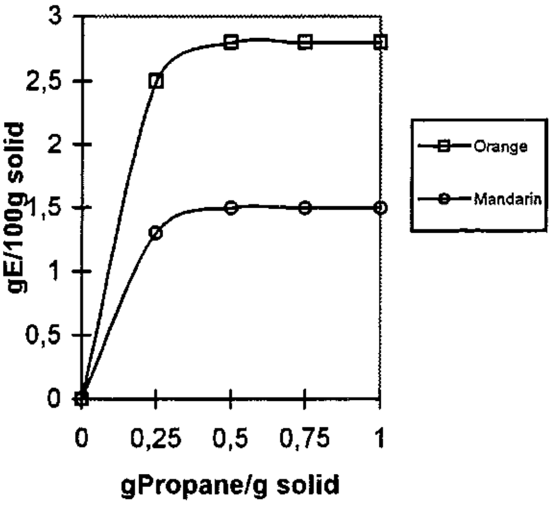

Figure 4: Extraction of citrus peels by propane at subcritical conditions (25°C and 50 bar).

Acknowledgement

This work was financially supported by the Hungarian National Science Fund (OTKA) under grant number, TO23970 and T25814

References

1. Sies, H. "Oxidativ Stress: Oxidant and Antioxidant," Academic Press, London, 1991.
2. Stahl E.; Quirin, K.W.; Gerard, P. "Verdichtete gaze zur extraction und raffination, springer," Heidelberg, 1987.
3. Stahl, E.; Schutz, E.; Mangold, H.K. *J. Agric. Food Chem.* **1980**, 28, 1153.
4. Rizvi, S.S.H. "Supercritical fluid processing of foods and biomaterials," Blackie Academic Professional, London, 1994.
5. Sargenti, S.R.; Lancas, F.M. *J. Chromatogr. Sci.* **1998**, 36, 169.
6. Illés, V.; Szalai, O.; Then, M.; Daood, H.G.; Perneczki, S. *J. Supercritical Fluids* **1997**, 10, 209.
7. Peng, D.Y.; Robinson, D.B. *Ind. Engin. Chem. Fundam.* **1976**, 15, 59.
8. Bender, E. "Proceedings of the 5th symposium on thermophysical propertiers," Amer. Soc. Mech. Engin., New York, 1970. 227.
9. Biacs, P.; Daood, H.G. *J. Plant. Physiol.* **1994**, 143, 520.

Extraction of Natural Products with Superheated Water

Anthony A Clifford*, Annamaria Basile, Maria M. Jiménez-Carmona and Salim H.R. Al-Saidi
School of Chemistry, University of Leeds, Leeds LS2 9JT, UK

Superheated water under pressure at 150°C has been used to extract oxygenated compounds from plant materials. Rosemary (*Rosmarinus officinalis*), clove buds (*Syzygium aromaticum*) and lemon oil have been studied. During this process, monoterpenes are extracted slowly and only very small amounts of the sesquiterpenes, waxes and lipids are removed. Some comparisons are made with steam distillation and supercritical fluid extraction. The experiments conducted on a laboratory scale indicate that extraction by superheated water could be a viable process for the production of high quality plant extracts.

Introduction

In a search for alternatives to organic solvents for extraction and other processes, a number of workers have used liquid water under pressure above 100°C, but below its critical temperature of 374°C. Under these conditions it is referred to as superheated water or subcritical water. Organic compounds are much more soluble in water under these conditions than at room temperature firstly, because usually solubilities rise with temperature, and secondly, because water becomes less polar at higher temperatures as its structure breaks up and its relative electric permittivity (dielectric constant) falls [1]. A number of studies of solubilities in superheated water have been carried out, although no solubility data on compounds from natural products could be found. For example, one of these showed that biphenyl forms a 10 mass % solution in water at 300°C [2]. It was later shown [3] that the heavier solutes, benz[*e*]pyrene and nonadecylbenzene reach the same concentration at 350°C. More recent work has been carried out on polyaromatic compounds and pesticides, between 25°C and 200°C, which have been used to develop a simple, approximate, empirical equation for low solubilities [4].

Both subcritical water [5] and supercritical water [6] have been used for the oxidative destruction of organic compounds with molecular oxygen. More recently, superheated water has been used to extract pollutants with a wide range of polarities from environmental samples [7-10]. The elution of organic compounds from sorbents of varying polarity has also been studied [11] as has the partitioning of organic compounds from gasoline and diesel fuel [12]. Another recent application of superheated water is to achieve reversed-phase chromatographic separations by using pure water or water mixed with organic solvents at elevated temperatures [13,14]. Extraction of used automotive tyres with both supercritical and subcritical water has been studied and these experiments also involved breakdown of natural rubber [15]. Other processes studied involving natural products have been the hydrolysis of vegetable oils [16] and starch [17]. A small study on the extraction of rosemary by water at 125°C [18] showed that the oxygenated compounds were preferentially extracted.

Materials and Methods

Rosemary leaves were collected from plants growing in England in the period between October and December. This is not the best period to carry out studies on rosemary leaves, because the oil content is at the lowest level and so the studies are comparative only. Dried clove buds were purchased locally and were the produce of Madagascar. These were thoroughly mixed to produce as consistent samples as possible. Lemon oil was obtained from a Sicilian industrial source.

All standard compounds and the internal standards for chromatography, NaCl and Na_2SO_4 were provided by Aldrich (Gillingham, Dorset, UK), except for isobornyl acetate that was supplied by Lancaster (Morecambe, Lancashire, UK) and eugenyl acetate that was prepared from eugenol and acetic anhydride in the presence of acetic acid and dimethylaniline by the Fiore acetylation method. Carbon dioxide was 99.99% pure and supplied by BOC Ltd (London, UK). Dichloromethane, hexane and ethanol were HPLC solvents supplied by the Aldrich Chemical Company.

All extractions with superheated water were performed using the stainless steel apparatus shown schematically in Fig. 1, which is similar to one described earlier [8]. Distilled water was first purged for two hours with nitrogen to remove dissolved oxygen. The water was then delivered at a constant flow-rate by Pump 1, which was a L6000A pump (Merck-Hitachi, UK), through a needle valve to a stainless steel pre-equilibrating coil (1 m x 0.76 mm I.D. x 1.6 mm O.D.) and, finally, to a 10.4 mL extraction cell (Keystone Scientific, Bellefonte, PA). Both the coil and the cell were placed in a gas chromatographic oven (Carlo Erba Fractovap) and kept at constant temperature. The extraction cell was mounted vertically inside the oven with the water flowing from top to bottom. The outlet of the extraction cell was connected by stainless steel tubing to an outlet needle valve mounted just outside the oven wall, which was used as an on-off valve during an extraction and to control the flow during the filling of the cell. A 11 cm-long, 100 mm I.D., stainless steel restrictor (Coopers Needle Works, Birmingham, UK) was required to maintain pressure in the system, so that water remained liquid at all temperatures used. The outlet was inserted in a collection vial. Since hot water may cause losses of volatiles, a cooling loop (cooled with room temperature water), made from a 40-cm length of stainless steel tubing, was connected between the outlet needle valve and the restrictor. A second pump, Pump 2, which was also a L6000A pump, was connected to the cooling coil via a shut-off valve. This was used to flush through any organic compounds which were precipitated in the cooling coil as the temperature of the water cooled.

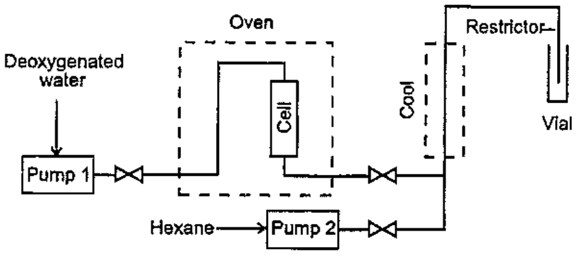

Figure 1. Experimental system for superheated water extraction

For extraction of solid material, the cell was filled with a weighed amount and a glasswool plug inserted at the outlet end to prevent the frit being plugged. After assembling the extraction cell in the oven, the cell was pressurized with ~20 bar of water by opening the inlet needle valve from the pump. The valve was then closed, the oven was brought up to the desired temperature as quickly as possible and let equilibrate for 20 minutes. The inlet and outlet valves were then opened, water pumped through the cell at a given flow rate and the extracts collected in the vial. For kinetic experiments the vial was replaced at given time intervals. In the case of lemon oil extraction, a 50 mL cell packed with stainless steel turnings was used and lemon oil pumped by a L6000A pump into the bottom the cell and flowed up over the packing to collect at the top of the cell after extraction. Following the extraction, 3 mL of hexane was pumped through the cooling coil to sweep any precipitated compounds from the cooling coil. A further 15 mL of hexane were added to each of the extracts in a separating funnel and about 1 g of NaCl was added to facilitate the breaking of the emulsion. The hexane layer was then separated, dried with ~3 g of anhydrous sodium sulfate and an appropriate amount of internal standard, *n*-nonane for rosemary and lemon oil extraction or vanillin for clove extraction, added before gas chromatographic analysis.

Supercritical fluid extraction (SFE) was carried out using a commercial system (ISCO SFX-210, ISCO, Lincoln, NE, USA). The extraction cell volume was 10 mL and the restrictor had an internal diameter of 75 μm and a length of around 40 cm, adjusted to give the required pressure in the cell. A long wide restrictor was used to avoid blocking, given the large amount of extract from clove. The extract was trapped in 10 mL of dichloromethane in a collection vial, ready for analysis. Kinetic experiments were carried out by changing the collection vial at timed intervals.

Soxhlet extraction was carried out in standard apparatus by standard methods for 24 hours. Steam distillation was performed in a simple laboratory quickfit apparatus. The receiving vessel contained 10 mL of hexane and cooled with room temperature water and during the distillation, the volume of hexane was kept approximately constant by adding more solvent. At the end of the process, the condenser was washed out with 5 mL of hexane in order to recover any extracted compounds deposited in it.

The analyses of the extracts were performed using standard gas chromatographic methods. For compound quantitation, calibrations were established graphically, by injecting solutions made of known amounts of internal standard and pure compound.

Extraction of Rosemary

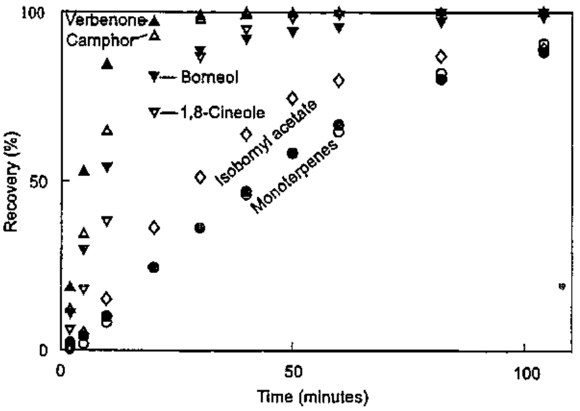

Figure 2. Extraction of rosemary leaves with superheated water at 150°C

A full description of the experiments on rosemary is given elsewhere [19]. Fig. 2 shows recovery curves for extraction from 4 g samples of rosemary at 150°C with a flow rate of 2 mL per minute. They are plotted as the percentage of a final mass recovered at a given time. The final mass is obtained using an extrapolation formula [20]. The monoterpenes extract slowly, with α-pinene shown as the open circles and camphene and limonene, whose extraction curves are indistinguishable on this figure, shown as filled circles. The ester isobornyl acetate (open diamonds) is extracted somewhat more rapidly than the monoterpenes. A more rapidly extracted group is formed by the cyclic ether 1,8-cineole (open inverted triangles) and the alcohol borneol (closed inverted triangles). The ketones are removed most rapidly. Of the latter, verbenone (closed triangles), which has a double carbon-carbon bond conjugated with the ketone bond, extracts more rapidly than camphor (open triangles). Very small and unquantifiable amounts of heavier hydrocarbons were extracted.

Table 1. Comparison of yields rosemary using steam distillation and water extraction at 150°C in mg per 1 g, with standard deviations in parentheses

	Steam Distn.	Water Extrn.
α-pinene	0.080(0.019)	0.163(0.056)
camphene	0.019(0.005)	0.039(0.011)
limonene	0.007(0.001)	0.025(0.011)
1,8-cineole	0.082(0.022)	0.161(0.010)
camphor	0.033(0.008)	0.060(0.002)
borneol	0.010(0.002)	0.017(0.003)
verbenone	0.016(0.003)	0.025(0.002)
isobornyl acetate	Undetected	0.004(0.001)

A comparison was made of extraction at 150°C and steam distillation both for a period of 60 minutes. A single sample was mixed thoroughly and used for both experiments. The flow rate for extraction was 2 mL per minute and the amount of water passed in the steam distillation was approximately the same. Both the extractions and steam distillations were carried in triplicate and the results are reported in Table 1. The extract obtained by superheated water extraction gives higher yields, especially of the oxygenated compounds. The yields are low by commercial standards and reflects the fact that the rosemary was not grown in an ideal climate and not collected at an ideal time of year.

Extraction of Clove Buds

Superheated water extractions were carried out on 4 g samples of clove buds at 150°C with a flow rate of 2 mL per minute. Percentage recovery curves versus time are shown in Fig. 3 for the three main compounds obtained. Surprisingly, it was found that caryophyllene extracted extremely rapidly, in spite of the fact that it is a non-polar compound. However, only a small proportion of the available caryophyllene is extracted, as is described below.

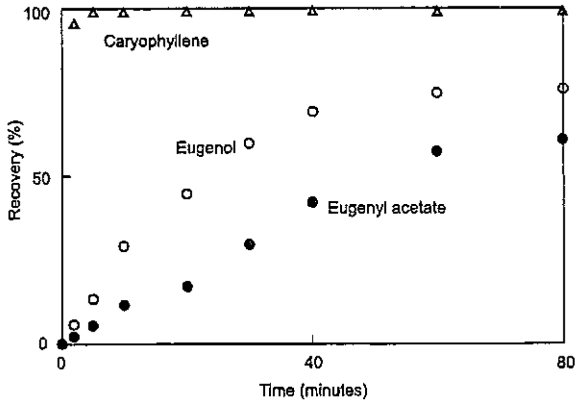

Figure 3. Extraction of clove buds with superheated water at 150°C

Table 2 shows the yield obtained by exhaustive extraction by four methods. Steam distillation was carried out on a 10 g sample for 4 hours using ~200 mL of water. Soxhlet extraction was also carried out on 10 g with dichloromethane 24 hours. Superheated water extraction (SWE) was carried out on 4 g at a flow rate of 2 mL at 150°C for 100 minutes. Supercritical fluid extraction (SFE) was carried out on 6 g with 1 mL per minute of CO_2 at 55°C and 200 bar for 330 minutes. Standard deviations are not shown, but the experiments were carried out in triplicate and had a precision of about 5%, which was ascribed to variations in the clove samples. As can be seen the final yields are mostly within the experimental precision, but it can be seen that the yield of caryophyllene is less with the methods that use water.

Table 2. Comparison of the yields in mass percent of the three main compounds obtained from the same sample of clove buds by different methods.

	Eugenol	Eugenol acetate	Caryo-phyllene	Total
Steam distn.	14.74	3.28	0.13	18.17
Soxhlet	13.35	2.65	1.38	17.38
SWE	15.30	2.94	0.18	18.34
SFE	16.42	3.39	1.73	21.54

Extraction of Lemon oil

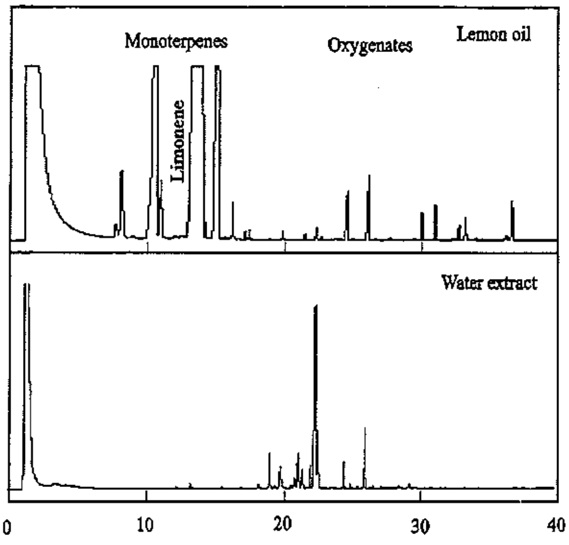

Figure 4. Chromatograms from the extraction of lemon oil with superheated water at 150°C

Because superheated water extracts oxygenated compounds more readily than monoterpenes, it can provide a method of deterpenating essential oils. Lemon oil was extracted with water at 150°C with a water flow rate of 2 mL per minute and an oil flow rate of 0.1 mL per minute. Fig. 4 shows the gas chromatograms obtained for the original oil and the water extract. As can be seen, the water extract contains the oxygenated compounds, but little of the monoterpenes, although they form some 95% of the original oil. Compounds of higher molar mass are also not extracted. Work in this area is continuing.

Conclusions

This study suggests that extraction by superheated water may be an effective way of obtaining aroma compounds from plant materials, whilst leaving behind the monoterpenes, higher hydrocarbons and lipids. It also suggests that it may be a useful solvent for deterpenating essential oils. In particular cases, however, thermal sensitivity of the products and separation of the products from water may be a problem, although with the high-yielding clove buds, the extracted oil spontaneously separated at low temperature.

Comparison with steam distillation for rosemary indicates that yields are a little higher and the extract contains a higher proportion of oxygenated flavour and fragrance compounds, i.e. is of higher quality. A process may be competitive with steam distillation, with lower energy costs, as it is not necessary to evaporate the water and heat can be more efficiently recycled.

Advantages over supercritical fluid extraction are it is not necessary to partially dry the plant material, plant waxes are not extracted and capital costs would be lower, as the pressures involved (5 bar at 150°C) are less.

Acknowledgments

The authors are grateful for financial support from the BBSRC (UK) and Sultan Qaboos University (Oman).

References

1. Haar, L.; Gallagher, J.S.; Kell, G.S. "NBS/NRC Steam Tables," p. 266, Hemisphere, Washington, DC, 1984.
2. von Bröllos, K.; Peter, K.; Schneider, G. M. *Ber. Buns. phys. Chem.* **1970**, 74, 682-686.
3. Sanders, N. D. *Ind. Eng. Chem. Fundam.* **1984**, 25, 169-171.
4. Miller, D.J.; Hawthorne, S.B.; Gizir, A.M.; Clifford, A.A.. *J. Chem. Eng. Data* **1998**, 43, 1043-1047.
5. Zimmermann, F.J. *US Patent* 2,665,249, 1954.
6. Modell, M. *US Patent* 4,338,199, 1982.
7. Hawthorne, S. B.; Yang, Y.; Miller, D. J. *Anal. Chem.* **1994**, 6, 2912-2920.
8. Yang, Y.; Bøwadt, S.; Hawthorne, S. B.; Miller, D. J. *Anal. Chem.* **1995**, 67, 4571-4576.
9. Yang, Y.; Hawthorne, S. B.; Miller, D. J. *Environ. Sci. Technol.* **1997**, 31, 430-437.
10. Hartonen, K.; Inkala, K; Kangas, M.; Riekkola, M.-L. *J. Chromatogr. A* **1997**, 785, 219-226.
11. Yang, Y.; Belgazi, M.; Lagadec, A.; Miller, D.J. Hawthorne, S.B. *J. Chromatogr.* **1998**, 810, 149-159.
12. Yang, Y.; Hawthorne, S. B.; Miller, D.J. *J. Chem. Eng. Data* **1997** 42, 908-913.
13. Smith, R. M.; Burgess, R. J. *J. Chromatogr. A* **1997**, 785, 49-55.
14. Miller, D. J.; Hawthorne, S. B. *Anal. Chem.* **1997**, 69, 623-627.
15. Funazukuri, T.; Takanashi, T.; Wakao, N. *J. Chem. Eng. Japan* **1987**, 20, 23-27.
16. Holliday, R.L.; King, J.W.; List, G.R. *Ind. Eng. Chem. Res.* **1997**, 36, 932-935.
17. Brunner, G. *Proc. 5th Mtg. On Supercritical Fluids*, Nice, March 1998, 413-424.
18. Miller, D. J.; Hawthorne, S. B. **1997**, private communication.
19. Bartle, K.D.; Clifford, A.A.; Hawthorne, S.B.; Langenfeld, J.L.; Miller, D.J.; Robinson, R. *J. Supercrit. Fluids* **1990**, 3, 143-149.
20. Basile, A.; Jiménez-Carmona, M.M.; Clifford, A.A. *J. Agric. Food Chem.* **46**, 5205-5209.

Processing carotenoid-containing liquids with supercritical CO_2

R. Eggers* [a], A. Pietsch [a], C.A. Lockemann [b], F. Runge [b]
[a] *Technical University Hamburg-Harburg,* Process Engineering II / Heat- and Mass Transfer,
Eissendorferstr. 38, D 21073 Hamburg, [b] *BASF AG, D 67056 Ludwigshafen,*
r.eggers@tu-harburg.de *fax ++49 (0)40 42878 2859*

The deoiling of different carotenoid-containing liquids has been investigated with a high-pressure spray process using CO_2 in the range of 25-40 MPa and 40-80°C. The carotenoid content in palm oil, model systems and in a lycopene oleoresin was enriched significantly. High-pressure phase equilibria of ternary systems with high carotenoid concentrations have been investigated. The different isomeric forms of the carotenoids behave differently and influence the separation process. Together with high-pressure viscosity and surface tension measurements, the equilibria form a sound basis of the ternary system properties to be discussed in the context of spray-extractions.

Introduction

Carotenoids are widely used in nutritional and pharmaceutical products due to their coloring, antioxidant and other properties. At present the supercritical extraction of natural carotenoids receives increasing attention because of the value of carotenoids and a potential market for natural qualities in combination with a non-toxic technology.
Generally, investigations concentrate on the extraction of solid carotenoid sources like carrots and tomatoes with supercritical CO_2. Examples are listed in Tab. 1. Several researchers have studied the solubility of β-carotene, the most widely known and sold carotenoid, in pressurized CO_2 [1,2,3]. Low carotenoid solubilities and limited concentrations in the feed materials are drawbacks of these high-pressure processes.
Liquid starting materials like vegetable oils or oleoresins can contain carotenoids in higher concentrations. Since the solubilities of vegetable oils are much higher than the reported binary solubilities of β-carotene, a supercritical deoiling process is suggested. If the CO_2 extracts mainly the vegetable oils and related components from the carotenoid-containing liquid, raffinates rich in carotenoids should be obtained. The process is determined both by kinetic effects and the distribution coefficients of carotenoids between the two phases. Except for values with palm oil and synthetic β-carotene in one publication [4] the distribution coefficients are not known so far. In a process aiming at the production of enriched concentrates, counter current packed columns cannot be used while adhesive and viscous or even solid raffinates form. Therefore a cocurrent high-pressure spray-extraction process is suggested [5]. The presented study gives experimental separation results and a basis of the ternary system properties.

Table 1 : Examples of research CO_2 - extractions

Carotenoid	Source	p MPa	T °C	Concentration Feed /Prod. wt%	Carotenoid Yield % C.in Feed	Lit.
β-Carotene	Sweet Potatoes	41	38	0.02 / ?	68	[6]
α,β-Carotene	Carrots	50	40	0.03 / 2.09	88	[7]
Lycopene	Tomato Skins	70	60	0.05 / 0.47	83	[8]
Lutein	Marigold Petals	70	60	1.47 / 8.14	63	[9]
β-Carotene	Palm Oil	24	50	0.05 / 0.07	69	[10]

Materials and Analytic Methods

Most investigations were conducted with dispersions of synthetic β-carotene in corn oil (Lucarotin® 30 M, BASF Health & Nutrition, Denmark). Dilutions were made with addition of commercially available corn oil (Mazola, CPC Germany). The β-carotene in the original dispersion is mainly isomeric all-E (~95%). Some of the dispersion was isomerized with a thermal treatment resulting in an isomer composition of approximately 55% (all-E), 22% (9Z) and 15% (13Z). Natural carotenoid sources used were Lycomato® with 6% lycopene (Lycored, Israel), Caromin® with 20% and 30% β-carotene (Carotec, Malaysia) and FloraGLO® with 20% Lutein (Kemin Foods, USA). Some Lycomato was diluted with refined soy oil (Hobum, Germany) to lower the lycopene concentrations.
The content of β-carotene and lycopene was analyzed photometrically (Shimadzu 240) and the distribution of isomers with HPLC (Waters 590, Rh7725i, YMC-C30, TSP UV-vis 150). The phosphorus was solubilized (HNO_3, microwave), quantified (PE-Plasma 2000GES with ICP) and converted to an approximated content of phospholipids with the usual multiplication factor of 30.

Experimental Methods

The high-pressure equipment used in the main experiments is shown in Fig. 1 and Fig. 2. The phase equilibrium apparatus (static-analytical method) in Fig. 1 was operated as follows: one liter of liquid material with the carotenoids was filled into the cylindrical pressure vessel and a high-pressure pump charged CO_2 into the system. After equilibration of pressure and temperature, the liquid phase was recirculated for at least 5 hours to intensify phase contact. Sampling of both phases was possible. The total solubility in the CO_2-rich phase was measured by reducing pressure of a sample volume of 30-50 liters (STP) and weighing the precipitating substances. The amount of CO_2 was quantified with a gas meter and the content of carotenoids with the analytical methods described above. A hydraulically driven piston in the bottom part of the pressure vessel allowed sampling without pressure loss.

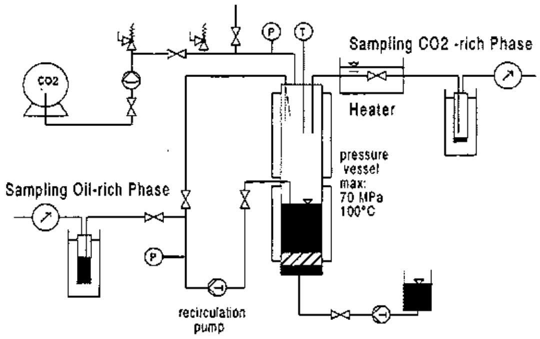

Figure 1. Schematic representation of the setup for measuring solubilities and distribution coefficients

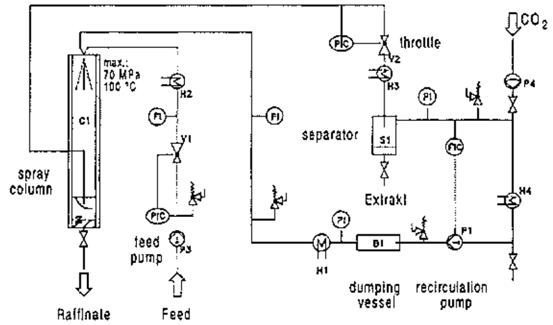

Figure 2. Schematic representation of the high-pressure spraying apparatus

The extraction experiments were performed in a high pressure spraying plant on a semi-industrial scale depicted in Fig. 2. The heated liquid feed was compressed by a reciprocating pump P3, contacted with the supercritical CO_2 in a twin-fluid atomizer and sprayed into a cylindrical high-pressure vessel C1. The inner diameter of this vessel was 50 mm and the length of the spraying zone was 2 m. At the bottom a raffinate phase was separated from the loaded CO_2-stream. The CO_2 was reduced in pressure and separated from the extract in a subsequent separator S1. Most of the plant components are described in detail elsewhere [11].

In order to test minor material quantities, screening extraction experiments were conducted. A porcelain trough (90x9x9 mm) was filled with 0.5 g of the carotenoid-containing liquid and placed inside a horizontal high-pressure tube. Supercritical CO_2 flowed through the tubing at a rate of 3.5 kg/h. After a certain time, the CO_2 flow was diverted through a bypass line and the porcelain trough removed for analytical purposes.

Further investigations were performed in less complex apparatuses. A high-pressure shear viscosimeter (Haake, Germany) operating on the base of the Searle-system was used to determine viscosities. Surface tensions were determined with the pendant drop method [12] in a high-pressure view cell (Sitec, Switzerland) using oil densities with dissolved CO_2.

Results and Discussion

The total solubility of dispersions with corn oil and of Lycomato was investigated in the range of 25-60 MPa at 40° and 80°C. The obtained values are the same as those of typical vegetable oils (Fig. 3) and show the well-known temperature inversion effect at approximately 32-35 MPa.

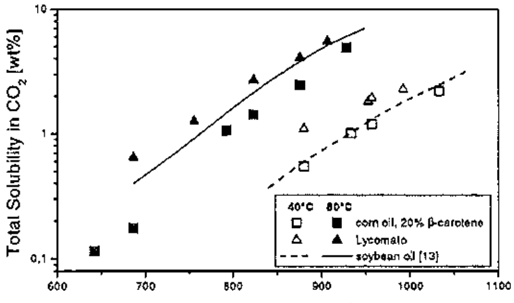

Figure 3. Solubility of carotenoid-containing liquids in supercritical carbon dioxide

The feasibility of the proposed separation process is determined not only by total solubility in CO_2 but also by the equilibrium distribution of the carotenoids between the two phases. The partition coefficient k is defined as the ratio between the mass concentrations in the CO_2-rich and in the liquid phase on a solvent-free basis. A rough estimation of the partition coefficient from separation data with a countercurrent column process [10] renders 0.3 at 24 MPa and 50°C. Comparison with the binary solubility data β-carotene-CO_2 illustrates a significant entraining effect of vegetable oils on carotene solubility in supercritical CO_2.

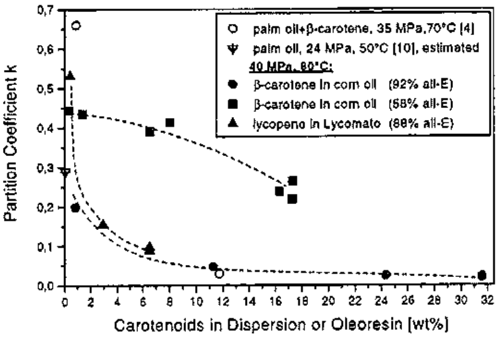

Figure 4. Partition coefficients of carotenoids on a solvent-free basis

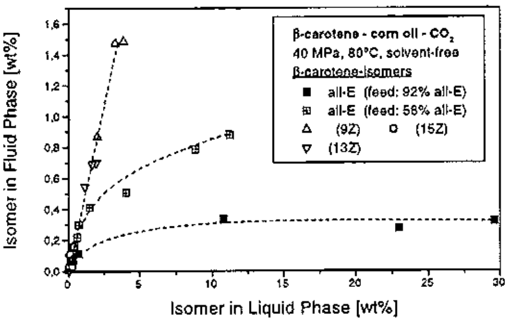

Figure 5. β-carotene-isomers – corn oil – CO_2

Experimental values at 40 MPa and 80°C are depicted in Fig. 4. The model system with (all-E)-β-carotene shows a significant decrease of the k-value with increasing concentration in the liquid phase. This effect is due to saturation of the supercritical phase and is in accordance with data points from Stoldt [4]. An unfavorable increase of the partition coefficient occurs in the presence of Z-isomers. These isomers show a higher solubility and also increase the dissolved amount of (all-E)-isomers. The effect of higher solubility of Z-isomers in vegetable oils and in pure supercritical CO_2 [3] is known and explained by the absence of crystallizability. The increase of (all-E)-solubility in mixture with Z-isomers has not been explained so far but could be due to isomerization of previously dissolved Z-isomers. The k-values of lycopene in the system Lycomato-CO_2 are close to the values of (all-E)-β-carotene, which is reasonable since the chemical structures of these carotenoids are related and Lycomato contains mainly (all-E)-lycopene. The (all-E)-portion of β-carotene in crude palm oil (sterilized fruits) is in the range of 40-55% [14] and explains the relatively low value estimated from separation data [10]. The partition coefficients increase remarkably with temperature and slightly with pressure.

Conclusions to enhance separation efficiency:

- Higher pressures and temperatures (p > 35 MPa) lead to higher solubilities.
- Higher feed concentrations lead to lower partition coefficients.
- The (all-E)-isomers show the lowest partition coefficients.

Solubility data with complex and partly unknown mixtures of chemical substances do not allow quantification of the soluble amount. Therefore additional experiments were performed. Simple screening tests with small quantities of material showed the good extractability of the model system as to be expected (Fig. 6). The residue diminished linearly with the duration of the extraction and the analyzed carotenoid concentrations matched mass-balance calculations.

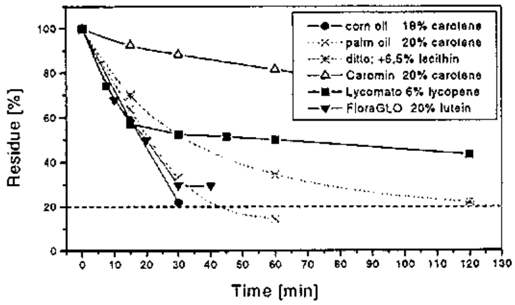

Figure 6. Screening extraction at 50 MPa, 60°C

FloraGLO contains a high percentage of soy oil and behaved similarly. The extraction kinetics of Lycomato changed indicating that the non-carotenoid fraction is not homogeneous. An extraction performance similar to vegetable oils is limited to approximately 50% of the material. The mass reduction of Caromin is very slow and a significant increase of the carotenoid concentration was not observed. The production process of Caromin includes short path distillation and removes many of the substances also soluble in CO_2. Both Caromin and Lycomato contain significant amounts of phospholipids and show high viscosities. The influence of phospholipids was studied by addition of soy lecithin to a dispersion. Phospholipids hinder the extraction and accumulate with the carotenoids.

Conclusions:

- Carotenoids can be refined from oily dispersions with supercritical CO_2.
- High concentrations of phospholipids should not be present.

The size of the phase surface area determines the rate of mass transfer. Since internal packing, such as structured packing in a counter-current column do not work for highly viscous or even solid materials, the formation of small droplets in a spraying process was chosen to obtain a sufficient surface area. The interfacial tension between vegetable oils and CO_2 decreases with CO_2 pressure [12] and thus supports droplet formation. Additionally dispersed β-carotene (5 wt%) did not affect the advantageous low interfacial tension in the system palm oil - CO_2. New viscosity data of the liquid materials used are given in Tab. 2. The viscosity increases with pressure and decreases with temperature and dissolved CO_2.

Table 2: Viscosity of feed materials / mPas

Atmospheric pressure	**60°C**	**80°C**
Palm oil	18	11
Corn oil, 20% β-carotene	84#	75#
Lycomato	410	160
Caromin	12000*	1200*
50 MPa; corn oil, 20% carotene		
Without CO_2	124#	101#
25% CO_2 dissolved	33#	27#

* type of flow behavior not known
# non Newtonian flow – shearing with 100-200 rpm

Conclusions:

- Elevated temperatures (~80°C) are important to reduce the high viscosities of Caromin and Lycopene.
- Dissolved CO_2 diminishes surface tension and viscosity and enhances droplet formation.

Table 3: Spraying results at 40 MPa and 80°C, 50 kg CO_2 /h, ratio CO_2/Feed: ~30

Material	**Carotenoid content [wt%]**		
	Feed	Raffinate experimental	Raffinate equilibrium*
Crude palm oil	0.06% β-carotene	0.09 (100°C)	~0.09
Caromin	26% β-carotene	27	data missing
Lycomato	6% lycopene	10	30
Corn oil	16% β-carotene (43% (all-E))	22	23
Corn oil	20% β-carotene (95% (all-E))	55 / 100 *	34

*explanations in the text

Results of high-pressure spray extraction experiments on a semi-industrial scale are listed in Tab. 3. The experimental and the theoretical equilibrium-based concentrations in the raffinate are compared. Generally the tendency of the previous screening experiments was confirmed. The carotenoid content in Caromin did not increase significantly due to a lack of soluble substances. The deoiling of Lycomato did not reach the equilibrium value in accordance with the screening results. The enrichment of partly isomerized carotene in corn oil and crude palm oil matched the equilibrium values, while the material with mainly (all-E)-carotene led to highly enriched raffinates. Because this isomer crystallizes easily sprayed material accumulated along the inner walls of the pressure vessel. This raffinate was rendered nearly oil-free by maintaining the CO_2 flow after shutting off the liquid feed pump.

Final Conclusions

- The isomeric form of β-carotene influences not only the distribution coefficient but also the raffinate structure.
- In liquid carotenoid-vegetable oil systems, the high-pressure spraying process leads to enrichment or even isolation of carotenoids.
- Decisive advantages of the spray extraction consist in the ability to handle solid raffinates and the formation of a large mass-transfer area even for viscous oleoresins.

Acknowledgement

We thank Dr. V. Meyn (Institut für Erdölforschung, Clausthal-Zellerfeld, Germany) for his assistance in measuring viscosities under pressure.

References

1 Subra, P.; Castellani, S.; Ksibi, H.; Garrabos, Y. *Fluid Phase Equilibria*, **1997,** 131, 269-286.
2 Johannsen, M. J.; Brunner, G. *Chem. Eng. Data* **1997**, 42, 106-111.
3 Mendes, R.L.; Fernandes, H.L.; Roxo, C.H.; Novais, J.M. Pajavra, A.F,. p.423-430, *FICSF** **1997.**
4 Stoldt, J., Doctoral Dissertation, Technical University Hamburg-Harburg, Germany, **1995** (in German).
5 Eggers, R.; Wagner, H., *J. Supercritical Fluids* **1993,** 6, 31-37.
6 Spanos, G.A.; Chen, H,; Schwartz, S.J. *J. Food Science* **1993**, 58(4), 817-820.
7 Chandra, A,; Nair, M.G. *Phytochem. Anal.* **1997**, 8, 244-246.
8 Favati, F.; Galgano, F.; Damiano, N., Larzarini, G., p. 121-128, *FICSF** **1997.**
9 Ambrogi, A., Eggers, R. p. 129-135, *FICSF** **1997.**
10 Ooi, C.K.; Bhaskar, A,; Yener, M.S.; Tuan, D.Q.; Hsu, J.; Rizvi, S.S. *JAOCS* **1996,** 73(2), 233-237.
11 Wagner, H., Doctoral Dissertation, Technical University Hamburg-Harburg, Germany, **1995** (in German).
12 Jaeger, P.T.; v. Schnitzler, J.; Eggers, R., *Chem. Eng. Technol.* **1996,** 19, 197-202
13 Quirin, K.-W. *Fette, Seifen, Anstrichmittel* **1982**, 84, 460.
14 Trujillo-Quijano, J.A.; Rodriguez-Amaya, D.B.; Esteves, W.; Plonis, G.F. *Fat Sci.Technol.* **1990**, 92(6), 222-226.

*) *FICSF:* Proceedings Fourth Italian Conference on Supercritical Fluids and their Applications, Italy 7/10 Sept. 1997, Ed. Reverchon, E.

Countercurrent Extraction with Supercritical Carbon Dioxide: Behavior of a Complex Natural Mixture

Dipl.-Ing. Dieter Buß*, Prof. Dr.- Ing. Gerd Brunner
Technische Universität Hamburg-Harburg, Eißendorfer Str. 38, 21073 Hamburg
Fax.: 0049-40-42878-4072; e-mail: buss@tu-harburg.de

Squalene (2,6,10,15,19,23-hexamethyl-2,6,10,14,18,20-tetracosahexaene), known as spinacene, is a naturally occurring triterpenoid hydrocarbon, usually used in its natural form in health foods or in its hydrogenated form (squalane) in cosmetic preparations as a moisturizing or emollient agent. Academic interest arises because of its role as an precursor in the biosynthesis of sterols and of the naturally occurring tetracyclic and pentacyclic triterpenes [5, 11, 12, 13].

Olive oil deodorizer distillate (OODD), a by-product of the olive oil industry, contains squalene in a concentration range of 10 to 30 Ma.-%. Other components are: 34 Ma.-% free fatty acids, 24 Ma.-% fatty acid esters (methyl and ethyl), 5.6 Ma.-% sterols, and 6.4 Ma.-% others (glycerides, tocopherols, hydrocarbons, etc.).

To investigate the possibility of separating squalene from OODD by means of supercritical carbon dioxide extraction, VLE measurements and a theoretical separation analysis were carried out. VLE data provide information about the operating parameters of the process. The object of the theoretical separation analysis is the simulation of the separation process and the determination of data for a scale-up. Experimental results have to be correlated with results of the VLE measurements. Extraction experiments were run on a 7 m laboratory plant in countercurrent mode.

Results show, that changing composition in the column has a major effect on the distribution coefficients K_i and on the separation factors α_{ij}. As a consequence, the concentration of squalene in the extract was limited and the concentration of FFA could not be reduced to a desired level.

Introduction

Squalene is a medium value chemical that is used as both as a health food tonic and for pharmaceutical preparations [6]. It was first discovered in 1906 in shark liver oils and is produced from fish liver oils by molecular distillation [7] and has been synthesised.

The chemical is a highly unsaturated open chain isoprenoid hexaene hydrocarbon polymer, the parent molecule of natural rubber, and structurally related to carotene. It has a chain length of C_{30}, ($C_{30}H_{50}$), with six double bonds per molecule. These bonds giving the molecule a strong susceptibility to oxidation and polymerisation, thickening to a viscous mass when exposed to air.

One reason that limits the use of squalene in cosmetic applications is the uncertainty of its availability as a result of international concern for the protection of marine animals that are the primary source of natural squalene. This consideration turned our interest toward a vegetable origin source of squalene, namely a by-product of the olive-oil industry, the distillated fraction obtained from the deodorizing step. It has a squalene content of about 10 to 30 Ma.-%

Supercritical fluid extraction is nowadays widely used both as a preparative method in analytical chemistry and as a large-scale separation process. In the last few years numerous applications have been developed in the field of processing natural oils such as: extraction of essential oils and aromas [3] and extraction and purification of polyenoic unsaturated fatty acids and fat-soluble vitamins [2, 8, 9].

Materials and Methods

The olive oil deodorizer distillate was supplied by a Portuguese factory (Fabrica Torrejana de Azeites). It contained squalene in a concentration range of 10 to 30 Ma.-%. Other components were 34 Ma.-% free fatty acids, 24 Ma.-% fatty acid esters (methyl and ethyl), 5.6 Ma.-% Sterols, and 6.4 Ma.-% others (glycerides, tocopherols, hydrocarbons, etc.).

During the extraction experiments, numerous samples of the extract and of the raffinate were collected, analyzed, and used for further VLE measurements.

The phase equilibrium measurements were performed using a static-type apparatus. Details on the apparatus and the sampling process were already described by Stoldt and Brunner [4, 10]. The equilibrium cell was a 1000 cm^3 stainless steel autoclave provided with a mechanical stirrer and two capillary lines (1/16" stainless steel tubing) for sampling the liquid phase (bottom) and the vapor phase (top). The pressure drop in the autoclave during the sampling process was compensated by injecting a similar mixture maintained at the same P, T-conditions from a second autoclave of lower volume, 500 cm^3. Usually, three samples were taken from the liquid phase and from the vapor phase in order to get a reliable value.

Extraction experiments were carried out in a 7 m laboratory scale plant of 17.5 mm inner diameter, equipped with a 6 m regular packing of the type Sulzer EX. A detailed description is given elsewhere [3].

Results and Discussion

Phase Equilibrium and Solubility

The OODD was divided into tree pseudo-components: 1) CO_2, 2) free fatty acid esters (FFE) and squalene, 3) free fatty acids (FFA). The phase equilibrium of these pseudo-components under extraction conditions 370 K and 23 MPa is shown in the triangular diagram (Fig. 1). The binodal-curve is interpolated by connecting the points of the feed (F), raffinate (R) and extract (E). Equilibrium compositions of the two phases are connected by the equilibrium tie lines.

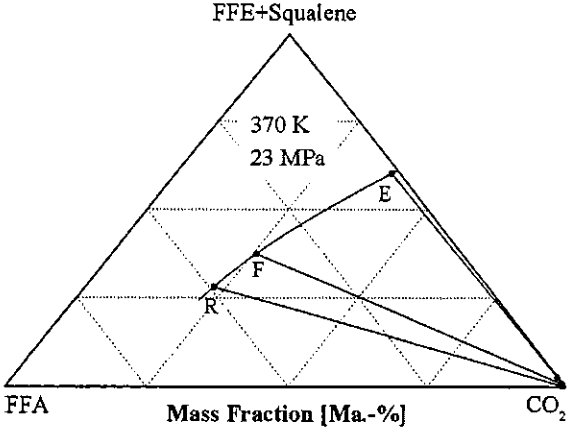

Figure 1. Phase equilibrium in the pseudo-ternary system CO_2 – (FFE + squalene) – FFA.

For processes like extraction at near-critical or supercritical conditions, it is necessary to know the behavior of each component in the mixture at different state conditions (T, P, composition). This is especially important for natural product systems, such as edible oils, which contain a large number of different components.

The OODD consists of components with partly very different properties as far as solubility in supercritical CO_2 and K-factors are concerned. It can already be seen from the triangular diagram, that the changing composition leads to a substantially higher solubility of the extract, which is poor in FFA, but rich in FFE and squalene. The changing solubility is illustrated by Fig. 2, in which solubilities of the feed and of the extract are compared for temperatures of 330 and 370 K and over the pressure range of 15 to 30 MPa.

FFE are much more soluble in supercritical CO_2 than FFA or squalene. The enrichment of FFE in the extract therefore leads to a loading of the gas phase which is 5 times higher than the solubility of the feed material.

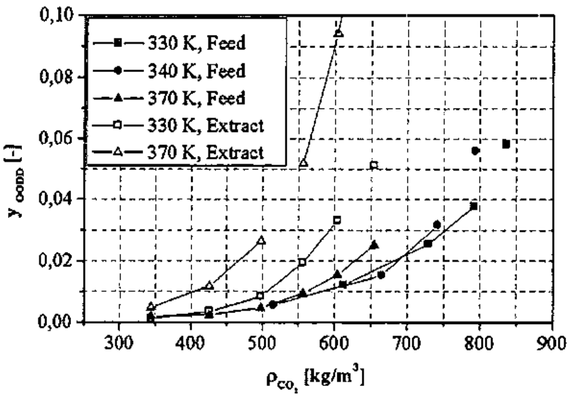

Figure 2. Solubility of the feed and of the extract as a function of temperature and CO_2-density.

The solubilities were correlated with the density of CO_2 using the Chrastil equation, modified by Adachi and Lu [1]. The Chrastil equation can be written as:

$$c = \rho^{e} \exp(a/T + b) \tag{1}$$

where c is the concentration of a solute in kg/m³ of a gas, ρ is the density of the gas in kg/m³, e, a, b are solubility constants. In the modified equation proposed by Adachi and Lu, e is density dependent:

$$e = e_0 + e_1\rho + e_2\rho^2 \tag{2}$$

where e_0, e_1 and e_2 are constants.

The solubility constants were calculated minimizing relative standard deviation between the experimental and calculated solute concentrations. They are summarized together with the standard deviations in Tab. 1. Good fit of the equation to the data achieved for all measured systems is illustrated by standard deviations of 1.01 for the feed and 0.35 for the extract. However, the correlation should not be extrapolated outside the experimental conditions, as the solubility constants e_0, e_1 and e_2 are sensitive to density.

Table 1. Solubility constants in Chrastil-Adachi-Lu equation.

Solute	A [K]	b [-]	e_0 [-]	e_1 [m³/kg]	e_2 [m³/kg]	σ [%]
Feed	-1273	54.6	-11.1	7.7E-3	3.3E-6	1.01
Extract	-3527	70.2	-13.5	11.1E-3	5.6E-6	0.35

K-factors

In particular, distribution of the component of interest between equilibrium phases determines the concentration enhancement by extraction. This is measured by the K-factor:

$$K_i = y_i/x_i \qquad (3)$$

which can strongly depend on pressure, temperature and composition:

$$K_i = f(T, P, x_i, x_j, \ldots, y_i, y_j, \ldots) \qquad (4)$$

In order to get a description for the change of K-factors with changing composition along the height of the column, the K-factors of the main components of OODD were measured in the feed and in the extract. The extract had a composition of 42 Ma-% squalene, 50 Ma.-% FFE and 8 Ma.-% FFA. Fig. 3 shows the effect of different compositions and CO_2 densities at 370 K on the K-factors of squalene, oleic acid and ethyloleate. It can be observed, that the K-factors of ethyloleate decrease sharply from 4.2 in the feed to 1.1 in the extract at 556 kg/m^3. Simultaneously the K-factor of oleic acid increases from 0.8 to 1, which means that the concentration of oleic acid can't be reduced to a lower level under these conditions. The K-factor of squalene decreases from 1.1 (enrichment in the gas phase) to 0.9 (enrichment in the liquid phase), which means that the behavior of squalene is almost inverted during the extraction process. As far as the enrichment of squalene and the elimination of FFA is concerned, the process has come to its limit under these conditions. This also corresponds with the effect, that selectivity usually declines with increasing capacity of a solvent.

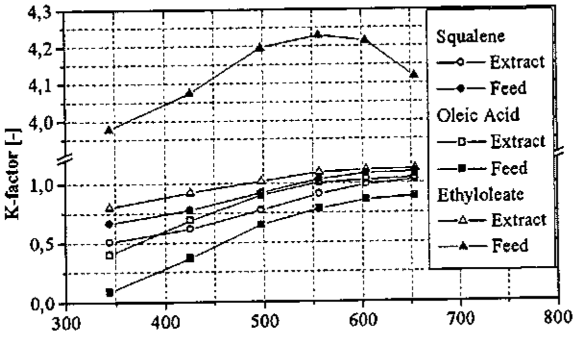

Figure 3. K-factors of squalene, oleic acid and ethyloleate in the feed and in the extract at 370 K and different CO_2-densities.

Concentration profiles of an extraction column provide information about the efficiency of the process and about the actual needed height of the column. If the column has no possibility for sampling along its height, the concentration profile can be theoretically derived from available VLE data. In our case, based on separation analysis, it could be assumed that the extraction column would have 6 theoretical stages of a height of 1 m. The concentration of the components at each theoretical stage can be approximately derived from the triangular diagram (Fig. 1), as these points have to be on the binodal-curve. This leads to a dependence of the concentration of the regarded components on the height of the column as shown in Fig. 4. Hollow symbols are representing the gas phase and solid symbols are representing the liquid phase. It can be seen, that there is mainly a separation of free fatty acids from free fatty acid esters. The esters are enriched in the extract, while the concentration of FFA can be decreased to less than 10 Ma.-%. The concentration of squalene in the extract can only be increased up to 42 Ma.-%, which is in accordance with all column experiments (see Fig. 6).

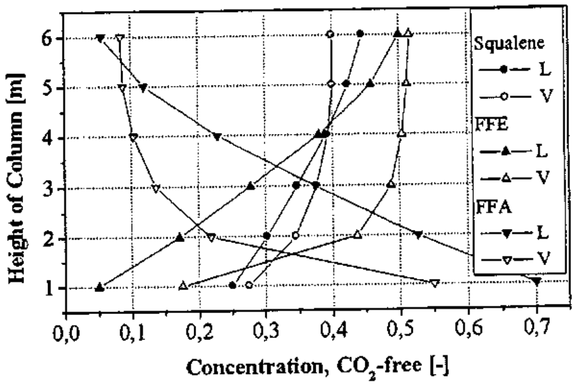

Figure 4. Changing of the concentration of squalene, FFE and FFA with height of column.

The most important information from the column profile is the crossing of the concentration lines of squalene at the 4th theoretical stage and those of FFA between the 5th and 6th theoretical stage. Here, the K-factor of squalene is changing from >1 to <1 while the K-factor of FFA is changing from <1 to >1 (Fig. 5). After an enrichment of squalene in the gas phase concerning the feed material, squalene is more and more enriched in the liquid phase with changing composition in the column. The squalene concentration reaches a maximum at the 5th stage. As a consequence it will be impossible to get to higher concentrations in the extract under the same conditions as well as the concentration of FFA can't be further decreased.

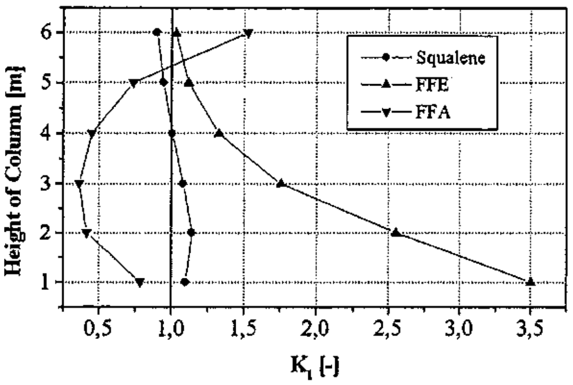

Figure 5. Changing of the K-factors of squalene, FFE and FFA with height of column.

Column Experiments

A series of column experiments were carried out to verify the results from VLE measurements and to determine the effect of different temperature/ pressure combinations and of the raffinate to extract ratio on both squalene concentration of the extract and yield. The raffinate to extract ratio was adjusted by the reflux ratio. The feed material determines the mass balance over the relation of FFE and Squalene to FFA. A deliberate deviation from the optimal raffinate to extract ratio enables a shift of the purities in favor of one of the two product streams. As Fig. 6 indicates, the best results were achieved at a raffinate to extract ratio of 2.5 with no further improvement of the extract purity. With correctly adjusted raffinate to extract ratio, the reflux ratio determines the selectivity of the separation process. The best quality of the extract could be obtained for reflux ratios greater than 4. The general trend was unique for all experiments even with different temperature/pressure combinations.

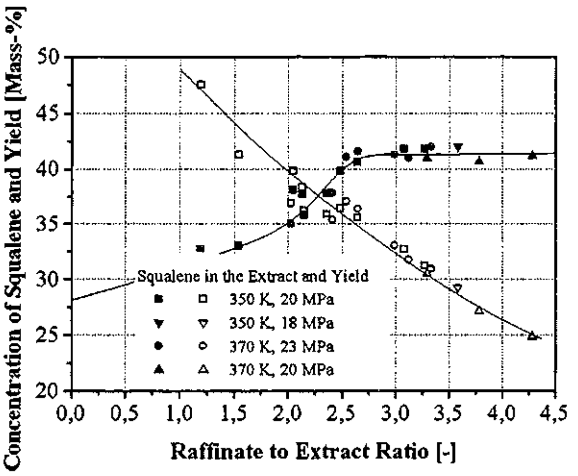

Figure 6. Extract purity and yield as a function of the raffinate to extract ratio.

Conclusions

The enrichment of squalene from olive oil deodorizer distillate was investigated by means of countercurrent extraction using supercritical CO_2 as solvent. VLE measurements were performed to enable an analysis of the separation process. The solubility of the feed and of the extract was also correlated for all operating conditions.

Squalene could be enriched to 42 Ma.-% in the extract as well as the concentration of FFA could be decreased to 8 Ma.-%. Further improvement of the product quality will only be possible with a second step of extraction by an enrichment of squalene in the raffinate, as VLE data indicate clearly.

Acknowledgements

The financial support from the European Union project CT 96-1075 is gratefully acknowledged.

References

[1] Adachi, Y.; Lu, C.-Y.: *Fluid Phase Equilibria*, 1983, 14, 147–156.
[2] Bondioli, P.; Mariani, C.; Lanzani, A.; Fedeli, E.; Müller, A.: Squalene recovery from olive oil deodorizer distillates. *JAOCS*, 1993, 70, (8), 763–776.
[3] Budich, M.; Werner, S.; Wesse, T.; Leibküchler, V.; Brunner, G.: Optimization study of countercurrent gas extraction: The deterpenation of citrus oil with supercritical carbon dioxide. *Journal of Supercritical Fluids*, in press.
[4] Brunner, G.: Gas Extraction. Steinkopff Darmstadt, 1994.
[5] Ceruti, M.; Viola, F.; Balliano, G.; Grosa, G.; Caputo, O.; Gerst, N.; Schuber, F.; Cattel, L.: *Eur. J. Med, Chem.*, 1988, 23:533.
[6] Gopakumar, K.; Thankappan, T. K.: *Seafood Export Journal*, 1986, March, 17.
[7] *Nippon Oil Technol. Soc.*, 1949, 2, (2-3), 48/65.
[8] Riha, V.: Gegenstromtrennung von Fettsäureethylestern mit überkritischem CO_2. Doctoral Thesis, TU Hamburg-Harburg, Germany, 1994.
[9] Saure, C.: Untersuchungen zur Anreicherung von Squalen und Tocopherolen mittels Gegenstromextraktion mit überkritischem Kohlendioxid. Doctoral Thesis, TU Hamburg-Harburg, Germany, 1996.
[10] Stoldt, J.; Saure, C.; Brunner, G.: Phase Equilibria of Fat Compounds with Supercritical Carbon Dioxide. *Fluid Phase Equilibria*, 1996, 116, 399–406.
[11] Strandberg, T. E.; Tilvis, R. S.; Miettinen, T. A.: *J. Lipid Res.*, 1990, 31:1637.
[12] Strandberg, T. E.; Tilvis, R. S.; Miettinen, T. A.: *J. Lipids*, 1989, 24:705.
[13] Strandberg, T. E.; Tilvis, R. S.; Miettinen, T. A.: *Biochim. Biophys. Acta*, 1989, 1001:150.

Supercritical CO_2-Extraction for Production of Extracts from Plant Materials containing Cholagoga Substances

T. Gamse and R. Marr

Institute for Chemical Engineering and Environmental Technology
University of Technology Graz, Inffeldgasse 25
A-8010 Graz, Austria
fax: + 43 316 873 7472
email: GAMSE@glvt.tu-graz.ac.at
*Corresponding author

The use of supercritical CO_2 for producing extracts from plant material is a good alternative to solvent extraction or steam distillation, because the extracts are completely free from solvent and also the temperatures normally used in CO_2 extraction are very moderate, so that no heat sensitive substances are destroyed or modified. Valerian, dandelion, St. Mary's thistle and yarrow were chosen as plant materials because they contain cholagoga active agents. The aim of this project was determination of extraction efficiency depending on pressure and temperature.

Introduction

Most of the research dealing with supercritical fluid extraction (SFE) has been done with different plant materials [1-19]. The interest in using SFE for producing natural extracts is nowadays growing again because of stronger limitations for residual solvent content in the products more investigations have to be done for solvent removal which increases as well plant as operation costs. Therefore the difference in investment costs between a solvent and a high pressure extraction plant get smaller and especially the low operation costs for a SFE plant are the reason for the increase of industrial SFE plants. Up to now there were only industrial plant for decaffeination of tea and coffee and for hop extraction. But in the last few years further industrial plants for different plant materials were installed.

The plant materials containing cholagoga substances were chosen for this project, because these active agents are interesting for pharmaceutical industry. Cholagoga substances are divided in cholocinetica compounds, which stimulate emptying of gall-bladder, and in choleretica substances, which stimulate the liver for stronger secretion of bile. Although it is possible to produce a lot of this agents synthetically many pharmaceutical producers go back to natural resources because the synthetic products do often not have the same effect than natural ones.

Materials and methods

Materials: The carbon dioxide with a purity higher than 99,94 % (v/v) and a dewing point lower than -60°C was purchased from Linde (Graz) and stored in a tank with a capacity of 3200 L. Equation of Bender [20,21], a 20 parameter equation of state, was used for calculation of CO_2 density at different pressure and temperature levels. For Soxhlet-and fexIKA extractions n-hexane in p.a. quality from Merck company was used. The plant materials of valerian (RD. valerianae CS. Ph. EUR), dandelion (RD. Taraxaci CS. ÖAB), St. Mary's thistle (HB. Cardui mariae CS. FL) and yarrow (HB. Millefolii CS. ÖAB) were organised in pharmaceutical quality by Kottas-Heldenberg & Sohn, Drogenhandel Ges.m.b.H. (Austria).

Methods:

Soxhlet extraction for 4 hours was performed for all plant materials using n-hexane as solvent to determine the maximal extractable amount of substances. n-hexane was chosen as solvent, because its polarity is comparable to supercritical CO_2 and therefore the same kind of substances are extracted. The total amount of extractable substances was achieved by evaporating the solvent from the solvent-extract mixture at the end of the Soxhlet extraction and weighing the amount of extract.

fexIKA extraction: This extraction method is a further development of the Soxhlet extraction. As shown in Fig. 1 the solvent is vaporised in the bottom flask and passes the material situated in the top flask. At the top of this flask the solvent is condensed and the liquid wets the material which has to be extracted. After a certain amount of solvent is vaporised the bottom flask is cooled down and the resulting under-pressure sucks the solvent - extract mixture into the bottom flask. Then the next cycle starts with heating up and vaporising the solvent. The advantage in comparison to the Soxhlet extraction is that when material of fine particle size has to be extracted not filter cake, which will not be extracted, is produced because the coming up steam causes strong turbulences in the solid material and therefore also better extraction results.

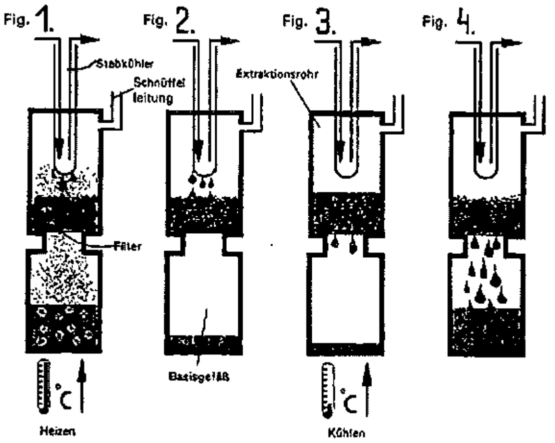
Fig. 1.
Fig. 2.
Fig. 3.
Fig. 4.
Stabkühler
Schnüffel leitung
Extraktionsrohr
Filter
Basisgefäß
°C
Heizen
°C
Kühlen

Figure 1: Operating procedure of fexIKA extraction

CO_2 extraction: All extraction test were performed in a high pressure extraction plant, designed by Applied Separations company (see Fig. 2). Liquid CO_2 of 60 bar enters the air-powered pump and extraction pressure is adjusted by regulating pressure of compressed air. The great advantage of this plant is that two extractions can be performed parallel at same pressure and temperature conditions so that a direct comparison of extraction results is possible. The two extraction vessels with a volume of 300 ml each can be operated up to 690 bar and 250°C. This extraction chambers have a filter at the bottom for distributing the supercritical CO_2 over the whole extraction area to avoid channelling in the solid material and a filter at the top to prevent that solid particles are withdrawn by the leaving CO_2 stream. For depressurisation of CO_2 to atmospheric pressure as well outlet valves as metering valves for accurate adjustment of the flow rate are installed. The metering valves are heated in a thermostated block so that no blocking might occur because of the low temperatures by the Joule-Thompson-effect. The sample vials are situated in an ice-water bath so that all extracted substances are collected.

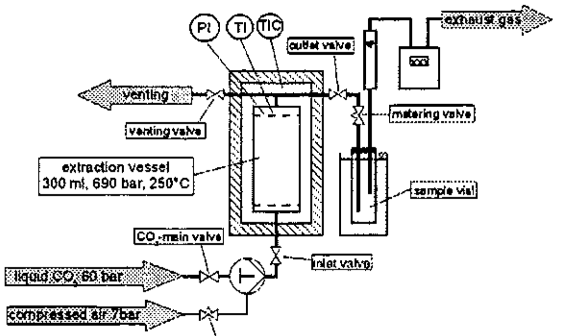
PI
TI
TIC
exhaust gas
outlet valve
venting
venting valve
metering valve
extraction vessel
300 ml, 690 bar, 250°C
sample vial
CO₂-main valve
inlet valve
liquid CO₂ 60 bar
compressed air 7bar
compressed air nozzle

Figure 2: Schemata of the high pressure extraction plant

The gaseous CO_2 leaving the sample vials passes calibrated rotameters for determining the actual flow rates and gas meters for the total CO_2 flow over extraction time. As well temperature of the thermostating oven as of extraction vessel is measured.

For determination of extraction progress at the beginning every 15 minutes sample vials were changed and later on every half an hour. By weighing the sample vials the extraction progress was calculating based on the results from Soxhlet- and fexIKA-extraction, which were set as 100 % of extractable mass.

Results and Discussion

Valerian The extraction yields after 4 hour extraction time are given in Tab. 1.

Temperature	Pressure	Extraction yield
25°C	100 bar	45.92 %
	200 bar	57.58 %
	300 bar	59.07 %
	400 bar	51.10 %
40°C	100 bar	40.20 %
	200 bar	67.36 %
	300 bar	67.82 %
	400 bar	75.46 %
60°C	100 bar	12.35 %
	200 bar	79.08 %
	300 bar	82.82 %
	400 bar	96.39 %

Table 1: Extraction yields of valerian

It is obvious that an increase in pressure results always in higher extraction yields correlating with increase in CO_2 density and therefore higher solubility. Higher temperatures at low pressure levels occur a strong decrease in density and therefore solubility but at higher pressure levels density decrease is the lower effect than increase of vapour pressure of extractable substances so that higher extraction yields are obtained (see Fig. 3).

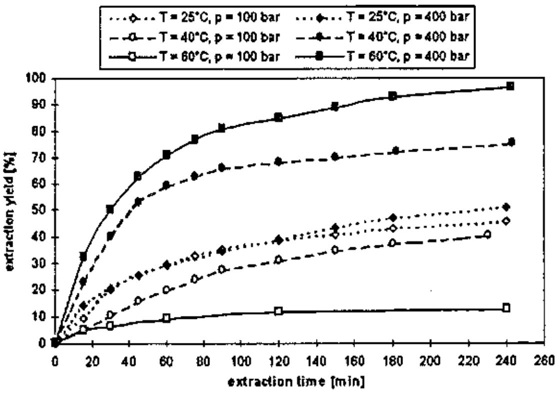

Figure 3: Effect of pressure and temperature on extraction yield of valerian

At constant temperatures a linear dependency between density and total extraction yield was obtained which rises to higher extraction yields at higher temperatures as shown in Fig. 4. A further increase in temperature which would result in better extraction results is not suitable because the extractable active agents are heat sensitive and would be destroyed at higher temperatures. The anomaly at 25°C was also obtained for all other plant materials and it might be a result because of the high CO_2 density so that at these conditions repulsive forces are active.
Best extraction results were obtained at 400 bar and 60°C with 96.39 % extraction yield.

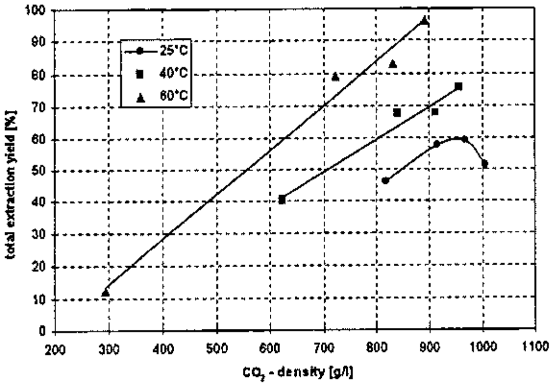

Figure 4: Dependency of extraction yield over CO_2 - density

Dandelion The influence of pressure and temperature is not so significant as given in Tab. 2 and also the maximum extraction yield of 64.44 % at 400 bar and 60°C is relatively low. The effects on pressure and temperature are the same as for valerian extraction.

Temperature	Pressure	Extraction yield
25°C	100 bar	27.36 %
	200 bar	41.80 %
	300 bar	41.43 %
	400 bar	40.23 %
40°C	100 bar	23.99 %
	200 bar	37.37 %
	300 bar	37.97 %
	400 bar	42.28 %
60°C	100 bar	3.37 %
	200 bar	41.24 %
	300 bar	51.06 %
	400 bar	64.44 %

Table 2: Extraction yields of dandelion

St. Mary's thistle Again a linear dependency between total extraction yield and density is occurred increasing with higher extraction temperature. The maximal extraction yield of 76.30 % was obtained at 400 bar and 60°C as given in Tab. 3.

Temperature	Pressure	Extraction yield
25°C	100 bar	34.09 %
	200 bar	42.67 %
	300 bar	50.75 %
	400 bar	47.51 %
40°C	100 bar	22.22 %
	200 bar	47.82 %
	300 bar	49.00 %
	400 bar	55.08 %
60°C	100 bar	5.54 %
	200 bar	50.12 %
	300 bar	64.11 %
	400 bar	76.30 %

Table 3: Extraction yields of St. Mary's thistle

Yarrow The maximal extraction yield of 94.72 % of yarrow at 400 bar and 60°C is comparable with the results of valerian. Data of extraction tests of yarrow are given in Tab. 4.

Temperature	Pressure	Extraction yield
25°C	100 bar	48.76 %
	200 bar	62.78 %
	300 bar	52.05 %
	400 bar	53.73 %
40°C	100 bar	11.48 %
	200 bar	61.98 %
	300 bar	69.39 %
	400 bar	75.95 %
60°C	100 bar	7.78 %
	200 bar	74.58 %
	300 bar	84.27 %
	400 bar	94.72 %

Table 4: Extraction yields of yarrow

Gaschromatographic analysis A certain amount of the CO_2 extracts was solved in n-hexane and analysed by gas chromatographic method using a flame ionisation detector (GC-FID). Also the extracts of Soxhlet and fexIKA-extractions were analysed and compared with the CO_2 extracts. A characterisation of all substances by gas chromatographic method with mass spectrometer detector (GC-MS) was not possible because the library of the GC-MS was not suitable for natural substances.

Only for valerian the substances isovaleric acid and caryophyllene could be determined. The content of active agents in the extract over extraction time changes dramatically. At the beginning extracts with high contents of these two substances are produced and later on only by-products are present. Up to 2.5 hours extraction time the concentration of these two substances in the extract is much higher than in the comparable Soxhlet and fexIKA extracts. Therefore CO_2 extraction is suitable for producing extracts with high concentration of active agents if extraction lasts only for about 2.5 hours.

Conclusion

CO_2 extraction is a very sufficient process for extracting and concentrating active agents from plant materials containing cholagoga substances like valerian, dandelion, St. Mary's thistle and yarrow. The extraction yields are a little bit lower than with solvent extraction but on the other hand the concentration of the active agents in the extract is much higher which is of interest for pharmaceutical industry. Based on these experimental data and because of the excellent extract quality the use for pharmaceutical applications are tested.

This project was funded by the Jubiläumsfonds of the Österreichische Nationalbank (ÖNB project number 6545)

References

1. Marrone, C.; Poletto, M.; Reverchon, E.; Stassi, A.; *Chem. Eng. Sci.* **1998**,53(21),3711-3718
2. Beutler, H.J.; Lenhard, V.; Lürken, F.; *Fat Sci. Technol.* **1988**, 90, 550-555
3. Bunzenberger, G.; Lack, E.; Marr, R.; *VDI Berichte* **1983**, 50, 508-516
4. Caragay, A.B.; Little, A.D. *Perfumer & Flavorist* **1981**, 40, 890-891
5. Coenen, H.; Kriegel, E.; *Chem. Ing. Tech.* **1983**, 11, 890-891
6. Eggers, R.; Tschiersch, R.; *Chem. Ing., Tech.* **1978**, 50, 11, 842-849
7. Lack, E.; Marr, R.; *Sep. Sci. Technol.* **1988**, 23(1-3), 63-76
8. Reverchon, E.; Sesti Osseo, L.; in: G. Brunner, M. Perrut (Eds.), Proceedings of the Third International Symposium on Supercritical Fluids, Vol. 2, **1994**, p.189-196
9. Reverchon, E.; Della Porta; G.; Gorgolione, D.; Senatore, F.; in: G. Brunner, M. Perrut (Eds.), Proceedings of the Third International Symposium on Supercritical Fluids, Vol. 2, **1994**, p.389-394
10. Poiana, M.; Sicari, V.; Tramontana, A.; Mincione, B.; in: G. Brunner, M. Perrut (Eds.), Proceedings of the Third International Symposium on Supercritical Fluids, Vol. 2, **1994**, p.395-400
11. Fontan, I.M.; Equivel, M.M.; Bernardo-Gil; M.G.; in: G. Brunner, M. Perrut (Eds.), Proceedings of the Third International Symposium on Supercritical Fluids, Vol. 2, **1994**, p.423-428
12. Swift, D.A.; Kallis, S.G.; Longmore, R.B.; Smith, T.N.; Trengove, R.D.; in: G. Brunner, M. Perrut (Eds.), Proceedings of the Third International Symposium on Supercritical Fluids, vol. 2, **1994**, p.487-490
13. Knez, Z.; Skerget, M.; in: T.Yanno; R.Matsuno and K.Nakamura (Eds.), Proceedings of the 6th International Congress on Engineering and Food, Vol. 2, **1993**, p.826-828
14. Caroso, A.L.; Moldao-Martins, M.; Bernardo-Gil, M.G.; in: T.Yanno; R.Matsuno and K.Nakamura (Eds.), Proceedings of the 6th International Congress on Engineering and Food, Vol. 2, **1993**, p.829-831
15. D'Andrea, A.; Di Fabio, A.; Nicoletti, M.; in: D.Barth, J.M.Blanchard, F.Cansell (Eds), Proceedings of the 4th Meeting on Supercritical Fluids and Environment, **1997**, p.181-184
16. Reverchon, E.; Della Porta, G.; in: D.Barth, J.M.Blanchard, F.Cansell (Eds), Proceedings of the 4th Meeting on Supercritical Fluids and Environment, **1997**, p.185-194
17. Reverchon, E.; Della Porta, G.; Lamberti, G.; Taddeo, R.; in: Proceedings of the 4th Italian Conference on Supercritical Fluids and their Applications, **1997**, p.47-56
18. Benvenuti, F.; Gironi, F.; in: Proceedings of the 4th Italian Conference on Supercritical Fluids and their Applications, **1997**, p.65-72
19. Osseo, L.S.; Reverchon, E.; in: Proceedings of the 4th Italian Conference on Supercritical Fluids and their Applications, **1997**, p.515-525
20. Bender, E.; in: Proceedings Fifth Symposium on Thermophysical Properties of American Society of Mechanical Engineers, **1970**, p.227-235
21. Sievers, U.; *VDI - Fortschr. - Ber. VDI-Z.*, **1984**, Reihe 6, Nr. 155; Düsseldorf VDI-Verlag

SUPERCRITICAL CARBON DIOXIDE EXTRACTION OF ESSENTIAL OIL : THE CASE OF TWO ROMANIAN *LAMIACEAE*

D.Barth*, L.Philippon, E.Pop(1)
Laboratoire de Thermodynamique des Séparations,E.A.2287
ENSIC, 1 rue Grandville, BP 451, 54001 F - NANCY
barth@ensic.u-nancy.fr, fax : 33.3.83.35.08.11
(1)Babes-Bolyai University, CLUJ-NAPOCA (Romania)

Supercritical fluid extraction and a comparison of essential oil from some mint hybrids have been previously reported. This is one of our reasons to apply a modern method to a novel and interesting vegetable mater. This paper presepaper presents results of our study in supercritical fluid extraction from different new hybrids of the genus *Mentha* : *Mentha* M_A and *Mentha* M_E. The process parameters influence has been studied : pressure, temperature, flow of carbon dioxide through the bed of mint plants.Some caracteristics of the plant have been examined : particle size and also the cultivation conditions. The extracts were analyzed by gas capillary chromatography and the major components have been identified by the retention times comparison.

Introduction

Supercritical fluids, demonstrated their qualities and superiority to other fluids, being widely studied and applied on research, pilot and plant level , particularly concerning mint [1]-[4]. To obtain a concentrated extract with the flavour and fragrance that of the genuine plant is a delicate task. Compositions obtained by steam distillation (essential oils), or by solvent extraction (concrete, absolute) do not give a correct picture of the complex terpenoidic system present in the genuine plant and responsible for olfactory and/or pharmacologycal properties. Supercritical CO_2 extraction avoid thermal degradation and solvent pollution, giving compositions closer to vegetable matrix than other methods do. Supercritical CO_2 offers great possibilities for selective extraction, fractionation and purification of essential oils thanks to the possibility to adjust the composition of the extract by varying the solvent density and, consequently, its solvent power. *Lamiaceae* family, one of the most valuable from plant kingdom, is divided in two groups: one rich in essential oils, with a large scale of applications in food, pharmaceutic and cosmetic industry and other rich in iridoids, important for their antitumoral, hepatoprotector, imunostimulating, anthalgique, antibiotic and other pharmacological effects. The genus *Mentha*, one of the most studied from *Lamiaceae* consists of approximately 25 species and a great number of hybrids [5]. Apart from their morphological variability, most mint species are characterised by a certain essential oil diversity. Crossing experiments in this genus permitted to obtain a wide variety of compositions and, consequently, of olfactory and pharmacological properties. Thai is why mint may be considered« MotherNature`sChemicalFactory »

Romanian research was oriented to obtain new and performant mint hybrids, resistant to deseases and unfavorable climatic conditions, with a good yield of essential oil, and new valuable compositions [6]-[8]. Supercritical fluid extraction and a comparison of yield and composition of supercritical fluid extract and essential oil from some mint hybrids have been previously reported [7,8]. These are one of our reasons to apply supercritical carbon dioxide extraction to interesting vegetable mater. This paper presents results of our study about two different new hybrids of the genus *Mentha*:*Mentha* M_A and *Mentha* M_E.

Materials and methods

a)Plant material.

Mint hybrid, named *Mentha* M_A and *Mentha* M_E in this paper, were obtained by E.Pop[8], cultivated at Grid (country of Brasov), harvested 1996 and 1997,dried,vacuum packeged and stored in cool dry place.

b)Supercritical carbon dioxide extraction

This is a home made apparatus, composed of a CO_2 conditioning section (maximum CO_2 flow rate: 3-5 kg/h,), an extraction column (height = 40 cm., diameter=23 mm.) and a series of three separators [10] where the solutes are recovered. Carbon dioxide is supplied by Carboxyque Française being of industrial grade. Carbon dioxide flow rate is measured by a mass flow meter (Coriolis effect,type DH006 from Rosemount). A gas totaliser is placed after the separators to measure the volume of CO_2 exiting the system. The column is fed, at atmospheric pressure, with the feed. The system is closed and CO_2 is pumped into the column until the pressure of the experiment was reached. The content of the column is equilibrated during a 10 min period after which extraction started. Pressure and temperature of the separators are mentioned in Table 1. The valves at the bottom of the separators were regularly opened and the precipitated solutes were recovered and weighed. Each sample was analyzed by gas chromatography. At the same time the sample was recovered, the amount of gas passed through and carbon dioxide flow rate, were registered.

c) Gas capillary chromatographic analysis

GC analysis is used for kinetic supercritical fluid extraction control and for components identification. All GC analyses were performed using a Chrompack CP 9002 equipped with a CP-Sil 5 CB capillary column (lenght: 10 m, internal diameter: 0.25 mm, inlet pressure : 35kPa.) and a micro catharometer detector. Oven temperature was initially at 50 °C for 5 minutes, temperature was then raised up to 250 °C at a heating rate of 8 °C/min then isotherm for 5 minutes. The temperature of the detector and the injector was 200°C and 250°C, respectively. The carrier gas flow (helium) was of 3 ml./min.. The splitratio was regulated at 5 ml/min. The samples were dissolved in hexane, or heptane and injected (the injection volume was of 0.5 to 5 µl., depending on dilution).The identification of the individual components was accomplished by comparison with pure standard components retention times:α-thujene, sabinene, myrcene, 1,8 cineole, trans-sabinene hydrate (*Mentha* M_A) , menthol (*Mentha* M_E), menthone, α-terpineole, menthyl acetate, trans-caryophyllene.

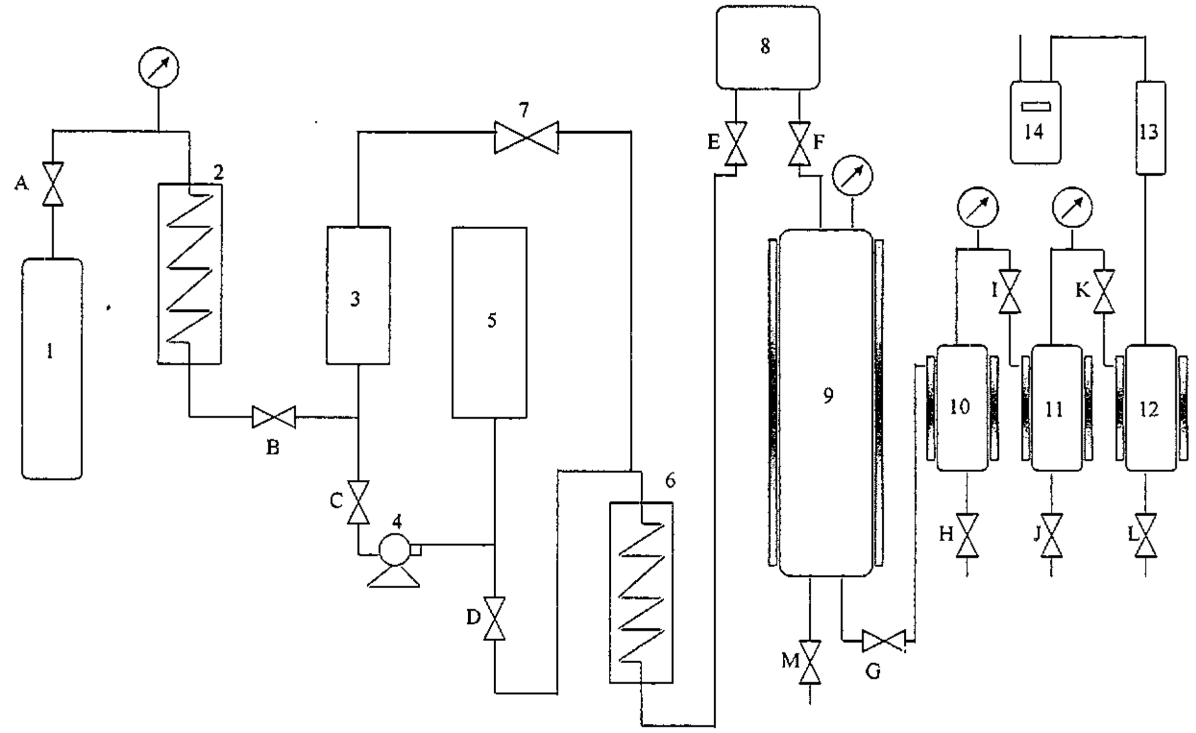

Figure 1.Schematic presentation of the experimental apparatus
1. CO_2 cylinder, 2. Heat exchanger, 3. Liquid CO_2 reservoir, 4. High pressure pump,
5. Pulsations dampener, 6. Heat exchanger,7. Pressure regulation valve, 8.Mass flow meter, 9.Extraction column, 10. , 11. and 12. Precipitation cyclones, 13. Flowmeter, 14. Gas totaliser

Results and Discussion

A valuable extract is considered that which are the closest possible to the vegetable matter. Because the oxygenated monoterpenes have a foundamental contribution to the flavour and fragrance of the extract, the percent of these ones was used as a quality parameter [11]; at the same time the coextraction of unwanted compounds must be reduced as much as possible.

In a preliminary study [9], the essental oil of two have been studied *Nepeta* species :*Nepeta transcaucasica* Grossh. and *Nepeta cataria* L.. The extracts obtained by hydrodistillation and SC-CO2 were analyzed by GC-MS and compared. It seems that the CO_2 extracts have a composition near to the plant. The composition of the extracts are not the same. The yields have also been compared .For example, in the case of *Nepeta Cataria,* the yield of hydrodistillation was 0.49, that of supercritical extraction (P = 100 bar, T = 40°C, Δt = 210 min.) is 0.87. The experimental conditions are mentioned in table 1. Considering, *Mentha M_A* , we have studied the yield (Figure 2) depending on extraction pressure and the influence of the size particle feed (Figure 2). The yield is higher whith at 93-94 bar than at 90 bar . It seems that a decrease of the particle size does not contribute to an increase of the yield. The extracts are analyzed by GC and the percentage area of some identified components are plotted versus time (Figures 3 to 5). When the extraction pressure is 92-94 bar, it is possible to obtain an oil with a better quality, regarding the light components composition. Regarding the evolution of heavy compounds (heavier than bicyclogermacrene) versus time, we could observe that the heavy compounds extraction is increasing as the particle size of the feed is decreasing(Figure 3). Two other process parameters are important : CO_2 liquid or supercritical, downflow or upflow CO_2 through the bed of mint plants.(*Mentha* M_E)The extraction yield is better with liquid (1.59%) than with supercritical CO_2 (1.1%) , but more heavy compounds are extracted. The yield of oil in the CO2 upflow mode reaches 1.1% comparing to 0.66% in the CO2 downflow mode. This result does not agree with the litterature[1].

Mentha hybrid	Exp. N°	Feed Particle size (mm.)	Feed Mass (g.)	Extraction Pressure (bar)	Extraction Temperature (°C)	Δt(1) (min.)	Δt(2) (min.)	Separators* P(bar),T(°C)	CO2 Flowrate (kg./h.)
MA 3.5	5	0.59	15.98	90	50	30	230	I :80,1.7 II :40,4	0.189
MA 3.5 (28/06, 06/07)	7	0.59	16.11	92-94	50	15	240	I :80,1.7 II :40,4	0.212
MA 3.3	8	0.315	19.86	92-94	50	15	240	I :80,1.8 II :40,4	0.234
ME 2.2a	9	0.59	16.26	92-94	50	15	210	I :80,1.8 II :40,3.8	0.215
ME 2.2b	10	0.59	15.84	92-94	26.6	15	240	I :80,1.8 II :40,3.8	0.215
ME 2.2b	11	0.59	13.34	92-94	50	50	180	I :80,1.8 II :40,3.8	0.238

Table 1. CO_2 experimental conditions and results.((1),(2) :equilibrium and extraction duration respectivelly)

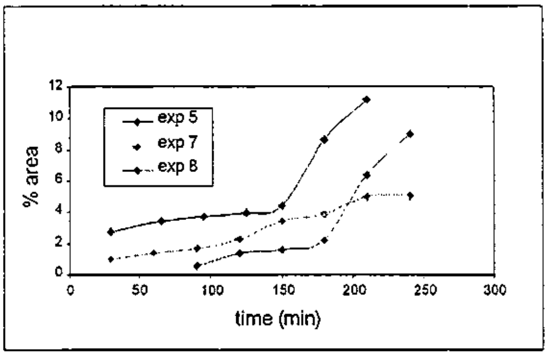

Figure 2. *Mentha* M_A
% area heavy compounds versus time
(> bicyclogermacrene)

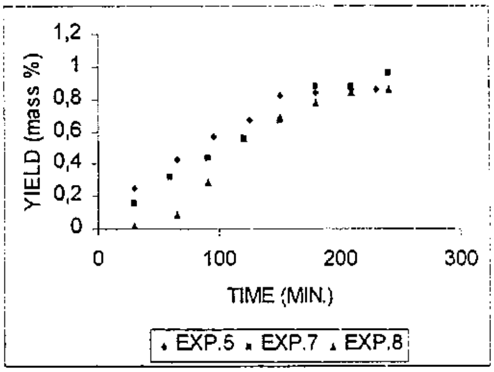

Figure 3. *Mentha* M_A.
Yield (%) versus time

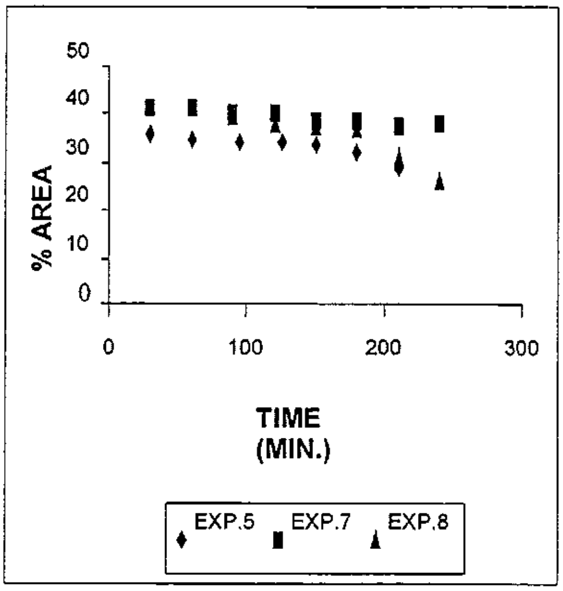

Figure 4.*Mentha* M_A
% area trans-sabinenehydrate versus time

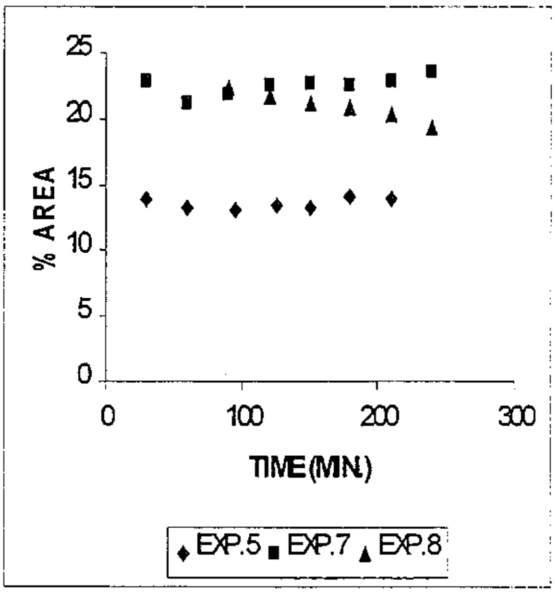

Figure 5.*Mentha* M_A
% area trans-sabinenehydrate acetate versus time

Conclusion

All extracts obtained are yellow liquids at room temperature, with a flavour very similar to the starting material, in opposition to corresponding essential oils which have an unpleasant flavour. iunie The yield of extract as function of extraction time followed for all experiments a kinetic law typical of essentiel oil extraction,being similar to those obtained by other researchers [4]. Upflow of carbon dioxide through the bed of cut plants is more effective than downflow. Liquid carbon dioxide favorites coextraction of large percentages of heavy molecular weight compounds, as shown by the experimental data, this fact is in accordance with the litterature[4].

References

1.Barton P. ;Hughes R.E.Jr. ;Hussein M.M.The Journal of Supercritical Fluids 1992,5(3),157-162.
2.Hawthorne, S.B. ; Riekkola, M.L. ; Serenius, K ;Holm Y. ; Hiltunen, R. ; Hartonen, K J.Chromatography 1993,634,297-308.
3.Reverchon E. ; Ambruosi A. ; Senatore F. Flavour and Fragrance Journal,1994,9,19-23
4.Reverchon, E. ; J. Supercrit. Fluids, 1997, 10,1-37.
5.Kokini, S.,Modern Methods of Plant Analysis, New Series, 1991, 12, 63.
6.Barbu, C., Acta Phytotherapica Romanica, 1995,2,17
7.Pop, E., Third Roumanian International Symposium on Cosmetic and Flavour Products, 1997, 3-6 iunie Iaşi, Romania.
8.Pop, E.,Revista de chimie Bucuresti, 1997,7,587
9.Barth D.,Pop E. ;Hubert N. ;Mihaiescu D.,Gainar I., 5th Meeting on Supercritical Fluids (Eds.M.Perrut ,P.Subra) 1998,2,655-660
10.Perrut,M.,Brevet Francais, nr. 85 104 68 09 07 1985.
11.Reverchon E. ;Della Porta G. ;Senatore F., J.Agric.Food Chem.,1995,43,1654

GVC-Fachausschuß „High Pressure Chemical Engineering“, March 3-5, Karlsruhe, Germany, 1999 GVC FZK '99

Prepurification of Esterase EP10 by Treatment with Supercritical Carbon Dioxide (SC-CO_2)

D.-J. Steinberger*, A. Gießauf, T. Gamse and R. Marr

Institute for Chemical Engineering and Environmental Technology
University of Technology Graz, Inffeldgasse 25
A-8010 Graz, Austria
fax: + 43 316 873 7472
email: steinberger@glvt.tu-graz.ac.at
*Corresponding author

A crude preparation (0,2 U/mg) of esterase EP10 from *Burkholderia gladioli* was purified by treatment with SC-CO_2. The enzyme preparation showed high stability (activity increase to 120,7 %.) against 30 pressurisation / depressurisation steps at 35°C and 150 bar. Incubation for 24 hours in SC-CO_2 at 150 bar and 35°C had less effect on enzyme activity (103,8 %) than incubation at 75°C (residual activity: 62,3 %). By using a purified enzyme preparation (0,4 U/mg) of esterase EP10 no significant effect has been observed. High pressure extraction of crude esterase EP10 with CO_2 at different temperatures, pressures and incubation times exhibited various amounts of activity increase, reaching the highest ones at 500 bar and 1 hour at 50°C (25,3 %) and 25°C (33,4 %). Several fatty acids have been identified in the SC-CO_2 extract by gas chromatography. The addition of entrainers except hexane cause an activity decrease. Fluorescence spectra indicated no conformational change and several biochemical assays no chemical modification of esterase EP10 after treatment with SC-CO_2.

Introduction

Supercritical fluid extraction (SFE) represents a rapidly growing and useful technology with wide fields of applications. The use of enzymes as catalysts in supercritical fluids has been described in the scientific literature since the mid-1980's by Randolph et al.[1], Hammond et al. [2] and Nakamura et al. [3]. The aim of the initial studies was to demonstrate that enzymes are active in SC-CO_2 and which factors cause enzyme inactivation or decrease of enzyme activity.

Only one publication [4] deals with the fact, that SC-CO_2 treatment leads to a significant activity increase (21% and 35%) of a crude α-Amylase mixed with E.coli or Baker yeast at a weight ratio of 9:1 during a sterilisation step at 200 atm and 35°C for 2 hours. But Kamihira at al. [4] did not attach importance to these results. SC-CO_2 is known to be an unpolar solvent. Crude enzyme preparations usually consists of many impurities like carbohydrates, fatty acids, triglycerides, phospholipides and other proteins. Proteins, peptides and amino acids are polar substances that are generally insoluble in SC-CO_2. After SFE they are found in the residue [5].

The aim of this study was to investigate if SC-CO_2 extraction is an appropriate technique to purify crude enzyme preparations of esterase EP 10 from Burkholderia gladioli as well as to analyse the presence of free fatty acids in the extract obtained by this process. To exclude the possibility that during processing enzymes become modified the sample is characterised by fluorescence spectroscopy and biochemical methods. In addition attempts have been made to investigate whether pressurisation / depressurisation steps have influence on enzyme stability of crude and purified enzyme preparations. Besides long term stability studies at higher temperatures were made to report about the activity alteration of crude and purified esterase EP10. To study the influence of entrainers on the prepurification effect, polar and unpolar organic solvents were added to the extraction process.

Materials and Methods

Materials: All chemicals used if not otherwise stated were purchased from Merck (Darmstadt) and were of p.a. (pro analysi) quality. The carbon dioxide with a purity > 99,94 % (v/v) and a dewing point lower than -60°C was purchased from Linde (Graz) and stored in a tank with a capacity of 3200 L. 2-Nitrophenyl butyrate (o-NPB) was supplied by Fluka (Buchs). Esterase EP10 (EC 3.1.1.1) from *Burkholderia gladioli* crude (0,2 U/mg lyophilisate; given by the supplier) and chromatographically (HIC) purified (0,4 U/mg lyophilisate, given by the supplier) was a gift (activities given by the manufacturer) from the Department of Biotechnology, University of Technology Graz. Specification of esterase EP-10: recombinant enzyme overpressed in E.coli BL21 [DE3]. Lipase from Aspergillus niger was supplied by Fluka (Buchs). Hexane (HPLC quality), 2,4,6-trinitrobenzensulfonic acid purum (TNBS) and 5,5'-dithiobis(2-nitrobenzoic) acid were purchased from Fluka (Buchs). 2,4-Dinitro-phenyl-hydrazine was supplied by Sigma Aldrich and bovine serum albumin (purity > 98 %, fatty acid free) was a gift from Hämosan (Austria). Coomassie Brilliant Blue G-250 was provided from Serva. Celluloseacetate filters (not sterile, 0,22 µm) were supplied by Roth (Karlsruhe). Karl Fischer solutions were purchased from Merck (Darmstadt).

Methods: Following assay was used for enzyme activity measurements before and after treatment with SC-CO_2:

Esterase Assay: 10 µL of a substrate solution (84 µL o-NPB dissolved in 916 µL ethanol absolute) was added to 990 µL of an enzyme solution (100 µg esterase EP-10 / mL in 0,1 M Tris(hydroxymethyl)-aminomethan / HCl pH = 7,0). The linear increase of absorbance at 420 nm after seven minutes of incubation was used to determine the enzyme activity.

Crude EP10: 0,26 U / mg lyophilisate; purified EP10: 0,44 U / mg lyophilisate

All absorbance measurements were performed at 25°C with a Shimadzu UV 160A spectrophotometer equipped with a Lauda RM6 temperature control.

Tryptophan fluorescence: Fluorescence spectra of the intrinsic fluorescence of the clear solutions of the proteins (0,1 mg / mL) were recorded with a Perkin Elmer LS50B spectrofluorimeter (instrument settings: excitation wavelength 280 nm, emission wavelength 300-420 nm, excitation / emission slits: 3 nm, scan speed 400 nm /min). The emission spectra recorded are the average of 10 scans.

The proteins were dissolved in the same buffer solution as used for activity measurements and the emission spectra were recorded at 30°C.

Water content of the proteins were determined by Karl Fischer titration at 55°C.

For the characterisation of the enzyme powder following assays were used: Bradford assay for the determination of the protein concentration of the enzyme preparation [6]. Carbonyl assay for identification of oxidant modification in the protein [7]. Sulfhydryl assay to calculate the amount of sulfhydryl groups per mg enzyme powder [8]. TNBS-reactive lysine was estimated according to Kakade and Liener [9].

Gas chromatographic extract analysis: Esterification of the extract was performed as described in [10] for the analysis of free fatty acids. Fatty acid methyl esters were separated by a HP 5890 Series II GC equipped with a flame ionisation detector (detector temperature 300°C) and a temperature controlled autosampler (column: DB-WAX (J&W Scientific) 60 m x 0,323 mm; with a film thickness of 0.5µm, split 1:10). Hydrogen was used as a carrier gas at a flow rate of 0,934 ml / minute. Following temperature program was used : 210°C (4 minutes), 210-240°C (5°C / minute) and 240°C. Peaks were identified by external and internal standardisation using a fatty acid methyl ester mixture from Supelco.

Long term stability: The enzymes were balanced on a filter paper and the folded filter was put into an enzyme reactor (140 mL) placed in a water bath (temperature: 75°C and 35°C). The temperature inside the reactor was measured by means of a platinum sensor. CO_2 was compressed by a piston pump up to 150 bar and the enzyme was incubated at these conditions for 24 hours. During the depressurisation step, temperature never remained under 50°C / 25°C. After incubation the enzyme was stored at -18°C.

Pressurisation / Depressurisation experiments: The same reactor as described above was utilised. The enzyme was now incubated for 1 hour in SC-CO_2 at 150 bar and 35°C. Afterwards it was depressurised to atmospheric pressure (this step lasted about 6 minutes) and again pressurised to 150 bar. This working step was repeated for 30 times. After that, the enzyme was stored at -18°C in the deep freezer.

High pressure extraction: The extraction experiments were carried out in a Spe-ed-SFE (Applied Separations) high pressure CO_2-extraction plant. After the vessel was put in the oven of the extraction plant, the CO_2-inlet pipe was fixed at the bottom of the extractor and the outlet pipe at the top. Extraction experiments were carried out at different pressure (200 bar, 350 bar, 500 bar) and temperature levels (25°C, 50°C, 60°C) and different extraction times (30 min, 60 min, 120 min). The CO_2 flow rate was always about 4,4 L / min. Pressurisation and depressurisation steps were carried out slowly and lasted about 10 ± 3 minutes. During depressurisation the temperature never remained under 20°C. After high pressure extraction the enzyme was stored at -18°C in the deep freezer.

Addition of entrainers: Different solvents (methanol, ethanol, acetone, isobutanol, hexane, heptane, octane) were placed at the bottom of the extraction vessel, whereas the enzyme was placed at the top of the vessel, in a manner that there was no direct contact between the modifier and the enzyme. The amount added to the CO_2 was about 0,7 % (w/w) for each entrainer. The extraction conditions when using an entrainer were always set to 50°C, 500 bar and 1 hour extraction time.

Results and Discussion

Effect of long term incubation on enzyme stability: While enzyme activity of the purified enzyme preparation did not change markedly (residual activity: 93,7 % at 75°C and 98,7 % at 35°C), the activity of crude esterase EP10 decreased to 62,3 %, when incubating at 75°C, but did not change significantly at 35°C (103,8 %). Temperature enhancement seems to have more influence on enzyme stability of crude EP10 than incubation time.

Effect of 30 pressurisation / depressurisation cycles on enzyme stability:
Fig.1 shows the enzyme activities after 30 pressurisation / depressurisation cycles with SC-CO2 at 35°C and 150 bar. Each incubation step lasted 1 hour. The experiment had no effect on the purified enzyme preparation and the appearance of the white powder did not change at all. The 30 pressurisation / depressurisation cycles did not generate any activity loss, in contrary. The enzyme activity of crude esterase EP10 increased significantly to 20,7 %. The crude enzyme preparation became a bright yellow dry enzyme powder by supercritical fluid treatment. An important fact is, that after each depressurisation step the enzyme was contacted with fresh CO_2. This led to a better cleaning effect of the enzyme.

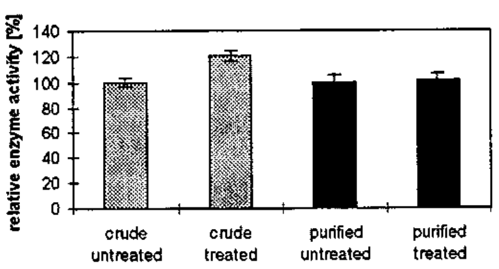

Figure 1. Comparison between enzyme activity of crude and purified esterase EP10 before and after 30 pressurisation / depressurisation steps at 35°C and 150 bar with SC-CO_2.

High pressure extraction with SC-CO_2: To find the best extraction conditions for crude EP10, three different temperatures, pressures and extraction times were investigated. While two variables were kept constant, the third one was varied. Table 1 shows the results of this investigation.

Table1. Enzyme activity of crude EP10 (≈ 50 mg) after high pressure extraction with SC-CO_2. The enzyme activity of the untreated enzyme was set to 100 %.

conditions	**activity [%] mean ± SD**
25°C, 1h, 500 bar (ρ = 1035g/L)	133,4 ± 4,79
50°C, 1h, 500 bar (ρ = 963 g/L)	125,3 ± 7,39
60°C, 1h, 500 bar (ρ = 934 g/L)	110,7 ± 3,94
50°C, ½ h, 500 bar (ρ = 963g/L)	104,1 ± 5,45
50°C, 1h, 500 bar (ρ = 963 g/L)	125,3 ± 7,39
50°C, 2h, 500 bar (ρ = 963 g/L)	114,5 ± 4,90
50°C, 1h, 200 bar (ρ = 784 g/L)	112,2 ± 4,92
50°C, 1h, 350 bar (ρ = 899 g/L)	113,6 ± 7,81
50°C, 1h, 500 bar (ρ = 963 g/L)	125,3 ± 7,39

The highest enzyme activity increase (25,3 %) was achieved with supercritical CO_2 at 50°C, 500 bar and 1 hour extraction time and with liquid CO_2 at 25°C, 500 bar and 1 hour extraction time to 33,4 %. In the field of high pressure extraction, CO_2 density plays an important role. The larger the density of CO_2 the higher prepurification effect can be observed. The activity enhancement of crude EP10 treated at 60°C and 500 bar for one hour amounts to 10,7 %. At this temperature thermal instability gets more and more important. An optimal extraction time was found at 1 hour. Extracting for only 30 minutes does not yet show full purification effect (4,1 % activity increase). Whereas longer extraction times (e.g. 2 hours) already cause increasing inactivation of the enzyme and no further impurities can be removed.

Solubility of unpolar substances in SC-CO_2 also depends on pressure. When extracting crude EP10 at 200 bar and 350 bar at 50°C for one hour the results did not show significant differences (112,2 % and 113,6 %) although CO_2 density enhances from 784 g/L to 899 g/L. Increasing pressure from 350 bar to 500 bar gives an enhancement in purification effect from 113,6 % to 125,3 %. That means that an efficient purification of crude esterase EP10 is only obtained at pressures higher than 350 bar or / and CO_2 densities higher than 900 g / L.

There is also a great difference in appearance of crude esterase EP10, before and after treatment with SC-CO_2 (extraction at 50°C, 500 bar, 1 hour). The crude enzyme preparation has a yellow colour and a fatty consistence (water content: 6,7 ± 0,42 (w/w)), while the treated enzyme preparation shows a brighter yellow tint and a powdery consistence.

To investigate the influence of SC-CO_2 extraction on purified preparations of EP10, two experiments were carried out under the same extraction conditions as those which had given the highest activity increase with the crude preparation of EP10.

The enzyme activities of both extractions were slightly higher (at 50°C: 108,1 ± 6,58 %; at 25°C: 109,0 ± 5,72 %) in comparison to the untreated reference sample (100 %), but did not reach the values of the crude preparation. In fact, the chromatographically purified white enzyme powder (water content: 9,5 ± 0,38 (w/w)) has less unpolar impurities which are soluble in SC-CO_2 than the crude preparation.

Fig. 2 shows the residual enzyme activity of crude preparation of esterase EP10 when extracting the enzyme at 50°C, 500 bar for one hour and adding an entrainer with an amount of 0,7 % (w/w) for each solvent.

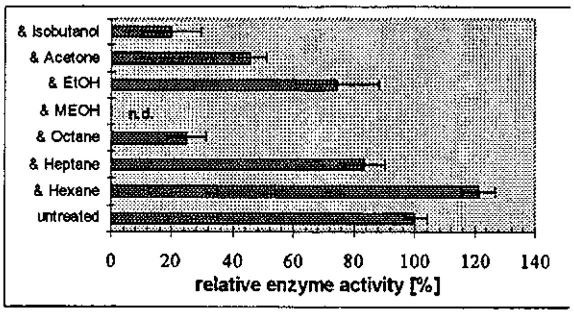

Figure 2. Comparison between residual activities of crude esterase EP10 after SC-CO_2 with different entrainers (0,7 (w/w)) at 50°C, 500 bar and 1 hour and crude esterase EP10 untreated.

While unpolar solvents strengthen the unpolar nature of SC-CO_2, polar entrainers can also solve polar impurities like carbohydrates. But neither the polar modifiers (ethanol, methanol, acetone, isobutanol) nor the unpolar entrainers (hexane, heptane, octane) caused a further activity increase (except hexane) on the contrary they inactivated the enzyme. One possible reason might be, that during pressurisation droplets of the entrainer were dragged along by the CO_2 stream and therefore moistens the enzyme. But this effect could not be determined, because no sight glasses are installed in the reactor.

Characterisation of the enzyme powder:

Bradford assay: The protein concentration of crude and purified esterase EP10 was analysed and compared with those enzyme preparations which were extracted at 50°C, 500 bar and 1 hour without adding an entrainer. The protein content of the crude preparation is much higher than of the purified one, because all other foreign proteins are also detected by this method. The value of the purified preparation (3,58 % (w/w)) represents the real amount of esterase EP10 in the preparation. Because of the purification effect of the SC-CO_2 extraction the protein content of the crude preparation of EP10 changes to a 4,53 % higher amount (protein content of the untreated preparation was set 100 %). The protein content of the purified preparation did not increase significantly (1,12 %). This is due to the fact that the prepurification effect of SC-CO_2 extraction is markedly higher in case of crude EP10 than purified EP10.

Carbonyl assay / Sulfhydryl test / TNBS test: The amount of carbonyl groups / sulfhydryl groups / amino groups of crude preparation of esterase EP10 was measured before and after treatment (50°C, 500 bar, 1 hour) with SC-CO_2.

The results are the values per gram enzyme preparation and are listed in Table 2.

Table 2. Values of carbonyl groups / sulfhydryl groups / amino groups of crude preparation of esterase EP10 before and after treatment (50°C, 500 bar, 1h) with SC-CO_2.

	Carbonyl Assay [µmol carbonyl groups/g]	Sulfhydryl test [µmol sulfhydryl groups/g]	TNBS test [nmol NH_2 groups/g]
crude, untreated	19,8 ± 0,83	0,25±0,001	9,4 ± 0,34
treated (50°C, 1h, 500 bar)	22,4 ± 0,71	0,27±0,005	10,9 ± 0,21
increase [%]	16,0	13,1	8,0

The values of the treated enzyme preparations are in each instant a small amount higher (8,0-16,0 %) than those of the untreated ones. The reason is that through treatment with SC-CO_2 a prepurification effect of the enzyme preparations has been obtained.

Fluorescence spectroscopy: No changes of fluorescence emission maxima (< 1,5 nm) of the tryptophan residues before and after SC-CO_2 treatment can be observed, indicating that no conformational change of the protein occurs. High pressure extraction with SC-CO_2 does not cause any sustained changes of the enzyme.

Fatty acid analysis: During the high pressure extraction of esterase EP-10 an oily, yellow extract was separated. The extract contained the following free fatty acids:

As the main components palmitic acid (C16:0), stearic acid (C18:0) and oleic acid (C18:1) were identified. In the extract also myristic acid (C14:0), palmitoleic acid (C16:1) and linoleic acid (C18:2) were present.

Conclusion

The results show that a crude preparation of esterase from *Bukholderia gladioli* can be purified by treatment with SC-CO_2. The separation of fatty acids leads to a higher protein content in the enzyme powder and a significant higher enzyme activity.

Several biochemical and biophysical methods show that no conformational change during the extraction appears.

A further intention in future will be to check other crude preparations of different enzymes, in particular those which have unpolar impurities and are commonly used in industry.

References

1. Williams, D.F. *Chemical Engineering Science* **1981**, 36, 11, 1769-1788.

2. Paulaitis, M.E. *Reviews in Chemical Engineering*, **1983**, 1, 2, 179-250.

3. Randolph, T.W. *Trends in Biotechnology*, **1990**, 8, 78-82.

4. Kamihira, M.; Taniguchi, M. and Kobayashi, T. *Agriculture Biological Chemistry*, **1987**, 51 (2), 407-412.

5. Weder, J.K.P. *Cafe Cacao The*, **1990**, 34 (2), 87-96.

6. Bradford, M.M. *Analytical Biochemistry*, **1976**, 72, 248-254.

7. Fields, R. and Dixon, H.B.F. *Biochemical Journal*, **1971**, 121, 587-589.

8. Ellman, G.L. *Archives of Biochemistry and Biophysics*, **1959**, 82, 70-77.

9. Kakade, M.L. and Liener, I.E. *Analytical Biochemistry*, **1969**, 72, 273-280.

10. Sattler, W.; Puhl, H.; Hayn, M.; Kostner, G.M. and Esterbauer, H. *Analytical Biochemistry*, **1991**, 198, 184-190.

Supercritical Fluid Extraction of the Oil from the Tucumã Pulp (*Astrocaryum vulgare* Mart.) using Carbon Dioxide

Luiz Ferreira de FRANÇA*[1]; Torsten CHRISTENSEN[2]; Gerd BRUNNER[2].
[1]LAOS/DEQ/CT/Universidade Federal do Pará (UFPA), Rua Augusto Corrêa, nº 01- CEP 66050-970, Belém, Pará, Brasil.
[2]Technische Universität Hamburg-Harburg, Eissendorfer Str., 38, 21073, Hamburg - Germany

The fruit of the Tucumã palm (*Astrocaryum vulgare*, Mart.) is a rich source of oil. Its dried pulp has got an oil-content ranging from 33 to 47,5 % corresponding to an oil-content of about 16 % in the fresh pulp. This oil of high nutritional value is edible and tasty. It contains about 51,000 UI of vitamin A activity, corresponding to 2,000 ppm of carotene. This carotene content is much higher than that of other fruits. Extraction experiments were carried out at temperatures of 40, 55 and 70°C under their respective pressures (200, 250 and 300 bar). A high pressure experimental apparatus with a continuous flow through a fixed bed was used, allowing an independent control of temperature, pressure and flow rates. About 20 g of dry tucumã pulp, with a medium diameter of 0.5 mm, was placed in a 1.76 cm diameter fixed bed with a height of 18 cm. The experiments have been carried out at three flow rates, 5, 10 and 15 l/min (measured under room conditions). In the constant extraction rate period, the oil concentration at the outlet of the extractor did not change at 5 and at 10 l/min flow rates. This concentration was taken as the saturation concentration or solubility. The extracted oil was analyzed by spectrometry and gas chromatography of the methyl esters. A sharp increase in the carotene concentration in the oil was observed during the extraction. This increase started when the extracted oil reached a weight of 4.5 g, corresponding to 75% of the extractable oil. At this point the extraction curve changes from the linear part to the non linear one.

Introduction

The Palm fruits from the Amazon region are abundant and promising sources of high nutritional vegetable oils. Tucumã (*Astrocaryum vulgare*, Mart.) is a palm fruit similar to the Palm Oil fruit (*Elaes guineensis*), which grows near to rivers but in areas not covered with water. The fruit, with a weight ranging from 30-35g, consists of the pulp and the pit (kernel and hard peel), each one of them having 50% of the total weight. Its dried pulp has got an oil content ranging from 33-47,5%, about 16% of the fresh pulp. The kernel contains 30-50% corresponding to an oil-content of about 10% of the whole [1, 2, 3].

The oil from the Tucumã pulp is an edible and tasty oil with high nutritional value. It contains about 51,000 UI of vitamin A activity, corresponding to 2,000 ppm of carotene which is higher than that of other fruits [3]. Moreover it has a high amount of tocopherol and high content of unsaturated fatty acid compounds. Because of this the Tucumã palm has become the object of some studies in the recent years. Today, only a few of these palms are cultivated and exploited, and the processing of many fruits is still on a small commercial scale.

As the carotene is a thermolabile and unsaturated molecule, the use of high temperatures or chemical products can destroy it, either by degradation or by oxidation. Because of this, the use of supercritical CO_2 has been studied as an alternative method to extract the high value product, such as carotene and tocopherol [4, 5, 6]. In this extraction many fat soluble compounds such as carotene and tocopherol, which are poorly soluble in CO_2, are often coextracted in higher amounts, much higher than expected. This is because the lipids act as a entrainer [6].

Previous studies have been conducted to determine the quality of oil extracted from many oil palm fruits such as buriti (*Mauritia flexuosa*) and dendê (*Elaes guineensis*) . During the extraction, these investigations showed a significant increase in the carotenoid concentration in the oil, reaching highly concentrated fractions in the decreasing extraction rate period [7,8].

The objective of this paper is to study the extraction rate of oil from the dried tucumã pulp using supercritical CO_2 as a function of pressure, temperature and solvent flow rate. The effect of the pressure and the temperature on the solubility is discussed. extraction conditions on. In addition, the composition of lipids and carotenes is evaluated.

Materials and Methods

Materials. The tucumã fruits were picked from palm trees located in fluvial areas, with marine influences, in the municipal district of São Caetano of Odivelas and on the island of Marajó, in Pará. The fruits were treated with vapor, for about 30 minutes in order to facilitate the separation of the pulp from the pit and to inactivate the enzyme lipase which causes the decomposition of the oil. After the separation, the pulp was dried in a oven with circulating air (FABBE, Brazil, mod. 179) for 36 hours at 60°C. Then the pulp was ground in a comminuting mill (Geratetechnik, Germany, Mod. A-70) and passed through a 1,0 mm sieve. The dried material was packed in plastic bags and kept in a refrigerator at about 278 K. The 99,9 % carbon dioxide was delivered by S. A. White Martins (Belém, Brazil).

Apparatus. The extractions were performed with the apparatus shown in Figure 1, which has been described previously [8]. A ½" steel tube (ID = 1.76 cm, H = 20 cm) containing the raw material, was inserted into a 1000 cm^3 stainless steel autoclave extractor. Between the steel tube and the internal wall of the autoclave there was a seal to assure no by-pass of the flow. The recycle valve in the gas compressor was used to control the gas flow. A thermostatic bath (Haake Mess-Technik GmbH, Karlsruhe, Germany, Model: N3) has been used to maintain the operation temperature constant inside the jacket of the extractor and the extractor temperature was measured by a NiCr-Ni thermocouple with a precision of ± 0.5 K (SAB GmbH & Co, Viersen, Germany, Model: MTE-303). The pressure inside the extractor was monitored by a bourdon manometer with a precision of ± 0,1 MPa (Wika Alexander Wiegand GmbH, Klingenberg, Germany, Model: 332.30, 0 - 40 MPa). In the control valve, the oil and gas phases were separated by simultaneous pressure reduction and heating, and the oil was collected in the glass tube inside the separator, (a 130 cm^3 small stainless steel vessel). The gas is passed through a flow totalizer (Bopp & Reuter Mess-Technik, Alemanha) before being exhausted.

Raw material characterization. In order to characterize the tucumã dried pulp the following analysis was made: a) density, by the picnometry method, using as a fluid the finest fraction of the dried kaolin sieving (53-74 μm diameter) [9]; b) Humidity, by drying the material at 105°C, until constant weight; c) lipids, by AOAC 920.39 standard method [10]; and d) protein by AOAC 320.176 standard method [10], using 6.25 factor.

Carotene determination. The extracts (20-30 mg) were analyzed using a spectrophotometer UV/Vis (CELM, Brazil, Mod. E225D). They were diluted in 10 ml of petroleum ether (CHEMCO, Brazil, 30-60°C) and the absorbance was read at 450 nm. The carotenes in the extracts were calculated in terms of β-carotene using a standard absorbance curve calibrated with β-carotene (> 99 %, Merck, Darmstadt, Germany). The standard curve was prepared with 0.1 g of β-carotene diluted up to 100 ml in petroleum ether. Aliquots taken from this solution were then diluted to 5 different concentrations. The absorbance was read at 450 nm.

Chromatographic analysis. About 0.1-1g of the extract was saponified with NaOH 0.5 M, under reflux for one hour. Then the solution was washed several times with hexane. To this aqueous solution HCl 1.0 M was added, until pH = 1 was reached. The fatty acid was extracted from this solution by a mixture of hexane and diethyl ether (1:1). Later the solvent was evaporated at 60°C and the fatty acids were esterified with methanol and a small amount of sulfuric acid, used as catalyzer, by boiling it for two hours under reflux. 1.0 mL of hexane and 2.0 mL of diethyl ether were added for each 6.0 mL of solution and completed with water up to 50 mL. This solution was shaken vigorously and later put to rest. The organic phase is separated with a capillary pipette and injected into a gas chromatograph (HP, mod. 5890 A), equipped with a flame ionization detector and a Carbowax 20 M column (25 m x 0.32 mm x 0.30 μm). The carrier gas was helium (1.89 mL/min). The temperature was kept at 383 K for 1 min, then risen to 443 K at 10 K/min and kept at this temperature for 2 min, then risen again until 446 K at 1.5 K/min and finally up to 453 K at 1 K/min, and kept at this temperature for 7 min. The temperature of the detector was 493 K and that of the injector was 383 K. The analysis was performed comparing the obtained peaks with those obtained by standard solutions of fatty acids methyl esters. The unidentified peaks were not taken into consideration.

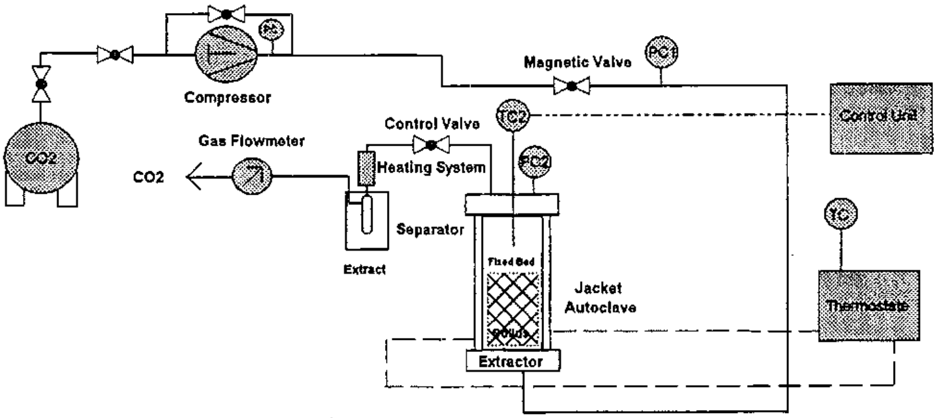

Figure 1. Flowsheet of the extraction apparatus

Results and Discussion

The solid material used in all extractions had the characteristic shown in Table 1. The mean diameter before the extraction was 0.55 mm and after it was 0.35 mm.

Table 1: Characteristic of the tucumã dried pulp

humidity	2.60 % w/w
density	0.724 g/cm^3
total amount of lipids	30.52 % w/w
total amount of proteins	5.46 % w/w

The extraction experiments have been carried out with 20.0 g of tucumã dried pulp, at 313, 328 and 343 K under their respective pressures (20, 25 and 30 MPa), using a gas flow corresponding to 10.0 L/min, under room conditions. The average height of the fixed bed in the tube was 18.0 cm before and 13.5 cm after the extraction. The extracted material was then submitted to a soxhlet extraction to verify the remaining amount of oil. The residual humidity was also determined. The extractions were executed twice at the same temperature and pressure. The average values and their medium deviation can be found in Table 2.

Table 2: Survey of the total amount of extracted oil

P MPa	T [K]	Amount of extracted oil [g]			Humidity
		CO_2	hexane	total	[%]
30	313	6.17 ± 0.01	0.21 ± 0.02	6.38	1.37 ± 0.28
25	313	6.14 ± 0.02	0.22 ± 0.04	6.36	1.24 ± 0.16
20	313	6.19 ± 0.01	0.22 ± 0.01	6.41	1.32 ± 0.14
30	328	6.16 ± 0.03	0.22 ± 0.03	6.38	1.43 ± 0.13
25	328	5.99 ± 0.04	0.40 ± 0.07	6.40	1.59 ± 0.21
20	328	4.29 ± 0.03	2.08 ± 0.18	6.37	1.72 ± 0.13
30	343	6.18 ± 0.01	0.23 ± 0.05	6.41	1.35 ± 0.12
25	343	5.72 ± 0.06	0.72 ± 0.17	6.45	1.69 ± 0.07
20	343	3.05 ± 0.07	3.29 ± 0.14	6.34	1.97 ± 0.10

The experimental error was: ± 0.5 K for temperature and ± 0.1 MPa for pressure.

All extractions showed good reproducibility, and the first part of the extraction curve was linear, characterizing the period of the constant extraction rate which goes up to 4.5 g of extracted oil. From this point on, the extraction curve presented a decreasing extraction rate period. In the case where the extractions were not performed completely, the extraction curves was a straight line until 4.5 g (see Figure 2). Extraction rates obtained in all extractions, at different temperatures, at 30 MPa, presented similar values. These values were slightly higher than that obtained at 25 MPa and 313 K. Since the extraction rate is directly propocional to the solubility at constant solvent flow rate, the solute vapor pressure increase should make up for the density decrease, when the temperature increases. In fact, this intersection point for the isotherm solubility has been observed for soybean oil in CO_2 at about 28 MPa [11].

The smallest extraction rate was observed at 20 MPand 343 K. The extraction curves obtained at 20 MPa and 313 K were identical to those obtained at 25 MPa, for 328 and 343 K. The extraction curves with different configurations are presented in Figure 2.

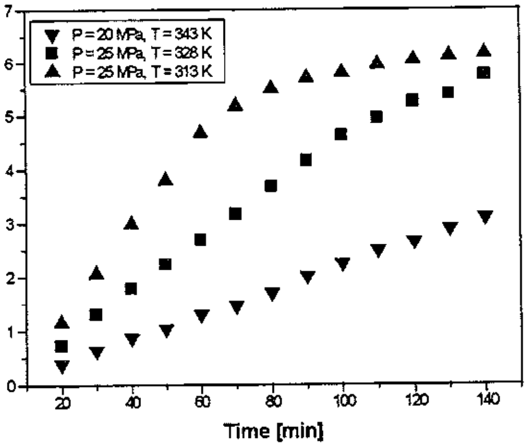

Figure 2: Experimental extraction curves. The data points represent an average of two determinations, with 18 g/min.

Two experiments, one with a higher flow rate, 27 g/min, and another with a lower flow rate, 9 g/min, were carried out to verify the behavior of the outlet oil concentration. The condition was that of the maximum mass transfer rate, 30 MPa and 343 K. The plot corresponding to the mass of the extracted oil *versus* mass of CO_2 had no change in the range from 9 to 18 g/min (10 L/min, under room conditions). But at 27 g/min a decrease of the slope was observed. Therefore it can be assured that the solubility for the intermediate flow rate was reached. Since the other experiments were done using a flow rate of 18 g/min, the outlet oil concentration can be taken as the solubility. A linear regression was performed on the experimental data corresponding to the linear part and the average values for each condition are presented in Table 3.

At constant temperature the solubility increases as the pressure increases. Nevertheless, at 313 K, the increase in solubility is small in the range from 25 to 30 MPa, it is smaller than that observed at other temperature. At 30 MPa, the solubility values were approximately the same, for the three studied temperatures. A similar behavior has been observed for primrose oil solubility within the range from 313 to 333 K [12]. The effect of pressure on tucumã oil solubility is shown in Figure 3. A comparison with the canola seed oil solubility data reported in literature shows a good agreement at 343 K for all pressures. A good agreement is also observed at 20 MPa for all temperatures.

Table 3: Tucumã oil solubility in supercritical CO_2, in mg/g CO_2.

Pressure [MPa]	Temperature [K]		
	313	328	343
30	5.42 ± 0.22	5.09 ± 0.16	5.74 ± 0.11
25	5.01 ± 0.09	3.39 ± 0.05	2.70 ± 0.04
20	3.00 ± 0.04	1.86 ± 0.03	1.27 ± 0.03

In Figure 4, the tucumã oil solubility is plotted as a function of temperature, at studied pressures. At 20 and 25 MPa, the solubility decreases with the increase in the temperature, whereas at 30 MPa the solubility decreases until the minimum value at 328 K, and then increases with the increase in the temperature. The dependence of the solubility on the temperature changes because at low pressures the solution enthalpy is negative whereas at high pressures it is positive [14].

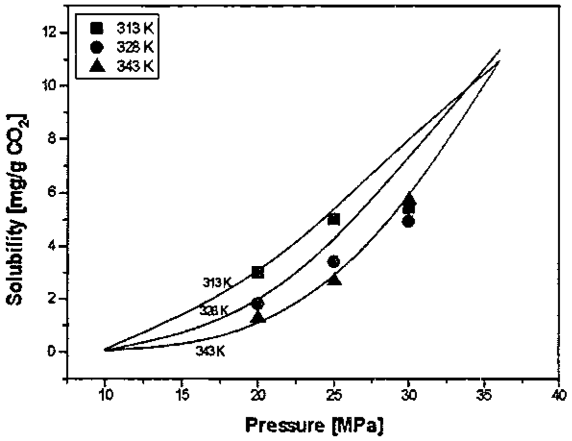

Figure 3: The effect of the pressure on the tucumã oil solubility. The lines represent data of literature for canola seed oil [13]

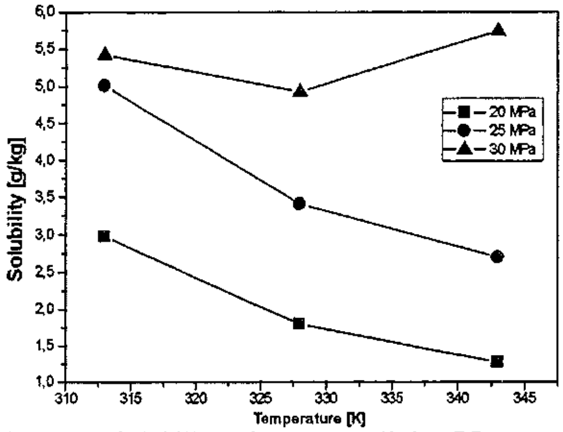

Figure 4: Solubility of tucumã oil in CO_2 as a function of temperature.

Carotene. To evaluate the behavior of carotene concentration in the oil during the extractions by CO_2, the oil from the soxhlet extraction was used as reference. This oil presented about 2000 ppm of carotene. A sharp increase in the carotene concentration during the extraction could be observed. This increase starts at about 4.5 g of the extracted oil. At this point the extraction curve changes from linear to non linear. All extractions showed the same behavior: a constant carotene content until 4.5 g and a sharp increase after that. The carotene concentration at the end of the extractions was always about 10,000 ppm. In Figure 5, the configuration of the carotene concentration for several extractions is depicted.

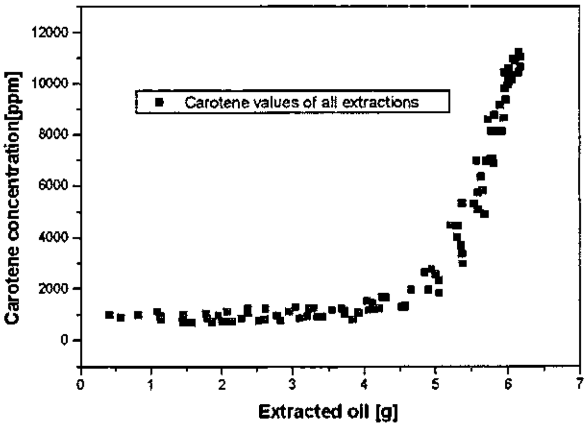

Figure 5: Carotene yield *versus* amount of extracted oil

It could be observed that pressure and temperature do not influence the configuration of the carotene concentration in the extracted oil. All extractions which have been carried out completely lead to an entire depletion of the carotene from the raw material.

The course of the carotene concentration offers the possibility to separate the extract in two fractions: one with 75% of the oil, containing 1,000 ppm of carotene and other with 25% of the oil, containing more than 5,000 ppm.

Fatty acid methyl ester. In order to verify the change in the oil composition in relation to the fatty acids, a Gas Chromatography (GC) analysis was carried out on the taken samples. The examined samples were those obtained at 328 K, at different pressures, 30, 25 and 20 MPa To compare the results of different extractions the fatty acid distribution was plotted against the amount of extracted oil. The results are depicted in Figure 6.

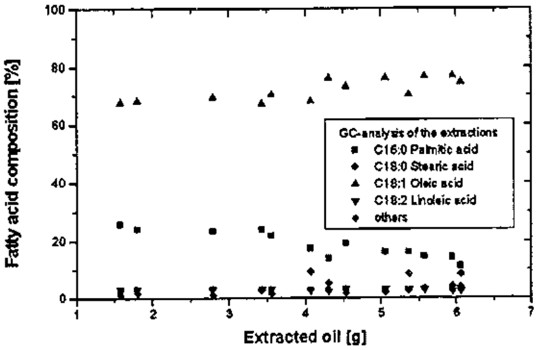

Figure 6: Fatty acid distribution *versus* amount of extracted oil.

The composition of the fatty acids only shows a slight change. The palmitic acid concentration is increasing during the extraction. The concentration of linoleic acid and stearic acid remains nearly constant. Other fatty acids which represent lower molecular fatty acids, from C8 to C14, show a slight increase during the extraction.

References

[1] R. Rodrigues Lima, L. Carlos Trassato, and V. Coelho, O Tucumã: Principais Características e Pontencialidade Agroindustrial, Boletim de Pesquisa n. 75, EMBRAPA-CPATU (1986).

[2] B. Cavalante, Frutas Comestíveis da Amazônia, Ed. CEJUP, Museu Paraense, Emílio Goeldi (1991).

[3] H. Serruya, M. H. da Siva Bentes, and J. G. Ribeiro Tostes, Análise dos Componentes Principais de Algumas Palmaceas da Amazônia, Proceedings of 6° Encontro de Profissionais de Quimica da Amazônia (1988).

[4] A. Birtigh, M. Johannsen, and G. Brunner, J. Sup. Fluids, 8 (1), 46 (1995).

[5] Z. Shen, M. V. Palmer, S. S. T. Ting, and R. J. Fairclough, J. Agric. Food Chem, 44 (10), 3033 (1996).

[6] P. Manninen, J. Pakarinen, and H. Kallio, J. Agric. Food Chem, 45 (7), 2533 (1997).

[7] L. F. França, and M. A. A. Meireles,Ciênc. Technol. Aliment., 17 (4), 384 (1997).

[8] L. F. França, G. Reber, M. A. A. Meireles, N. T. Machado, and G. Brunner, J. Sup. Fluids, accepted for pubication (1988).

[9] B. Buczek, and D. Geldart, Powder Technology, 45, 173 (1986).

[10] Official Methods of Analysis of the Association of Official Agricultural Chemist, 16ª Ed., 1995.

[11] E. Sthal, W. Quirin, A. Glatz, D. Gerard, and G. Rau, Ber. Bunsenges. Phys. Chem., 88, 900 (1984).

[12] F. Favati, J. R. King, and M. Mazzanti, J. Am. Oil Chem. Soc., 68 (6), 968 (1991).

[13] M. Fattori, N. R. Bulley, and A. Meisen, J. Am. Oil Chem. Soc., 65 (6), 968 (1988).

[14] G. Brunner and S. Peter, Sep. Sci. and Tech., 17 (1), 199 (1982).

Dipl.-Ing. Wagner Meß- und Regeltechnik GmbH
Pirazzistraße 18 · 63067 Offenbach/Main
Tel. 0 69/ 82 97 76 - 0 · Fax 0 69 / 82 97 76 - 10

WAGNER
Meß-und
Regeltechnik

Massflow- and Pressure Meters/Controllers for Gases and Liquids

up to 700 bar !!!

We are specialised in instruments for high pressure application. World wide service and support. Please contact us for detailed brochures and more information.

- **Massflowmeters and - controllers for gases up to 700 bar**
- **0,1 - 5 mln/min up to 1250 ln/min N2**
- **SS 316**
- **Seals Viton, Kalrez, EPDM**
- **Fluidtemp. up to 70°C, higher on request**
- **Analog versions for 0-5(10)V, (0)4-20 mA reading and setpoint**
- **Digital versions for RS 485 connections and DDE server software for Windows applications**
- **special Vary-P-valves**

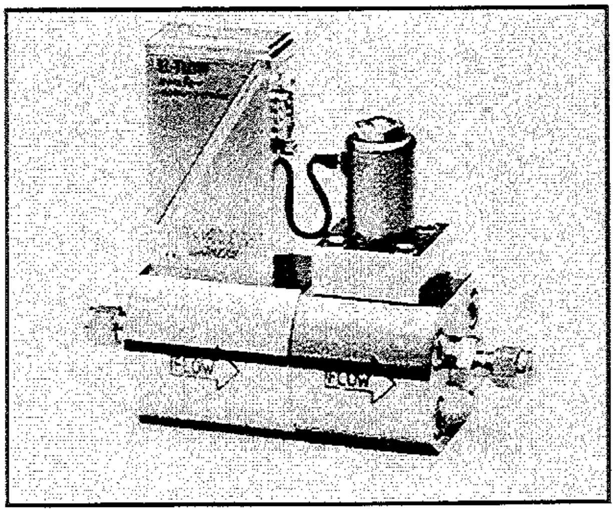

Flowcontroller F-232M

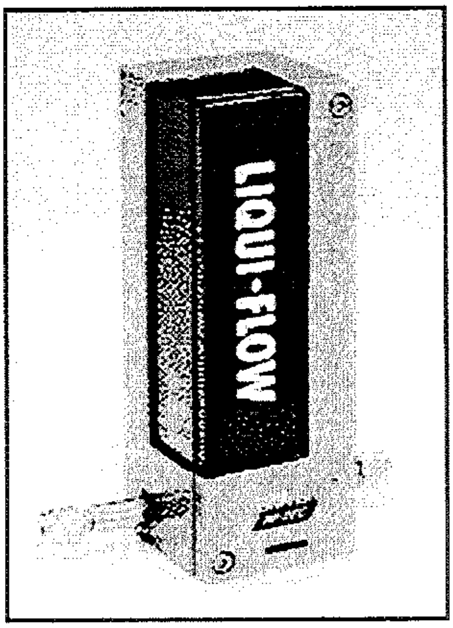

Liquid Flowmeter L1

- **Massflowmeters and -controllers for**
- **liquids up to 400 bar**
- **0,0125 – 0,25 g/h up to 20 kg/h H2O**
- **SS 316**
- **Seals Kalrez, PTFE, others on request**
- **Fluidtemp. up to 70°C**
- **Analog versions for 0-5(10)V, (0)4-20 mA**
- **Digital RS232 connection with DDE server software for Windows combined with E-7000 readout systems**
- **Special Vary-P-valves**

Particle Formation

Powder Generation by high pressure Spray Processes

Eckhard Weidner
Ruhr-University, Process Technology IB6/126, Universitätsstr. 150, 44780 Bochum,
Tel. 0234 700 6680, Fax 0234 7094 277, email: weidner@vtp.ruhr-uni-bochum.de

The use of supercritical fluids to generate solid particles with specific properties is investigated world-wide by numerous groups. Often the aim is, to obtain particles with micron and submicron size. Several methods for „powder generation by supercritical fluids" are known and meanwhile a broad range of applying the different methods to inorganic and organic compounds is covered. These methods are compared in terms of their technological properties (mode of operation, gas consumption, pressure, volume of high pressure equipment, separation of solids from gas and liquid). Considering large-scale applications, a continuous operation mode with reasonable gas consumption is favored. Such a process is described for manufacturing powder coatings by a continuous process for mixing and powder generation. A plant, with a capacity of 20kg/h of powder, and the process features will be presented. The process may not only be applied to reactive mixtures like coatings, but also for powder generation from non-reacting polymers, blends and other compounds, like e.g. emulsifiers, fats or natural products.

In addition to particle size reduction, gas driven spray processes also offer new possibilities for producing enlarged particles. This is exemplified by the so-called CPF-technology (Concentrated Powder Form). By spraying gas saturated solutions and admixing a solid carrier material with the spray, powderous agglomerates with unusual high liquid concentrations of up to 90wt% are obtained. One function of the gas, which must be at least partially soluble in the liquid, is to generate small droplets. These droplets may infiltrate porous substrates or may agglomerate solid, non-porous carrier materials. Infiltration and agglomeration is promoted by the expanding gas which causes an intensive mixing between liquid and solid substrate. Properties as liquid concentration, release and dispersion of active ingredients may be adjusted to customer needs.

Processes for Particle generation with compressed gases

Even in the first publications on solubility phenomena under near-critical conditions the formation of „snow" by expansion of a binary solution was described [1]. Precipitation of solids from liquid solutions by addition of pressurized gases was already proposed at the beginning of this century [2]. In the 70's and 80's processes based on these (perhaps meanwhile forgotten) observations were developed. These processes, that have been studied intensively by numerous groups, are:

- High pressure micronisation [e.g. 3,4]
- RESS (Rapid Expansion of a Supercritical Solution [e.g. 5]
- GAS (Gas Antisolvent Process) [e.g. 6]

In the past 10 years modifications and additional processes have been proposed:

- PCA (Precipitation with a compressed Anti-solvent) [1]
- SEDS (Solution Enhanced Dispersion of Solids)
- PGSS (Particles from Gas Saturated Solutions) [7,8]

Based on this methods a large number of applications, both for organic and inorganic substances were developed. The particles and powders are to be used for electronic, ceramic, food, pharmaceutical, coating, textile, cosmetic, polymer, chemical or biotechnological applications.

A principle flow scheme of the high pressure micronisation process and the RESS-process is shown in fig. 1.

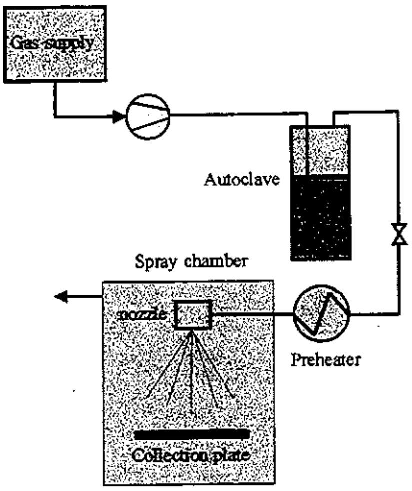

Fig. 1: High Pressure Micronisation, RESS-Process

---

[1] A description and a survey on the state of the art for the different processes is given in [9].

In a pressure vessel, the substance to be powdered (in most cases a solid) is dissolved in a supercritical gas. Due to the limited solvent power of the gas rather high pressures have to be applied to dissolve a certain quantity. Characteristic conditions are pressures up to 600 bar with rather low mass concentrations of a tenth of a percent up to some percentage of the substance to be powered. Thereby gas consumption may reach some hundred kilograms per kilogram of powder. The supercritical solution is expanded in a nozzle. To avoid plugging, the solution is preheated. During expansion, temperature and pressure decrease rapidly, causing the dissolved matter to precipitate in a fine dispersed form. Quantitative collection of the particles that are diluted in a large amount of gas is a challenging task, that has to be solved if large quantities of powders are to be produced.

The GAS/PCA/SEDS-process overcomes the limited solvent capacity of supercritical gases for substances with high molecular weight by using a classical, liquid solvent. The solvent is saturated with the substance to be powdered. This solution is diluted by contacting it with a supercritical gas. The above mentioned processes differ in the way how this contact is achieved (e.g. spraying the solution in a supercritical gas, spraying the gas into the liquid solution and so on). The solvent power of the classical solvent is reduced by the gas, initiating precipitation of the substance to be powdered. The following steps are filtration and drying of the fine dispersed solid material. The dried powder has to be removed from the autoclave and the drying gas must be separated from the used solvent.

The restrictions arising from the difficult product and gas-recovery in the RESS- and GAS/PCA/SEDS -processes are avoided by the PGSS-method (fig. 2).

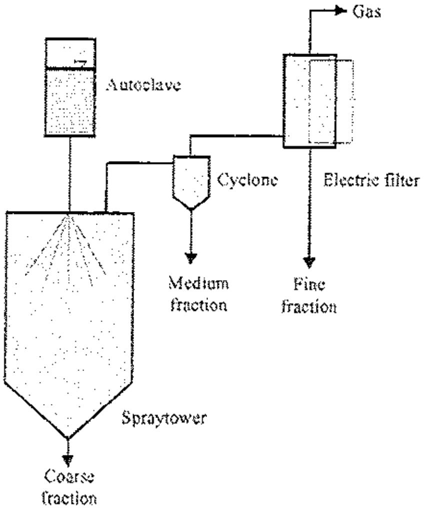

Fig. 2: PGSS-Process

In a laboratory setup, the substance to be powdered is melted in an autoclave. A pressurized gas is dissolved in the melt and forms a solution. At moderate pressures (typically between 70 and 200 bar) gas concentrations of 5 to 50 wt% in the melt/solution are obtained. The dissolution of gas in a liquid substance is even possible, when the gas possesses no solvent capacity for the substance to be powdered. The gas saturated solution is expanded in a nozzle. Cooling and volume increase of the released gas causes the substance to precipitate in a fine dispersed form. The rather low amount of gas (<0,1kg.....1kg of Gas/kg of powder) makes sedimentation in a spray tower and centrifugal forces in a cyclone an useful tool for powder separation. Small particles might be collected by electrical forces or fine filters.

In tab. 1 some features of the described processes are summarised and compared.

	RESS	GAS/SAS/ PCA	PGSS
Establishing gas containing solution	discont.	semicont.	cont.
Gas demand	high	medium	low
Pressure	high	low to medium	low to medium
Solvent	none	yes	none
Volume of pressurized equipment	large	medium to large	small
Separation Gas/Solid	difficult	easy	easy
Separation Gas/Solvent	not required	difficult	not required

Tab. 1: Technological features of RESS, GAS and PGSS-process - Comparison

From this comparison it can be said, that the PGSS-process offers certain advantages if a competitive, large-scale production is considered. The amount of required gas is low and the separation of gas and powder can be achieved by approved methods. An important feature is the possibility for a fully continuous operation. This will be further illustrated on a process for producing powder coatings.

Continuous production of powder coatings by the PGSS-process

The classical process (fig. 3) for manufacturing of powder coatings comprises to establish a premix (A,B,C,D) of the ingredients (binder, hardener, filler, colour, stabilizer, lubricants, degassing agent).

This premix is melted and homogenized in an extruder (2-4).

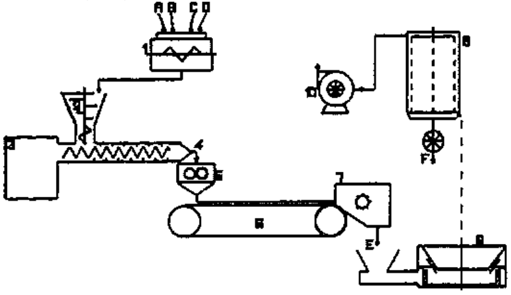

Fig. 3: Classical process for manufacturing powder coating [10]

The fluid mixture is cooled, solidified, grinded, air-milled and sieved to the wanted particle size (5-8). Some drawbacks of this process come from powder losses, from the economical obtainable minimum particle size (50 to 100µm) determined by the milling costs and from the reactivity of the fluid mixture, which may cause gel formation in the extruder.

An alternative procedure was proposed by Mandel [11]. The extrusion-, cooling- and milling-steps are substituted by a stirred autoclave and a spray tower. In the autoclave a mixture of the powder coating with supercritical carbon dioxide is established. This mixture is then sprayed in order to obtain an uniform powderous product. The costs of this process are prohibitive by the large high pressure vessel required for homogenization, the relative long residence time of the reactive mixture in the autoclave (minutes to hours) and the discontinous mode of operation.

A continuous method is presented in fig. 4 [12]. The reaction partners (binder and hardener) are stored in a fluid state in different feed vessels (1) at ambient pressure. Additives might be admixed to either of the main compounds, depending on miscibility and the rheological properties. Pumps (2), designed for the specific fluid properties (membrane pump, extruder, gear pump) feed the fluids to a static mixer (6), where they are mixed intensively and quickly (a couple of seconds to some ten seconds) with each other and with compressed, preheated CO_2 (3,4,5). The mixture is expanded from pressures between 70 to 250 bar down to approximately atmospheric pressure through a nozzle which is mounted in a spray tower (7). A coarse fraction (>50µm) might be collected at the bottom, while the smaller particles are withdrawn at the top together with the gas. This fraction (> 1µm) is separated in a cyclone. Smaller particles can be removed by a fine filter. This fraction is unwanted in case of powder coatings and can be avoided by adjusting the operation conditions of the system. The described system, the mode of operation and several powder coating formulations have been developed and tested in the last couple of years.

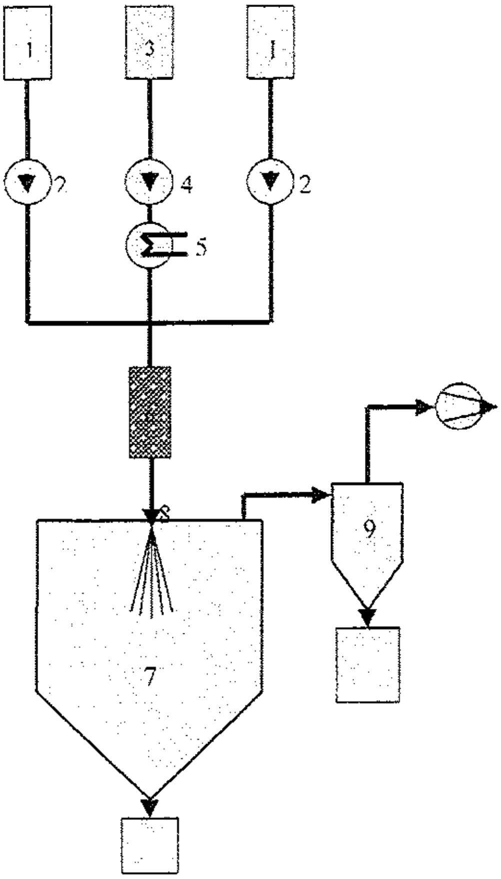

Fig. 4: Flow scheme for a continous mixing and powder generation process for powder coatings

The process was applied successfully separately to binder and hardener materials, like PMMA, Polyesters, Polyurethanes, Polycarbonates to stoichiometric combinations of both and to „complete" coating formulations".

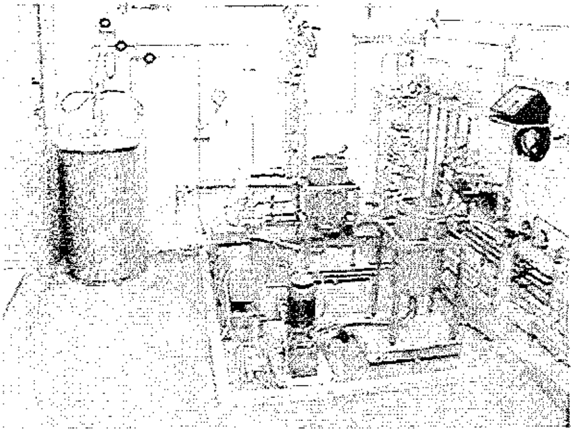

Fig. 5: Plant (semi-technical scale)

The semi-technical plant shown in fig. 5 has a capacity of 15 – 20 kg/h of powder. A key problem is the determination of the temperature for the mixing process. In fig. 6 a thermogram of a powder coating formulation is shown.

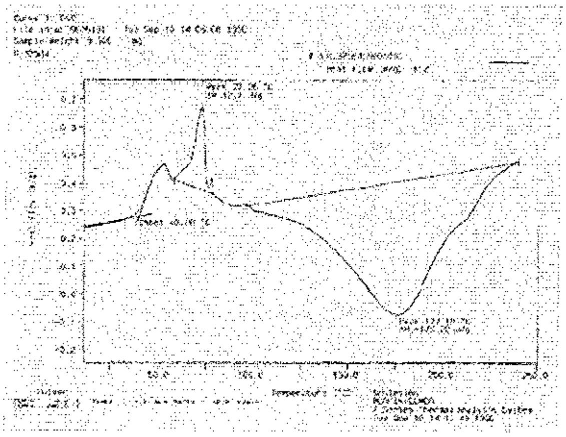

Fig. 6: Thermogram (DSC) of a powder coating formulation

The first two peaks (positive enthalpy) indicate the melting of hardener (approx. 50°C) and binder (approx. 75°C). The negative peak shows the reaction between the two compounds (177°C, starting at approx. 100°C). From this observations it can be concluded that the mixture is liquid above 75°C. If the temperature is maintained below 100°C a reaction in the static mixer can be avoided. It was found, that this was only the first indication: Due to lowering of melting points in presence of a soluble gas, the temperature range for mixing is broadened. It was possible to obtain powders at mixing temperatures of up to 10K below the melting point of a pure component.

The following features and parameters were investigated

- Continuous dosage of polymer melts with large differences in viscosity and melting points.
  Pure components are melted separately at temperatures/viscosities suitable for pumping. These temperatures might be higher than the reaction temperature. By admixing colder CO_2 in the static mixer a reaction can be suppressed
- Efficiency of the mixing process by spectroscopy and application tests of the powder coatings.
- Dependency of particle size, particle size distribution and morphology from process conditions (temperature, pressure, flow ratios, type of nozzle).
- Applicability of the obtained powders in standard spray units for powder coating.
- Solubility of CO_2 in the polymer melts and CO_2-consumption of the process (0,2 – 1 kg of Gas/kg of powder).
- Separation of the powder from the gas.

In fig. 7 the particle size distribution for a powder coating formulation on polyester basis is presented. This free flowing powder with a mean particle size of 15µm was withdrawn from the cyclone and analysed without further fractioning. The size distribution is sufficiently narrow. In the spray tower only some product from the start-up was found, while the fine filter was empty.

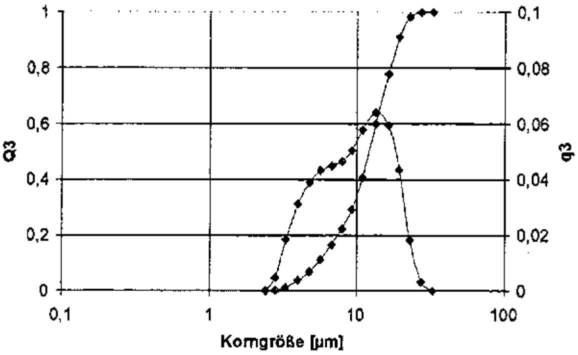

Fig. 7: Particle size distribution for a powder coating formulation on polyester basis

The different test procedures for powder coatings, including application, film formation and hardening on metal surfaces were passed successfully. The continuous mixing and powder generation process is considered as a competitive alternative to the existing extruder technology. It opens the field to powder coatings with lower melting temperatures, smaller particle sizes at higher yield, and thus for coatings with favorable properties.

The above described high pressure spray processes aim towards particle size reduction. By a process, developed in the past 3 years a size increase may also be achieved.

High Pressure Spray Agglomeration – CPF-Technology

This process comprises the following steps:

- Dissolution of a pressurized gas in the liquid to be applied, thus lowering the viscosity and the surface tension
- Release of the gas by expansion in a nozzle forms small droplets of the liquid
- Admixing of a solid, powderous carrier, which is intensively mixed with the droplets by the expanding gas
- Infiltration of the droplets into porous carriers and/or agglomeration of non-porous carrier materials by the liquid
- Separation of the formed powders by sedimentation, centrifugal forces or filters.

A principle flow scheme[13,14] of a continuosly operated plant is given in fig. 8. The liquid feedstock (temperature 20 – 60°C) is mixed continuously with the pressurized gas, e.g. CO_2 (typical temperatures between ambient and 50°C) in a static mixer. After expansion in a nozzle, a powderous carrier is added co- or crosscurrently. The liquid containing particles are then formed in an air/oxygen-and solventfree atmosphere of high turbulence. The turbulence is caused by the expanding gas. Due to the Joule-Thomson-Effect, the temperature in the spray tower might be very low (ambient to –50°C).

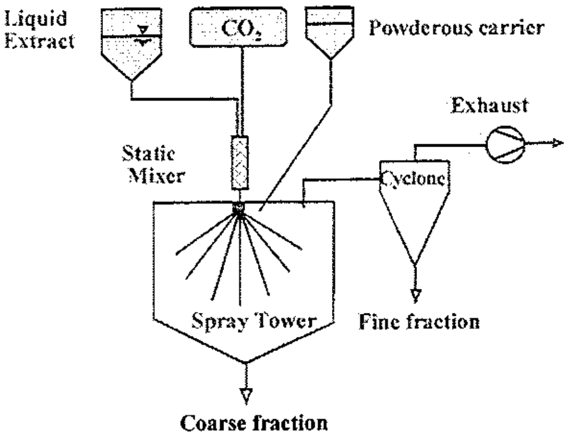

Fig. 8: Flow scheme of the CPF-process

The powder formation and maximum liquid loading was tested for several combinations of liquids (extracts of celery, oregano, laurel, pepper, ginger, nutmeg, basil, tumeric, paprika, rosemary, lemon oil, strawberry aroma, cheese aroma, butter fat, α-Tocopherol, whiskey and vinegar) and solid carriers (silic acid, maize starch, waxy maize starch, potato starch, cellulose, maltodextrose, extraction residues, powdered spices, citric acid, powdered sugar, titanium dioxide, sodium chloride, polymers and emulsifiers). Two examples are presented in fig. 9.

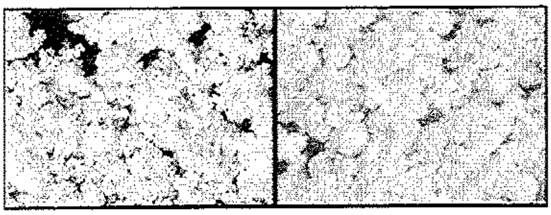

Fig. 9: Powders by CPF
left: Celery (79%), fine dispersed silic acid
right: Strawberry Aroma (60%) on porous silic acid

Celery extract was sprayed with CO_2 on a fine dispersed silic acid with a bulk density of 50 kg/m³ and a mean particle size of 20µm. The obtained powder, with a loading of 79wt% of liquid celery extract has a bulk density of 250 kg/m³. The sizes of the agglomerates reach up to 300µm. Strawberry aroma was sprayed with a spherical silic acid, with a particle size of approx. 200µm. As can be seen in fig. 9, the particles do not agglomerate, but the liquid has infiltrated the porous structure.

The CPF-process can be applied to low and high viscous liquids. Solid carriers with a broad range of particle sizes and bulk densities (50 – 850kg/m³) can be used. The maximum loading with liquid depends on the properties of the carrier and reaches up to 90wt%. The substances are treated only at mild conditions: low saturation and spraying temperatures, solvent- and airfree. The pressure range is 70 to 200 bar. Gas consumption is 0,5 – 2 kg of Gas/kg of powder. The process is realised in a continuously operated plant with a capacity of some hundred kg of powder per hour.

Primary aim during the development of the CPF-process was to obtain free-flowing powderous products. In almost all fields of applications mentioned in the introduction, the powder properties are as important for the acceptance as the powder form itself. This leads to secondary aims for the CPF-powders that are to be applied in the food and pharmaceutical industry. It was studied how the release and dispersion of the liquid in aqueous media depends on the solid carrier, liquid loading, addition of emulsifiers and addition of fat with different melting points. In fig. 10 the release and dispersion of lipophilic thyme extract in aqueous medium is shown in dependence of the solid carrier material.

Silic Acid	Cellulose	Maize Starch	Maltodextrose	Emulsifier
Partly cloudy green sediment oily droplets	Cloudy, yellow sediment oily droplets	Milky, white sediment oily droplets	Clear, no sediment oily film	Cloudy, no sediment no oily droplets slightly foaming

Fig. 10: Release and dispersion of thyme extract in aqueous medium

From the colour of the sediment and from the film/droplet formation it is concluded, that the release increases from the left to the right in fig. 10. A complete release is achieved, when a water-soluble carrier as maltodextrose is used. By applying an emulsifier (Lamemul by Grünau in this case) results in a complete release and the oily phase is dispersed almost homogenously in water. The characteristic features of the products obtained with the CPF-technology can be summarised as follows:

A complete release of active ingredients can only be achieved when water soluble carriers are used. Dispersion of released oily compounds require the addition of emulsifiers. Similar results were obtained with starches with emulsifying properties. Increasing loading of the powders with lipophilic active compounds leads to decreasing release. The emulsifiers are preferably added to the liquid compound, instead of adding it in powderous form to the carrier material. Combinations of emulsifiers are not recommendable, they might interfere with each other. Addition of fats with different melting points result in a temperature dependent release. High melting fats hinder the release in cold water.

Outlook

Numerous processes for powder generation by spraying gas pressurized solutions or mixtures have been proposed. The specific properties of nearcritical gases allows to obtain fine dispersed solids. One of the first goals, studied and achieved by high pressure micronisation/RESS and the GAS process, was to produce particles with submicron dimensions. Meanwhile it turned out, that also the size reduction to particles of some microns to some hundreds of microns are a promising outlook for the use of high pressure spray processes. This technology is of special interest for substances with low melting temperatures, high viscosities and waxy or sticky properties. These compounds are difficult and expensive to comminute by classical mechanical methods. Also reactive mixtures are considered as potential candidates for using compressed and soluble gases as auxiliaries for particle generation. In this case, not only the thermodynamics of the system, but also the chemical behavior is of importance for designing suitable processes. For a scale-up to large quantities of powders a continuous operated process with low gas consumption is favorable. For powder generation by spraying gas saturated solutions a competitive process was developed. Experimental results indicate, that this method can also be applied to other reactive and non-reactive systems. The next step is to transfer the results obtained in the semi-technical plant into a larger unit.

A process, based on spraying gas saturated liquids has found already it´s way to industrial realisation. The CPF-technology results in powderous agglomerates with an unusual high liquid content. It was demonstrated, that almost any liquid might be applied to solid carrier materials. Those products might be of interest in almost all industrial areas, especially if release and dispersion might be adjusted to the intended use of the product.

Acknowledgments: The author wishes to thank for the support from Herberts, Raps and from (in alphabetical order) B. Altmann, C. Blatter, H. Dirscherl, S. Grüner, A. Kilzer, Z. Knez, K. Kokot, A. Mey, Z. Novak, S. Peter, M. Petermann, K-H. Simmrock, R. Steiner, U. Streiber, B. Weinreich, V. Wiesmet.

Literature

[1] J.B. Hannay, J. Hogarth, On the Solubility of Solids in Gases, Proc. Roy. Soc. London 29 (1879): 324

[2] R. Zsigismondy, W. Bachmann, Über neue Filter, Z.Anorg. Allg.Chem., 103 (1918): 119

[3] E.Stahl, K.-W.Quirin, D.Gerard, Verdichtete Gase zur Extraktion und Raffination, Springer (1987): 250 - 251

[4] W. Best, F.J. Müller, K. Schmieder, R. Frank, J.Paust, DP 29 43 267 (BASF AG)

[5] D.W. Matson, R.C. Petersen, R.D. Smith, Formation of Silica Powder from the Rapid Expansion of Supercritical Solutions, Adv. Ceramic Mat., Vol.1 No.3 (1986): 243 - 246

[6] P.M. Gallagher, M.P. Coffey, V.J. Krukonis, N.Klasutis, Gas Antisolvent Recrystallization: New Process to Recrystallize Compounds Insoluble in Supercritical Fluids, Amer. Chem. Soc. Symp. Series, No. 406 (1989): 335-353

[7] E. Weidner, Z. Knez. Z. Novak, PGSS (Particles from Gas Saturated Solutions) - A new Process for Powder Generation, 3rd. Int. Symp. on Supercritical Fluids, Straßburg Oct. 17 - 19 1994, Proc. Tome 3, 229 - 235

[8] E. Weidner, Z. Knez, R. Steiner, Powder Generation from Polyethyleneglycols with Compressible Fluids, 3rd Int. Symp on High Pressure Chem. Eng., Zürich 7.-9.October 1996, Preprints, 223-228

[9] B. Bungert, G. Sadowski, W. Arlt, Innovative Verfahren mit komprimierten Gasen, CIT 69, 298 - 311

[10] Kittel, H.: Lehrbuch der Lacke und Beschichtungen, Band VIII Teil 2, Verlag W.A.Colomb, Berlin und Oberschwandorf 1980

[11] F. Mandel, Manufacturing of Powder Coatings via the Utilization of Supercritical Carbon Dioxide, 4th Int. Symp. on Supercrit. Fluids, Sendai 11.-14. May 1997, Proc. Vol. B, 493-497

[12] M. Petermann, Dissertation Erlangen 1999, in preparation

[13] S. Grüner, Entwicklung eines Hochdrucksprühverfahrens zur Herstellung hochkonzentrierter, flüssigkeitsbeladener Pulver, Dissertation Erlangen 1999, in press

[14] B. Weinreich, S. Grüner, H. Dirscherl, R. Steiner, E. Weidner, Zeitschrift für Fleischwirtschaft, in press

Fine phospholipid particles formed by Precipitation with a Compressed fluid Antisolvent

C. Magnan, N. Commenges, E. Badens, G. Charbit *
Laboratoire d'Etudes et d'Applications de Procédés Séparatifs
Service 512, Faculté de Saint Jérôme
Avenue Escadrille Normandie Niemen, 13397 Marseille cedex 20, France
Tel : (33) 491 28 89 00 Fax : (33) 491 02 35 72
Email : gerard.charbit@leaps.u-3mrs.fr

Phospholipids may be used to produce liposomes which act as controlled drug delivery systems. This study aimed to develop a micronization process of soy lecithin in order to obtain fine particles of phospholipids showing low dispersion of size and free of organic solvent. The PCA process was performed using ethanol as auxiliary solvent and carbon dioxide as compressed fluid antisolvent. Microparticles, with size ranging from 14 to 40 µm, could be produced under semi-continuous mode, when CO_2 and the liquid solution flow co-currently. Infra Red spectra of the particles seems to show that they are free of residual solvent.

Introduction

Microencapsulation of drugs in bioerodible substances allows to control their rate of release. Since they may form liposomial structures, phospholipids, from lecithin, are used for that purpose. Soy lecithin is cheaper than egg yolk lecithin, and is for that reason preferentially used to generate liposomes. However, processing with raw lecithin yields liposomes having inadequate features so that preliminary treatments are needed.

In the conventional method soy lecithin is first dissolved in an organic solution ; next the solvent is eliminated by evaporation. Phospholipids thus obtained are dispersed in water with the help of a highly shearing turbine in order to generate liposomes. However the technique come up against a difficulty : phospholipids from the second step of the process, form a gel containing a few amount of organic solvent. It has been stated that the liposomes are of better quality (more homogeneous in size distribution) when the raw phospholipids do not form a gel but fine particles. This drawback prompted us to develop a new method using supercritical or near critical fluids in order to obtain fine particles of phospholipids exempt of organic solvent.

The GAS and the PCA processes are mild techniques allowing the production of micron-sized particles and are for this reason the object of a growing number of studies [1]. Both methods rely on the insolubility of the supercritical fluid in an auxiliary organic solvent. A solution formed from the solvent and the solid solute, is contacted with the supercritical fluid which acts as an antisolvent and reprecipitates the solute in fine solid particles. A last step of washing by the CO_2 allows the removal of the solvent and the recovery of dry particles.

This study is aimed at the PCA process as a novel route to form fine particles of phospholipids from soy lecithin.

Materials and methods

Preliminary studies concern :

- the phase diagrams of the CO_2/solvent/lecithin system,
- the volumetric expansion of the liquid phase occurring during the dissolution of CO_2 in the liquid phase.
-

The phase diagrams were determined by direct visualization of the phase transitions. We focused on the transition from gas/liquid/solid to supercritical phase/solid. As shown in figure 1 the equipment used was a high pressure pump equipped with a movable piston and a sapphire window. A camera and a video monitor complete the set-up.

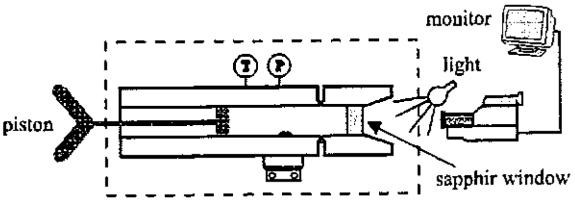

Figure 1. Apparatus for phase diagrams study

Measurements were performed as follows : a known composition mixture of CO2, lecithin and liquid solvent was introduced into the cell. At a fixed temperature short movings of the piston were achieved, leading to variations of the pressure without changing the global composition of the system. The phase transition pressure was registered taking care that equilibrium was established.

Concerning the determination of the volumetric expansion, experiments were performed in the case of chloroform ; the main equipment was a sapphire vessel equipped with a graduated scale. The liquid solution being initially placed in the vessel, an amount of CO2 was introduced and dispersed ; the raising of the liquid level was noted after equilibrium was reached.

In the case of ethanol, the volumetric expansion was determined theoretically from the Peng Robinson EOS in combination with values of molar fractions and molar volumes of both the liquid and the gas phases experimentally determined by Chang *and al.* [2].

The PCA experiments of micronization were carried out on a semi-continuous mode with a co-current flow of the solution of phospholipids and of pure CO_2 (antisolvent). The experimental set-up is shown in Figure 2.

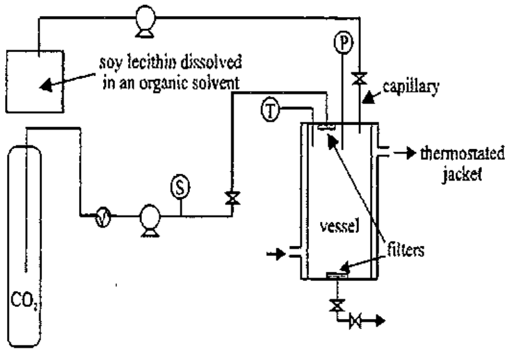

Figure 2. PCA experimental set-up

The procedure was as follows : first the vessel was pressurized with pure CO_2. Next, the liquid solution and CO_2 were simultaneously introduced thus causing the precipitation of the solute. The precipitation, was followed by a washing step achieved by injection of pure CO_2 to eliminate the residual organic solvent. The introduction of the liquid phase is made through a 125 µm diameter capillary in order to form small droplets and thus to improve the mass transfer between the two phases. Due to the CO_2 dissolution within the liquid droplets, the saturation of the phospholipids is reached and the supersaturation induces the precipitation of phospholipids. The PCA process was carried out at temperature varying from 308 to 323 K and pressure varying from 8 to 12 Mpa.

The Infra-Red analysis of the particles was performed in order to detect the presence of organic solvent and the observations were carried out with a Scanning Electron Microscope (SEM) JEOL 6320 F. The sample was first metallized with a small gold surface 200 Å-thick.

Results and Discussion

Preliminary studies

Figures 3 and 4 represent the experimental diagrams Pressure vs. Temperature obtained for the ternary systems CO_2/ethanol/lecithin and CO_2/chloroform/lecithin respectively. Curves in full line show the transition gas/liquid/solid and supercritical phase/solid. The key parameters of this study were:

- The lecithin type : the S20, S75 and S100 lecithins provided by LIPOID contained respectively 20%, 75% and 100% of Phosphatidyl Choline (PC).
- The global composition of the system: CO_2/solvent/ lecithin.

Three main conclusions may be drawn from these results :

- At a given temperature, the phospholipids concentration does not influence significantly the transition onset pressure.
- From the strict point of view of the working pressure, chloroform is more suitable than ethanol since it allows to work at a lower pressure for a fixed temperature. More being more volatile it should be eliminated more easily.
- No significant difference exists between the two types of lecithin S75 and S100.

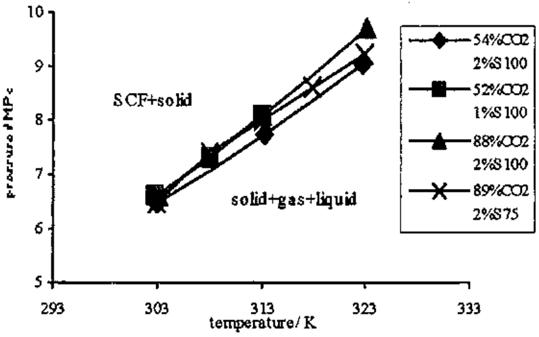

Figure 3. Phase diagram of the CO_2/ethanol/lecithin system

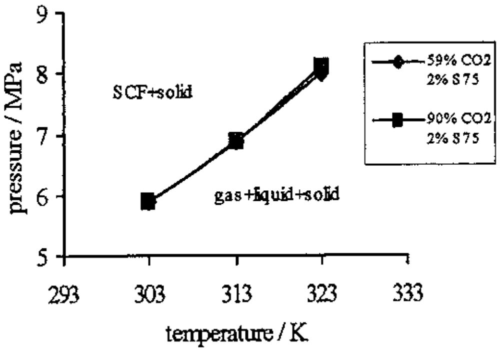

Figure 4. Phase diagram of the CO_2/chloroform/lecithin system

The supercritical phase/solid region corresponds to the best operating conditions of pressure and temperature for the PCA process. In this part of the experimental field, solid particles can be collected and the organic solvent can be easily eliminated with CO_2 in the supercritical phase.

Figures 5 and 6 represent the volumetric expansion of the liquid phase in the case of chloroform and ethanol. The volumetric expansion is defined as the ratio of the liquid volume variation to the initial liquid volume. Figure 5 represents experimental results contrary to figure 6 which represents calculated results.

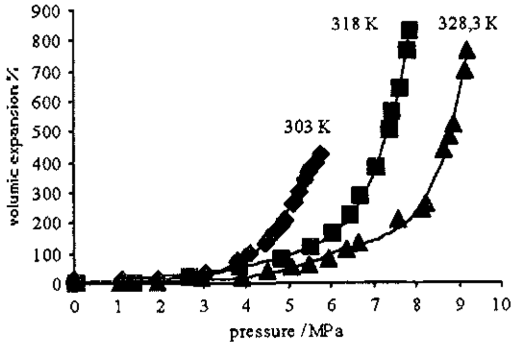

Figure 5. volumetric expansion of the liquid phase with chloroform as solvent

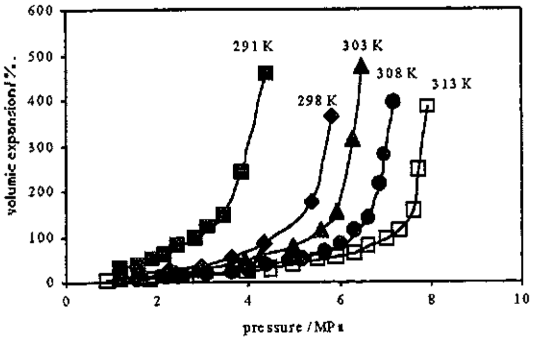

Figure 6. volumetric expansion of the liquid phase with the ethanol as solvent

Different observations can be made :

As shown in figure 5, the volumetric expansion can reach up to 900 %.

As previously mentioned, one can note that chloroform is a better solvent because a similar volumetric expansion is observed at lower pressure than for ethanol.

The results are consistent with those of Kordikowski *and al.* [3] who has determined the volumetric expansion of different solvents versus the molar fraction of CO_2 dissolved.

PCA experiments

As mentioned above, chloroform is more suitable than ethanol but, because of its toxicity, its use was avoided and ethanol was preferred. Table 1 summarizes the experimental conditions of the runs ; in every case the liquid flow rate was of 10 ml.h^{-1}.

P / MPa	T / K	Type of lecithin	Solute concentration / wt %
10	303	S 100	10
10	303	S 100	20
10	303	S 75	2
10	303	S 75	15
10	303	S 75	20
12	308	S 75	15

Table 1. Experimental conditions for the PCA process

Fine and dry particles of phospholipids were formed in every run. The experimentation field is thus wide enough to give some freedom for operating ; one should particularly point out the extent of the solute concentration range.

During these experiments one difficulty was encountered, it appeared that the phospholipids were very unstable ; they were rapidly denatured by oxidation in the presence of air. This reactivity results from the high specific area of the micron-sized particles formed. As a consequence, it was necessary to maintain the micronized phospholipids under a CO_2 atmosphere as long as possible before observation.

Figure 7 represents a SEM photography obtained for a pressure of 12 MPa, a temperature of 308 K and a concentration of S75 lecithin of 15 wt %. The particles have a size ranging from 14 to 40 µm, they are roughly spherical and more or less agglomerated.

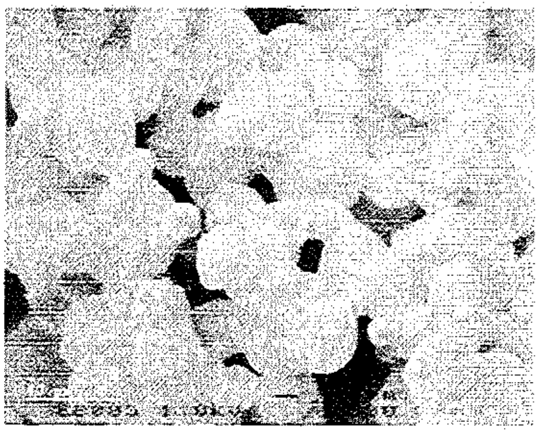

Figure 7. SEM photography of micronized phospholipids

Samples of precipitated phospholipids were analyzed by Infra Red spectroscopy in order to check the presence of residual traces of solvent. The absorption band of the alcohol function which spans from 500 to 800cm^{-1} does not appear in our spectra. This result may be of a great importance if further deeper analyses confirm that the solvent is completely eliminated. As a matter of fact, in these circumstances the use of more suitable solvents may be considered even if they are more toxic.

More, the IR spectrum of the precipitated lecithin was compared to that of the egg yolk lecithin. As shown in Figure 8 the spectra are very similar and may be superimposed ; this finding shows that the lecithin was not modified when processed by the PCA technique.

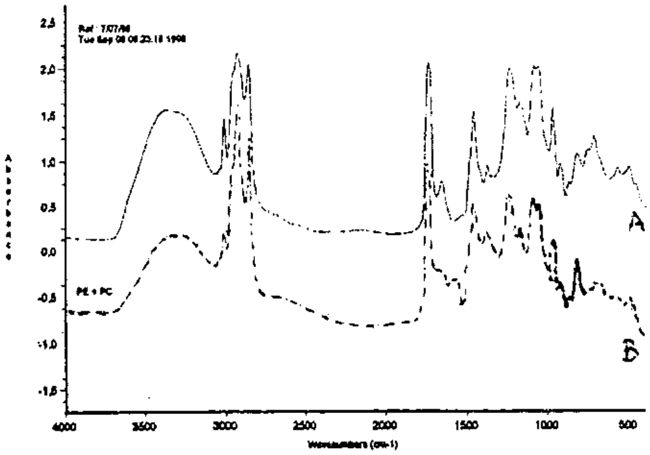

Figure 8. Infra red Spectra of the precipitated soy lecithin and of egg yolk lecithin

Conclusion

Dry and fine particles of phospholipids, with size ranging from 14 to 40 μm, were obtained from soy lecithin by the PCA method. The process is effective over a wide range of experimental conditions.

As concerns the supercritical fluid precipitation techniques, it was stated elsewhere that ethanol is one of the less interesting solvents. This statement is confirmed by the present study, but because of the non presence of residual solvent in the micronized particles, the use of others solvents may be considered for further experiments. They could give similar results at lower working pressures.

The drawback encountered concerning the instability of the precipitated phospholipids may be evaded by processing the following step (dispersion of the phospholipid powder in water) in the same vessel, that is to say without opening it.

References

1. Reverchon, E. "Supercritical Antisolvent Precipitation : its application to microparticle generation and products fractionation", *Proc. of the 5th Meeting on Supercritical Fluids*, **1998**, Nice, 221-236
2. Chang, C.J. ; Day, C.Y. ; Ko, C.H. ; Chiu, K.L. "Densities and P-x-y diagrams for carbon dissolution in methanol, ethanol, and acetone mixtures", *Fluid Phase Equilibria*, **1997**, 243-258
3. Kordikowski, A. ; Schenk, A.P. ; Van Nielen, R.M. ; Peters, C.J. "Volume expansions and vapor-liquid equilibria of binary mixtures of a variety of polar solvents and certain near-critical solutes", *3rd congres I Fluidi Supercritici e le loro applicazioni*, **1995**, Griganno, Trieste, 29-34

Acknowledgements

The authors are indebted to the Pharmaceutical Laboratories LAPHAL for financial support

Gas Antisolvent Crystallization - from Fundamentals to Industrial Applications

Andreas Weber*, Claudia Weiß, Juri Tschernjaew[1), Rolf Kümmel

Fraunhofer Institut Umwelt-, Sicherheits-, Energietechnik UMSICHT Osterfelder Str. 3 D-46047 Oberhausen
email: web@umsicht.fhg.de, fax +49 208 8598 290

[1) Degussa AG, Rodenbacher Chaussee 4, D-63403 Hanau

Gas Antisolvent Processes offer several benefits for the production of high-quality solids e.g. for nutritional or pharmaceutical use. In recent years the crystallization with supercritical fluids has gained growing interest, since it allows an effective micronization of solids without any loss of product quality. Taking the process into industrial applications is still a risky task and affords a lot of experimental groundwork. Within this presentation a short overview shall be given about our work in recent years followed by some concepts useful for plant design in future.

Introduction

The principle of the presented PCA process (Precipitation with Compressed Antisolvents) is the dispersion of a solution into a compressed antisolvent. At subcritical conditions, the antisolvent is absorbed by the liquid drops, while at supercritical conditions the primary solvent dissolves in the compressed antisolvent. Both processes lead to a high supersaturation of the primary solution, causing precipitation of the solute. The properties of the solid product can be influenced in a wide range by the process temperature and the pressure as well as by the dispersion procedure. Variation of the process parameters temperature and pressure allows a fine control of the process in order to carry out different crystallization tasks.

So far this process has been carried out only on a laboratory scale in relatively small batches [1,2]. On a production scale, allowing the circulation of the working media (primary solvent, antisolvent) it will gain attractivity. The aim of this work is to work out technical applications of the PCA-process and to find models to allow scale-up calculations.

Methods and Materials

All experiments were carried out on a pilot plant described in Fig.1. The crystallizer A1 was a stainless steel autoclave (UHDE GmbH, volume 6 l, max. pressure 50 MPa). Pressure and temperature were measured at the top of the autoclave and controlled in a range of ±1°C and ±0,02 MPa. The antisolvent was compressed by a jetting pump P1 (max. flow rate 30 kg/h) and fed into the autoclave from the top. It was released at the bottom and expanded through a control valve into a separator S1, where the dissolved primary solvent was collected and the expanded antisolvent was fed back into tank D1.

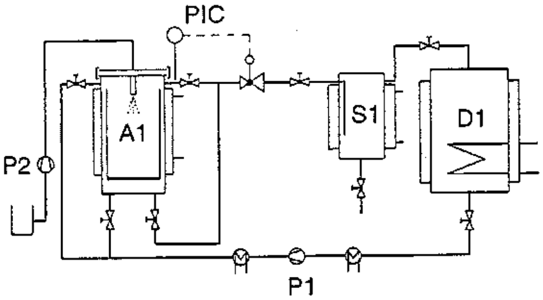

Fig. 1: Apparatus for PCA experiments; A1 crystallizer, S1 separator, D1 antisolvent-storage-tank, P1 and P2 high-pressure pumps

The primary solution was fed with a high-pressure diaphragm pump P2 (LEWA, max. Feed 6 l/h) through a nozzle (diameter 100 - 300 µm) at the top of the autoclave. The crystallized particles were collected on a paper filter (Schleicher und Schüll White Ribbon) at the bottom of the autoclave, and the excess solvent was passed through into the separator.

The antisolvent was circulated in a loop at a rate of 10 to 40 kg/h until the desired pressure was reached in the crystallizer. The pressure in the separator was kept constant at 4.5 to 5.0 MPa. At designated temperature and pressure conditions the primary solution was injected through the nozzle. The CO_2 stream was left on for another 20 - 40 minutes after injection in order to dry the precipitated product.

The yield was calculated by analysis of the primary solvent collected in the separator. The particles were characterized by optical and scanning electron microscopy. Additional investigations were carried out by differential scanning calorimetry to determine phase interactions in the products obtained by simultaneous precipitation. The chemical composition of the products was determined by HPLC, UV spectrometry, XRFS and miscellaneous analytical methods.

Materials

Carbon dioxide (99.9%, Messer Griesheim) was used as antisolvent. In the experiments ascorbic acid (99%, reagent grade, Aldrich), paracetamol (BP93 grade, Kramer & Martin), urea (98%, Aldrich), and chloramphenicol (99%, for biochemistry, Merck) were crystallized. The primary solutions were prepared in ethanol (abs., denaturated, Bernd Kraft).

Results

In recent years experiments were carried out on different substances with different objectives [3,4]. It was possible to resolve these tasks on a pilot plant just by changing the process parameters like temperature, pressure and the choice of the appropriate primary solvent.

Micronization

In several experiments ascorbic acid, paracetamol, urea, aspirine, and saccharose were micronized by PCA. The resulting products consisted of crystalline particles with a mean diameter in between 1 and 10 µm and a comparably small particle size distribution. Best results were obtained between 7.5 and 10.0 Mpa, at a process temperature between 35 to 40 °C. Within these conditions, the particle size is affected by the general parameters pressure, temperature and the concentration of the solute in the mother liquor.

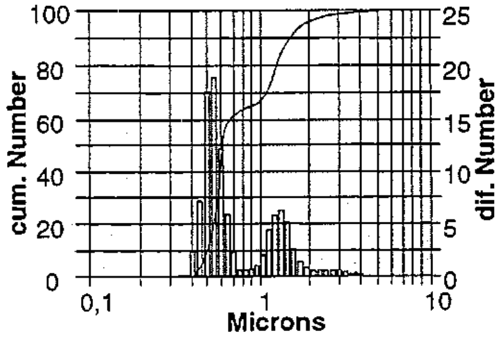

Fig. 2: Particle size of micronized ascorbic acid (the bimodal distribution is a consequence of measuring needle shaped crystals by light scattering)

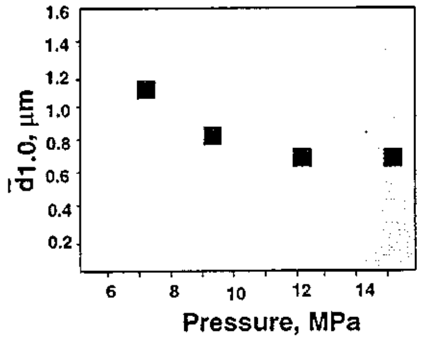

Fig. 3: Particle size of micronized ascorbic acid in dependance of the process pressure

Microcomposites

A unique feature of the used process is the generation of microcomposites by coprecipitation of two or more solid components. This technique can be used to prepare sophisticated solid materials which are useful as controlled release systems for medical or microbiological uses, or as precursors for ceramic materials. Experiments with organic systems as urea-chloramphenicol or ascorbic acid-paracetamol showed that variation of the process parameters can lead to dramatic changes of the product morphology [5]. In spite of this handicap, modes of operation were found which lead to homogeneous microcomposites at high product yields. Optimal conditions were found between 8.0 and 10.0 Mpa and 40 °C.

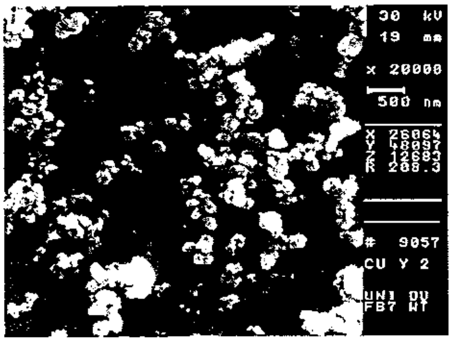

Fig. 4: Nanocomposites of Cu-acetate and Y-acetate by PCA from ethanol

To apply the process to prepare precursors for high performance ceramics, experiments were carried out on Copper-, Barium- and Yttrium Acetate.-Coprecipitation of these components lead to composite particles of 50 to 150 nm which showed a unique homogeneous distribution of each of the elements.

Recovery of natural products

Further investigations were made on the precipitation of lecithine from egg yolk extracts, which was part of a novel process for the production of lecithine. A product yield of above 85 % was achieved. The gained lecithine was free from the used solvent to the desired extent.

Modelling

For the theoretical analysis of the PCA Process, the dispersed mother liquor in the compressed antisolvent was regarded. Therefore a simulation tool which describes the time-resolved concentration of each component in a single droplet was used. Presupposing that the nonequimolar diffusion of the components results in a change in the droplet radius, the problem to be solved is a moving boundary problem.

The crystallization of the dissolved substance is a consequence of the diffusion of two of the components (solvent and antisolvent) in the system. To characterize the crystallization, a population balance is to be solved simultaneous to the concentration profiles of each component. The result is the time dependent evolution of the crystal size.

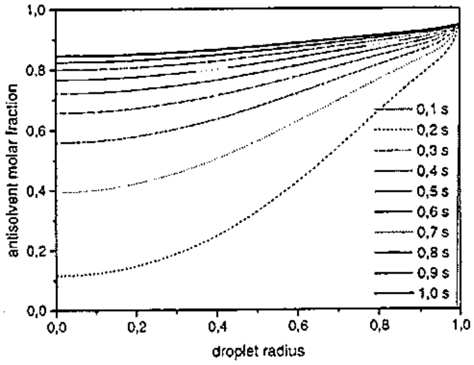

Fig. 5: Time-resolved profile of the antisolvent concentration in a droplet

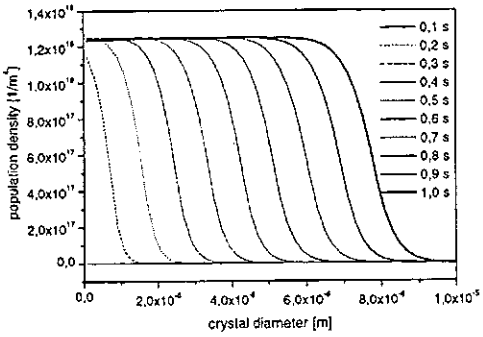

Fig. 6: Population balance in a droplet

Processing Costs

The processing costs may be calculated considering the energy consumption for compression and the temperature stabilization of the vessels, payoff of the equipment and labour costs [7]. Depending on the process conditions the production costs span from 6 Euro/kg to 12 Euro/kg.

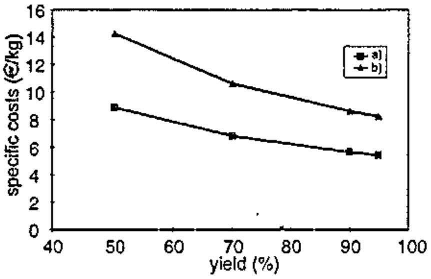

Fig. 7: Specific production costs at a different process yield
a) antisolvent to solution feed ratio 3:1, capacity 125 kg/h
b) antisolvent to solution feed ratio 2:1, capacity 250 kg/h

Together with other considerations like simple fluid dynamical approaches to spray density and droplet size or properties of the resulting solid material these results are helpful to estimate capacity and design of possible crystallization equipment. Further work heading for a complete set of modeling tools is being carried out at the moment.

Conclusions

Gas antisolvent crystallization is an attractive process for high quality solids e.g. pharmaceutical products, polymers, cosmetics or nutritional products.

An advantage is the multipurpose character of the Process. Many different crystallization tasks can be carried out on a single plant just by variation of the process conditions. This can bring about an optimal operation time. Because of the compact setup cleaning and inertization of the plant is reduced to a minimum.

Our future work will concentrate on the development of further applications and will take into account possible advancements to reduce the still high processing costs.

References

1. Tom, J.W.; Debenedetti, P.G.; *J. Supercritical Fluids* 7 (1994), 9
2. Schmitt, W.J.; Salada, M.C.; Shook, G.C.; Speaker, S.M. *AIChE Journal* 11 (1995) 2476
3. Tschernjaew, J.; Weber, A; Berger, T.; Kümmel, R. *Chem. Ing. Tech.* 69 (3) (1997) 349-352
4. Weber, A.; Beutin, M.; Tschernjaew, J.; Kümmel, R. *Proc. 1st European Symposium of Process Technology in Pharmaceutical and Nutritional Sciences,* March 10-12, 1998, 121-130
5. Weber, A.; Beutin, M.; Tschernjaew, J.; Kümmel, R. *Proc 4th int. Workshopon Grystal Growth of Organic Materials,* Bremen, Sept. 1997, 214-221
6. Bird, R.B.; Steward, W.E.; Lightfoot, E.N. *Transport Phenomena*, John Wiley & Sons, New York, 1960
7. Weber, A.; Tschernjaew, J.;Berger, T.; Bork, M. *Proc. 5th Meeting on Supercritical Fluids,* Nice (France), 23-25 March 1998, 281-285

GVC-Fachausschuß „High Pressure Chemical Engineering", March 3-5, Karlsruhe, Germany, 1999 GVC FZK '99

Understanding Gas Antisolvent Processes of Biocompatible Polymers and Drugs with Supercritical CO_2

A. Bertucco*, P. Pallado**
*Università di Padova, Istituto di Impianti Chimici, via Marzolo, 9, 35131 Padova, Italy
**Exenia Group S.r.l., v. L. Da Zara, 13 – 35020 Albignasego (PD), Italy
email: bebo@polochi.cheg.unipd.it

The use of supercritical fluids to obtain products of interest in the pharmaceutical industry is a great potential. In this work, the precipitation process of bio-compatible polymers and drugs by supercritical anti-solvent techniques using CO_2 as the anti-solvent (GASP processes) is considered and discussed with reference to the phase equilibria. Experiments are carried out in a windowed cell to measure the volume expansion of the liquid solution and the precipitation pressure of the heavy product. Several bio-polymers and drugs are considered in different organic solvents. In order to elucidate the variables relevant to interpret the precipitation effect, a simplified thermodynamic model is applied, which leads to results consistent with the experimental evidence. It is concluded that the CO_2 content in the liquid solution plays the key role in the process and that precipitation occurs when the liquid density reaches a maximum; the density values for different compounds are slightly different, but in terms of pressure the difference may be significant.

Introduction

Among the currently developed techniques that exploit the unique properties of supercritical fluids for the production of particles of micron and sub-micron size, the ones based on the anti-solvent effect are particularly promising. They allow to obtain the precipitation of the heavy compounds of interest from an organic solution by adding a supercritical component, which is able to exert an anti-solvent action towards them. In the literature different applications of this idea have been proposed after the pioneering work of Gallagher et al. [1], which are referred to as SAS or GAS or PCA [2]; in this work we will generically use the acronym GASP.

The main advantages of GASP techniques are well known: the anti-solvent effect is applicable with many classes of compounds, such as hydrocarbons, inorganic materials, drugs, polymers; any solvent except water is able to dissolve the most attractive supercritical fluid (CO_2) at any extent; a pressure lower than 100 bar is usually enough to carry out the process; it is possible to precipitate the compounds of interest completely and in a single step.

These techniques are extremely attractive for the processing of pharmaceuticals, as can be seen in a recent review by Subramaniam [3], and argued by the number of related patents currently issued. The development of products of bio-compatible materials obtained by GASP is indeed a field of great potential (see for example Benedetti et al. [4] and Winters et al. [5]). In particular, these techniques are studied to carry out co-precipitation processes, for example to produce controlled drug-delivery systems, where one or more drugs are conveniently dispersed within an inert matrix (the bio-polymer).

At present the development of such techniques, not only in the field of pharmaceuticals, is mainly performed by trial-and-error procedures, because little knowledge of the phenomena involved is available. Deeper understanding of phase equilibria, mass transfer and nucleation aspects would be highly helpful in view of reducing the experimental effort required to select the best process conditions and to scale them up to the industrial level.

In this work, the precipitation of bio-compatible polymers and drugs by GASP with CO_2 is addressed and discussed with special respect to the phase equilibria occurring in the system. Preliminary results of this kind are reported by Vaccaro et al. [6]; here, more data are presented and interpreted in the frame of a simple thermodynamic model.

Materials and Methods

Several bio-polymers and drugs were studied in different organic solvents: Ethylcellulose in Acetone and Ethylacetate, HP55 in Acetone, HYAFF11 in Dimethylsulphoxide (DMSO), Salbuthanole and Pentamidine in DMSO. Iper-pure liquid CO_2 was always used as the anti-solvent.

Experiments were carried out in a view cell (Jerguson type) where the precipitation pressure of the heavy compound and the volume expansion of the liquid solution were measured at constant temperature. The sketch of the experimental set-up and the operating procedure are reported in Vaccaro et al. [6]. Special care was taken to operate the system at quasi-equilibrium conditions.

In all the systems considered the anti-solvent effect was achieved completely in a narrow pressure range, so the precipitation pressure can be defined, according to Gallagher et at. [7], as the level where the "onset of nucleation" is seen by the unaided eye. The volume expansion is expressed by:

$$\Delta V = \frac{V - V^0}{V^0} \qquad (1)$$

where V^0 and V are the total liquid volumes at ambient and variable pressures, respectively.

Model

In order to elucidate the role of variables relevant to the precipitation process, a simple thermodynamic model was applied. It is based on an equation proposed by Chang and Randolph [8]:

$$s(T,p,x) = s(T,p=1,x=0)\,\frac{\overline{v}_{OS}}{v_{OS}^{0}} \tag{2}$$

In Eq. (2) s is the solubility, x the mole fraction of the supercritical component in the liquid phase and $v_{OS}^{0}, \overline{v_{OS}}$ are, respectively, the pure compound and partial molar volumes of the solvent (OS) in the liquid phase. If the solvent amount in the vapor phase is neglected, the relation between volume expansion and molar volume is given by:

$$\frac{V-V^{0}}{V^{0}} = \frac{v}{v_{OS}^{0}}\left(1+\frac{x}{1-x}\right)-1 \tag{3}$$

where v is the molar volume of the liquid at mole fraction x.

Partial and total molar volumes in Eqns. (2) and (3) were calculated by the Peng-Robinson equation of state, at the experimental temperature. As the related pure component parameters are missing for all the bio-polymers and drugs considered, it was not possible to account for their effect. Therefore, the Peng Robinson equation was applied to the binary systems CO_2–OS; one binary adjustable parameter fitted to vapor-liquid equilibrium data was used.

We note that the proposed model is independent of the heavy compound identity, and is therefore applicable to dilute systems only.

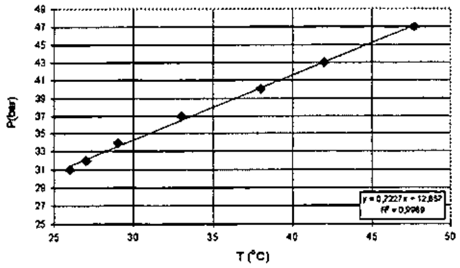

Figure 1 Precipitation pressure of Ethylcellulose as a function of temperature for the system CO_2-Acetone- Ethylcellulose.

Results and Discussion

The experimental measurements carried out in this work confirm the results reported by Vaccaro et al. [6]: the precipitation pressure depends on the solute, the solvent and the temperature, but the volume expansion of the liquid solution is not affected by the solute. The volume expansion measured at the precipitation pressure is a function of the solute. For a given solute and solvent, two major results were found in all the cases considered:

- the temperature dependence of the precipitation pressure values can be approximated by a straight line, as can be seen from Fig. 1 for Ethylcellulose in Acetone. This allows reducing the number of experiments for a given system.
- when the volume expansion is plotted against the precipitation pressure (i.e. at different temperatures), a constant value is found with good approximation, as reported in Fig 2.

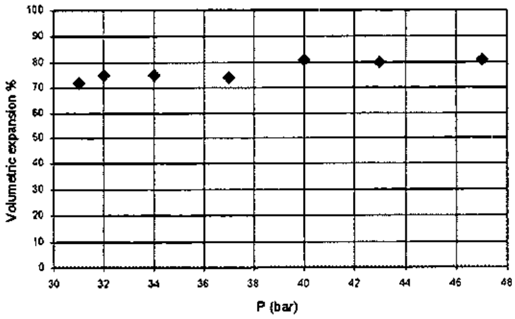

Figure 2: Volume expansion of the liquid as a function of precipitation pressure at different temperatures for the system CO_2-Acetone- Ethylcellulose.

According to these results it is concluded that, as different solutes show different precipitation pressures, from a thermodynamic point of view they cannot be precipitated together. To be able to obtain simultaneous precipitation, the process must be carried out at kinetically limited conditions; for that, GASP techniques where the liquid solution is injected in an anti-solvent environment are more favorable than batch GASP operation.

We remark that the proposed thermodynamic model is not able to predict different precipitation pressure values for different compounds in the same solvent at a given temperature. However, it is very useful in defining the process key variable to interpret experimental results.

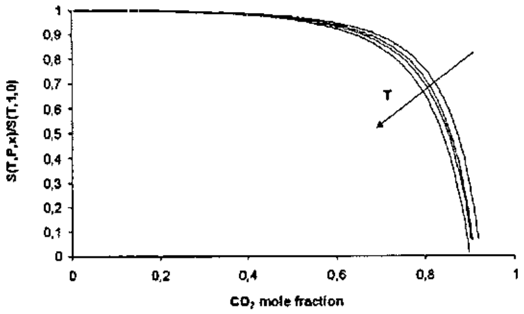

Figure 3: System CO_2-Acetone: solubility s of a generic heavy compound in the liquid as a function of CO_2 mole fraction x. The plot is normalized to the value at x=0. Temperatures: 25, 35, 40, 50°C.

To clarify this point, we applied Eq. (1) to the binary system CO_2-Acetone at various temperatures and plotted the calculated solubility as a function of the mole fraction of CO_2 in the liquid phase, x, rather than as a function of pressure. The curves are very close one another (see Fig. 3). In addition, if also the volume expansion is reported versus x, again one single curve is practically obtained, as depicted by Fig. 4. It means that the CO_2 content in the liquid phase is not only the driving force for the expansion, which is somehow expected, but also that it triggers the precipitation of the heavy compound, and almost independently of temperature.

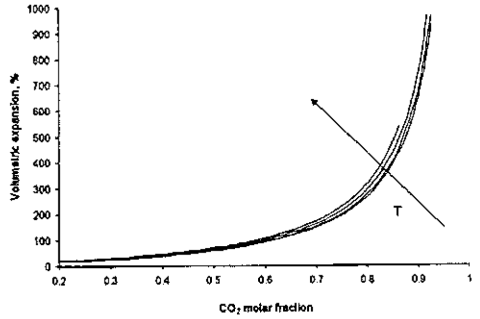

Figure 4: System CO_2-Acetone: profiles of volume expansion as a function of CO_2 mole fraction. Temperature: 25, 35, 40, 50°C.

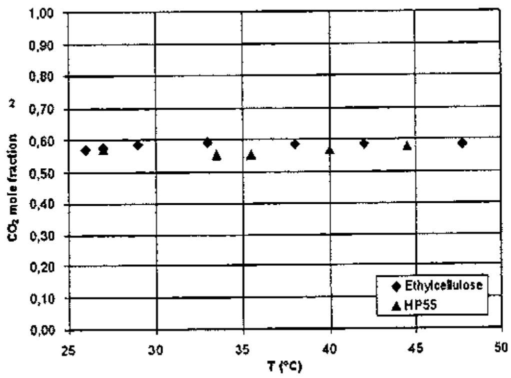

Figure 5: Predicted CO_2 mole fraction in the liquid phase at precipitation conditions. Systems: CO_2-Acetone-HP55 and CO_2-Acetone-Ethylcellulose

This result is confirmed if experimental data at precipitation conditions are presented as a function of temperature. It is clear from Fig. 5 that the value of x obtained by applying the Peng-Robinson equation of state at the measured precipitation pressures and temperatures is reasonably an invariant within the temperature range investigated. Data for two bio-polymers are reported; note that the two lines are close to each other because, in this particular case, the two polymers show similar precipitation pressures.

Another important result can be evidenced if the liquid density is used as the independent variable. Fig. 6 clearly shows that precipitation takes place at a density value relatively high and independent of the temperature and of the solute. We recall that the density is not measured but calculated by the Peng-Robinson equation for the binary system CO_2-OS at the experimental temperature and pressure.

The major result of density calculations is that the saturated liquid density shows a maximum with respect to x, as can be seen in Fig. 7 for the system CO_2-Acetone. It is noteworthy that the value at maximum is close to the one where precipitation conditions occur. This conclusion is confirmed by results presented in Fig. 8, calculated according to Eq. (2) and the Peng-Robinson equation: here, the drop of the solubility curve starts when a maximum density value is reached. Finally, for the CO_2-DMSO system, the curves of Fig. 9 are obtained in terms of volume expansion versus density.

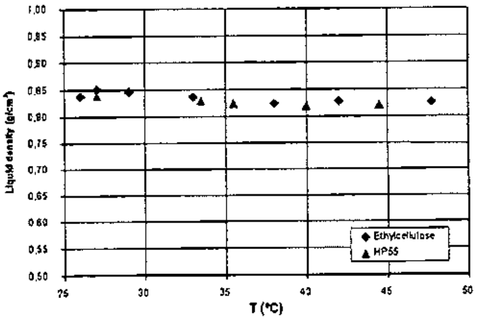

Figure 6: Predicted liquid density at precipitation conditions. Systems: CO_2-Acetone-HP55 and CO_2-Acetone-Ethylcellulose

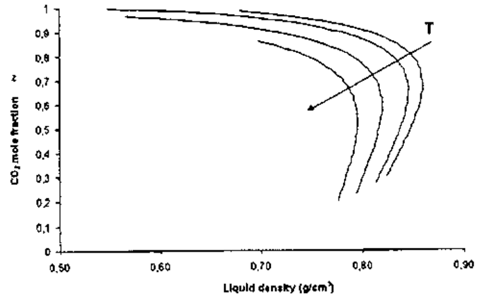

Figure 7: Mole fraction of CO_2 in the liquid versus the saturated liquid density. System: CO_2-Acetone. Temperatures: 25, 35, 40, 50°C

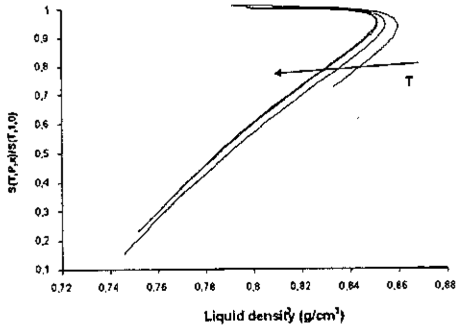

Figure 8: Solubility of a heavy compound versus the saturated liquid density. System: CO_2-Acetone. Temperatures: 25, 35, 40, 50°C

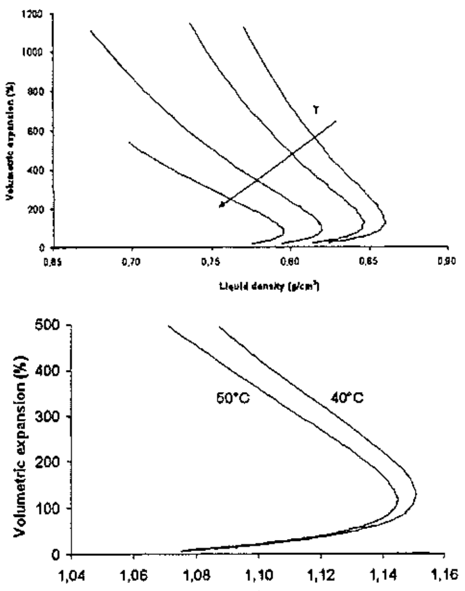

Figure 9: Volume expansion of the liquid versus the saturated liquid density. Systems: CO_2-acetone at 25, 35, 40 and 50°C (upper); CO_2-DMSO at 40 and 50°C (lower).

We note that the experimental data reported by Vaccaro et al. [6] for Ethylcellulose, Eudragit and HP-55 in Acetone at 40°C are consistent with the curves of Fig. 9. There, it was found that a single curve could represent acceptably all three systems, and that the points corresponding to the precipitation pressure were always located within 1-2% of the maximum density value. New data confirming this result in the case of a drug are presented in Fig. 10.

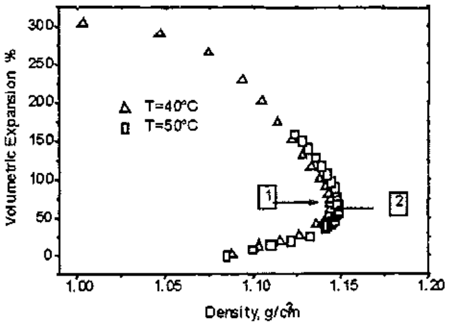

Figure 10: Volume expansion as a function of liquid density for the system CO_2- DMSO-Salbuthanole at two temperatures. Precipitation conditions are evidenced.

It is important to point out that, even if precipitation at given temperature and solvent takes place at a very similar liquid density for different compounds, indeed they show different precipitation pressures. This is so because the liquid density value around its maximum is rather insensitive to pressure. The model used in this work is unable to predict such a behavior. To account for the solute effect, an equation of state should be used, able to treat systems containing highly volatile components (such as CO_2), normal boiling fluids (the organic solvents) and long-chain molecules (the bio-polymers and the drugs). Such a model is currently not available in the literature and is matter of present research work [9].

Conclusions

The phase equilibria behavior of systems typical of a GASP process was analysed through both experimental measurements and a thermodynamic model. The well known result that, for a given solvent and solute, the precipitation is affected by the operating pressure and temperature, was interpreted in terms of the density of the liquid solution. It was shown that precipitation occurs when the saturated liquid density reaches a maximum. The content of the supercritical fluid (CO_2) in the liquid phase plays the key role in the process, since it determines the value of the liquid density. In the approximation of dilute solutions such a result was predicted theoretically. Our experimental measurements showed that precipitation is always obtained at a density which is close to the maximum and depends slightly on the compound, while the precipitation pressure may differ significantly for different compounds. Therefore, simultaneous precipitation of polymers and drugs with this technique can be achieved only operating at kinetically limited conditions.

Acknowledgements

We thank Mr. Marco Baggio for help in running experiments. Also the financial support of the Italian MURST (fondi ex-40%) is gratefully acknowledged.

References

1. Gallagher, P.M.; Coffey, M.P.; Krukonis, V.J., and N. Klasutis, N., in: *Supercr. Fluid Science & Technol.*, K.P. Johnston and J.M.L. Penninger Editors, **1989**, *ACS Symp Ser. 406*, 334-354
2. Bungert, B.; Sadowski G.; Arlt, W. *Fluid Phase Equil..*, **1997**, *139*, 349-359
3. Subramaniam, B.; Rajewski, R.A.; Snavely, K. *J. Pharm. Sci..*, **1997**, *86*, 885-890
4. Benedetti, L.; Bertucco, A.; Pallado, P. *Biotech. Bioeng.*, **1997**, *53*, 232-238
5. Winters, M.A.; Knutson, B.L.; Debenedetti, P.G.; Przybycien, T.M.; Stevenson, C.L.; Prestrelski, S.J. *J. Pharm. Sci.*, **1996**, *85*, 586-594
6. Vaccaro, F.; Pallado, P.; Bertucco, A. *Proc. 4th Italian Conf. Supercritical Fluids and their Applications*, p. 327-334, Capri (I), **1997**
7. Gallagher, P.M.; Coffey, M.P.; Krukonis, V.J. *J. Supercr. Fluids*, **1992**, *5*, 130-142
8. Chang, C.J.; Randolph, A.D. *AIChE J.*, **1990**, *36*, 939-942
9. Favati, F.; Elvassore, N.; Bertucco, A.; Fermeglia, M. submitted to *Chem. Eng. Sci.*, **1999**

Experimental and theoretical investigations of the formation of small particles from the rapid expansion of supercritical solutions (RESS)

Michael Türk*, Britta Helfgen, Stephan Cihlar and Karlheinz Schaber
Institut für Technische Thermodynamik und Kältetechnik, Universität Karlsruhe (TH),
Richard-Willstätter-Allee 2, 76128 Karlsruhe, Germany
mail to: tuerk@ttk1.ciw.uni-karlsruhe.de; fax: ++49-(0)721-60 71 02

RESS is an innovative and promising technology to produce small particles with narrow particle size distribution and it offers interesting applications for heat-sensitive organic compounds such as certain pharmaceuticals. At our laboratory, experiments are carried out with a RESS-apparatus suitable for temperatures up to 600 K and pressures up to 60 MPa [1]. Until now carbon dioxide has been used as solvent and naphthalene, cholesterol and benzoic acid as solutes [1,2,3]. In the present investigation, first experimental results for the system trifluoromethane/benzoic acid are reported and compared with the results for the system carbon dioxide/benzoic acid. Besides the experimental investigations the RESS-Process is modelled numerically considering the three parts capillary inlet - capillary - freejet. The one-dimensional time-independent flow model for the pure solvent includes heat-exchange in the capillary and the freejet, friction in the capillary and isentropic flow in the capillary inlet area. The calculated pressure and temperature changes along the expansion path are used to calculate the solute solubility in the solvent and the supersaturation of the real mixture. The results are theoretical supersaturations of 10^7 at residence times of $\approx 10^{-7}$ seconds and the classical nucleation theory leads to nucleation rates of about 10^{26} $cm^{-3} \cdot s^{-1}$ in the freejet. Furthermore, it is shown that the steady-state condition needs to be checked on a case-by-case basis once the solvent has changed as well as the supercritical solution has expanded significantly and that particle formation is dominated by coagulation-controlled growth.

Introduction

RESS is an promising technology to produce small particles with narrow particle size distribution and it offers interesting applications for heat-sensitive organic compounds such as certain pharmaceuticals. The rapid expansion of a supercritical solution through a capillary nozzle leads to a large cooling rate, resulting in high supersaturations with homogeneous nucleation and particle growth. The influence of the various process parameters (temperature and pressure in in the pre- and post-expansion chamber, nozzle geometry and temperature) on particle size has been studied in experimental and theoretical work, but until to date, the modelling can give only rough interpretations of the experimental results [4-9].

Experimental

The flow apparatus used in the present investigation was designed for experiments in the temperature range from 300 to 600 K and for pressures up to 60 MPa. The gaseous solvent is cleaned in a column, condensed, subcooled and pressurized to the desired pressure with a diaphragm pump. In a controlled water bath, the supercritical solvent is heated to the extraction temperature in a preheater, and then passed through an extraction column, which is packed with the solute. The mole fraction of the solute in the solvent can be measured offline at the exit of the extraction unit. After passing through the heated sampling valve the supercritical solution enters a heated high pressure vessel to reduce the flow velocity, and the preexpansion temperature is adjusted by a heating jacket. The preexpansion temperature and pressure are measured by a platinium resistance thermometer and a digital pressure gauge. The supercritical mixture is expanded into the expansion chamber through a heated, laserdrilled capillary nozzle with an inner diameter of about 55 µm and a length of 350 µm. For all experiments carried out, the expansion jet is sprayed always to ambient pressure and temperature. In contrast to the usual offline measurement technique, the particles precipitated are measured inside the expansion chamber online and in-situ with the 3-Wavelength-Extinction measurement technique. This multiple wavelength extinction technique, based on different attenuation of laser light of different wavelengths passing a particle cloud, has been used to determine the median diameter x of the particles. The particles are collected on a membrane filter and the gaseous solvent is vented. Additional samples for visual analysis of the particles by Scanning Electron Microscope can be taken directly behind the 3-WEM. A more detailed description of the experimental procedure is given in literature [1,2,3].

Results and Discussion

Table 1 shows the median particle size x of the systems a) carbon dioxide/benzoic acid and b) trifluoromethane/benzoic acid. Thereby, the extraction pressure p_E was equal to the preexpansion pressure p_0 and the extraction temperature T_E was $\approx$ 318 K. For both mixtures investigated, the experiments lead to similar results. In case of the lower preexpansion pressure ($p_0 \approx$ 13 MPa), the particle size varies between 580 nm and 1360 nm and for the higher preexpansion pressure ($p_0 \approx$ 20 MPa) between 430 nm and 1090 nm. Furthermore, at nearly the same preexpansion pressure and increasing the preexpansion temperature, the particle size increases, whereas the expansion from the higher pressure, at nearly the same preexpansion temperature, leads to markedly smaller particles. The particle size also depends on the solvent.

Table 1: Results for the systems investigated, T_{Nozzle} = 448 K, $D_{Nozzle} \approx$ 55 µm and $L_{Nozzle} \approx$ 350 µm.

a)			b)		
p_0 [MPa]	T_0 [K]	x [nm]	p_0 [MPa]	T_0 [K]	x [nm]
12.8	350	576	12.9	352	958
13.4	382	990	13.0	386	1147
13.5	408	1137	12.9	418	1362
19.9	351	500	19.9	351	434
20.0	385	752	20.0	384	555
19.9	415	1104	20.0	417	1089

According to the conditions p_0 = 20 MPa, T_0 = 380 K and T_{Nozzle} = 430 K, calculations with an one-dimensional time-independent flow model are performed. The model includes heat-exchange in the capillary and the supersonic freejet, friction in the capillary and isentropic flow in the capillary inlet area. Over the reduced distance x/L along the expansion path the flow is described by mass, momentum, and energy balances, plus an accurate equation of state. The unknown velocity at the capillary inlet is determined by Ma = 1 at the capillary exit. A more detailed description of the model is given in literature [2]. Because of the low solute concentration ($y^* < 10^{-3}$) along the expansion path the modelling of the gas dynamics can be performed by considering the pure supercritical solvent. The thermodynamic properties of the pure solvent are calculated by means of the extended generalized Bender-Equation of State [10]. It is shown elsewhere, that this equation of state is able to give a satisfactory presentation of the p, V, T - behaviour and of the caloric properties [3,10,11]. The differential equation system with the variables pressure, density, temperature, and velocity is solved with a numerical algorithm. The calculated pressure and temperature changes are used to calculate the supersaturation, S, of the real mixture.

$$S = \phi(T, p, y_E) \cdot y_E / (\phi(T, p, y) \cdot y) \qquad (1)$$

In Eqn. (1) ϕ is the solute fugacity coefficient in the dilute mixture, y_E the equilibrium mole fraction at extraction conditions and y the equilibrium mole fraction at prevailing expansion conditions. The variables y and ϕ are calculated by means of a modified Peng-Robinson-Equation of State [12].

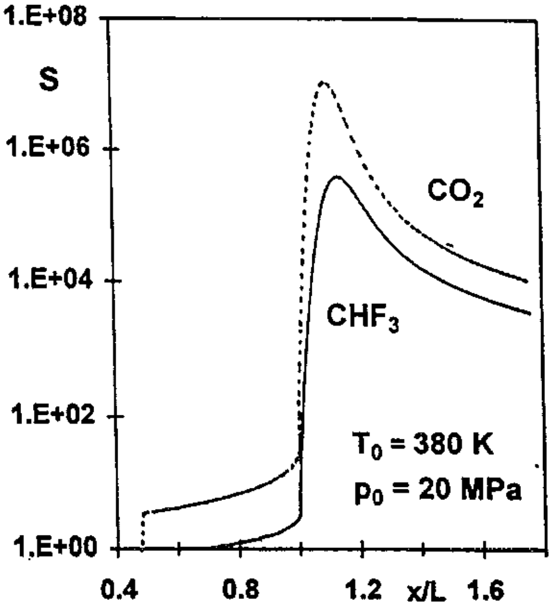

Fig. 1: Maximum theoretical supersaturation along the expansion path for the mixtures investigated (x/L = 1 at capillary exit).

Fig. 1 shows the evolution of the theoretically attainable supersaturation, S, for benzoic acid in carbon dioxide as well as for the same solute in trifluoromethane. In case of the former solvent, the supersaturation at the capillary nozzle exit is around ten and increases rapidly in the initial stage of the freejet up to values of about 1×10^7. Whereas for benzoic acid in trifluoromethane the supersaturation is always about ten times lower. In addition, typical orders of magnitude for the residence times in the capillary nozzle as well as in the supersonic freejet are in the range 10^{-6} s to 10^{-7} s.

In order to describe the kinetics of particle formation, the following expression for the nucleation rate J:

$$J = \theta \cdot Z \cdot \alpha_C \cdot n \cdot \pi \cdot r^{*2} \cdot c \cdot n \cdot \exp[-\Delta G^{*}/(k \cdot T)] \qquad (2)$$

was used. In Eqn. (2) θ is the non-isothermal factor (= 1 in case of dilute mixtures), Z the Zeldovich nonequilibrium factor, α_C the condensation coefficient (= 0.1, [13]), n the number of condensable molecules (= $\rho_M \cdot y_E \cdot N_A$), r^* the critical nucleus size corresponding to the maximum value of ΔG^* (= $4/3 \cdot \pi \cdot \sigma \cdot r^{*2}$), c the velocity (= $(8 \cdot k \cdot T/(\pi \cdot m)))^{0.5}$, and m the mass of the solute. Eqn. (2) is based on the classical nucleation theory arguments [14] and is more appropriate than the expressions for the nucleation rate [e.g. 6, 15] usually used in the literature. For the systems of interest, solvent dissolution in the incompressible solid is neglectible, and a value of 0.02 N/m for the solid-fluid interfacial tension σ was assumed.

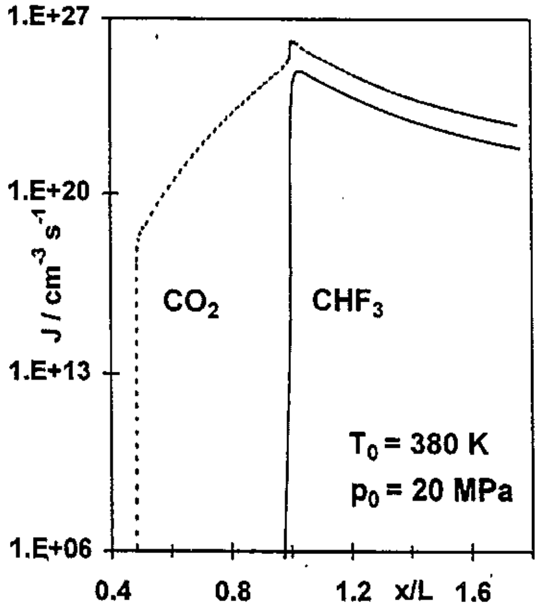

Fig. 2: Calculated nucleation rate along the expansion path for the mixtures in question (x/L = 1 at capillary exit).

Fig. 2 compares the calculated nucleation rate for the two mixtures investigated along the expansion path. In case of benzoic acid in carbon dioxide the calculations lead to a rapid increase of the attainable nucleation rate at the beginning of the capillary with values of 10^{17} cm$^{-3}\cdot$s^{-1} and a maximun nucleation rate of 2×10^{26} cm$^{-3}\cdot$s^{-1} in the initial stage of the freejet. On the other hand, for the mixture trifluoromethane/benzoic acid, the calculated nucleation rate is always less than 1 cm$^{-3}\cdot$s^{-1} inside the capillary nozzle and increases abruptly in the initial stage of the freejet up to 5×10^{24} cm$^{-3}\cdot$s^{-1}. From Fig. 2 it follows that in case of trifluoromethane/benzoic acid particle formation occurs probably in the initial stage of the freejet. Whereas, in case of the system carbon dioxide/benzoic acid, particle formation inside the capillary nozzle could not be excluded.

As mentioned above, the residence time of the supercritical solution is partly less than 10^{-6} s, so the use of Eqn. (2) derived for steady-state conditions, must be proved. This can be done with an equation valid for non-isothermal nucleation [13]:

$$t_S = \theta / (2 \cdot \alpha_C \cdot n \cdot v \cdot [2 \cdot \sigma/(\pi \cdot m)]^{0.5}) \qquad (3)$$

and proving the steady-state condition: $t_S/t_R \ll 1$. This means that relaxation time for attainment of a steady distribution of sub-critical clusters, t_S, is always less than residence time, t_R. In case of carbon dioxide/benzoic acid, the calculated values of t_S are less than 2.5×10^{-8} s inside the nozzle, which is four times smaller than the residence time and the steady-state condition might be satisfied. By contrast t_S increases up to 10^{-6} s in the initial stage of the freejet, therewith the steady-state condition is not satisfied. For the mixture trifluoromethane/benzoic acid, the prove of the validity of the steady-state condition leads to values for t_S/t_R nearly equal or greater than 1 in the freejet. Thus, these calculated nucleation rates must be interpreted with caution and the example shows, that the steady-state condition needs to be checked on a case-by-case basis once the solvent has changed as well as the supercritical solution has expanded significantly.

Due to the high attainable supersaturations, particle formation occurs by homogeneous nucleation and the particles grow either by coagulation or by condensation until the supersaturation disappears. Particle growth will be coagulation-controlled if $t_R \gg t_C$, where t_R is the residence time and t_C is the characteristic time between particle collision. An expression for the latter time is given by Lesniewski and Koch [16]:

$$t_C = 0.6053 \cdot r^{*2.5} \cdot [1/(v \cdot k \cdot T)]^{0.5} \qquad (4)$$

where v is the molecular volume of the particle. For the systems investigated, the values of t_C calculated for typical expansion conditions, are more than an order of magnitude smaller than t_R and thus particle growth might be coagulation-controlled.

Conclusions

RESS-experiments were performed with the mixture carbon dioxide/benzoic acid as well as trifluoromethane/benzoic acid. The experiments lead to particles in the range between 0.4 μm and 1.1 μm with the particle size depending on the solvent and the preexpansion conditions. In addition, the RESS-process was modelled numerically considering the three parts capillary inlet - capillary nozzle - freejet. The one-dimensional flow model for the pure solvent includes heat-exchange in the capillary and the freejet, friction in the capillary and isentropic flow in the capillary inlet area. Due to the rapid expansion of the supercritical solution through a capillary nozzle, the large decrease in density leads to calculated supersaturations of $10^5 < S < 10^7$ in the freejet and to corresponding nucleation rates of 10^{24} $cm^{-3} \cdot s^{-1}$ to 10^{26} $cm^{-3} \cdot s^{-1}$. From the calculated nucleation rates follows that in case of carbon dioxide/benzoic acid particle formation inside the capillary nozzle could not be excluded, whereas for the system trifluoromethane/benzoic acid particle formation occurs probably in the freejet. Furthermore, the use of the classical nucleation rate expression, derived for steady-state conditions, must be always proved critically and the influence of non-steady-state nucleation effects on attainable nucleation rates needs to be checked carefully. Due to very high attainable supersaturations particle growth is dominated by coagulation.

Acknowledgments

Part of this work was supported by the state government of Baden-Württemberg and by the grants Scha 524 / 5-1, 5-2, 5-3 of Deutsche Forschungsgemeinschaft (DFG), which is gratefully acknowledged.

References

1. S. Cihlar, M. Türk, K. Schaber, Micronization of organic solids by rapid expansion of supercritical solutions, Proceedings of the World Congress on Particle Technology 3, Brighton, UK, 6 - 9 July 1998, No. 380.

2. B. Helfgen, M. Türk, K. Schaber, Micronization by rapid expansion of supercritical solutions: Theoretical and experimental investigations, Proceedings of the AIChE Annual Meeting, 15. - 20. 11. 1998, Miami Beach, FL

3. M. Türk, Formation of small organic particles by RESS: - Experimental and theoretical investigations -, J. Supercrit. Fluids, in press

4. R. S. Mohamed, P. G. Debenedetti, R. K. Prud'homme, Effects of process conditions on crystals obtained from supercritical mixtures, AIChE J., 35 (1989) 386

5. J. W. Tom, P. G. Debenedetti, Particle formation with supercritical fluids - A Review, J. Aerosol Sci., 22 (1991) 555

6. X. Kwauk, P. G. Debenedetti, Mathematical modelling of aerosol formation by rapid expansion of supercritical solutions in a converging nozzle, J. Aerosol Sci., 24, (1993) 445

7. G. R. Shaub, J. F. Brennecke, M. J. McCready, Radial model for particle formation from the rapid expansion of supercritical solutions, J. Supercrit. Fluids, 8 (1995) 318

8. E. Reverchon, P. Pallado, Hydrodynamic modelling of the RESS process, J. Supercrit. Fluids, 9 (1996) 216

9. C. Domingo, D. Berends, G. M. van Rosmalen, Precipitation of ultrafine organic crystals from the rapid expansion of supercritical solutions over a capillary and a frit nozzle, J. Supercrit. Fluids, 10 (1997) 39

10. B. Platzer, G. Maurer, A generalized equation of state for pure polar and nonpolar fluids, Fluid Phase Equilib. 10 (1989) 223

11. M. Türk, Untersuchung der kalorischen Eigenschaften und der zwischenmolekularen Wechselwirkung für eine gasförmige Mischung aus Difluorchlormethan und Tetrafluordichlorethan, Dissertation, Universität Karlsruhe (TH), 1993

12. W. J. Schmitt, R. C. Reid, Solubility of monofunctional organic solids in chemically diverse supercritical fluids, Chem. Eng. Data, 31 (1986) 204

13. G. S. Springer, Homogeneous nucleation, Adv. Heat Transf. 14 (1978) 316

14. P. Treffinger, F. Ehrler, K. Bier, Spontane Kondensation in Überschallströmungen, Fortschritt-Berichte VDI, Reihe 7, Nr. 251

15. P. G. Debenedetti, Homogeneous nucleation in supercritical fluids, AIChE J., 36 (1990) 1289

16 T. K. Lesniewski, W. Koch, Production of rounded Ti - and Al - hydroxide particles in a turbulent jet by coagulation-controlled growth followed by rapid coalescence, J. Aerosol Sci., 29 (1998) 81

GVC-Fachausschuß „High Pressure Chemical Engineering", March 3-5, Karlsruhe, Germany, 1999 GVC FZK '99

Formation of Submicron Particles by Rapid Expansion of Supercritical Solutions

H. Kröber*, U. Teipel, H. Krause

Fraunhofer Institut für Chemische Technologie (ICT), P.O. Box 1240, D-76318 Pfinztal, Germany;

* e-mail: hkr@ict.fhg.de, Fax: +49-(0)721-4640-581

A pilot plant is presented, which has been built to prepare fine particles (< 1 µm) by the Rapid Expansion of Supercritical Solutions (RESS - process). In this study supercritical carbon dioxide was used to recrystallize cholesterol. The investigations were carried out by using two different Laval-nozzles. The particles obtained have a mean particle size in the range of about 300 to 500 nm. It turned out that neither changes of the concentration of the dissolved cholesterol in carbon dioxide and pre-expansion conditions (pressure and temperature) nor different nozzles have a provable influence on the particle size of the micronized particles. Merely, the pre-expansion pressure has a slight influence on the size of the particle obtained, it seems so that an increase in pressure results in smaller particles.

Introduction

Fluids at pressures and temperatures slightly higher than the critical point (supercritical fluids) were first found to dissolve solids with low vapour pressure more than a century ago by Hannay and Hogarth [1]. Supercritical fluids combine liquid-like density, higher diffusion coefficient and lower viscosity than common organic solvents. The solubility of non-volatile solutes in supercritical fluids can be much higher than the value calculated assuming ideal gas behaviour at the same temperature and pressure.

The RESS - process (Rapid Expansion of Supercritical Solutions) is a new technique for the production of crystalline uniform particles. When a solution consisting of a compressed gas as solvent and a dissolved solid is rapidly depressurized, the dissolved solid becomes insoluble in the low pressure gas. The rapid expansion of supercritical solution exploits this phenomena. During the process, a loaded supercritical fluid is expanded through a nozzle, creating high supersaturation in the jet. Fast nucleation and growth of the crystalline particle occurs. If carbon dioxide is used as a supercritical fluid the RESS - process offers advantages over conventional size reduction methods. Because of the low critical data of carbon dioxide ($p_C = 7.38$ MPa, $T_C = 304$ K) mild process conditions can be chosen to work on heat sensitive products. After the process the solvent is in the gaseous condition for which reason solvent free products can be achieved. By varying process parameters, the particle size distribution and the morphology can be influenced. Important process parameters are: concentration of the dissolved solid, pre- and post-expansion pressure, pre- and post-expansion temperature and the geometry of the nozzle. This technology will find application in the production of pharmaceutical substances and energetic materials.

Solids formation by the rapid expansion of supercritical solutions has been under investigations by several authors. Matson et al. [2, 3] studied ceramic precursor processing to obtain powder with better sintering characteristics. In the field of particle size reduction, they searched for alternatives to milling and solution crystallization, especially for pharmaceutical and thermally labile organic substances. Krukonis [4], Lele and Shine [5] and Debenedetti et al. [6] worked out processes to alter the morphology of polymer particles and to produce intimate blends of polymers with other materials. Gerber et al. [7] describes the influence of the post-expansion pressure on the particle size of anthracene.

These investigations show that the fundamental processes in the RESS-process are not sufficiently understood so far. For that reason the objective of this study is to describe the effects of nozzle diameter and conditions (pressure, temperature and concentration) before the nozzle upon the quality (e.g. particle size and morphology) of the solid product.

Materials

Fig. 1 shows the pressure-temperature phase diagram of carbon dioxide. A fluid whose temperature and pressure is simultaneously higher than the critical point is supercritical. At the critical point the boundary between the liquid and vapour phase disappears, the surface tension becomes zero and the properties of the fluid change dramatically. Especially the density of the fluid increases strongly in the near of the critical point and with that also the dissolution power of the fluid. This behaviour allows the use of compressed fluids in extraction processes.

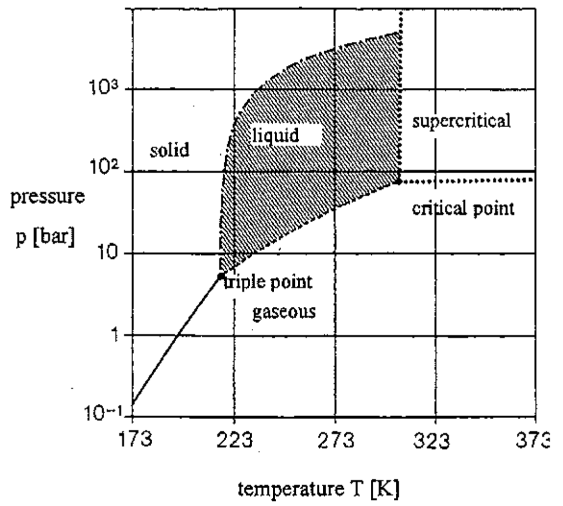

Figure 1: pressure-temperature phase diagram of carbon dioxide [8]

Several supercritical fluids have been used in the RESS-process. Carbon dioxide is a common one for low molecular weight solutes [4] because of its low critical pressure and temperature and the fact that it is inexpensive, non-toxic and non-flammable. In contrast to supercritical water the use of supercritical carbon dioxide does not require special material in the plant..

For our investigations cholesterol (Merck, purity: 97 %) was used as a model substance for pharmaceutical substances. Cholesterol counts among the category of the steroids and is a biological derivate of isoprene. The used carbon dioxide had a purity of 99.95 %.

To be able to carry out a RESS-process, it is necessary that the phase equilibrium of cholesterol dissolved in carbon dioxide is known as a function of temperature and pressure. This relationship is drawn from the literature and shown in Fig. 2:

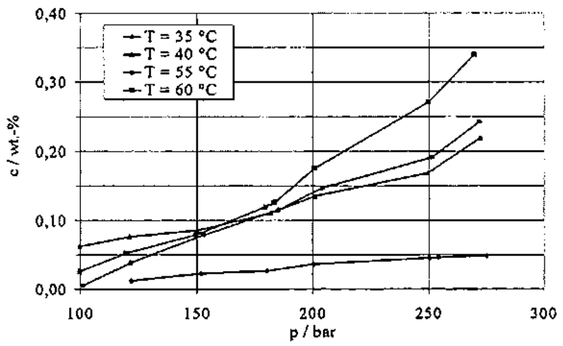

Figure 2: phase equilibrium concentration (mol fraction) of cholesterol dissolved in carbon dioxide [9]

Experimental Methods

The experiments were performed in a pilot plant which consists of three sections (as shown in Fig. 3 schematically): the CO_2-supply unit, the extractor and the separation vessel. The extractor is closed with two sintered metal filters (pore size 0.1 µm) to avoid discharging of the solid material. The maximum pressure in the plant is limited to 30 MPa, the extraction temperature to 353 K.

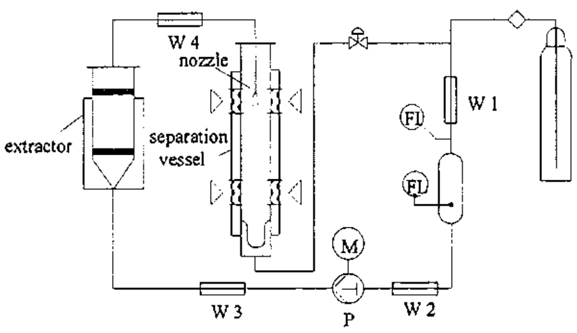

W: heat exchanger
FL: liquid CO_2 reservoir
P: jetting pump
FI: mass flow meter
D: pressure control

Figure 3: flow sheet of the experimental setup

Liquid carbon dioxide is cooled down (W1 and W2) to avoid cavitation in the membrane pump (P). After the compression to pre-expansion pressure, the fluid is heated to the extraction temperature (W3). In the extractor (V = 0.6 l), the supercritical fluid is charged with cholesterol. To avoid dropwise condensation during the expansion it is necessary to overheat the solution in an additional heat exchanger (W4). In the separation vessel the supercritical solution is expanded through a nozzle. In our experiments we used two different Laval nozzles with a 100 and 150 µm diameter, respectively. The particle formation can be observed through three sapphire windows which are placed on different positions in the separation vessel. The expanded gas will be condensed (W1) and recompressed or let off. After the experiment, the separation vessel is opened and the particles were collected. The size of these particles was measured by photon correlation spectroscopy (Malvern Zetasizer 3000).

Before measuring the particle size by photon correlation spectroscopy, the sample has to be prepared in the following way. 10 mg cholesterol are dispersed in a 0.05 wt.-% Tween 80/water-solution and treated with ultrasonic for 45 minutes. This dispersion is measured in the Zetasizer at 293 K. The refractive indices of cholesterol and water are 1.53 and 1.33, respectively. The particle size $x_{50,3}$ of each sample is calculated as a mean value of at least five measurements. The standard deviation for the particle size was calculated and it varied between 5 and 23 nm.

Results and Discussion

This work is part of a project in which cholesterol as a model substance is being studied in order to understand, and eventually, predict the effects of process variables upon the morphology and size distribution of the solid products obtained by expanding supercritical solutions. In this paper, we describe the effects of nozzle diameter and condition (pressure, temperature and concentration) before the nozzle upon the solid product.

The raw cholesterol (160 g), characterized by a mean particle size of 20 µm, was charged into the extractor and extracted with CO_2. The extraction pressure $p_{extr.}$ was between 15 and 20 MPa; the extraction temperature worked out between 308 K and 343 K. The supercritical solution was overheated up to 436 K and expanded through a Laval nozzle from pre-expansion pressure to atmospheric pressure and 298 K. The pre-expansion pressure p_0 was between 15 and 20 MPa. Our investigations was carried out with two different nozzles with diameters of 100 µm and 150 µm. The concentration of cholesterol in CO_2 is determined by measuring the whole mass of CO_2 consumed during the process and the decrease of the cholesterol in the extractor. Under these conditions the concentration of cholesterol in CO_2 was measured between 0.050 and 0.093 wt.-% for the 100 µm nozzle and between 0.031 and 0.089 wt.-% for the 150 µm nozzle, respectively.

In Fig. 4 the mean size of the particles obtained is presented in dependence of the concentration and nozzle diameter.

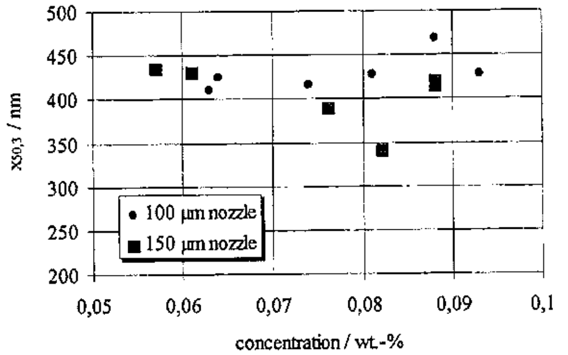

Figure 4: mean particle size of cholesterol obtained in the RESS-process (T_0 = 436 K, $p_0 = p_{extr}$ =20 MPa)

The results presented in this diagram show that the influence of the concentration and nozzle diameter on the particle size is not significant and systematic for the investigated cholesterol-carbon dioxide system. The mean particle size $x_{50,3}$ varies between 300 and 470 nm.

It is possible that the missing influence of the concentration on the size of the particles obtained can be explained by the low mass of cholesterol solved in CO_2. Unfortunately it was not possible to increase the concentration of cholesterol over 0.093 wt.-% because the retention time of the CO_2 in the extractor was not long enough to achieve the equilibrium concentration given by extraction pressure and temperature.

The influence of the pre-expansion pressure on the particle size is shown in Fig. 5. The extraction temperature $T_{extr.}$ is specified as a second parameter which was kept constant during the experiment. Because of the different pressure the concentration in the supercritical solution is not constant within one experimental campaign. The mean particle size is again in the range of 300 to 500 nm.

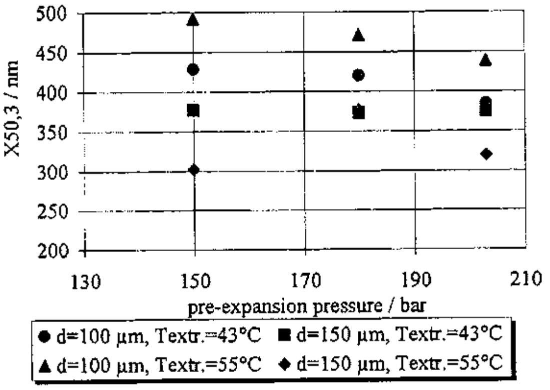

Figure 5: mean particle size of cholesterol obtained in the RESS-process in dependence of the pre-expansion pressure (T_0 = 436 K)

These presented results reveal a trend of the particle size in dependence on the pre-expansion pressure. An increasing pressure results in smaller particles even though the differences in particle size are not strongly marked. This behaviour is inconsistent with results presented by Smith et al. [10]. According to his remarks the number of molecules forming a cluster should increase with increasing expansion pressure. Despite of the fact that the size of a cluster is not identical with the particle size the general tendency should be comparable.

Supplementary, SEM-pictures of cholesterol particles obtained by the RESS-process were prepared. These pictures are not included in this paper but show that the recrystallized particles have a different morphology, shape and size as the original cholesterol. The pictures confirm the results received by the photon correlation spectroscopy, in general.

For raw cholesterol the mean volume diameter is about 20 µm and the particles are plate-like and rod shaped. The recrystallized particles are smaller and more or less filamentous. The thickness of these particles is between 50 and 300 nm, their length is up to 4 µm. The particles are agglomerated to very porous structures with a mean size of about 20 µm. It can be seen that different process conditions do not have an influence on the shape and morphology of the recrystallized particles.

Summary

A pilot plant was built to study the influence of different process parameters on the particle size produced by the RESS-process (Rapid Expansion of Supercritical Solutions). Particles in the range of about 400 nm were obtained for the system cholesterol/carbon dioxide.

In this study the influence of process parameters upon the size of the particles obtained was shown. In detail the conditions (pressure, temperature and concentration of cholesterol in carbon dioxide) before the expansion of the supercritical solution and the nozzle diameter was varied. It was seen that the mean size of the particles measured by photon correlation spectroscopy (PCS) was about 400 nm. In our investigations with the system cholesterol/CO_2, we did not find a significant and systematic influence of the concentration and nozzle diameter on the particle size. The pre-expansion pressure seems to have a little effect upon the particle size. It was shown that the mean particle size decreases with increasing pressure. SEM-pictures showed us that the recrystallized particles are more or less filamentous. The thickness of these particles is between 50 and 300 nm, their length is up to 4 µm. The particles are agglomerated to very porous structures with a mean size of about 20 µm. Different process conditions do not have an influence on the shape and morphology of the recrystallized cholesterol particles.

References

1. Hannay, J. B.; Hogarth, J.; "On the solubility of solids in gases", *Proc. Roy. Soc.*, **1879**, 29, 324ff
2. Matson D. W.; Petersen R. C.; Smith R. D.; "Formation of silica powder from the rapid expansion of supercritical solutions", *Advanced Ceramic Materials*, **1986**, 1, 242-246
3. Matson, D. W.; Petersen, R. C.; Smith R. D.; "The preparation of polycarbosilane powders and fibers during rapid expansion of supercritical fluid solutions", *Materials Letter*, **1986**, 4, 429-432
4. Krukonis, V.; "Supercritical Fluid Nucleation of Difficult-to-Comminute Solids", *AIChE meeting San Francisco*, **1984**, 140ff
5. Lele, A. K.; Shine A. D.; "Dissolution and Precipitation of Polymers Using a Supercritical Solvent", *Am. Chem. Soc.*, **1990**, 31, 677-678
6. Debenedetti. P. G.; Kwauk, X.; Tom, J. W.; Prud'homme, R. K.; "Particle formation following the rapid expansion of supercritical solutions", *AAAR meeting, Philadelphia*, **1990**, paper 3A.4
7. Gerber, P.; Teipel, U.; Krause, H.; "Solids Formation by Rapid Expansion of Supercritical Solutions", *Proc. Tech. Proceedings 12*, **1996**, High Pressure Chemical Engineering, Elsevier Science B.V., 369-372
8. Fachverband Kohlensäure-Industrie e.V.; *"Eigenschaften der Kohlensäure"*, 4. Auflage, **1992**
9. Kosal, E.; Lee C. H.; Holder G. D.; "Solubility of Progesterone, Testosterone and Cholesterol in supercritical Fluids", *J. Supercritical Fluids*, **1992**, 5, 167-179
10. Smith, R.; Wash, R.; "Supercritical Fluid Molecular Spray Film Deposition and Powder Formation", *U.S. Patent No. 4.582.731*, **1986**

Effect of Process Parameters on the Supercritical Antisolvent Precipitation of Microspheres of Natural Polymers

E. Reverchon*, I. De Rosa and G. Della Porta
Dipartimento di Ingegneria Chimica e Alimentare, Università di Salerno,
Via Ponte Don Melillo, 84084 Fisciano (SA), Italy
FAX 39 089964116, E-mail reverch@dica.unisa.it

Several polysaccharides are currently used as drug delivery system in form of microspheres and various routes have been used to prepare such microparticles. In this work, continuous supercritical antisolvent precipitation (SAS) has been used to produce sub-micronic particles of various natural polymers: inulin, dextran, and poly-hyaluronic acid (HYAFF 11). Supercritical carbon dioxide as the supercritical antisolvent and dimethylsulphoxide (DMSO) as the liquid solvent has been used. The effect of pressure, temperature and liquid solution concentration has been studied on the morphology, particle size and particle size distribution of polymer particles.

Introduction

Supercritical antisolvent precipitation (SAS) is a new technique used to produce micronic and submicronic particles with controlled particle size and particle size distribution [1]. When process conditions are well chosen, due to the very fast diffusion of the supercritical antisolvent, the liquid phase is rapidly expanded and eliminated causing the solute precipitation in form of very small particles with a narrow particle size distribution (PSD). CO_2 is commonly used as supercritical antisolvent, but other compounds have also been used [2-4]. The process is characterized by very mild conditions of temperature, no solvent residues and smaller particles are obtained when compared to the common industrial comminution techniques like jet milling, liquid antisolvent precipitation and crystallization [1].

SAS precipitation has been performed using different process arrangements. Among these, the continuous operation seems the most promising with respect to particle size and particle size distribution control and industrial application [1].

Until now, SAS has been applied to several fields: explosives and high-energy propellants [2], coloring matter [5], superconductor and catalyst precursors [6-8], pharmaceutical compounds [9-14] and some polymers [15] and biopolymers [16-20]. Among the tested biopolymers: the poly-L-lactic acid (PLLA) [16, 17] and poly-hyaluronic acid methyl esters (HYAFF-7, 11) [18-19] have been successfully processed and microparticles have been obtained; whereas the SAS of poly-DL-lactide acid (PDLA), polylactide acid-co-glycolide acid (PGLA) [17] and polycaprolactone (PCL) [20] was unsuccessful since these biopolymers were extracted by supercritical CO_2.

The scope of this work was to use continuous SAS processing to produce micro and sub-microparticles of controlled size and distribution of polysaccharides. These natural polymers can be used as drug delivery systems in form of microspheres, nanoparticles and films with the possibility of reducing toxicity and improving patient compliance. The morphologies of SAS processed polysaccharides have been studied and the influence of the SAS process parameters on particles size and particle size distribution has been analyzed.

Apparatus, Materials, Methods

The experimental apparatus consists of two high-pressure pumps (Gilson 305) that deliver the liquid and the supercritical antisolvent; an injection nozzle of 60 μm of internal diameter is used to spray the liquid solution to the precipitation chamber (500 cm^3 volume). A stainless steel frit at the bottom is used to collect the precipitated powder. A second vessel located after the precipitator operates at lower pressures and is used to recover the liquid solvent. A rotameter and a wet test meter are used to measure the instantaneous and the overall CO_2 delivered, respectively. More details on the apparatus were given elsewhere [6, 7].

Supercritical CO_2 is preliminary fed at a constant flow rate to pressurize the precipitator; then, the experiment starts when the liquid solvent is fed to the precipitator chamber through the nozzle. After 15 min, the liquid solvent flow is stopped and the liquid solution is fed through the injector. The precipitation process starts and continues for several minutes until the flow of the liquid solution is stopped. Supercritical CO_2 continues to flow in the chamber to wash out the supercritical solution formed by CO_2 and the liquid solvent. This operation can be very long (90 min or more) to avoid the re-condensation of the liquid inside the chamber.

Inulin (molecular weight 5000, extracted from Dahilia Tubers) and Dextran 40 (molecular weight 40000) were supplied by ICN Biochemicals (USA). HYAFF-11 was supplied by Fidia Pharmaceuticals (Italy). Dimethylsulfoxide (DMSO) (purity 99.5%), was bought from Carlo Erba Reagenti (Italy). CO_2 (purity 99.9%) was supplied by SON (Italy).

The approximate solubilities of inulin, dextran and HYAFF-11 in DMSO are 350, 20 and 35 mg/ml, respectively. The untreated inulin polymer was formed by some micron long irregular particles. The untreated dextran were formed by irregular spheres with a diameter ranging between 1 and 100 μm. The untreated HYAFF-11 polymer were formed by very long fibres (some mm).

Samples of processed biopolymers were observed by a LEO 420 Electron Scanning Microscope (SEM). The samples were covered with 250 Å of gold using a sputter coater (Agar mod. 108A). Particle size and particle size distribution were calculated using an image analysis software (Sigma Scan Pro, Jandel Scientific). More than 200 particles were measured for each PSD calculation.

Results and discussion

Continuous SAS experiments reported in this work have all been performed using DMSO as the liquid solvent and operating at 40 °C, to avoid problems connected to the glass transition of polymers and its lowering in presence of supercritical CO_2. The range of precipitation pressures explored was from 95 to 150 bars. Pressures larger than 100 bar assure that DMSO asymptotic expansion has been obtained [1]. The experiments were performed using liquid flow rates between 0.7 and 1 ml/min. The ratio between CO_2 flow rate and liquid solution was fixed at 20.

At pressures larger than 100 bar the three biopolymers showed a similar basic morphology at the various SAS conditions we tested: they all were precipitated as spherical nanoparticles. However, HYAFF-11 in some cases showed a tendence to organize these nanoparticles in long fibres in which the original spherical structure of single elements was still visible. Inulin particles were largely higher than the ones produced using the other two polymers. Examples of spherical nanoparticles are shown in Figure 1 and 2 that proposed a SEM images of HYAFF-11 precipitated at 150 bar, 40°C from a solution of 10 mg HYAFF-11/ml DMSO and inulin precipitated at 150 bar 40°C from a solution of 50 mg inulin/ml DMSO, respectively.

We performed a series of experiments at pressures ranging from 100 to 150 bar. In this range of operating conditions the effect of pressure on the particle size and particle size distribution was not measurable. When we performed experiments at fixed pressure (150 bar) by varying the concentration of the injected liquid solution, we found an increase of the mean particle size. Particles ranging from about 0.1 to 6 μm were produced by increasing the concentration of the injected solution. An even more relevant increase of the corresponding particle size distribution was obtained. This experimental evidence is in line with the results we obtained on some others compounds processed by SAS. Among these: yttrium acetate [6], samarium acetate [7], zinc acetate [8], salbutamol [12], tetracycline [13], amoxicillin [14]; the influence of concentration was much more relevant for inulin than for dextran-40 and HYAFF-11. This difference could be explained taking into account that polymers are characterized by very high molecular weights and molecular weight distributions.

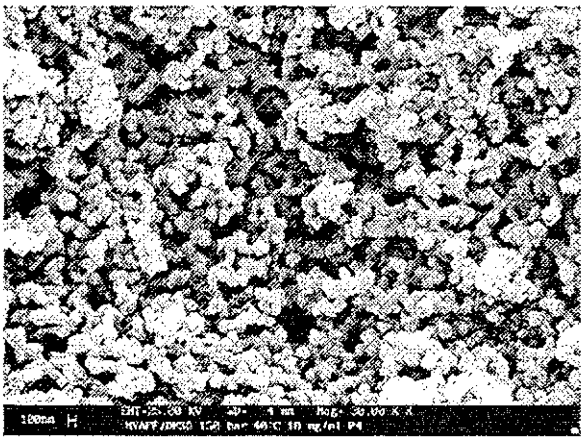

Figure 1. SEM image of HYAFF-11 particles obtained by SAS operating at 150 bar, 40°C and 10 mg/ml. H = 100 nm

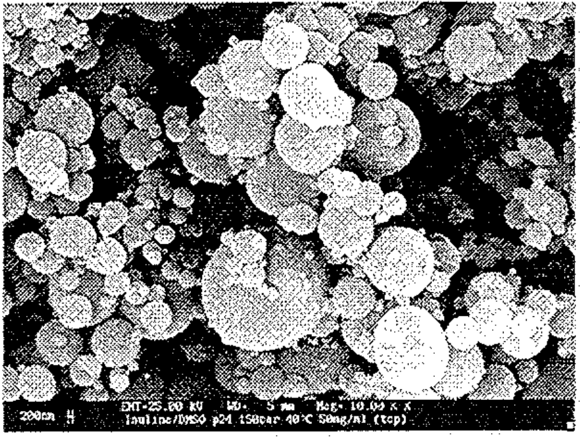
200nm
EHT=25.00 kV WD= 5 mm Mag= 10.00 K X
Inuline/DMSO p24 150bar 40°C 50mg/ml (top)

Figure 2. SEM image of inulin particles obtained by SAS operating at 150 bar, 40°C and 50 mg/ml. H = 200 nm.

These two characteristics can play a role during the nucleation and growth phenomena that characterise the precipitation. Therefore, the precipitation of the polymer with low molecular weight (inulin) was much more influenced by liquid solution concentration.

Another relevant factor to be considered during SAS of polysaccharides is connected to the stability of the produced powders. It is well known that polysaccarides have a strong affinity with water; therefore, they are moisture sensitive. This effect is even more pronounced when they are in form of nanoparticles. Indeed, we have experienced the collapse of polysaccharides nanoparticles (mainly dextran and inulin) when they were expose to air at ambient room conditions but with a high relative percentage of humidity.

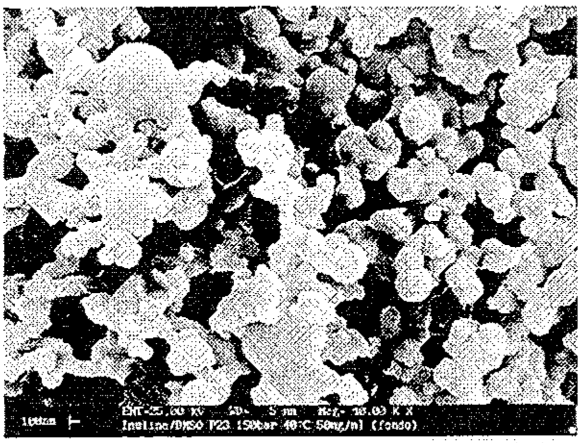
100nm
EHT=25.00 kV WD= 5 mm Mag= 10.00 K X
Inuline/DMSO P23 150bar 40°C 50mg/ml (fondo)

Figure 3. SEM image of inulin particles produced at 150 bar, 40°C and 50 mg/ml after exposure at air. H = 100 nm.

An example of the influence of humidity on polysaccharide nanoparticles is shown in Figure 3 where a SEM image of inulin nanoparticles is reported. These particles were produced at 150 bar, 40°C, 50 mg/ml DMSO and exposed for several minutes to air with a high percentage humidity. The result of this operation was the marked coalescence of the nanoparticles in large aggregates, though the original spherical structure is still present. SEM images of dextran or inulin exposed to air for some days revealed a complete coalescence of the particles and the formation of an homogeneous mass of material.

Conclusions

In conclusion, our experiments were successful in demonstrating the SAS processability of some polysaccharides. We obtained nano- and micro-particles and were able to control (within certain ranges) particle size and particle size distribution.

Since they are a moisture sensitive material the powers obtained by SAS have to be stored in dry conditions.

References

1. Reverchon, E.; *J. Supercrit. Fluids*, **1999**, in press.
2. Gallagher, P. M.; Coffey, M. P.; Krukonis, V. J.; Klasutis, N.; Supercritical fluids Science and Technology, *ACS Symp. Series*, **1989**, 406, 334-354.
3. Schimtt, W. J.; Salada, M. C.; Shook, G. G.; Speaker, S. M. III, *AIChE J.*, **1995**, 41, 2476-2486.
4. Tan, C.-S.; Chang, W.-W., *Ind. Eng. Chem. Res.*, **1998**, 37, 1821-1826.
5. Gao, Y.; Mulenda, T. K.; Shi, Y.-F.; Yuan, W.-K., *J. Sup. Fluids*, **1998**, 13, 369-374.
6. Reverchon E., Celano C., Della Porta G., Di Trolio A., Pace S., *J. Material Research*, **1998**, 13 (2), 284-289.
7. Reverchon E., Della Porta G., Pace S., Di Trolio A.; *Ind. Eng. Chem. Res.*, **1998**, 37, 952-958.
8. Reverchon E.; Della Porta G.; Sannino D.; Ciambelli P., *Powder Technology*, **1998**, in press.
9. Yeo, S. D.; Lim, G. B.; Debenedetti, P. G.; Bernstein, H., *Biotech. Bioeng.*, **1993**, 41, 341-346.
10. Jaarmo, S.; Rantakyla, M.; Aaltonen, O., In *Proceed. of the 4th Int. Symp. on Supercritical Fluids*, K. Arai Eds., Sendai (Japan), **1997**, pp 263-266.

11. York, P.; Hanna, M. Salmeterol xinafoate with controlled particle size, Internat. Patent C07C215/60, **1994**.
12. Reverchon, E.; Della Porta, G.; Pallado, P., *Pharm. Res.*, **1998**, submitted.
13. Reverchon E., Della Porta G., *Powder Technol.*, **1998** submitted.
14. Reverchon E., Della Porta G.; Falivene, M.G.; *J. Pharm. Sci*, **1998** submitted.
15. Dixon, D. J.; Luna-Bercenas,G.; Johnston, K. P.; *Polymer*, **1994**, 35, 3998. Randolph, T. W.; Randolph, A. D.; Mebes, M.; Yeung, S., *Biotech. Progress*, **1993**, 9, 429-435.
16. Bleich, J.; Muller, B. W.; Waβmus, W., *Internat. J. Pharm.*, **1993**, 97, 111-117.
17. Benedetti, L.; Bertucco, A.; Pallado, P.; *Biotech. Bioeng.*, **1997**, 53, 232-238.
18. Saim, S.; Subramaniam, B.; Rajewski, R. A.; Stella, V. J.; *Pharmaceut. Res.*, **1996**, 13, S273.
19. Bodmeier, R.; Wang, H.; Dixon, D. J.; Mawson, S.; Johnston, K. P.; *Pharm. Res.*, **1995**, 13, 1211-1217.

Research with SITEC Modular Pilot Units

Pilot units are a very important tool in order to check the feasibility of this technology for your product range or to search for new or higher quality products. Also the next development step namely the optimization of the process conditions which is the
basis for scale up can be done using such a unit.

In **Supercritical Fluid Extraction (SFE)** a compressed gas (at supercritical conditions) is used as solvent. SFE can be applied to selectively extract certain components out of solid or liquid products and is a good tool to extract thermolabile high molecular components or to produce new high quality products.

Both **Rapid Expansion of Supercritical Solutions (RESS)** and **Gas Anti-Solvent Recrystallisation (GAS)** are fascinating techniques to produce very fine, very uniform powders which are very interesting for pharamceutical products.

Supercritical Reactions with high selectivity, enhanced conversion rates and homogeneous reactions based on unlimited solubility of reactants.

Sterilisation: High pressure treatment of food or drugs leads to the destruction of microorganisms. The **SITEC** standard models (desk-top and laboratory models) are suitable tools to do such research work.

All **SITEC** Laboratory and Pilot Units for above mentioned technologies are based on well known and tested basic modules. Therefore the pilot units can easily be adapted to your requirements.

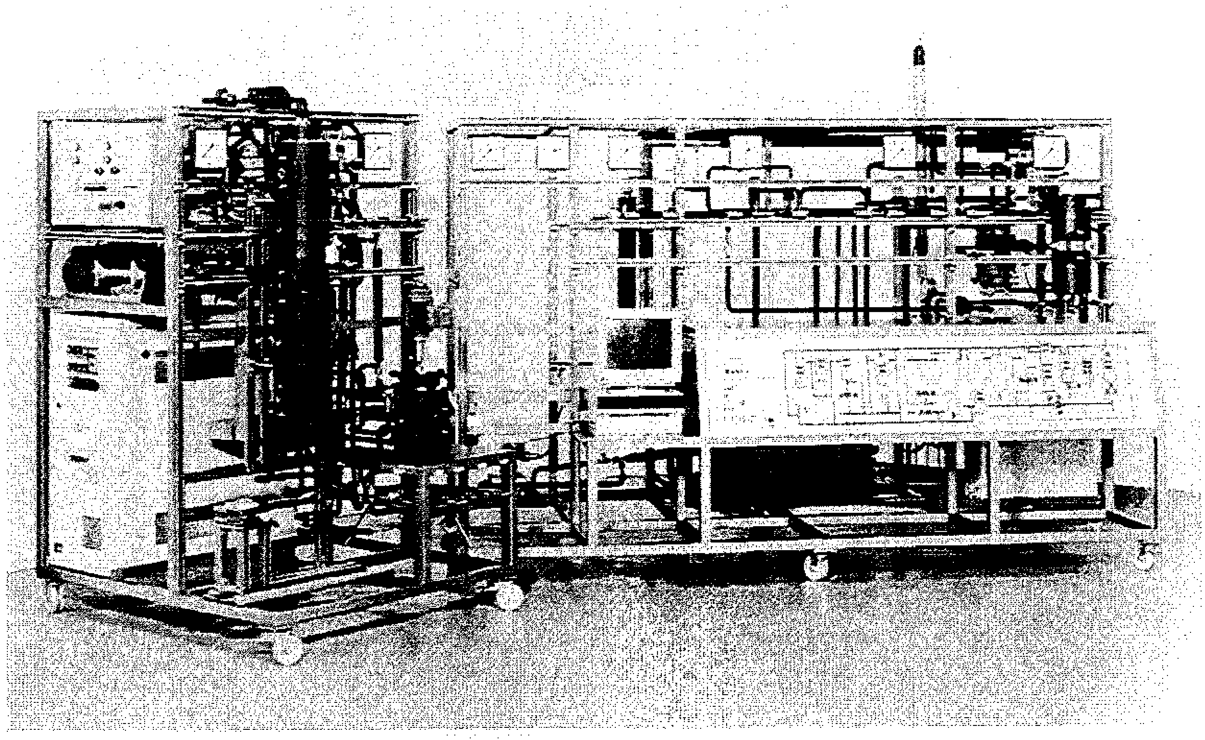

SITEC-Sieber Engineering AG
Aschbach 621
CH – 8124 Maur / Zürich
Switzerland

Tel.: +41 (1) 982 2070
Fax: +41 (1) 980 1538
e-mail: sieber@sitec-hp.ch
homepage: http://www.sitec-hp.ch

Separation Techniques

Separation of Fine Chemicals through Continuous Supercritical Fluid Simulated Moving Bed (SF-SMB) Chromatography

O. Di Giovanni[a], W. Dörfler[a], M. Mazzotti[a], M. Morbidelli[b*]

[a]Institut für Verfahrenstechnik, ETH Zürich, CH-8092 Zürich, Switzerland
[b]Laboratorium für Technische Chemie, ETH Zürich, CH-8092 Zürich, Switzerland
fax number: ++41-1-632 1082; e-mail: morbidelli @tech.chem.ethz.ch

Continuous chromatographic separation processes, based on the Simulated Moving Bed (SMB) technology, have gained increasing industrial importance. The use of supercritical fluids as eluents presents numerous advantages over the conventional application in gas and liquid phase. Particularly, in the case of SF-SMB the use of a supercritical eluent allows an elution strength gradient to be applied through a pressure gradient, thus optimizing separation performance. In order to best exploit this possibility, a thorough understanding of the nonlinear adsorption behaviour of solutes in supercritical solvents is needed. A quantitative prediction of experimental data must take into account the competitive adsorption of the supercritical solvent and the non-idealities in fluid and adsorbed phases. Since the adsorbed amount can be measured only as excess amount the application of established models, like the RAST (Real Adorpion Solution Theory), has to be carefully considered.

Introduction

The evolution of pharmaceutical, agrochemical and food industries is clearly towards purer products and cleaner processes, due to stricter regulations and growing environmental concerns.

Preparative chromatography has been increasing its importance as a separation and purification process in the above mentioned industries, since it is flexible, non-energy intensive and achieves high purity performances. Batch preparative chromatography can be scaled up to continuous production scale chromatography through the Simulated Moving Bed (SMB) technique with further advantages in terms of process performance. Nowadays, the liquid phase SMB technology is extensively adopted in these industries for difficult applications, such as the resolution of racemates.

Supercritical fluids, in particular supercritical carbon dioxide, have replaced organic solvents in many cases, because they are non-toxic and easily recycled, while allowing mild operating conditions, easy recovery of products and minimization of waste solvent disposal. Moreover, the easy tunability of properties, such as density, viscosity and solubility, makes supercritical solvents attractive media for many separation and reactive processes.

Combining these two concepts leads to supercritical fluid chromatography (SFC), i.e., chromatography using supercritical eluents. The aim of this work is to contribute to lay down the basis for its application to production scale separations, through the supercritical fluid SMB (SF-SMB) technology [1,2]. Several fundamental and applicative issues related to this technique are still open and the following specific objectives have to be reached:

1) the thermodynamic description of competitive adsorption of supercritical mixtures;
2) the analysis and assessement of preparative SFC through modeling and experiments;
3) the development of optimal and robust design criteria for SF-SMB units;
4) the optimal operation of a pilot SF-SMB unit.

Supercritical Fluid Chromatography (SFC)

The first and most important step in the development of this new technology is the characterization of nonlinear adsorption equilibria of the system solute-supercritical solvent-stationary phase. All the data available in the literature show that under supercritical conditions adsorption isotherms depend on total pressure [3]. In particular the solute loading on the stationary phase decreases, when increasing the density of the the mobile phase. This behaviour is different from what observed in adsorption from the gas and the liquid phase and it may be explained based on different phenomena, including non-idealities and competition of the solute.

The non-ideality of the fluid phase has been for long time considered the only explanation to this phenomenon. In fact larger fluid phase density yields greater solubility, i.e. higher affinity for the solute for the fluid phase in comparison to the adsorbed phase.

Moreover the nonideality of the adsorbed phase itself may be not negligible at such high pressure.

The competition of the supercritical solvent for the adsorption sites is also always responsible for such an effect, but only a few authors take this phenomenon into account in the analysis of adsorption isotherms from supercritical mixtures. On the other hand adsorption isotherms of carbon dioxide on various adsorbents have been published, showing that also the solvent has a non negligible affinity with the stationary phase.

In determining adsorption isotherms one must be aware that at high pressure only the excess amount adsorbed can be measured, yielding the so called *excess isotherm* [4], which exhibits a characteristic maximum as a function of carbon dioxide pressure. The relation between the real amount adsorbed (n) and the excess amount (n^e) is:

$$n^e = n - V_{ads}\,\rho \qquad (1)$$

where V_{ads} is the volume of the adsorbed phase, which cannot be measured, and ρ is the fluid phase density. The fact that the experimental values are just excess values gives a further explanation for the loading decrease at high density.

To account for these new features, an extension of the Real Adsorption Solution Theory (RAST) to excess isotherm data [5] is required. The main difficulty is the definition of a mixing law that allows the total amount adsorbed from a mixture to be expressed as a function of the pure component isotherms.

The measurement of multicomponent adsorption equilibria can be carried out using different techniques and procedures. On the one hand a high pressure magnetic suspension balance may be used for direct gravimetric measurements. On the other hand chromatographic methods, such as pulse experiments, frontal analysis and perturbation methods, may applied using a small-scale packed SFC column. The experiments may be performed both in pure carbon dioxide and in the presence of a modifier. The results of the measurements are correlated using the above mentioned thermodynamic model, thus achieving a proper physico-chemical characterization of the system under investigation. Due to the ever increasing interest for the chromatographic separation of chiral compounds, the model separation selected is the enantioseparation of a biological active substance, e.g. Naproxen or Ibuprofen.

Supercritical Fluid Simulated Moving Bed (SF-SMB)

In the SF-SMB technology, the well known advantages of supercritical fluid chromatography, namely easy separation of products and solvent and full compatibility of the most common solvent (i.e. CO_2) with any product bound to be used on humans, are coupled with the SMB performance improvements due to the possibility of tuning the elution strength of the mobile phase. The importance of tuning the elution strength of the mobile phase stems from the different roles played by the different sections of the SMB unit. On the one hand, since the objective of section 1 is the desorption of any adsorbed species, its operation is favored by a large elution strength of the mobile phase. On the other hand, since the objective of section 4 is the adsorption of any species still present in the fluid phase, its operation is most convenient when the elution strength of the mobile phase is small. It follows that in general the best choice corresponds to a compromise between the opposite needs in section 1 and 4.. However, the SF-SMB technology allows for a novel approach to this optimization problem, based on the enforcement of an elution strength gradient in the SBM unit. This can be achieved by imposing different pressure levels in the four sections of the unit, which can be realized by locating a pressure control valve after each column, between outlet and inlet valves. Thus, since the density of the supercritical mobile phase decreases with decreasing pressure, the Henry costants of the components increase according to the following equation:

$$H_i = H_{i,0}\left(\frac{d_0}{d}\right)^{b_i} \qquad (2)$$

where the subscript *0* refers to reference conditions and b_i is an empirical parameter that depends only on the chromatographic system, i.e., the supercritical eluent, the stationary phase and the specific solute *i*. Accordingly, by imposing a decreasing pressure gradient from section 1 to section 4, we realize also a decreasing gradient of the elution strength of the mobile phase, thus achieving the optimal condition. This analysis applies straightforwardly to systems characterized by linear isotherms, i.e. operated under rather dilute conditions. The extension to SF-SMB operated under competitive nonlinear adsorption conditions requires the adoption of the nonlinear detailed thermodynamic description discussed above.

It is worth noting that this is particularly important, since SMB advantages with respect to preparative chromatography are due to the possibility of operating under overload conditions, where nonlinear adsorption behavior is observed.

References

[1] J.Y. CLAVIER, R.M. NICOUD, M. PERRUT, " A new efficient fractionation process: The Simulated Moving Bed with Supercritical Eluent" in P.Rudolph von Rohr, Ch. Trepp (Eds.), High Pressure Chemical Engineering, Elsevier Science, London, 1996.

[2] M. MAZZOTTI, G. STORTI, M. MORBIDELLI, "Supercritical Fluid Simulated Moving Bed Chromatography", *J. Chromatogr. A*, 786 , 309 (1997).

[3] I. KIKIC, P. ALESSI, A. CORTESI, S.J. MACNAUGHTON, N.R. FOSTER, B. SPICKA, "An Experimental Study of Supercritical Adsorption Equilibria of Salicylic Acid on Activated Carbon.", *Fluid Phase Equilibria*, 117, 304 (1996).

[4] S. SIRCAR, "Excess Properties and Thermodynamics of multicomponent gas adsorption", *J. Chem. Soc. Faraday Trans.*, 81 , 1527 (1995)

[5] G. GAMBA, R. ROTA, G. STORTI, S. CARRA, M. MORBIDELLI, "Adsorbed Solution Theory Models for Multicomponent Adsorption Equilibria", *AIChE J.*, 35, 959 (1989).

Alcohol Reduction from Excess Wine by Supercritical CO_2-Extraction

T. Gamse*, F.Steinkellner and R. Marr

Institute for Chemical Engineering and Environmental Technology
University of Technology Graz, Inffeldgasse 25
A-8010 Graz, Austria
fax: + 43 316 873 7472
email: GAMSE@glvt.tu-graz.ac.at
*Corresponding author

The extraction of alcohol and aroma compounds from excess wine, which means a low quality and therefore low price wine, by supercritical CO_2-extraction has been tested. In a continuous operating high pressure extraction plant the influence of extraction parameters like pressure, phase ratio, kind of phase contact and kind of packings were determined to reduce the alcohol content of excess wine from initially 11.3 vol% to a raffinate concentration of about 3 vol%.

Introduction

The coming into force of the alcohol limit of 0.5 ‰ for road users at the beginning of 1998 in Austria resulted in different gastronomically areas in dramatically decrease of turnover. As well the wine dresser association Krems as the federal office for viniculture in Eisenstadt confirm, that an market introduction of a "light wine" with an alcohol content of about 4 to 5 vol% including the whole wine aroma has excellent chances on the market and is demanded by the gastronomy.

The separation of ethanol form aqueous solutions using supercritical CO_2 has been studied by different research groups [1-13].

For producing alcohol-free wine or alcohol-reduced wine different patents exist, which are mainly a combination of distillation and high pressure extraction with supercritical CO_2. A patent for producing alcohol-free wine was developed at the Institute for Chemical Engineering and Environmental Technology, University for Technology Graz [14]. For this process in the first step only the aroma compounds are extracted from wine by CO_2-extraction. In a subsequent distillation column ethanol is separated from the raffinate of the CO_2-extraction. Remixing of the extracted aroma compounds into the bottom product of the distillation column produces alcohol-free wine with high content of aroma compounds. Another patent [15] describes the other way round by separating ethanol together with the aroma compounds in a distillation column. The aroma compounds from this top product are extracted in a high pressure extraction plant and recycled into the bottom product of the distillation, so that again alcohol-free wine is produced.

The disadvantage of both processes is that a distillation step is included, which means thermal treatment of the material and therefore loss or change of thermal sensitive compounds. Up to now about 280 substances in wine have been detected and especially the aroma substances are available in very low concentrations, but even small changes in composition of these aroma compounds might result in completely different smell and taste of wine.

The aim of this new process is to extract with supercritical CO_2 ethanol and aroma compounds from wine of poor quality without thermal treatment. The amount of excess wine per year depends on certain circumstances, especially climate conditions, which results in large or small quantities with low market price. In the European Commission excess wine is also distilled for production of ethanol. This excess wine of pour quality represents the raw material for this process.

Using supercritical CO_2 a selective extraction of only ethanol is not possible because also most of the aroma compounds are extracted. One possibility is to use two extraction columns, one operating at lower pressure to remove the aroma compounds and the second at higher pressure level to extract ethanol. The disadvantage of this method are the high investment costs of two high pressure extraction columns. Another possibility is to extract at high pressure level as well aroma compounds as ethanol and separate these substances by a subsequent fractionated separation. Depending on phase equilibria and solubility behaviour in the first separator at higher pressure level substances with lower solubility (ethanol) are removed from the CO_2 stream and the second separator is operated at low pressure and maybe different temperature to collect the compounds with high solubility in CO_2 (most of the aroma compounds). For the case that the fraction of the first separator contains many aroma substances a purification by chromatographic method using again CO_2 as solvent might be necessary.

First of all it was necessary to determine CO_2 extraction efficiency, which means is it possible to achieve an alcohol content in the raffinate of about 3 vol% starting with an initial concentration of

11.3 vol%. This low raffinate concentration was chosen to be flexible in further processing to achieve an alcohol reduced wine of 4 to 5 vol% alcohol. By this way it is possible to remix the product of the second separator even if certain amounts of ethanol are present. Further it is possible to recycle not only the separated aroma compounds from the second separator but also to add small amounts of the original wine to the raffinate for increasing the light wine quality by adding these aroma compounds which might get lost in the separation steps.

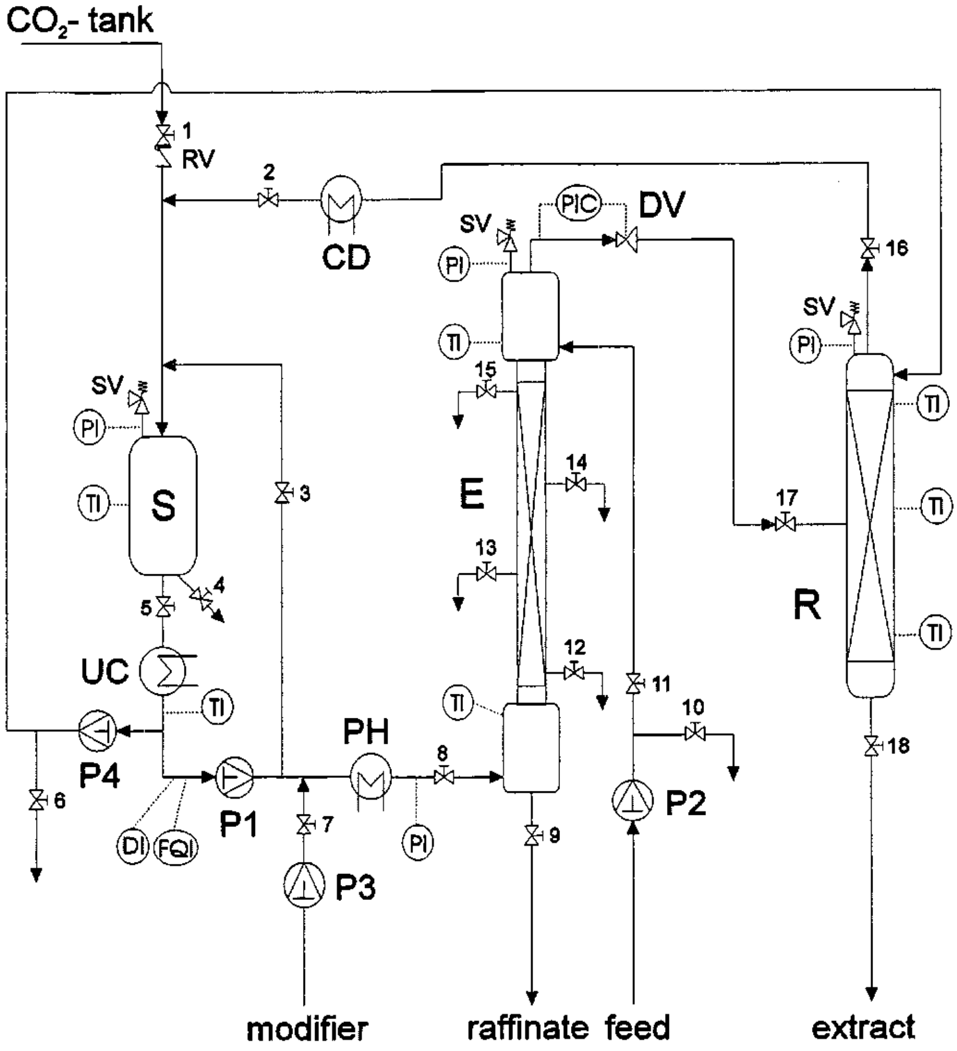

Figure 1: Schemata of the continuous operating high pressure CO_2 extraction column

Materials and Methods

Materials: The carbon dioxide with a purity higher than 99,94 % (v/v) and a dewing point lower than -60°C was purchased from Linde (Graz) and stored in a tank with a capacity of 3200 L. Equation of Bender [16, 17], a 20 parameter equation of state, was used for calculation of CO_2 density at different pressure and temperature levels.

The Federal Viniculture Office Eisenstadt supplied the white wine, called "Grüner Veltliner", mainly produced in the Austrian regions of Burgenland and Niederösterreich. All detailed analysis of as well CO_2-extract as raffinate and all sensorial tests by a wine commission were performed in Eisenstadt.

The alcohol content of samples taken along the height of the extraction column and of the raffinate was analysed in a thermostated Paar densimeter by relative density. This means the density of taken wine samples is compared to the density of water at 20°C. Before density measuring the solved CO_2 had to be removed form samples, which was achieved by putting the sample flasks into an ultrasonic bath for about 2 minutes.

Experimental set-up: A flow-sheet of the continuous operating high pressure CO_2 extraction column is shown in Fig.1. The extraction column (inner diameter 35 mm, active height 2 m, maximum operating pressure 180 bar, maximum operating temperature 100°C) includes top and bottom settlers for phase separation. These settlers are equipped with sight glasses to determine and adjust the boundary layer. For the case the column is operated with continuous liquid phase and dispersed CO_2 phase, the boundary layer in the top settler is controlled with the help of a video camera, which transmits the pictures to a monitor. The monitor is situated close to the raffinate valve at the bottom of the column and therefore accurate adjustment of the boundary layer by regulating the raffinate valve is possible.

Liquid CO_2 from the storage tank (S) passes an undercooler (**UC**), is compressed with a Lewa diaphragm pump (**P1**) with adjustable flow (flow rate 2 - 20 l/h, maximum pressure 250 bar) and heated up to extraction temperature in a preheater (**PH**). If necessary modifier can be added to the CO_2 stream with pump **P3**. The CO_2 stream enters at the bottom of the column and liquid feed is injected at the top of the column by a Lewa diaphragm pump with adjustable flow (flow rate 0 - 15 l/h). Raffinate is withdrawn at the bottom of column and the loaded CO_2 from the top of the column is expanded by a Kämmer pressure regulated expansion valve (**DV**) into the regeneration column (maximum operating temperature 100°C, maximum operating pressure 100 bar). This regeneration column exist of four segments (inner diameter 50 mm, segment height 500 mm, Sulzer DX packings) so that three positions for the inlet in the column can be chosen. All segments are equipped with double wall for thermostating and the bottom segment has additionally an inside heating tube. At the top of the regeneration column liquid CO_2 can be injected with pump **P4** for better regeneration and CO_2 is recycled into the storage tank passing a condenser (**CD**) to reach liquid state again.

Besides raffinate and extract samples can be taken along the column height to determine extraction course. The instrumentation includes measuring of temperature, pressure, CO_2 flow rate by a mass flow meter (see Fig. 1) as well as thermostats for constant operating temperatures. All apparatus are equipped with safety valves.

Operation conditions: Temperature in the extraction column was set constant at 25°C because as determined in preliminary tests higher temperatures cause foaming of wine and this foam is that stable that it will not separated in the top settler and enters the regeneration column, which reduces extraction efficiency. The regeneration column was operated at 45°C and no liquid CO_2 reflux was necessary for CO_2 purification. Different pressure stages (90 bar, 110 bar, 130 bar, 160 bar) were tested at different phase ratios and phase control. Different phase ratios of CO_2 to aqueous feed were adjusted (50, 15, 7.5, 5 and 3,75 kg/kg) by changing the liquid flow rate (0.5, 1, 2, 3 and 4 kg/h) and constant CO_2 flow rate of 15 kg/h.

Results

Bubble column: The column was operated without inlets as bubble column with CO_2 as dispersed phase. Extraction temperature was set constant at 25°C. The results at different phase ratios and pressures are given in Fig. 2 and it is obvious that the influence of phase ratio is dominant while changes in extraction pressure have nearly no influence. The best separation efficiency of 60.5% could be achieved with a phase ratio of 30 kg/kg and 160 bar resulting in an ethanol concentration in the raffinate of 4.48 vol%. Increasing of separation efficiency could not be achieved by further increase of phase ratio because of problems with flooding.

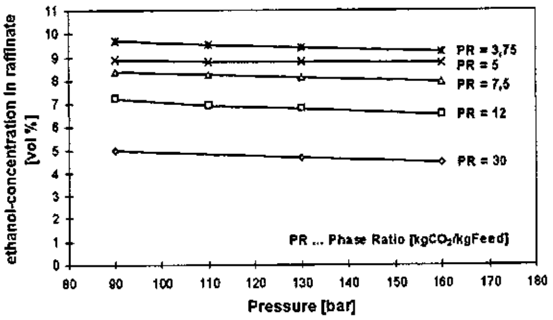

Figure 2: Influence of pressure and phase ratio on raffinate concentration

Pall® rings For increasing extraction efficiency metallic Pall® rings (dimensions 10 x 10 x 0.3 mm, Raschig company) were used. The disadvantage of these inlets is the relatively high pressure drop and therefore phase inversion occurred when using CO_2 as dispersed phased because of the small density difference between aqueous feed and CO_2. Therefore the aqueous feed had to be dispersed in the continuous CO_2 phase. As given in Fig. 3 again phase ratio is the dominant effect on extraction efficiency and changes in pressure have nearly no influence comparable to the results operating the column as bubble column. The ethanol concentration in the raffinate could be lowered to 2.88 vol% at 160 bar and a phase ratio of 30 kg/kg with a CO_2 flow rate of 15 kg/h. Starting with an initially concentration of 11.3 vol% an extraction yield of 74.6 % could be achieved and the goal of the project could be reached to lower the ethanol content in the raffinate to about 3 vol%.

Temperature effect For a phase ratio of 7.5 kg/kg experiments with increasing temperature from 25°C to 32°C were carried out. In contrast to the bubble column experiments no problems with foaming occurred when operating the aqueous feed as dispersed phase. As shown in Fig. 3 higher temperature lowers the ethanol concentration in the raffinate. Extraction yield could be increased by 8% for 32°C extraction temperature.

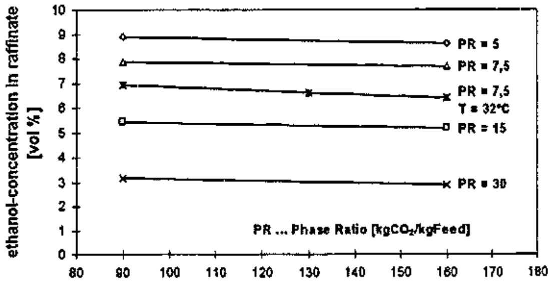

Figure 3: Influence of pressure, temperature and phase ratio on extraction efficiency using Pall® rings

Calculation of HETP values Based on equilibria data for the system water - ethanol - CO_2 the HETP values (height equal to one theoretical plate) are calculated supposing water and CO_2 as inert flows, which means that solubility of CO_2 in water and of water in CO_2 are neglected. As shown in Fig. 4 an increase in phase ratio lowers the HETP values dramatically. Changing phase ratio from 3.75 kg/kg to 30 kg/kg lowers the HETP value at 90 bar extraction pressure by 60.9 % and at 160 bar by 55.9 %. This is a result of the much better phase contact and therefore better mass transfer. Comparing these data with the results of the bubble column the HETP values with Pall® rings and highest phase ratio (30 kg/kg) are 25,9% (90 bar) and 22,7 % (160 bar) lower. This shows the efficiency of the Pall® rings by increasing phase contact and therefore mass transfer.

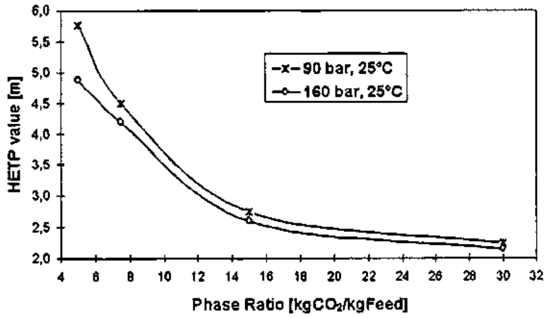

Figure 4: Influence of pressure and phase ratio on HETP values with Pall® rings

Conclusion

The aim of the project, to remove not only aroma compounds but also most of the alcohol from wine was reached. The raffinate concentration of about 3 vol% could be achieved when operating the column with Pall® rings and dispersed aqueous feed at 160 bar and 25°C. The raffinate concentration of 2.88 vol% under this conditions corresponds to an extraction efficiency of 74.6 % and a calculated HETP value of 2.14 m. This means that nearly one theoretical step is sufficient, which could be realised in the available high pressure extraction plant.

References

1. Brignole E.A.; Andersen P.M.; Fredenslund, A. *Ind. Eng. Chem. Res.* **1987**, 26, 254-261
2. Bunzenberger, G.; "Zur Stofftrennung mit Kohlendioxid unter Druck in flüssig-flüssig und flüssig-fest-Systemen", **1988** Thesis TU Graz
3. Bunzenberger, G.; Marr, R.; in: M. Perrut (Eds.), Proceedings of the International Symposium on Supercritical Fluids, vol. 2, **1988**, p.613-618
4. Brignole, E.A.; *Fluid Phase Equilibria* **1986**, 29 133-144
5. Giacomo, G.D.; Brandani, V.; del Re, G.; de la Ossa, E.M.; in: Proceedings of 2nd International Symposium High Pressure Chemical Engineering, **1990**, p.231-236
6. Furuta, S.; Ikawa, N.; Fukuzato, R.; in: Proceedings of 2nd International Symposium High Pressure Chemical Engineering, **1990**, p.345-351
7. Gilbert, M.L.; Paulaitis, M.E.; *J. Chem. Eng. Data* **1986**, 31, 296-298
8. Yoon, J.H.; Lee, H.; Chung, B.H.; *Fluid Phase Equilibria* **1994**, 102, p.287-292
9. Fernandez, S.; Lopes, J.A.; Machado, A.S.R.; Nunes da Ponte, M.; Reves, J.C.; in: G. Brunner, M. Perrut (Eds.), Proceedings of the Third International Symposium on Supercritical Fluids, vol. 2, **1994**, p.491-495
10. Medina, I.; Martinez, J.L.; in: G. Brunner, M. Perrut (Eds.), Proceedings of the Third International Symposium on Supercritical Fluids, vol. 2, **1994**, p.401-406
11. Brunner, G.; Kreim, K.; *Chem. Ing. Tech.* **1985** 57 (6), 550-551
12. Brunner, G.; Kreim, K.; *Ger. Chem. Eng.* **1986**, 9, 246-250
13. Gamse, T.; Rogler, I.; Marr, R.; *J. Supercrit. Fluids* **1999**, 14, 123-128
14. European Patent No. 0 228 572 B1
15. European Patent No. 0 397 642 A1
16. Bender, E.; in: Proceedings Fifth Symposium on Thermophysical Properties of American Society of Mechanical Engineers, **1970**, p.227-235
17. Sievers, U.; *VDI - Fortschr. - Ber. VDI-Z.*, **1984**, Reihe 6, Nr. 155; Düsseldorf VDI-Verlag

Hydrodynamics In Countercurrent Packed Columns At High Pressure Conditions

P.C. Simões*, M.J. Cebola, R. Ruivo, M. Nunes da Ponte
Departamento de Química, Centro de Química Fina e Biotecnologia, Faculdade de Ciências e Tecnologia,
Universidade Nova de Lisboa, 2825 Monte da Caparica, Portugal
EMAIL: pcs@dq.fct.unl.pt FAX: +351 1 2948385

The design of countercurrent packed columns operating at supercritical conditions requires knowledge about their hydrodynamic behaviour. This subject still receives less attention than mass transfer or phase equilibria studies at high-pressure conditions causing a dearth of reliable hydrodynamic models. We have built a new apparatus for the hydrodynamic study of a structured gauze packing column operating in a countercurrent way. Preliminary results on the hydrodynamics of two different systems are presented in this paper. The deacidification of olive oil by supercritical carbon dioxide was chosen as a case study due to its commercial interest. Flooding conditions were poorly detected with this system due to the present low capacities of the fluid pumps. Experimental data was also collected for a model system consisting of squalene, $C_{30}H_{50}$, and oleic acid. Flooding data were determined for certain extraction conditions of temperature and pressure. The density difference between the two contacting phases appears to be an important factor as flooding is concerned. The model system, with a lower liquid density, flooded easier than the olive oil system.

Introduction

One of the main applications of supercritical fluids is in the field of separation processes, particularly in the extraction of high-value substances from natural products. When dealing with liquid mixtures, continuous supercritical fluid extraction (SFE) is usually carried out in countercurrent packed columns like conventional liquid-fluid separation processes. Packing is provided to help establish the two-phase contact mechanism. When one wants to quantify the separation efficiency of such columns, knowledge on the mass transfer and hydrodynamic behaviour is fundamental. If the first issue has been studied during the last years with some effort, evaluation of the hydrodynamics of packed towers at such high-pressure conditions is still a relatively unstudied subject despite being of key importance to establish the ultimate capacity of the column.

Some of the work reported in the literature on mass transfer characteristics of SFE packed columns was also concerned with hydraulic characteristics; their interested was devoted to observe the physical contact between the two phases on the packing surface [1,2]. To our knowledge, only relatively few studies entirely devoted to hydrodynamics at high-pressure conditions were until now presented in the literature. Meyer and Brunner [3] studied the hydrodynamic behaviour of common oils in supercritical carbon dioxide. A Sulzer type gauze structured packing was used in these experiments and flooding conditions of the column were visually observed as well as determined by measuring the pressure drop across the packing section. Mention was made on the importance of the density difference between the two phases to the loading capacity and extraction efficiency of a packed column. Bernad et al. [4] measured the liquid hold-up and liquid axial dispersion for the countercurrent flow of water and SC carbon dioxide on a *Sulzer BX* stainless steel structured packing. The column was able to operate as a bubble column (the dispersed phase being the carbon dioxide-rich phase) as well as a trickle bed column (liquid phase dispersed). Finally, Woerlee [5] carried out a general study on the application of hydrodynamic models to SFE packed columns. Experimental data was collected for a laboratory-type structured gauze packing and a aqueous solution/carbon dioxide system. In this work hold-up and pressure drop were measured for several operating conditions. A relatively overlooked problem was emphasised by the author: the large influence that the physical properties may have on the loading capacity of high-pressure columns. Severe physical property changes (on density, viscosity, and diffusivity) occur when using supercritical fluids and the influence of these changes on column efficiency is still fairly understood.

The design of a supercritical fluid extraction process needs fundamental data on phase equilibria, mass transfer and also on the hydrodynamics of the extractor. Models that may be applied for such unconventional conditions are essential. Although some of the published work [3,5] deals with this subject, much more work is needed until reliable models are available. Towards this goal, we have built a new apparatus that allows one to study the hydrodynamic behaviour of packed columns at high-pressure conditions. The main goal will be to collect experimental data for further model development. Here, we describe the hydrodynamic apparatus and present preliminary results for two different systems: the deacidification of olive oil by supercritical carbon dioxide and the model system squalene / oleic acid / carbon dioxide. These systems show different liquid phase properties and thus different hydrodynamic behaviours were obtained.

Experimental

Apparatus:

The experimental apparatus used for the hydrodynamic study is schematically shown in Fig. 1. The main piece of equipment is the stainless steel extraction column, *EC* (see Fig.1 for abbreviations). It consists of four stainless steel tubes of 50 cm high and 2.4 cm of internal diameter (the thickness of the tube wall is 0.8 cm), connected to each other by means of three hexagonal cross-section pieces. The total height of the column, including the entrance and exit parts is 2.45 m. The hexagonal sections are fitted with entrance points for temperature and pressure measurement, and phase collection along the column. Sapphire windows ($1^{1}/_{4}$ in of diameter) are located at the bottom and top hexagonal pieces for visual observation of hydrodynamics. The column is filled with structured *Sulzer EX* gauze packing elements of 5.5 cm high each. The total packing height is estimated as 2 m. Specifications of the packing are 1710 m^2/m^3 of specific surface area and 0.86 m^3/m^3 of fractional void volume.

The column has been operating until now as a stripping column, the liquid feed introduced by means of a liquid piston pump *LP* (LDC Analytical) above the packing section at the top of the column. Fresh carbon dioxide is introduced by the bottom of the column by means of a metering pump *MP* (*Lewa* pump). The inlet point of the CO_2 stream is located in between the level of the liquid residue deposited in the bottom section of the column and the point where the packing ends. The liquid level inside the column is maintained at a constant position by manually opening the raffinate valve, V_{raf}. Control of the liquid level is made by simple visualisation through the sapphire window located at the bottom of the column. A thermocouple, introduced at about the middle section of the bottom sapphire window column, was found to be useful in controlling the amount of liquid inside the column due to the different thermal capacities of the liquid and gas phases when wetting this thermocouple.

The sapphire windows were also used to visualise the hydrodynamic phenomena, *i.e.*, to determine the flooding points and the flow mechanisms through the packing section, at such high-pressure conditions. A differential pressure sensor, ΔP, (*Rosemount* 1151 HP) was connected to two of the hexagonal pieces at the middle of the column, and measured the pressure drop over a section of 1.05 m of packing bed.

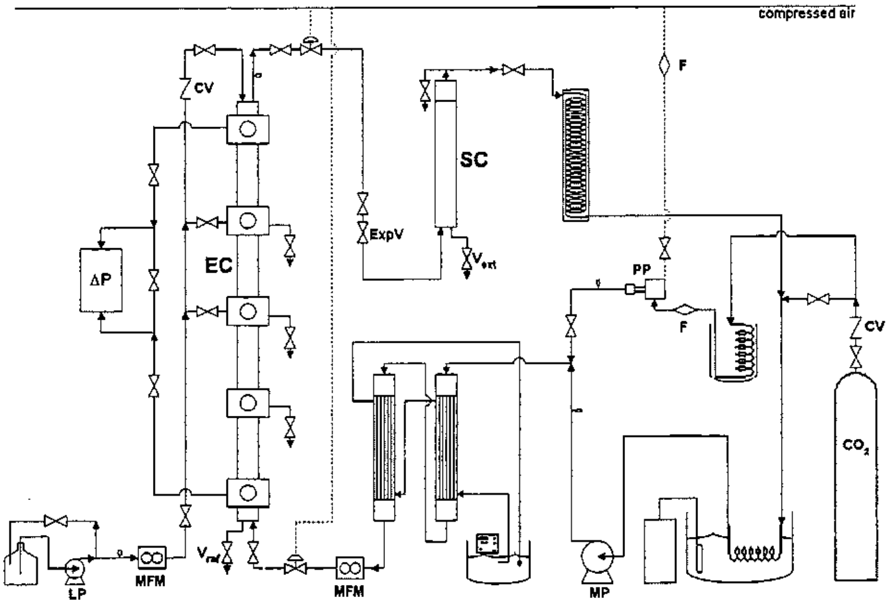

Figure 1. Schematic diagram of the hydrodynamic apparatus.

Method:

Before hydrodynamic characteristics are evaluated for each set of operating conditions (pressure, temperature and gas to liquid flow ratios), steady state condition is achieved in the extraction column. Pressure in this column is maintained by means of expansion valve, *ExpV*, located downstream the gas outlet flow. Separation of dissolved substances is accomplished in a second column, *SC*. Liquid level inside the column is maintained at a constant level during the run. When steady state is reached, a change is made on one of the following properties: pressure, gas flow or liquid flow. Flooding point is visually observed at the top of the column when a meniscus appears in the sapphire window zone. The hold-up of dispersed phase may be measured in the end of a run by shutting off the column from the rest of the apparatus and let the dispersed phase to coalesce and drop by gravity to the bottom leg of the column.

Materials:

Carbon dioxide was supplied by *Air Liquide* with a purity of 99.995%. Olive oil was of commercial virgin grade and purchased locally. Squalene and oleic acid were supplied by Merck (98% and 70% by weight, respectively).

Results and Discussion

Due to technical difficulties arisen with the differential pressure sensor, the flooding conditions were determined by visual observation only.

The first runs were made with virgin olive oil as the feed. The global composition of this oil was 1 wt% of free fatty acids, the rest made of triglycerides. The deacidification process of olive oil by supercritical carbon dioxide was previously studied [6] and mass transfer and phase equilibria data are available for this system. Here, our goal was to assess the limiting conditions of flow in the packed column.

The extraction temperature was set at 313K. The liquid feed rate was first kept at a low value, 0.13 kg/h, and the gas flowrate fixed at 7 kg/h. The extraction pressure was then slowly increased from 13 MPa till 24 MPa, the other parameters kept constant. Olive oil flowed down wetting the packing surface. The gas flowed upwards through the channels of the packing in a continuous way. No flooding situation was detected in this run. This is an interesting result, since one important factor when discussing the packing effectiveness in separation towers is the density difference, $\Delta\rho$, between the two phases. Some authors point out that a safe value for this difference should be observed in order to have an efficient mechanism flow through the packing section. Brunner, for instance, considers a difference of 100 kg/m^3 to be a reasonable limiting value [7]. Few comments were made until now about this proposed limit. Concerning our experiment, at 24 MPa and 313K, the pure carbon dioxide density is 873 kg/m^3. The density of the commercial olive oil measured at 313K was 913 kg/m^3; this means that the phase density difference for this run was around 40 kg/m^3. Although the phase densities were estimated from the pure substance values and, as a consequence, no composition influence on their densities was taken into consideration, the low figure obtained for $\Delta\rho$ is indicative that the olive oil system may be processed at low density differences without flooding occurs.

A flooding point was possible to be determined for this system by forcing the operating conditions to reach the actual flow capacities of the apparatus. The experimental flooding data is shown in Table 1. Due to the actual undersized capacities of the fluid pumps we were unable to detect other flooding points.

Table 1. Flooding data for structured packing Sulzer EX, as determined for the olive oil and squalene / oleic acid systems. *G* stands for the CO_2 flow and *L* for the liquid flow.

Pressure [MPa]	Temperature [K]	G [kg/h]	L [kg/h]
Olive oil/CO_2 system			
20.3	313	17.5	0.37
Squalene/oleic acid/CO_2 system			
11.0	313	12.8	0.24
		11.3	0.36
		4.9	0.72
		5.2	0.89
		3.5	1.48
15.0	333	12.8	0.36
		7.3	0.78
		4.8	1.40

The second system to be studied was a mixture of 75 wt% of squalene and 25 wt% of oleic acid. The flooding capacity of the packed column was determined for two operating conditions, 11.0MPa/313K and 15.0MPa/333K.

First, at 313K we checked the limiting value of $\Delta\rho$ for a normal two-phase flow through the packing. The flowrates were fixed at 0.15 kg/h for the liquid, and 6.3 kg/h for the gas flow. An absence of liquid flowing down in the bottom of the column was detected at a pressure of 16.4 MPa, suggesting the possible formation of a second liquid/gas interface inside the column. At these conditions, the density difference, estimated from the pure substance data, is 60 kg/m^3, which is higher than the olive oil value. The density of the mixture at 313K was determined to be 860 kg/m^3, which is lower than the olive oil density at the same temperature. As before, the real composition of the two phases was not taken into consideration for the density calculation.

The flooding data obtained for the squalene/oleic acid/carbon dioxide system is presented in Table 1. The use of higher liquid flowrates lowers the maximum gas capacity through the packed column. The influence of the density difference of the two phases in the loading capacity of the column is better understood in Fig. 2 where we show a flooding diagram of our structured packing. For comparison, we have included hydrodynamic data available in the literature for other high pressure systems.

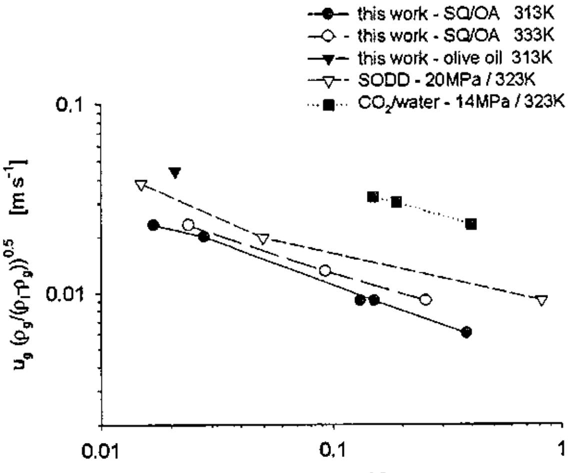

Figure 2. Flooding diagram of EX gauze packing at supercritical conditions. Literature data: Soybean oil deodoriser distillate (SODD)/CO_2 - ϕ_{column} = 3.5cm [7]; CO_2/water - ϕ_{column} = 3.6 cm, unspecified gauze packing [5].

At 15.0MPa/333K the density difference between the two phases is higher than at 11.0MPa/313K; consequently, the gas loading capacity of the column at the highest temperature is increased. There is a relative concordance between our experimental data and literature data, even if they refer to different test systems and column dimensions.

Conclusions

A new apparatus for hydrodynamic research in countercurrent packed columns at supercritical extraction conditions was built. Flooding points for two systems showing different liquid phase composition and density were measured. Deacidification of virgin olive oil by supercritical carbon dioxide was possible to operate in a broad range of extraction pressures. For the model system squalene/oleic acid in carbon dioxide flooding was detected at much lower pressures. The influence of the solubility of the carbon dioxide-rich phase in the hydrodynamic behaviour will be studied further on.

Acknowledgements

Financial support by Fundação para a Ciência e Tecnologia, under project grant number PBIC/C/QUI/2364/95, is gratefully acknowledged. The authors also acknowledge Müller Extract Company GmbH&Co., Fábrica Torrejana de Azeites, Stazione Sperimentale per le Industrie degli oli e dei Grassi, and Technische Universitat Hamburg Harburg, as partners of the project contract Nr. FAIR CT 96-1075 (European Commission *RTD Life Science and Technologies programme*) and the European Commission for the financially support of this work.

References

1. Rathkamp, J.; Bravo, J.L.; Fair, J.R. *Solv. Ext. and Ion Exchange* **1987**, 5(3), 367-391.
2. Lim, J.S.; Lee, Y.-W.; Kim, J.-D., Lee, Y.Y. *J. Supercrit. Fluids*, **1995**, 8(2), 127-137.
3. Meyer, J.T.; Brunner, G. In *Proceedings of the 3rd. International Symposium on Supercritical Fluids*; Brunner, G.; Perrut, M., Eds.; I.S.A.S.F.: Strasbourg, France, 1994; Tome 2, 217-222.
4. Bernad, L.; Barth, D.; Perrut, M. In *Proceedings of the 2nd International Symposium on High Pressure Chemical Technology*; Vetter, G. Ed.; Dechema: Erlangen, Germany, 1990; 553-558.
5. Woerlee, G.F. Ph.D. thesis, Delft Technical University, Delft, 1997.
6. Carmelo, P.J.; Simoes, P.; Nunes da Ponte, M. In *Proceedings of the 3rd. International Symposium on Supercritical Fluids*; Brunner, G.; Perrut, M., Eds.; I.S.A.S.F.: Strasbourg, France, 1994; Tome 2, 107-112.
7. Brunner, G. In *Proceedings of the 4th International Symposium on Supercritical Fluids*; Saito, S.; Arai, K., Eds.; I.S.A.S.F.: Sendai, Japan, 1997; Tome C, 745-756.

SYNTHESIS OF HEAVY HYDROCARBONS (C_{26} AND C_{28}) AND PURIFICATION BY SUPERCRITICAL CARBON DIOXIDE EXTRACTION

D. BARTH(1)*, **S. GANDOLFO**(1), **A. BREMBILLA**(2), **D. PETITJEAN**(1), **M. DIRAND**(1)

(1)Laboratoire de Thermodynamique des Séparations, E.A.2287
(2)Laboratoire de Chimie-Physique Macromoléculaire UMR 7568-CNRS-INPL
E.N.S.I.C.-1, rue Grandville-BP451-54001-NANCY (France)
barth@ensic.u-nancy.fr-fax :33 3 83350811

Two components, n-hexacosane and n-octacosane have been chemically synthesized. N-octacosane was prepared by reaction between bromooctane and dodecanedioyl dichloride via an organozincic intermediate, to form the corresponding Blaise's diketone. The reduction of this latter compound by a Wolff-Kishner reaction led to the n-alkane. The same synthesis way was used in order to obtain n-hexacosane. The synthesized alcanes have been purified by supercritical carbon dioxide extraction. The experiments were not so easy because the feed and the solute are solid under atmospheric conditions. We have tried to optimize the separation and the withdrawn of the solute by using cyclonic separators. The purity of the extract was established by several ways : melting point, calorimetric analysis, gas chromatography, X ray diffraction and the purity of the purified products was compared to the commercial products.

Introduction

The evaluation of the cristallization point of fuels can be only accessed from the knowledge of the thermodynamic properties of the higher n-alkanes which compose them, and if any, whose crystalline structures have been solved[1,2]. An equimolecular binary mixture n-octacosane/n-hexacosane should be a good model for the study of the complex paraffinic deposits which form in the oily fluids. To this end, it is essential to have at one's disposal, the highest purity material.

The commercial products contain, as main impurities, branched-chains and/or linear chains of closely related homologues which are extremely difficult to eliminate. The purpose of this work deals with the synthesis of the two components. The solubility of n-alcanes in supercritical carbon dioxide are well known in the litterature. It is the reason why we have choosen to purify the synthesized alcanes by supercritical CO_2 extraction.

1. Materials and Methods

^1H and ^{13}C NMR spectra were recorded on a Bruker AC-200P spectrometer for deuteriochloroform solutions. Chemical shifts are given in δ scale downfield from TMS I.R.F.T spectra were measured with a Bruker IFS 25 spectrophotometer.

The differential scanning calorimetry analyses were realized by using a Setaram DSC 111 Calorimeter of Tian Calvet Type.The X-ray diffraction experiments were carried out with a counter diffractometer.

Products were analyzed by gas chromatography on a Carlo Erba GC 6000 equipped with a capillary column (WCOT ULTI-METAL, 10m., 0.53 mm.).The FID temperature was 330°C, the injector was an on-column. The oven temperature was at 50°C during 3 min., then a temperature gradient was operating (10°C/min.), then an isotherm at 300°C. The samples were diluted in 0.5 ml.of n-heptane and 0.5 µl.of solution was injected.

1.1. Materials

1, 10-decanedicarboxylic acid, thionyl chloride, 1-bromooctane, 1-bromoheptane, anhydrous ether and n-hexacosane with a purity greater than 99% , were purchased from Aldrich and used without purification. Zinc chloride, and n-octacosane were issued from Fluka and their purity was >98 %. Chloroform (>99%), acetic acid (>99%), toluene (>99.5%) were purchased from Prolabo and 1-octanol (>98%) from Janssen.

First step of the chemical synthesis :Dodecanedioyl dichloride.

A mixture of 80.08 g. of the diacid, 100 ml. of thionyl chloride was refluxed for 24 hr. At 80°C. The excess of thionyl chloride were removed by distillation under atmospheric pressure. Distillation under reduced pressure (170°C, 1 mm Hg.) provides 80.9 g (molar yield : 87%) of pure dodecanedioyl dichloride.

The infrared spectrum exhibited a strong peak in the carbonyl region, at 1799 cm^{-1} assigned to acid chloride.

Second Step of the chemical synthesis : 9, 20-octacosane dione and 8,19 hexacosane dione.

At this moment, the chemical synthesis of the two alcanes are managed at once.

a) Grignard reagents :

1-bromooctane (35 ml.) (or 1-bromoheptane (32ml.)) and an excess of magnesium turnings (5 g.) were allowed to react in 126 ml. of anhydrous ether to give a 90% yield of Grignard reagents.

b) Diketones

Zinc chloride (21.6 g, 0.158 mole) was weighted into a 250 ml three necked round-bottomed flask. The mouth of the flask was connected to a vacuum pump. The system was evacuated to full pump vacuum and flame dried. The zinc chloride was slowly fused to a clear melt with a Bunsen flame. After cooling the flask to room temperature under vacuum, the vacuum pump line was removed and 66 ml of anhydrous ether was added. The mixture in the closed system was stirred magnetically until the fused zinc chloride had dissolved and the solution became colorless. To this solution, the Grignard reagent was added rapidly. A thick, gray paste was obtained with strong refluxing. After 20 mn stirring, ether was removed and 33 ml of anhydrous benzene were added to the pasty mixture. Dodecanedioyl dichloride 15.18g.(or 15.15 g. for C_{26}) in 140 ml of anhydrous benzene was added to the organozinc reagent over a period of 15 min. The solution was stirred and refluxed for 3 hr under nitrogen. The mixture (gray paste) was then hydrolyzed with 2N hydrochloric acid. The organic layer was separated and benzene removed on a rotary evaporator. The crude product was washed with water, dried and purified by recrystallization from benzene. 9, 20-octacosane dione was obtained in 69.7% molar yield, m.p. 97°C and 8,19 hexacosane dione in 71.3% molar yield, m.p. 92 °C.

The products were caracterized by 4 methods: melting point (Köfler), thin layer chromatography (only one spot for each product), I.R.(wave number corresponding with C=O linked to $-CH_2$), ^{13} C N.M.R. (Table 1)

δ (ppm)	group	carbon n°	number of carbons
14.37	CH_3	1	2
22.92	α,$CH_2(-CH_3)$	2	2
24.16	β,γ, $CH_2(-CH_3)$	3	4
29.56	$CH_2(-CH_2)$	4	10
31.98	β $CH_2(-C{=}O)$	5	2
43.08	α CH_2 $(-C{=}O)$	6	4
211.94	C=O	7	2

Table 1 . 8,19 hexacosane dione ^{13} C N.M.R.

The third step of the chemical synthesis : n-octacosane and n-hexacosane .

9,20-octacosane dione (9 g.) (or 10 g. of 8,19 hexacosane dione), 22.5 ml. of hydrazine monohydrate, 2.25 ml. Of glacial acetic acid and 305 ml. of 1-octanol were refluxed under stirring at 140-150°C for 9 hours. The formed water and the excess of hydrazine were removed with a Dean-Stark apparatus. A solution of sodium octanolate (11 g. of sodium in 120 ml of 1-octanol) was added to the hydrazone. The mixture was then refluxed at 140 °C for 24 hours 1-octanol was removed under reduced pressure(1mm.Hg.). The resulting yellow product was extracted with chloroform and the suspension was filtered off. The products were purified on a silica column chromatography and the fractions analyzed by thin layer chromatograply. Fractions with one spot were collected together and dried in order to eliminate the solvant (toluene) :

-two hours under vacuum,

-two hours under vacuum at 40°C,

-six hours under vacuum at 60°C

At this step, we obtained 1.9 g.of C_{26} (reduction molar yield :22.9%) and 4.55 g. of C_{28} (reduction molar yield : 48.9%).The by-products should be : diketone,ketone,octanol , toluene and… ?.

1.2 Supercritical carbon dioxide extraction apparatus (Figure1)

The solid feed was introduced in the autoclave, with a stainless steel frit at the outlet column (height :30cm.,internal diameter :23 mm.), then the autoclave was closed. CO_2 (P = 5 MPa, T = 20°C) is cooled (T=5°C), pumped (P_{max} = 25 MPa, CO_2 flowrate$_{max}$=3.5kg./h.) then heated to be a supercritical fluid or a liquid . It flowed through the thermostated extraction column . At the outlet column, the mixture CO_2-solutes was expanded through three valves and were separated in cyclonic separators[3].At last, CO_2 was vented through a rotameter and a gas meter. An originality of the process was to withdraw the solutes at atmospheric conditions everytime we need. The solutes were weighted and analyzed by capillary gas chromatography if they are mixtures. The temperature of the first and second separator should be different from the top to the bottom. The third separator temperature was the same at the bottom of the second separator.

Results and Discussion

Supercritical Fluid extraction

Due to the synthesis and first steps of purification, it is obvious to think that the impurity of n-octacosane is 9,20-octacosane dione and that it is not soluble in SC-CO_2. According to the results published in the litterature, mentionned on figure 2, we have calculated the octacosane solubility, y* considering the experimental conditions : CO_2 flowrate, temperature and pressure. As the withdrawing of solid samples is not so easy, we have choosen the experimental parameters as : 55°C and 110 bars for the autoclave. Some conditions of the separators have been kept constant : Separator 2 (40°C,2MPa.), Separator 3 (40°C,1MPa.) (C_{28} melting point temperature at atmospheric condition : T_f =58°C). We have tested several feeds and the results are mentionned on table 2. Some difficulties appear during the first experiments; the tube were often blocked occuring a bad mass

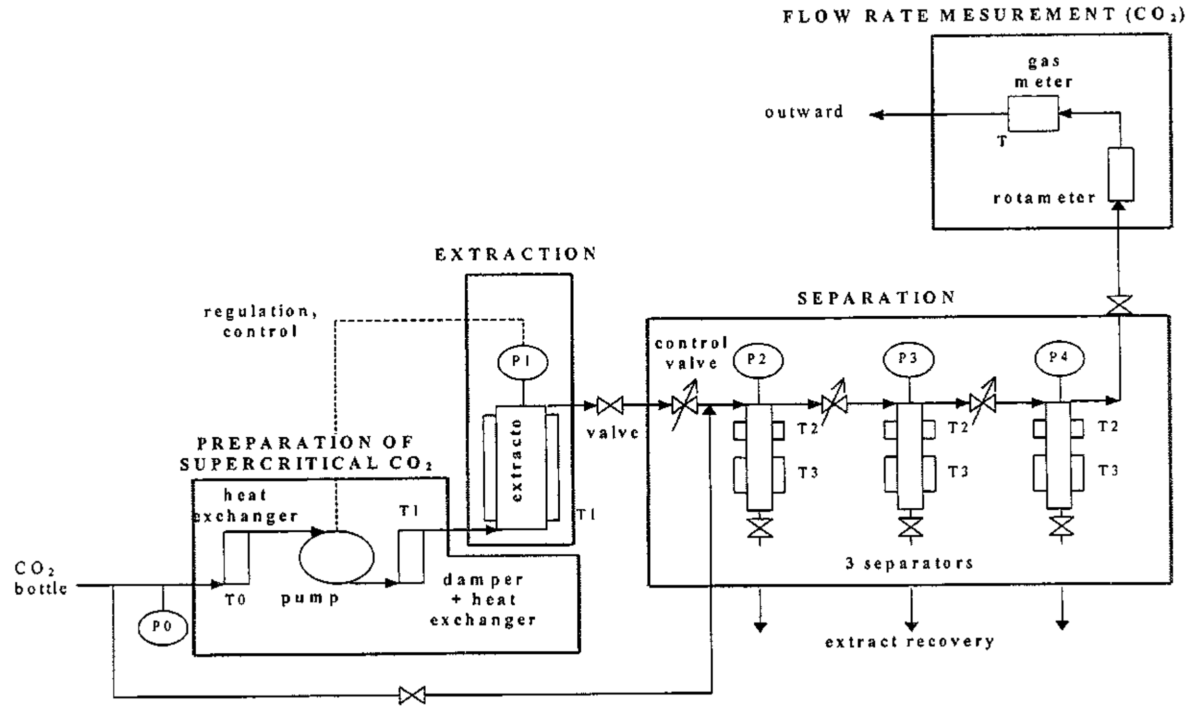
FLOW RATE MESUREMENT (CO_2)
gas meter
outward
T
rotameter
EXTRACTION
SEPARATION
regulation, control
P1
control valve
P2
P3
P4
valve
extracto
T2
T3
PREPARATION OF SUPERCRITICAL CO_2
heat exchanger
T1
CO_2 bottle
T0
pump
damper + heat exchanger
P0
3 separators
extract recovery

Figure 1 .Schematic diagram of extraction process

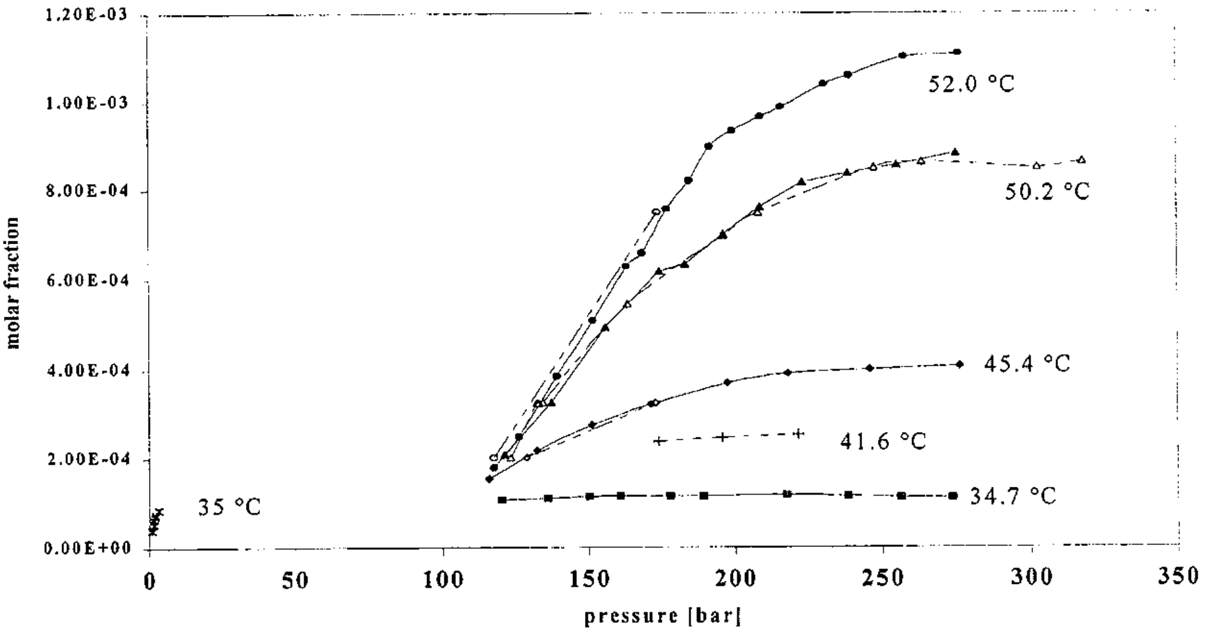

Figure 2. C28 molar fraction versus pressure for several temperatures[4-6]

alcane	N°	type	Feed (mg.)	$\Delta t^{(1)}$ (min.)	$V(CO_2)^{(2)}$ (l.)	Separator1 P (MPa)	Separator1 T (°C)	M $S1^{(3)}$ (mg.)	M $E^{(4)}$ (mg.)
C_{28}	1	Fluka	114	45		8	40	71	0
C_{28}	2	Synth.	173	70		8	40	24	47
C_{28}	3	Synth	343	158	856	8	40	32	62
C_{28}	4	Synth	442	154	965	8	40	101	119
C_{26}	5	Synth	329	161	758	8	40	54	30
C_{26}	6	Synth	466	150	739	8	40	131	0
C_{26}	7	Synth	523	160	812	8	40	354	0
C_{26}	8	Aldrich	253	160	772	8	40	227	0
C_{28}	9	Fluka	290	158	888	8	40	108	41
C_{28}	10	products	756	50	280	8	40-40	62	325
C_{28}	11	products	493	135	776	5	40-40	28	208
C_{28}	12	products	430	158	759	5	70-25	23	111
C_{28}	13	products	412	140	731	5	70-6	192	111
C_{28}	14	products	343	140	443	8	70-6	98	81
C_{28}	15	products	228	140	1156	5	40-15	66.8	28.8
C_{28}	16	products	178	120	956	5	40-15	44	27
C_{28}	17	products	282	140		8	40-40	122	57
C_{28}	18	products	180	160		8	40-40	44	14

Table 2 : Supercritical fluid extraction result
(1) : extraction duration, (2) : carbon dioxide volume, (3) : separator 1 extracted mass, (4) : raffinate mass
products : crude materials, without purification by liquid chromatography

balance (loss from 10% to 70%). By heating the valves ,the tubes were not so often blocked. Nevertheless, the extract has a very nice appearance : a very fine powder , sparkle and white.We have tried to obtain a better yield recovery regarding the poor quantity of product obtained by the chemical synthesis. We have the possibility to modify the temperature of the first and second separator, and also to have a temperature for the bottom and an other for the top(table 2), but we don't obtain any succesful results.(loss from 26% to 69%).

Characterisation of the product

The gas chromatographic analysis shows that the synthesized products are not pure before and after the supercritical carbon dioxide purification. Some of the impurities have been identified . There is no diketone and no octanol present in the two synthesized products. In the case of octacosane, one impurity is unknown, the other is triacontane. An internal standardization with docosane has contributed to estimate the purity at 99.5 % .

The meelting point and transition temperatures have been measured by differential scanning calorimetry analysis.The melting point temperature is higher after the supercritical purification , so we could observe the disappearance of some impurities. But, the literature temperatures [2,7] are higher.Moreover,we have observed by X-ray diffraction analyses that the structure of the synthesized product is similar to this of the commercial product.

Conclusions

Two heavy alcanes have been chemically synthesized, puified by supercritical carbon dioxide,the purity has been established by several ways and compared to commercial products. According to the results, if we want to obtain more pur product, we have certainly to purify 1-bromooctane and 1-bromoheptane in order to have no other neighbouring alcanes.

References

1.Dirand M ; Chevallier V., Provost E., Bouroukba M., Petitjean D., Fuel, 77, 1998, 1253
2.Provost E., Chevallier V., Bouroukba M., Petitjean D., Dirand M., J.Chem.Eng.Data, 43, 1998, 749
3.Perrut M.,Brevet Français,N°85104680907, 1985
4.McHugh M.A. ;Seckner A.J. ;Yogant J. ; Ind.Eng.Chem.Fundam., vol.17, n°1, 1984, 21
5.Griscik G.J., Rousseau R.W., Teja A.S., J.of Crystal Growth, vol.155, 1995, 112
6.Craig S.R., Hastie G.P., Roberts K.J., Sherwood J.N., J.Mater.Chem., vol.4, n°6, 1994, 977
7.Handbook of Chemistry and Physics, DR Liede, 78 th Edition, 1997-1998

Present Situation of Research and Technology of Textile Cleaning in Compressed CO_2

Josef Kurz*, Andrea Hilbink, Bernd Gosolits
HOHENSTEIN INSTITUTES
Schloss Hohenstein · D-74357 Bönnigheim · Germany
Fax: -7143-271-8746 · email: j.kurz@hohenstein.de

The results of worldwide research show that in principle textile cleaning with compressed CO_2 is possible. The matter of examination was the resistance of textile fibres, dyeings or textile makings like buttons. A sufficient dirt removal with the help of compressed CO_2 can be guaranteed at the moment only for nonpolar substances like lipids. For the removal of polar substances like salts, suitable tensids have not yet been developed.

1. Introduction

Tetrachloroethylene is the most commonly used solvent in textile drycleaning worldwide. As this solvent is critical in regard to environment and toxicology, there are international efforts to find alternatives. Solvents based on hydrocarbon as a scientific and technically perfected alternative are available since 1995. The next step towards ecological and generally recognized as safe textile drycleaning is the development of textile cleaning procedures applying compressed CO_2.

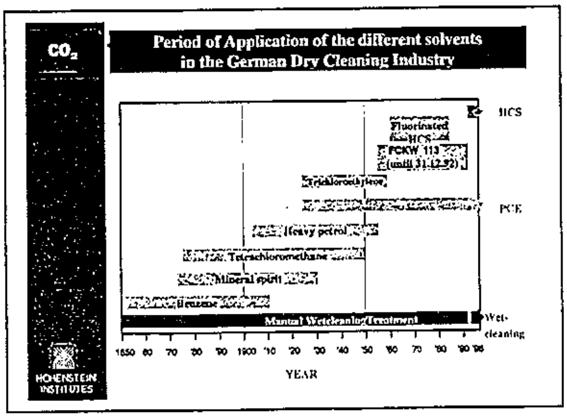

Figure 1: Period of application of the different solvents in the German dry cleaning industry

2. International research activities

2.1 Studies about the cleaning characteristics of compressed CO_2 with regard to textiles

❖ *Los Alamos National Laboratory (USA):*

The Los Alamos National Laboratory was one of the first research institutions worldwide which systematically studied textile cleaning with the aid of compressed CO_2. The characteristics of a limited number of natural and artificial fibers, buttons and accessories were studied. Moreover there was a series of test with regard to the cleaning properties of compressed CO_2 [1], [2], [3].

❖ *North Carolina State University, Raleigh, USA:*

Prof. Joseph M. DeSimone from North Carolina State University, Raleigh, has been working in the field of emulsion and dispersion polymerization with compressed CO_2 for many years so far.

Suitable tensides had to be developed on the basis of fluorinated hydrocarbons and silicones. The transfer of these tensides into the field of dry cleaning was examined [4], [5].

❖ *Deutsches Textilforschungszentrum Nord-West DTNW e.V., Krefeld, Germany:*

This German Textile Research Institute has developed a method for textile dyeing in compressed CO_2 some years ago. The experience in this field was being transferred to the dry cleaning sector [6], [7].

2.2 Development of Textile Drycleaning Machines

❖ *Global Technologies LLC and Hughes Environmental Systems, Inc, USA:*

Global Technologies closely cooperates with Los Alamos National Laboratory.

In cooperation with Hughes Environmental Systems a machine technology was being developed, which is now licensed to manufacturers of dry cleaning machines (e. g. Electrolux, Sweden). These dry cleaning machines work with the so-called fluid-jet-agitation (Figure 2). The required mechanical action is being produced by injection of compressed CO_2 into a fixed dry cleaning drum.

- *Micell Technologies Corp., Raleigh, USA:*

Prof. DeSimone from North Carolina State University, Raleigh is a founding member of this company. Micell has developed a dry cleaning machine with rotating drum, which can be operated at 55 to 65 bar and standard room temperature.
A cleaning cycle shall take 35 min.

3. Results of the research work at Hohenstein

Within the framework of a joint research project, which started in 1997, the Hohenstein Institute is working intensively on the development of a textile dry cleaning process with the aid of compressed CO_2.
The present tests have been carried out in a pilot plant with a rotating cleaning drum (Figure 2).
In cooperation with the research partners Böwe GCS, Augsburg and Linde AG, Höllriegelskreuth, this pilot plant shall be further developed into a prototype 10 kg-dry cleaning machine within the next few weeks.

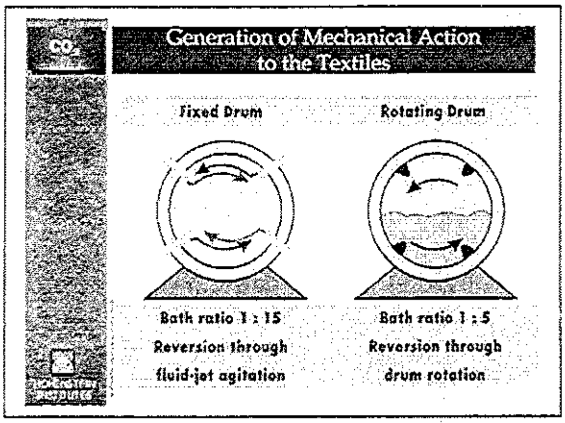
CO_2
Generation of Mechanical Action to the Textiles
Fixed Drum
Rotating Drum
Bath ratio 1 : 15
Reversion through fluid-jet agitation
Bath ratio 1 : 5
Reversion through drum rotation

Figure 2: Generation of Mechanical Action to the Textiles

Extensive tests on the resistance of textile materials, showed that compressed CO_2 is suitable for both, dry cleaning of textile fibres and leather substitutes or laminated textiles.
This was proved by means of scanning electron microscopy and physical measuring methods.
For this purpose, scanning electron micrographs were taken from each tested sample before and after cleaning in compressed CO_2 and have then been compared with each other (Figure 3).

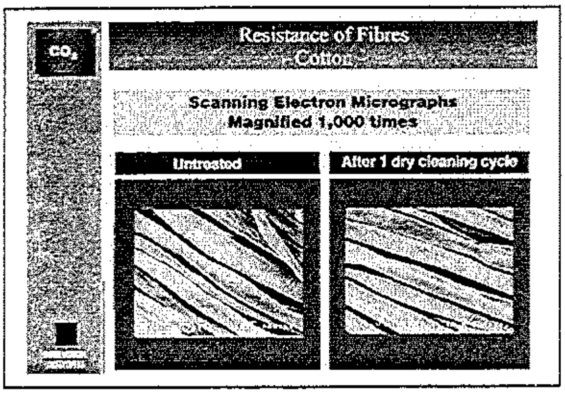
CO_2
Resistance of Fibres
Cotton
Scanning Electron Micrographs
Magnified 1,000 times
Untreated
After 1 dry cleaning cycle

Figure 3: Resistance of Fibers – Cotton

The physical tests ranged from the determination of area shrinkage after dry cleaning to colour fastness tests and others.
An assessment of the measuring results can only be made in comparison to the results of dry cleaning in tetrachloroethylene.
Due to their specific structure of matter and material properties, leather substitutes must undergo additional quality checks to ensure that the special features, i. e. a high physical strength and a soft, supple handle, do not suffer during dry cleaning treatments.
Leather substitutes consist of different individual materials. If only one of these components was damaged under dry cleaning in CO_2, the distinct quality features would be lost. For this reason further physical tests, as for example tests on abrasion and rubbing fastness were carried out (Figures 4 and 5).

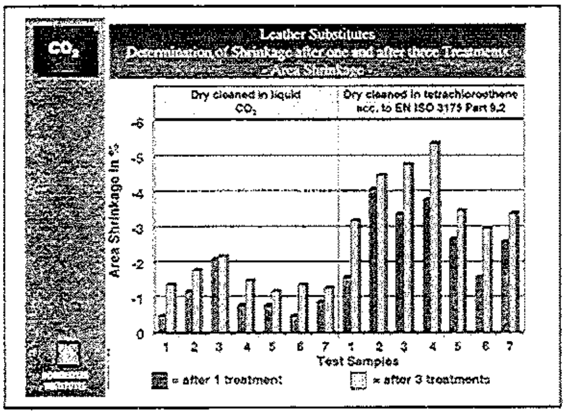

Figure 4: Leather Substitutes – Determination of Area Shrinkage

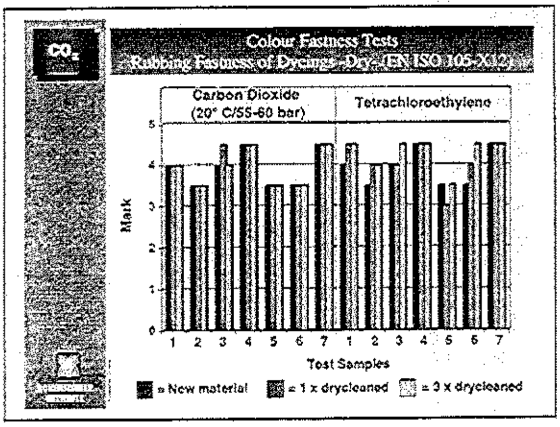

Figure 5: Colour Fastness Tests/Rubbing Fastness of Dyeings

Laminated textiles are composite materials. This means that textile fabrics are laminated to membranes in different ways. It is of special importance, that the combination of textile and membrane, for example by means of adhesives, does not suffer damage during dry cleaning.
A damage of the laminate construction leads to decreased air permeability respectively water impermeability of the membrane. This causes a limitation of the breathability of the laminates and thus reduces the wear comfort of the nonwovens.
Figure 6 shows different kinds of laminate after dry cleaning in compressed CO_2. The membrane of sample no. 2 has been damaged through the dry cleaning process. The water impermeability of the material was lost. However, the same effect shows after dry cleaning in tetrachloroethylene.

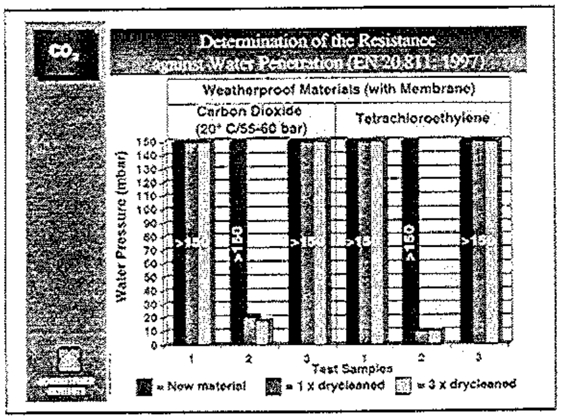

Figure 6: Determination of the resistance against water penetration

Buttons, sequins and zippers can also be treated in compressed CO_2. However, the boundary conditions are important for the resistance of the materials.
Too fast stress-relaxation can cause material deformations (Figure 7).

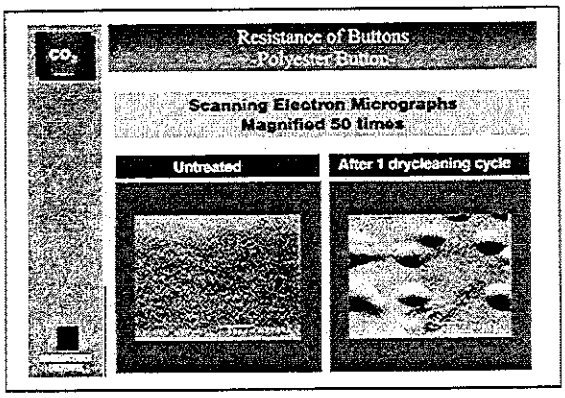

Figure 7: Resistance of Buttons – Polyester

Besides the tests on material resistance, further testing comprised colour fastness of different kinds of materials and resistance of dyestuffs.
The following dyestuff classes were tested:

- reactive dyestuff on cotton
- direct dyestuff on cotton
- acid dyestuff on polyamide
- sulfide dyestuff on cotton

All tested dyeings showed a good resistance in both tetrachloroethylene and compressed CO_2.

To evaluate the dirt removal in CO_2 it is necessary to distinguish between different kinds of soil. Skin fat and similar non-polar substances can easily be removed in pure CO_2 (Figure 8). Whereas it's solvent power does not suffice to remove polar dirt components, such as proteins and salts (Figure 9).
However, there is no considerable difference regarding the removal properties of compressed CO_2 and pure tetrachloroethylene for salts.
Dry cleaning processes in tetrachloroethylene can only remove polar substances like salts when adding cleaning intensifiers (tensides). A distinct increase of the salt removal properties of compressed CO_2 should also be feasible by using adequate tensides.
At a pressure below 70 bar, pure CO_2 is too covalent to remove these substances from the textiles.

Under higher pressure the polarity of CO_2 increases and leads to enhanced removal quality regarding polar substances. However, the operation of dry cleaning machines under such high pressures is inefficient.

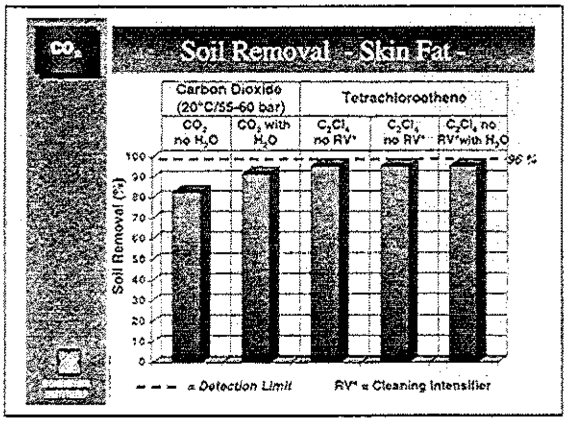

Figure 8: Soil Removal – Skin Fat

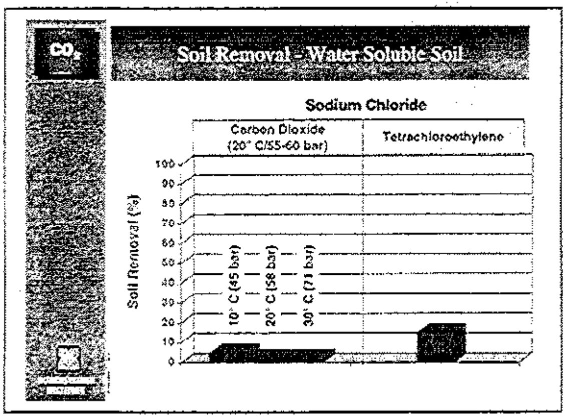

Figure 9: Soil Removal – Water Soluble Soil

For this reason, the next step must be to develop tensides, which fulfil all requirements with regard to the textiles and which improve the removal quality of compressed CO_2 for these polar substances when applied with solubilized water.
If this can be managed successfully, the CO_2-technology constitutes a real alternative to conventional dry cleaning.

4. References

[1] Spall, W. D. „Carbon dioxide as an environmentally conscious dry cleaning solvent.“
Los Alamos National Laboratory, **1997**

[2] Williams, S. G.; Laintz, K. E.; Spall, W. D.; Bustos, L.; Taylor, C. „Fabric compatibility and cleaning effectiveness of dry cleaning with carbon dioxide“.
Los Alamos National Laboratory Report Number La-UR-96-822, **1997**

[3] Chao, S; Purer, M; Townsend, C.
„Dry Wash – A revolutionary garment dry cleaning technology with liquid carbon dioxide“.
Hughes Aircraft Company, **1996**

[4] McClain, J.B.; DeSimone, J. M. et al
„Design of Noninonic Surfactants for Supercritical Carbon Dioxide“
SCIENCE, **1996**, 274 (2049 - 2052)

[5] Guan, Z.; DeSimone, J. M.
„Fluorcarbon-Based Heterophase Polymeric Materials – Copolymer Surfactants for Carbon Dioxide Applications“
Macromolecules, **1994**, 27, 5527 - 5532

[6]Gebert, B.; Knittel, D.; Schollmeyer, E.
„Überkritisches Kohlendioxid als Ersatz für Perchlorethylen“
Melliand Textilber., **1993**, 151 - 152

[7] Knittel, D.: Gebert, B.; Schollmeyer, E.
„Überkritisches Kohlendioxid für die Textilreinigung – Ein neues Medium ist in der Erforschung“
WRP, **1996**, 3, 40 - 46.

EXTRAPOLATION OF SUPERCRITICAL FLUID PROCESSES FROM LAB AND PILOT TO PRODUCTION SCALE : PROBLEMS AND SOLUTIONS

Philippe MENGAL*, Jean-Yves CLAVIER**, Michel PERRUT**
* HITEX, Parc d'Innovation Bretagne Sud, rue du Commerce, CP 65, 56038 VANNES Cedex - France
** SEPAREX S.A., 5 rue Jacques Monod, BP9, 54250 Champigneulles – France
Email : separex@francecom.net – Fax : 33-3.83.31.24.83

Introduction :

Extrapolation of experimental results obtained at lab and/or pilot scale to production equipments is a major challenge for chemical engineers, especially when new technologies are developed, as it is the case for supercritical fluid applications for which very few results have ever been published.
Illustrated by problems met on various processes including solid extraction (SFE) and liquid fractionation (SFF), we present some rules that could be followed during design, operation, maintenance and cleaning of large-scale plants using supercritical carbon dioxide and co-solvents.

Design of large-scale units :

Basic chemical engineering for supercritical fluid equipment design can be found in a recent book by BRUNNER[1], but few data are presently available for calculation of main equipments to be assembled into large scale SF plants. In fact, two different types of units are required by the clients : either flexible equipments easy to adapt to many applications unknown during the design and construction well-defined equipments dedicated to a specific application. Obviously, the design is not at all the same, leading to much more complex equipments in the first case than in the second, with the corresponding difference in investment cost and sophistication. As an example, we would present the flowsheet of a flexible SFE/SFF equipment built in 199è by SEPAREX and prresently operated by HITEX (figure 1) : it is possible either to process a solid (SFE) in batch mode on one, two or three extraction autoclave(s), or a liquid (SFF) in continuous or batch mode onto the fractionation column with raffinate decompression into one or two of the extraction autoclave(s) ; moreover, when it is mandatory to collect the light fraction of the extract that might be entrained by the gaseaous fluid downward the separation steps (for example when procesing aromas), an adsorption bed is set inside one or two extraction autoclave(s), with regeneration of the adsorbant by the fluid in supercritical phase, the recovered axtract fraction being collected in the separators. For such a complex flowsheet, a convivial software is required to facilitate the operation and to avoid mistakes in the main valves positionning. But, on this unique equipment, many different processes can be easily and rapidly implemented, without modifications of the hardware.

Heat exchangers

Double-tube counter-current heat exchangers are used on pilot and semi-industrial plants but cannot be used on units where the SF flowrate exceeds 1,000 $kg.h^{-1}$: shell-and-tube heat exchangers are required for providing a sufficient transfer area. According to our experience, we recommend :

- Obviously, process fluid always on tube side and heating/cooling medium on shell-side ;
- Horizontal SF heater (when SF is pumped in liquid phase) or cooler (when SF is compressed in a gas phase), after SF pump/compressor, with one pass on shell-side and two passes on tube side, U-tubes being acceptable as the SF is clean at that point ;
- Vertical reheater(s) downward fluid decompression between the high pressure operation and the separators with one pass on tube side for downward high speed flow of process fluid in order to avoid extract deposition and plugging ;
- Vertical the fluid prior to recycling by pumping) with one condensor (when required to liquefied pass on tube side and downward flow of process fluid so as to avoid plugging by extract entrained from the separators.

Extraction autoclaves

Most attention is paid to closure systems permitting a fast and easy opening/closure, as solid extraction is realized in batch mode and requires a great number of repetitive operations to fill and to withdraw the baskets containing the raw materials. First of all, these closure systems must be very safe and reliable so as to avoid any risk of moving them when the autoclave is pressurized. Generally, a redundancy is proposed through automation and passive safety blocking the closure systems when some pressure remains inside the autoclave.

Fluid compression

Two possible fluid cycles can be used :

- Liquefied gas pumping : in most small and medium scale equipments, a volumetric high pressure pump is used to compress the fluid in liquid phase ; generally, membrane pumps are preferred for flowrates up to 1,000 kg/h meanwhile piston-plunger pumps are used for larger capacities where they are much less expensive than the precedent type. It is important to notice that these pumps have check-valves presenting a significant pressure drop at full capacity : this requires a sub-cooling of the liquefied gas of at least 3°C below the boiling temperature at the inlet pressure (~40 to 50 bar in most cases) to avoid cavitation in the pump head that must also be cooled.
- However, it happens in some processes that the extract-fluid separation is not performed by depressurization below the critical pressure, but by temperature change or fluid scrubbing or adsorption, as it is performed in the very large scale decaffeination plants : the total pressure drop being small, centrifugal pumps can be used, delivering very large flowrates (higher than 20,000 kg/h) at a much lower cost than any volumetric pump.
- Gas compression : Instead of liquefying the gas prior to pumping it in liquid phase, it is also possible to compress it as a gas through a compressor. However, these equipments are generally considered as more expensive than pumps and more costly in maintenance, although savings can be made as no refrigeration machine and condensor are required. Moreover, some problems may occur if the extract-fluid separation is not total, especially if waxy materials re entrained in the gas phase to the compressor.

Operation of large-scale units

Solid extraction processes (SFE)

According to our experience, many issues may happen along long-term exploitation :

- Fine particle migration and plugging may cause basket sintered disk deformation ; this is the most widely encountered problem as most operators do not take enough care to the raw material granulometry during grinding ; We strongly recommend to avoid very fine particles by grinding monitoring and/or screening the raw materials prior to filling the baskets ; a paper filter may be an aid in certain cases to prevent this problem. In other cases, the raw material may agglomerate in form at a thick "cake", what drastically reduces the SF-material contact and extraction efficiency ; this may also lead to total plugging of the basket and deformation of the sintered disks. When such "sticking" materials are processed, a pelletization step is required, as for hops treatment. When pelletization is not available, we can recommend to blend the raw material powder with an inert granular material that will prevent this agglomeration.
- In the worst case, basket disk plugging may lead to basket deformation and blockage inside the extraction autoclave, causing important damage to the autoclave wall during withdrawal ; this may be avoided by controlling the pressure drop between the inlet and outlet of the vessel with SF flow stop when it reaches a value that indicates such plugging, below the pressure drop that irreversibly damage the basket and/or the sintered disks.
- Basket deformation may happen due to shocks during handling, and autoclave wall damage may be caused by shock with the basket bottom during introduction : this may lead to a drastic loss of efficiency of the extraction due to SF by-pass between the basket and autoclave walls when the external gasket of the basket is not totally efficient to force SF to percolate through the basket. With certain autoclave lid designs, such damage may cause a leakage to atmosphere when the rays appear on the zone of main gasket ; so we believe it is important to operate with adequate means of basket handling and careful manpower.

Supercritical Fluid Fractionation (SFF) :

In most cases, SFF is much easier to operate than SFE as pressure vessels are not often opened and closed. However, column packing plugging may happen and lead to flooding : it is generally a slow process with deposition of a solid or highly viscous material onto the packing, that progressively reduces the open section of the column and creates zones no longer swept by the fluid, what generally "catalyses" the deposition, until the moment where brutally flooding appears, requiring operation stop and unit cleaning !

This phenomenon is not easy to detect and to prevent, as, in most cases, it does not appear at pilot-scale where experiments are generally conducted during short periods.

To avoid this, it may be necessary to pretreat the feed (filtration, ...), to change the operating conditions (possibly increased temperature) or to operate preventative column cleaning regularly.

SF recycle loop

For all industrial-scale processes, SF is recycled for obvious economical and ecological reasons. This means that the separation of the extract from the fluid prior to its recycle must be as perfect as possible to avoid extract deposition throughout the recycle loop, especially the colder parts (condensor and sub-cooler, liquefied gas reservoir, or compressor), that may lead to plugging and stop the unit for a long time. Moreover, some problems, unknown at lab or pilot-scale, may appear as some tiny impurities may accumulatein the fluid phase (inert gases, pollutants,...).

Maintenance of large-scale units

Industrial production with supercritical fluids requires a high reliability operation of high pressure equipments with drastic safety requirements as hazards must be eliminated : this requires a **preventative** maintenance as many parts must be inspected and changed periodically ; moreover, a rigorous operation plan must be enforced to eliminate any risk of deterioration of the basic parts, and safety sensors must be continuously logged. This preventative maintenance and inspection firstly concerns the high-pressure pump(s) (check-valves and membrane(s) are highly sensitive to abrasion or perforation by solids), autoclave closure systems and gaskets (to prevent solvent leakage) and baskets (external gaskets to avoid solvent by-pass ; sintered disks plugging to avoid deformation or rupture). Of course, pressure vessels must be inspected and submitted to pressure tests according to official standards. Moreover, the main process valves must be often checked as they are the key of safe operation during autoclave opening for raw material change. Sensors must be recalibrated periodically, in comparison with traceable reference sensors, and data logging validated. Finally, I would stress on the fact that maintenance is greatly eased when a great attention is paid to extract-solvent separation to avoid entrainment of some fraction of extract through the fluid recycle loop, and if an efficient cleaning is frequently operated.

Cleaning large-scale units

One of the most important issue for operating a supercritical fluid process on a large-scale flexible unit is probably ***cleaning***, especially when food or pharmaceutical products are treated. Obviously, it is much more difficult for pharmaceutical processing than for foodstuffs and we will focus our attention here on those pharmaceutical products, as it is clear that drastic simplifications of this procedures can be accepted for foodstuffs processing, happily ! It can also be considered that less strict requirements are imposed for phytopharmaceuticals than for synthetic drugs in their final form.

For pharmaceutical processing, it has to be proven that no contamination by previously processed compounds may occur ; but according to GMP (pharmaceuticals) even when the plant is dedicated to only one product, it is also required to avoid cross-contamination from one lot to the other. Although cleaning is always an issue on any type of process and equipment operated in GMP, it is much more severe for supercritical fluid process and equipment as the operator must ***prove*** that the equipment is cleaned rid of previous compounds ; this constraint is generally matched by the famous "***swab***" technique consisting in scrubbing the equipment wall with a specific swab that is further extracted with a solvent which is evaporated, leaving a dry residue easy to weigh and analyze. In the special case of SF equipment, most parts cannot be opened between each lot manufacture and the swab technique cannot be used. Moreover, as most high pressure parts - like valves - are not Clean-In-Place (CIP), cleaning procedure validation is really a troublesome burden !

According to our experience, we are convinced that the only GMP-acceptable cleaning technique requires:

- Between batches :
  Rinsing the whole unit with an adequate liquid solvent , dismantling and cleaning dead-ends, rinsing again with the liquid solvent, with sampling for cleaning validation, drying with gaseous nitrogen or CO_2 to eliminate solvent vapor and rinsing with liquid/supercritical CO_2 that is finally vented to atmosphere in order to eliminate most extracted impurities, (mainly liquid solvent) ;
- Between different products :
  Total or partly dismantling of the equipment, cleaning of each part, swabbing the pressure vessels, ..., reassembling the equipment, rinsing with an adequate liquid solvent with sampling for cleaning validation, drying with gaseous nitrogen or CO_2 to eliminate solvent vapor and rinsing with liquid/supercritical CO_2 that is finally vented to atmosphere in order to eliminate most extracted impurities, (mainly liquid solvent).
  Cleaning validation is obtained through liquid solvent samples analyses (dry weight of residue and residue identification are the key-parameters) and swab characterization according to the classical technique.

It is extremely important to consider the cleaning issue at the very beginning of any SF equipment design, especially – but not only – for those dedicated to food or pharmaceutical products : this shall influence many choices so as to avoid piping/instruments dead-ends and all zones that could not be swept easily by the process fluids. For example, we developed very low volume multi-tubing/multi-instrument connections, and very low volume high speed separators in form of cyclonic chambers. Moreover, adequate parts must be installed to permit an easy rinsing of the whole unit with liquid solvent : the ports locations must be carefully determined so that a total drainage is rapidly completed.

Reference :

[1] BRUNNER G., "Gas Extraction", Springer, ISBN 0-387-91477-3, 1994.

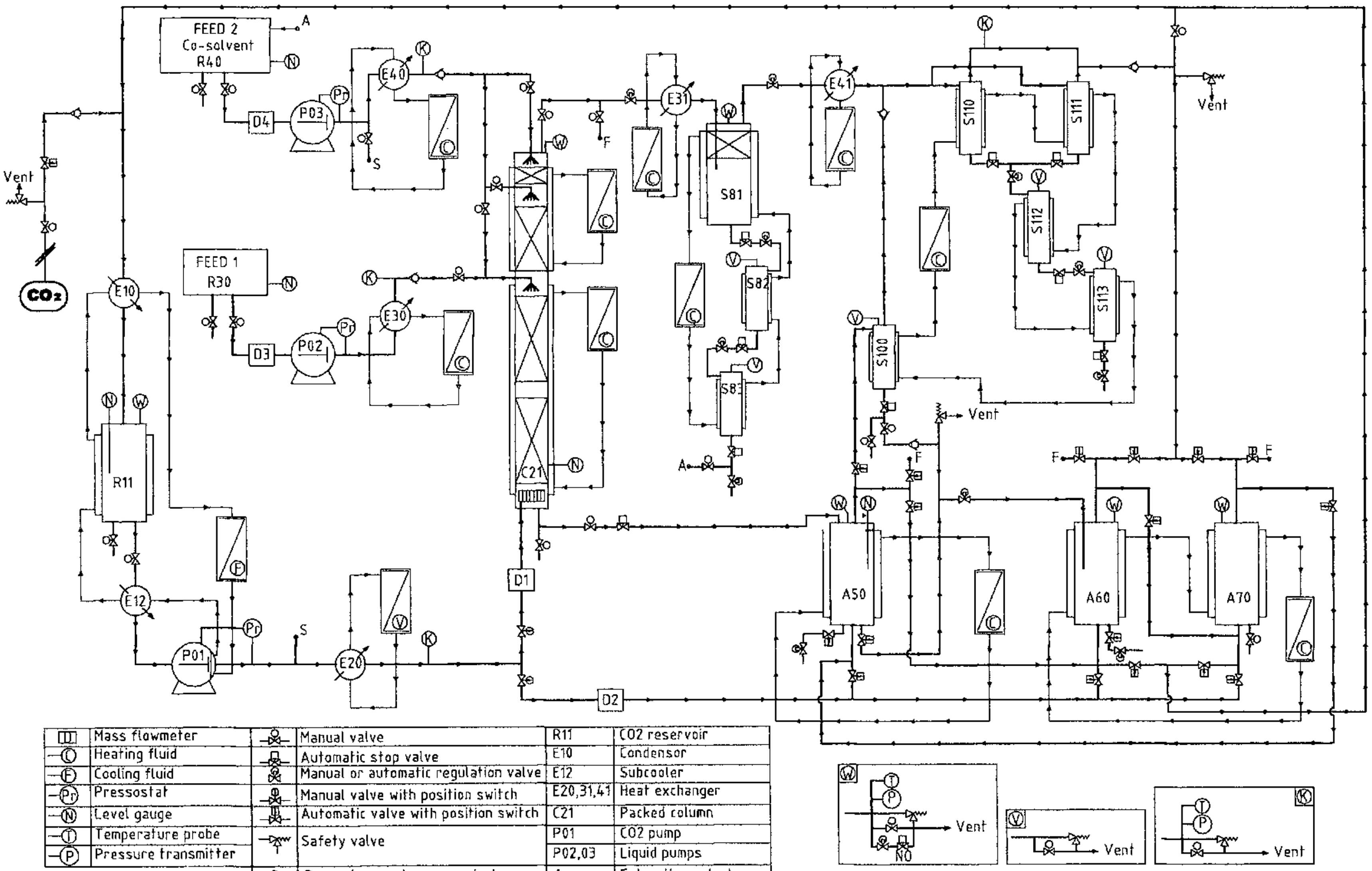
FEED 2
Co-solvent
R40
A
N
E40
K
Pr
P03
D4
S
C
W
F
E31
S81
E41
S110
S111
S112
S113
V
Vent
CO2
E10
FEED 1
R30
P02
D3
E30
C21
S82
S83
S100
R11
E12
P01
E20
D1
D2
A50
A60
A70
T
P
NO

◫	Mass flowmeter		Manual valve	R11	CO2 reservoir
Ⓒ	Heating fluid		Automatic stop valve	E10	Condensor
Ⓕ	Cooling fluid		Manual or automatic regulation valve	E12	Subcooler
(Pr)	Pressostat		Manual valve with position switch	E20,31,41	Heat exchanger
Ⓝ	Level gauge		Automatic valve with position switch	C21	Packed column
Ⓣ	Temperature probe		Safety valve	P01	CO2 pump
Ⓟ	Pressure transmitter			P02,03	Liquid pumps
		S	Separators and pressure locks	A	Extraction autoclaves

Figure 1 : General flowsheet of industrial scale SFE/SFF unit

GVC-Fachausschuß „High Pressure Chemical Engineering", March 3-5, Karlsruhe, Germany, 1999 GVC FZK '99

Separation of Stereoisomers in a SMB-SFC Plant Determination of Isotherms and Simulation

Dipl.-Ing. T. Giese*, Dipl.-Ing. A. Depta, Dr. M. Johannsen, Prof. Dr.-Ing. G. Brunner
Arbeitsbereich Verfahrenstechnik II, Technische Universität Hamburg-Harburg, Germany
Fax.:0049-40-42878-4072; e-mail: t.giese@tu-harburg.de

The combination of two techniques, Simulated Moving Bed (SMB) and Supercritical Fluid Chromatography (SFC) leads to an apparatus with unique features. Besides the known advantages of the SMB process like reduced solvent consumption and its continuity the use of supercritical carbon dioxide as mobile phase offers an easy product recovery by depressurizing the supercritical fluid without any additional rectification steps. Details of the new apparatus are shown. Due to the large number of process parameters a simulation of the SMB process is necessary to achieve optimal operating conditions. As the most important thermodynamic information for a SMB process the adsorption isotherms for two phytol isomers are measured with frontal analysis and correlated with a quadratic isotherm equation. Using a plug flow model with axial dispersion and mass transfer resistance experimental chromatograms are simulated. A fast dynamic model for the simulation of SMB is used to calculate the region of complete separation taking different column configurations into account.

Introduction

The increasing trend towards drugs of highest purity promotes preparative-scale chromatographic techniques. Most of these separations are performed using preparative liquid elution chromatography on a single column. The well known disadvantages of this concept are the dilution of products, the high solvent consumption and its discontinuity. The Simulated Moving Bed (SMB) concept can overcome two of these drawbacks: it is a continuous countercurrent process with reduced solvent consumption [1, 2]. Fig. 1 shows the functional scheme of the SMB process with the resulting internal concentration profile for the separated components A and B.

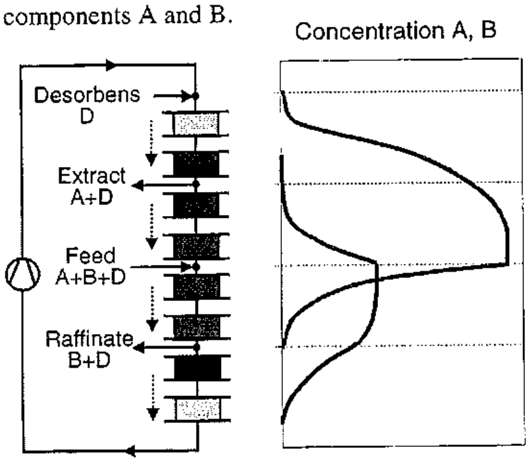

Figure 1: Functional scheme of the SMB process

The SMB concept is derived from the true countercurrent movement bed process (TMB) of the fluid and the solid phase. Due to enormous technical problems of moving a solid under pressure, the movement of the solid is simulated. By moving the inlet and outlet ports downwards, the movement of the solid phase upwards is simulated.

If for SMB process a supercritical fluid is used as solvent the product recovery can easily be achieved by depressurizing the gas. Another unique feature of the SMB-SFC process is the opportunity to change the elution strength of the mobile phase in order to optimize the separation performance.

The SMB Technique was originally developed by UOP [3] for the separation of hydrocarbons. In the last decade, this technique has been applied for the a number of other separations such as: sugars [4], racemic drugs [5] and isomers [6]. All these studies have been carried out using liquid solvents. Up to now, only one group is known who published results of a SFC-SMB separation [7]. The aim of this project is to develop this technique for the separation of pharmaceutical or finechemical products.

The SFC-SMB plant

The SFC-SMB plant (Fig. 2) consists of up to eight custom made columns (inner diameter 30 mm) with dynamic axial compression and variable bed length. They are designed for pressures up to 400 bar and temperatures up to 200°C.

The five in- and outgoing streams (feed, desorbens, raffinate, extract and recycling) are guided by five 8+1 way valves (SD8UW, Valco, Switzerland). Between two columns shut-off valves (Labor-Ventil Typ 1, Nova Swiss, Switzerland) are located. All these valves are coupled with air actuators. The raffinate and extract fractions are collected in high pressure fluid cyclones made at the TUHH. The cyclones have an inner diameter of 20 mm and an integrated product storage tank. Both, columns and cyclones are electrically heated. Temperatures are measured with PT 100 resistors. The carbon dioxide is pumped by an air driven pump (type G60 L, Maximator, Zorge, Germany) that pumps up to 18 kg/h. The pump sucks cooled, liquid carbon dioxide

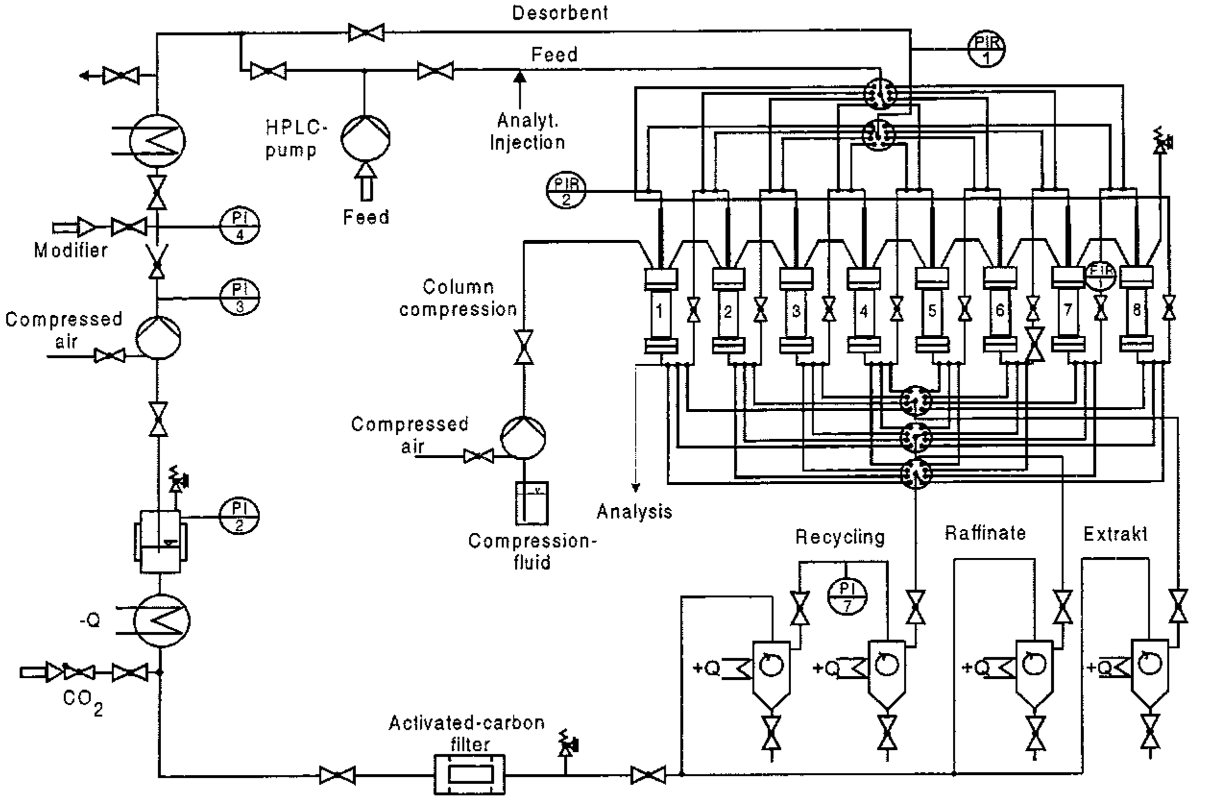
Desorbent
Feed
HPLC-pump
Analyt. Injection
Feed
PIR 1
PIR 2
PI 4
Modifier
PI 3
Compressed air
Column compression
1
2
3
4
5
6
7
8
FIR
Compressed air
PI 2
Analysis
Compression-fluid
Recycling
Raffinate
Extrakt
PI 7
-Q
+Q
CO$_2$
Activated-carbon filter

Figure 2: Scheme of the SFC-SMB plant

from the bottom of an autoclave (500cm^3). Then the carbon dioxide passes a pressure regulating valve (Tescom), that regulates the pressure to 240 bar.

Modifier (Isopropanol p.A., Merck KG, Darmstadt, Germany) is added by a doublehead-HPLC pump (Kontron). Heating is done in a temperature-controlled water bath. The stream is divided into two parts: one for the desorbent and the one for the feed. The liquid feed material is pumped with a single head HPLC pump (Kontron) into the system. All connections are made with 1/8" stainless steel tubing (Dockweiler, Oststeinbek, Germany) and fittings from Autoclave Engineers, Valco and Swagelok.

The system is controlled by a pentium 233 PC in combination with a control cabinet build at the TUHH.

Determination of adsorption-isotherms for phytol

The apparatus is shown in Fig. 3: Liquid carbon dioxide is compressed up to the desired pressure with a pneumatically driven pump. The flow of liquefied gas is lowered to operating pressure with a pressure-reducing valve. This process is done in a modified PM-101 module (NWA). With a double head HPLC pump (Kontron) isopropanol (IPA) as modifier is pumped into the system. Operating temperature is achieved with a heating cabinet (Binder, Germany) containing the column and five 6-port Rheodyne valves. A supercritical mixture of carbon dioxide and phytol is filled in a syringe pump (Isco, USA) to serve as feed. For adsorption a 4 x 250 mm column filled with LiChrospher Si 60 from Merck is used. After detection with UV-vis detector (SPD-10A, Shimadzu, Japan) at λ=221 nm the pressure is reduced in a two stage expansion module (PE-103, NWA) to ambient pressure. The gas flow is measured with a gas meter.

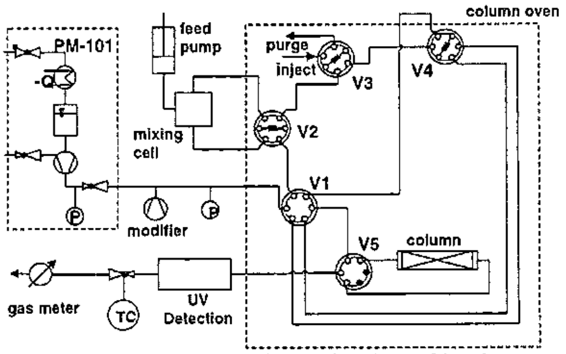
column oven
PM-101
feed pump
purge
inject
V3
V4
mixing cell
V2
V1
modifier
P
V5
column
gas meter
TC
UV Detection

Figure 3: Apparatus for determination of isotherms

The apparatus allows the measurement of adsorption isotherms with frontal analysis and a perturbation method. The following data are determined with frontal analysis. Due to the anti-langmuir behavior of the isotherms at lower concentrations the desorption fronts are integrated.

The experimental data are correlated with a quadratic isotherm equation, because both isotherms have a point of inflection (Fig. 4, Fig. 5).

$$q = q_s \frac{c(b_1 + 2b_2 c)}{1 + b_1 c + b_2 c^2} \qquad (1)$$

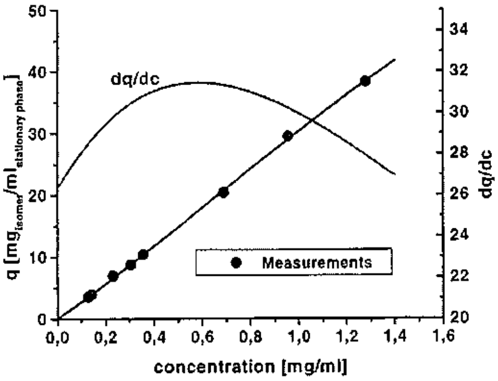

Figure 4: Adsorption isotherm of phytol cis-isomer at 225 bar, 40 °C, 1.8 mass% IPA

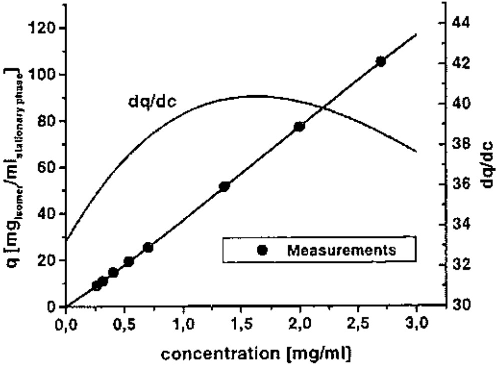

Figure 5: Adsorption isotherm of phytol trans-isomer at 225 bar , 40 °C, 1.8 mass% IPA

The measured data correspond well to the correlation. The derivative of the correlation is shown to demonstrate the point of inflection. The presented isotherms are mixture isotherms, because the data are determined directly from the binary phytol mixture and not from the pure isomers.

Simulation of batch chromatograms

For the simulation of batch chromatograms a plug flow model with axial dispersion and a linear mass transfer resistance is used. The solution of the resulting mass balance equations is performed with a finite difference method [8]. Interactions between the two isomers are neglected for the simulation of the chromatograms. The pressure drop of about 30 bar in the column leads to an increase in density of 3% under experimental conditions. This small change in density is taken into account by using a mean density. There have been found only minor differences between a more detailed model for the pressure drop and this simplification.

Although interaction between the isomers are neglected the simulated chromatograms agree well with experimental data (Fig. 7). For other applications or the higher concentration region a more detailed model like IAS theory is necessary.

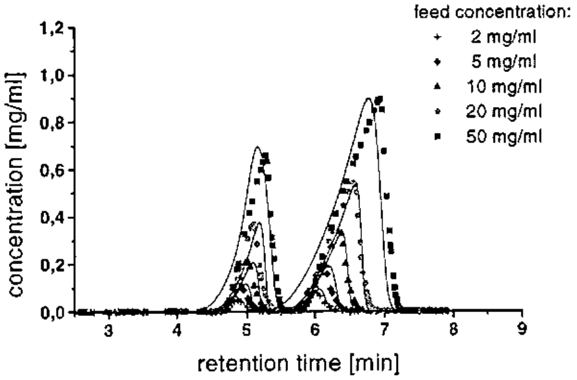

Figure 6: Experimental and simulated phytol chromatograms at 225 bar, 40 °C, 1.8 mass% IPA, column: 4 mm x 250 mm, LiChrospher Si 60

Simulation of the SMB process

Because of its significant shorter computation time a simpler equilibrium axial dispersed plug flow model is used for the simulation of the SMB process. All kinetic effects are lumped into the apparent dispersion coefficient 'D_{ap}'. The numerical solution of the mass balance equations (Eq.2) is done with a finite difference method first developed by Rouchon [9] for the simulation of a single bed and adapted to the conditions of the SMB process by Kniep et al. [10].

$$\frac{\partial c_i}{\partial t} + u\frac{\partial c_i}{\partial z} + \frac{1-\varepsilon_{ges}}{\varepsilon_{ges}}\frac{\partial q_i}{\partial t} - D_{ap,i}\frac{\partial^2 c_i}{\partial z^2} = 0 \qquad (2)$$

Following the ideas of Ruthven [11] and Storti [12] one can describe the TMB process as well as the SMB process with four key parameters: the net flow ratios m_j (Eq. 3).

$$m_j = \frac{Q_{zone}^{TMB} - Q_s \varepsilon_p}{Q_s(1-\varepsilon_p)} = \frac{Q_{zone}^{SMB} t_{shift} - V_{column}\varepsilon_{total}}{V_{column}(1-\varepsilon_{total})} \qquad (3)$$

$$j = \text{Zone I to Zone IV}$$

Using these parameters the region of complete separation of a binary mixture can be shown in a (m_2, m_3)-plane. For the most common adsorption isotherm equations i. e. Langmuir and bi-Langmuir multicomponent isotherms analytical solutions exists for the complete separation region. These analytical solutions are based on equilibrium theory and therefore neglecting mass transfer resistance and axial dispersion. In addition, the number of columns the SMB process consists of is not taken into account by the analytical solution, because it is based on the TMB process. The mentioned algorithm is fast and robust enough to calculate the region of complete separation in the (m_2, m_3)-plane numerically considering the effects of axial dispersion and a discrete number of columns in a SMB process.

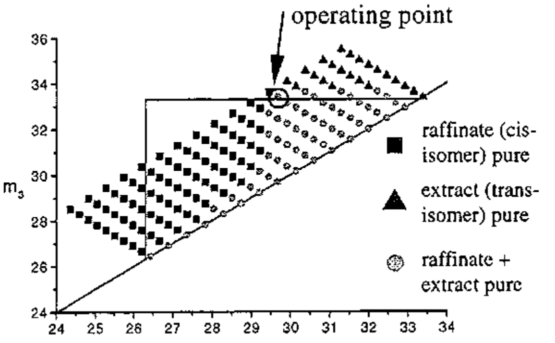

Figure 7: Region of complete separation for C_{feed}=5.0mg/ml phytol (225 bar; 40 °C, 1.8 mass% IPA) compared to infinite dilution situation and an infinite number of theoretical plates (black triangle). Column configuration: 2/2/2/2; 300 theoretical plates per column

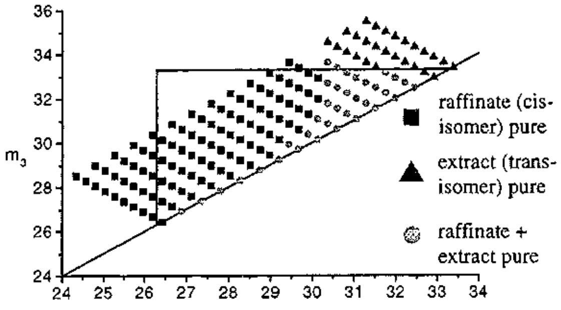

Figure 8: Same parameters as in Fig. 8 but column configuration: 1/1/1/1; 1000 theoretical plates per column

The use of only 4 separation columns leads to a smaller region of complete separation and therefore to a decrease in productivity. The optimal operating point for the 8 column configuration (m_2=29.68; m_3=33.39, shown in Fig. 8) is simulated with the dynamic SMB model for 4 and 8 columns (Fig. 10 and Fig. 11).

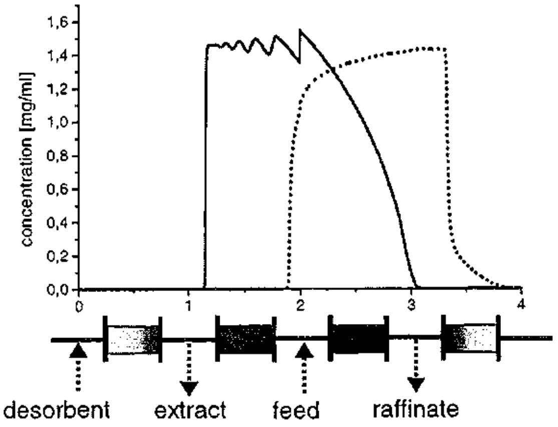

Figure 9: SMB concentration profile just before switching 1/1/1/1 column configuration, each column 1000 theoretical plates, operating point as shown in Fig. 8; extract purity: 93.5%, raffinate purity >99%

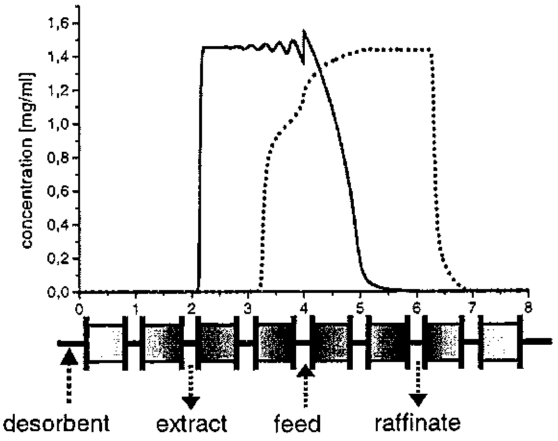

Figure 10: SMB concentration profile just before switching 2/2/2/2 column configuration, each column 300 theoretical plates, both isomers separated with more than 99.9% purity

Conclusions

The experimental chromatograms under supercritical conditions can be described well, with the measured adsorption data, correlated with a quadratic isotherm equation. Taking a finite number of theoretical plates and the number of columns into account the (m_2, m_3)-plane can be calculated The optimal operating points and the resulting concentration profiles for a 8 and 4 column configuration are shown.

Acknowledgment

The financial support from F. Hoffmann La-Roche AG, Kaiseraugst, Switzerland is gratefully acknowledged. The authors also thank Merck KGaA for the gift of stationary phases and sample material.

References

[1] Gottschall, K. PREP 1995, Washington DC.
[2] Strube, J. Chem.-Eng.-Tech. 70 (1998), 1271.
[3] Broughton, D.B. US Pat.3291726 (1966).
[4] Deckert, P. Chem.-Eng.-Tech. 69 (1997), 115.
[5] Schulte, M. J. Chromatogr. A 769 (1997) 93.
[6] J. Blehaut et al. LC GC Int. 9 (1996), 226.
[7] Clavier, J.Y. Int. Symposium on Supercritical Fluid Chromatography and Extraction Indianapolis, 1996.
[8] K. Kaczmarski et al., J. Chromatogr. A 756 (1996), 73-87
[9] P. Rouchon et al., Sep. Sci. Technol. 22 (1987), 1793-1833
[10] H. Kniep et al., PREP 1996
[11] D. M. Ruthven et al., Chem. Eng. Sci. 44
[12] G. Storti et al., AIChE J. 39 (1993) , 471-492

Hydrodynamic Behavior of Aqueous Systems in Countercurrent Columns at High Pressures

Dipl.-Ing. R. Stockfleth*, Prof. Dr.-Ing. G. Brunner
Arbeitsbereich Verfahrenstechnik II, Technische Universität Hamburg-Harburg, Germany
E-Mail: stockfleth@tu-harburg.de Fax.: 0049 (0)40 42878 4072

The hydraulic capacity of a countercurrent column with gauze packing was examined at pressures between 8 MPa and 30 MPa and temperatures between 313 K and 373 K. The systems used were water + carbon dioxide and surfactant solution + carbon dioxide. A distinctive change in the flooding mechanisms from "liquid layer flooding" to "bubble column flooding" was observed between $0.15 < \Phi = L/G(\rho_G/\rho_L)^{0.5} < 0.4$. The foamability of the surfactant solution decreased significantly with increasing pressure. Its influence on the flooding behavior could not be proved. The liquid hold-up ranged between 2 % and 5 %. The dry pressure drop adhered to the Ergun equation [1].

Introduction

The objective of this work is the examination of the hydrodynamic behavior, i. e. flooding, liquid hold-up, and pressure drop of columns with Sulzer gauze packing operating in countercurrent mode. The hydrodynamic behavior is investigated at temperatures between 313 K and 373 K and pressures between 8 MPa and 30 MPa. The systems used were water + carbon dioxide and (water + 129.2 mg/l Triton-X-100, a nonionic surfactant) + carbon dioxide.

There have been numerous investigations of the hydraulic capacity of columns for low pressure operating conditions, which usually yield semi-empirical correlations for the estimation of the hydraulic capacity. An early and very fundamental work on this subject is that by Sherwood et al. [2]. The concept developed by Sherwood et al. [2] exhibits general validity - it was for example successfully applied by Gieseler [3] to correlate flood points in blast furnaces. Billet [4] reports several newer flooding point and pressure drop correlations for vacuum and normal pressure. Krehenwinkel [5] and Krehenwinkel and Knapp [6] investigated the hydrodynamic behavior and mass transfer in columns with random packing at pressures up to 10 MPa under absorption conditions. Woerlee [7] briefly investigated the hydrodynamics and mass transfer in packed columns at ambient conditions and at conditions relevant for the gas extraction. Meyer [8] examined flooding points, pressure drop, and physical properties of the systems soybean oil distillate + carbon dioxide and fish oil + carbon dioxide. A major conclusion from his work was, that it is necessary to measure the hydraulic capacity of the column and the physical properties of the liquid and gaseous phase at high pressures, because the semi-empirical correlations obtained at low pressure conditions are not valid for the high pressures and therefore high gas densities encountered in gas extraction processes.

Experimental Apparatus

The apparatus shown in Fig. 1 is operated at pressures between 8 and 30 MPa and temperatures between 313 and 373 K. It consists of two main parts: The column has a height of 1.89 m and is equipped with four long windows for the visual observation of the two-phase flow through the packing and an equilibrium autoclave equipped with a stirrer. The column is filled with 0.9 m packing.

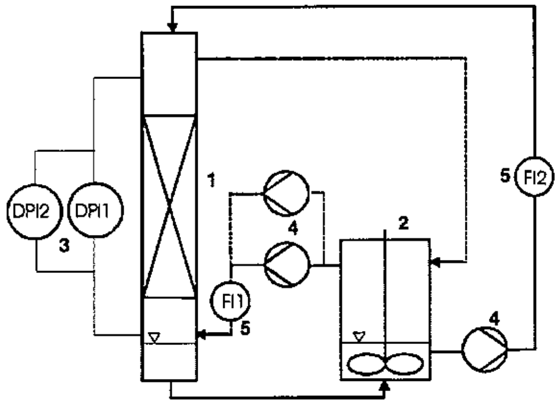

Figure 1: Flowsheet of the Experimental Apparatus
1 - Column, 2 - Autoclave, 3 - Differential Pressure Transducers 4 - Gear Pumps, 5 - Flow Meters
Full Line - Liquid Cycle, Dashed Line - Gas Cycle

The coexisting phases are brought into equilibrium by circulating and stirring. This is necessary to observe the hydrodynamic phenomena independently of the mass transfer phenomena. Three high pressure gear pumps (two for the supercritical phase and one for the liquid phase) convey the two phases from the autoclave to the column and from there they flow back into the autoclave after passing through the packing.

Materials and Methods

Deionized water with an electrical conductivity smaller than 1 µS was used. The carbon dioxide had a purity of 99.95 % and was supplied by

Kohlensäurewerke Deutschland. Laboratory grade Triton-X-100 (t-Octylphenoxypolyethoxyethanol) supplied by Sigma Aldrich was used to make the water susceptible to foaming. The geometric properties of the packings used are shown in Table 1. The two diameters d_p and d_h are calculated with the following equations:

$$d_p = 6\frac{1-\varepsilon}{a_S} \qquad (1)$$

$$d_h = 4\frac{\varepsilon}{a_S} \qquad (2)$$

Table 1: Geometric Data of the Packings [8]

	Column Diameter	Porosity	Specific Surface Area	Particle Diameter	Hydraulic Diameter
Packing	d [m]	ε [-]	a_s [m²/m³]	d_p [mm]	d_h [mm]
CY	0.025	0.9584	1127	0.2215	3.088
EX	0.025	0.86	1710	0.4912	1.886

The entire apparatus is placed in two modified heating ovens, which are used to bring the apparatus to the desired temperature. Due to the significant mass and heat capacity of the column and autoclave this process takes six hours when increasing and ten hours when decreasing the temperature. Next the column was filled with liquid from a storage tank. The carbon dioxide is then conveyed to the column by a two-stage compressor until the desired pressure is reached. The stirrer in the autoclave is turned on and the phases are circulated through the column until the pressure and the temperature are constant. At this point it can be assumed that the liquid and supercritical phase are in equilibrium, the preparations are complete and the experiment is started. A flow rate for the supercritical phase and for the liquid phase are selected. The phases are circulated at constant liquid phase level in the bottom until a constant value for the pressure drop has been reached. This usually takes five minutes unless the column floods in which case it was in most cases impossible to obtain a constant value for the pressure drop. Then the bottom valve is closed and the gear pumps are shut off. The dynamic liquid hold-up is measured by the drainage method [9]. When the liquid level in the bottom does not change anymore - this usually happens after ten minutes - the previous liquid level (before shutting off the gear pumps) is subtracted from the current liquid level thus yielding the volume of the liquid hold-up after multiplication with the cross-sectional area A. The next experiment is conducted at the same flow rate of the supercritical phase, but with increased liquid flow rate. This procedure is repeated until the flooding point or the capacity limit of the gear pumps is reached. Then the flow rate of the supercritical phase is changed and the procedure is repeated. Finally, the dry pressure drop is measured by circulating the supercritical phase at different mass flow rates through the wetted but dry packing.

For the measurement of the foamability of a surfactant solution under high pressure the apparatus was slightly modified. The packing was removed and the supercritical phase was conveyed into the column through a tube with a diffuser stone made from 20 µm sintered metal particles at the end. The bottom valve of the column was closed and the surfactant solution was poured into the column as usual until the liquid level was 2 cm above the top of the diffuser stone. The gear pump for the supercritical phase was turned on and the system was given enough time to reach a steady state foam height, then the pump was shut off and the foam was given time to collapse. Next the procedure was repeated with a different flow rate.

Visual Observations

The packing is not completely wetted. The water flows down the packing in rivulets at all flow rates. The only exception is if the columns floods. The redistribution devices of the packing collect the rivulets from the wall and make them flow into the packing again. The most important finding was the observation of two different flooding mechanisms. The "liquid layer flooding" is the commonly known flooding mechanism. The liquid layer on top of the packing grows higher than a certain limit. If the liquid layer on top of the packing exceeded 8 cm this was called a flooding point. This may seem somewhat arbitrary, however, it was observed, that if the liquid layer exceeded 4 cm it also exceeded 8 cm after some time had elapsed. The phenomenon "bubble column flooding" is similar to the emulsification described by Kafarow [10]. At first nothing is observed except that the pressure drop increases slowly but consistently. Then the liquid front reaches the lowest long window. The lower part of the packing is filled with liquid and the supercritical phase bubbles discontinuously through the liquid. The upper part of the packing still exhibits a normal flow regime. Since the amount of liquid entering the packing is greater than the amount leaving the packing, the liquid front advances to the top of the packing and higher. Obviously the pressure drop is significantly higher when "bubble column flooding" occurs than when "liquid layer flooding" takes place. A distinctive difference in the flooding mechanism for flooding points with $\Phi < 0.15$ and with $\Phi > 0.4$ was observed. All flooding points with $\Phi < 0.15$ were "bubble column flooding points" and all flooding points with $\Phi > 0.4$ were "liquid layer flooding points". The flooding points for $0.15 < \Phi < 0.4$ were partially "liquid layer flooding points" and partially "bubble column flooding points" indicating that this is an area of transition from one flooding mechanism to the other. Billet [4] states that the gaseous phase becomes the disperse phase at $\Phi = 0.4$ confirming our observation and interpretation.

During the foaming experiments the formation of foam plugs was observed at lower pressures. A foam plug is a piece of foam that separates from the main body of the foam and travels up in the column driven by the flow of the supercritical phase until it has drained enough to rupture and slide down onto the main body of the foam. These plugs severely inhibited the measurement of the steady state foam height.

Results and Discussion

The dry pressure drop over the wetted but dry packing is an important piece of information for the evaluation of the wet pressure drop. The knowledge of the dry pressure drop allows the determination of the difference between total pressure drop and dry pressure drop, and this difference is the part of pressure drop which is caused by the liquid flowing countercurrently to the supercritical phase. Many correlations for the total pressure drop and for flooding points use the dry pressure drop as input information [4, 11, 12]. Similar to the pressure drop in pipes the pressure drop over the packing is a function of the resistance factor and the dynamic head [13]:

$$\frac{\Delta p_0}{H} = \psi \frac{(1-\varepsilon)\rho_G u^2}{\varepsilon^3 d_p} \tag{3}$$

Where Δp_0 denotes the dry pressure drop, H the height of the packing, ψ the resistance factor, ρ_G the density of the supercritical phase, and u the superficial velocity of the supercritical phase. For convenience the subscript G (gaseous) is used for the supercritical phase to maintain a notation similar to publications investigating hydrodynamics at low pressures. The resistance factor is a function of the Reynolds number yielding the dimensionless relationship (see for example [11]):

$$\psi = f\left(\mathrm{Re} = \frac{u d_p \rho_G}{(1-\varepsilon)\eta_G}\right) \tag{4}$$

One of the most commonly applied relations of this type is the Ergun equation [1]):

$$\psi = \frac{150}{\mathrm{Re}} + 1.75 \tag{5}$$

Fig. 2 shows the measured dry pressure drop with supercritical carbon dioxide in the Sulzer EX packing. For comparison other authors' data have been included in the diagram. The Reynolds number varies only tenfold from 100 to 1000; due to the limited capacity of the gear pumps a higher variation was not possible. The Ergun equation is a good correlation for the measured values - almost all values lie within the ± 20 % interval. Krehenwinkel's values, although obtained at different conditions with a different packing, fall into the ± 20 % interval as well.

The hold-up and the wet pressure drop are closely correlated. The liquid hold-up decreases the free diameter of the flow channels for the supercritical phase, thereby increasing the effective velocity and the pressure drop. If the free diameter of the flow channels is lower than a critical value the two phases start to interact. This point is called loading point. Beyond this point the two phases interact. Several microscopic processes can be held responsible for the increased interaction and thereby increased liquid hold-up and pressure drop. These microscopic processes are entrainment of liquid droplets, interfacial shear stress, and the formation of waves which will eventually destabilize the liquid film. Woerlee [7] developed a model for the entrainment. Bänziger [14] examined the formation of droplets in structured packings at high but subcritical pressures. Mersmann [12] conceived the "liquid-film-gas-shear-stress-model". However, the applicability of this model is limited [3, 8, 11] indicating that the interfacial shear stress is not - or at least not solely - decisive for loading and flooding. There have been several investigations on the formation of waves on the surface of falling liquid films. Moser [15] and Moser and Trepp [16], investigated the stability of a falling liquid film of α-Tocopherol + carbon dioxide as countercurrent supercritical phase. The wave formation caused by countercurrent gas flow is examined by Shearer and Davidson [17].

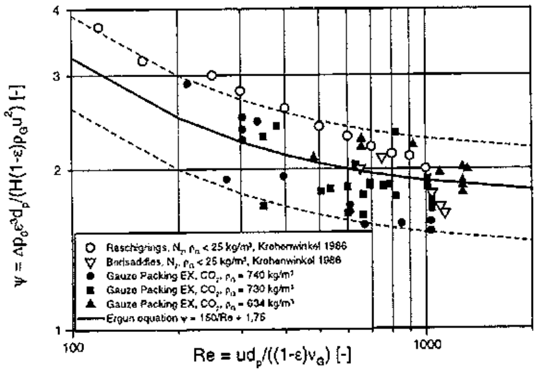

Figure 2: Resistance Factor versus Reynolds Number for Sulzer EX Packing

The dashed line represents the ± 20 % interval of the Ergun equation.

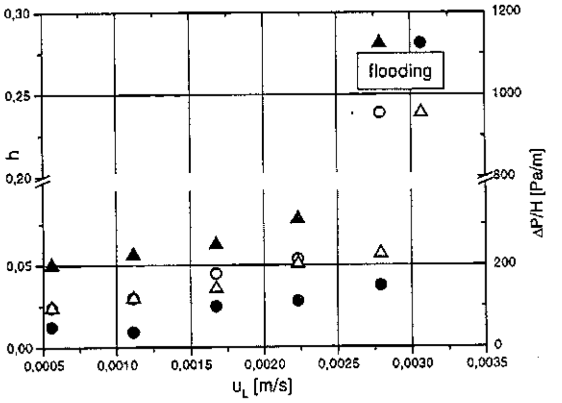

Figure 3: Liquid Hold-up and Pressure Drop versus Liquid Load for the System Water + CO_2 in Sulzer EX Packing

Solid: Pressure Drop   Circles: u = 0.01 m/s
Open: Liquid Hold-Up   Triangles: u = 0.02 m/s

Fig. 3 shows the liquid hold-up and the pressure drop for the system water + carbon dioxide in Sulzer EX packing. As expected the liquid hold-up and pressure drop are rising slightly with increasing liquid load until the flooding point is reached. If these date are compared with other authors' data (e. g. [4], [11]) it becomes apparent that the loading region is very small and not detectable in Fig. 3. The system changes abruptly from no interaction between the two phases to flooding. In this case "bubble column flooding" occurred, so the values for the pressure drop and the liquid hold-up at the flooding point have no absolute but only a relative meaning since they would have grown indefinitely until all liquid from the autoclave was piled up in the packing and above.

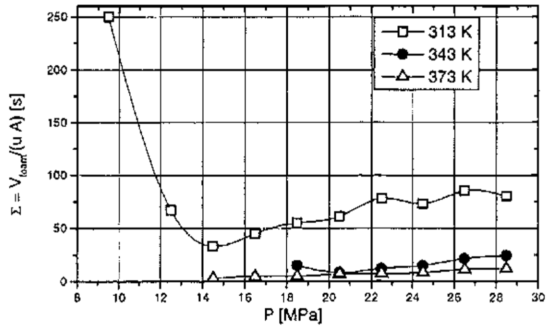

Figure 4: Foamability versus Pressure for the System Water + 129.2 mg/l Triton-X-100 + CO_2

Fig. 4 shows the results of the foaming experiments. The water contained 129.2 mg/l Triton-X-100 which is half the value of the critical micelle concentration at standard temperature and pressure [18]. The ordinate shows the residence time of the supercritical phase in the foam; this measure for the foamability was suggested by Bikerman [19]. As already pointed out, the experiments at lower pressures did not yield consistent results due to the formation of foam plugs. However, from this diagram it can be deduced that the pressure has a significant impact on the foamability of the surfactant solution. For 313 K there seems to be a minimum foamability at 14.5 MPa.

Fig. 5 shows a flooding diagram for the Sulzer CY packing with the system pure water + carbon dioxide and surfactant solution (water + 129.2 mg/l Triton-X-100) + carbon dioxide. There is no detectable difference in the qualitative (visual) and quantitative flooding behavior between the two systems, which is in contradiction to other authors' experimental results ([5], [20]) and the generally accepted rule that foaming significantly decreases the hydraulic capacity of columns [21]. The considerable decrease in foamability with increasing pressure as shown in Fig. 4 could explain this extraordinary behavior. The surfactant solution exhibits a severely restricted tendency to form a stable foam under high pressures in comparison to ambient pressure. Therefore, the foamability of this specific surfactant solution does not affect the flooding behavior at high pressures. The packing geometry however, has a decisive impact on the hydraulic capacity of the packing as changing from EX to CY will increase the possible load of the supercritical phase by a factor of five.

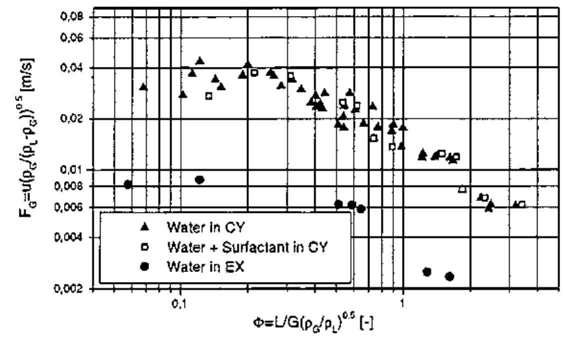

Figure 5: Flooding Diagram for the Systems Water + CO_2 and Surfactant Solution + CO_2 in Sulzer CY Packing compared with the System Water + CO_2 in Sulzer EX Packing

Conclusions

It was demonstrated that there are two different flooding mechanisms and the flow parameter as suggested by Sherwood et al. [2] determines according to which mechanism the column will flood. Foaming liquids seem to be not as bothersome in gas extraction columns as in columns operated at normal conditions, because the foamability decreases decisively with increasing pressure.

References

[1] Ergun, S.; Chem. Eng. Prog. **48**, p. 89-94, 1952

[2] Sherwood, T. K.; Shipley, G. H.; Holloway, F. A. L.; Ind. Eng. Chem., 7, p. 765-769, 1938

[3] Gieseler, M.; *Durchströmungsverhalten von Packungen und Schüttungen aus Koksen unterschiedlicher Größe und Gestalt in Gegenwart einer flüssigen Phase hoher Viskosität*, Thesis, Clausthal, 1972

[4] Billet, R.; *Packed Towers*, VCH, Weinheim, 1995

[5] Krehenwinkel, H.; *Experimentelle Untersuchung der Fluiddynamik und der Stoffübertragung in Füllkörperkolonnen bei Drücken bis zu 100 bar*, Thesis, Berlin, 1986

[6] Krehenwinkel, H.; Knapp, H.; Chem. Eng. Tech., **10**, p. 231-242, 1987

[7] Woerlee, G. F., *Hydrodynamics and Mass Transfer in Packed Columns and their Applications for Supercritical Separations*, Thesis, Delft, 1997

[8] Meyer, J.-T.; *Druckverlust und Flutpunkte in Hochdruckgegenstromkolonnen betrieben mit überkritischem Kohlendioxid*, Thesis, Hamburg, 1998

[9] Lim, J. S.; Lee, Y.-W.; Kim, J.-D.; Lee, Y.-Y.; Chun, H.-S.; J. Supercrit. Fluids, **8**, p. 127-137, 1995

[10] Kafarow, W. W.; *Grundlagen der Stoffübertragung*, Akademie Verlag, Berlin, 1977

[11] Mackowiak, J; *Fluiddynamik von Kolonnen mit modernen Füllkörpern und Packungen für Gas/Flüssigkeitssysteme*, Salle + Sauerländer, Frankfurt am Main, 1991

[12] Mersmann, A.; Chem. Ing. Tech., **37**, p. 218-226, 1965

[13] Brauer, H.; *Grundlagen der Einphasen- und Mehrphasenströmungen*, Sauerländer, Frankfurt am Main, 1971

[14] Bänziger, G.; *Untersuchung des Fluidverhaltens in geordneten Packungen unter Hochdruck*, Thesis, Zürich, 1995

[15] Moser, M., *Fallfilmstabilität und Grenzflächenspannung in Systemen mit einer überkritischen Komponente*, Thesis, Zürich, 1996

[16] Moser, M.; Trepp, C.; Chem. Eng. Tech., **20**, p. 612-616, 1997

[17] Shearer, C. J.; Davidson, J. F.; J. Fluid Mech., **22**, p. 321-335, 1964

[18] Gutwald, S.; *Über die Wirkweise mechanischer Schaumzerstörer mit Prallverdichtung*, Thesis, München, 1996

[19] Bikerman, J. J.; *Foams*, Springer, Berlin, 1973

[20] Mersmann, A.; *Druckverlust und Schaumhöhen von gasdurchströmten Flüssigkeitsschichten auf Siebböden*, VDI Verlag, Düsseldorf, 1962

[21] Perry, R. H.; Green, D. W.; *Perry's Chemical Engineers' Handbook*, 7th Edition, McGraw-Hill, 1997

TREND EVALUATION FOR SUPERCRITICAL APPLICATIONS BY PATENT STATISTICS

Erwin Schütz, Drosselweg 2, D-83308 Trostberg

The development of technology for supercritical fluids as solvents was accompanied by an increasing flow of patent applications. The total number of filed patents is now between 2000 and 2300 which is suitable for statistical analysis. A databank has been built up with the purpose of collecting bibliographic as well as technical details allowing the retrieval of individual and global informations. After a dozen of related publications in the US during the thirties, supercritical fluid extraction of food and flavours during the seventies was the core of development activities that were located in Germany. Japan followed since 1983 with developments in the food and chemical sector. Till now SFE is the most frequently used technique with supercritical fluids, but SCWO and techniques for particle generation gain more and more attention. Until 1987 the field was dominated by patents for food applications, since that time a tremendous increase in chemical process proposals has happened. Particle generation and production and treatment of polymers are the most frequent techniques. The total trend for development of new supercritical applications is still positive.

Introduction

Probably the first patent for the application of pressurised carbon dioxide for extraction purposes was filed in 1904 by *Sachs* [1] (Fig. 1).

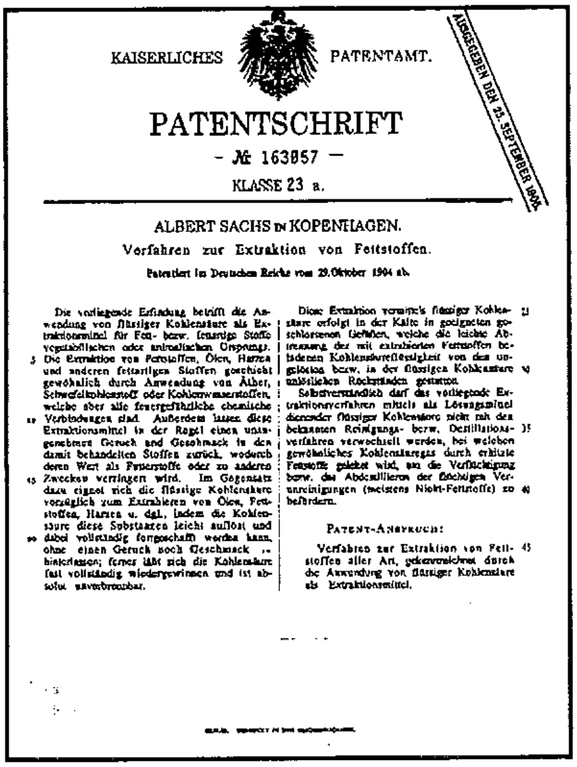

KAISERLICHES PATENTAMT.

AUSGEGEBEN DEN 23. SEPTEMBER 1905

PATENTSCHRIFT

— № 163057 —

KLASSE 23 a.

ALBERT SACHS IN KOPENHAGEN.

Verfahren zur Extraktion von Fettstoffen.

Patentiert im Deutschen Reiche vom 29. Oktober 1904 ab.

Die vorliegende Erfindung betrifft die Anwendung von flüssiger Kohlensäure als Extraktionsmittel für Fett- bezw. fettartige Stoffe vegetabilischen oder animalischen Ursprungs. Die Extraktion von Fettstoffen, Ölen, Harzen und anderen fettartigen Stoffen geschieht gewöhnlich durch Anwendung von Äther, Schwefelkohlenstoff oder Kohlenwasserstoffen, welche aber alle feuergefährliche chemische Verbindungen sind. Außerdem lassen diese Extraktionsmittel in der Regel einen unangenehmen Geruch und Geschmack in den damit behandelten Stoffen zurück, wodurch deren Wert als Futterstoffe oder zu anderen Zwecken verringert wird. Im Gegensatz dazu eignet sich die flüssige Kohlensäure vorzüglich zum Extrahieren von Ölen, Fettstoffen, Harzen u. dgl., indem die Kohlensäure diese Substanzen leicht auflöst und dabei vollständig fortgeschafft werden kann, ohne einen Geruch noch Geschmack zu hinterlassen; ferner läßt sich die Kohlensäure fast vollständig wiedergewinnen und ist absolut unverbrennbar.

Diese Extraktion vermittels flüssiger Kohlensäure erfolgt in der Kälte in geeigneten geschlossenen Gefäßen, welche die leichte Abtrennung der mit extrahierten Fettstoffen beladenen Kohlensäureflüssigkeit von den ungelösten bezw. in der flüssigen Kohlensäure unlöslichen Rückständen gestatten.

Selbstverständlich darf das vorliegende Extraktionsverfahren mittels als Lösungsmittel dienender flüssiger Kohlensäure nicht mit den bekannten Reinigungs- bezw. Destillationsverfahren verwechselt werden, bei welchen gewöhnliches Kohlensäuregas durch erhitzte Fettstoffe geleitet wird, um die Verflüchtigung bezw. das Abdestillieren der flüchtigen Verunreinigungen (meistens Nicht-Fettstoffe) zu befördern.

PATENT-ANSPRUCH:

Verfahren zur Extraktion von Fettstoffen aller Art, gekennzeichnet durch die Anwendung von flüssiger Kohlensäure als Extraktionsmittel.

Figure 1. First patent about extraction with liquefied CO_2.

Until the year of 1970 in total 50 patents were published, most coming from US and mostly with claims about extraction with liquefied or supercritical hydrocarbons or CO_2. The extraction and purification of fats and oils was the most frequent application field. The broad development began 1964 with the filing of a german patent by *Studiengesellschaft Kohle* (inventor: *Zosel)* with priority in Austria [2] published 1969. The topic was supercritical fluid extraction.

Data Material and Methods

The source for the generation of the databank was literature research, research at patent offices and the use of online- databanks [3,4,5], which are partially open for everyone's use [6,7]. None of the sources allows alone a 100 % reliable search. The coverage of patents by the databank is estimated to be 80 percent of the total existing files of the field. Subcritical fluids and liquefied gases with related applications are included. The databank was built up for MS Excel in a table form. By the use of standardised formats and the creation of selective keywords the statistical evaluation of bibliographic data and some technical relations is possible. As a criterion for the chronological view the year of application was used. Because of the time delay between priority application and the publication times ranging from 6 to 18 months there is a uncertainty of one or more years regarding national data and priority time. For the statistical evaluation only one family member of a patent was used, continuations and divisions were only taken into consideration when the older files were abandoned. This evaluation covers patents until publication in November 1998.

Results

Global Patent view

Fig. 2 shows the number of patents filed in total for the major contributing countries. Because of the uncompleted research of application years later then 1996 the general statistics were not evaluated after that time. Until that time in the US and Japan about 600 patents have been filed, whereas Germany (both parts) and Austria contributed about half that number. The total number covered by the databank until 1996 reaches 1750. Since 1991 the number of patents filed per year seems to be constant.

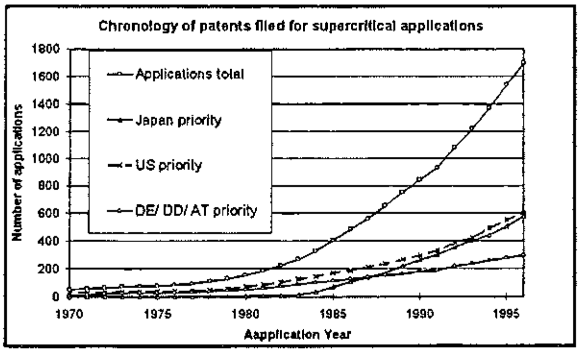

Figure 2. Chronology of patents filed for supercritical applications

The view of the applications per year leads to somewhat more information about what is actually happening (Fig. 3.) There was a significant decrease in the number of filed patents in 1991 and there is evidence that the total number of patents filed per year is not more increasing since 1995.

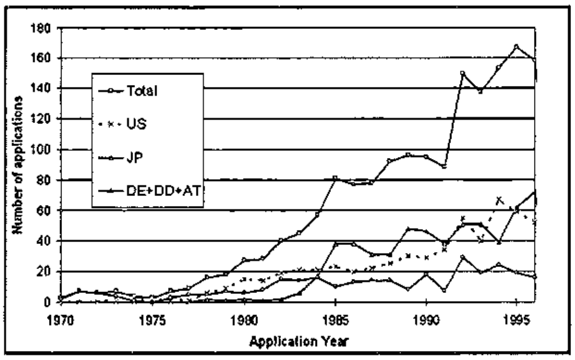

Figure 3. Total patent applications per year

Regarding the behaviour of nations it is visible that Japan started its activity somewhat after the US and Germany but was the most active country in the field of SCF during the most recent years .

Patent view of selected branches

The development of different fields applying supercritical fluids was split into food (including alcohol, caffeine and tobacco), chemistry, textiles as a sub - branch and pharmaceuticals including medicinal products. In Fig. 4 the chronological situation is demonstrated. Food applications dominated the statistics until 1988. From that time there is a slow decrease in patent numbers. In 1996, food is the least important field of the selected groups. It was overtaken by chemistry which increased especially in the recent year 1995 and is still increasing. Chemistry seems to be now by far the most interesting field for developers.

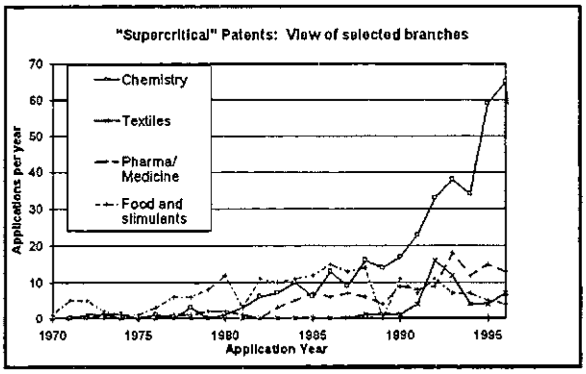

Figure 4. Chronological patent view of selected branches with supercritical application

Processes in the pharmaceutical and medicinal field began their development later, the number increased to a maximum in 1993 and is fairly constant since that time. Textile treatment, mainly consisting of processes for textile dyeing and dry cleaning, had a boom in 1992 and 1993; since that time the interest has been significantly reduced.

View of processes

Fig. 5 shows some of the most import processes used. The patent analysis is somewhat difficult in this case because the homogeneity of keywords is not very distinct regarding differing process variants. The most frequent operation supercritical fluids are used for is extraction (SFE). The number of patents filed per year was increasing nearly steadily until 1995. There is a decline in 1996 which is not yet shure to be a longer lasting trend.
Other major contributors are impregnation (including textile dyeing), with a maximum in 1992, now less important and supercritical water oxidation (SCWO) with a maximum in 1994.

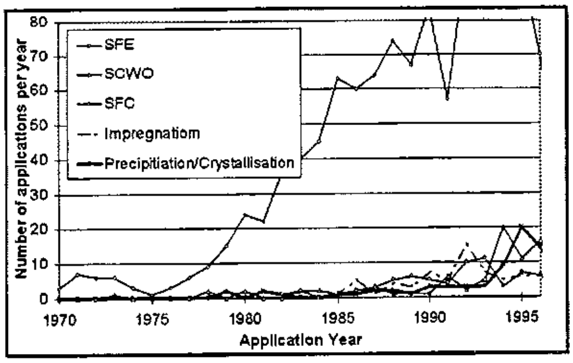

Figure 5. Patents containing techniques using supercritical fluids

The latter (about 15 patents per year) is still in active progress. Supercritical fluid chromatography (SFC) is an older field which developed strongest in the years 1992 and 1993. From the statistical view the field of particle generation is most difficult to record, because it contains crystallisation and precipitation (antisolvens) techniques, sedimentation, furnishing and coating application as well as spray drying. It is visible that this field has its strongest development since 1995, maybe the maximum of activity is not yet reached.

A more detailed view of the situation and a determination of the most recent trends is given in Table 1 and 2. Here the number of recently (since 1996) filed patents is compared with the total number of supercritical applications as well as with the global number of patent applications.

Table 1. **Patent - Statistics of supercritical applications**

1. Fields with the highest **relative** patent number after 1996

[%] related to : 1758 patents 201 patents

[%] related to global patent number: 100% 4,4%

Group analysis	Total number	[%]	Number 1996-1998	Trend 96/98
SFE Medicine	8	0%	2	568%
SFE Analytics	40	2%	10	568%
SFE Measurement Control	10	1%	3	682%
SFE Drying	51	3%	10	446%
Folder 3: Chemistry	**386**	**22%**	**84**	495%
Polymers	201	**11%**	41	464%
Reactions without Polymeres	120	7%	30	568%
Supercritical Water Oxidation	83	5%	19	520%
Folder 4: Materials	**173**	**10%**	**31**	407%
Particle processing	41	2%	11	610%
Semiconductors, Electronics	18	1%	5	631%
Sterilisation, mostly supercritical	16	1%	3	426%

Table 1. New and relatively strongly growing applications for supercritical fluids.
[%] = number of special patents related to total number of supercritical patents. (Answers the question: which supercritical application has most patent applications?)
Trend = patents in a time period related to estimated increase in global patent number. (Answers the question: which fields are new?)

The table shows selected fields with a performance better then the average of the totally covered fifty supercritical application groups. Indicated is the total number of patents and their percentage to the total supercritical field. The column called „Trend 96/98" shows a chronological comparison of actual patent number compared with the estimated global increase in patents. It does not tell anything about the **absolute** number of patents filed in this time range. Using this criterion, measurement/ control-developments for SFE are nearly seven times as frequently filed as the average of, but the number of patents is only three. In SFE the analytical applications gained more interest. In chemistry, the fields of polymers production, reactions in supercritical fluids and supercritical water oxidation developed strongly. Also particle processing and semiconductors treatment had a high impact.

In Table 2 the absolute and relative number of new patents is combined by multiplying the „trend" figure with the percentage. Here SFE is still a strong group. Chemistry has developed to the same level and includes the most important new developments. Materials, particle processing and surface treatments are also developing stronger then the average.

2. Fields with the highest **rel. and absolute** pat. number after 1996

Group analysis	Total number	[%]	Number 1996-1998	[%] x Trend
Folder 1: SFE	1204	**68%**	96	**1,24**
SFE Pharmaceuticals	105	6%	13	0,17
SFE Chemistry	173	**10%**	24	**0,31**
SFE Analytics	40	2%	10	0,13
SFE Purification	193	**11%**	28	**0,36**
SFE Drying	51	3%	10	0,13
SFE Chemical Engineering	235	**13%**	18	**0,23**
Folder 2: Impregnation	**72**	**4%**	**11**	0,14
Folder 3: Chemistry	**386**	**22%**	**84**	**1,09**
Polymers	201	**11%**	41	**0,53**
Reactions without Polymeres	120	7%	30	**0,39**
Supercritical Water Oxidation	83	5%	19	**0,25**
Folder 4: Materials	**173**	**10%**	**31**	**0,40**
Particle processing	41	2%	11	**0,14**
Furnaces, surfaces	47	3%	8	0,10

Table 2. Recent trends of supercritical applications
[%] x Trend = Attempt for description of both relative and absolute patent status. (Answers the question: which patent field is topical and strong in patent number?)

In summary the fields of

- SFE with purification processes and processing of chemicals,
- chemistry with polymers and reactions
- materials processing

are either well introduced techniques or in recent times strongly developing.

- chemistry with polymers and reactions
- materials processing

are either well introduced techniques or in recent times strongly developing.

Companies and persons related to supercritical developments

The view of patents of course leads not to an adequate overview over the total research activities going on because it is strongly connected with commercial projects and does underestimate the academical side of university research. Table 3 shows the most frequently occurring companies and organisations.

Under the 38 names are only three academic/ research organisations which is not unusual but is underlining the fact that the strongest impetus for developments came from industrial side. The first two companies - *Kraft* including *General Foods* and *HAG AG* and *SKW Trostberg AG* - launched nearly exclusively patents for food processing, whereas the third - *Mitsubishi Heavy Industry* - was covering a broad spectrum relating to chemical applications.

Patent applicant/ owner	Number of filed patents
KRAFT/ GENERAL FOODS/ HAG AG	31
SKW TROSTBERG AG	31
MITSUBISHI HEAVY IND	27
HITACHI	26
UNION CARBIDE	24
KOBE STEEL	23
SEITETSU KAGAKU CO LTD	23
HASEGAWA CO LTD	22
AGENCY OF IND SCI & TECHNOLOGY	21
KRUPP GMBH	21
SHELL OIL	19
STUDIENGESELLSCHAFT KOHLE	19
HEWLETT-PACKARD	18
IDEMITSU PETROCHEM	18
MATSUSHITA ELECTRIC WORKS	18
SUMITOMO SEIKA CHEM	17
HOPFENEXTRAKTION HVG BARTH RAISER	16
MITSUBISHI CORP	16
SHOKUHIN SANGYO HIGH SEPARATION SYST	16
MUELLER A (MUELLER EXTRACT)	15
MORI SEIYU KK	14
BASF	13
DU PONT DE NEMOURS	13
NIPPON STEEL CHEM	13
CIBA GEIGY	12
HOECHST	12
HUGHES AIRCRAFT	12
NIPPON SANSO	12
PHILLIPS PETROLEUM	12
CHLORINE ENGINEERS CORP	11
KERR-MCGEE CHEM CORP	11
LION CORP	11
US DEPT ENERGY	11
BAYER	10
EXXON	10
JAPAN TOBACCO	10
MOBIL OIL	10
SUMITOMO HEAVY IND	10
XEROX	10

Table 3. Patent assignees for supercritical applications

Table 4 shows the most frequently named inventors of a total index of more then 2600. They are inventors on 450 patents, about 20 % of the total patent number. A technical problem of the evaluation is the variability in spelling especially japanese names. So in a second row a second number in- or excluding similar spellings was listed. The first three japanese inventors, *Ogasawara (Ogasahara)* and *Inada* are connected with the companies *Seitetsu Kagaku* and *Sumitomo Seika*, as well as the third name. The latter is also appearing on patent applications of *Hitachi Ltd.*

Inventor name	Number of Patent appl.	Name similarity
Ogasawara J	26	23?
Inada S	25	22?
Takahashi S	23	30?
Vollbrecht H	20	
Horizoe H	19	
Gehrig M	16	
Hubert P	16	
Coenen H	15	
Peter S	15	
Schuetz E	15	
Tsubakimoto G	15	16?
Vitzthum O	15	
Arai K	14	
Mueller A	14	
Cully J	13	
Imamura H	13	
Yokogawa H	13	
Heidlas J	12	
Kubota M	12	
Nielsen KA	12	
Forster A	11	
Hong GT	11	
Matsuzaka H	11	
Morikawa K	11	
Roethe KP	11	
Schollmeyer E	11	
Yokoyama M	11	
DeSimone JM	10	
Kitakura Y	10	
Makihara H	10	
Matsuya T	10	
Rosahl B	10	

Table 4. Most frequently appearing inventors

The list may be useful for literature search and getting familiar with the field of supercritical fluids.

Summary

Patent research is an useful instrument for the determination of the state of the technique and for the evaluation of new trends in process technology. Application of supercritical fluids especially for chemistry are belonging to the more interesting fields for future developments.

References

[1] Gehrig M., personal communication (1997)
[2] Deutsches Patent 1493190, Studiengesellschaft

NATURAL AND FORCED CONVECTION IN PRECISION CLEANING AUTOCLAVES

Authors : Vincent PERRUT, Michel PERRUT
SEPAREX S.A., 5 rue Jacques Monod F-54250 Champigneulles
Email : separex@francecom.net - Fax : 33-3.83.31.24.83

Chloroalkanes substitution by liquid carbon dioxide for precision cleaning is a major environmental challenge that requires innovative solutions to reach both high quality cleaning and acceptable costs. One technical problem consists in causing a strong convection inside the cleaning autoclave in order to boost mass transfer of pollutants to the fluid and to entrain particles. Several techniques have been proposed : Forced convection through a motor-driven blade stirrer, ultrasonic agitation, free connection. In this paper, a special autoclave design is disclosed, permitting both forced and free convection of the liquid carbon dioxide and experimental results are presented to show convection efficiency on cleaning.

Introduction

As halogenated solvents are widely banned either for health and environmental hazards, both textile dry cleaning and mechanical and electronical parts degreasing and cleaning are becoming a worldwide issue. In spite of drastic efforts to find non hazardous solvents (hydrocarbons, perfluorinated hydrocarbons or ethers, ...) or to re-investigate cleaning processes using water + surfactants, carbon dioxide is becoming one of the most attractive substitute to chlorinated and CFC solvents. Many patents and articles are now appearing, mainly in USA where a very significant effort is made to substitute perchlorethylene for dry cleaning and trichlorethylene for part degreasing, by liquid CO_2. However, the industrial development of processes using CO_2 requires both :

- Optimized cleaning cycles minimizing residence time of the items in the cleaning zone ;
- Adequate surfactants for a high quality cleaning with minimized CO_2 and energy consumptions [1-3] ;
- Fully automated cleaning machine that should be easily operated and maintained by non-specialists.

SEPAREX has developed a cleaning machine [4] adapted to treatment of mechanical or electronical parts made of metals, polymers, composites, ... using liquid CO_2 as solvent : it is fully automated for an easy operation, including fast closure of the autoclave. Carbon dioxide is not recycled, and it can be added a surfactant and/or a co-solvent in a period of the cleaning cycle.

The volume of the cleaning autoclave is 60 liters.

Process and machine description

As the process and plant will be operated in mechanical or electronical shops, it is absolutely necessary that operation and maintenance be very easy and take the least time as possible. It is the reason why we choose to simplify the process :

- No CO_2 recirculation, what means that no CO_2 pump is necessary ;
- No heating/cooling medium circulation.

This leads to the general flowsheet presented on figure 1 :

Liquid CO_2 from the storage (10 to 20°C, 50 bar) is introduced in the cleaning autoclave (1), possibly added with a co-solvent or a surfactant through a small pump (2). In the cleaning autoclave (1), a basket (3) is designed to receive the parts to be cleaned : the liquid CO_2 is subjected to natural convection induced by a gas-lift, as described later, and/or to forced convection induced by a turbine (4) moved by a variable-speed motor (5) through a magnetic driver. The cleaning autoclave closure system is fully automated and the basket can be moved in and out by a hoist (Cf. picture 1). CO_2 exits the autoclave through the bottom and is further reheated in the electrically-heated exchanger (6) prior to oil separation in a high performance cyclonic separator (7). CO_2 flowrate is controlled by an automated needle valve (8) under control of a mass flowmeter (9). In order to avoid a low temperature exploration that might destroy or heavily damage the parts, nitrogen or dry air is introduced in the autoclave at the end of the cleaning cycle, prior to final CO_2 venting.

High reliability and safety are obtained by failsafe systems as common practice in CO_2 extraction plants. The cleaning cycle and all process operations are managed by a computer, including safety functions.

In fact, the main originality consists in the autoclave design (see picture 1) that is described in a recent patent application [4] : according to the schematic view presented on figure 2, the basket (3) containing the parts to be cleaned is a cylinder, closed at the bottom by a metal grid, of a diameter slightly lower than the internal autoclave diameter so as to maintain a cylindrical annular passage for the fluid ; the bottom of the autoclave is designed with an open annular channel in which is set an electrical resist (10). At the beginning of the cleaning procedure, liquid CO_2 is introduced from a nozzle or a distributor (11) fixed on the autoclave lid and fill the autoclave until it reaches a level N, just below the basket upper section. At that moment, the resist (10) is turned on : the heat provokes a partial vaporization of CO_2 in contact with the resist, what induces a gas-lift convection through the passage between the basket and the autoclave walls. The two-phase fluid mixes with the colder "fresh" CO_2 arriving through (11) and condenses to a liquid phase that falls again onto the pieces. During this cleaning time, a small flowrate of CO_2 is added through (11) meanwhile a similar amount of fluid is withdrawn at the bottom port (12) in order to maintain a quasi-constant quantity of CO_2 inside the autoclave. It is to be noticed that most pollutants dissolved in CO_2 while leaching the parts are precipitated onto the resist as CO_2 density is decreased and are carried away with the exiting fluid prior to their further recovery in separator (7) (cf. figure 1).

Experiment

In order to evaluate the efficiency of the natural (gas-lift) and forced convection on cleaning, a wide experimental plan was realized, using very difficult conditions in order to evaluate the impact of the various parameters : in fact, parts were covered with very high quantities of oil, that are much more important than currently found on work pieces.

Materials

All experiments are made with the same metal parts, chosen as complex nuts, tees and connections currently used in plumbing, made of cast iron, carbon steel, stainless steel and brass (see picture 2). At first, they are immerged in the selected oil and then collected in the basket in which they are cleaned with liquid CO_2.

CO_2 is European Standard Quality from CARBOXYQUE.

Two contaminants are used :

- A soluble machine oil : TEXSOL H3 from Texaco mixed with water (5% oil) taken after use on a lathe.
- An engine oil : CARTER 220 from Elf.

Measurements

After cleaning with liquid CO_2, the pieces are subjected to a very intense cleaning in an ultrasonic bath using chloroform ($CHCl_3$) as solvent ; the resulting solution is carefully evaporated in a rotating evaporator and the liquid residue is weighed (± 0.1 g).

CO_2 Cleaning Cycle

• CO_2 filling (45 kg)	4 min
• Cleaning (3 different processes)	0 to 60 min
• Slow emptying	15 min
• Nitrogen sweeping	10 min

CO_2 Cleaning Processes

- Process 1 : soaking the pieces in the autoclave.
- Process 2 : soaking (1/3 of cleaning time) then emptying and rinsing with a new complete filling of CO_2 (45 kg).
- Process 3 : circulation of CO_2 through the autoclave. The amount of added CO_2 is the same as for Process 2 (45 kg).

CO_2 Cleaning Methods :

- no agitation.
- natural convection (figure 2).
- forced convection (figure 3).

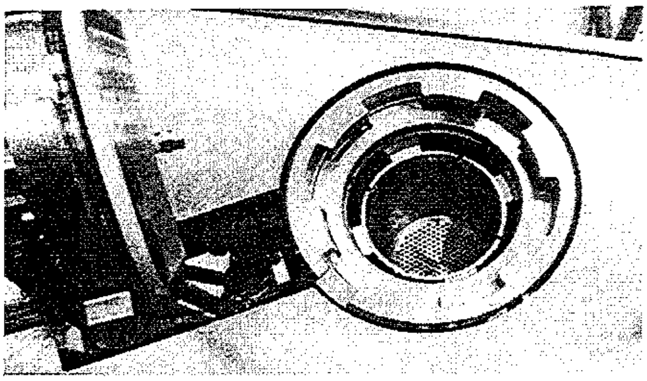

Picture 1. Cleaning Autoclave (60 liter)

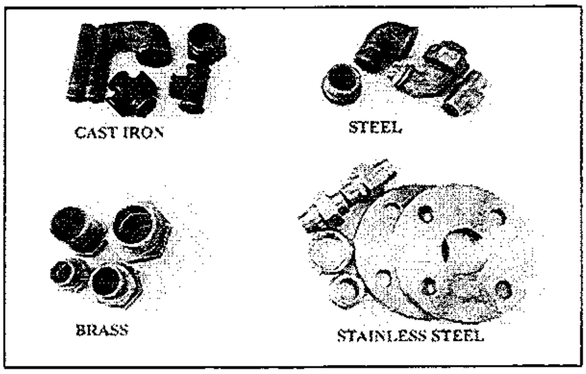

Picture 2 : parts to clean

Results

Efficiency of the different processes and methods

Figures 4 and 5 compare the processes and methods of cleaning for the machine oil and the motor oil, with a cleaning time of 40 minutes.

Concerning the comparison of cleaning processes, the most important differences are reported for the machine oil removal with natural convection, where processes 2 and 3 reduce the amount of remaining oil by half. But almost no changes are noticed in the other cases.

The impact of the different cleaning methods is more important. Natural and forced convections improve very significantly the elimination of the two oils ; and they have the same efficiency to remove the machine oil in process 2 or 3.

But the differences between these two methods for engine oil cleaning demonstrates that the shear forces induced to remove oil from the surface of the parts are more important for the forced convection than for natural convection.

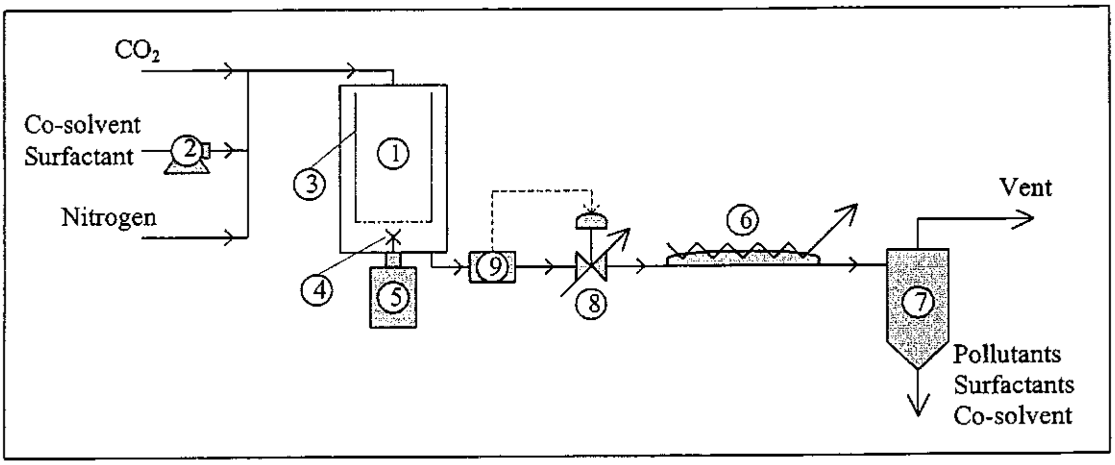
CO₂
Co-solvent
Surfactant
Nitrogen
①
②
③
④
⑤
⑥
⑦
⑧
⑨
Vent
Pollutants
Surfactants
Co-solvent

Figure 1. General flowsheet

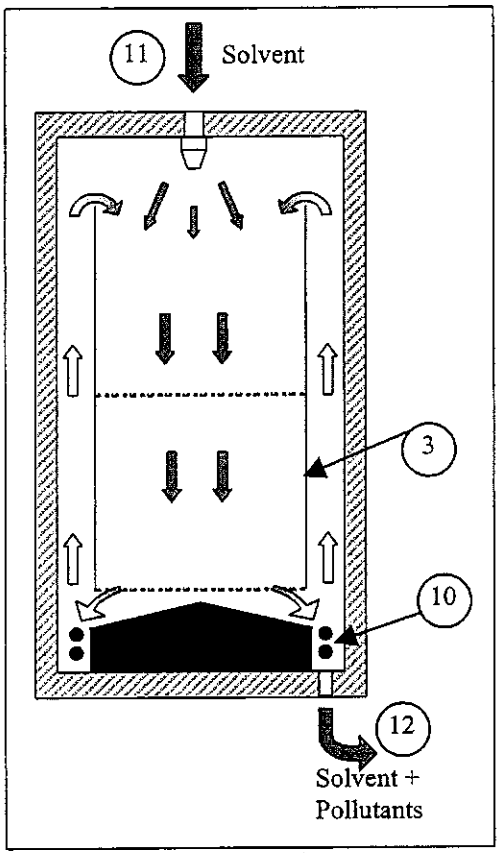
11
Solvent
3
10
12
Solvent +
Pollutants

Figure 2. Natural convection

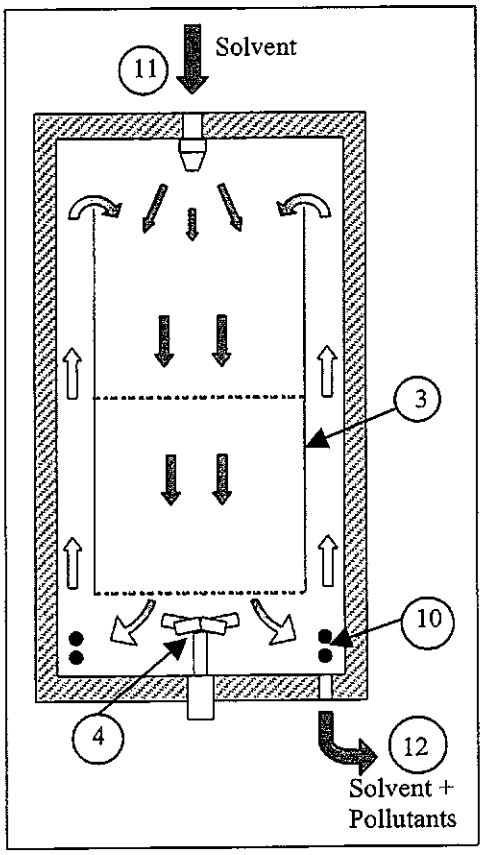
11
Solvent
3
10
4
12
Solvent +
Pollutants

Figure 3. Forced convection

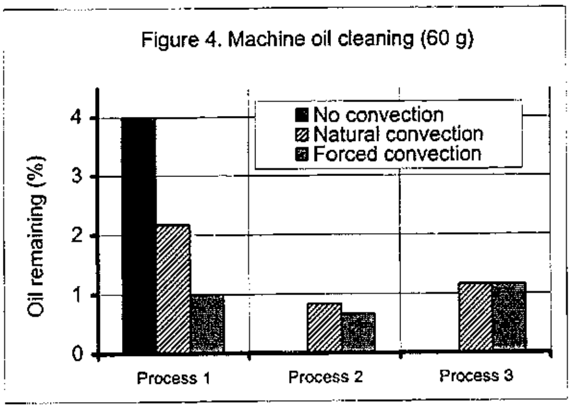

Figure 4. Machine oil cleaning (60 g)

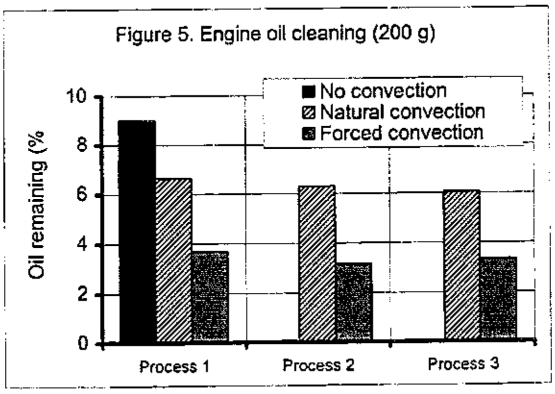

Figure 5. Engine oil cleaning (200 g)

Influence of the amount of oil to eliminate

A known quantity of engine oil is poured on the parts to clean. The cleaning parameters are as follows : process 1, natural convection, 40 minutes cleaning time. The results are presented on figure 6. They suggest that the same amount of oil remains on the pieces as far as the quantity put before is sufficient to cover completely the surface of the parts. This means that this cleaning technique leaves a layer of oil with the same thickness whatever the quantity of oil may be before.

This confirms the results shown on figure 5, the amount of oil remaining depends on the mechanical energy for cleaning but not on the oil / CO_2 ratio.

Figure 6. Engine oil cleaning : Influence of the amount of oil put on the pieces

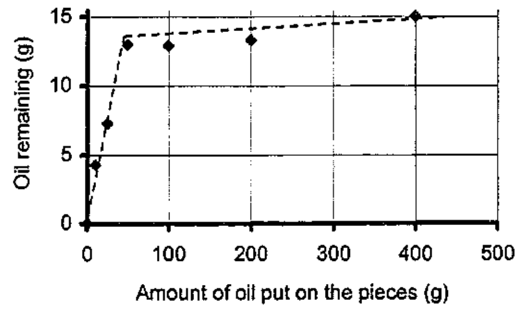

Figure 7. Engine oil cleaning : Influence of Cleaning Time

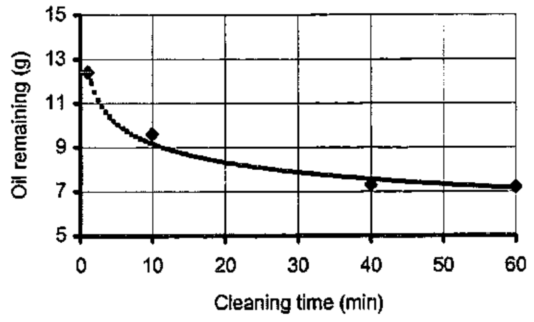

Influence of cleaning time

25 g of engine oil are poured on the parts to be cleaned. The cleaning parameters are as follows : process 1, natural convection, 0 to 60 minutes cleaning time. The results submitted on figure 7 show that the maximum efficiency for the process is reached after 30 to 40 minutes cleaning.

Surfactants

Some potential surfactants are tested to improve the cleaning efficiency of the machine. The selected conditions are as follows : process 2 (in order to rinse the parts), forced convection and 40 minutes cleaning. The pollutant is a mixture 50:50 of the two oils (50 g). About 50 g of surfactant (concentration in CO_2 : 0.1%) is added during filling in the autoclave.

The following surfactants are tested :

- Fomblin Z-DOL (Ausimont SpA) : hydroxy-terminated perfluoroalkylpolyether (Mn = 530 dalton) ;
- Q2-5211 (Dow Corning) : glycol-silicone copolymer used as superwetting agent ;
- FS1265 (Dow Corning) : fluorosilicone ;
- Tegopren 5878 (Goldschmidt AG) : polyether siloxane ;
- KRYTOX FSL (DuPont de Nemours) : carboxy-terminated perfluoroalkylpolyether (Mn = 2500 dalton) ;
- Citral : from lemon oil.

No surfactant improves the quality of cleaning (the amount of residues is always higher than without surfactant). This means that other types of surfactant must be found to improve the cleaning process. Another study of the behavior of such products should be necessary by observation in a sapphire cell.

Industrial development

Presently, SEPAREX is working on its pilot plant on various types of parts mainly originated from high-tech applications including instrumentation, opto-electronics, guidance systems, electronic boards, television parts, ...

Cleaning is very efficient and most organic compounds are removed ; however, as found in the results presented here, the cleaning efficiency is often lower than the efficiency observed with chlorinated solvents :

- A thin film of oil may remain at the surface, that is not always an issue ... and is sometimes wanted to avoid oxidation during the part storage ;
- Some stains of additives may appear, depending on the oil/grease composition, what suggests the need for addition of a surfactant active in liquid CO_2, to be selected case-by-case.

Finally, this study demonstrates that a very simple and inexpensive system leads to attractive results, especially when natural convection is efficient enough, what avoids any mechanical agitation. However, ultrasonic agitation may probably be beneficial to this natural convection system without complexifying the equipment.

References

1. Micell Technologies, Raleigh (North Carolina-USA), Technical note, 1997.
2. University of Texas/Air Products and Chemicals, Patent EP 0 814 112, 29/12/97, Priority : US 667, 132, 20/06/96.
3. Unilever, Patent WO 96/27704, 12/09/96, Priority 06/03/95.
4. Perrut, M. ; Perrut, V. ; French Patent 98.03451, 20/03/98.

Cleaning of Metal Parts and Components by Compressed Carbon Dioxide

N. Dahmen*, J. Schön, H. Schmieder, E. Dinjus
Forschungszentrum Karlsruhe, Institut für Technische Chemie CPV, P.O.Box 3640,
D- 76021 Karlsruhe, Germany
EMAIL : nicolaus.dahmen@itc-cpv.fzk.de
FAX : +49 7247 82 2244

A process was developed for the cleaning of metal parts and components by use of compressed carbon dioxide in the liquid and supercritical state. Laboratory studies were performed to determine the solubility of cooling lubricants and to investigate the effect of added detergents. Using samples from industrial production, cleaning parameters were scanned for a wide range of types from different metal working processes, where a variety of contaminants had to be removed. In some cases optimized parameters were determined in order to estimate cycle times as a basis for a process design.

Introduction

Industrial cleaning of components is a frequent step in technical production. It serves to clean small metal parts of adhering cooling lubricants and other kinds of dirt after manufacture and prior to further processing. The use of compressed carbon dioxide is a promising alternative for conventional cleaning processes such as the treatment with aqueous detergents, flammable or chlorinated hydrocarbons. During the last years the costs increased considerably for the traditional processes caused by waste water treatment, emission law and explosion prevention, respectively. One advantage of CO_2 as solvent are the inert properties, avoiding the forgoing problems. The use of pure CO_2 allows an unproblematic regeneration in a cyclic process, satisfying the demands for encased processes and closed circuits. In contrast to conventional processes, no secondary waste is generated.

The ability of compressed carbon dioxide for deoiling processes was successfully tested by the removal of oils from glass and metal grinding sludge [1,2], which is available commercially. By deoiling grinding sludge with CO_2 oil of good quality is produced, which can be recycled into the process, as has been demonstrated by oil manufacturers. In the further developments the process was extended to remove oil adhering to metal parts and components. In literature experiments are described using model systems [3] and industrial parts as well [4]. The process development described here was performed using samples from industrial production using 50 products and semi finished products from the industry:

- Material: steel, brass, aluminum, copper, sintered metals and composite materials
- Working process: drilling, machining, cutting, deforming, punching, casting ....
- Geometry: threads, internal threads, bore holes, blind holes.....
- Pollution: cooling lubricants, greases, pastes, particles

For the experiments the dimensions and the number of parts was limited by the size of the high pressure vessels used.

In the table, some properties of conventional cleaning compounds and CO_2 are compiled. In comparison to conventional cleaning agents, compressed carbon dioxide shows low values of viscosity and surface tension, allowing the cleaning of parts with complex and small dimensioned geometry and also of sintered materials [5].

Compound	Density ρ $g\,cm^{-3}$	Viscosity η $mPa\,s^{-1}$	Interfacial tension σ $mN\,m^{-1}$
Aqueous	≈ 1	≈ 1	30-72
Flammable	0.75-0.9	1.25-3.0	24-30
Halogenated	1.43-1.62	0.58-0.88	26-32
CO_2	0.4-0.9	0.03-0.1	5-30

Solubility of metalworking fluids

The time needed for dissolving of the oils and fats in CO_2 is determined mainly by their solubility and the mass transfer rate. Metal working fluids often consist of complex mixtures of different hydrocarbon components and additives. Looking at cutting oils on mineral or synthetic hydrocarbon basis it was found that solubility is not very different and comparable to squalane, which can act as a model compound for such oils [6]. This class of oils covers a wide range of metal working fluids in metal cutting processes. Larger differences are observed for other oils like mineral white oil consisting of low molecular weight liquid paraffin showing a markedly higher solubility or for native oils showing a significantly lower solubility. For other processes where cooling lubricants with increasing content of high molecular weight components (drawing punching fats and greases) are used, solubility is reduced markedly. This is also valid for the variety of additives like the commonly used fatty acids, esters, sulfur- and phosphor containing compounds, and detergents. In addition, insoluble solid particles like abrasive are contained. Finally residual working fluids from previous machining processes can be found on the parts due to carrying over of the fluids.

Use of detergents

To come to the desired cleanness in a reasonable time the addition of entrainers and detergents is useful [7]. The application of surfactants would have:

1. to assist the separation of pollutants from the surfaces to be cleaned
2. to disperse insoluble components and fractions

In a recent investigation the influence of a CO_2-soluble amphiphile on a non polar squalane phase and on a polar water phase characterised by the interfacial tension was studied. In the experiments a non ionic polydimethylsiloxane with polyether end groups was used (Fig. 2)[8]. α,ω-Siloxan 60 is a linear siliconepolyether with a medium molecular weight of 5440 g/mol. This type of surfactant is not commercially available. α,ω-Siloxan 60 consists of 60 dimethylsiloxane groups, forming the 'CO_2-philic' part. The polymer end chains consist of 1-2 ethylenglycole groups and 6-7 propyleneglycole groups as 'CO_2-phobic' tails with a medium molecular weight 500 g/mole.

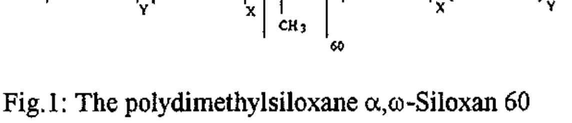

$$H-\left[O-(C_3H_6)\right]_Y-\left[O-(C_2H_4)\right]_X-\left[\underset{CH_3}{\overset{CH_3}{Si}}-O\right]_{60}-\left[(C_2H_4)-O\right]_X-\left[(C_3H_6)-O\right]_Y-H$$

Fig.1: The polydimethylsiloxane α,ω-Siloxan 60

The interfacial tension was determined using the pendent drop method. A drop of squalane or water, respectively, is generated pending at a capillary and exposed to pure or surfactant containing (1 wt,%) CO_2. With increasing pressure interfacial tension is reduced. The most pronounced changes occur near the critical isochore of CO_2. With rising pressure a value of ca. 25 mN/m is reached in the CO_2-water system at 50°C (Fig.3). In the CO_2-squalane system a value of zero is approached; here complete miscibility of the both components is attained.

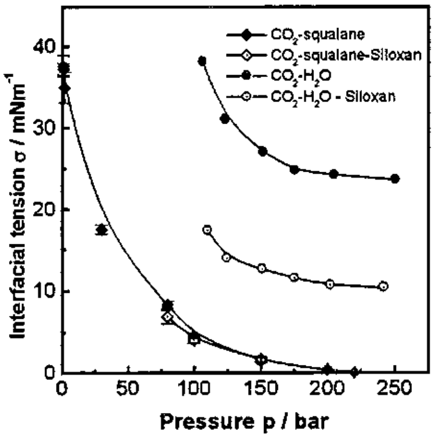

Fig.2: Interfacial tension in the CO_2-squalane and -water system with and without Siloxan 60 at 50°C

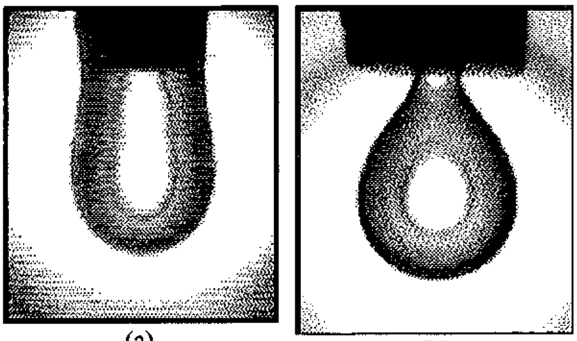

(a) (b)

Fig. 3: Images of drops of squalane in pure CO_2 (a) and with addition of the Siloxan 60 (b) at 150 bar and 50°C

From Fig. 3 it becomes evident that interfacial tension in the squalane systems is not changed, while it is drastically reduced in the water system by addition of Siloxan 60. This is due to its hydrophilic character of the polyether end groups, which in addition leads to a displacement of oil from the surface of metal parts. This was observed also at the capillary tip of the experimental device (Fig. 3. (b)).

With regard to the metal cleaning process this is a desired effect, but not sufficient for a surfactant aided cleaning process. In a next step, the scavenger effect of CO_2-soluble dispersing agents will be investigated, which have to exhibit a more lipophilic chemistry in order to emulsify the substances removed during the cleaning process. Furthermore synergistic effects of different surfactants will be studied which are common in conventional aqueous cleaning processes.

Cleaning experiments

The experiments were performed in two devices. Single parts of small geometry were basically investigated in a laboratory extraction setup using SFE extraction cells up to 50 ml volume [2]. Here the influence of pressure, temperature, flow rate and specific CO_2-throughput were studied. Larger parts and complete batches were treated in a bench-scale plant, containing a fixed 4 dm^3 autoclave and a 12 dm^3 rotating autoclave (Fig. 4). CO_2 is taken from a liquid CO_2-storage and is compressed by means of a high pressure pump, permeating the components to be cleaned and dissolving adhering residues. Then, the compressed fluid is expanded and the substances removed before are separated quantitatively. The CO_2-gas is liquefied by cooling and fed back to the pump. Max. operating conditions are 50 MPa at 100°C with 30 kg/h CO_2-flow.

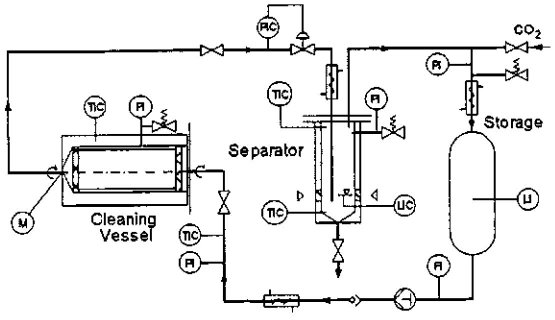

Fig.4: Scheme of the bench scale plant

Especially in the treatment of oil impregnated sintered materials pressure and temperature dependence of the deoiling rate is important, because an optimum in solubility and mass transfer rate has to be found.

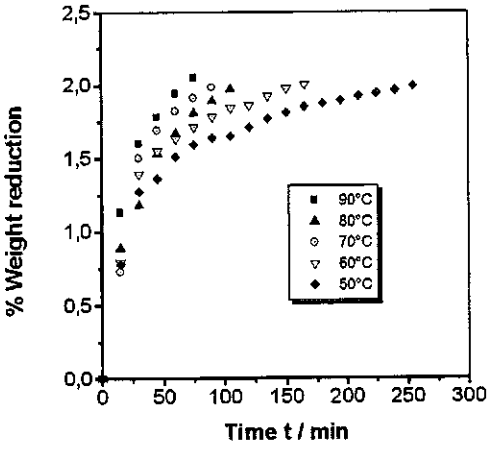

Fig.5: Extraction rate for sintered material in dependence of temperature at a density of 0.75 g cm^{-3}

In Fig.5 the influence of temperature at constant solvent density on the extraction rate is shown. An increase in temperature from 50 to 90°C results in a reduction of extraction time by a factor of 3. The task was to reduce the oil content by 2 wt.%.

The time needed for a cleaning cycle depends also on CO_2-throughput and -flow rate. They have to be optimized, especially in the case of oil-impregnated sintered materials, where alternating static and dynamic treatment is applied. Each cleaning cycle in the Fig. 6 lasts for the same time, but differs significantly in the specific CO_2-throughput depending on the ratio of static and dynamic cycle times. The oil content to be removed amounted to ca. 3 wt.%.

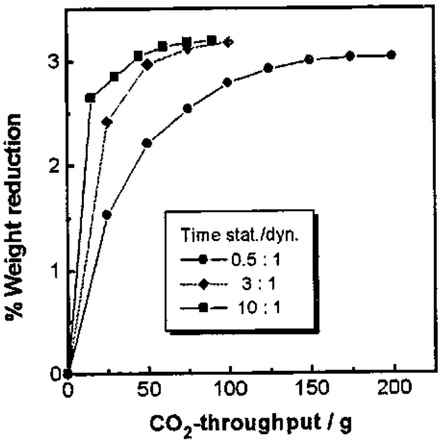

Fig. 6: Extraction efficiency of deoiling sintered material using static and dynamic cycles

The cleanness depend strongly on the type of cooling lubricants used and the kind and amount of other contaminants. Parts from metalworking, where pure oils or fats are used (cutting, drawing) can be cleaned without problems. Parts from processes, where solids occur (polishing, lapping), are more problematic because of the poor solid carrying capacity of the carbon dioxide. To come to satisfying results, additional energy has to be introduced to the system by mechanical or hydrodynamic methods. Especially for the treatment of loose goods it already turned out to be necessary to use the rotation autoclave for a constant cleaning result.

Pure CO_2 can only be a solvent for a limited number of cleaning applications. To extend the range of applications entrainers or detergents can be used as in conventional cleaning processes. To fit a specific cleaning problem, new classes of surfactants has to be identified or even to be synthesised.

---

[1] J. Schön, N. Dahmen, H. Schmieder, K. Ebert, ACS Symposium Series 670, ACS, Washington, 1997, 270-279

[2] J. Schön, N. Dahmen, H. Schmieder, E. Dinjus, Proceedings of the 20th Int. Symp. On Capillary Chromatography, May 26-29, 1998, Riva del Garda

[3] E. Björklund, C. Turner, L. Karlsson, L. Mathiasson; *J. Supercritical Fluids* **1996**, 9, 56-60

[4] J. McHardy, T.B. Stanford, L.R. Benjamin, T.E. Whiting, S.C. Chao; *SAMPE Journal*, **1993**, 29 (5), 20-27

[5] K. Abaroudi, C. Maillet, F. Trabelsi, F. Recasens; Proceedings of the 5th Meeting on Supercritical Fluids, March 23-25, Nice, France, 1998, 181-186

[6]N. Dahmen, J. Schön, H. Wilde, H. Schmieder, Process Technology Proceedings, 12, Elsevier, Amsterdam-Lausanne-New York-Oxford-Shannon-Tokyo, 1996

[7] J.C. Meredith, K.P. Johnston; Proceedings of the NATO ASI Supcercitical Fluids – Fundamentals and Applications; July 12-24, Kemer, Turkey, 1998

[8] N. Dahmen, J. Schön, H. Schmieder, S. Veith, O. Muth, T. Hirth; Proceedings of the 5th Meeting on Supercritical Fluids, March 23-25, Nice, France, 1998, 187-191

To Revert Grinding Sludge into Oil and Metal
- An Application for Supercritical Fluid Extraction in a Technical Scale -

Dr. U. Leffrang*, K. Büttner and R. Schwing
HIM*TECH* Hessische Industriemüll Technologie GmbH
Kreuzberger Ring 58, D – 65205 Wiesbaden, Germany

The separation of metal grinding sludge into oil and metal by using supercritical carbon dioxide (EMSIC process) has been developed by the Research Center Karlsruhe for Technology and Environment (FZK). HIMTECH, an engineering and consulting company in the field of industrial and hazardous waste, has brought the EMSIC process together with FZK to a technical and economical maturity level.

The disposal of most of the metal grinding sludge is restricted to disposal on landfills, the thermal utilisation within the cement industry or the incineration in hazardous waste incineration plants at the moment. Besides that mechanical and chemical-physical procedures for the utilisation of grinding sludge have been developed in the last few years. All these procedures have in common that only one of the contained fractions (mostly the metal fraction) can be utilised.

The EMSIC process is a new method for the treatment of metal grinding sludge by high-pressure extraction in carbon dioxide, which makes the separation of the contained grinding oil in a reusable quality possible for the first time. This allows the material utilisation of both of the contained fractions of these hazardous wastes from the metal processing industry: metal and oil.

Introduction

Metal grinding sludge is waste from processes of the mechanical forming like grinding or honing, which contain fine metal particles, abrasion dust, cooling lubricants (grinding oil) and other pollution. The quantity ratio of these contained substances depends on the treatment process and the treated material - therefore great variations appear: the oil contents may vary between 15 and 50 % by weight, the metal contents between 30 and 60 % by weight.

At present and in future considerable amounts of metal grinding sludge are generated. Besides coarse metal cuttings approximately 150,000 to 200,000 tons of grinding sludge per year are generated in the Federal Republic of Germany only; about 70,000 tons of these sludge result from treatment processes with non water-mixed cooling lubricants [1]. These grinding sludge are especially suitable for the proposed EMSIC process (de-oiling of metal grinding sludge in supercritical CO_2).

Additionally to the disposal costs of the grinding sludge also the required replacement of the high-quality cooling lubricants (grinding oil) causes high operation costs in the metal processing companies. This leads to a great interest in a process that recirculates the oil content of these grinding sludge to the production process and meets the requirements of the actual legislation and licensing practice (closed cycle for material economy).

In addition to the direct regaining and recycling of the oil within the metal treatment process an economical interest can be found in the simultaneous utilisation (smelting etc.) of the de-oiled metal fraction.

State of Disposal Technology

At present, the disposal of most of the metal grinding sludge is performed by disposal on landfills, thermal utilisation within the cement industry or the incineration in hazardous waste incineration plants.

Momentary, the importance of disposal on landfills is decreasing because the disposal landfills are running short anyway and the limits for the disposal on landfills are getting stricter.

The incineration within cement plants or hazardous waste incineration facilities is not free of problems, too. It causes emissions, which lead to pollutant loads, and is only an energetic utilisation and not material utilisation in maximum.

In the last years mechanical and chemical-physical processes for the regaining of grinding sludge have been developed. A simple mechanical process for the utilisation of the metal fraction has been established for metal grinding sludge with water-mixed cooling lubricants. Within this process the metal grinding sludge is mixed with metal cuttings and compacted in high-pressure presses to solid pellets. The application of this process for the oil-containing grinding sludge causes the following problems: at the one hand, often the necessary cuttings have to be bought, which causes a mixture of different recycled grinding oils and prevents a recycling of the grinding oil in the metal processing industry. At the other hand, the residual oil content of the metal fraction reached with this process is often too high to utilise the metal.

Other chemical-physical processes for the separation of the grinding oils from the metal grinding sludge are based on the vacuum-thermal drying, where the grinding oils are distilled in a vacuum at a temperature of approx. 200 - 300°C. The grinding oil is damaged by the elevated temperature of this process, that a reuse of the oil is impossible. At present, the separated oil is transferred to the waste oil disposal.

Another process for the utilisation of metal grinding sludge is the sintering process, where the upcoming grinding sludge is sintered at a temperature of approx. 1,300°C. Afterwards the stripped grinding oil is incinerated in a secondary combustion chamber. This process recirculates the metal into the metal cycle, but the grinding oil can, of course, not be reused.

All these processes have in common, that only one of the fractions contained in the metal grinding sludge can be utilised (mostly the metal fraction).

Besides that, the part of the grinding oil, which is discharged by the disposal of the grinding sludge, has to be replaced by fresh grinding oil. This results in considerable costs for every metal processing company.

Therefore a modern recovery concept is required with one clear aim: The optimal economic use of grinding sludge.

The EMSIC process described here allows the recycling of both fractions (grinding oil and metal) to a direct material utilisation. This leads to the required significant cost saving for the metal processing company and fulfils the conditions of the closed cycle for material economy in an ideal way.

The EMSIC Process

The proposed EMSIC process has been developed by the Research Center Karslruhe (FZK) and secured under license by HIMTECH. The EMSIC process is a new method for the treatment of metal grinding sludge by high-pressure extraction in carbon dioxide, which makes the separation of the contained grinding oil in a reusable quality possible for the first time.

The extraction process using supercritical CO_2 has been successfully applied for many years in different areas, e.g. in the food and pharmaceutical industry. Examples are the decaffeinating of coffee or the extraction of flavours from herbs and spices [2,3].

Supercritical carbon dioxide has solvent properties for grinding oils, which are comparable to the conventional solvents such as benzene or carbon tetrachloride without the same negative environmental features [4]. Supercritical CO_2 is to be understood as carbon dioxide above the critical point (critical temperature: approx. 31.3 °C, critical pressure: approx. 73.8 bar).

At the EMSIC process the grinding oils are extracted from oil-containing metal grinding sludge in a high-pressure extractor at temperatures of approx. 50°C and pressures between 150 and 300 bar by supercritical carbon dioxide. The oil containing supercritical carbon dioxide is expanded in a separator, where the grinding oil is recovered as a carbon dioxide-free product and can be reused directly for metal processing.

After the separator the separated CO_2 is liquefied, redensified, thermostated and as supercritical CO_2 reused for extraction. The metal fraction which remains after the extraction and which is polluted with eventually added filter additives and remainders of grinding tools can be recirculated in the metal processing. Figure 1 shows the principle flow sheet of the EMSIC process.

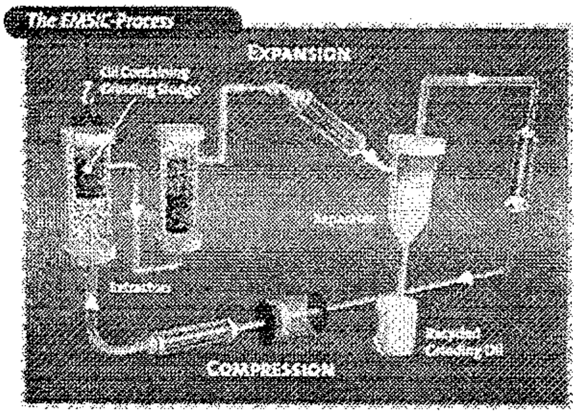

Figure 1. Principle Flow Sheet of the EMSIC Process

Advantages of the EMSIC Process

The low temperatures of the EMSIC process cause no thermal stress to the grinding oil. The residual oil content of the treated metal is always lower than 1% at a reasonable expenditure of energy.

Analyses of independent oil laboratories showed, that the grinding oil recycled by the EMSIC process has the same composition like the cooling lubricant the metal processing companies circulate in their central cooling and lubrication systems. In consequence, the grinding oil recycled by the EMSIC process can directly be released into the central lubrication systems.

Due to the treatment process in the metal processing company the additive content in the cooling lubricants decreases. This results, that fresh additives have to be added to the central lubrication system in certain intervals anyway. Therewith the additives for the grinding oils recycled by the EMSIC process are also added automatically.

Beside the simple re-use of the grinding oil due to the low thermal load during the procedure the EMSIC process can offer some remarkable benefits. The material recovery of the metal fraction (remaining oil content < 1 %) is possible. Due to that the EMSIC process serves as an ideal recovery solution as grinding oil and metal fraction are directly returned to the production cycle.

Additionally the EMSIC process offers an ecologically safe solution due to the avoidance of secondary waste.

Technical Feasibility

Based on the experience of the FZK [5], HIMTECH, an engineering and consulting company in the field of industrial and hazardous waste, has brought the EMSIC process together with FZK to a technical and economical maturity level.

This has been demonstrated by the separation of metal grinding sludge from different metal processing companies in a technical relevant scale of several tons. The oil content in the remaining metal fraction after separation was below 1 %.The recycled oil was always in a reusable quality.

The trust of the respective companies in the recycled grinding oil is only guaranteed, if their "own" grinding oil is not blended with other oils - the best solution is to return their "own" oil to them directly. To guarantee that, an EMSIC plant has to be operated batch wise, which allows a separate treatment of different kinds of grinding sludge.

By variation of the operation parameters the EMSIC process can be easily adapted to the different kinds of grinding sludge.

The EMSIC facility will consist of different extractor units and can be adapted to the necessary application (quality and amount of grinding sludge to be treated) by adding additional units. Big or small extractors in various sizes designed as a single or multi line facility are possible. This modular concept allows a high flexibility and simple adaptation of the process to the required application.

This leads to different applications: large extractors for a stationary facility at low operation costs with a larger logistic effort for the handling and management of the grinding sludge, the generated grinding oil and remaining metal fraction; small extractors for the installation in a container as a mobile system with higher operation costs but a reduced logistic effort. Figure 2 shows the computer simulation of a mobile EMSIC plant.

The EMSIC process in general offers a high operational safety by using proven technology and a high security potential by using CO_2 as extraction media. The operation costs can be reduced by a re-circulation of extraction media.

For interested organisations HIMTECH offers a full service in the field of the EMSIC process. It includes competent, individually orientated service packages, experimental demonstration in a technical relevant scale as well as design and delivery of turn-key facilities.

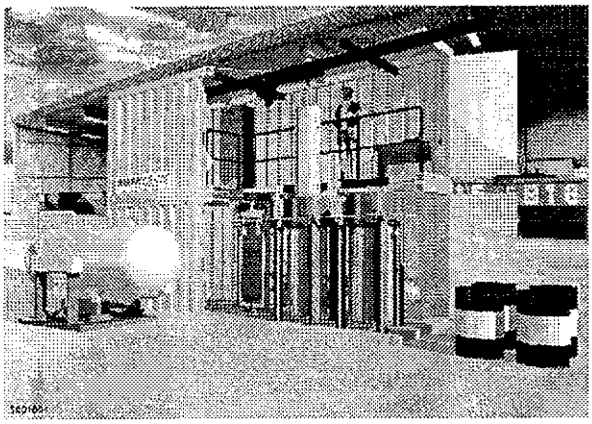

Figure 2: Computer Simulation of a
Mobile EMSIC Plant

Outlook

The EMSIC-process is perfectly suitable for the solution of the problems described in the chapters before.

The applicability of the EMSIC process is made evident by the interest of potential operators / clients in an innovative, economically and ecologically useful alternative to the present disposal. A few enterprises even consider a changeover to non water-mixable grinding oils, which could be utilised by the EMSIC process as soon as the process is established. There even exists a world-wide potential for EMSIC plants; as well as for plants for public use - this means, for waste producers with waste amounts which are too small for an own plant - as for company-owned plants for waste producers with the according large amounts of waste.

References

1. H. Kissler, Contribution to the Seminar of the FhG Institute Center, Stuttgart, 1997.
2. G.M. Schneider, E. Stahl, G. Wilke (Editors), “Extraction with supercritical gases”, Verlag Chemie, Weinheim, 1980.
3. M.A. McHugh, V.J. Krukonis, “Supercritical Fluid Extraction, Principles and Practice”, Butterworth, Boston 1986, 1993.
4. N. Dahmen, J. Schön, P. Schwab, H. Wilde, H. Schmieder, KfK Nachrichten 1994, 2, 128 – 132.
5. J. Schön, N. Dahmen, E. Dinjus, H. Schmieder, U. Leffrang, R. Schwing, Contribution to the “Werkstoffwoche”, Munich 1998.

Author Index

Abeln, J. 83, 111
Al-Salidi, S.H.R. 189
Arlt, W. 31, 51

Badens, E. 231
Barth, D. 205, 271
Bartle, K.D. 43
Basile, A. 189
Baur, S. 103
Behme, S. 31
Berger, T. 67
Bertucco, A. 239
Beuermann, S. 19
Biacs, P.A. 185
Boukis, N. 101
Brand, J.I. 97
Brembilla, A. 271
Bromilow, I. 43
Brunner, G. 123, 197, 215, 283, 287
Buback, M. 19, 35
Bungert, B. 51
Busch, M. 35
Buß, D. 197
Büttner, K. 305

Canel, M. 137
Casal, V. 103
Cebola, M.J. 267
Charbit, G. 155, 231
Chatzidoukas, Ch. 27
Chen, L. 173
Christensen, T. 215
Cihlar, S. 243
Clavier, J.-Y. 279
Clifford, A.A. 189
Commenges, N. 231
Crampon, C. 155

Dahmen, N. 301
Daood, H.G. 185
de Franca, L. F. 215
De Rosa, I. 251
de Vries, T.J. 23
Della Porta, G. 251
Depta, A. 283
Di Giovanni, O. 259
Diefenbacher, A. 151
Dinjus, E. 101, 111, 301
Dirand, M. 271
Dmoch, R. 43
Dörfler, W. 259
Eggers, R. 59, 193

Fischer, K. 167
Friedrich, C. 101

Gamse, T. 201, 209, 263
Gandolfo, S. 271
Germanus, J. 163
Giese, T. 283
Gießauf, A. 209
Gmehling, J. 167
Gnayfeed, M.H. 185
Gosolits, B. 275
Götz, Ch. 47
Gray, K.W. 131
Groß, T. 173

Härröd, M. 126
Harting, P. 163
Helfgen, B. 243
Hilbink, A. 275
Hirth, Th. 39
Hitzler, M.G. 131

Illés, V. 185
Isemer, Ch. 19

Jiménez-Carmona, M.M. 189
Johannsen, M. 283

Karger, N. 173
Keller, J.U. 63
Keurentjes, J.T.F. 23
Kinzl, M. 15
Kiparissides, C. 27, 55
Kiran, E. 5
Kleideiter, G. 75
Kluth, M. 111
Knez, Ž. 133
Knoll, W. 75
Krause, H. 247
Kröber, H. 247
Kruse, A. 111
Kurz, J. 275
Kümmel, R. 235

Lechner, M.D. 75
Leffrang, U. 305
Liu, K. 123
Lockemann, C.A. 193

Lüdemann, H.-D. 173
Luft, G. 15, 47

Macher, M.-B. 127
Magnan, C. 231
Majer, V. 145
Mantelis, Ch. 27
Marr, R. 201, 209, 263
Mazzotti, M. 259
Meehan, N. 131
Mengal, P. 279
Møller, P. 127
Morbidelli, M. 259
Muth, O. 39
Myers, P. 43

Neau, E. 156
Novak, Z. 133
Nunes da Ponte, M. 267

Pagalos, N. 27
Pallado, P. 239
Penninger, J.M.L. 89
Perrut, M. 279, 297
Perrut, V. 297
PetitJean, D. 271
Petrich, G. 111
Philippon, L. 205
Pietsch, A. 193
Pilz, S. 91, 107
Pladis, P. 55
Poliakoff, M. 131
Pop, E. 205

Rau, A. 47
Rave, H. 63
Reverchon, E. 251
Richter, T. 119
Robson, M.M. 43
Ross, S.K. 131
Ruivo, R. 267
Runge, F. 193

Schaber, K. 243
Sadowski, G. 31, 51
Sadri, E. 111
Schmaltz, C. 19
Schmidt, H. 103
Schmieder, H. 83, 111, 301
Schmitz, S. 47
Schneider, G.M. 159
Schön, J. 301
Schütz, E. 293
Schwing, R. 305
Sezer, A.O. 97
Simões, P.C. 267

Smail, F. 131
Staudt, R. 63
Steffen, W. 67
Steinberger, D.-J. 209
Steinkellner, F. 263
Stockfleth, R. 287

Teipel, U. 247
Tschernjaew, J. 235
Tuma, D. 159
Türk, M. 151, 243

van Boxtel, H.C.M. 35
van den Hark, S. 127
Vogel, H. 39, 119
von Schnitzler, J. 59
Vorstman, M.A.G. 23

Wahl, A. 19
Weber, A. 235
Weidner, E. 177, 225
Weiss, C. 235
Wiesmet, V. 177
Wilken, M. 167